

**NASA TECHNICAL
MEMORANDUM**



NASA TM X-3274

NASA TM X-3274

**CASE FILE
COPY**

9TH AEROSPACE MECHANISMS SYMPOSIUM

Held at

John F. Kennedy Space Center

Kennedy Space Center, Fla. 32899

October 17-18, 1974



NATIONAL AERONAUTICS AND SPACE ADMINISTRATION • WASHINGTON, D. C. • AUGUST 1975

STANDARD TITLE PAGE			
1. Report No. NASA TM X-3274		2. Government Accession No.	
4. Title and Subtitle 9TH AEROSPACE MECHANISMS SYMPOSIUM		3. Recipient's Catalog No.	
		5. Report Date AUGUST 1975	
7. Author(s)		6. Performing Organization Code	
9. Performing Organization Name and Address NASA John F. Kennedy Space Center Kennedy Space Center, Florida 32899		8. Performing Organization Report No.	
12. Sponsoring Agency Name and Address National Aeronautics and Space Administration Washington, D.C. 20546		10. Work Unit No.	
		11. Contract or Grant No.	
		13. Type of Report and Period Covered Technical Memorandum	
		14. Sponsoring Agency Code	
15. Supplementary Notes Held at John F. Kennedy Space Center on October 17-18, 1974			
16. Abstract This symposium includes presentation of both successes and failures in the design and development of mechanisms for space and aeronautical research programs. Emphasis is given to aerospace mechanisms which have been either flight qualified or flight demonstrated.			
17. Key Words Aerospace Systems Servomechanisms Mechanisms Devices		18. Distribution Statement Unclassified - Unlimited CAT 37	
19. Security Classif.(of this report) Unclassified	20. Security Classif.(of this page) Unclassified	21. No. of Pages 404	22. Price \$10.50

NOTICE

This document was prepared under the sponsorship of the National Aeronautics and Space Administration. Neither the United States Government nor any person acting on behalf of the United States Government assumes any liability resulting from the use of the information contained in this document, or warrants that such use will be free from privately owned rights.

The citation of manufacturer's names, trademarks, or other product identification in this document does not constitute an endorsement or approval of the use of such commercial products.

PREFACE

The 9th Aerospace Mechanisms Symposium, held at the John F. Kennedy Space Center, Florida, October 17 and 18, 1974, was sponsored jointly by the National Aeronautics and Space Administration, Lockheed Missiles and Space Company, Inc., and California Institute of Technology. This symposium is devoted exclusively to an interchange of ideas and information on aerospace mechanisms.

Contributions were from NASA Research Centers, U.S. universities, and U.S. manufacturers.

ACKNOWLEDGMENTS

This report and the conduct of the symposium benefited from the dedicated contribution of many individuals and organizations. In addition to the key role played by the Committee for Aerospace Mechanisms Symposium, I wish to recognize the efforts of the local arrangements committee at the John F. Kennedy Space Center. They include: Barbara M. Westfeldt, Nadine Y. Socks, Fred Christ, Kirby Key, W. Wheeler, W. C. Jones, Norm R. Perry, L. Blocker, W. Munsey, R. Cato, R. Miller, G. Brown, Jean S. String, James M. Taylor, Thurman Killian, F. Markley, Al Lavender, Diana Holden, Beverly Wesche, and Grace Palmer.

O. H. Fedor
Host Chairman,
John F. Kennedy Space Center

9TH AEROSPACE MECHANISMS SYMPOSIUM

MORNING SESSION - October 17, 1974

Chairman: K. A. Faymon
NASA Lewis Research Center

1. FORWARD BEARING REACTOR MECHANISM FOR TITAN IIIE/CENTAUR D-1T
SPACE LAUNCH VEHICLE 1

Richard A. Jones, General Dynamics Corp., Convair Aerospace Div.
2. A MANIPULATOR ARM FOR ZERO-G SIMULATIONS 19

Shepard B Brodie, Christopher Grant, and Janos J. Lazar, Martin-
Marietta Corp., Denver Div.
3. STRUCTURAL EVALUATION OF DEPLOYABLE AERODYNAMIC SPIKE BOOMS 31

B. J. Richter, Lockheed Missiles & Space Co., Inc.

Chairman: E. E. Sechler
California Institute of Technology

4. AEROSPACE LUBRICATION TECHNOLOGY TRANSFER TO INDUSTRIAL
APPLICATIONS 45

Thomas J. Loran and Bill Perrin, Ball Brothers Research Corp.
5. A STRUT WITH INFINITELY ADJUSTABLE THERMAL EXPANSIVITY AND LENGTH . 59

Paul T. Nelson, TRW Systems Group
6. IN-FLIGHT FRICTION AND WEAR MECHANISM 69

E. J. Devine and H. E. Evans, NASA Goddard Space Flight Center
7. METAL WITH A MEMORY PROVIDES USEFUL TOOL FOR SKYLAB ASTRONAUTS . . 81

G. A. Smith, Fairchild Space and Electronics Co.

AFTERNOON SESSION

Chairman: A. C. Bond
NASA Lyndon B. Johnson Space Center

8. THE SKYLAB PARASOL 99

Jack A. Kinzler, NASA Lyndon B. Johnson Space Center

9. THE PERFORMANCE OF COMPONENTS IN THE SKYLAB REFRIGERATION SYSTEM .	115
Charles E. Daniher, Jr., McDonnell-Douglas Astronautics Co.	
10. REFURBISHMENT OF THE CRYOGENIC COOLERS FOR THE SKYLAB EARTH RESOURCES EXPERIMENT PACKAGE	133
Jerry C. Smithson and Norman C. Luska, NASA Lyndon B. Johnson Space Center	
11. SKYLAB TRASH AIRLOCK	149
Larry R. Price, McDonnell-Douglas Astronautics Co.	
Chairman: F. F. Martin NASA Goddard Space Flight Center	
12. A PRECISION SIX-METER DEPLOYABLE BOOM FOR THE MARINER-VENUS- MERCURY '73 MAGNETOMETER EXPERIMENT	161
Harry F. Burdick, NASA Goddard Space Flight Center	
13. DISPERSION DEVELOPMENT PROGRAM	175
D. J. Carlson, R. J. Lusardi, and W. H. Phillips, Chrysler Corp., Defense Div.	

MORNING SESSION - October 18, 1974

Chairman: K. C. Curry NASA Jet Propulsion Laboratory	
14. A NEW CONCEPT FOR ACTUATING SPACE MECHANISMS	187
William C. Strange, NASA Goddard Space Flight Center	
15. THE MECHANICAL DESIGN OF AN IMAGING PHOTOPOLARIMETER FOR THE JUPITER MISSIONS (PIONEER 10 AND 11)	199
James C. Kodak, Santa Barbara Research Center	
16. MAGNETICALLY SUSPENDED REACTION WHEELS	211
Ajit V. Sabnis, George L. Stocking, and Joe B. Dendy, Sperry Flight Systems	
17. USE OF COMPUTER MODELING TO INVESTIGATE A DYNAMIC INTERACTION PROBLEM IN THE SKYLAB TACS QUAD-VALVE PACKAGE	235
Raymond J. Hesser and Robert Gershman, McDonnell-Douglas Astronautics Co.	

Chairman: A. Giovannetti
NASA Ames Research Center

18. MODERN MECHANISMS MAKE MANLESS MARTIAN MISSILE MOBILE - SPIN-OFF
SPELLS STAIRCLIMBING SELF-SUFFICIENCY FOR EARTHBOUND HANDICAPPED . 247

George N. Sandor, David R. Hassel, and Phillip F. Marino,
Rensselaer Polytechnic Institute

19. LOADCELL SUPPORTS FOR A DYNAMIC FORCE PLACE 265

C. W. Keller and L. M. Musil, Lockheed Missiles & Space Co., and
John L. Hagy, Shriners Hospital

20. DEVELOPMENT OF A BONE-FIXATION PROSTHETIC ATTACHMENT 281

L. J. Owens, NASA John F. Kennedy Space Center

AFTERNOON SESSION

Chairman: D. Buchanan
NASA John F. Kennedy Space Center

21. A UNIQUE CHALLENGE: EMERGENCY EGRESS AND LIFE SUPPORT EQUIPMENT
AT KSC 295

Henry M. Waddell, Jr., Rockwell International

22. A DAMPER FOR GROUND WIND-INDUCED LAUNCH VEHICLE OSCILLATIONS . . . 313

J. G. Bodle and D. S. Hackley, General Dynamics Corp., Convair
Aerospace Div.

23. HOLDDOWN ARM RELEASE MECHANISM USED ON SATURN VEHICLES 335

J. D. Phillips and B. A. Tolson, NASA John F. Kennedy Space Center

24. CRAWLER TRANSPORTER STEERING AND JEL SYSTEM 359

V. L. Davis, NASA John F. Kennedy Space Center

25. MOUNT MECHANISMS FOR THE SATURN V/APOLLO MOBILE LAUNCHER AT JOHN F.
KENNEDY SPACE CENTER 373

Harry Balke, Harry Balke Engineers

26. AUTOMATED PARKING GARAGE SYSTEM MODEL 387

Carl R. Collins, Jr., JPL, California Institute of Technology

1. FORWARD BEARING REACTOR MECHANISM FOR TITAN IIIE/ CENTAUR D-1T SPACE LAUNCH VEHICLE

Richard A. Jones
General Dynamics/Convair Aerospace
San Diego, California

SUMMARY

This paper describes a load sharing system between the Titan/Centaur launch vehicle and its aerodynamic shroud. The system provides a precise spring constant and is capable of being inactivated during flight. Design requirements, design details, and the test program are discussed. The conventional English system of units was used during this development program for all principal measurements and calculations.

INTRODUCTION

The Titan IIIE/Centaur D-1T is the nation's newest space launch vehicle. The vehicle has recently been developed through the marriage of the newest booster in the Titan III family with the latest version of Centaur, the nation's first high energy upper stage vehicle. The Titan/Centaur vehicle was developed to launch the Viking spacecraft to Mars in 1975. It is also to be used to launch the Helios solar probe payloads and two Mariner-Jupiter-Saturn payloads in 1977. The configuration is characterized by a newly developed bulbous 4.27 meter (14 foot) diameter Centaur Standard Shroud (CSS) which covers the payload, the Centaur, and part of the Titan/Centaur interstage structure. The shroud is attached to and cantilevered from the interstage structure. The Titan/Centaur vehicle is shown in Figure 1.

In order to gain the cost effectiveness of commonality, the Centaur D-1T utilizes the same propellant tanks as those used on the version of Centaur which is flown on the Atlas booster. The propellant tanks, in addition to containing the Centaur propellants, are pressure stabilized in order to react vehicle external loads. For the Atlas/Centaur the loads are normally critical at 1) launch due to payload lateral excitation, 2) at the time of maximum aerodynamic pressure, 3) at booster engine shutdown,

and 4) at the various Centaur engine starts and shutdowns. For the Titan/Centaur, those four critical load times are identical to the Atlas/Centaur except for the maximum aerodynamic pressure load. The tanks are not subjected to aerodynamic loads because they are protected by the CSS. However, the other three critical load conditions, which are mainly payload weight originated, cause higher loads in the Titan/Centaur propellant tanks because the Titan/Centaur vehicle has a greater payload weight capability than the Atlas/Centaur. Analyses showed that the common propellant tanks could withstand all the larger Titan/Centaur loads except the launch lateral transient load imposed by the payload. Under this load condition, the aft end of the tanks became structurally critical due to the bending moment resulting from the relatively long cantilever support of the payload.

Two methods to alleviate that situation were considered; first, to increase the tank pressures and second, to provide a lateral load sharing device with the shroud. The first method had the disadvantage of requiring increased tank skin gages, revision to the pneumatic system, and revisions to many other related vehicle components and systems. In short, the propellant tanks would no longer be common. The second method, in addition to the advantage of preserving commonality of the tanks, had a further advantage of supporting the shroud during the aerodynamic load period of flight. Since CSS-to-payload and CSS-to-Centaur relative deflections are critical, CSS weight would be excessive if it had to be designed as a cantilevered structure attached at its aft end. A lateral support for the CSS to share airloads with the Centaur structure reduced the required CSS stiffness and thereby reduced its weight.

Conceptually, the ideal load sharing device would consist of a series of closely spaced springs between the Centaur vehicle and the CSS. This ideal system is shown schematically in Figure 2.

DESIGN REQUIREMENTS

The lateral support system was named the Forward Bearing Reactor (FBR) and the following requirements were established for its design:

- A. The lateral support system was to be mounted at the forward end of the Stub Adapter, which is near the forward end of the cylindrical portion of the Centaur vehicle. See Figure 1.

- B. The maximum lateral limit load capability of the Centaur vehicle at the station location described above is 88,965 Newtons (20,000 pounds). The maximum allowable deflection at that location is plus or minus 2.54 centimeters (1 inch), based on CSS-to-payload clearance limitations and allowable motions designed into components spanning between the CSS and Centaur. Therefore, a maximum spring constant was established for the FBR system to be 35,293 Newtons per centimeter (20,000 pounds per inch). Additionally, in order to facilitate overall vehicle loads analyses, it was required that this spring constant be constant over the full range of deflection of plus or minus 2.54 centimeters (1 inch).
- C. The FBR had to withstand a thermal environment of -54°C (-65°F) to $+71^{\circ}\text{C}$ ($+160^{\circ}\text{F}$) and a pressure environment of sea level to 1 millimeter of mercury.
- D. The presence of an FBR during the aerodynamic heating phase of flight is objectionable because of the asymmetric loads introduced into the CSS. Therefore, a requirement was established that the FBR system had to be made incapable of load transmittal after maximum aerodynamic loads were reduced but before significant aerodynamic heating had begun.
- E. The FBR system had to provide sufficient clearance so that there would be no "hang-up" or "bumping" during CSS jettison.
- F. The system chosen to render the FBR system incapable of load transmittal in flight had to be redundant. The system also had to be self-containing (no debris) and if there was a shock environment associated with the system, the shock levels had to be low.
- G. Any material left on the Centaur vehicle after jettison had to either be local and confined close to the vehicle or, if the material protruded outboard, it had to be non-metallic. This was required so as to not cause interference with antenna patterns from the antennas located just aft of the FBR system.
- H. The FBR system had to be capable of sustaining an axial deflection of the vehicle moving aft with respect to the CSS of 1.75 centimeters (0.69 inch) at liftoff and 1.47 centimeters (0.58 inch) during the period of maximum aerodynamic pressure. This is caused mainly by cryogenic shrinkage of the Centaur propellant tank.

- I. There was a design goal to make the system light with minimum system weight remaining with the vehicle. Since the CSS is jettisoned rather early in flight, the trade-off factor with payload weight is more favorable for CSS weight than for vehicle weight.

CONCEPTS

Several concepts were studied to identify a system to meet the above requirements. The concepts are listed below with a brief description of each.

Struts with Elastomeric Links and Elastomeric Spheroids

These two concepts were basically similar; they both employed elastomeric material to provide the precise spring constant required. However, preliminary studies and analyses indicated that it might not have been possible to design an elastomeric device which would have a linear spring constant over the temperature and load range required. The development program to determine the shape of the elastomeric material, if any, that would satisfy the requirements was considered risky.

Struts with Pneumatic Cylinders

This concept consisted of a pneumatic pressure compartment within a strut to provide the desired spring constant. The disadvantages of this system included its complexity because of the required gas storage provisions, piping, valving, etc. Although not studied in any great depth because of the system complexity, other obvious disadvantages were the difficulties of obtaining a linear spring constant, and possible system leakages which would result in pressure variation. Also, pressure variations caused by the wide temperature range would cause difficulties in providing a precise spring constant.

Pneumatic Tube

This concept consisted of a pressurized rubber "donut" shaped tube which transferred loads by bearing through the use of rollers or teflon slide pads. In addition to the disadvantages associated with pneumatic systems listed previously, it was found analytically that a relatively high pressure was required to obtain the design spring constant. In an

effort to achieve a near linear spring constant, tapered tubes and multiple concentric tubes each having a different pressure were considered. There was also a concern that, even though a low friction slide pad was provided, the tube would not maintain its shape when a relative CSS-to-Centaur axial deflection occurred simultaneously with a load transfer. The complexity and development risk were considered too great to choose this concept.

Thin Flat Sheet of Stainless Steel Cut by a Linear Explosive

This system had the advantage of combining the forward annular compartment seal with the load transfer device. However, it was felt that it would be difficult to obtain a precise linear spring constant. This concern would be compounded as the sheet developed shear buckles. The linear explosive device technology existed; however, no developed, tested system could be found which would operate in a plane around a curve. Utilizing a system operating in a series of straight lines had the disadvantages of leaving too large a metallic "shelf" which violated the antenna pattern requirement.

Struts with Conical Washers

This system consisted of a series of struts which contained conical or "Belleville" washers to obtain the desired spring constant, and a pyrotechnic device to inactivate the strut load carrying capability. Due to the length of strut required to package the number of conical washers required plus the pyrotechnic device, it was not possible to use radial struts. Therefore, a series of six struts spanning the CSS/Centaur vehicle annulus at an angle was proposed. This was the system chosen for development and is discussed in detail in the following sections.

FORWARD BEARING REACTOR SYSTEM DESCRIPTION

Total System Description

The FBR system consists of a series of six double acting spring struts located symmetrically around the CSS/vehicle annulus as shown in Figure 3. The struts are located nearly tangent to the Centaur Stub Adapter to facilitate load introduction. Load introduction into the CSS at a much greater angle is acceptable because of the existence of a deep frame located there for other reasons. Two of the struts are located in the plane of the Titan Solid Rocket motors to share the majority of the launch lateral loads developed by the unbalanced thrust buildup of the motors. The quantity of

four additional struts was chosen because the strut load magnitudes are small enough to be easily reacted by the CSS and Centaur, preferential load introduction structure is located on the stub adapter at these locations, and it preserved the required symmetry of the system.

The struts are installed with the inboard end 1.60 centimeters (0.63 inches) forward of the outboard end. As the Centaur vehicle moves aft relative to the CSS (due mainly to Centaur propellant tank cryogenic shrinkage) the struts move more into a station plane. Rotation of the strut ends about the attachment fittings is accomplished by use of spherical strut end fittings.

Strut Configuration

The individual struts as shown in Figure 4 are nominally 71.12 centimeters (28 inches) long. The strut has a separation plane inclined 1.4 radians (80 degrees) to the strut centerline. That portion of the strut to the right of the separation plane is the stub adapter mounted inboard portion; that portion to the left of the separation plane is the CSS mounted outboard portion. The precise spring constant is obtained by compressing the stack of 22 conical washers installed in the outboard portion of the strut. The washers are stacked in series rather than in parallel to reduce the frictional losses and non-linearity associated with a parallel stack. If a compression load is applied to the strut, the load is transmitted through the piston to the compression thrust washer. This compresses the conical washer stack against the tension thrust washer, which then transmits the load into the barrel. A tensile load is transmitted through the piston into the cap which loads the tension thrust washer. This in turn compresses the conical washer stack against the compression thrust washer which then transmits the load into the housing.

The conical washer chosen has the following properties:

$$OD = 8.00 \text{ cm (3.15 in.)} \quad t = .4999 \text{ cm (.1968 in.)}$$

$$ID = 4.09 \text{ cm (1.61 in.)} \quad \text{Spring Rate } K_w = 277,050 \text{ N/cm} \\ (157,000) \text{ lb/in}$$

$$\text{Therefore:} \quad \frac{1}{K_{\text{Stack}}} = \frac{22}{K_w}$$

Knowing from previous tests that the strut spring constant, K , without the conical washers is approximately 255,875 Newtons per centimeter (145,000 pounds per inch):

$$\frac{1}{K_{\text{Strut}}} = \frac{1}{K} + \frac{1}{K_{\text{Stack}}} = \frac{1}{K} + \frac{22}{K_w}$$

$$K_{\text{Strut}} = \frac{K K_w}{K_w + 22K} = \frac{255,875 (277,050)}{277,050 + 22 (255,875)} = 12,003 \text{ N/cm} \quad (6802 \text{ lb/in.})$$

The spring constant of the CSS, K_{CSS} , was determined to be approximately 882,326 Newtons per centimeter (500,000 pounds per inch) and the Stub Adapter spring constant, K_{SA} , was determined to be approximately 1,764,552 Newtons per centimeter (1,000,000 pounds per inch). Extreme accuracy of the spring constants was not required because the total system spring constant is not sensitive to the support structure. Because of the geometrical configuration of the struts, it can be shown that for any direction of shear load the equivalent of three struts placed parallel to the direction of loading will react the load. Therefore, the system spring constant is determined as follows:

$$\frac{1}{K_{\text{SYS}}} = \frac{1}{K_{\text{CSS}}} + \frac{1}{K_{\text{SA}}} + \frac{1}{3K_{\text{Strut}}}$$

$$= \frac{1}{882,326} + \frac{1}{1,764,552} + \frac{1}{3 (12,003)}$$

$$K_{\text{SYS}} = 33,932 \text{ N/cm} \quad (19,229 \text{ lb/in.})$$

It can be shown that using 21 conical washers in lieu of 22 exceeds the maximum 35,293 Newtons per centimeter (20,000 pounds per inch) requirement. The linearity of the strut spring constant in tension and compression is shown in Figure 5. This load/deflection curve was obtained by testing one of the struts flown on a recent vehicle. All flight struts are similarly tested and the curves from strut to strut are very uniform. Note that there is very good agreement between the theoretical strut spring constant of 12,003 Newtons per centimeter (6802 pounds per inch) and the test values. The spring constant in tension is less than 2.5 percent low and in compression is less than 0.5 percent low. The strut spring constant without conical washers of 255,875 Newtons per centimeter (145,000 pounds per inch) was obtained by testing an old strut design. It is suspected the present strut spring constant is lower, and

this brings the theoretical value even closer to the test values. As an additional data point, tests run on conical washer stacks with spring rates four to five times higher also exhibited good linearity, except for a small non-linear zone near the point where the load shifts from tension to compression.

The two strut segments are held together at the separation plane by use of a pyrotechnically actuated frangible bolt. Since the two redundant pyrotechnic cartridges must be installed late in the launch countdown, pyrotechnic cartridge access holes are machined into the strut body. The mechanically redundant frangible bolt is stronger (and therefore is larger) than required for this application; however, it is a flight qualified device used in many other applications on Centaur and was used in this application to gain the advantages of commonality.

The frangible bolt is shown in Figure 6. Separation is initiated when either or both of the cartridges are actuated generating a gas pressure on the face of the primary piston (3) which applies a force on the elastomeric coupling (6). The coupling amplifies the force, as a fluid would, and loads the secondary piston (7) by a factor of 3.15 to 1. The secondary piston in turn reacts against the secondary piston on the opposite side, which pushes against the insert (5) and subsequently the housing (1), putting the fracture plane in tension. As internal forces build up, the bolt breaks at the fracture plane and the bolt halves are driven apart by the stored energy within the system. The bolt has an ultimate breaking strength of 182,377 Newtons (41,000 pounds) to 204,618 Newtons (46,000 pounds).

Strut tension loads are transmitted directly through the frangible bolt; compression loads, which apply a shear force along the face of the separation plane, are reacted by a pair of shear pins extending across the separation plane. It is undesirable to load the frangible bolt in shear because of its low capability to carry shear through the frangible groove and also because the bolt is clamped on spherical seats in a loose fit hole. When either or both pyrotechnic cartridges are actuated, the bolt fractures through the groove and, as stated previously, a high velocity is imparted to the two halves. The velocity of the half on the inboard end is arrested by bottoming out on a rubber "O" ring. The shear pin assembly is attached to the outboard half and as the bolt half is driven away from the separation plane it withdraws the shear pins. The bolt half/shear pin assembly velocity is arrested by bottoming out on a metallic stop. The

possibility of rebound so that the shear pins reposition themselves back across the separation plane is prohibited by use of spring fingers which snap in place after the assembly passes by.

In order to meet the requirement that the FBR cannot transmit load during significant aerodynamic heating, the strut is separated by the frangible bolt 100 seconds after launch. At that time a conservative analysis showed that there could be as much as 20,017 Newtons (4500 pounds) tension or compression load in the struts. It was found during the test program of the original strut design that when the frangible bolt was actuated with that compression load on the strut, it often failed to separate. Due to the large deflection of the strut at this load (approximately 1.75 centimeters)(0.69 inches) the separation plane remains loaded through many degrees of rotation, rather than achieving immediate separation. As a consequence, frictional forces prohibited strut release. The surface finish was a high temperature curing solid film lubricant applied to hard anodized aluminum separation fittings. It was found that after the lube was applied, its surface consisted mostly of a concentration of the phenolic resin binder material. After the surfaces were carefully hand burnished (removing the surface concentration of binder material), acceptable strut separation was obtained. However, this was not an acceptable solution for production parts because of the problem of describing to the factory how much (or how little) to burnish and the improbability of obtaining consistent parts. Too little burnishing would not remove the binder material from the surface; too much burnishing would remove all of the very thin coating (0.00051 to 0.00127 centimeter) (0.0002 to 0.0005 inch). Therefore, a test program was initiated to determine if a surface finish could be found which would guarantee strut separation and would be producible.

Many different bearing surface finishes and lubricants were tested including anodized and hard anodized aluminum alloy, hardened steel with polished finishes, chrome plated steels, teflon coating, and various greases. The test program was accomplished using a set of three plates sandwiched and clamped together. The center plate was pulled while the two outer plates were held. The loads for the center plate to first move, and then to continue moving, were recorded. Based on the relative values so obtained, the best surface finish, by far, was a combination of a special grease consisting of 10 percent by weight of molybdenum disulfide powder mixed with a 90 percent by weight of silicone grease, applied to aluminum alloy separation fittings which had a hard, dense chrome plating electrodeposited on the bearing surfaces.

There are several reasons why this combination was best. The molybdenum disulfide powder has a low coefficient of friction, and also has an extremely high compressive load allowable. The silicone grease is a viscous carrier which flows as the surfaces slide, and it retains this property down to the lower temperature limit of -54°C (-65°F). The effectiveness of the molybdenum disulphide powder was demonstrated during the slip tests. Load values measured with the molybdenum disulphide powder plus silicone grease were only 25% to 30% of loads measured with silicone grease alone. The bearing surfaces were chrome plated to provide hard, smooth surfaces for the powder to act upon. The chrome is applied by an outside vendor using his proprietary method of electrodeposition at a low temperature. The plating thickness is 0.000127 to 0.00127 centimeter (0.0005 to 0.005 inch), has a Rockwell "C" hardness of 70-72, and a surface finish of 12-16 RMS. These properties are similar to those achieved by the conventional high temperature electrodeposited chrome plating per QQ-C-320; however, it does not contain the numerous surface microcracks that the conventional chrome plating does. Another advantage is the absence of warping or the possibility of hydrogen embrittlement (where applicable) inherent in the high temperature process.

The sliding action then occurs due to the sliding of one hard smooth surface upon the other, the surfaces being held apart by, and riding on the low coefficient of friction molybdenum disulphide powder. The relatively fine powder is effective because the surfaces are very hard and smooth and contain no surface microcracks.

Retract System

After the frangible bolt is actuated and the separation plane shear pins are driven away from the separation plane, the strut segments are rotated away from each other. The inboard segment is rotated and held in a position along the Stub Adapter; the outboard segment is likewise rotated and held in position along the CSS. The rotation is sufficient to preclude any further load transfer and to provide sufficient clearance during CSS jettison. See Figure 7 for a structural arrangement of the rotation components.

The inboard segment has a spring looped around the strut body. Upon strut separation, the spring rotates the strut about the spherical end bearing and holds it in place in a saddle mounted on the Stub Adapter. The

outboard segment is retracted and held in place by a pair of spring/cable assemblies. The primary system consists of a spring cylinder mechanism mounted on the CSS which is attached to a cable that is routed around a pulley and attached to the strut near the separation plane. The cable of secondary spring/cable assembly is looped around the strut body further outboard on the strut, is routed around another pulley in the opposite direction from the primary system, and is then attached to a stretched spring which is mounted on the CSS. When the strut separates, both systems pull it outboard until it slams into a block of aluminum honeycomb. At that point, the primary system cylinder mechanism locks in place precluding the cable from being pulled back out of the cylinder. The secondary system assists in holding the strut outboard and also applies a forward force to hold the strut up off the annular seal located just below the struts. See Figure 8 for a photograph of one strut installed in flight configuration.

TESTING

Three types of tests were performed on the strut system: component tests on a one-strut configuration, system tests on a complete six-strut configuration, and one flight test to date.

Component Testing

Component tests were performed on one strut and its retraction hardware mounted in a test fixture which simulated the end mounting fittings, the retract hardware mounts, and the annular seal mounted just aft of the strut. When there is a burst pressure acting on the seal, it bears on the struts and applies a forward load. Testing was accomplished at the temperature and pressure extremes, with both tension and compression loads on the strut, with and without pressure on the seal, and by actuating one pyrotechnic cartridge and also actuating both pyrotechnic cartridges. All these tests were successful except the strut failed to separate when the original design was tested when loaded in compression. The solution for this failure has been discussed previously. When the separation plane surfaces were modified as discussed, separation tests when loaded in compression were successful.

"Off limits" testing was also accomplished. These tests included actuation of only one pyrotechnic cartridge which contained 80% of the standard charge, a test at -18°C (0°F) and high humidity which formed ice/

frost, and a test with the grease left off the separation plane surfaces. Both the 80% cartridge test and the ice/frost test were successful; however, the no grease test, when actuated with the strut loaded in compression, was unsuccessful.

Other component tests included structural testing to limit and ultimate loads, and tension/compression cyclic loading. No problems were encountered during this testing.

Systems Testing

Both functional and structural testing was performed on the FBR at the system level using flight configuration hardware. Five functional system tests were performed. All five tests were performed with cryogenics in the Centaur fuel and oxidizer tanks, plus two of the tests occurred while a CSS/Centaur relative shear load was applied. All struts separated and retracted normally on each test as indicated by strain gage and breakwire instrumentation.

Data were obtained on FBR total system load versus CSS-to-Centaur relative deflection during many of the Titan/Centaur system structural test runs. Two types of tests were performed, one in which a shear load was applied only to the CSS, and the other where a shear load was applied to the CSS plus a shear in the reverse direction applied to the Centaur. This latter test was required in order to develop the full 88,964 Newtons (20,000 pounds) shear load in the FBR system. Using only the CSS shear load application to obtain the 88,964 Newtons (20,000 pounds) load at the FBR station would have resulted in overloading the CSS locally where the load was applied.

Typical data from each of the two types of tests are shown in Figure 9. Included in the figure is a plot of FBR total load versus CSS-to-Centaur relative deflection for the CSS shear load only test. These data illustrate the linearity of the system. All other test data were similarly linear. All the data plots like that shown in Figure 9 were generated by computer using strain gage data from each strut. The computer first determined the total system load at various CSS-to-Centaur relative deflections by vector summing the individual strut loads. The CSS-to-Centaur relative deflections were also calculated by the computer using the strain gage data together with the pretest load/deflection calibration data of each strut. Finally, the computer plotted the load/deflection data as shown in Figure 9.

Note that the spring constant calculated from the data in Figure 9 is very close to the analytical prediction of 33,932 Newtons per centimeter (19,229 pounds per inch). As noted in the Figure, the test data is slightly (less than 5%) higher. This was typical of all the test data and was attributed to the spring constant of the support structures (the CSS and Centaur) being a little greater than that approximated in the original analysis.

Flight Tests

The FBR system has flown once to date on the first Titan/Centaur launch vehicle. All telemetry data indicated that the FBR system functioned satisfactorily, and that the maximum in-flight shear load was approximately 31,137 Newtons (7000 pounds) occurring both at launch and during the maximum aerodynamic pressure period of flight.

CONCLUDING REMARKS

The spring strut system described herein is a simple and effective method of sharing load between two concentric structures with a known, precise spring constant. The additional requirement to remove the load transfer capability remotely in flight added complexity. However, the basic spring strut principle can be adapted by the mechanical designer to other load transfer applications where a precise linear spring constant is required of the load transfer device.

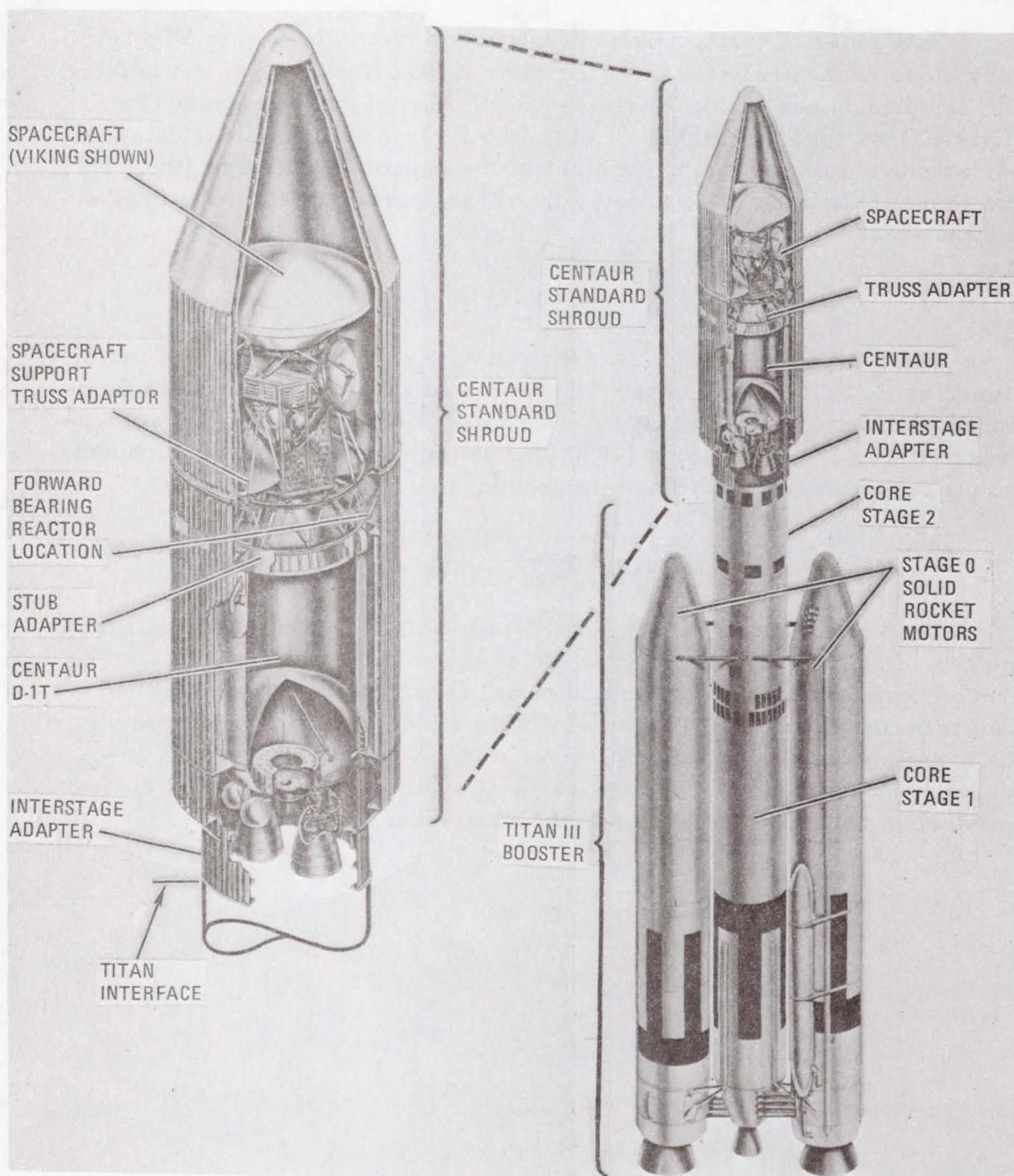


Figure 1. Titan-Centaur vehicle.

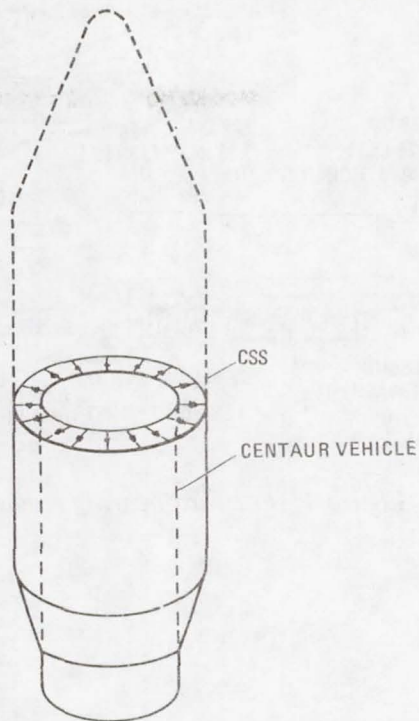


Figure 2. Conceptual ideal load-sharing device.

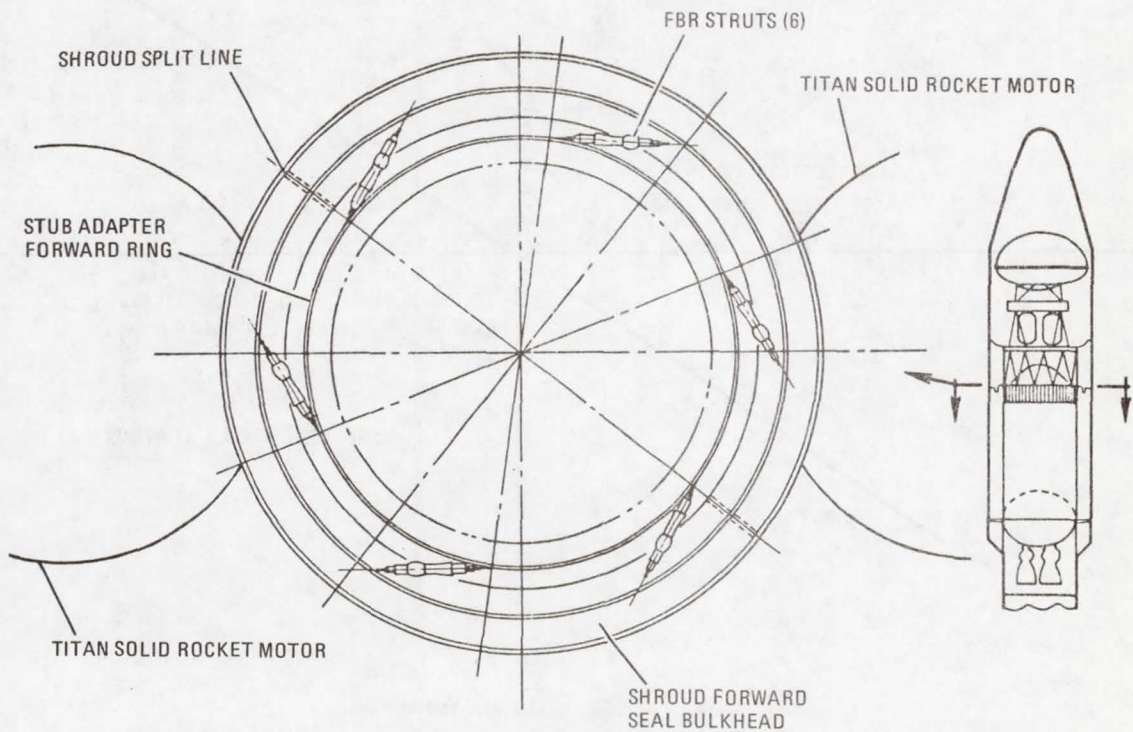


Figure 3. Forward bearing reactor strut system.

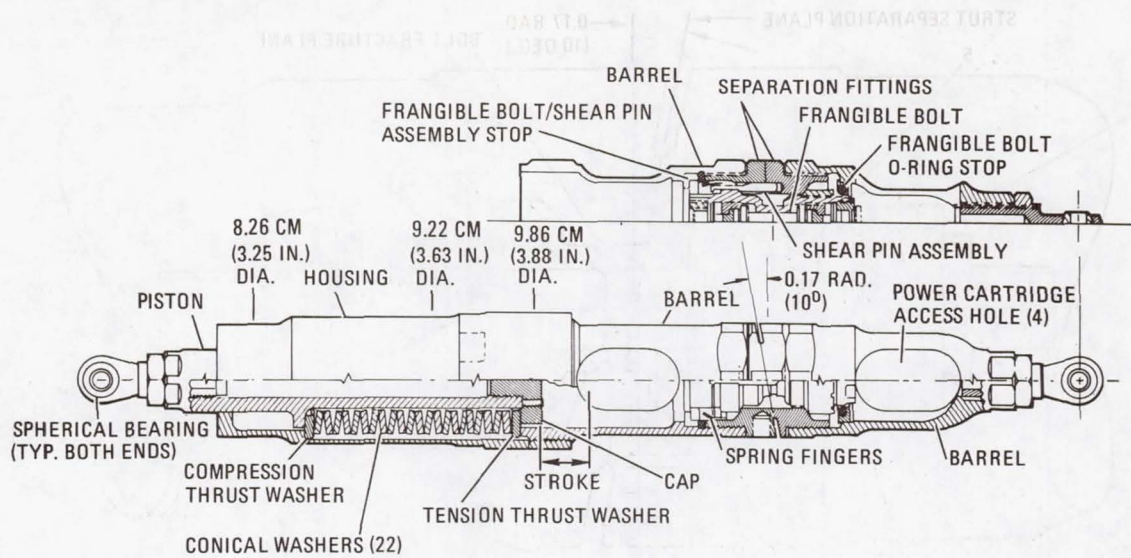


Figure 4. Forward bearing reactor strut configuration.

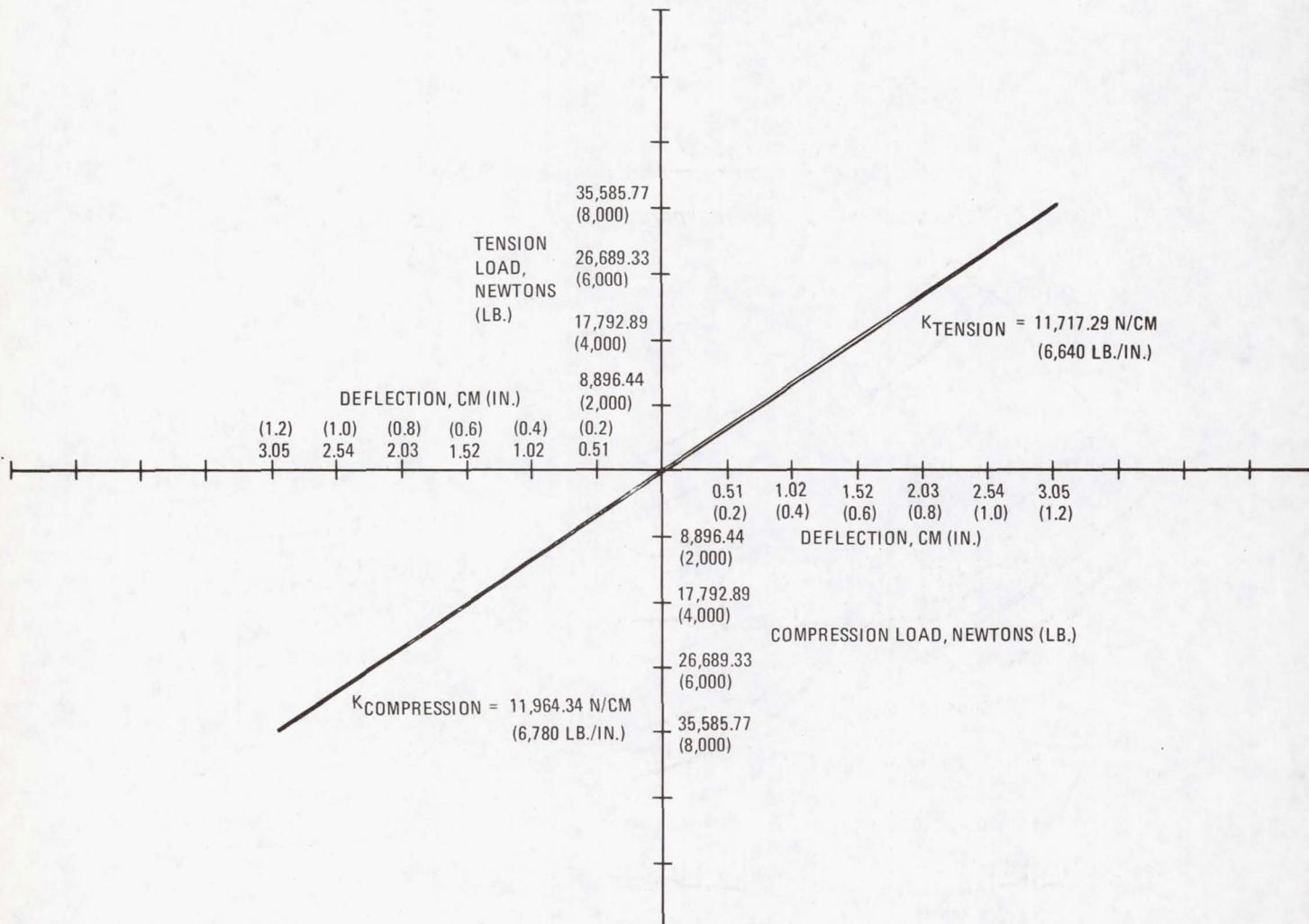


Figure 5. Strut load versus deflection test data.

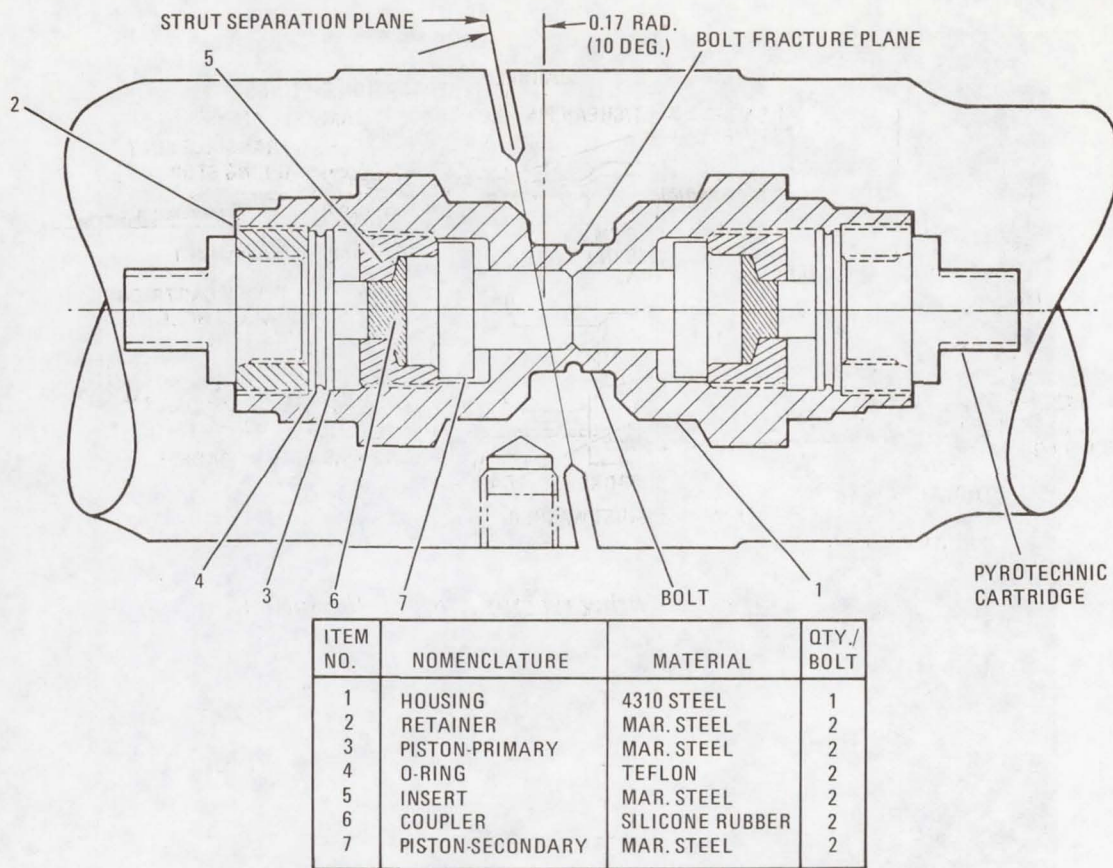


Figure 6. Forward bearing reactor separation bolt assembly configuration.

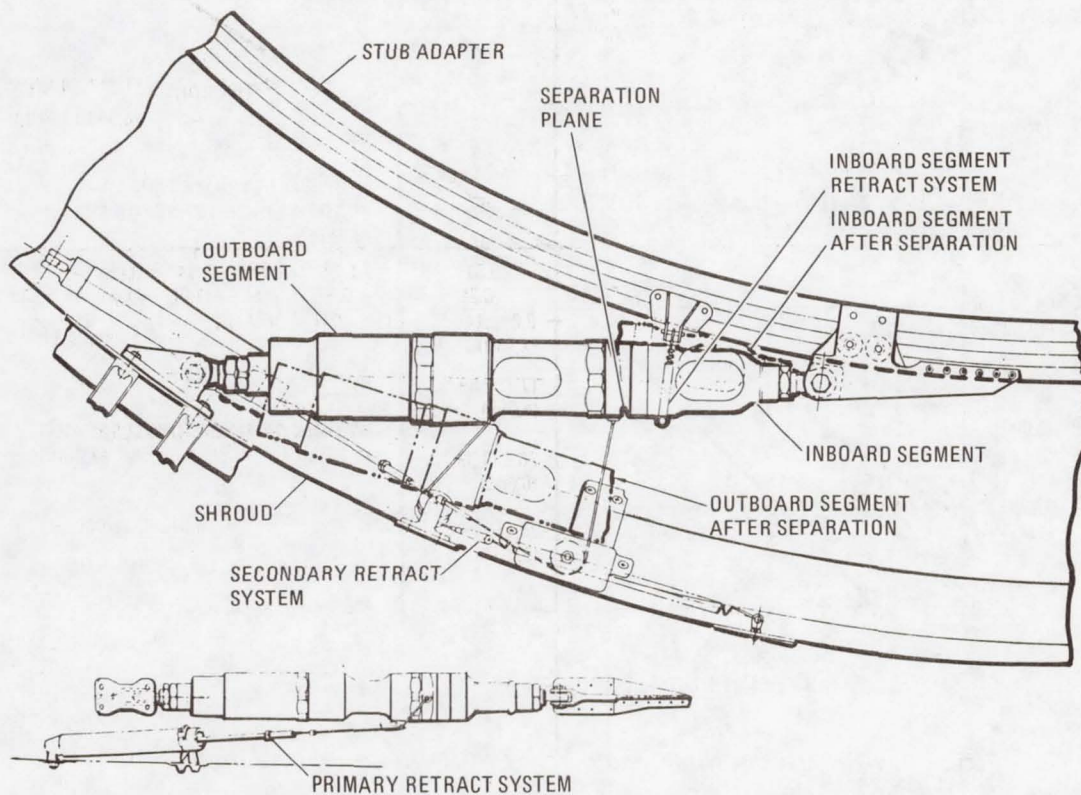


Figure 7. Forward bearing reactor strut retract system.

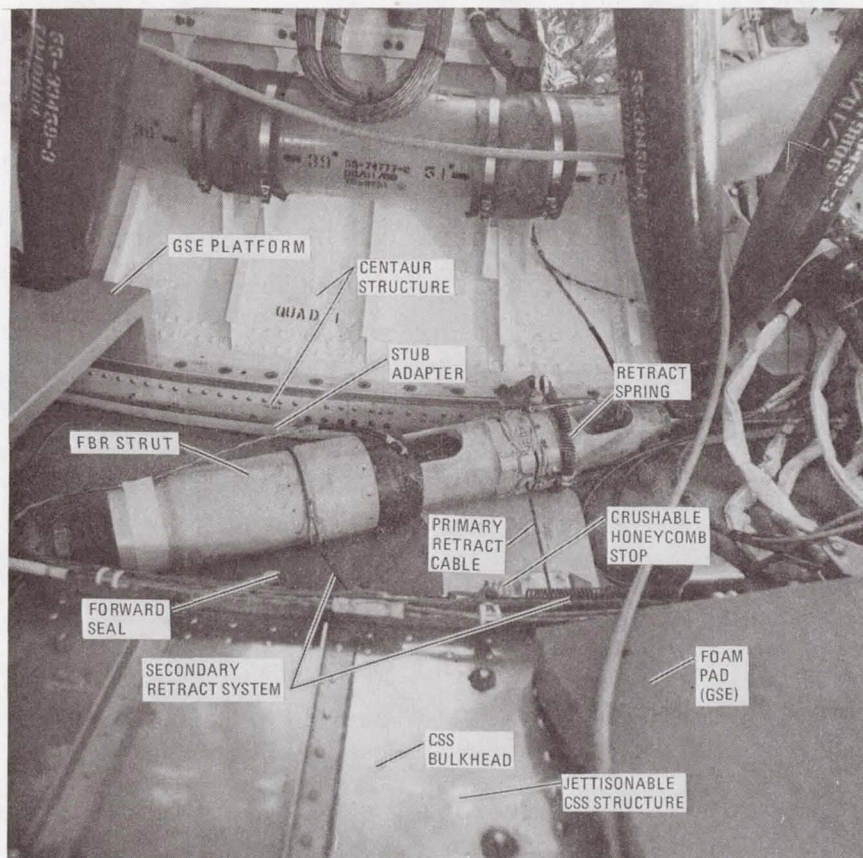


Figure 8. Single FBR strut installed in flight configuration.

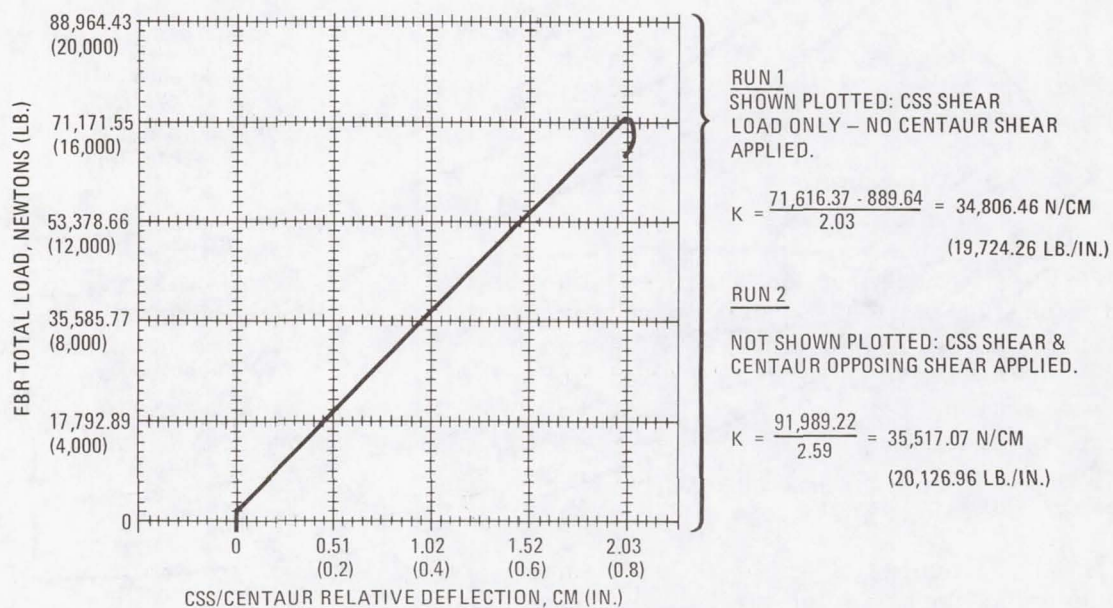


Figure 9. FBR system total load versus CSS/Centaur relative deflection.

2. A MANIPULATOR ARM FOR ZERO-G SIMULATIONS

By Shepard B. Brodie, Christopher Grant,
and Janos J. Lazar

Martin Marietta Corporation
Denver Division
Denver, Colorado

INTRODUCTION

Martin Marietta has designed and fabricated a 12-ft counterbalanced Slave Manipulator Arm (SMA), to be used for resolving the questions of operational applications, capabilities, and limitations for such remote manned systems as the Payload Deployment and Retrieval Mechanism (PDRM) for the Shuttle, the Free-Flying Teleoperator System, the Advanced Space Tug, and Planetary Rovers. As a developmental tool for the Shuttle manipulator system (or PDRM), the SMA represents an approximate one-quarter scale working model for simulating and demonstrating payload handling, docking assistance, and satellite servicing. For the Free-Flying Teleoperator System and the Advanced Tug, the SMA will provide a near full-scale developmental tool for satellite servicing, docking, and deployment/retrieval procedures, techniques, and support equipment requirements. For the Planetary Rovers, it would provide an oversize developmental tool for sample handling and soil mechanics investigations.

The design of the SMA was based on concepts developed for a 40-ft NASA technology arm to be used for zero-g Shuttle manipulator simulations.

COUNTERBALANCE CONCEPT

The SMA uses an articulated counterbalance scheme for shoulder and elbow and a self-counterbalanced design for the wrist. The articulated counterbalance scheme is essentially a second arm at the end of the shoulder extension with one or two counterbalance weights which are driven (via mechanical linkage) in phase with the lower arm (elbow to wrist). This system provides an arm whose shoulder and elbow torques need not, in any orientation, overcome the force of gravity on either the upper or lower arm, and whose motion is completely unrestricted.

The concept of articulated counterbalance is difficult to grasp intuitively, especially when the arm is in an orientation where the tip of the slave is on the counterbalance side of the fulcrum (Figure 1). An analytical proof of this scheme follows.

The slave arm with articulated counterbalance can be modeled as shown in Figure 2.

The counterbalance weights are w_1 and w_2 . The tubes of the slave are represented by w_3 and w_5 . The elbow joint is w_4 ; and the wrist joints, wrist extension, and terminal device are lumped in w_6 .

For the system to be balanced, the total moments about A and B should be equal. This is given by Equation [1], Table 1. The system can also be considered a rigid body whose governing moment equation for balance about the shoulder is given in Equation [2], Table 1. The distances D_1, D_2, \dots can be written in terms of the arm segments L_1, L_2, \dots and the cosine of angles α and β . Substituting these expressions into Equations [1] and [2], and solving the two equations simultaneously, we get Equations [3] and [4], Table 1.

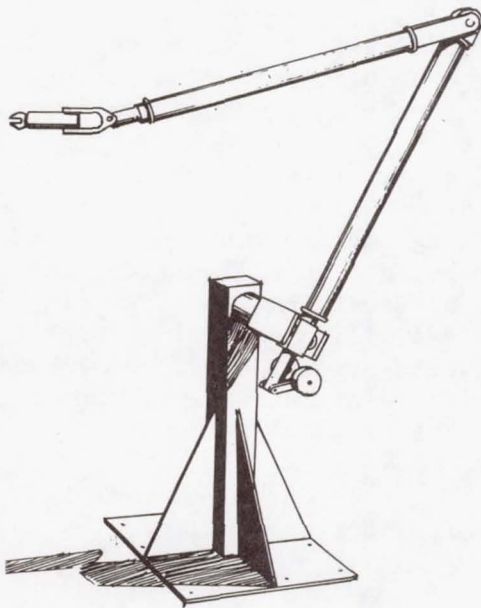


Figure 1. Manipulation in Cross-Over Position

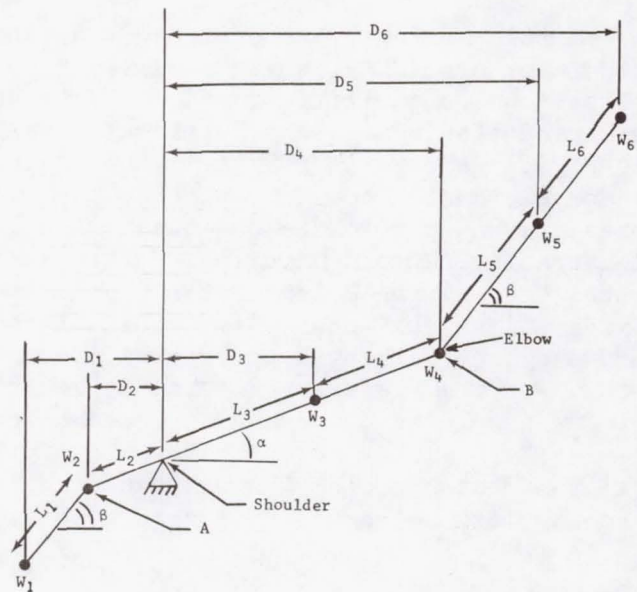


Figure 2. Articulated Counterbalance Model

Table 1. Counterbalance Equations

$w_1(D_1 - D_2) = w_5(D_5 - D_4) + w_6(D_6 - D_4)$	$w_1D_1 + w_2D_2 = w_3D_3 + w_4D_4 + w_5D_5 + w_6D_6$
Equation [1]	Equation [2]
$L_1 = L_5(w_5 + 2w_6)/w_1$	$L_2 = L_3[w_3 + 2(w_4 + w_5 + w_6)](w_1 + w_2)$
Equation [3]	Equation [4]

It can be seen that both α and β have cancelled in the solution of the balance equations. Thus, if Equations [3] and [4] are satisfied with proper values of the lengths and weights, the system is entirely counterbalanced at all angles of α and β . It can be shown that the system is also independent of roll angle so long as the slave arm and counterbalance arm roll as one about the centerline of the upper arm tube.

The SMA counterbalance linkage configuration is a three-bar direct-drive system that was selected to meet the design requirements for low friction and high stiffness. Each of the three bars is mounted on a separate crank plate. These assemblies were put together to form a crankshaft-rod type system. The pin locations in the plates are 120° apart. Figure 3 is a schematic of the linkage system. An optimization program was used to determine the yoke and mass sizes for minimum increase in inertia as seen by the joint drives. Figures 4 and 5 are photographs of the SMA.

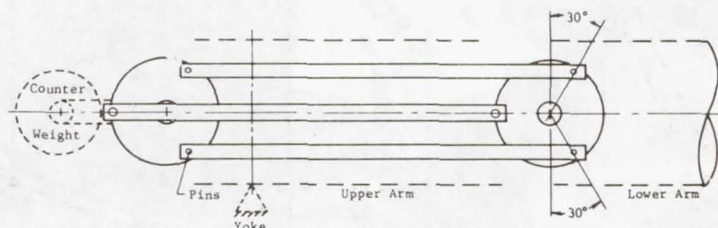


Figure 3. Counterbalance Linkage Concept

DRIVES

Table 2 illustrates the general joint capabilities. The drives are the most significant portion of the design because of their close approximation to flight hardware. All joints contain 60V dc motors, potentiometers, tachometer-generators, and fail-safe 28V dc friction brakes. The gear ratios are in the range of 115:1. Each joint is servo controlled, and may accept commands from manual or computer sources. Of particular interest in the drives during simulations are joint flexibility/stiffness, gear backlash/backdrive, finite motor torque, friction/stiction, and response.

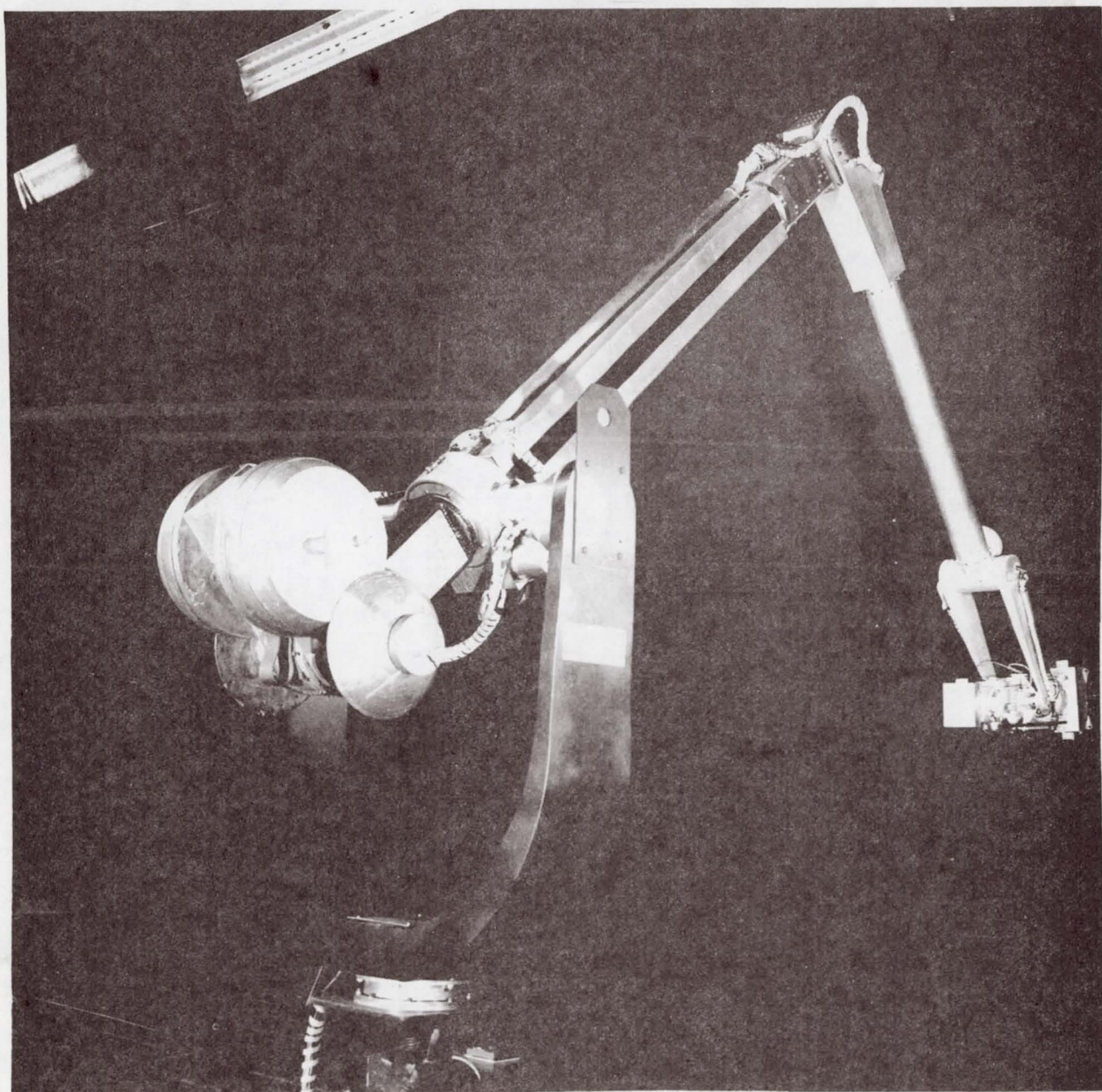


Figure 4. Slave Manipulator Arm

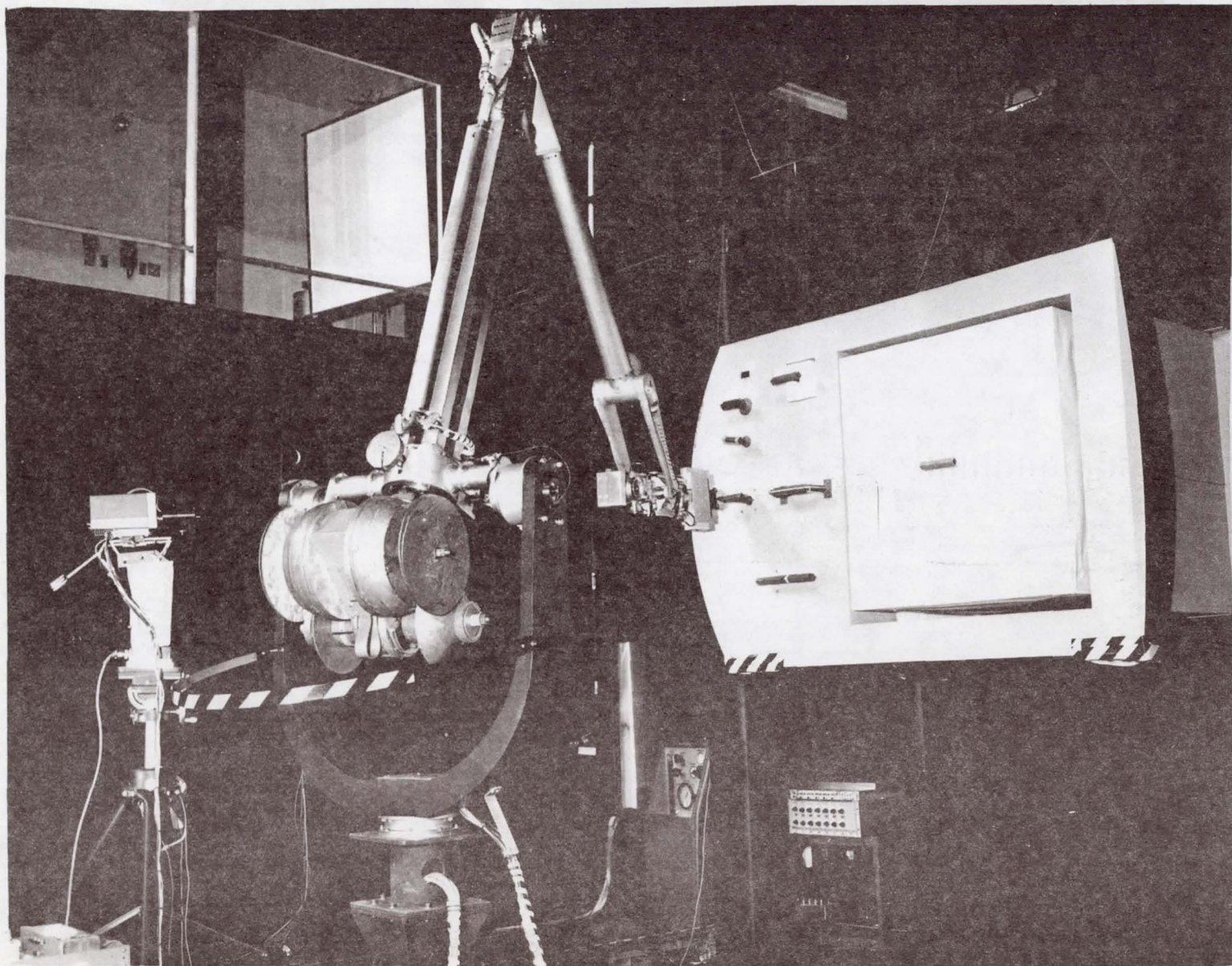


Figure 5. Slave Manipulator Arm Working at Task Panel

Table 2 Electro-Mechanical Joint Capabilities

	<u>Shoulder</u>			<u>Elbow</u>		<u>Wrist</u>		
	Pitch	Yaw	Roll	Yaw	Pitch	Yaw	Roll	
Design Stall Torque Ft-lbs	100	100	66	66	30.5	30.5	15	
Joint Travel in Degrees	± 200	+150 - 75	± 200	+ 10 -160	± 80	± 130	± 200	
Design Slew Angular Velocity Rad/sec	0.1	0.1	0.03	0.15	0.2	0.2	0.1	
Actual Backdrive Torque Brake On Ft-Lbs	69	60	--	75	40	42	40	

The wrist consists of three degrees-of-freedom. Counterbalancing is accomplished by the proper placement of equipment around each axis, as shown in Figure 6. By placing the pitch axis at the center of gravity of the roll drive and the end effector/TV camera assembly, the pitch axis is balanced. By locating the yaw axis at the center of gravity of the pitch motion equipment and the pitch/yaw drive assembly, the yaw axis is balanced. The pitch and yaw drives are separated from their respective drive centers by the use of steel drive tapes. All equipment is mounted on the main wrist support member which pivots around the yaw axis. Figure 7 is a photograph of the SMA wrist.

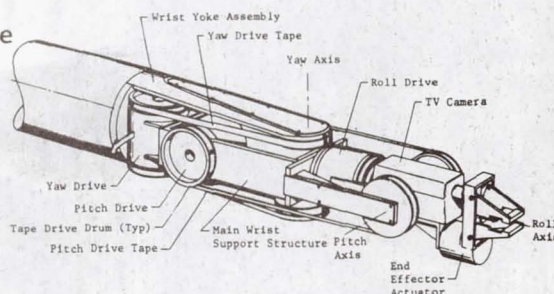


Figure 6. Self-Counterbalanced Wrist Assembly

END EFFECTOR

The end effector is an electro-mechanical device utilizing a 60V dc motor to drive a screw thread which actuates the linkage opening and closing the jaws. The closing force of the jaws is 6.8 kilograms (15 pounds) [11 kilogram-meters (or 80 ft-lbs) of torque] and is capable of being actuated in less than one second. The jaws are designed to grasp a 0.025-meter (one-inch) square bar placed at a 45° angle to the horizontal. This configuration may be changed by exchanging the jaws with the desired shape. Figure 5 illustrates the end effector/grasp bar relation.

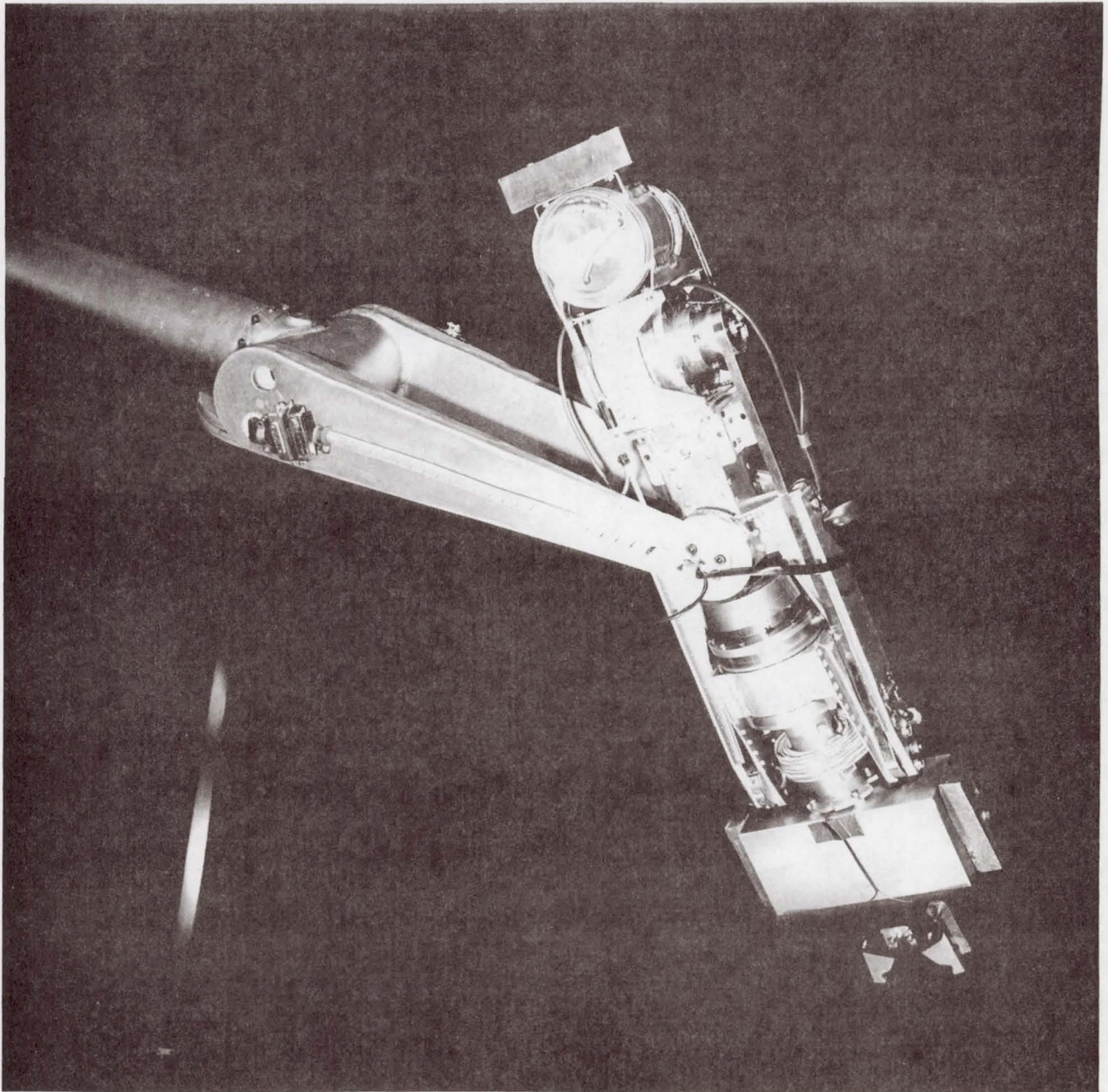


Figure 7. Slave Manipulator Arm Self-Counterbalanced Wrist Assembly

TELEVISION SYSTEM

The television system used on the arm itself is located immediately behind the end effector. The mounting bracket will accept either one or two videocon tubes for monaural or stereo TV viewing. The resolution point begins approximately 0.02 meter (one inch) behind the jaws of the end effector and continues forward. The electronics for the videocon tubes are located at the wrist-forearm attach point.

BASE SUPPORTS

The base assembly is made up of six components. These components may be assembled in combination to provide six locations for shoulder yoke orientation. The shoulder yoke may be located at 1.22, 2.13, or 3.66 meters (4, 7, or 12 feet) from the floor to the shoulder pitch (yaw) axis in either a vertical or horizontal position. The base plates are constructed of structural steel and weigh a total of 431 kilograms (950 pounds).

TEST CONDUCTOR'S CONTROL CONSOLE

The Test Conductor's Control Console (TCCC) provides the equipment necessary to (1) power up the SMA, (2) select operating modes, (3) monitor system operation and provide limit warnings, (4) allow manual SMA control, (5) bring the SMA to a safe stop in an emergency, (6) control the associated analog computer, and (7) house the system electronics. Figure 8 is a photograph of the TCCC.

The TCCC was designed to be as flexible as possible to accommodate experimental configuration changes and operational improvements. Plug-in circuit boards are used extensively and all cabling is terminated in connectors so that large sections (such as an entire panel) can be completely removed for modification or maintenance. System reliability is enhanced by the use of solid-state switching in all signal circuits.

Power for the SMA and TCCC is obtained from 117V ac and 28V dc mains. The internal power supplies provide dc voltages of +60, +15, -15, +10, -10, and +5.

The TCCC makes provision for several modes of operation including both rate and position servo control. In the normal operating situation with an analog computer in the loop, the command signals (either rate or position) from controllers located in the Operator's Station (OS) are routed to the computer. The computer represents a servo rate command which is amplified in the TCCC and applied to the proper joint servomotor. As an alternative, the computer may utilize the joint position potentiometer outputs to produce a

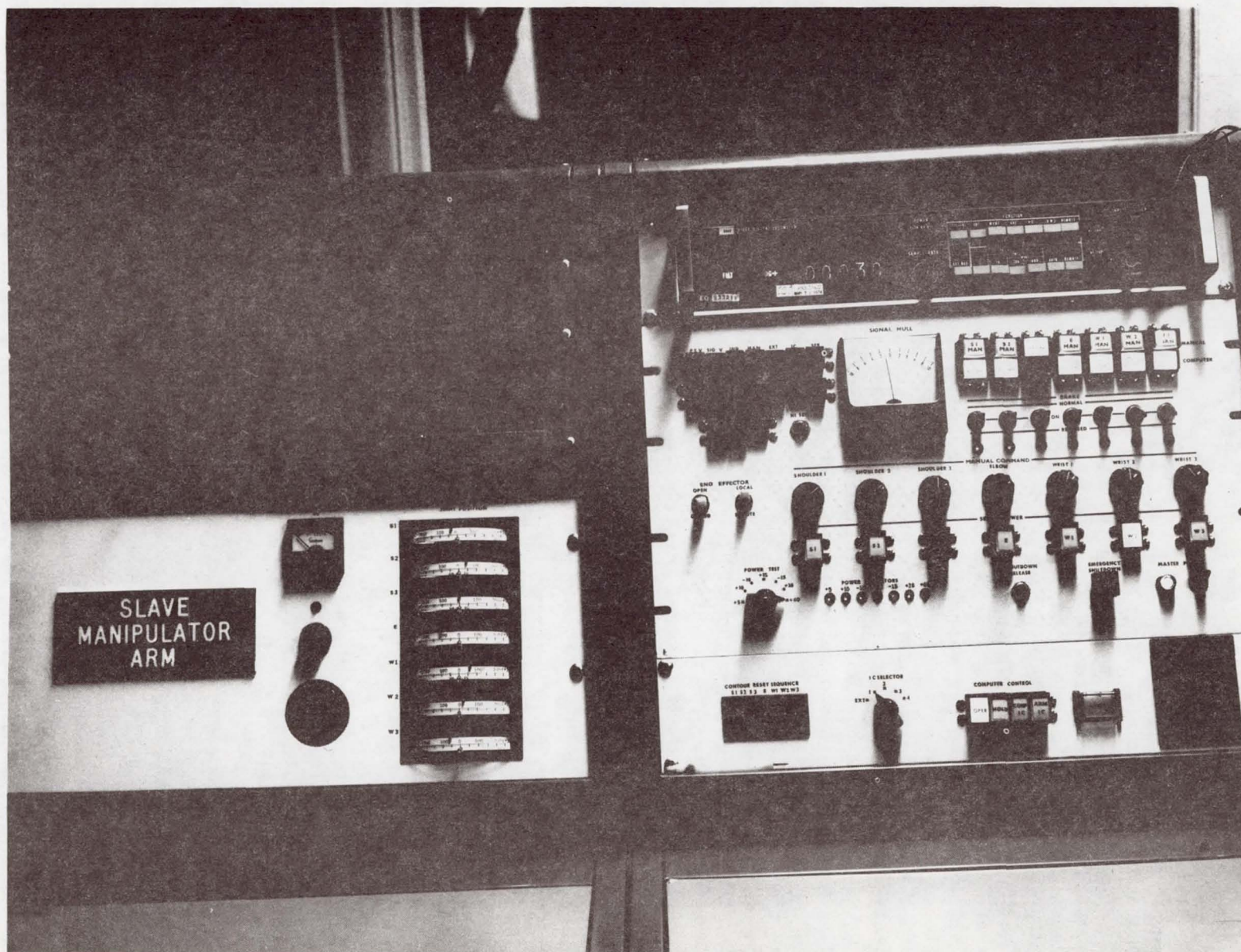


Figure 8. Slave Manipulator Arm Test Conductor's Control Console

servo drive signal based upon arm position. Either of these situations are termed the OPERATE mode.

Once an exercise has been completed, it is necessary to return the SMA to some initial position. First, the SMA is placed in the HOLD mode by a pushbutton on the TCCC. In HOLD, control of the servo loop is removed from the computer and transferred to the TCCC. Local control from the console is a position loop. In the HOLD mode, the joint position pot output is used as the position command so that the servo drive signal is always zero. Next, the SMA servos are placed in the RESET mode by the TCCC. The initial conditions are determined by the settings of a group of potentiometers, one for each SMA axis. The output voltage of the pot represents a specific joint position. Four sets of initial conditions are obtainable from the TCCC. In the RESET mode, each servo position command is integrated between the position at the beginning of RESET and the desired end position. The rate of return is controllable from the TCCC. In addition, there is a reset sequencer which allows each joint to be reset individually or in any desired sequence. The reset sequencer logic operates in 10 asynchronous steps. For example, if the reset thumbwheel switches on the TCCC are set up so that joints E and W2 are reset during step 2, both joints will remain in the HOLD mode during steps 0 and 1, then go into the RESET mode during step 2, and return to HOLD in steps 3 through 9. The reset sequencer will not progress to step 3 until both E and W2 reach their desired initial condition points.

Two other modes of operation are possible. The first of these is the ALIGN mode. This sequence causes the position track and hold circuits to sample the present joint positions and then throw the mode control into the HOLD mode. ALIGN occurs automatically when the system is powered up and can be activated at any time during use. The last mode is MANUAL operation. In this mode position commands come from 3-turn potentiometers on the TCCC Main Control Panel. SMA joints may be placed in the MANUAL mode individually while other joints remain under computer control. In the MANUAL mode, the other mode controls have no effect on that particular joint.

The Mode Control logic is accomplished by a read only memory (ROM) which either accepts or rejects an action of a mode control pushbutton depending upon system conditions. For example, it is generally undesirable to go to OPERATE before completing RESET. Thus, the ROM will not permit a mode change directly from OPERATE to RESET.

Other provisions are included for system safety. A power interrupt circuit removes servomotor power and applies the electromagnetic joint brakes when activated. Power interrupt can be initiated manually by observers located in various parts of the facility or automatically when a joint angle limit occurs. When a joint angle is approaching its limit, an early warning is provided by the limit circuitry. An audible boxing sound occurs and a red warning light flashes to indicate an approaching limit. At this time the operator can reverse the action and drive normally back to a safe condition at which time the warnings cease. If the limit is exceeded, however, the power interrupt will be initiated as described above. It is then necessary to bring the SMA out of the limit under manual control.

The TCCC contains a digital voltmeter to monitor the various dc voltages in the system. Selector pushbuttons are provided for all power supply voltages and the following signal voltages for each joint: (1) position pot, (2) computer output, (3) reset pot, and (4) manual control pot.

3. STRUCTURAL EVALUATION OF DEPLOYABLE AERODYNAMIC SPIKE BOOMS

By B. J. Richter*

ABSTRACT

An extendable boom consisting of a series of telescopic cylindrical tube segments and overlapping lock joints is being developed for use as an aerodynamic spike mounted atop a missile. Two candidate design concepts differing mainly in the particular overlapping lock joint designs are currently undergoing a combined analytical/experimental evaluation. Some of the results of this evaluation are presented in this paper.

INTRODUCTION

In order to increase its range by reducing aerodynamic drag, a missile is to be flown with a completely mechanical and self-contained deployable aerodynamic nose spike system. A typical aerodynamic flow pattern induced by the aerospike mounted atop a missile's nose fairing is illustrated in figure 1. The worst expected loading condition for the deployed spike boom results from aerodynamically induced static and dynamic pressures and is statically equivalent to a 2300 lb compressive axial load and a 360 lb lateral load both applied at the extended boom tip. The aerospike system consists of a series of telescopic cylindrical boom segments, an inertial initiator, and a gas generator, which are housed in the stowed configuration inside a case mounted in the missile nose fairing. In the extended position the telescopic boom segments obtain their axial and lateral rigidity from a series of overlapping lock joints.

Two extendable boom design concepts are currently being evaluated and differs from each other mainly in the design of the overlapping lock joints employed. Each concept is being evaluated both analytically and experimentally and after the evaluation is complete, one of the design concepts will be chosen as baseline for the missile. The progress on some of the structural aspects of the current analytical/experimental investigation of these two extendable boom design concepts is the subject of this paper.

STRUCTURAL DESIGN REQUIREMENTS

The following lists some of the more important structural design requirements which the aerospike boom must meet.

1. The extended length must be 50 ± 1 inch.
2. The stowed length must be ≤ 11.5 inches.

*Lockheed Missiles & Space Company, Inc., Sunnyvale, California.

3. The extended boom must be capable of supporting a 2300 lb compressive axial load and a 360 lb lateral load both applied at the boom tip.
4. The deployment process must minimize axial impact stopping loads imposed upon the housing/nose cap structure.
5. The overlapping joints shall act to laterally align the individual boom segment centerlines of the fully extended aerospike within 0.5 inch of the missile centerline.
6. The first cantilevered lateral bending frequency of the fully extended and locked aerospike boom with a 2 lb tip disc shall be ≥ 35 Hz.
7. The entire deployment and locking process shall take place within 1 second after the inertial initiator ignites the gas generator.

MECHANISM OPERATION

The deployable aerodynamic spike system consists of a series of N telescopic boom segments, an inertial initiator, a gas generator, and a housing which is attached inside the missile nose fairing. This system is illustrated schematically in the stowed configuration in figure 2a. After the missile is launched the inertial initiator senses an appropriate missile acceleration profile and ignites a gas generator. The gases produce a history of internal pressure which initially acts to break a hold-down bolt. The gas pressure then acts on the individual telescopic boom segments S_i and accelerates them into an extended and locked configuration as illustrated in figure 2b. The positioning and the locking of the boom segments are accomplished by a series of overlapping lock joints J_i . The positioning must be such that the centerlines of the individual segments S_i be laterally aligned within specified tolerance limits with the missile centerline, and that the final extended length $L = 50$ inches.

After the aerospike boom has been extended and locked into place, it is subjected to a history of aerodynamically induced heating and loading. The joints J_i are then required to transfer loads (i.e., axial loads, bending moments, and shears) from one segment to the next. As an example, two ways in which the bending moment M shown in figure 3a can be transferred from segment S_{i+1} across joint J_{i+1} to segment S_i are illustrated in figures 3b and 3c. In these figures e represents the axial engagement or joint overlap distance. The first way is illustrated in figure 3b. In this case the moment is reacted by a couple cF . In the second case, shown in figure 3c, the moment M is reacted by the couple cP . The couple forces F are the resultants of surface stresses distributed in the joint region which act parallel to the tube centerline. The couple forces P are the resultants of surface stresses distributed in the joint region which act perpendicular to the tube centerline. There also exists a third way which is simply a combination of the above two ways.

If the deployed aerospike boom segments and joints were not a mechanism (e.g., if the segments could be welded together), then a moment M would be reacted as in classical beam bending theory. The bending stresses σ would be given by

$$\sigma = M/(\pi R^2 t), \quad (1)$$

where R and t are the tube radius and thickness, respectively. For $\sigma = 100,000$ psi, $R = 2$ inches, and $t = 0.1$ inch the allowable theoretical bending moment capability M_A of the boom is found, using (1), to be

$$M_A = 125,000 \text{ in. -lb} \quad (2)$$

Because the aerospike is a mechanism, however, the joint design produces actual allowable bending moment capabilities far below the theoretical value given by (2). These reduced bending allowables will be discussed in more detail later in this paper.

One important parameter which determines how a particular joint functions is the engagement distance e . This parameter is geometrically related to the three parameters L , ℓ , and N which are defined in figure 2. Since L and ℓ are fixed by the requirements such that $L = 50$ inches and $\ell = 11.5$ inches, a unique relation exists between e and N . From geometric considerations (fig. 2) this relation is found to be

$$e = 11.5'' - 50''/N, \quad (3)$$

with the further requirements that $0 < e < 11.5$ inches. Hence, the smallest number of segments that will satisfy (3) is $N = 5$. This corresponds to an $e = 1.5$ inches. An $N = 6$ corresponds to an $e = 3.2$ inches. These two cases form the geometric basis of the two design concepts which are discussed in this paper.

Design concept I employs five steel cylindrical tube segments with tube radii varying from 2.14 to 1.50 inches and corresponding tube wall thickness varying from 0.141 to 0.078 inch. The manner in which joint J_{i+1} locks together segments S_i and S_{i+1} is illustrated schematically in figure 4 (the angle β in fig. 4 is exaggerated and typically is about 1.5°). Segment S_{i+1} approaches the joint region J_{i+1} with a velocity v relative to S_i as shown in figure 4a. Surface AB of S_{i+1} initially encounters surface CD of S_i as shown in figure 4b. At this time the engagement is e_0 . The two segments then swage together; the engagement e_0 decreases to e ; and S_{i+1} comes to a halt relative to S_i . The two segments are then held together entirely by frictional stresses developed during the swaging process.

Design concept II employs six steel cylindrical tube segments with tube radii varying from 2.19 to 0.97 inches and corresponding tube wall thicknesses varying from 0.12 to 0.060 inch. The manner in which joint J_{i+1} locks together segments S_i and S_{i+1} is illustrated in figure 5. Segment S_{i+1} approaches the joint region with a velocity v relative to S_i as shown in figure 5a. Temporary relative stopping occurs when surface BC engages surface DE and surface HI engages surface JK. The radii of the various engaging surfaces are such that

$$r_{BC} - r_{DE} = r_{KJ} - r_{HI} = \Delta r \quad (4)$$

where Δr represents a radial interference. This interference fit causes frictional stresses to be generated in the contact regions which act to oppose the relative motion. The temporary motion again proceeds when the internal tube pressure builds up to a level high enough to overcome the frictional forces. Final joint locking occurs when surface AB impacts surface DF. At this time a ring of 24 locking fingers snaps into place along FG. The purpose of these locking fingers is to prevent any subsequent

relative motion in the opposite direction. This fully extended and locked joint configuration is illustrated in figure 5b.

EXPERIMENTAL INVESTIGATIONS

1. Axial engagement experiments were conducted on the two types of joint concepts. The geometries of the test specimens used for the types I and II joint concepts are shown respectively in figures 6a and 6b. Loading was applied with a hydraulic load cell. For the type I test specimen the force F required to reduce the initial engagement of 1.5 inches by amount δ is shown as the upper dashed curve in figure 7a. For increasing δ the applied force F increased from zero to a maximum of 10,000 lb and then fell off towards zero as δ approached 1.5 inches. For decreasing δ the experimentally determined $F(\delta)$ curve was found to be the lower dashed curve in figure 7a.

For the type II joint the applied force F required to partially engage the interference surfaces BC/DE and HI/JK (see fig. 5) ranged from zero up to a maximum of 2,000 lb. This force held constant at 2,000 lb as long as the surfaces BC/DE and HI/JK remained fully engaged.

2. An experiment was conducted on the design concept II joint configuration shown in figure 6b in order to investigate how a lateral force and bending moment are transferred across the joint. A hydraulically applied force P (see fig. 6b) was cycled between ± 650 lb, and the lateral deflection Δ and the hoop strain ϵ indicated in figure 6b were monitored. The results for a load history 1-2-3-4-5-6-2 are shown in figures 7b and 7c. These figures indicate that this type of joint initially transfers the joint bending moment in the manner shown in figure 3b until $P = 300$ lb (path 1-2 in figs. 7b,c). At this load level the interference frictional shear stresses (which were generated when the two segments were initially pulled together) are overcome and slipping occurs. The increased bending moment caused by the loading in the 300 lb to 650 lb range (path 2-3 in fig. 7) is then carried across the joint in the manner shown in figure 3c. Repeated cycling retraces the path 2-3-4-5-6-2.

ANALYTICAL INVESTIGATIONS

1. The axial force required to reduce the initial engagement e_0 by amount δ (see fig. 6a) can be computed by considering interference geometry, basic strength of materials, elastic behavior, and equilibrium of forces on the inner tube of figure 6a. This relation was found to be

$$F = k\delta(1 - \delta/e_0), \quad 0 \leq \delta \leq e_0 \quad (5)$$

where

$$k = 2\pi t E e_0 \tan \beta (\tan \beta \pm \mu)/R \quad (6)$$

with R and t being, respectively, the average tube radius and thickness. β is the cone half angle indicated in figure 4; μ is the interface coefficient of friction, and E is the material's Young's Modulus. The positive sign in (6) is for increasing δ while the negative sign is for decreasing δ . This relation is shown in figure 7a for $t = 0.0855$ inch, $R = 1.565$ inch, $E = 30,000,000$ psi, $e_o = 1.5$ inch, $\beta = 1.5$ degrees, and $\mu = 0.06$. The agreement of this rather simple formula with the experimental data is fairly good in view of the rather complex behavior of this joint.

2. A reasonable estimate of the load P at which slipping first occurs at point 2 (see figure 7b) can be obtained from elementary considerations as

$$P_{SLIP} = (F_e)(R + e)/(\pi h) \quad (7)$$

In this equation R is again the average tube radius; e and h are defined in figure 6b; and F_e is the force required to fully engage the two tubes. The axial force F_e was experimentally found to be 2,000 lb. Hence, for $R = 2.1$ inches, $e = 3.0$ inches, and $h = 13.0$ inches, equation (7) gives

$$P_{SLIP} = 250 \text{ lb} \quad (8)$$

A precise analysis of the lateral load configuration shown in figure 6b was undertaken, using BOSOR, a well known finite difference computer code for the analysis of shells of revolution (ref. 1). Two cases were analyzed. In the first case the contact regions BC/DE and HI/JK (see fig. 5a) were not allowed any relative motion (i. e., no slip). The ratios P/Δ and P/ϵ were computed to be 22,300 lb/inch and -10,000,000 lb/inch/inch, respectively. For the second case the contact regions were allowed to move relative to each other except for the radial contact deflection. The ratios P/Δ and P/ϵ were found to be 15,000 lb/inch and 1,670,000 lb/inch/inch, respectively. These ratios were then combined with the slip load given by (8) resulting in the analytical prediction of the load cycle 1-2-3-4-5-6-2 shown in figures 7b and 7c. The agreement between experiment and prediction is seen to be reasonably good.

3. Analytical predictions of the allowable moment carrying capability of each of the two joint concepts can be accessed using the following expressions. For joint concept I

$$M_A = \mu R k \delta (1 - \delta/e_o)/(\tan \beta + \mu)/\pi \quad (9)$$

where the various variables are those defined previously in equations (5) and (6). For joint concept II

$$M_A = 2\pi e R t \left(\frac{\lambda t \sigma}{3} - \frac{E \Delta r}{2\lambda R^2} \right) \quad (10)$$

where

$$\lambda^4 = 3(1 - \nu^2)/(R^2 t^2) \quad (11)$$

and where ν is Poisson's ratio, σ is the allowable stress of the tube material, and the remaining variables are as previously defined. Using $R = 2$ inches, $\delta = 0.2$ inch, $\mu = 0.2$, $k = 200,000$ lb/in., $\beta = 1.5$ degrees, $e = 1.5$ inches in equation (9) gives for a feasible type I joint,

$$M_A = 20,000 \text{ in.-lb.}$$

Using $R = 2$ inches, $t = 0.1$ inch, $e = 3$ inches, $E = 30,000,000$ psi, $\nu = 0.3$, $\Delta r = 0.003$ inch, $\sigma = 100,000$ psi in equations (10) and (11) gives, for a feasible type II joint,

$$M_A = 25,000 \text{ in.-lb.}$$

These joint allowables may then be compared with the typical theoretical moment carrying capability given by equation (2).

CONCLUDING REMARKS

This paper presents some of the results of an analytical/experimental evaluation of the behavior of two types of deployable aerospike boom designs. Some useful analytical design procedures have been developed and experimentally verified. Such analytical procedures have provided not only the basis for understanding how each type of boom/joint system functions physically, but also the tools necessary in guiding design changes which have led to the continual improvement of the load carrying capacity of the two types of design concepts.

Because of space limitations the results of many other completed investigations have been omitted. These deal with such topics as the study of the effects of aerodynamic heating upon the boom/joint performance, the dynamic characteristics of each design concept, and the study of the interaction between the boom deployment process and the housing/nose fairing structure.

REFERENCE

1. Bushnell, David: "Analysis of Ring-Stiffened Shells of Revolution Under Combined Thermal and Mechanical Loading," AIAA Jour., vol. 9, No. 3, Mar. 1971, pp. 401-410.

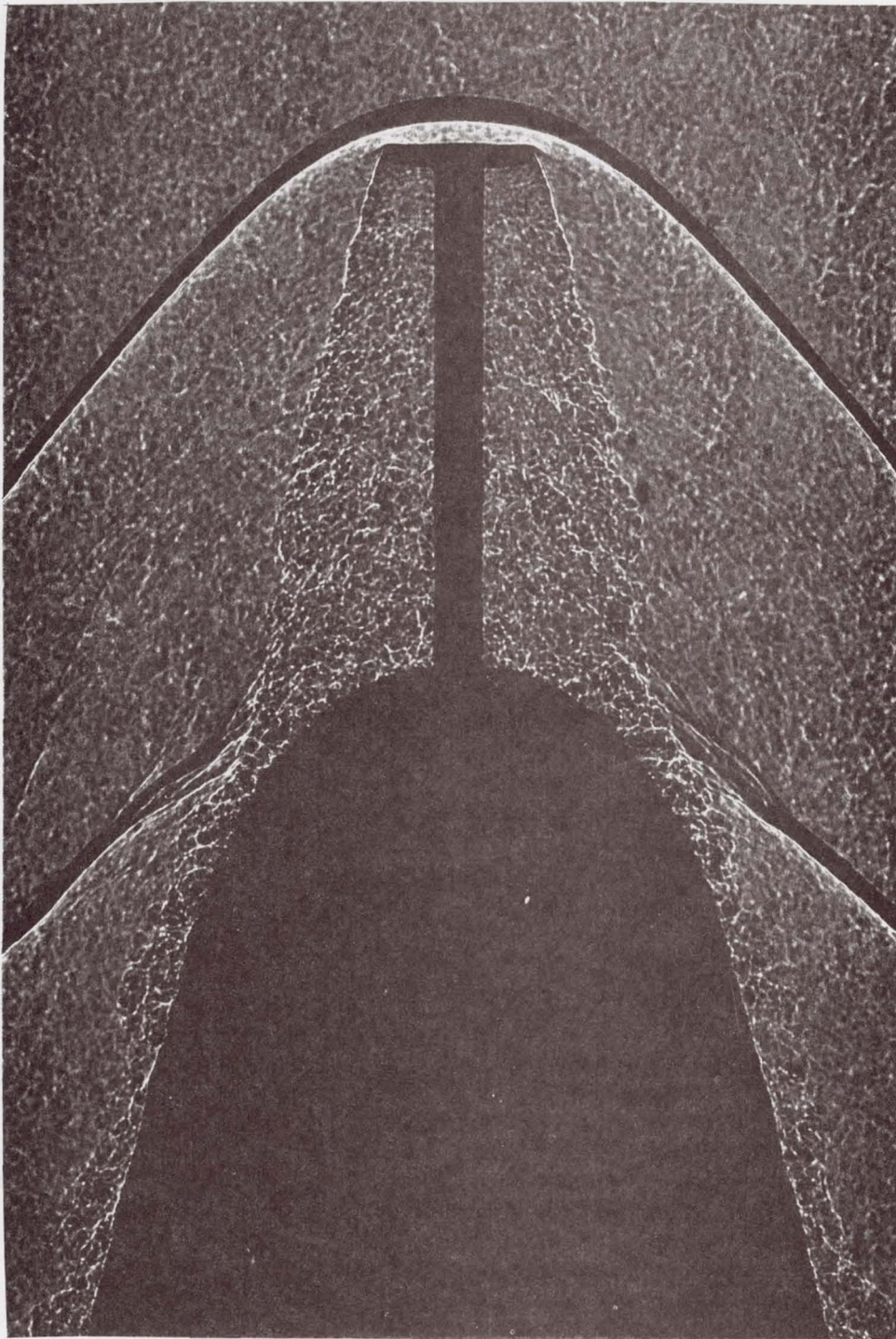
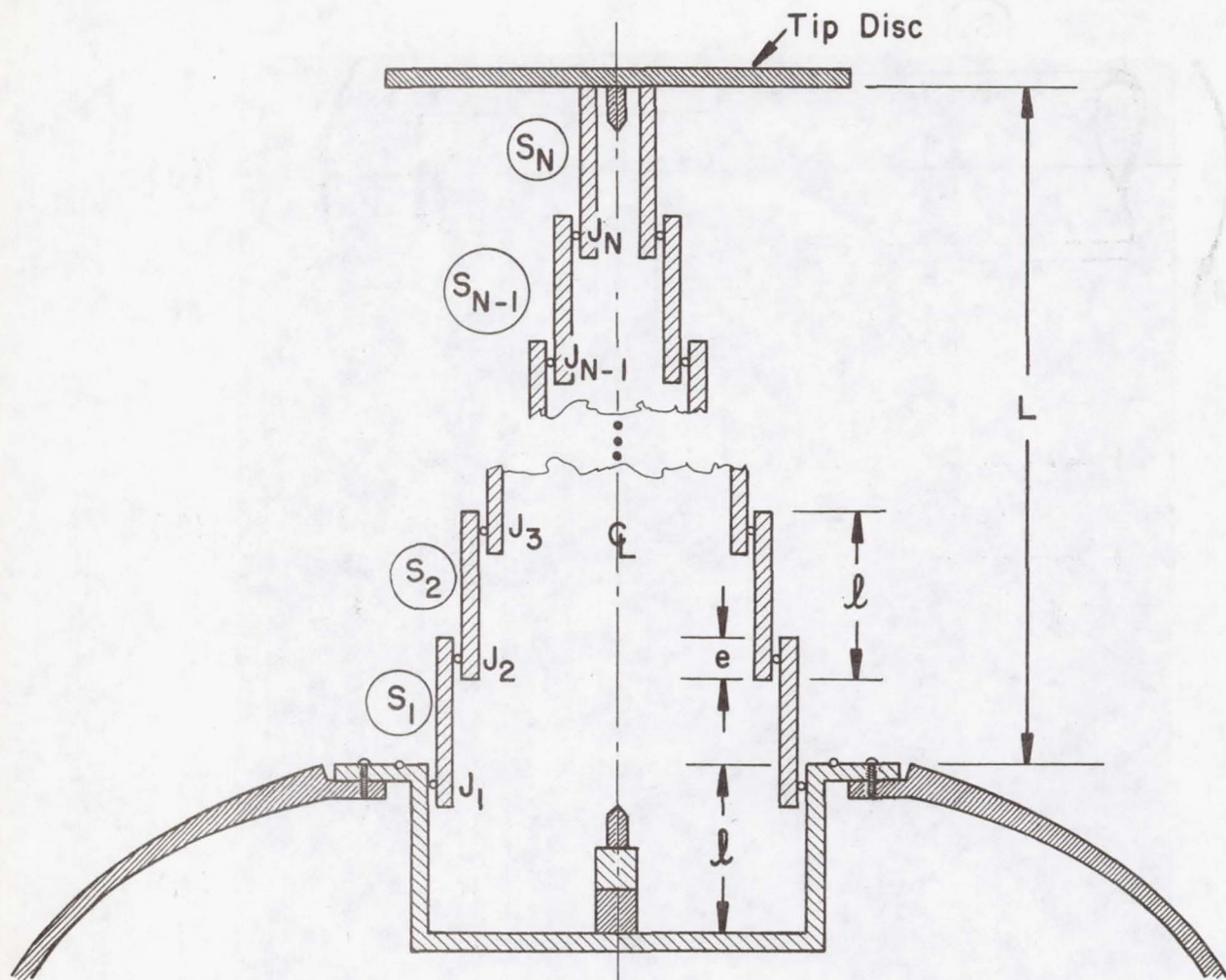
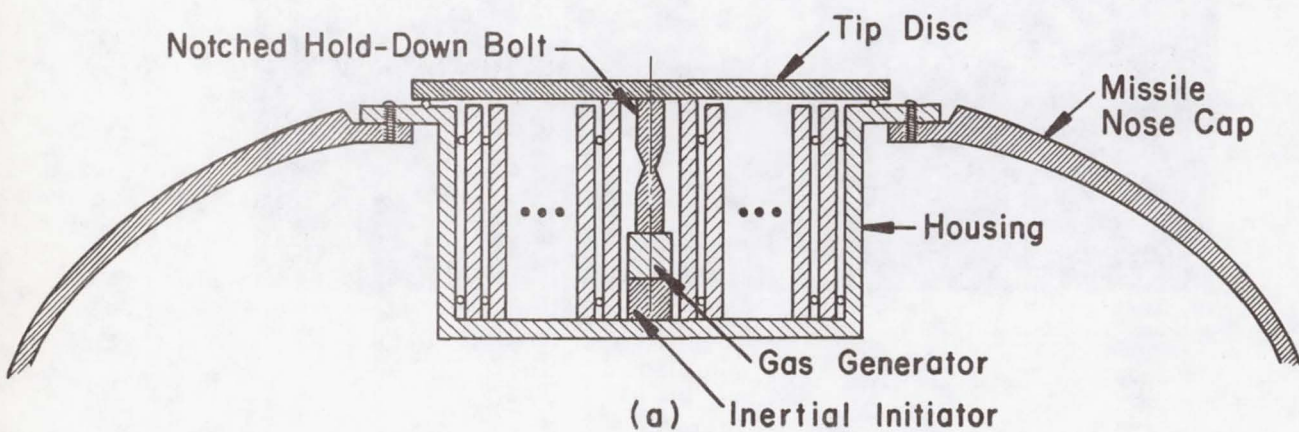


Figure 1. Aerospike-Induced Flow Pattern



(b)



(a)

Figure 2. - Aerospike configuration (a) stowed, (b) extended.

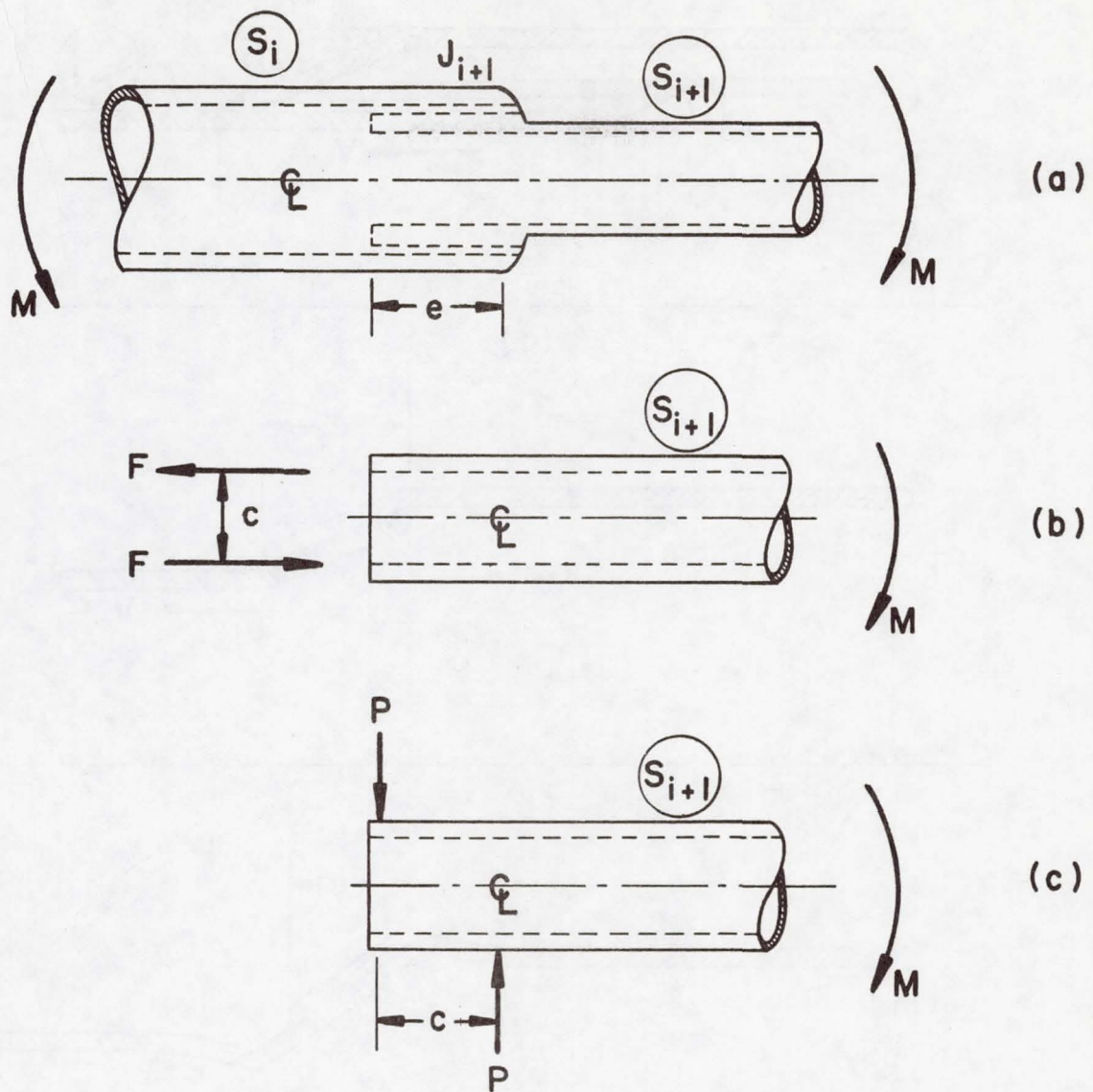


Figure 3. — Load carrying characteristics of a typical joint.

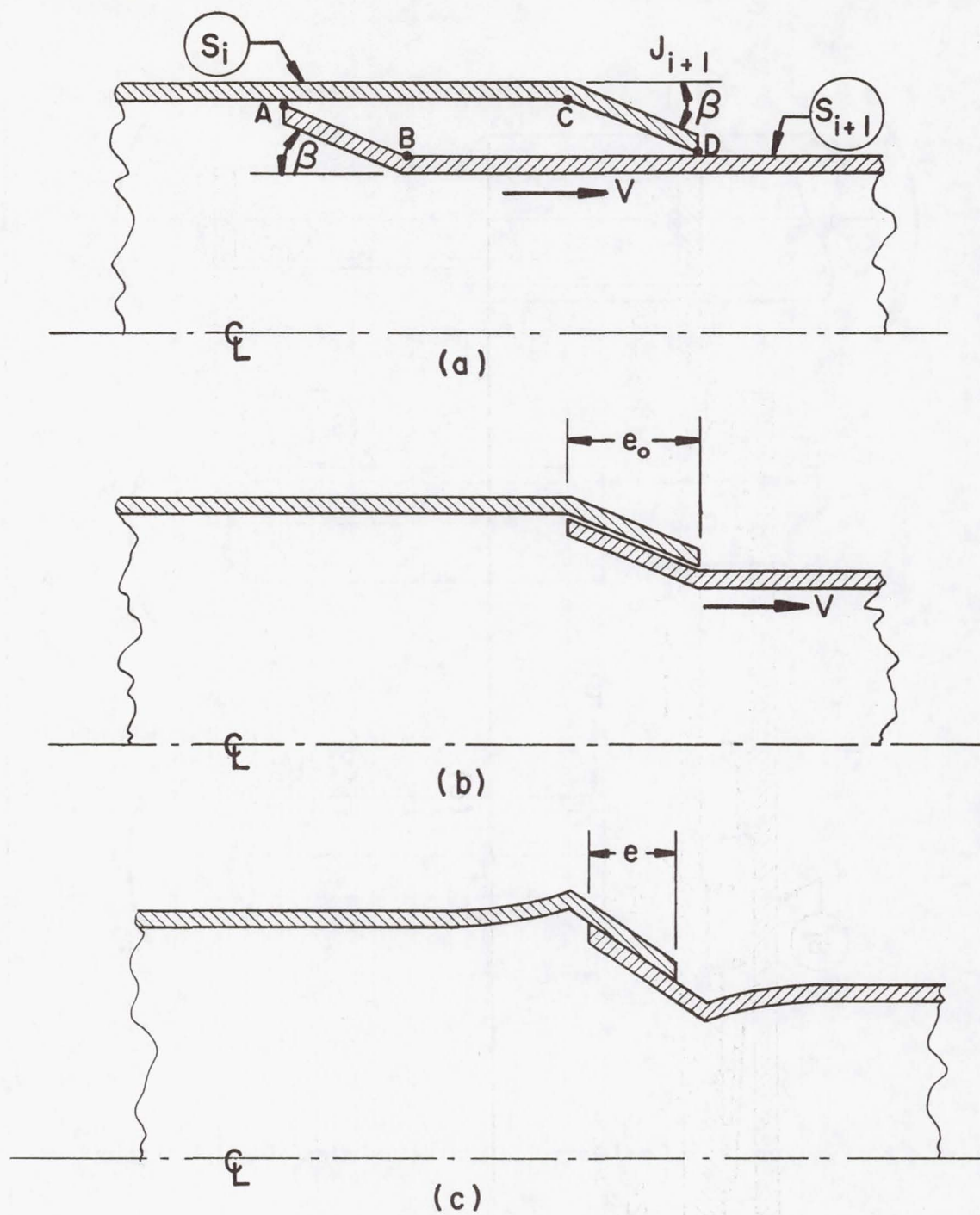


Figure 4. — Schematic operation of type I joint.

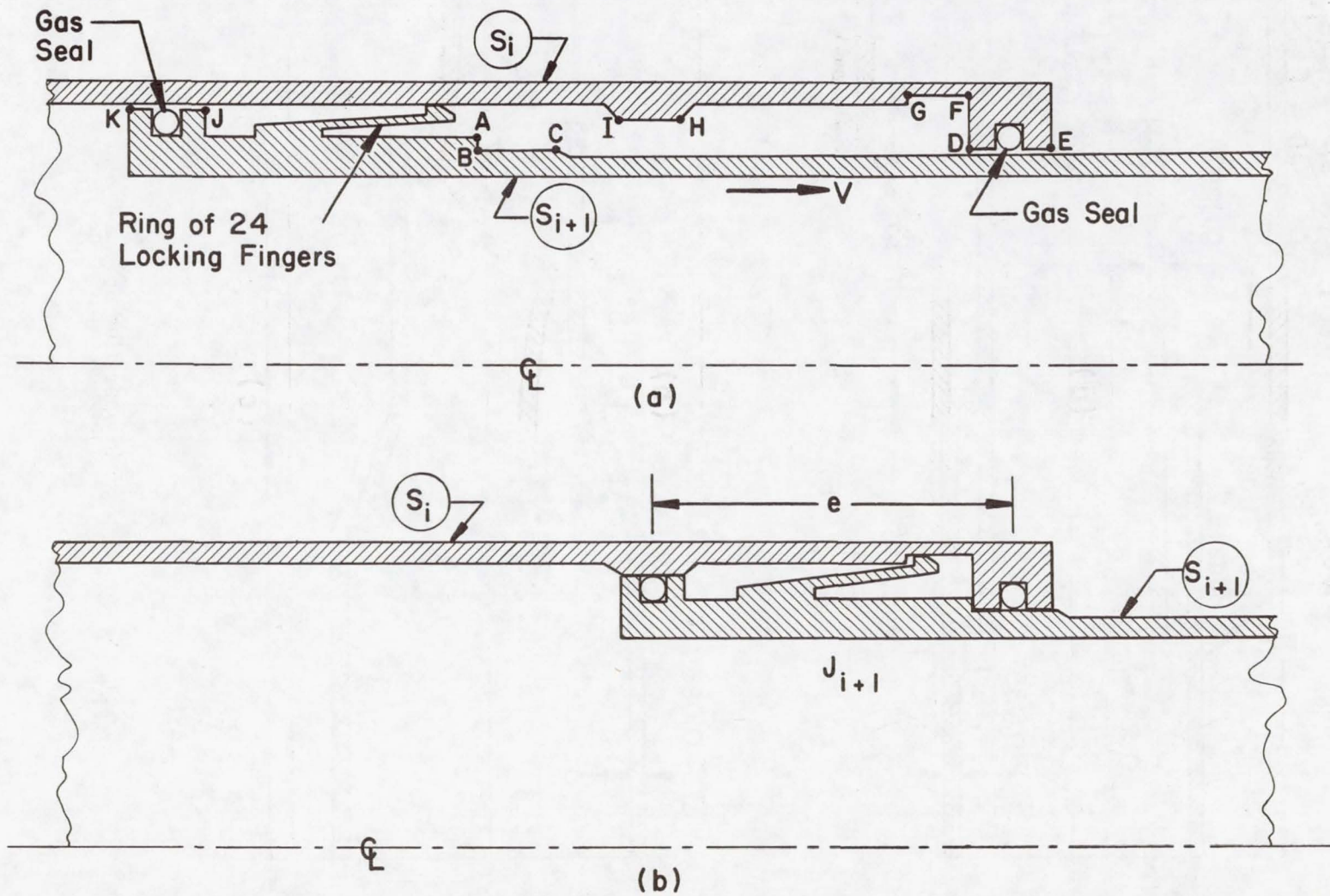
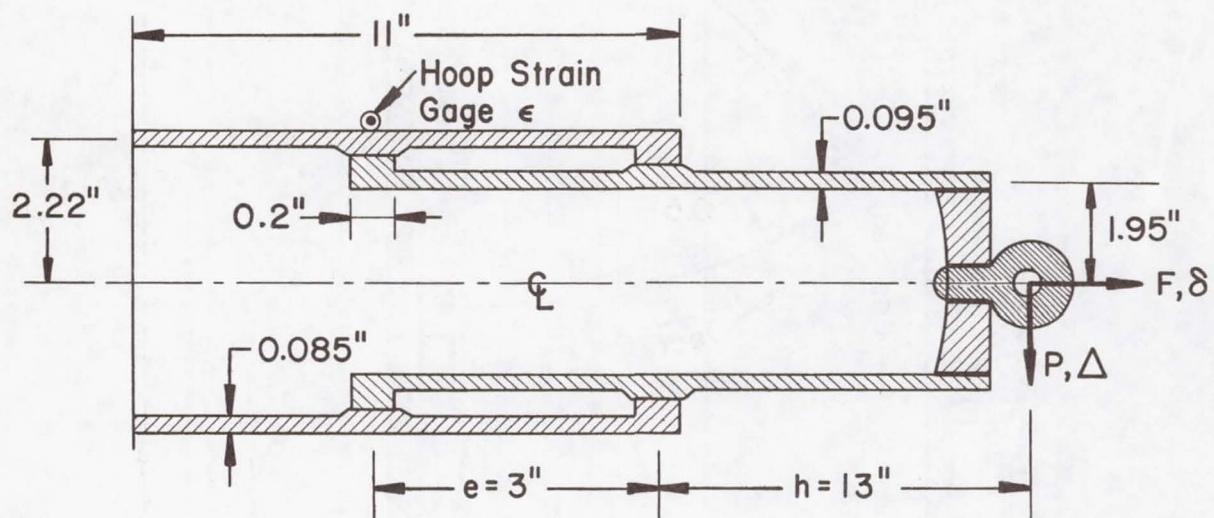
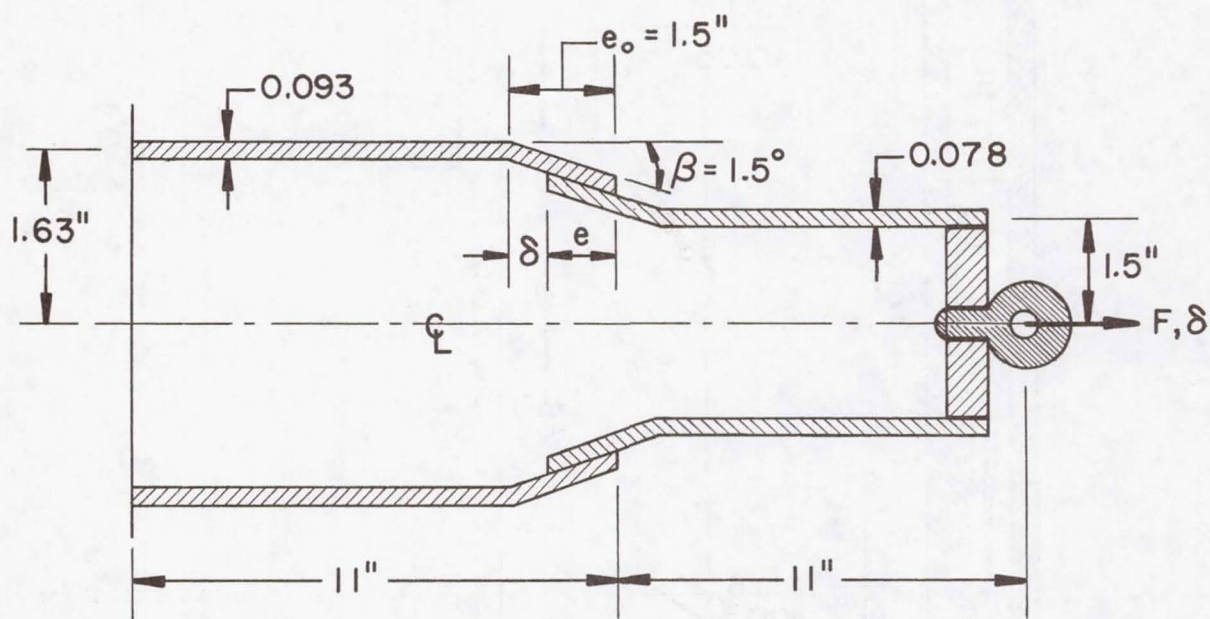


Figure 5. - Schematic operation of type II joint.



(b)



(a)

Figure 6. — Geometry of joint test specimens.

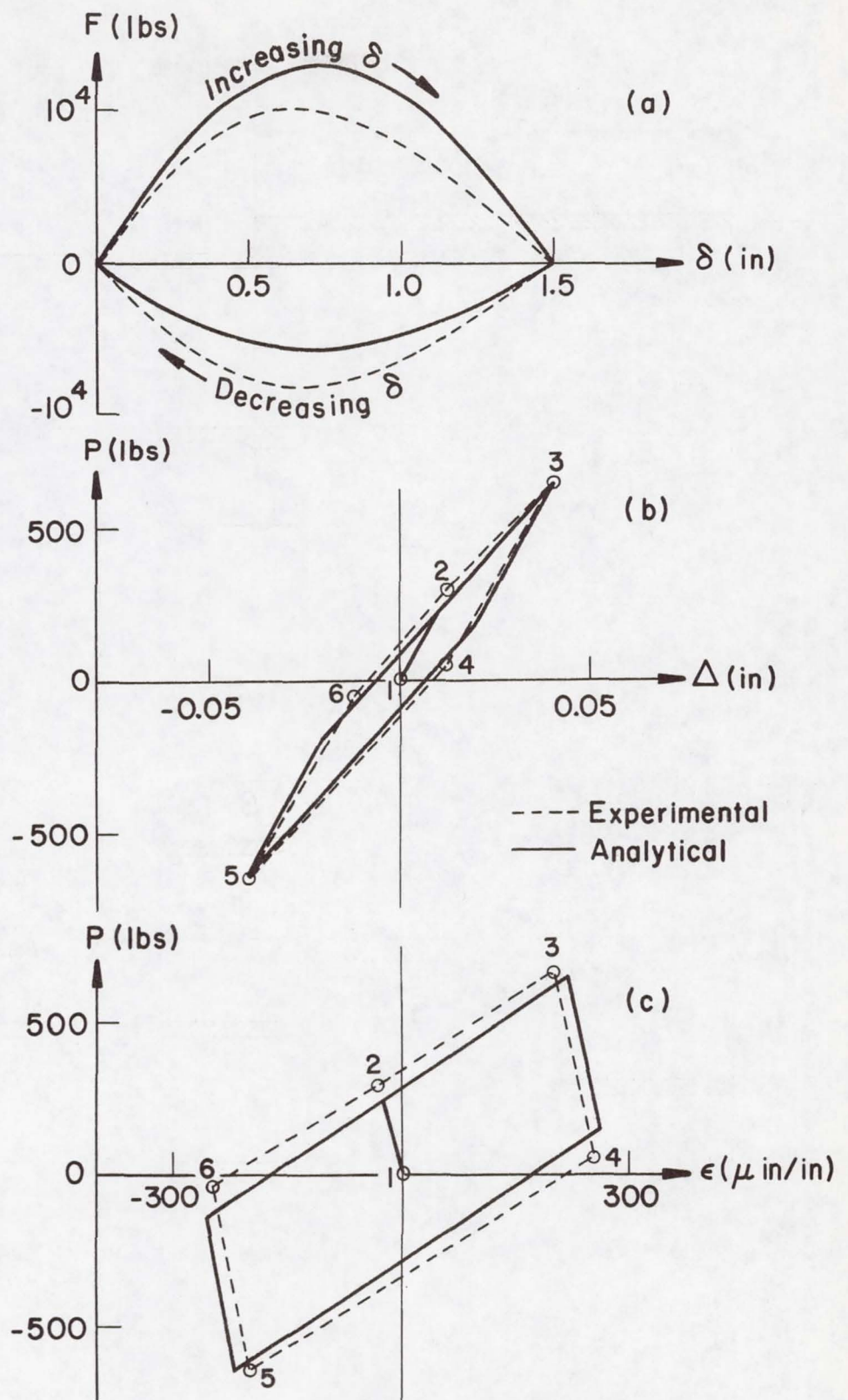


Figure 7. — Experimental comparison with analyses.

4. AEROSPACE LUBRICATION TECHNOLOGY TRANSFER TO INDUSTRIAL APPLICATIONS

By Thomas J. Loran and Bill Perrin

Ball Brothers Research Corporation
Boulder, Colorado

SUMMARY

Transferring technology from the highly specialized aerospace industry to high-volume, commercial markets is quite difficult. It has required several years for Ball Brothers Research Corporation (BBRC) to penetrate the industrial market. In the course of this, BBRC experienced problems that are unique to aerospace oriented organizations. To overcome these problems required overhaul of marketing concepts, licensing techniques, and internal product security. As one would expect, designs had to incorporate trade-offs of cost and functional life whereas normal aerospace mechanisms need reliability and function as prime considerations. The program must have upper management support since flexibility in pricing and modifying normal aerospace procedures are mandatory to satisfy the low-cost/high volume market requirement.

INTRODUCTION

We all know that the transfer of the technology gains made by our aerospace industry into the industrial mainstream has been (surprisingly) difficult. We are also aware of individual company efforts to spin off aerospace technology into the private sector that have ended in failure. Although many new products

resulting from the aerospace program have been featured in advertising, new product announcements, and special articles, many seem to disappear after a short period of time. NASA has recognized the magnitude of the technology transfer problem and among other things, has resorted to special TV announcements and the use of exclusive license arrangements to encourage the use of its technology. NASA's Technology Utilization Office is making an effective effort in coordinating our industry with the private sector. This paper discusses some of the difficulties BBRC encountered in entering new industrial markets with an aerospace lubrication and coating technology and the technical, financial, and managerial solutions that evolved and led to our success in this venture. We are pleased to review this experience with you and hope that others in our industry can benefit from it.

BACKGROUND

Ball Brothers Research Corporation started a lubrication and coating technology in 1959 during the initial design of the Orbiting Solar Observatory (OSO) Satellite. Our engineers recognized that moving and rotating satellite mechanisms such as bearings, motors, and slip rings could not be reliably sealed and therefore would be exposed to vacuum for several months. The known lubricants and coatings were unsuitable because of high evaporating rates and unstable constituents. BBRC determined the fundamental properties of materials needed for long life in vacuum and formulated lubricant materials and processes to satisfy those theoretical needs. Several aerospace companies subsequently recognized the success of the OSO Satellite and BBRC's Vac Kote lubrication technology (as it was called) and began to request the same lubrication technology for their mechanisms. A lubrication service and consulting activity thus began at BBRC.

In 1965 BBRC began an aerospace mechanism product line that featured the use of the Vac Kote lubrication technology. Within 3 years a multimillion dollar business was flourishing that involved the design, fabrication, and lubrication of mechanisms for spacecraft applications. In 1969 BBRC began to concentrate on diversifying beyond the pure aerospace activity. Several product lines based on BBRC's aerospace technology were initiated. These new business areas included ocean systems, low light television, military hardware, environmental monitoring, antenna design, low cost housing, and Vac Kote lubrication technology. A consulting firm specialized in evaluating potential new business activities was employed to assist BBRC in evaluating these new product areas with regard to business potential and to establish business goals, objectives, strategies, and budgets. The project team that had successfully developed the aerospace lubrication and mechanism business was assigned the task of diversifying the Vac Kote lubricating and coating business into industrial and commercial areas.

A five-year plan was developed for the Vac Kote business center that estimated the investment and potential sales. Figure 1 indicates the chart as drawn in 1969. The break-even point would be in 1971 and the business was projected to grow rapidly. The determination of the sales slope and cost curve depended upon a number of factors such as magnitude of market, company assets for investment, and the return on assets potential as determined by the consultants computerized cash flow formulas. This business area was originally composed of twenty people, including project engineers, production technicians, materials engineers, and marketing personnel.

SALES FORECAST

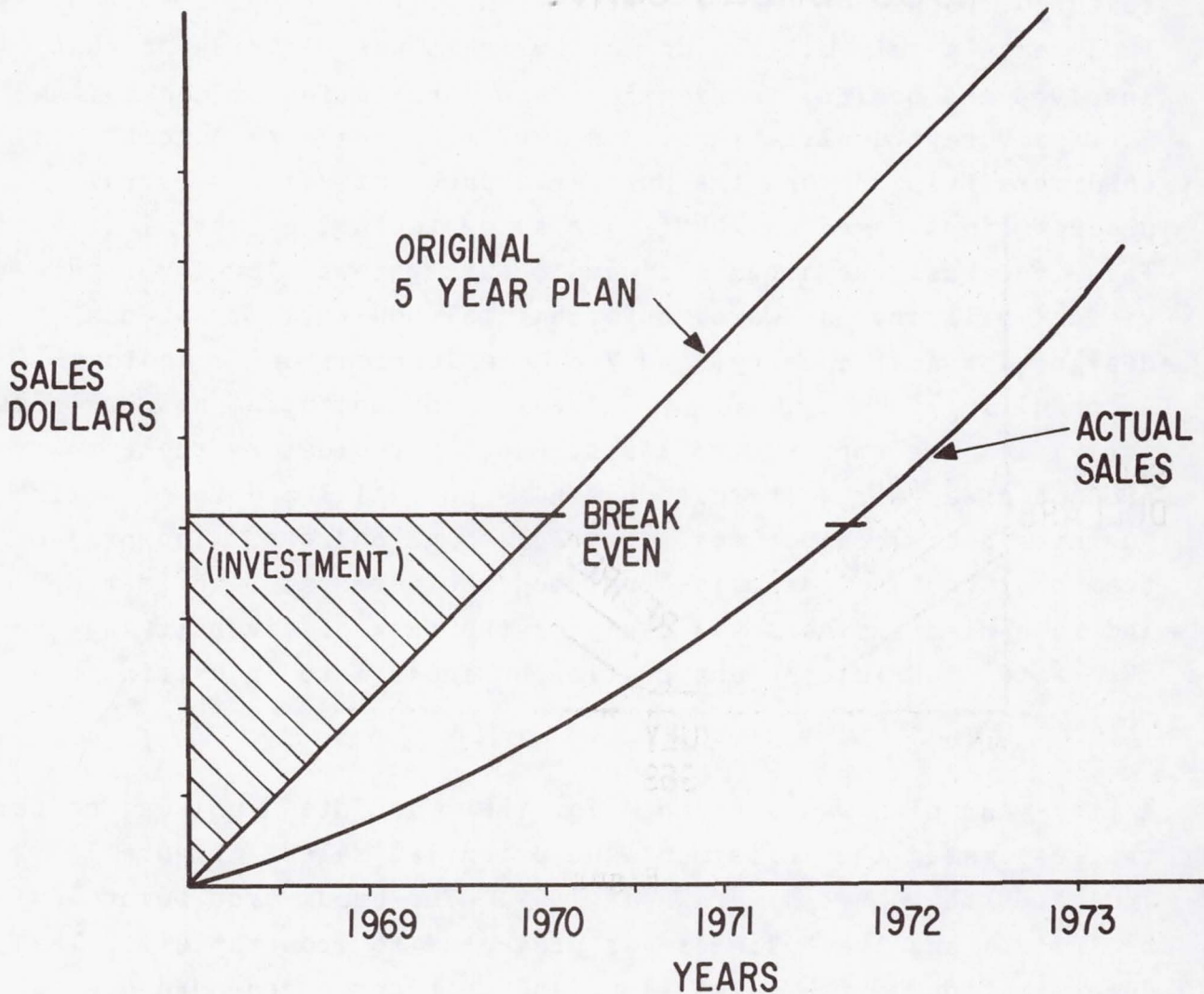


Figure 1

LESSONS LEARNED

Great difficulties (technical, financial, and managerial) were almost immediately encountered. We found that the "commercial" business was an entirely new ball game; our aerospace experience was actually detrimental to our pricing structure, sales methods, and customer service. The chart in Figure 2 indicates our rapid business demise.

1969 SALES CURVE

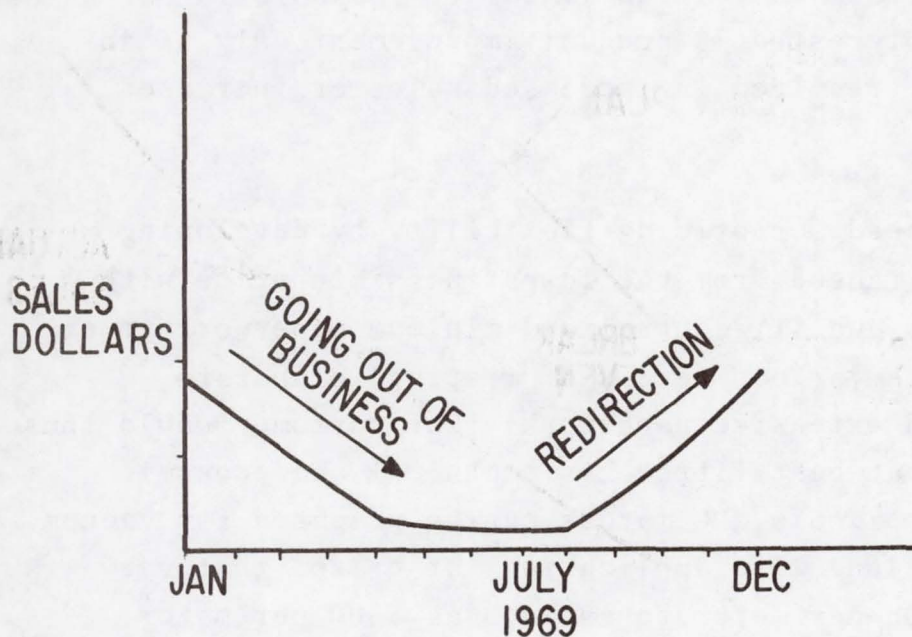


Figure 2

We found that industrial and commercial customers associated the word "Aerospace" with high costs and, unfortunately, they were right. We learned that our practice of maximum quality control, selection, and test of components to produce maximum reliability for the aerospace applications had to be modified. For aerospace applications we always recommend to the customer a complete program of analysis, immaculate processing, and confirmation testing required to produce high reliability. Flight history, engineering analysis, laboratory tests, and reliability

calculations support our material choices. **For** critical satellite applications, cost is usually a secondary concern. When potential commercial customers failed to respond to our proposals, we soon learned to ask the price range that would be consistent with the improvement in the performance and life of their products. With this change in approach we felt an immediate response in our sales. The customer was interested in product improvement only if increased reliability resulted in increased sales or increased profit.

We reacted to the need for pricing flexibility by developing price options that ranged from the lowest possible price with no testing, minimum quality control, and minimum paperwork to expensive options with various levels of testing, **elaborate** quality control, and extensive paperwork. Our customer could thus select a program that best fitted his technical and economic **requirements**. For example, DC motors can be prepared for vacuum operations and for long life applications at prices that vary from as little as 5¢ per motor to as much as \$500 per motor. The 5¢ treatment is achieved by simply processing the motor brushes. The brushes are heated and impregnated **with** special lubricants in quantities exceeding 10,000 per lot. For \$500 per motor, each individual brush is weighed before and after treatment to determine the lubricant absorption. The motor is then assembled and run until the brush **conforms** to the shape of the commutator. Extensive testing is then conducted. This ensures highly reliable motors for a specific, critical aerospace application. As a result of our flexible option pricing there is a complete range of prices between these two extremes.

Thus Lesson #1: A commercial customer will only purchase a product at a price that results in a profit for him.

Lesson #2 was much more subtle. We have learned that the team seeking to develop a new business area should have total responsibility for their destiny. The aerospace procedures manuals, proposal guides, and quality control levels should be available but not mandatory for use. To be responsive to the entirely different type of customer in the commercial marketplace (and thereby win sales), a program manager needs the flexibility to set policy "on the spot" and as required for the occasion. He must have the authority to provide free samples, quote prices, deliveries, terms, and conditions as the customer requires. Many times this is done on the scene in a customer's plant or on the telephone. Coordinating these judgments through the usual aerospace chain of command with enough of the details required for a good decision impedes and frustrates the effort and responsiveness of a business group. The aerospace management must trust the business judgment of the new business group and delegate policy making authority. Sufficient control exists by offering financial reward for the group for business success or "the parking lot" for failure. With this concept, upper level management sets broad business policy and monitors business performance on a quarterly or **semiannual** basis and does not become involved with the day-to-day decision making process.

Lesson #3: "Flexibility and diversity are mandatory!" Customer diversification and flexibility of business goals can either insure success or, if not used, guarantee failure. Originally only a few key companies were identified as potential customers. Cancellation of aerospace contracts taught us the need to expand the customer base. This one point is crucial - it resulted in the **failure** of some of BBRC's new business areas. Also, as you **diversify**, other opportunities that relate to the original goals occur. For example, our coating of movie film and aerospace components led us to the glass mold coating. This was

followed by rubber mold coatings and now we are pursuing plastic mold coatings. However one must not lose sight of the original goals; many contracts can easily take twice the time to develop than originally expected and the new business effort can easily be spread too thin with uncontrolled diversification.

We found that our technology base also had to be flexible to meet customer demands. To our surprise, our early aerospace formulations would solve very few commercial problems. Much to the consternation of our highly qualified engineers, the direction of the technical development had to be changed continually and sometimes the product tentatively "sold" prior to completion of laboratory testing in order to be timely. These decisions must be made by a commercially oriented program manager and are completely "against the grain" of conventional aerospace engineering practice. This can cause difficulties - especially if the technical people are not a part of the "commercial team" and thereby not continuously appraised of the total situation.

Lesson #4: The need for "establishing a team." We found that a team where an esprit de corps is created and proper rewards from the business success are given, significantly improves the probability of business success. With project, engineering, and production aware of the business direction of the team, changes in technical direction or production operations to respond to customer needs are understood and incorporated with minimum lost motion. The "team" also aids in the new product security. Every company has experienced loss of technology by personnel changing employment or leaving the company to start their own business. By limiting the number of people who have a "need-to-know" lowers the probability of losing technology that is not patented. Patents are not always the best method of protecting technology. Many foreign countries issue immediate patents where the USA usually takes 2-3 years. Therefore the technology can be

exposed prior to total development or at a time prior to the marketing thrust. Many times a trade secret is therefore a better sales method (classic example is Coca-Cola). Product security is then mandatory and with it the "team" concept becomes imperative.

SUCCESSFUL COMMERCIAL MARKET PENETRATIONS

The Vac Kote lubrication and coating business evolved into a variety of products as indicated in Figure 3. A brief description of a few of these products will serve to illustrate the diversity BBRC has attained in the commercial area.

A product line that evolved early in our activity was based on special treatments for brushes used in DC motors and tachometers that had been developed for Aerospace applications. Previous research and tests proved that the moisture in graphite and metal-graphite brushes evaporates within hours in vacuum and after this loss, rapid brush wear ensues. BBRC found that impregnating brushes with special low vapor pressure lubricants would appreciably extend life and lower motor noise levels in vacuum. This same technique has been applied to commercial brushes for use in air operation to extend life and reduce EMI. Hundreds of thousands of brushes and other motor parts are now being processed at low competitive cost for the commercial market. One large European manufacturer has licensed and incorporated the Vac Kote technology in his motor production line. The U. S. Navy is also evaluating these treatments for submarine motor-generator brushes.

The glass container industry in Los Angeles had severe plant pollution problems caused by smoke-creating mold release lubricants and were threatened with industry-wide closing. BBRC

Product Bulletin

BALL BROTHERS SERVICE CORPORATION
Muncie, Indiana 47302

"Glass Release" Coating

Glass Release is a semi permanent solid film lubricant used on the glass contacting surfaces of glass forming machine tooling. It is a non-toxic, water based material, consisting of special binders and high temperature release agents. The binder attaches firmly to the metal surface and holds the release agents, thus providing a smooth, abrasion resistant, solid coating. This coating is applied to rings, blanks, baffles, molds, bottom plates, plungers, trimmers and funnels before installation on the forming machine.


Substantial benefits such as improved percent pack, extended tooling life, reduced pollutant contribution and improved labor utilization can be realized from the Glass Release Process.

Glass Release is applied with a conventional paint spray-gun system under normal factory operating conditions. The glass machine tooling is sandblasted or glass peened, but not polished, before the coating is applied. The coated parts may be air dried at room temperature or during the normal tooling pre-heating step. However, for controlled results, it is best to place the treated parts in a 450° oven for approximately thirty minutes. The resultant coating thickness is in the range of .5 to 2.5 thousandths.

The Glass Release Coating will last approximately twenty-four hours without swabbing. However, it is recommended that a light swabbing be supplemented at thirty minute to one hour intervals to extend the life of the coated surface to a period in the order of a few days or in most cases where the tooling is replaced for other reasons.

The Glass Release surface is compatible with most oil based and non-smoking swabbing compounds. In either case, the amount of swabbing compound used is reduced considerably by the light application of

VAC KOTE: THE MOON LUBE



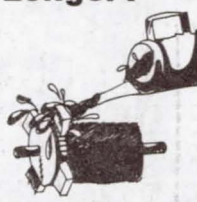
Vac Kote - the space-proven lubrication process from Ball Brothers Research Corporation - now has a new addition to its long list of credits. It was originally developed to provide lubrication of bearings, motors and ship-rings on the Orbiting Solar Observatory. Since then, it has been used on sixteen other major satellites.

Now, it has lubricated the stereo close-up camera designed and manufactured by Eastman Kodak Company and used successfully to take photographs on the lunar surface during the Apollo 11 landing.

When you have unique lubrication problems, in the vacuum of space - or in vacuum or nonvacuum ground applications - when you want to extend the wear-life of your hardware consider Vac Kote. Write for our brochure.

Ball Brothers Research Corporation,
Subsidiary of Ball Corporation, Lubrication Marketing, Boulder, Colorado 80502.
Phone: (303) 444-5300.

Would You Pour Water On Your DC Motor Brushes To Make Them Last Longer?



Water is what lubricates them now - but Ball Brothers Research Corporation has a better way! It's a revolutionary processing technique called Vac Kote.


At the contact points between brushes and commutators, temperatures often go to 150° C. and higher. Water boils off. Vac Kote doesn't - it keeps working. Tests show brush life is extended up to ten times the life of untreated graphite or silver-graphite brushes!

Vac Kote works in all wet gases, or hard vapors - without affecting electrical performance. Vac Kote will save you time and money - increase wear life - increase shaft life - and improve your product performance.

Curiously aroused? Write us and we'll send you data on Vac Kote - no, better yet, call us on our "hot line" - Area Code 303, 443-7755.

BALL BROTHERS PROTECTIVE FILM COATING

The New protective film coating that's out of this world.



A giant step for the film industry.

When the Apollo space program got off the ground, our researchers had an idea that would help the film industry take a giant step forward.

They realized that any coating mixing in the hostile environment of outer space would work wonders on Earth.

So they took the same technology they developed for the astronauts' 35 mm camera, the TV camera and the Lunar Rover and adapted it to films on Earth. The result, Ball Brothers Protective Film Coating for film use in cartridges, cassettes and reels that offers:

- a tough, clear coating tightly bonded to film
- two to five times longer film life
- scratch and wear resistance
- low friction, smooth projection, steady picture even with a 2400 foot continuous load cartridge
- an anti-static ingredient retarding dust and debris accumulation
- unimpeded optical sound tracks
- very low magnetic sound track wear
- application with conventional equipment
- competitive price

For more information send us the attached coupon. It's a small step to take for giant gains. Licensing inquiries invited.

BALL BROTHERS RESEARCH CORP.
Subsidiary of Ball Corporation
1303 441-4814

Ball Brothers P.O. Box 1023 Boulder, Colorado 80502

1st _____
City _____
State _____
Zip _____

Figure 3. Typical Aerospace Products Successfully Transferred to Commercial Use.

devised a semi-permanent coating that eliminated the pollution, increased personnel safety, and reduced personnel exposure to high temperatures and noise. An added bonus for using this coating was increased bottle production that is four times more profitable than the coating cost. Four plants in Los Angeles, as well as five others in the U. S. and three in France, are now licensed to use this coating. Other glass plants throughout the world are scheduled for tests in the near future.

A special low friction, clear, tough coating is being applied to movie film to provide scratch and abrasion protection. Three film processing companies have licensed the process. This coating evolved from materials used for cameras on the Apollo Program.

Using special non-metallic coatings to protect magnetic memory surfaces for the computer industry is another aerospace technology spin-off. These protecting films on computer drums and discs replace the function of rhodium coatings on nickel-cobalt surfaces. This coating has been used for four years on production drums for a major U. S. computer manufacturer. Based on the success in this industrial field, head and tape wear in the sterilizable Viking tape recorder was lessened.

LICENSING STRATEGIES

Recognizing some of our shortcomings such as limited marketing in new industries, high overhead and labor rates, and shortage of funds to staff a large business area suggested using a licensing sales mode. Licenses are difficult to sell because of legal negotiations, psychological blocks regarding payment of royalties, and foreign sales that complicate business relationships. However, the financial returns can be significant.

The license will sell if a customer can realize a large profit from the use of the product in his operation. BBRC's royalty fee is normally a small percentage of the profit that is realized by the use of our technology. Arriving at a fair dollar value can be difficult and involves extensive study of an industry to learn details about its costs. BBRC avoids the use of exclusive licenses for the obvious reason that the entire sales success from a product will then depend on the ability of only one organization or distributor. The licensing technique is especially attractive for business relationships with foreign companies since import duties and foreign restrictions can then be by-passed resulting in a lower priced product and increased sales.

CLOSING THOUGHTS

Interestingly, problem solving for industrial applications has provided a synergistic effect by creating improved lubrication systems for aerospace applications at much lower costs. Lubricants used first for private industry solved the high temperature motor brush problem on the Lunar Rover. The commercial film lubricant has proven effective in reducing friction, wear and signal loss in the metallic recording tape for the Viking Mars Lander Recorder.

Combining production schedules of commercial and aerospace contracts improves efficiency and lowers costs. Expedient processing techniques were found to be applicable for many aerospace mechanisms thereby saving the industry many dollars.

As in almost every human endeavor, a continuous positive attitude and perseverance are mandatory for success in a venture such as this. A book would be required to discuss the many discouraging

events that occurred along the way. The unflagging positive attitude provided the persistence to "go the extra mile" to success. An example of this is illustrated by the following experience that almost resulted in the loss of a very profitable product line.

After almost two years of product development, demonstration, and customer cultivation that had taken us "to the negotiating table" with our potential customers, a dark horse competitor entered the market with a product that was significantly superior to ours and at 1/4 the cost. At this crucial moment a decision to withdraw could easily have been made with the acknowledged loss of investment. Our confidence in our technical ability and our positive attitude resulted in continuing our efforts in product development. The new product proved to be so significantly superior to the new competitor's product that cost was no longer a factor and we regained our former position in this market.

The business goal of diversifying the lubrication work at BBRC has been accomplished with a minimum of corporate funds. The staff has been increased to accomodate the new business during a period when other aerospace lubrication organizations were declining. We believe that our success resulted from the above lessons.

5. A STRUT WITH INFINITELY ADJUSTABLE THERMAL EXPANSIVITY AND LENGTH

By Paul T. Nelson

TRW Systems Group

SUMMARY

TRW Systems has developed a tubular strut with an integral mechanism for adjusting its thermal expansivity and length. The stimulus for its development derived from the stringent thermal stability requirements anticipated for the metering truss in the Large Space Telescope (LST). Its application is not limited to the LST or even to spacecraft structures; its features may be advantageously applied to a general variety of structures and precision mechanisms where dimensional control of component elements in a dynamic thermal environment is required. Detail design, fabrication, and test of a developmental strut have been completed.

INTRODUCTION

A significant and ever increasing category of spacecraft structures has to be substantially inert to the dynamic thermal environment on orbit. The metering structure for the Large Space Telescope (LST) falls in this category. Since it is a precision optical structure, its allowable distortion due to temperature changes is near zero. A prime candidate for the metering structure is a cylindrical truss consisting of several circumferential rings interconnected by tubular strut members. Figure 1 illustrates this concept and shows how a temperature gradient change along the axis can cause dimensional changes in the rings and the struts. However, if the expansivity relationship of ring to strut is properly proportioned, as shown in the inset, the truss length will nominally remain constant. This is because the ring expansion is proportioned to compensate for strut expansion and is called athermalization. A severe constraint results on control of the expansivities (α_R , α_S) of the rings and struts, however.

A straightforward means of controlling the required ratio of α_R/α_S is to fabricate the circular rings to an acceptable expansivity range and then adjust, to suit, the expansivity of their interfacing struts. Strut expansivity can be precisely adjusted by the simple tuning principle described in this paper.

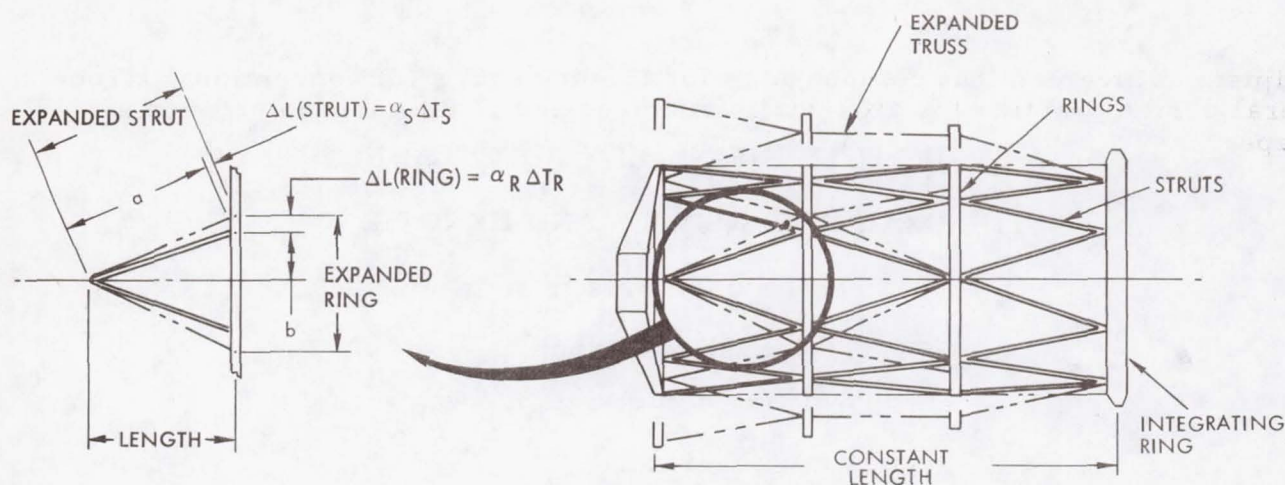


Figure 1. - Effect of temperature gradient change on an athermalized truss.

Graphite/epoxy is a prime material candidate for the LST metering truss. It is uniquely suited for this application because of its low coefficient of thermal expansion (CTE), high thermal conductivity, low specific heat, high specific stiffness, and high specific strength. Even with these outstanding material properties, when used in the LST metering truss and enclosed in multilayer insulation, tests indicate that variations in its CTE are intolerable. In fact, conventional design approaches using any common constructional materials available today, even with the most sophisticated fabrication methods, are expected to be inadequate for the critical structure in the LST because of its stringent thermal stability requirements. The expansivity tolerance band—due to variations in constituent materials and processing—cannot be held small enough.

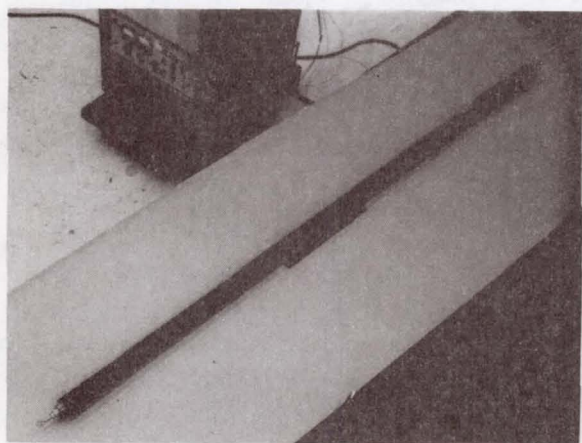


Figure 2. - Graphite/epoxy athermal strut with tunable end fittings.

Figure 2 shows a developmental structural member that is representative of a strut for a three-bay metering truss of LST size. The tubular portion of the strut is made of graphite epoxy with longitudinal graphite fiber orientation and Style 181 glass cloth on inside and outside diametrical surfaces. This construction yields a relatively low positive CTE, but, because of variations in materials and processing, it does not yield adequate repeatability in production for athermalization without a means for "tuning." The end fittings are metallic, nonferromagnetic, and incorporate a mechanism which provides adjustment capability to "fine tune" both the pin-to-pin length and "Effective CTE" of the strut. It is this

adjustment feature that compensates for the inadequacy of conventional structural design practice for athermal structures and is the main topic of this paper.

SYMBOLS

L	length
ΔL	change in length due to temperature change
ΔT	change in temperature
α	coefficient of thermal expansion

Subscripts:

Al	aluminum
eff	effective
G	graphite/epoxy
R	ring
S	strut
Ti	titanium
tot	total

ATHERMAL STRUT MECHANISM

The key to achieving precision control of thermal expansivity in the strut is the mechanism illustrated in Figure 3. The primary load path for a typical tension or compression load is from the graphite-epoxy tube through the bonded titanium collar, into the threaded aluminum sleeve, and finally through the titanium eyebolt. The sleeve and eyebolt locknuts serve to retain the adjustment after it has been made and also to eliminate backlash in the mechanism. The eyebolt locknut also serves as a linear bearing for the eyebolt.

To visualize the operating principle of the mechanism, consider a uniform temperature rise in the entire system. We are primarily interested in the axial change in length induced by a change in temperature (ΔT). In this particular system, the coefficient of thermal expansion of each component will expand in direct proportion to its CTE and effective length, and thereby each component influences the overall length of the strut. The key to controlling the thermal expansivity of the strut system is the relatively high reverse

expansion of the aluminum sleeve which compensates for the aggregate positive expansion of all the other components. The strut also has infinitely variable length adjustment within the limits of thread length. This is achieved by left-hand threads on one end of the complete strut and right-hand threads on the other; thus the strut length can be fine tuned in turnbuckle fashion and locked in place with the two jam nuts.

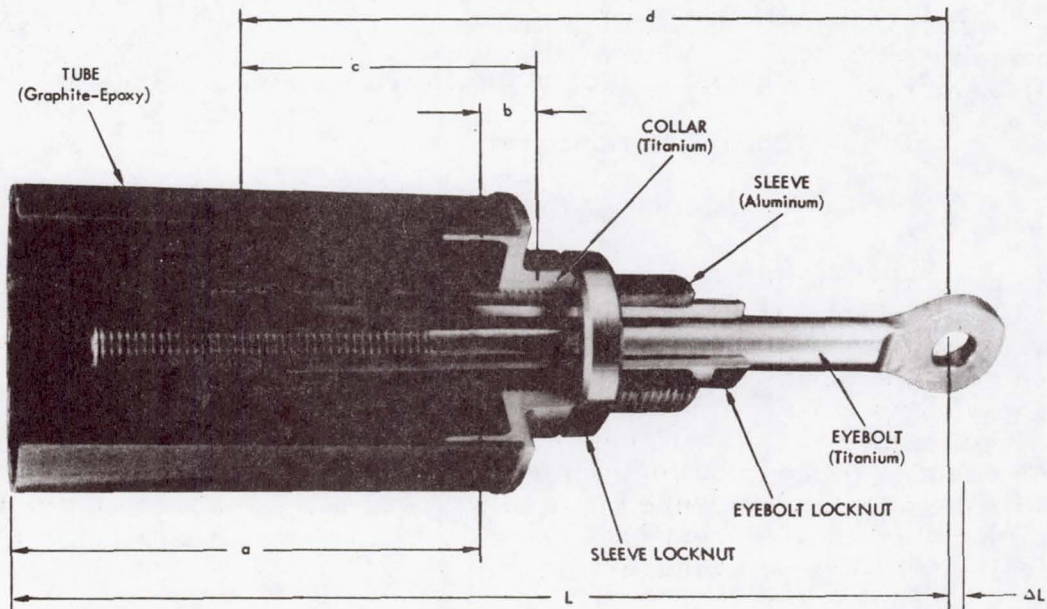


Figure 3. - View of sectional tunable end fitting.

If the procedure is followed of first adjusting the length to a nominal dimension and then adjusting thermal expansion, a further fine length adjustment will have a trivial effect on the calibrated expansivity of the strut system.

You will note that the change in length (ΔL) of the system represented in Figure 3 due to a uniform ΔT is the aggregate response of the components in the load path. In the concept reported here, the expansion of all components except the aluminum sleeve tends to increase the length of the strut. The precise increase in length (ΔL) of the complete strut system, the aggregate response of the system, is as follows:

$$\Delta L = (a\alpha_G + b\alpha_{Ti} - c\alpha_{Al} + d\alpha_{Ti}) \Delta T_S$$

The effective CTE of the system (as shown in Figure 3) is expressed by the following:

$$\alpha_{eff} = \frac{a\alpha_G + b\alpha_{Ti} - c\alpha_{Al} + d\alpha_{Ti}}{L}$$

From the above equation it is apparent that the effective expansivity of a strut is a function of: (1) the geometry (dimensions a , b , c , d , and L) and (2) the coefficients of thermal expansion (α_G , α_{Ti} , and α_{Al}) of the constituent materials. The effective coefficient of thermal expansion of the system can be made equal to "zero" for a given selection of materials by using a geometry in which the numerator of the above equation equates to zero. Since the " c " dimension can be adjusted about its nominal value, the effective CTE of the strut "system" can be adjusted accordingly, limited only by the adjusting range of the threads. The overall length " L " is unaltered by the CTE adjustment (changing " c ") because the thread series on the sleeve and eyebolt are identical; i. e., the thread pitches are the same.

FABRICATION

The graphite/epoxy tube is a six-ply unidirectional laminate of Modmor Type 1/5208 material. It was laid up on an aluminum alloy mandrel with a 0.30-mm taper over its length. A lamina of Style 181 glass cloth/5208 was laid up on both the inside and outside walls of the tube. The prepegged tubular laminate was vacuum bagged and cured for 3 hours at 107°C at 0.5×10^6 newton/m² autoclave pressure. This description is of the part that was tested and is not intended to imply a choice for the LST metering truss. The adjustable end-fitting components were made of stock aluminum and titanium alloys and were machined in a conventional manner. An extra assembly was made for sectioning (as shown in Figure 3) to more graphically illustrate the mechanism.

STRUT SYSTEM TESTS

Test Procedure

Tests performed on the strut assembly shown in Figure 2 included the full range of expansivity adjustment of both end fittings. The primary purpose of the tests was to verify the effectiveness of the thermal expansion tuning concept.

The test setup is shown on a 3.7-meter granite surface table, with the test article inside a specially built thermal chamber (as illustrated in Figure 4). The operating principle of the experiment is as follows. A quartz spacer reacts externally against a heavy weight cast iron anchor at one end of the thermal chamber, and another spacer with the strut in between bears against a laser retroreflector at the opposite end. A steel coil spring maintains about 45 newtons force against the retroreflector throughout the tests assuring continuing compliance of the retroreflector with test specimen dilation. The retroreflector base is free to move with the free end of the test article and quartz spacer.

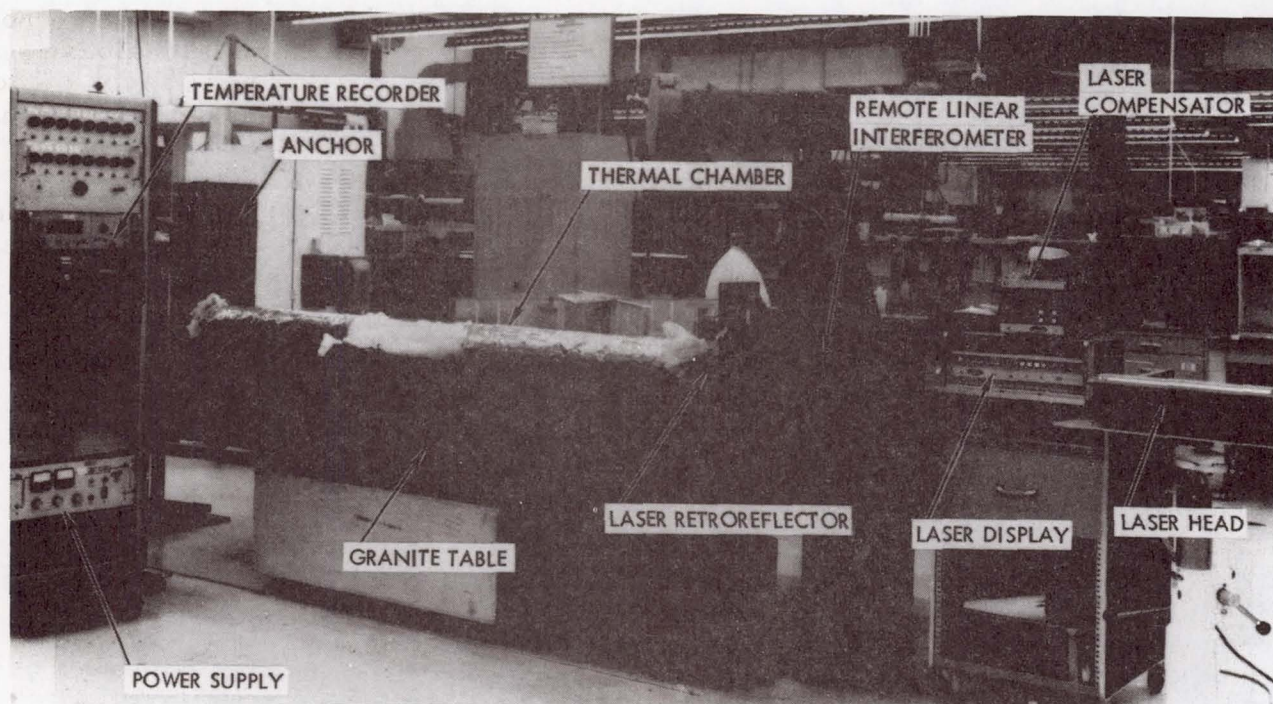


Figure 4. - Dilatometer for testing thermal expansivity of a long strut.

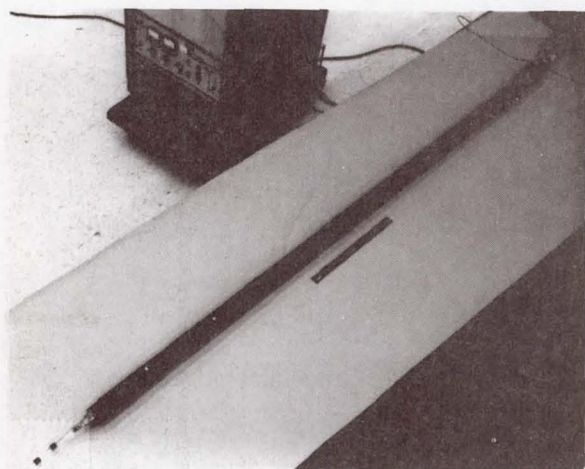


Figure 5. - Instrumented strut with quartz spacers at each end.

The externally positioned remote linear interferometer is the basic reference from which distance to the laser retroreflector is measured. The laser head and laser display were located in a convenient position for viewing. Figure 5 shows the instrumented strut with 15.24-cm quartz spacer rods at each end. Three thermocouples were mounted on the graphite/epoxy tube — one in the center, and one 15.24 cm from each end. A thermocouple was installed 7 cm from the outboard end of each quartz spacer. The reaction bar shown in Figure 6 assures a positive force against the anchor through the coil spring, the retroreflector, and quartz spacers, as well as the test article; it is held in place by the heavy cast iron angle plates.

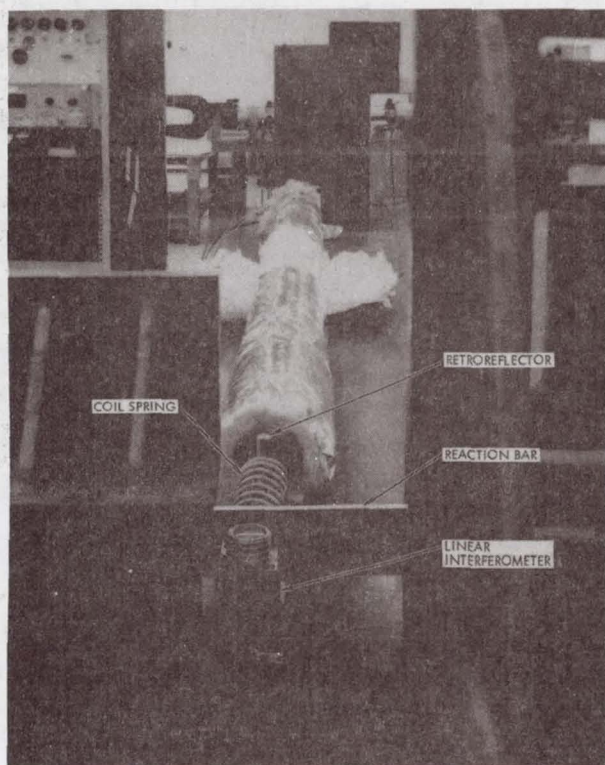


Figure 6. - View of dilatometer showing retroreflector spring reaction bar.

Figure 7 shows the laser retro-reflector setup. Its polished base was well lubricated with silicon oil to assure virtually friction-free motion. The thermal chamber was heated by electrical resistance heaters and wrapped with fiberglass and aluminum foil insulation. Insulation was partially stripped in the center because of a minor temperature imbalance in the test specimen. Stripping enhanced local cooling, providing a more even temperature distribution in the tube.

Vee-shaped support clips in the chamber held the tube specimen in the center of the chamber. End caps supported the quartz spacers (as shown in Figure 8) and allowed the spacers to move freely with test specimen and spacer dilation.

The validity of this test method was verified by a preliminary experiment in which an alternate method was also evaluated. The retroreflector and remote linear interferometer in the alternate method were mounted at

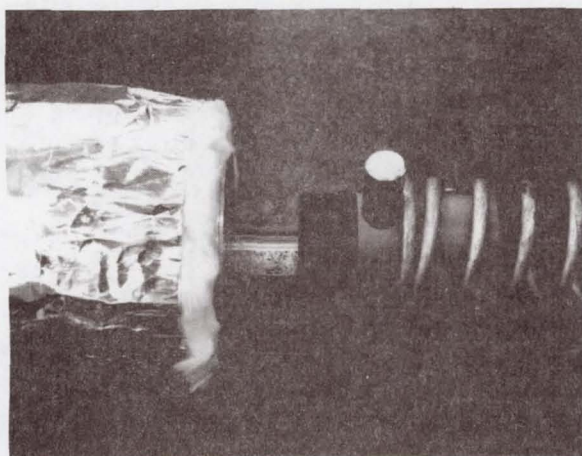


Figure 7. - Laser retroreflector setup.

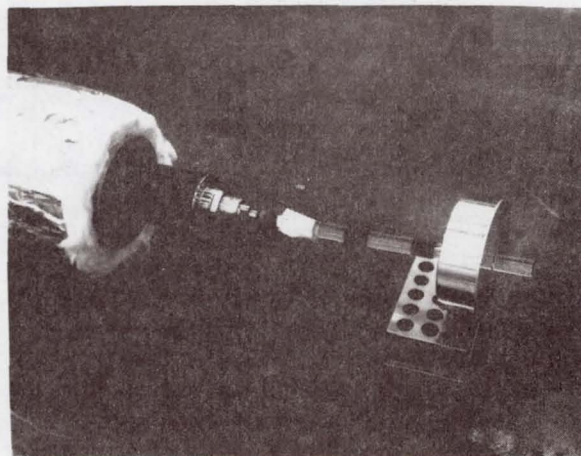


Figure 8. - End caps removed from chamber to show support of quartz spacers.

opposite ends of the test specimen which was not anchored at one end. Atmospheric turbulence in the environment surrounding the specimen, however, caused an unacceptable wavering in the laser display readout. On the other hand, an experiment directed toward a test as finally executed resulted in a very stable readout (within ± 0.025 micron), when the granite table was locally heated in the most critical area beyond tolerance to human touch. During this latter experiment, an aluminum tube was installed for protection of the laser beam to preclude atmospheric disturbance. When it was ascertained that any error due to table heating was negligible, the concept of an anchor at one end and movable retroreflector was verified. The linear interferometer could then be located close to the retroreflector (as shown in Figure 6) without the need for a protective tube for the laser beam. This latter approach appeared to be better and was accordingly selected. The experiment also confirmed that the effect of air turbulence to the laser beam over a short distance was negligible.

The strut assembly was installed in the test chamber with the quartz spacers and instrumentation. Thermocouples were installed on the graphite/epoxy tube (three places), on both end fittings, and on the quartz spacers. The length of the strut was adjusted by turning the eyebolts so that the distance between the quartz spacers (overall length) was 198 cm. This 198-cm length was nominally maintained for all of the tests. Each test run was started with the specimen relatively near room temperature. Temperature recordings were made for each thermocouple location and the laser display was reset to zero. With this pretest activity complete, the chamber was heated to a peak temperature and then allowed to level out and cool until all test specimen thermocouples and also quartz spacer thermocouples were stabilized. Temperatures were again recorded for end-of-run condition.

Test Results

Three end-fitting adjustment positions were tested: (1) sleeve full in; (2) sleeve at mid-position; and (3) sleeve full out. These positions correspond to minimum, median, and maximum effective CTE adjustments, respectively. The average temperature of the strut and quartz spacers at the beginning and end of the run are listed in Table 1. Temperature data and the corresponding change in length (ΔL) were taken when all thermocouples on the strut were within 2.8°C . Furthermore, both quartz spacers were within 2.8°C .

The average temperature differences (ΔT 's) for the strut and spacers are also shown in Table 1. The effective strut coefficient of thermal expansion (α_S) is shown in the extreme right column. It is computed from the following:

$$\alpha_S = \frac{\Delta L_{\text{tot}} - 2L_Q\Delta T_Q\alpha_Q}{L_S\Delta T_S}$$

In this case the length of each spacer (L_Q) is 15.24 cm and overall length of the strut (L_S) is 198 cm.

Table 1. - Temperature and expansion data from strut system test.

Test Configuration	Average Temperature at Start of Test (°C)		Average Temperature at End of Test (°C)		ΔT_O (°C)	ΔT_S (°C)	ΔT_{tot} (cm x 10 ⁻⁴)	α_S (ppm/°C)
	Quartz Spacer	Strut System	Quartz Spacer	Strut System				
Aluminum sleeve turned in line with flats	23.1	23.1	63.6	66.0	40.4	42.9	15.4	0.10
Aluminum sleeve at mid-position	22.8	22.8	83.8	86.6	61.0	63.8	59.0	0.39
Aluminum sleeve turned to maximum outward position	21.9	22.8	80.6	83.4	58.7	60.7	93.0	0.69

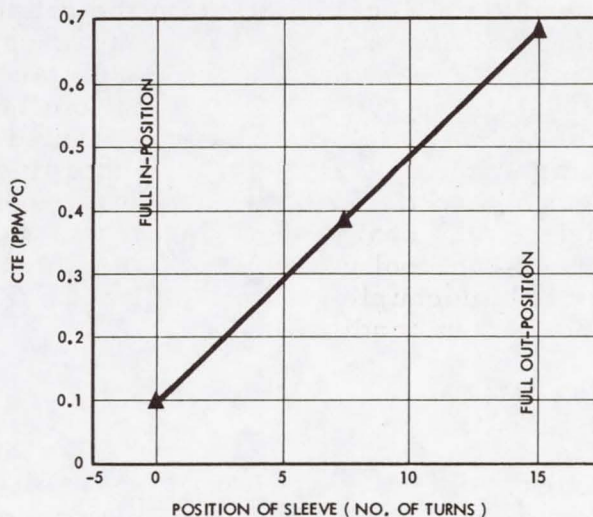


Figure 9. - Effective CTE versus position of aluminum sleeve.

A total number of 15 turns comprised the full range of adjustment. Therefore, the sensitivity of adjustment is as follows:

$$\frac{0.69 - 0.10}{15} = 0.039 \text{ ppm/}^\circ\text{C/turn}$$

Linearity of the adjustment is shown by the curve in Figure 9.

CONCLUDING REMARKS

The strut was "tuned" from 0.10 to 0.69 ppm/°C. Adjustment of expansivity is substantially linear in the adjustment range. A much wider range of expansion could be readily demonstrated by appropriate material and geometry selection. Clearly the adjustment range could be made to pass through zero and into negative values. Viability of this TRW tuning concept is proven and can be applied "in-principle" to a wide range of thermally inert structural or mechanical systems.

6. IN-FLIGHT FRICTION AND WEAR MECHANISM

By E. J. Devine and H. E. Evans

Goddard Space Flight Center

SUMMARY

A unique mechanism has been developed for conducting friction and wear experiments in orbit. The device is capable of testing twelve material samples simultaneously. Power, weight, volume, mounting, cleanliness, and thermal designs were particularly critical requirements that were successfully met. The device performed flawlessly in orbit over an eighteen month period and demonstrated the usefulness of this design for future unmanned spacecraft or Shuttle applications.

INTRODUCTION

It is well recognized that the increased tendency of cold welding (friction) and wear in vacuum are potentially serious hazards to mechanical devices operating in space. When exposed to the space environment, conventional lubricants rapidly evaporate, oxide films disappear once disrupted, and chemically clean metal surfaces can come into intimate contact. The result is drastically increased friction and wear due to adhesion (cold welding). (Reference 1) This cold-welding phenomenon in space is of great interest to unmanned spacecraft instrument and equipment designers and especially to the manned space effort because such procedures as repeated orbital docking and assembly may be affected by cold welding.

A very widespread and costly effort was undertaken to investigate this problem under laboratory simulation of the space environment. At one time, a count showed that approximately 100 groups (both government and industry) had been or were studying cold welding and wear. Most of these studies involve vacuum effects.

In contrast to the extensive laboratory investigations and in view of the recognized importance of the friction and wear

problem, it was surprising that very little data had been, or were planned to be, obtained in the actual space environment. The only previously planned experiments were carried out by the Jet Propulsion Laboratory (Reference 2) on the early Ranger flights and the Air Force Rocket Propulsion Laboratory using the Experimental Research Satellite (Reference 3).

OBJECTIVE

The major objective of this program was to determine the effect of the actual space environment on friction (cold welding) and wear of widely used spacecraft materials. In addition to verifying or disproving laboratory results, this experiment was planned to establish a better definition of the degree of vacuum required for an adequate simulation of the space environment.

APPROACH

It was decided that the disk and rider technique would be used for measuring cold-welding tendency and wear. Welding tendency was determined by measuring the strain induced in a cantilever beam supporting the rider. Semiconductor strain gages mounted on the beam were selected for this measurement. Seven disks and twelve riders were picked as a realistic sample size.

Cleanliness is mandatory when conducting experiments involving material surface effects. (Reference 4) Great care was required in designing the experiment to minimize the possibility of contaminating the material couples. Design of the drive train, instrumentation, and material selection had to be made with the objective of minimizing outgassing. The drive train had to be hermetically sealed and materials with vapor pressures less than 10^{-13} torr had to be used.

To minimize contamination by outgassing from the satellite and at the same time to give maximum exposure of the experiment to the space environment, it was necessary to mount the experiment on the outer surface of the spacecraft and to baffle it from any potential outgassing source.

Most of the laboratory test work was done at pressures of 10^{-8} to 10^{-9} torr; therefore, it was required that the orbit chosen for this experiment have an apogee that would expose the

spacecraft to a pressure less than 10^{-10} torr, preferably 10^{-12} torr. This condition would shed light on the degree of vacuum required for adequate simulation.

The materials selected for study are commonly used in spacecraft and also have properties that enable the effects of mutual solubility and hardness to be studied. Materials were:

- o Gold and silver
- o 7075 anodized aluminum and 440C stainless steel (Rc60)
- o 440C stainless steel (Rc60) and 440C stainless steel (Rc60)
- o 440C stainless steel (Rc60) and nitrided Nitralloy 135 mod steel
- o 440C stainless steel (Rc60) and 1020 carbon steel
- o Be-Cu alloy 25 no. 190 heat treat and 440C stainless steel (Rc60)

Two samples of each of these combinations were tested with the experiment module.

INSTRUMENTATION

The basic friction-test mechanism consisted of a hemispherical rider sliding on the flat face of a disk rotated at constant velocity. This geometry is simple and has been widely used in past investigations of vacuum effects on friction phenomena.

Parameters measured and telemetered were friction force, normal force, and displacement of the rider because of wear. These were measured by strain-gage transducers.

The rider-support arm was designed with two flexible sections: one sensitive to friction force and the other sensitive to normal force. These sections were instrumented with epoxy-bonded, diffused-silicon strain gages. The gages were arranged in a half-bridge configuration to increase the output signal and to cancel the apparent strain due to thermal expansion mismatch of the gage and substrate.

Normal load was applied by means of an independent, adjustable spring as shown in Figure 1. Normal load for the gold versus silver samples was 4.45 N (1 lb); all other metal couples were loaded to 8.90 N (2 lb). The occurrence of a given amount of wear (0.12 cm) of the rider would result in a corresponding motion of the load rod that would bring the rod in contact with the wear transducer, giving a single-point measurement of wear.

Seven disks were stacked on a common drive shaft and 12 rider assemblies were equally spaced around the periphery, giving a capability for measuring 12 material combinations. Surface velocity between disk and rider was approximately 0.10 cm/s.

In the event that the friction force on a particular couple reached a level such that excessive power was required, the rider was removed from contact by means of a sealed pyrotechnic actuator. The electrical signal for firing the actuator was generated when the friction gage output exceeded a level corresponding to a coefficient of 3.3.

The drive train for the device incorporated two state-of-the-art devices. A brushless motor with solid-state commutation required only 3.5W to drive the fully loaded device. The motor drove an intermediate gearhead of 16.3:1. The motor and gearhead were enclosed in a hermetically sealed package to avoid contamination of the friction experiment and at the same time to maintain conventional lubricants on the high-speed drive elements. Transmittal of power through the hermetic package, together with an additional 72:1 gear reduction, was accomplished by a harmonic drive mechanism.

Considerable attention was given to lubrication of the few slow-moving parts exposed to the space vacuum. The spline (gear) of the harmonic drive mechanism was gold-plated and a light burnish of molybdenum disulfide was applied, run in, and the excess removed. Linear ball bushings, which float the transducer load rods, were in-situ coated with molybdenum disulfide. The drive shaft support bearings were equipped with a self-lubricating duroid retainer and shields.

The strain-gage transducers were designed to meet the following requirements:

Load range	Normal force: 0 to 13.3 N (3 lb)
	Friction force: 0 to 26 N (6 lb)

Maximum strain 5000×10^{-6} cm/cm (limited by the bond strength)

Natural frequency 2000 Hz

Sensitivity Normal force: 13.5 mV/N
Friction force: 6.8 mV/N

These requirements dictated the use of semiconductor strain-gages for the required sensitivity. Literature search (Reference 5) indicated that radiation exposure in a one-year orbit would not significantly affect the gage output. Silicon gages of p-type material are more radiation-resistant and were accordingly selected. The gages had a nominal gage factor of 100.

Experimental studies were conducted in a search for a bonding technique that would eliminate organic materials. Although two of these approaches (ceramic bonding and soft soldering) showed promise, neither could be flight-qualified in the time available. As a result, a high-temperature epoxy bond was selected for this application.

The transducer substrate chosen was 17-4 PH stainless steel. The gages were used in a half-bridge configuration with one gage in tension and the other in compression. The gage output as a function of load (strain) deviated only slightly from linearity within the desired range of operation; therefore compensation for this effect was not required.

The gages were compensated for temperature effects. First, the two gages in a half-bridge were tested for gage-factor change with temperature. Any mismatch was eliminated experimentally by a shunt resistor across the gage showing the larger change. Even with the gages matched for gage-factor change with temperature, the bridge sensitivity dropped with increasing temperature. This effect was compensated by a resistor in series with the voltage supply to the bridge. At elevated temperatures, the bridge resistance increased, causing the current and the voltage drop across the series resistor to decrease. As a result, the voltage across the bridge and the bridge output rose to compensate for the loss of sensitivity. The compensated transducers readily met the specification of less than ± 3 percent of full output drift over a temperature range of -20° to 60°C . Typical transducer linearity is shown by Figure 2.

The relatively high output of the semiconductor strain-gage transducers made feasible the use of individual linear integrated-circuit amplifiers. Thus the complexity of commutation was avoided and redundancy was attained. Some penalty in power drain was inherent in the individual amplifier approach. It was desired that the amplifier stability and temperature drift performance would at least equal that of the transducers. This was, in fact, achieved by careful burn-in and selection. A sample of 500 commercial μ A709 amplifiers was burned in over a temperature range of -40° to 100°C ; 250 were selected because of minimum change in offset current.

The schematic for the strain-gage half-bridge, the series-shunt resistor-type temperature compensation, and the integrated-circuit amplifier is given by Figure 3.

Ancillary circuits are required for the following:

- o Converter regulators for supplying -3 V (± 0.5 percent) for the strain-bridge excitation, $\pm 9\text{ V}$ for unregulated amplifier power, and 5 (± 0.5 percent) V for temperature sensors
- o Thermistor temperature sensors for in-flight temperature monitoring
- o Shaft rotation sensor for status monitoring of the drive train
- o Timer for turning the experiment on and off at a 10 percent duty cycle to extend the lifetime of the material couples

The experiment was wired with solid conductor, teflon-insulated wire to minimize trapped gasses and to provide a control of the outgassed materials (Figure 4). Teflon and the minute amount of epoxy bonding material for the gages are the only organic materials permitted in the friction-measurement environs.

TEST PROGRAM

The instrument was qualified for launch vibration at the following levels:

	<u>Prototype</u>	<u>Flight Qualification</u>
Sine vibration	8g vector	5g vector
Random vibration	6g	6g

The prototype disclosed large displacements of the normal load rods when the vibration was parallel to the rod (thrust axis). As a result, vibration stops were incorporated to limit the excursion of the rod and thus prevent overstressing of the normal load strain-gages. Two units were subsequently qualified at flight levels with no significant shifts in the strain-gage transducers.

The experiment was qualified for thermal vacuum over a temperature range from 0° to 60°C and vacuum from 10^{-9} to 10^{-7} torr. These tests were conducted in an oil-free, ionization-pumped system and are the source of the vacuum-friction data discussed in the next section.

The instrument was integrated and tested on the OV-1-13 Satellite with the following results:

- o Electrical, RF, and magnetic interference tests showed no interference with the satellite systems or the other sensitive experiments.
- o Thermal-vacuum (including solar-simulation) tests established the worst-case condition as the cold temperature and demonstrated the capability of the passive temperature control to maintain a predicted range of 0° to 15°C.
- o Satellite vibration test with a 1g vector input resulted in no degradation. The vibration test demonstrated that the strain-gage transducers maintain remarkable stability under mechanical abuse. The other unknown factor was the stability with time. Table 1 gives stability data for a complete set of transducers measured at the beginning and end of an 8-month interval. The drift figures shown include both the transducer and integrated-circuit amplifier circuit. In only one case did the drift exceed the design specification, the drift in this instance being in the amplifier circuit.

IN-ORBIT OPERATION

The friction-and-wear device was operated in orbit throughout the 18-month life of the OV-1-13 Satellite. The experiment was turned on and data recorded on an average of one orbit per week. Because the duty cycle was designed for 3 minutes of operation out of 30, this schedule resulted in an average of 6.5 turn-on intervals per week. This totals approximately 500 intervals of 3-minute duration for a total running time of about 25 hours. Instrument performance was flawless throughout the mission.

REFERENCES

1. F. P. Bowden and D. Tabor, The Friction and Lubrication of Solids, Oxford, 1950.
2. J. B. Rittenhouse, L. D. Jaffe, R. G. Nagler, and H. E. Martens, "Friction Measurements on a Low Earth Satellite," Report 32-402, Jet Propulsion Laboratory.
3. "A Study of Space Propulsion System Experiments Utilizing Environmental Research Satellites," AFRPF-TR-65-73, Air Force Rocket Propulsion Laboratory.
4. D. R. Milner and G.W. Rowe, "Fundamentals of Solid Phase Welding," Met. Rev. 7 (28), 1962.
5. J. F. Kircher and R. E. Bowman, Effects of Radiation on Materials and Components, Reinhold Pub. Corp. 1964.

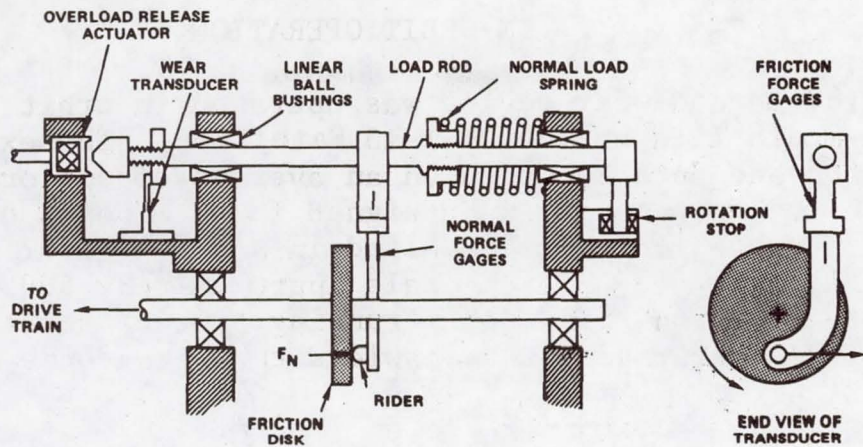


Figure 1 Schematic diagram of friction-test mechanism showing position of spring for application of normal load.

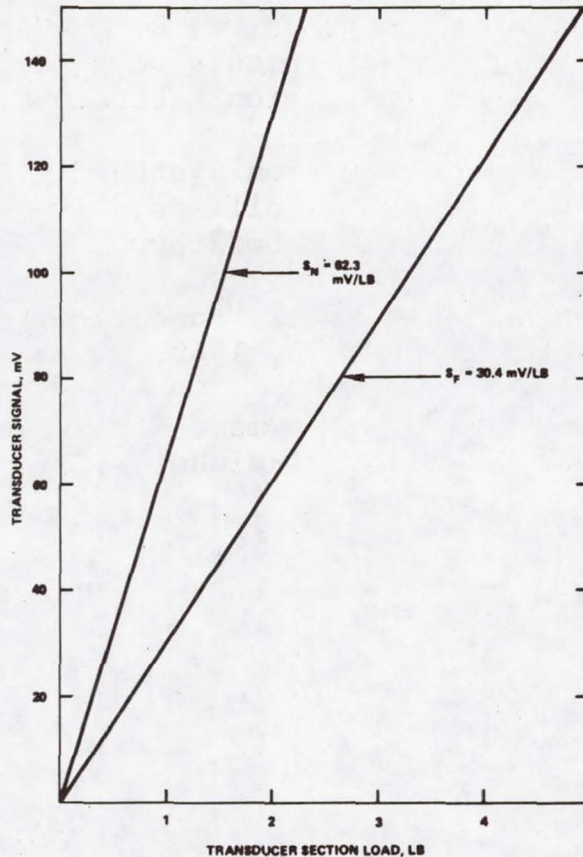


Figure 2 Transducer output as a function of load. Transducer substrate: 17-4 PH stainless steel; 3.00-V excitation; S_N = normal load; S_F = friction load.

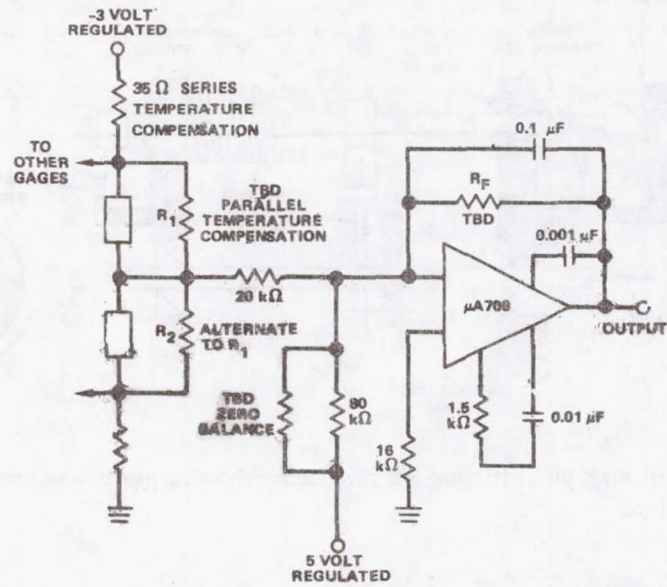


Figure 3. Schematic diagram of the half-bridge, the series-shunt resistor type temperature compensation, and the integrated-circuit amplifier of a strain-gage transducer.

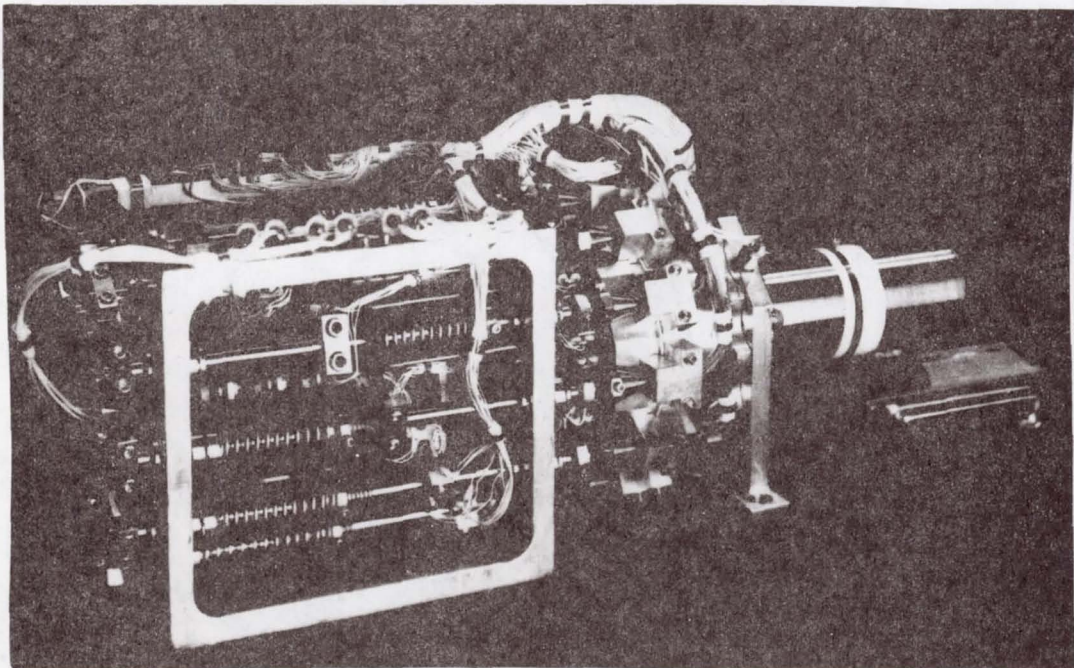


Figure 4. Friction-and-wear module.

Table 1
Stability of Strain-Gage and Amplifier Zero Levels at
Ambient Temperature.

Friction Force			Normal Force			Wear		
Initial	8 Months	Change*	Initial	8 Months	Change*	Initial	8 Months	Change*
—	—	—	0.340	0.378	0.8	2.529	2.486	-0.9
0.315	0.310	0.1	0.427	0.276	-3.0	2.506	2.496	-0.2
0.293	0.368	1.5	0.918	0.808	-2.2	2.574	2.516	-1.1
0.240	0.172	-1.3	0.442	0.385	-1.1	2.525	2.497	-0.5
0.322	0.352	0.6	0.282	0.238	-0.9	2.510	2.474	-0.7
0.240	0.188	-1.4	0.307	0.237	-1.4	2.463	2.479	0.3
0.210	0.233	0.5	0.329	0.343	0.3	2.536	2.520	-0.3
0.173	0.170	-0.06	0.439	0.419	-0.4	2.496	2.466	-0.6
0.154	-0.076	-4.6	0.503	0.400	2.0	2.515	2.471	-0.9
0.428	0.460	0.6	0.654	0.606	-1.0	2.416	2.403	-0.2
0.345	0.417	1.4	0.843	0.827	-0.3	2.484	2.422	-1.2
0.267	0.323	1.1	0.722	0.696	-0.5	—	—	—

*Percent of full scale.

7. METAL WITH A MEMORY PROVIDES USEFUL TOOL FOR SKYLAB ASTRONAUTS

by G. A. Smith

Fairchild Space & Electronics Company

SUMMARY

In 1970, Skylab planners decided to use extendible booms to convey film cassettes weighing 56.7 kg (125 lb) between the Airlock Module and the Apollo Telescope Mount. This paper describes the boom and its dispensing mechanism, and discusses problems encountered with the mechanism during the test program. These problems were mainly associated with operation in cold temperature, lubrication, and the motor/gearhead assembly. Another set of problems which arose during crew training in the MSFC water tank is also discussed.

Experience from this program leads to the conclusion that attention to detail is the cardinal rule for mechanisms designers. Such things as the correct choice of lubricant, the build up of tolerances, and the affect of differential contraction of metals can make or break a design.

INTRODUCTION

Two film transfer booms were used during six separate EVA's over the almost nine-month Skylab mission. At these times, film for five solar physics experiments was replenished and retrieved from two work stations on the Apollo Telescope Mount (ATM), and the touch of a button sent extendible, stainless steel booms carrying bulky cassettes at 0.15 m/s (6 in/s) across 9.1-m (30-ft) of space. One of the booms also performed an unscheduled task when it helped to salvage the mission by transferring foot restraints, clamps and a sunshade at the time the second protective cover was erected over the crippled spacecraft.

The booms and their dispensing mechanisms remained fixed to the shroud surrounding the Airlock Module (AM) throughout the mission; one boom's line of travel being between the AM and the Center Work Station (CWS), and the other between the AM and the Sun Work Station (SWS). Figure 1 diagrammatically shows the relative positions of the booms and the ATM.

BOOM DESIGN SPECIFICATION

The specification for the film transfer boom (which included the dispensing mechanism) was detailed and rigorous. Some of the general requirements are shown in Table 1 below:

TABLE 1
FILM TRANSFER BOOM SPECIFICATION

- The total weight of the boom and its dispensing mechanism shall be no greater than 39 kg (185.9 lb).
- The overall size of the boom and mechanism with the boom stowed, shall be no greater than 38 cm x 38 cm x 51 cm (14.9 in x 14.9 in x 20 in).
- The length between the base of the mechanism housing and the tip of the fully extended boom shall be 8.3 m (27.2 ft).
- The mechanism shall be motor driven, from a 26 ± 4 Vdc supply. The maximum power available will be 210 watts at 30 Vdc in a -29°C environment.
- The speed of boom extension and retraction shall not exceed 22.9 cm (8.9 in) per second at 30 Vdc and at a temperature of 71°C , and shall not be less than 7.62 cm (2.9 in) per second at 22 Vdc at a temperature of -29°C .
- At full boom deployment, a limit switch shall deactivate the motor. Similarly, a limit switch shall deactivate the motor at full retraction of the boom.
- The fully extended boom shall not deflect more than seven inches due to the temperature differential created by solar radiation on one side of the boom and shade on the other.
- The fully extended boom shall withstand a bending moment of 238 N -m (2100 in-lb).

In addition, the specification included the following unique requirements:

- It was required that the boom should be easily grasped by a gloved astronaut. (A 5.08-cm (2-in) diameter was regarded as a maximum size to grip.) This requirement also meant that no exposed sharp edges were allowed on the boom for fear of cutting a glove.
- The maximum temperature of the boom due to solar radiation was not to exceed 121°C . This limit was imposed to prevent damaging the astronaut's clothing.

- A 0.99 probability of completing a service life of no less than 200 cycles under any combination of specified environment was required of the boom and its dispensing mechanism.
- In the event of a motor failure, a back-up operational mode was required such that the boom could be extended and retracted by a hand crank. The torque required to operate the crank was to be no greater than 22.6 N-m (200 lb-in.).
- It was a requirement that a pressure-suited astronaut should be able to remove a boom unit from its location outside the Airlock Module and replace it with the spare. This was to be a one-handed operation.

DESIGN DESCRIPTION

Boom

Here was an obvious application for a tubular extendible element (TEE), the principle of which is to heat-treat a thin strip of metal such that it takes a tubular form when it is unrestrained. The technique of storing this type of tube is well known. It is simply opened out flat and rolled round a spool inside a dispensing mechanism.

It quickly became clear that the 238 N-m (2100 in-lb) bending moment requirement was a critical design parameter. Trade-off studies showed that to retract a steel boom thicker than 0.02 cm (0.008 inch) and wrap it flat around a spool required more power than was available, and the size of the dispensing mechanism would exceed the specified envelope. But, if 0.02-cm stainless steel strip was used, a conventional boom with a circular cross section would have too large a diameter for the astronaut to grip.

It was with these requirements in mind that the final boom configuration was designed as shown in Figure 2. This twin-lobe boom with its 5.08-cm (2-in) diameter lobes can be gripped by the astronaut, and the required strength is obtained by nesting two 0.02-cm elements one inside the other. The edges of the outer element that run the length of the boom were rolled inward slightly and dressed with an abrasive to eliminate the risk of cutting or snagging the beta cloth of the astronaut's glove.

Thermal considerations dictated a polished outer surface of the boom to achieve a low emittance (0.13) so that the temperature should be no higher than 121°C, and a black coating on the inside of the boom to achieve a high emittance (0.86) to keep the thermal gradient as low as possible across the boom and therefore to reduce thermal bending to a minimum.

DISPENSING MECHANISM

Mechanism Design

Figure 3 shows the envelope dimensions of the film transfer boom located in its funnel-shaped adapter that was permanently attached to the airlock shroud. A simplified internal view of the mechanism is shown in Figure 4.

A dc motor provides, through gearing, the necessary torques to extend and retract the boom. In the extend mode, each boom element is unreeled from a separate spool by an identical pinch drive system, which consists of an RTV-coated drive roller and a hard anodized, aluminum backup roller. Each boom element leaves its spool flat and passes round a drive roller where it is pinched between the drive and backup rollers. Both the spool and drive roller are driven, but the backup roller free-wheels.

When the boom is fully retracted, the combined diameter of an element and spool is greater than the diameter of the drive roller. Therefore, at the beginning of boom deployment, the drive roller has a tendency to turn faster than the spool. To prevent this and preclude the drive roller from slipping on the element, the spool is driven through a slip clutch. By this means, the high initial torque placed on the spool by tension in the element overrides the torque setting of the slip clutch, and the angular velocity of the spool approaches that of the drive roller. The slip clutch material, which bears against the stainless steel of the spool drive gear, is a teflon/molybdenum/lead composite which is stable over a wide temperature range.

When the boom elements leave the pinch drive rollers, they immediately start to assume their tubular shape. During the transition phase, when the boom elements are going from the flat to the formed twin-lobe configuration, they are very susceptible to buckling if subjected to a bending load. In this critical phase, they are supported by a fiberglass "shoe" molded to the natural shape of the element during its transition stage. The two elements extend, one on each side of the tapered shoe, and by the time they exit from the mechanism through a delrin collar, they have nested one within the other and are approximately 60% towards the final formed dimensions of the boom. The delrin collar gives external restraint and, together with the shoe, provides adequate support at the root of the fully deployed boom to withstand the 238 N-m (2100 in-lb) bending moment requirement.

To retract the boom, the polarity of the motor is reversed. During boom retraction, the spools are driven through one-way sprague clutches which free-wheel during boom deployment. To ensure a tight wrap on the spool, tension is maintained in the element by a technique similar to that used during boom deployment, only this time the slip clutch is on the drive roller.

The dispensing mechanism is normally driven by the motor. However, the motor can be isolated by operating a lever on the side of the mechanism housing which disengages a crown-toothed clutch in the mechanism's gearbox. The boom can then be extended or retracted using a manual crank handle. This was a contingency mode for operating the boom in case of a motor failure.

Three film transfer booms were located on the Skylab airlock shroud. Two were operated throughout the mission and the third was a spare that was not used. Because the two working units were exactly positioned to line up with their respective work stations, it was necessary to be able to replace either unit in the event of a failure. The specification required this to be a one-handed operation. To accomplish this, a latching handle was provided as shown in Figure 4. The handle can be gripped by one hand and a delrin trigger squeezed against a spring load, thereby lifting long aluminum links attached to the trigger and running down through the handle supports and to the base of the mechanism housing. The lift was transmitted to a horizontal load through a bell-crank, and the horizontal load, which pulled two scissor links whose four extremities were attached to pawls that traveled along slider blocks. The four pawls engaged in cutouts in the adapter funnel that was permanently attached to the shroud. The trigger was locked during launch to prevent the pawls from being dislodged due to vibration.

Motor/Gearhead Design

Power to extend and retract the boom was supplied by a dc motor. To meet the deployment and retraction speeds of the boom, and to produce sufficient torque to wind the boom into the mechanism (the boom has a natural tendency to self-deploy, and therefore the torque and power are higher in the retract mode), it was determined that the motor should deliver a minimum of 8.15 N-m (72 in-lbs.) of torque over a voltage range of 22 to 30 Vdc. In this voltage range, the speed of the motor/gearhead output shaft was required to be between 17,000 and 31,000 rad/s (45 and 82 rpm) for any temperature between -29 and 71°C. To achieve low output speeds, the motor was geared down through a four-pass planetary gearhead.

The motor/gearhead characteristics shown in Figure 5 indicate how well the assembly met the requirements at room and high temperature. However, at -29°C the motor did not supply quite enough torque at 17,000 rad/s and 22 Vdc. This affected the speed of boom deployment and retraction, about which more will be said later.

Various studies have been performed on motor brush materials suitable for a space environment, and with some success. But it has been found that these same brushes will not perform well in an earth environment because they are susceptible to oxidation and are hygroscopic. Therefore, dc motors with space-rated brushes fail repeatedly during testing in an earth atmosphere.

Unfortunately, brushes that are normally used for ground applications, lose moisture in space and become abrasive. They then score the armature, and curtail the motor's operating life in a space environment. In the case of Skylab, the motor was required to operate intermittently in space over a period of several months. It was decided therefore, to install space-rated brushes and find a way around the ground testing problem. This was done by sealing the motor in a can. The can was evacuated and back-filled with helium in order that a leak test could be performed after final assembly. The drive from the motor to the output shaft was effected through a nutating metal bellows, as shown in Figure 6.

DESIGN PROBLEMS AND THEIR SOLUTIONS

When first assembled, the qualification unit required the motor to deliver almost 22.6 N-m (200 in-lb) of torque to extend the boom at -29°C . It can be seen from the speed/torque characteristics that the motor/gearhead speed at 22.6 N-m is extremely low. Therefore, the boom deployment rate was lower than required, and the corresponding current of 10 amps at 22 Vdc exceeded the specified power budget. Furthermore, the output shaft and shaft bearings were not designed for this high load and both bearing and shaft failures occurred.

The problem was tackled in two ways; to reduce the loads in the mechanism at cold temperature, and to increase the torque-carrying capability of the motor/gearhead.

In the case of the mechanism, there were three main causes of high loading at -29°C .

- a. The delrin collar contracted round the boom at the point of exit from the mechanism housing. This forced the boom elements hard against the shoe and resulted in excessive drag.
- b. Considerable stiction forces became apparent in the gearbox at low temperatures. Gear-carrying stainless-steel shafts were supported in side plates which were separated by aluminum stand-offs, and the differential contraction of the aluminum and stainless steel resulted in shaft seizure.
- c. Increased drag of the slip clutches on the spools and drive roller.

Problems (a) and (b) were readily overcome by increasing the clearance of the delrin collar, and increasing the end-play in the gearbox shafts. Several environmental tests were performed to arrive at the optimum dimensions so that operation at 71°C would not be impaired.

Problem (c) was not so easy to resolve. Belleville washers were used behind the slip clutches to set the clutch torque values, and it was found that the spring force for any given deflection increased significantly at low temperatures. Therefore, a clutch set at room temperature would produce excessive drag at -29°C . To overcome this, the belleville washers were replaced by conical washers made from bimetallic strip, which have a more constant spring characteristic over the temperature range of interest.

The combination of these three fixes reduced the drive torque in the mechanism to 17.5 N-m at -29°C .

With regard to increasing the torque-carrying capability of the motor/gearhead, it was considered impractical to increase the size of the gearhead, for weight and cost reasons, so a closer look was taken at the mechanical design of the gearhead assembly. At high torque, the bearings on the output shaft were marginal, but more seriously, the dry film lubricant used was overstressed and broke down under load. Bearings packed with Braycote 803 grease were substituted. This grease has good outgassing characteristics and a higher load-carrying capacity than the dry film lubricant. One of its main disadvantages, however, is that it becomes too viscous below -29°C for most practical purposes.

With the change in lubricant, a problem in the output shaft itself became apparent. High loads at cold temperature snapped the shaft at its root. A step, designed to position the shaft against a bearing, had been machined at the root of the shaft. A classic stress raiser! The stainless-steel material was optimum, and an increase in shaft diameter would have necessitated a significant redesign. As an alternative solution, the shaft was machined to remove the step and leave as large a radius as possible. The step was replaced by a fitted washer.

As a further precaution, a solid-state circuit breaker was installed in the mechanism which limited the steady-state motor current to 12 amps. The breaker was designed to pass current spikes as high as 25 amps for up to 150 milli-seconds, but would open circuit when more than 12 amps were applied for longer periods. In this way, the torque on the motor output shaft, which is proportional to current, was limited to a safe level. Higher torques, which resulted from transient start-up currents, would not be transferred to the shaft because of the inherent spring-constant of the motor gearhead.

A combination of all of the above modifications produced an entirely reliable mechanism. The start-up torque in the mechanism at -29°C was reduced by approximately 25% and the motor torque-carrying capability was improved. But, more important, if for any reason a high start-up torque was called for, the motor would be shut down before a catastrophic failure occurred.

Other problems encountered during qualification testing centered around the pawls that latched the film transfer boom unit to its funnel-shaped adapter.

During Y-axis random vibration, the pawls intermittently unlatched. The causes of this anomaly were traced to two factors:

- a. Flexibility of the linkage connecting the latch handle to the pawls.
- b. An adverse tolerance build-up in the latching design.

The linkage was not modified, but a positive lock was designed into the latch handle to prevent the trigger from moving during vibration. In addition, a minimum acceptable engagement of each pawl in the adapter was established, and verified in a vibration retest. This minimum engagement was assured in flight units by following a detailed rigging procedure.

Another problem with the latching also occurred as an outcome of the vibration test. The pawls slide along stainless steel guides as they latch and unlatch, and originally, the guides were dry film lubricated. After vibration, the qualification unit was subjected to a 10-day temperature-humidity test. At the conclusion of the test, the guides were found to be corroded, and the pawls and guides had to be forced apart. It was determined that the guides had suffered surface damage during the 34 GRMS qualification level vibration and corrosion had set in over the damaged areas. Although a very effective lubricant, the process for applying the dry film changes the surface characteristics of steel and destroys its "stainless" qualities. Therefore, if the lubricant is removed, corrosion is likely. This was overcome by making new guides and coating them with 803 Braycote grease.

CREW TRAINING

Crew Extravehicular Activities (EVA's) were practiced in the water tank at the Marshall Space Flight Center, Huntsville. This alone presented a new set of problems, for now space hardware had to be adapted to an underwater environment. Figure 7 shows crew training in progress.

Because the training units had to be identical in external configuration and performance to the flight units, a simplistic approach was taken, namely to remove and/or replace all electrical components and to eliminate potential corrosion mechanisms wherever possible.

In the case of the electrical components, both extend and retract limit switches were permanently removed, and the limits of boom extension and retraction were controlled by hand valves. The electric dc motor was replaced by an air motor. An exhaust manifold was designed around the motor;

and air supply, and return and exhaust lines were routed from an external source.

To counteract the onset of corrosion as much as possible, aluminum parts were hard anodized (on the flight units many aluminum components were iridized to conduct electricity for electro-magnetic considerations). Stainless steel components were passivated. In addition, the one-way sprague clutches on the spools and drive rollers were packed with grease.

Problems occurred immediately when the mechanisms were first tested in a water tank. The RTV-coated drive rollers skidded on the boom elements and boom deployment was erratic. It was found that oil and grease were migrating to the elements from the air supply line, exhaust manifold, and sprague clutches.

Every last drop of oil and grease was removed from the boom and mechanism and tests were performed on an air motor using dry, oil-free air. But the motor, which was a standard off-the-shelf unit, relied on oil in the air supply to lubricate its bearings and the bearing life was severely curtailed as a result. The motor exhaust manifold was sealed and immediately the increased back pressure in the motor reduced efficiency. It was eventually decided to live with some leakage from the motor exhaust, but to limit the oil in the air supply and have spare motors on hand. This together with the following modifications enabled an effective training program to be fulfilled:

- The diameter of the back-up roller was increased and another back-up roller located next to it. Deploying the boom elements was like squeezing clothes through an old-fashioned wringer.
- To compensate for the increased load on the back-up roller, the hard-anodized hollow aluminum roller used in flight units was replaced by a solid shaft made of stainless steel.
- A silastic stripe was painted along the center of each boom element to increase the element's thickness at that point. This compensated for the fact that the boom elements tended to dip in the middle and assume their formed shape even when passing between the drive and back-up rollers.
- One last modification was to provide the drive rollers with "snow-treads". Grooves 3 mm (0.118 in.) wide by 1.5 mm (0.059 in.) deep were ground in the RTV, parallel to the roller axis and spaced 19 mm (0.74803 in.) apart round the circumference.

CONCLUDING REMARKS

It can be concluded that attention to detail is the cardinal rule for mechanisms designers. The boom mechanism design concept was sound from the outset and it was found to be adaptable to such opposite environments as space and water. But it was the seemingly small things that proved to be important--such things as the correct choice of lubricant, the build up of tolerances, and the effect of differential contraction of metals. The design of mechanisms is not for those who lack an eye for detail.

ACKNOWLEDGMENTS

The author wishes to thank the Fairchild team, and in particular James M. Talcott, for their contributions to a successful program. Thanks are also due to MDAC-E for their cooperation in this endeavor.

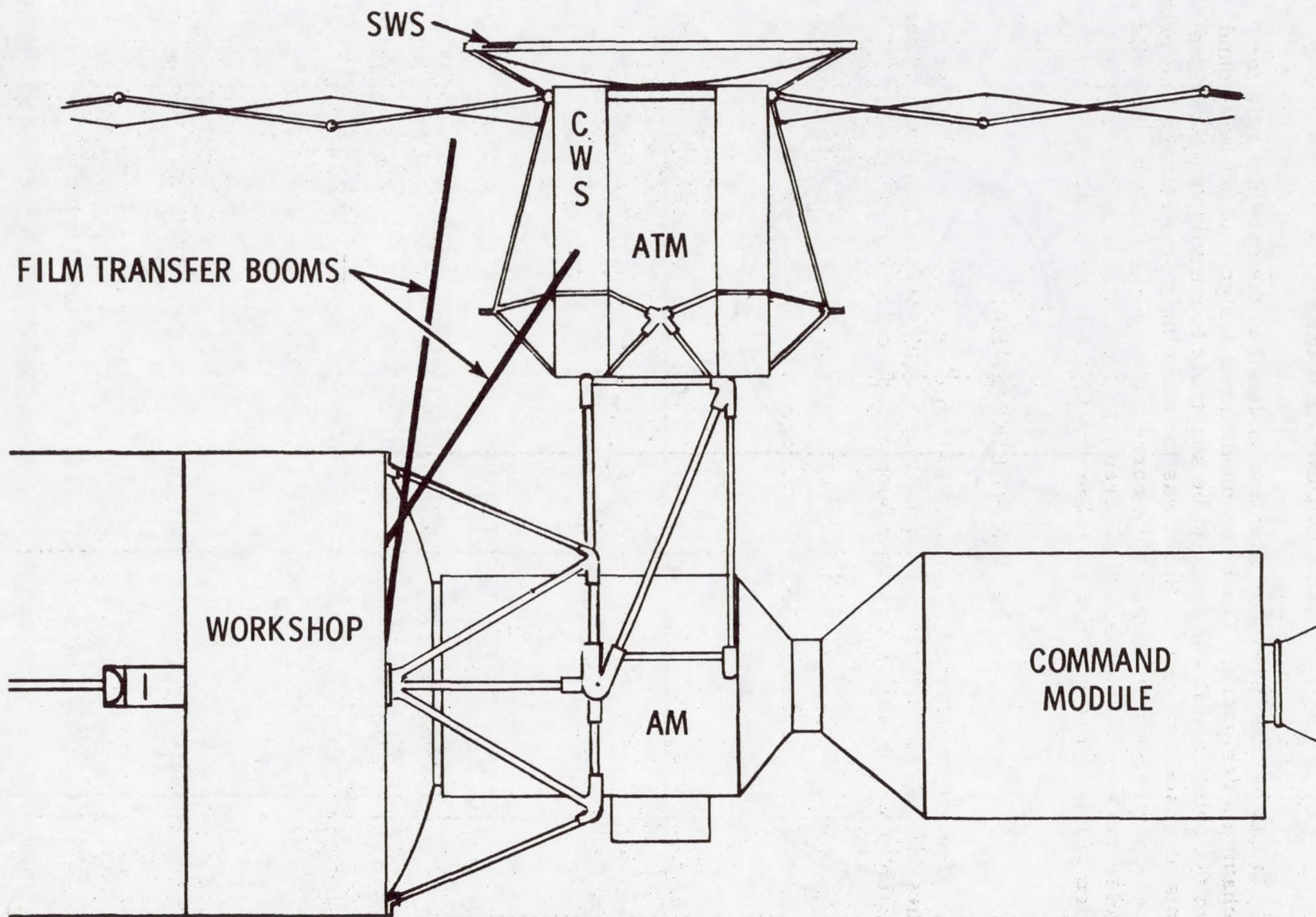
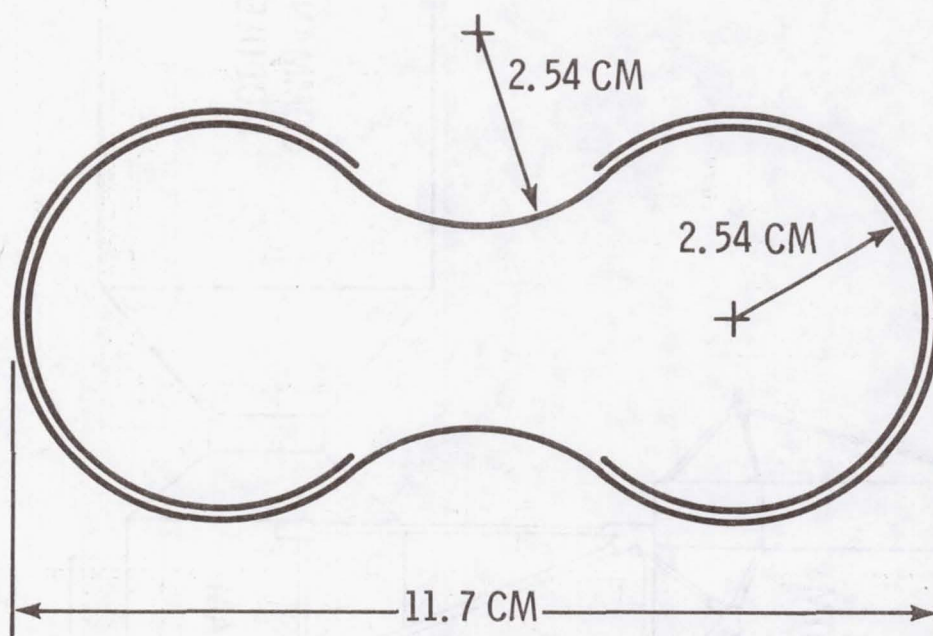


Figure 1. Skylab Orbiting Configuration with Film Transfer Booms Partly Extended



MATERIAL DESCRIPTION

STAINLESS STEEL CARPENTER CUSTOM 455
26.7 CM WIDE X .02 CM THICK

Figure 2. ATM Film Transfer Boom Configuration

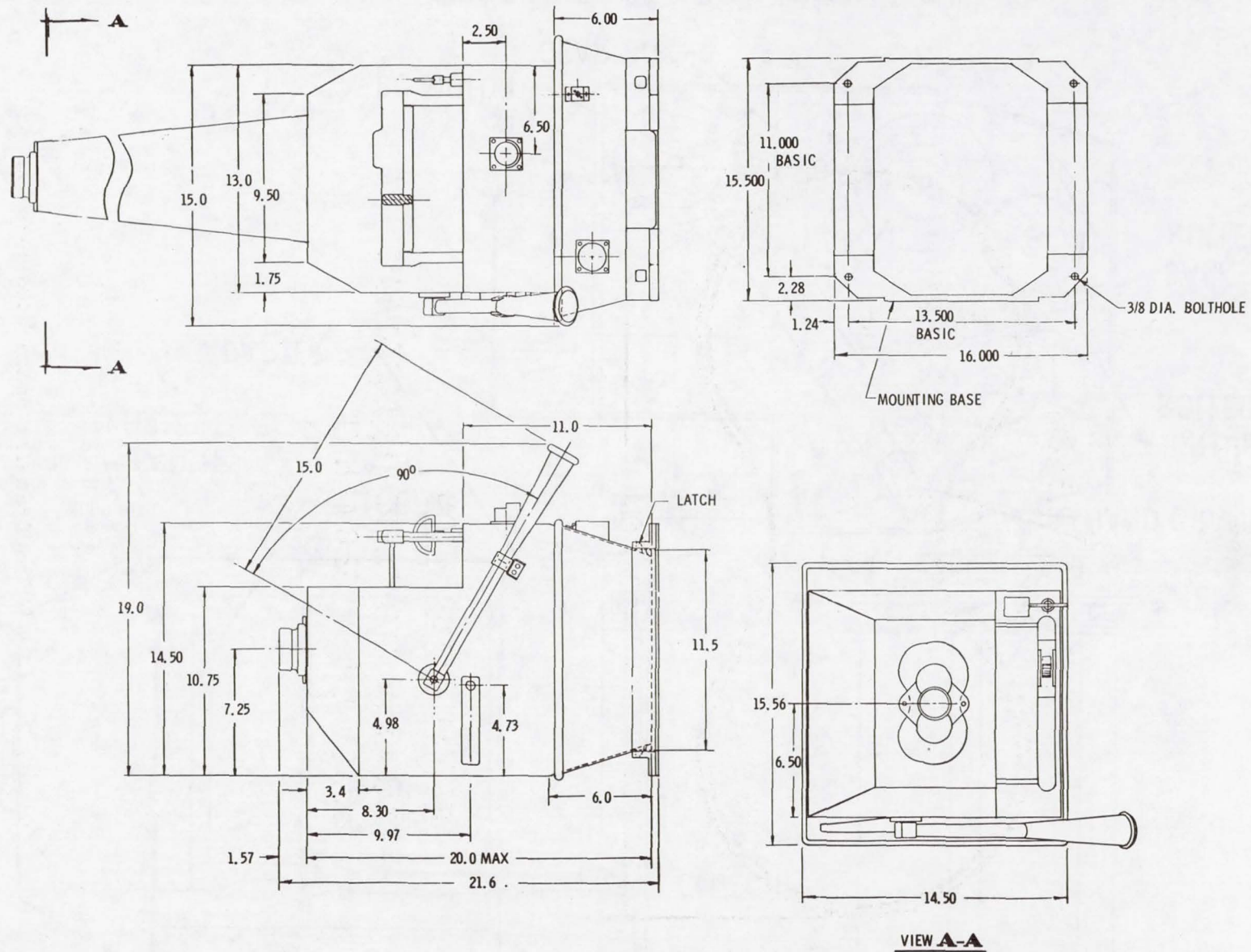


Figure 3. ATM Film Transfer Boom Envelope Dimensions

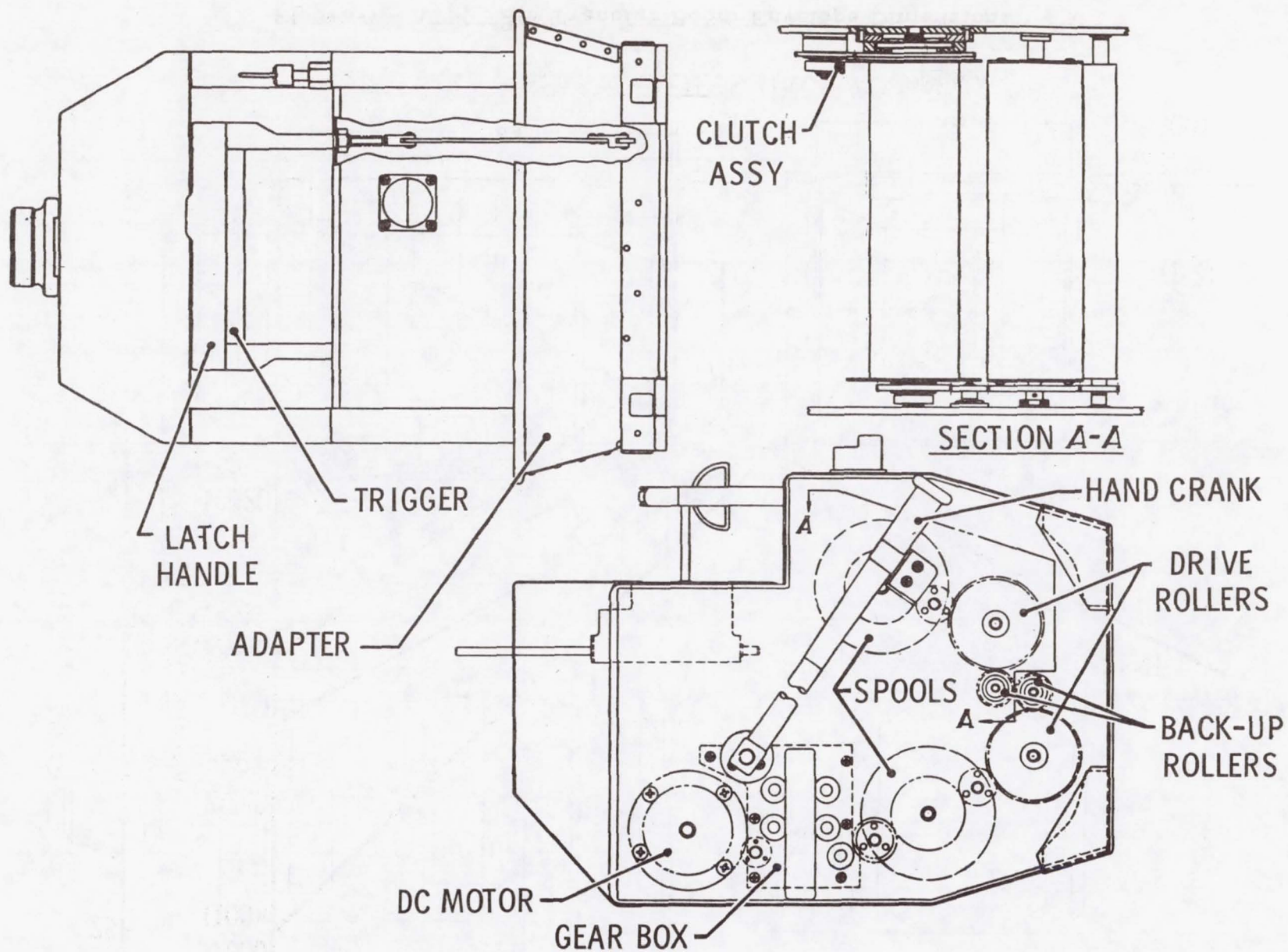


Figure 4. ATM Film Transfer Boom Internal Layout

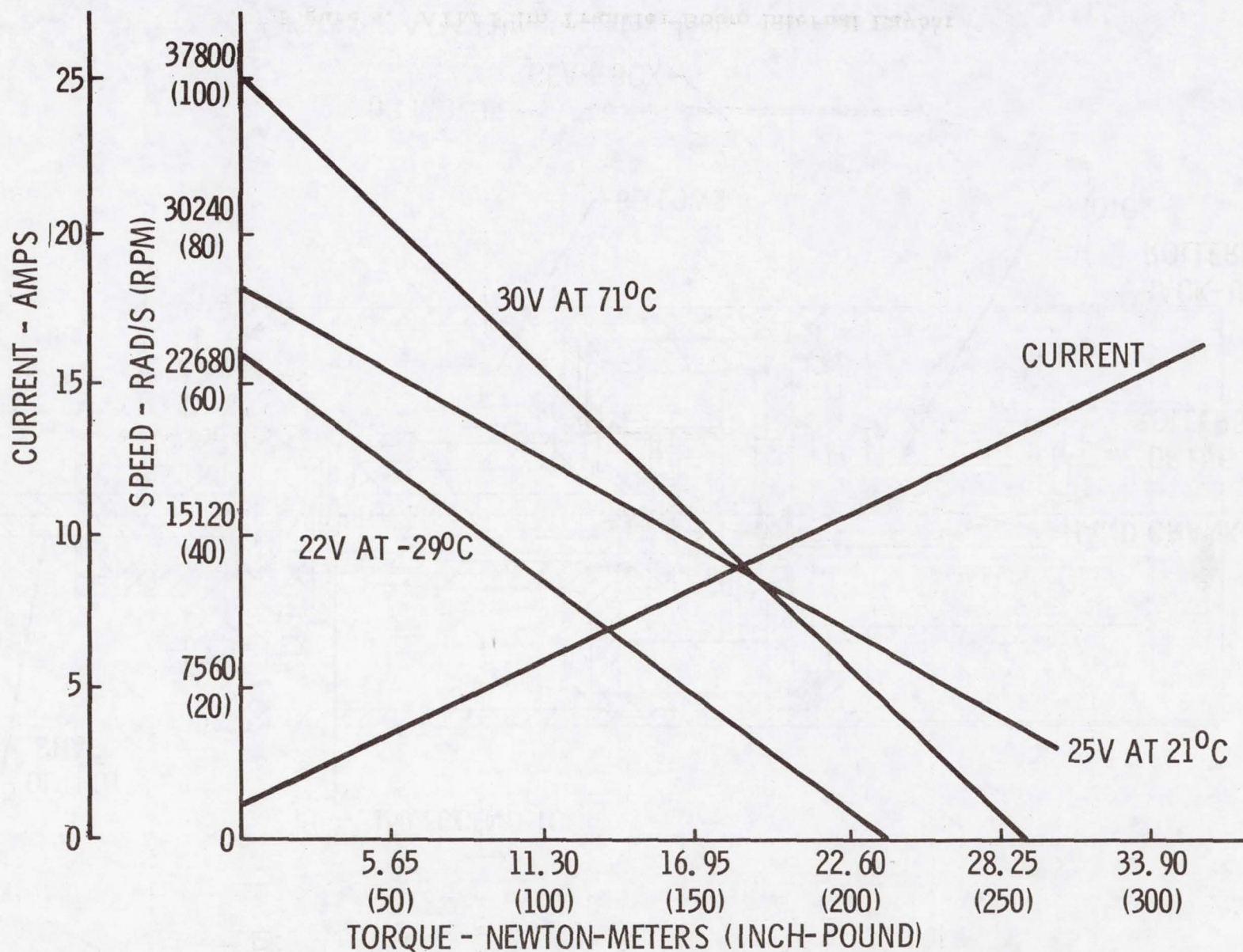


Figure 5. ATM Film Transfer Boom Motor/Gearhead Characteristics

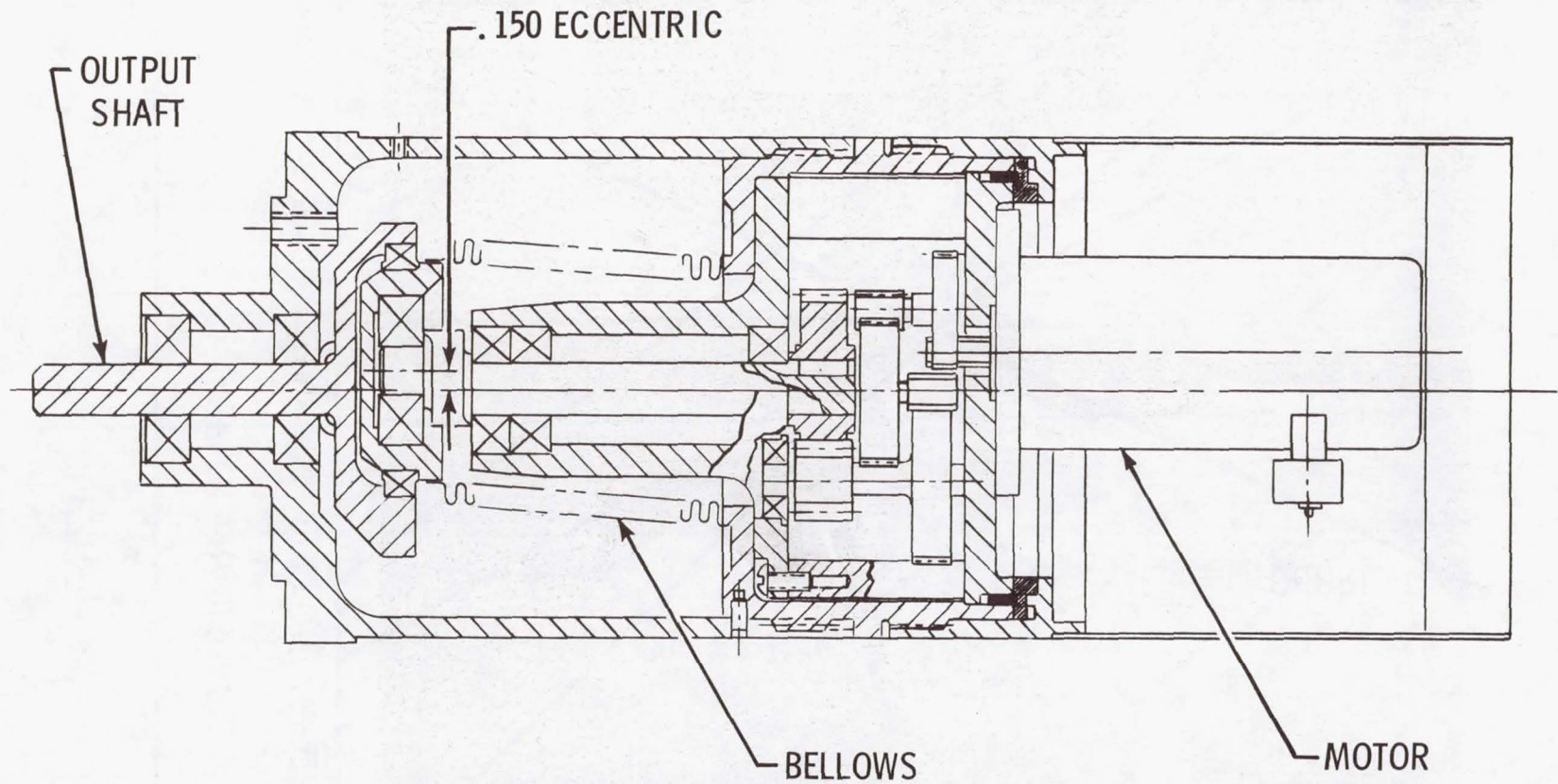


Figure 6. ATM Film Transfer Boom Motor Assembly

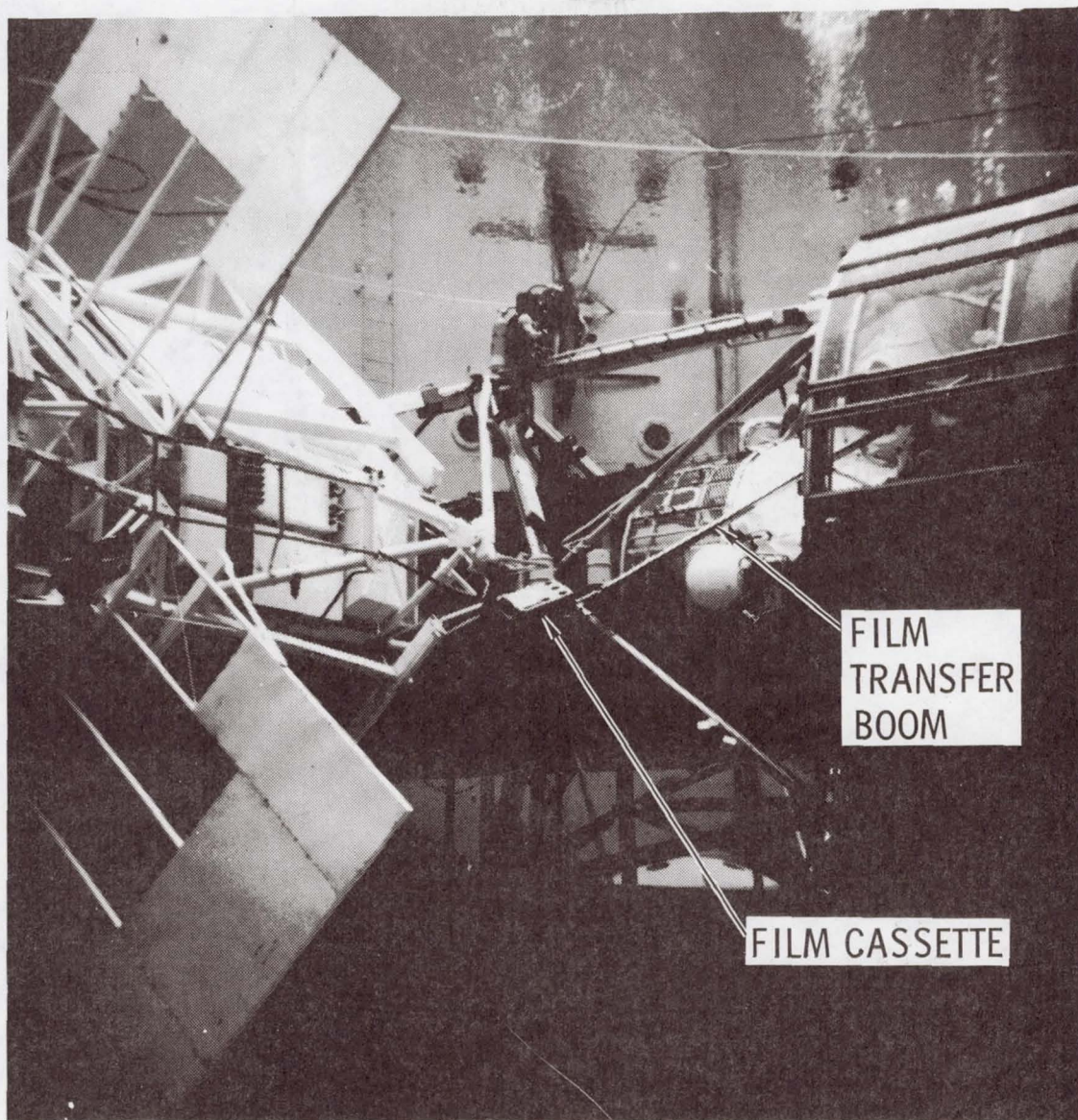


Figure 7. ATM Film Transfer Boom Underwater Testing

1945

1946

1947

1948

1949

1950

1951

1952

8. THE SKYLAB PARASOL

By Jack A. Kinzler*

SUMMARY

A need to provide an alternate thermal protection system for the Skylab space station cluster became apparent shortly after launch when severe damage occurred to the Orbital Workshop as it passed through the period of maximum dynamic pressure. Data indicated that the combination micrometeoroid and thermal shield on the sun-facing side of the vehicle had been destroyed. NASA management urgently requested all Centers and aerospace contractors to come forward with proposals for restoring Skylab to a habitable and operational mode as soon as possible. This paper discusses the simultaneous design, fabrication, and test of the Skylab Parasol System which was completed in 6 days of around-the-clock effort after which it was successfully deployed and served its purpose on the Skylab II Mission.

INTRODUCTION

The urgency of the effort necessary to produce a substitute thermal shield in a few days was based on NASA's concern for both foodstuffs and scientific film stored aboard the spacecraft where cabin temperatures approaching 316 degrees Kelvin (120 degrees Fahrenheit) were rapidly exceeding mission limitations. Consequently, the Skylab II crew launch was deferred approximately 10 days to permit the agency to consider various repair options and select the best candidate.

Numerous thermal shield concepts were advanced, some requiring extravehicular activity deployment, while others were deployable from inside the Orbital Workshop. The Skylab Parasol design was selected as the primary sunshade device based on simplicity of design, ability to fabricate quickly, and early demonstration of a working prototype which featured semiautomatic deployment from within the workshop under shirt-sleeve environment conditions.

The outstanding contributions to the parasol design, fabrication, and test given by Johnson Space Center directors, engineers, and technicians are gratefully acknowledged. Their combined efforts made the Skylab Parasol possible.

DESIGN REQUIREMENTS

The Skylab Parasol was designed to meet the following requirements: (1) provide a 6.7- by 7.3-meter (22- by 24-feet) canopy over the Orbital Workshop, (2) deploy from cabin in shirt-sleeve environment, (3) have 177.9-newton

*NASA Lyndon B. Johnson Space Center, Houston, Texas

(40-pound) push limit for ease of crew operation, (4) have jettison capability, (5) have container size limit of 30 by 30 by 152 centimeters (12 by 12 by 60 inches), (6) have maximum weight limit of 45 kilograms (100 pounds), (7) use readily available, proven materials, (8) simplify fabrication, and (9) use existing flight qualified hardware wherever possible.

SYSTEM DESCRIPTION

The design philosophy is best demonstrated by examining the overall mechanism and some of its detail parts. Figure 1 shows the packed parasol. An existing T027 photometer experiment canister was used as a container. This choice was based on appropriate size and the fact that an interface with the solar scientific airlock existed in the proximity of the unprotected portion of the Orbital Workshop. A modified inboard backplate utilized an existing seal design which permitted use of extension rods of the same basic design as those qualified for T027. The existing photometer ejection rod was also included to provide the capability to jettison. A teflon liner and a set of retractable exit flaps were added to the canister interior to protect the canopy material during extension. Major components of the parasol, other than the modified canister, were a 6.7- by 7.3-meter (22- by 24-foot) aluminized mylar/nylon laminate canopy that was essentially opaque to solar thermal energy, a canopy mast; a mast hub with four sets of deployment springs; four telescoping deployment tubes; seven extension rods; and the T027 canister support tripod. The combined stowage weight of the parasol, extension rods, and the container was 35.2 kilograms (77.5 pounds).

DEPLOYMENT

The following deployment sequence was used. Each step is referenced to steps of Figure 2.

1. Upon transfer from the Command Module to the Orbital Workshop, the parasol canister was attached to the scientific airlock port on the sun-facing side of the Orbital Workshop. Step A.
2. After appropriate venting, the scientific airlock port door was opened. Extension rods and a push knob were threaded on the mast in sequence, one at a time, as the parasol was extended gradually in the folded condition to a distance of 4.9 meters (16 feet). Release knobs attached to the tip ends (stowed inboard) of the telescoping tubes retained the telescoping tube assembly until full extension and latching had occurred. Step B.
3. At this point the crew released the telescoping tube array to permit further deployment out of the canister. A distance-calibrated final extension rod was installed, after which the canopy and telescoping tube deployment array were pushed to a position 6.4 meters (21 feet) beyond the outer surface of the Orbital Workshop where automatic deployment began via the deployment springs. Step C.

4. After completion of the automatic deployment sequence, the crew verified the deployment condition via an observer in the Command Module. Step D.

5. Upon full deployment, the crew returned the parasol to a position 20.3 centimeters (8 inches) above the Orbital Workshop's outer skin by reversing the extension rod deployment procedure. Using the rod clamp and orientation knob, the deployed parasol was repositioned by the crew to obtain optimum thermal protection and locked in place for the balance of the mission. Step E.

The actual deployment was deliberately done very carefully and slowly and took about 2 hours. Consequently, the parasol was extended out but not deployed while on the dark side of the orbit. The resulting cold condition prevented the immediate and complete deployment or flattening of the parasol fabric. However, as the spacecraft returned to the sun side, the material warmed up sufficiently to permit proper flattening out. Oscillation of the extension rods by the crew aided the final positioning process.

The Orbital Workshop external skin temperature of 364 degrees Kelvin (195 degrees Fahrenheit) dropped to 308 degrees Kelvin (95 degrees Fahrenheit) within 12 hours after parasol deployment. The internal cabin temperature of 316 degrees Kelvin (120 degrees Fahrenheit) dropped below 311 degrees Kelvin (100 degrees Fahrenheit) within a day and stabilized after 6 days at 297 degrees Kelvin (75 degrees Fahrenheit).

DESIGN DETAILS

Telescoping Tubes

The initial parasol demonstration model utilized easily obtainable, tapered, telescoping, friction-lock, fiberglass, fishing rods as a medium to deploy and support the canopy. Although considered a possible candidate for the flight article, a more substantial equivalent was produced by using stock readily available, 6061-T6 aluminum tubing, modified to produce the tube joint design depicted in Figure 3.

In order to compensate for the excess clearance between outside diameter and inside diameter of the standard 0.89-millimeter (0.035-inch) wall aluminum tubing series, a pair of convolutions was rolled into each tube's inside diameter which reduced the nominal stock clearance from 1.27 millimeters to 0.25 millimeter (0.050 to 0.010 inch) for a close sliding fit. This modification also provided a positive stop surface which interfaced at deployment with a similar convolution on the outside diameter of the mating tube.

An integral stop tang on the tubing is another major feature of this design. A pair of precision machined U-shaped slots was cut 180 degrees apart near the outboard end of each telescoping tube section, after which the resulting tangs were bent inward to form leaf-spring-like detents. It was necessary to machine a perpendicular surface on the previously rolled tube convolution to complete the positive stop mechanism. Minimal material thickness and uniformity of fit required special jigs for fabricating and verifying the operation of

the latch mechanism. Using mandrels, a conventional tube beading machine and a modified hand-flaring tool with appropriately radiused rollers, Johnson Space Center shop technicians perfected this detail as actual manufacturing was underway. All exterior tube surfaces were anodized and all interior surfaces were alodined to minimize galling and improve corrosion resistance.

Masthead Deployment Mechanism

The masthead deployment mechanism consists of a two-piece masthead and four sets of matched torsion springs (Fig. 4) mounted in a manner to guide as well as rotate the telescoping tube arrays through a 90-degree arc during canopy deployment. Due to the necessary offset location of the deployed canopy, versus the fixed location of the scientific airlock port in the Orbital Workshop, the deployment hub design required an asymmetric layout of the torsion spring sockets in conjunction with offset rigging of the canopy to achieve the desired results.

The initial demonstration masthead deployment system utilized four conventional, closely wound, extension springs with one end nested in each of the base telescoping tubes and the other clamped in counter-bores in the original hub. Although this design worked satisfactorily as a combination pivot and rotating force, it was superseded by the twin torsion type springs which was a stronger spring with better directional control. A pair of torsion springs made of 3.175-millimeter (1/8-inch) diameter music wire provided sufficient torque, 33.9 newton-meters (300 inch-pounds), to rotate the extended telescoping tube and canopy assembly through 90 degrees of rotation under zero-g conditions. Because the parasol components would be weightless when deployed in space, very low torsional force was considered necessary, while excessive torsional force was considered dangerous in that too rapid a deployment sequence might endanger other elements of the parasol system installation.

The two-piece masthead design featured a compact arrangement for terminating all eight springs in a small diameter hub, yet provided sufficient spacing width for stability. A combination of radiused grooves in the masthead collar, terminating in the opposed 90-degree blind drilled holes, permitted the torsion springs to overlap one another without affecting their function. A similarly designed split plug bushing was machined to fit the inside diameter of the telescoping tube to form a positive anchor for the other end of the torsion springs.

Canopy

The expediency of the parasol development effort dictated the selection of a fabric available at Johnson Space Center. The material chosen was a laminate of orange, 0.063-millimeter (0.0025-inch), rip-stop nylon bonded to 0.013-millimeter (0.0005-inch), aluminized Mylar (Fig. 5). Fabrication consisted of sewing adjacent 91.44-centimeter (36-inch) wide panels together, after which a hem around the periphery was reinforced with 2.54-centimeter (1-inch) nylon tape. A polybenzimidazole (PBI) line was sewn into the hem and provided a means of attaching the canopy in an offset manner to the ends of the telescoping deployment tubes.

The canopy was installed on the sun-facing side of the tubular deployment mechanism with the nylon side toward the sun. The basic nylon/Mylar material has an absorptivity/emissivity ratio (α/ϵ) of 0.47 and the vapor-deposited aluminized side an emissivity (ϵ) of 0.04.

DEVELOPMENT AND ACCEPTANCE TESTING

Determination of the type and scope of development and acceptance testing necessary to qualify the parasol for flight evolved quickly as the design details became known to members of the Johnson Space Center's test evaluation team. A command post was established on the floor of Johnson Space Center's central fabrication shop where all design, fabrication, and test requirements were coordinated around the clock over the 6-day period. This expedited arrangement resulted in completion of a data package containing a full drawing set, written assembly and test procedures, along with fully documented quality control coverage. The test program that evolved was aimed at providing sufficient tests to demonstrate the flight readiness of the parasol assembly. Test time was extremely limited and contingent upon hardware availability. Selected examples of a few of the materials, subsystems, and assembly verification tests that were performed are described as follows.

Telescoping Joint Tensile Tests

The objective of this test was to determine the tensile strength of the smallest diameter telescoping tube-joint of the telescoping tube assembly. An Instron tensile test device was used. The test specimen was a prototype joint fabricated from 9.53-millimeter and 12.7-millimeter (3/8-inch and 1/2-inch) diameter 6061-T6 aluminum tubing. Failure occurred at a load of 213.19 kilograms (470 pounds). At that point the inner tube pulled past the first boss of the telescoping joint. A load of 140.61 kilograms (310 pounds) was required to pull past the second boss and separate the tubing sections. The test indicated that the tube sections could not be pulled apart by a crew-generated force.

Deployment Development Tests

A series of successive deployment tests was performed in the high bay area of Johnson Space Center's central shops. The objective of this series was to evaluate the deployment characteristics of the spring-hub assembly, the telescoping tube array, the fabric packing configuration, teflon liner performance, and general packing density problems, if any. The setup consisted of an overhead crane, a suspended platform to which the parasol canister was attached, and a protected floor area to receive the deployed test article. To give the astronaut crew some firsthand experience, it was arranged for backup crewman, Bill Lenoir, to perform the deployment procedure while Jack Lousma and Owen Garriott acted as observers. Figure 6A shows deployment from the packed canister using extension rods under one-g conditions. The first test demonstrated the adequacy of the overall concept while causing some doubt about telescopic tube

latch-up. After deployment, the individual telescope tube lock tabs were inspected carefully and found to vary slightly in degree of built-in spring detent. The controlled adjustment of the lock tabs via appropriate tooling fixtures would alleviate the variance caused by the previously used hand-bending technique. The follow-on deployment demonstration tests provided additional confidence in the system's operation. Because of gravitational effects on the unequal mass distribution of weight within the canister package and resulting irregular deployment pattern, one test featured an alternate deployment where the parasol was not packed in the canister and was manually released from the platform with all telescoping tubes in the extended and locked position. Figure 6B depicts this deployment.

Canopy Material Test

The material selected for the parasol was subjected to a complete program of expedited materials testing ranging from verification of the "as received" mechanical properties to determination of the degradation of properties as a result of combined thermal/vacuum/ultraviolet radiation exposures which simulated on-orbit conditions. Accelerated exposure tests were conducted at Johnson Space Center, Marshall Space Flight Center, and TRW Systems in Redondo Beach, California. Properties measured included solar absorptance, total emittance, breaking strength, elongation, and tear strength. Before and after exposure, scanning electron microscope photomicrographs were taken at various magnifications to 5000x to determine the material surface conditions with respect to the formation of flaking or dust generation which could have generated contamination which would have interfered with Skylab experiments. Tests of out-gassed products were also performed under reduced pressure environments to ensure that the materials generated no potentially toxic products during launch and flight prior to deployment.

While ultraviolet-radiation-induced changes were observed in the materials' properties, in all cases testing verified that adequate integrity could be expected to be retained through the initial use period. Subsequent to deployment, additional ground testing verified acceptability to more than 2000 equivalent sun hours of orbital exposure.

As an additional precaution against possible long-term canopy degradation and to preclude higher internal temperature, an alternate thermal shield carried on the initial mission, a twin-boom sunshade, was deployed over the parasol on the second manned flight. At the conclusion of 9 months' exposure to a combined thermal vacuum/ultraviolet radiation environment, observations made by the crew of Skylab IV during final fly-around inspection indicated the protruding portion of the parasol that had been continuously exposed appeared to be in satisfactory condition.

Full Parasol Deployment at Vacuum (1×10^{-2})

The objective was to verify the operational readiness of the total parasol assembly under simulated space flight vacuum conditions. This test was conducted

in Chamber A of Johnson Space Center's Space Environment Simulation Facility. The parasol canister mounted to an I-beam structure within the chamber and a cable and pulley arrangement coupled with an appropriate drive motor and load cell system was used to activate the parasol and gather force data. A net was provided at the bottom of the chamber to catch the deployed parasol canopy and telescoping tubes. With a TV monitoring system in place, the cable drive system was actuated gradually and load cell readings were recorded. At 186.83 newtons (42 pounds) applied load, the drive switch was turned off and the load went to 44.48 newtons (10 pounds) indicating the push rod had moved. Each successive application of power again caused movement with extension force dropping to 22.24 newtons (5 pounds). Deployment continued to the point where the unevenly distributed weight of the deployed canopy material caused a significant bend in the telescoping tubes on the long side of the canopy. This condition resulted in the tubes that supported the short side of the canopy being released from the end of the canister last, thus causing a pitch-over toward the long side as the canopy came to rest in the net. This test condition, attributable to the one-g deployment, resulted in additional verification of the strength of the telescopic tubes since no damage was incurred.

CONCLUDING REMARKS

The Skylab Parasol is an outstanding example of the inherent advantages of a practical mechanical system design which features ease of fabrication and use of readily available materials. The choice of the parasol as the primary thermal protective device was based on readiness, demonstrated ease of deployment, and proven thermal effectiveness. The highly successful deployment on the Skylab II Mission, accompanied by crew reports on the ease of deployment, verified the operational aspects of the design. The drop in the Orbital Workshop interior temperature from 316 degrees Kelvin (120 degrees Fahrenheit) to 297 degrees Kelvin (75 degrees Fahrenheit) provided a habitable environment in which the flight crew was able to successfully complete its mission (Fig. 7).

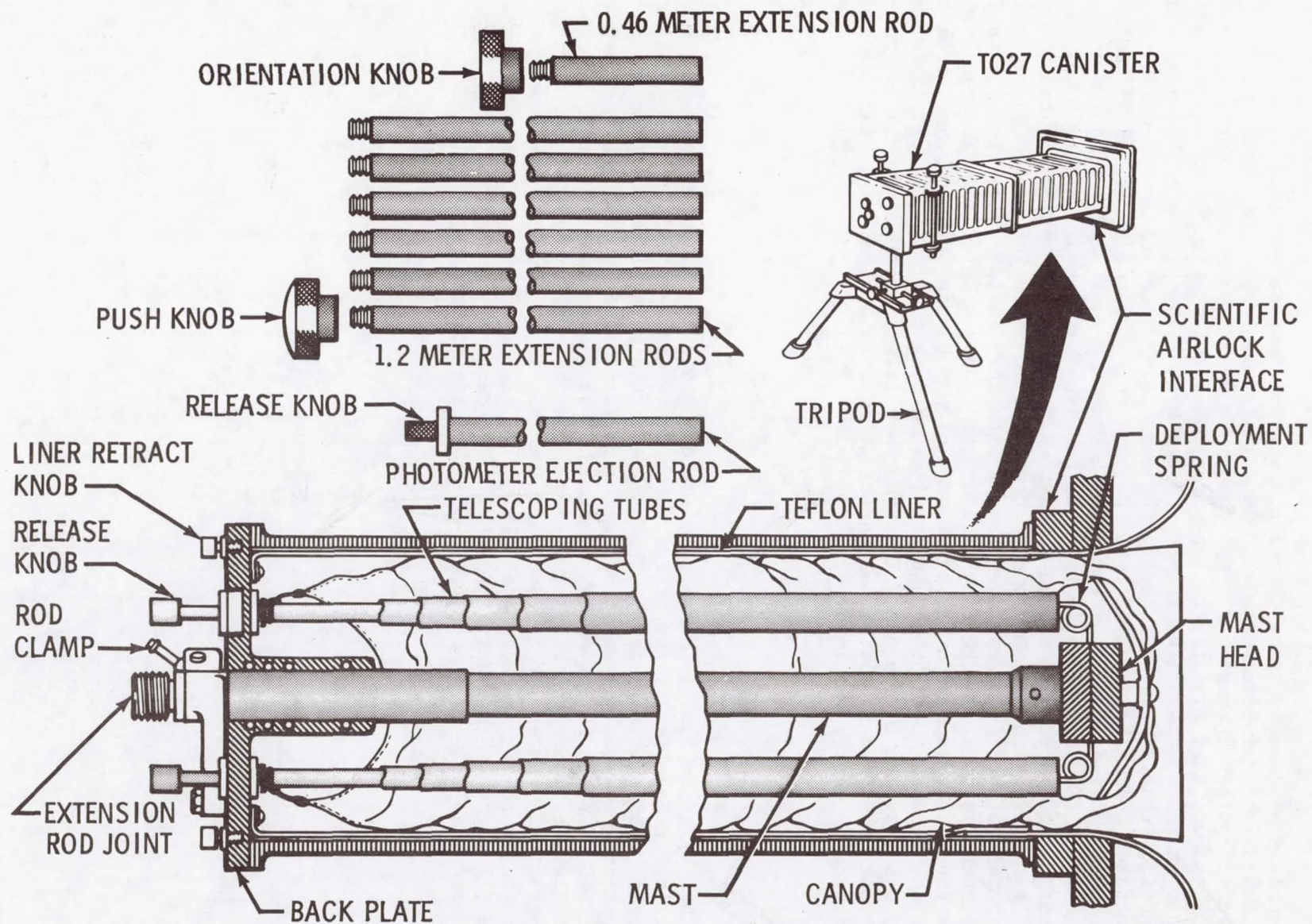


Figure 1. Parasol Packed Configuration

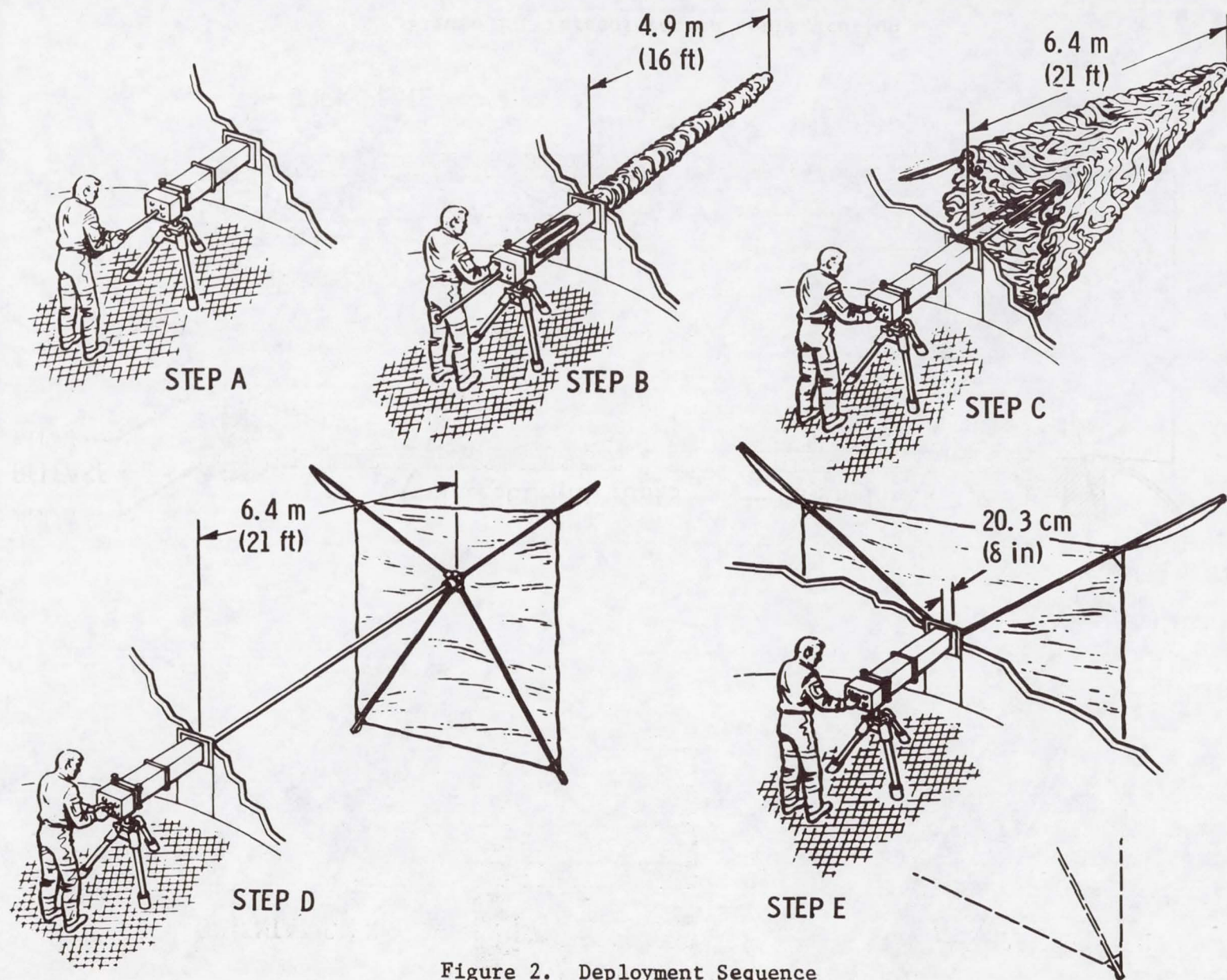


Figure 2. Deployment Sequence

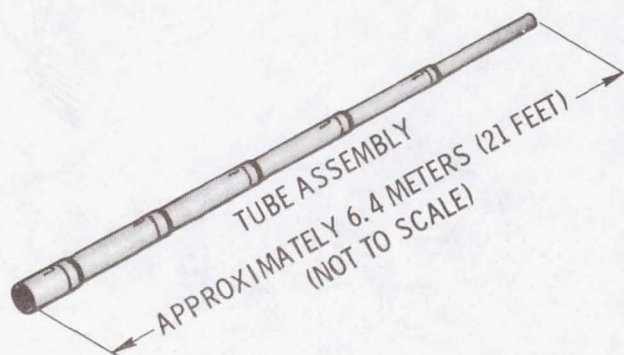
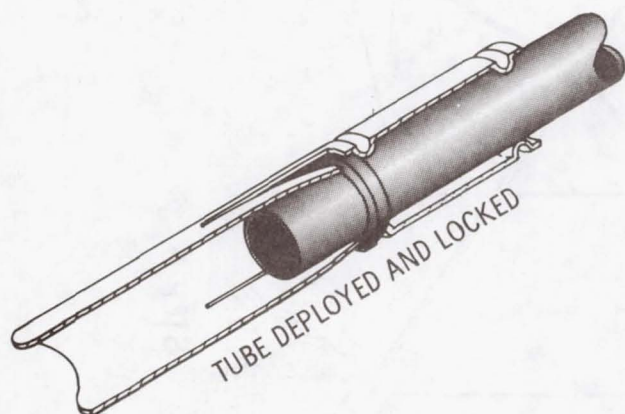
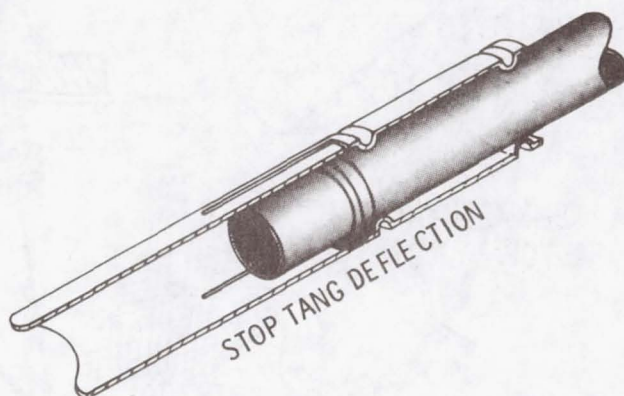
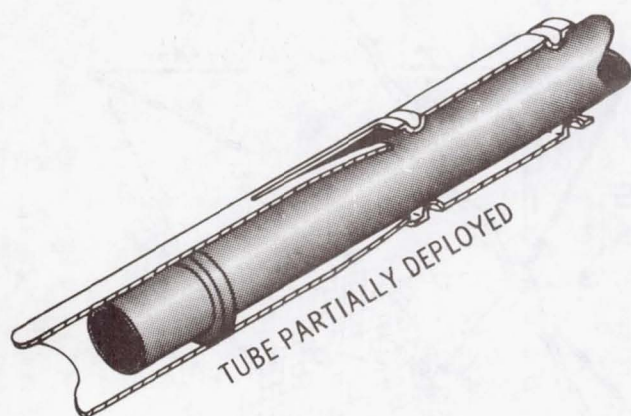


Figure 3. Telescoping Tube Details

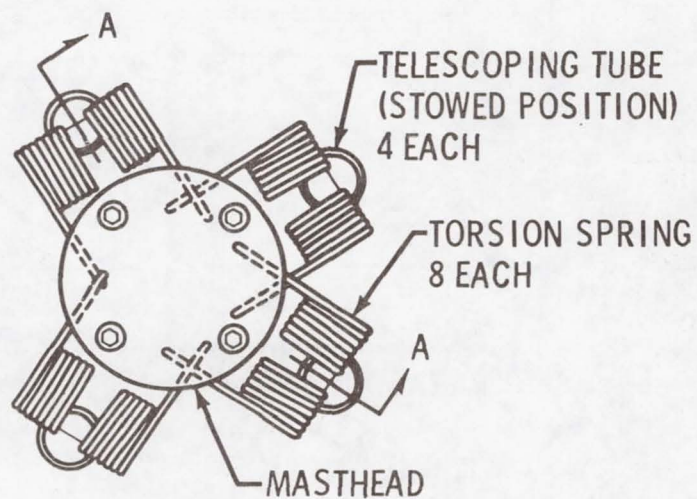
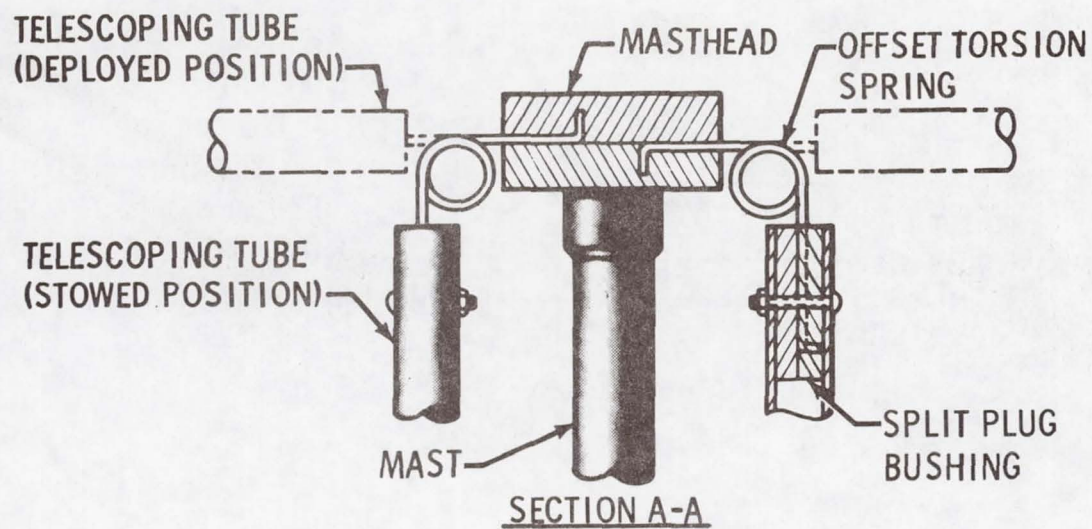


Figure 4. Deployment Mechanism

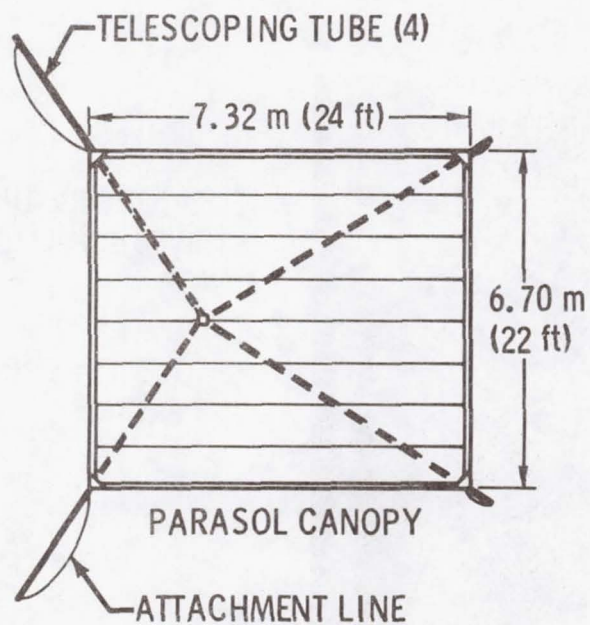
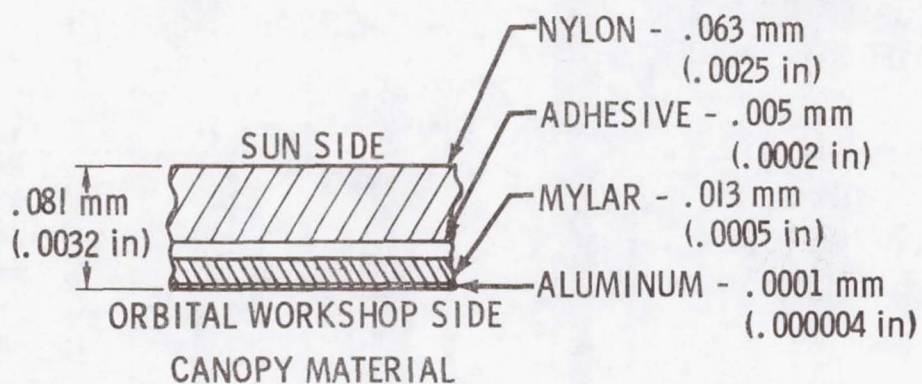


Figure 5. Parasol Canopy Details

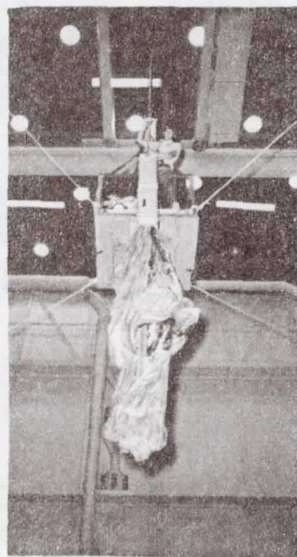
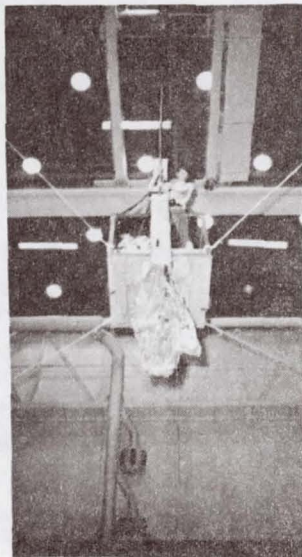


Figure 6A. Deployment of Canopy from Canister

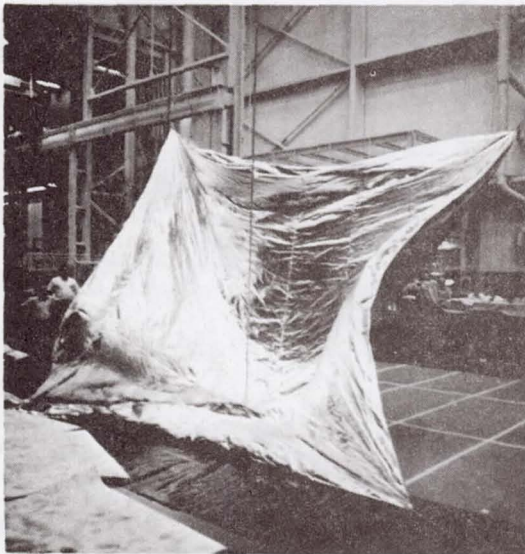


Figure 6B. Manual Release of Extended Canopy

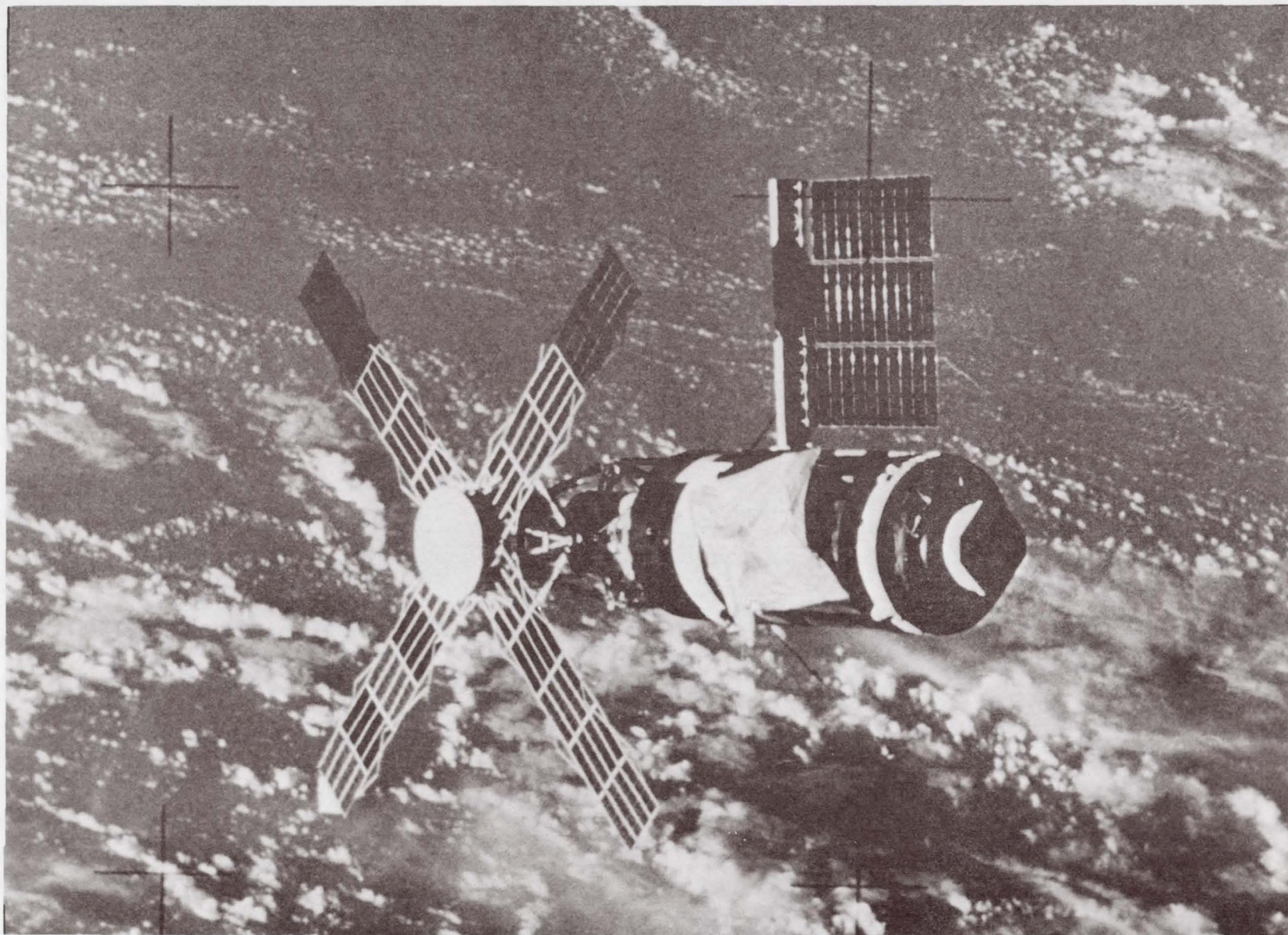


Figure 7. Skylab in Orbit with Parasol Deployed

9. THE PERFORMANCE OF COMPONENTS IN THE SKYLAB REFRIGERATION SYSTEM

By Charles E. Daniher, Jr.

Mc Donnell Douglas Astronautics Company

SUMMARY

The on-orbit performance of the Skylab Refrigeration System components is presented. Flight anomalies are analyzed and performance of the newly developed components is described.

Nine months of orbit data proved the practicality of the leak-free coolant system design. Flight-proven application of a thermal capacitor and development test results of the first all-mechanical, low-temperature mixing valve represent a significant advance in single-phase, low-temperature coolant loop design. System flight data suggest that additional instrumentation and fluid filters could have prevented system orbit performance anomalies.

INTRODUCTION

The Skylab Orbital Workshop (OWS) Module contained a refrigeration system (RS) that was designed to maintain 0.248m^3 (8.75ft^3) of frozen food at a temperature of $250\text{K} \pm 5.5\text{K}$ ($-10^\circ\text{F} \pm 10^\circ\text{F}$), freeze and maintain daily urine specimens (122ml/crewman) at 254K (-2.5°F), chill daily micturition (4liters/crewman) to less than 288.2K (59°F), and chill water, medical supplies, and biological specimens to $277\text{K} \pm 3.3\text{K}$ ($39 \pm 6^\circ\text{F}$). Temperature control was initiated 40 days before the launch of Skylab 1 (April 17, 1974) and was maintained until the end of the last mission 307 days later (February 8, 1974).

The spatial location of RS equipment is shown in figure 1. A food freezer-chiller, located in the wardroom, and a water chiller, located in the wardroom table, are shown. The Bioanalysis Lab contained the urine freezer and chiller. The forward area (second floor) contained the food storage freezer, the RS pumps, and electronic control modules. The RS radiator and an insulated thermal control assembly that housed the thermal capacitors, flow control valves, and ground cooling heat exchangers were located on the aft end of the OWS.

The RS fluid schematic is shown in figure 2. Heat-transport and temperature control were accomplished by controlling the flow of a single-phase liquid coolant (Coolanol 15) through freezers and chillers. The heat picked up by the flowing coolant was either rejected (1) to the space environment through the zinc-oxide coated 7.8m^2 (84ft^2) radiator, (2) to the ground cooling heat exchanger during ground operation, or (3) to the thermal capacitor

during periods when the radiator or ground cooling heat exchangers were not operating (during launch and transient thermal orbit operation). Dual redundant coolant loops were employed to preclude a single system coolant leak that would result in the loss of RS cooling capability (reference 1).

Extensive knowledge and experience was obtained during the design of this low-temperature 244 K (-20°F), single-phase, liquid-coolant refrigeration system. The purpose of this paper is to present the design failures, successes, and recommendations resulting from flight experience, with the hope that future designs will not follow paths leading to failure but rather follow the paths to success. This paper is limited to the following four design areas:

1. Design of leak-free coolant systems.
2. Design of thermal capacitors and their usage in thermal feedback control systems.
3. Design of a thermostatically actuated, mechanical flow-control valve for low-temperature mixing.
4. Flight anomalies of flow and pressure control components and possible remedies.

DESIGN OF LEAK-FREE COOLANT SYSTEMS

No detectable leakage of coolant, from either the primary or backup OWS RS cooling loops, showed in 307 days of ground and flight data (reference 1). In contrast, a similar redundant system on the Skylab leaked coolant from both loops and had to be refilled in flight. Neither the cause nor visible evidence of leaked coolant was found; however, the leaks were attributed to mechanical connections. The RS leak data show that it is possible to design a leak-free system. The suggestion is made that this leak-free performance resulted from the use of high quality fluid fittings and the application of stringent test criteria.

Design Philosophy and Hardware

The following discussion outlines the philosophy and hardware used in the RS design.

1. Minimize all mechanically separable connectors by brazing system coolant connections.
2. Where separable connections are required, use high-quality MC (Marshall Center) specifications for tube fittings, flares, O-rings, and K-seals.

3. Leak test braze fittings to 1×10^{-6} sccs He at 930.69 kPa (135 psig) and leak test mechanically separable connectors to 1×10^{-5} sccs as determined by mass spectrometer quantitative analysis.
4. Retorque B-nut connectors after pressure cycling to minimize the possibility of torque relaxation.

A typical braze union is shown in figure 3. The union was made of 340L CRES cond A. The braze material was 82-percent gold and 18-percent nickel and was held in the braze union bulb until melted out. A prime consideration was the effect of the melting temperature on components as a result of the required fitting brazing temperature of 1,311 K (1,900°F) for 35 sec. Testing revealed that the MC266J fluorosilicone rubber seal reached 394.3 K (250°F) during the braze operation; the seal can maintain its effectiveness to 505.4 K (450°F).

Mechanically separable connections to off-the-shelf hardware and to removeable equipment were made using either the braze adapter shown in figure 3, which was sealed with a fluorosilicone packing or a teflon-coated metal-K seal, or an MC flare tube connector shown in figure 4.

Leak testing of each coolant loop was accomplished using 930.69 kPa (135 psig) helium to a level of 10^{-5} sccs per joint. Care was taken to ensure that joints leak-checked with gas were dry and free of capillary liquid which could block potential leak paths. The system was also leak-checked by a pressure decay test with a decay of -0.124 kPa/hr (0.5 in H₂O/hr) allowable, using 930.69 kPa (135 psig) helium.

The RS contained a total of 413 joints of which 253 were braze fittings, 112 were O-rings or K-seals and 48 were MC flare fittings.

Leak Prediction

Symbols

P = pressure

V_G = maximum gas volume when accumulators are empty

K_B = effective metal bellows spring rate

X_o = bellows preload

A_B = effective bellows piston area

M_G = mass of accumulator gas charge

R_G = gas constant

T_G = absolute gas temperature

V_A = volume of coolant in accumulator

V_S = volume of coolant in one system loop with accumulator empty
 M_L = mass of liquid coolant loaded into system
 \bar{T}_L = average coolant temperature
 ρ_L = density of liquid coolant
 C_i = mass weighting constants
 ϵ = pressure error

Subscript

L = liquid coolant
 G = accumulator gas
 B = metal bellows
 S = per coolant loop

The prediction of flight coolant leakage was a mission data requirement. It is a paradox that leak-tight systems may not allow for the prediction of an unacceptable leak rate because of low gains on the measured parameters necessary to predict leakage.

$$\left(\text{i. e., low } \frac{\partial P_L}{\partial V_A} \text{ or low } \frac{\partial V_A}{\partial T_L} \right)$$

For example, the random error on the RS pressure measurements were such that 66 days were required to determine if a temperature-corrected pressure was actually a leak.

The off-the-shelf coolant accumulators did not incorporate a direct reading volume indicator. Thus, the volume of coolant had to be indirectly determined from the pressure on the coolant and the temperature of the accumulator gas. Pressure was maintained on the liquid coolant by a spring-loaded metal bellows and a non-condensing R-22 gas (figure 5).

The leak calculation procedure was to determine what the pressure on the coolant should be. This calculated pressure was then compared with the actual flight pressure and a pressure error number generated:

$$P_{\text{FLIGHT}} - P_C = \epsilon \quad (1)$$

The pressure on the coolant is described by

$$P_C = \underbrace{K_S X_o}_{\text{metal bellows preload}} + \underbrace{\frac{K_S V_A}{A_p^2}}_{\text{pressure due to bellows compression}} + \underbrace{\frac{M_G R_G T_G}{V_G - V_A}}_{\text{pressure due to accumulator gas}} \quad (2)$$

All leak detection schemes must assess the average coolant temperature to determine the volume of the coolant in the system and hence the amount of coolant that should be in the accumulator. The average coolant temperature is found from:

$$\bar{T}_L = \sum_{i=1}^n C_i T_i \quad (3)$$

C_i 's are mass-weighting constants. The RS coolant volume was divided into 16 isothermal nodes represented by combinations of flight temperature transducers (figure 5).

The volume of coolant in the accumulator was found from:

$$V_a = \frac{M_L}{\rho(\bar{T}_L)} - V_S \quad (4)$$

The leak calculation procedure is as follows:

1. Determine the average coolant temperature from equation (3).
2. Calculate the volume that should be in the accumulator from equation (4).
3. Calculate the coolant pressure using equation (2).
4. Calculate the pressure error using equation (1).

The mission leak-prediction results are shown in figure 6, with pressure error plotted against the day of the year (DOY).

Data evaluations were started on DOY 134 (May 14, 1973). The average value of the pressure error (μ) of 20.5 kPa (2.967 psig) was a systematic error that was probably due to variations in metal bellows spring constants K_S , the magnitude of the gas charge M_G , and uncertainty in coolant fill mass M_L .

The lower bound of measurement tolerance was established by adding the pressure transducer least bit error 2.14 kPa (0.31 psig) to the transducer

repeatability 2.07 kPa (0.3 psig). The allowable system leakage 197 cm³/year (12 in.³/year) was equivalent to a pressure decay of 0.0517 kPa/day (0.0075 psig/day). Figure 6 shows that no coolant leakage was detectable.

As a result of the difficulty in measuring system leakage, it is recommended that future systems either incorporate a high-gain accumulator (large $\partial P/\partial VA$) or incorporate volume-indicating instrumentation and provide sufficient temperature instrumentation to determine the average liquid temperature. Depending upon margins, the evaluation of possible leaks could be substantially reduced from the 66-day Skylab RS limit.

DESIGN AND USAGE OF THERMAL CAPACITORS

The RS used a phase-changing heat sink (thermal capacitor) as a heat storage device. Heat was transported to and from the liquid coolant that flowed through it at a constant rate of 56.7 kg/hr (125 lb/hr).

The phase-change material (PCM) was Undecane (C₁₁ H₂₄), a polymorphic odd-numbered paraffin with a liquid/solid fusion point at 247.60 K (-14°F) and a crystal structure change at 236.5 K (-34°F) (reference 2). At 247.60 K, the capacitor stored 36.68 cal/gr (66 Btu/lb); at 236.5 K it stored an additional 10.01 cal/gr (18 Btu/lb).

Design of Capacitors

The thermal capacitor was fabricated in three identical segments and plumbed in series as shown in figure 2. The construction of each segment is shown in figure 7 and consisted of:

1. A plate fin coldplate which transported heat between the coolant and the coldplate surface.
2. A PCM chamber which contained and allowed for expansion and contraction of the PCM, and transferred heat between the coldplate and the PCM.
3. A PCM that changes phase at 247.6 K (-14°F).

The PCM chamber was a special hex cell or honeycomb design. The hex cells were 0.3175 cm (1/8 in) across the flats and 2.54 cm (1 in) tall with 0.015-cm- (0.006-in) thick aluminum foil walls (figure 7C). Small cell size was desired to increase the effective thermal conductance to the PCM. Each hex cell was filled 80 percent with PCM and 20-percent air for ullage, (figure 7B). The ends of the hex cells were bonded to aluminum sheets, one end to the coldplate surface and the other to a thin sheet of aluminum.

The design captured a discrete expansion (ullage) volume into each cell. This was required because the wax volume increased 8 percent when melted. The original design did not capture the ullage but simply allowed for a

20-percent expansion in a chamber with open cell tops. When this original unit was slightly tilted and melted, the wax chambers ruptured. In zero gravity this same effect would result due to the Marangoni effect which observes that liquid will tend to flow towards regions of high surface tension (low temperature) (reference 2).

Capacitor Use in Thermal Feedback Control System

The thermal capacitor (TC) provided a means to filter cyclic inlet temperatures from the space radiator of $244.26 \text{ K} \pm 15 \text{ K}$ ($-20 \pm 27^\circ\text{F}$) to a cyclic amplitude of $242 \text{ K} \pm 4.4 \text{ K}$ ($-24^\circ\text{F} \pm 8^\circ\text{F}$) at the outlet of the third segment (figure 8).

The capacitor also provided deadband for the feedback controller. A temperature sensor located on the coolant tube downstream of the first capacitor segment (figure 2) was used to control the radiator bypass valve and maintain the two downstream thermal capacitor segments in a frozen state.

When the TC control temperature sensor reached 248.26 K (-12.8°F), indicating that the first segment had melted, the coolant flow was diverted to the radiator and the capacitor refrozen. Cooling was terminated when this same TC sensor reached 236.21 K (-34.5°F) at which time coolant flow was bypassed around the radiator and the first segment would then begin to melt again. This deadband resulted in a 93-minute limit cycle. The system response, (figure 8), shows the coolant temperature out of the third TC segment was maintained at less than 247.59 K (-14°F), the PCM fusion point.

Designers of future systems should consider liquid-coupled thermal capacitors as flight qualified components. Their effective use can greatly reduce the required radiating area and make possible the design of low-temperature refrigeration systems. In addition, capacitors provide substantial temperature filtering; they also provide their own controller deadband. The large thermal expansion and low thermal conductivity PCM's require a design of small hexagonal cells 0.32 cm by 2.54 cm ($1/8\text{-in}$ by 1-in) to increase the thermal conductance to the wax and with captured ullage to minimize the PCM expansion yield path to ullage.

LOW-TEMPERATURE FLOW CONTROL VALVE DEVELOPMENT

A thermostatically actuated flow control valve was developed to proportionally control flow through the radiator and thermal capacitor as shown in figure 9B. Proportional flow control was selected to meet an original requirement to limit frozen food temperature cycle amplitude. Flow and temperature instability showed up at the component test level; the proportional control valve was replaced with a binary flow control system and consequentially was not part of the RS. However, the oscillation (instability) problems were solved by degaining the valve area/stroke function at the hot port. Completion on this modification was too late to meet the Skylab launch schedule.

Degaining increased the stroke required to close the hot port and resulted in an increase in the valve control temperature bandwidth from 244.26 ± 1.66 K ($-20 \pm 3^\circ\text{F}$) to $247 \text{ K} \pm 3.3 \text{ K}$ ($-15 \pm 6^\circ\text{F}$). Although this performance did not meet the tolerance limits originally specified, this is the first flight-type, thermally-actuated valve to be developed for this low-temperature operating band. The low temperature flow control valve is shown in figure 9A. The total dry weight was 2.19 kg (4.84 lb), the length 25.4 cm (10.0 in), and the diameter 4.8 cm (1.89 in). This design functioned as follows:

An actuation medium, consisting of silicone fluid (DC-200) doped with (20 percent by volume) copper flake to improve thermal conductivity, was contained within an internally and externally finned actuator housing. The actuation medium linearly expanded and contracted, on heating and cooling respectively, as a function of the valve coolant mix temperature. This medium volume change was amplified and converted to a linear stroke by moving a bellows-sealed piston. The piston was connected to a slotted sleeve that masked and controlled the hot and cold coolant fluid passage openings. The fully open hot to fully open cold piston travel was 0.0889 cm (0.035 in). This travel took place between a 244.26 K (-20°F) to 247.59 K (-14°F) change in the actuation medium temperature. Over-temperature protection was provided by a second over-travel piston sealed by an over-travel bellows. This piston moved off its mechanical stops after the slotted sleeve had moved to the far left limiting position. Over-temperature protection to 322.03 K ($+120^\circ\text{F}$) was provided.

Early problems developed during valve testing. The actuation bellows squirmed, causing a shift in the temperature control band. The problem was solved by a hardware change using a close tolerance teflon guide cylinder for the bellows.

The valve also exhibited a temperature control instability with an amplitude of 8.33 K (15°F) and a period of 24 seconds. Instability was found to be a function of the radiator pressure drop and the difference in the hot and cold port temperatures. In the above case, instability occurred when the cold port temperature was 210.9 K (-80°F), the hot port was 250.37 K (-9°F), and the radiator pressure drop was 275.76 kPa (40 psid). This pressure drop had to be balanced by the hot-port, slotted-sleeve opening. The problem was the high area change to stroke gain at bypass port closure. The solution was to degain the bypass port by taking more valve stroke to change the port area from full open to full closed. The resulting performance is shown in figure 10 (reference 3). The condition being run was a simulated radiator temperature change at a high radiator pressure drop of 344.7 kPa (50 psid); minimum radiator temperature was 210.9 K (-80°F); and the bypass temperature was 266.48 K ($+20^\circ\text{F}$). As a result of this valve development, the following design recommendations are made:

1. Define port "load lines" early (pressure drop versus flow characteristics). If the evolving design is in such an unpredictable state (final radiator size not known), then a valve installation as shown in figure 9C should be considered. The maximum pressure drop imbalance is controlled by the design of the regenerator heat exchanger only. This approach was used successfully for the chiller valve shown in figure 2. When selected, the regenerator heat

exchanger approach allows the flow control valve development to proceed independent of the final radiator design.

2. Component-level testing should realistically simulate the flight system characteristics and should include the following:

Test conditions, that force the valve to perform its control function at the end of its stroke (at port closure), should be selected for stability analysis. For example: the coldest bypass port temperature 249.82 K (-10°F), the coldest radiator port temperature 210.93 K (-80°F), and the highest radiator pressure drop 310.23 kPa (45 psid) all combine to force the valve to flow control on the bypass port.

Testing should also include conditions that simulate the inlet port temperature design limits; this may reveal a fluid mixing instability. For example: this valve was tested with a bypass port temperature of 266.48 K (+20°F) and a radiator port temperature of 205.37 K (-90°F).

Testing should include the simulation of expected inlet temperature and pressure ramps to determine valve mix temperature tracking limits.

Data required for valve math modeling are:

1. Actuator stroke versus temperature (note bellows actuators usually have a hysteresis which provides deadband).
2. Port orifice coefficients versus stroke.
3. Actuator thermal time constant and effective capacitance.

FLIGHT ANOMALIES OF FLIGHT FLOW AND PRESSURE CONTROL COMPONENTS

The RS binary radiator flow control system functioned normally as shown in figure 8 until anomalous performance was observed on DOY 173. The expected and actual flight performance of the thermal capacitor outlet temperature and the coolant system differential pressures are shown in figure 11.

Description of Anomaly

At approximately 17:02:03 GMT, the system differential pressure decreased 34.47 kPa (5 psid), at a time when a switch to radiator flow was expected, due to a 248.26 K (-12.8°F) thermal capacitor control sensor signal. The expected differential pressure was 392.96 kPa (57 psid) which indicated that warm fluid was being diverted through a viscous radiator. The low differential pressure of 220.6 kPa (32 psid) and thermal capacitor inlet

temperature of 255.37 K (0°F) suggested that total flow was not flowing through the radiator and that a split flow (radiator and/or bypass legs path A and B, figure 2) was occurring.

The complete melt of the thermal capacitor occurred approximately 2 hours after the anomaly and an automatic switch to the backup coolant loop, caused by a food temperature sensor exceeding 255.93 K (+1°F), resulted in even worse performance. Apparently the secondary loop was also bypassing coolant flow around the radiator.

The potential leak paths are shown in figure 2. A leak through path B is caused by coolant flow past the bypass port poppet of the radiator bypass valve (RBV). Subsequent investigation indicated that a 25 μ particle, if trapped in the poppet seat, could cause the observed leak. Path A is through the radiator relief valve which could have lodged open due to contamination. Continuous cycling of the RBV by ground controllers may have been the cause for performance improvement since the RS primary loop returned to an acceptable split-flow performance mode (approximately 50 hours after the anomaly) and continued to function until the end of the last mission (February 8, 1974). The binary flow control system was disabled and the RBV left in the radiator flow position at that time.

Probable Causes and Recommendations

This anomalous performance might be prevented in future designs if the following two recommendations are implemented.

The first recommendation is to provide for particle filtering upstream of all valves that are contamination sensitive, and especially if they are located downstream of brazed heat exchangers. The brazed plate fin regenerator heat exchanger shown in figure 2 was a likely candidate for particle generation. This was assumed since vibrations and zero gravity could coincide to loosen and allow braze particles to enter the coolant flow stream. Better cleaning practices may reduce the number of particles generated but the judgement is that brazed heat exchangers will always be a potential source of particles large enough to cause a valve malfunction of the type observed.

The second recommendation is to provide a simple flow-sensitive reed switch to be located at points A and B (figure 2) and set to indicate flows above the allowable leakage values (in this case flows ≥ 0.91 Ks/Hr (≥ 2 lb/hr). This would allow for the positive ground checkout of the full radiator flow function. In retrospect, ground checkout procedures and existing instrumentation did not allow for the accurate determination of the full radiator flow condition when the RBV was commanded to the radiator flow position. Accurate assessment of the full bypass position was accomplished by noting the thermal capacitor inlet temperature when the ground cooling heat exchanger was operating. A partial flow of 259.26 K (+7°F) coolant to the radiator would have resulted in (1) condensation on the radiator surface and (2) a thermal capacitor inlet temperature higher than the coolant temperature out of the ground-cooling heat exchanger. The assessment of

the full radiator flow could not be determined in the same manner. Rather, it was determined by changes in system differential pressure between radiator and bypass RBV positions.

CONCLUDING REMARKS

Designers of future coolant systems should carefully evaluate cleaned heat exchangers as potential contamination sources and provide for coolant particle filtration. In addition, allowance should be made in the system for the incorporation of instrumentation, such as the flow-actuated reed switches, to verify required full and no-flow conditions.

REFERENCES

1. Skylab Final Technical Report. McDonnell Douglas Report MDC-G5170, May 1974.
2. Phase Change Materials Handbook. Interim Development Test Report, Nasa Report CR-61363, September 1971.
3. Radiator Control Valve. AiResearch Manufacturing Co., Report 72-8475, August 9, 1972.

ACKNOWLEDGMENT

The work discussed in this paper was sponsored by NASA Marshall Space Flight Center and Johnson Space Center under Contract NAS9-6555.

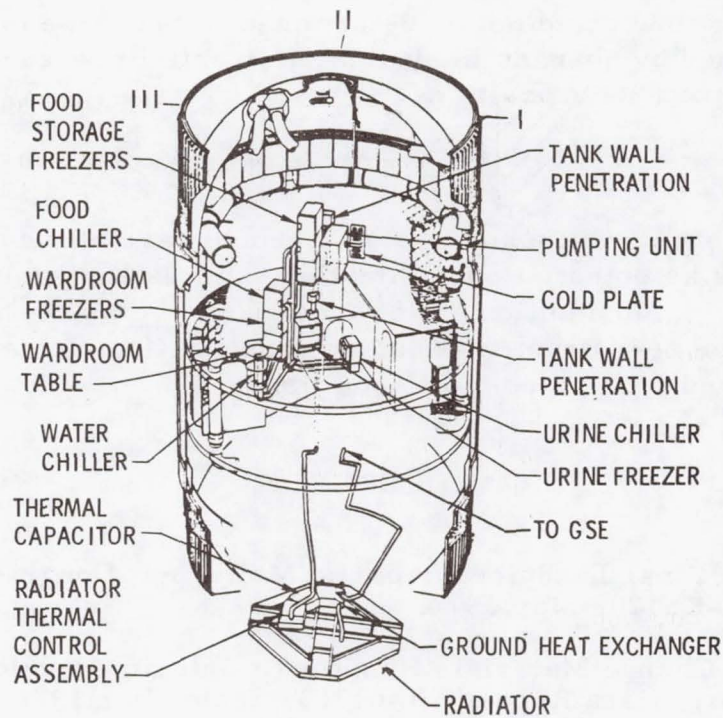


Figure 1. Skylab Orbital Workshop Refrigeration System

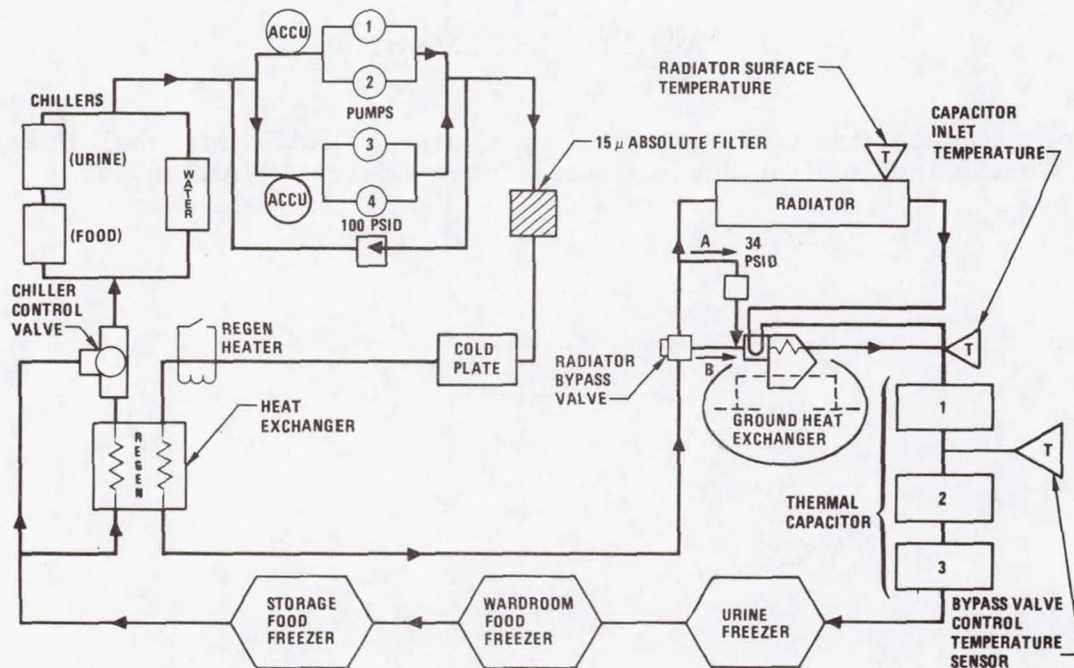


Figure 2. Refrigeration System Fluid Schematic

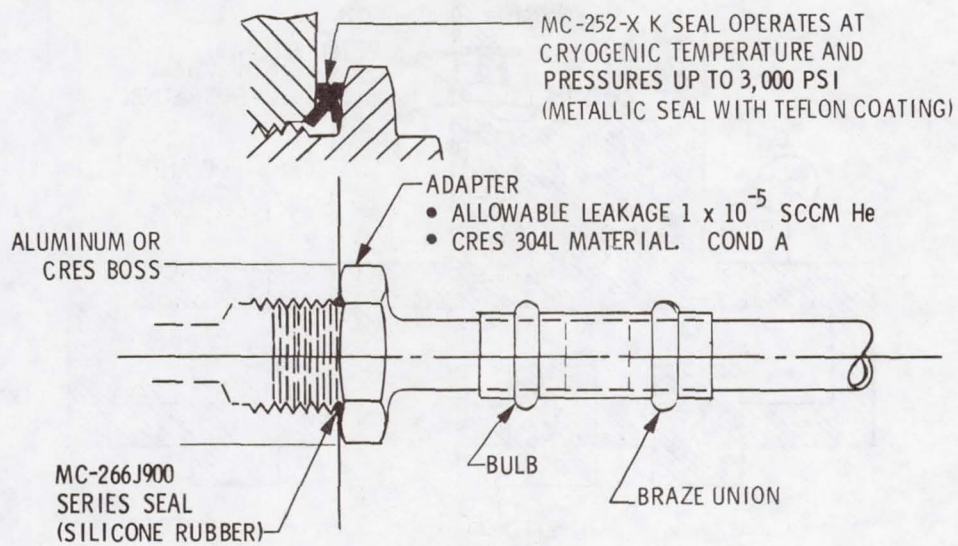


Figure 3. Refrigeration System Component-to-Boss Fluid Connection

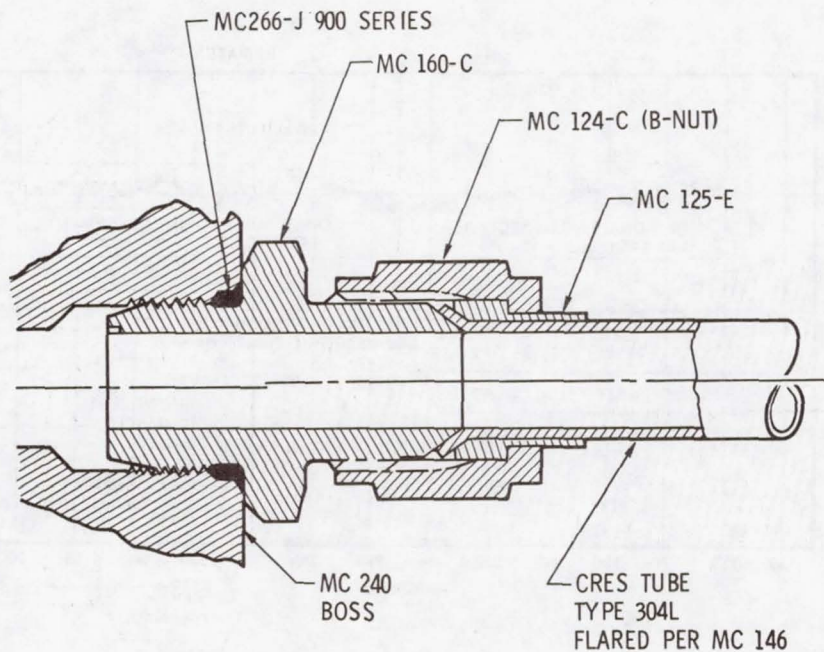


Figure 4. Refrigeration System Flare Tube Connector (MC)

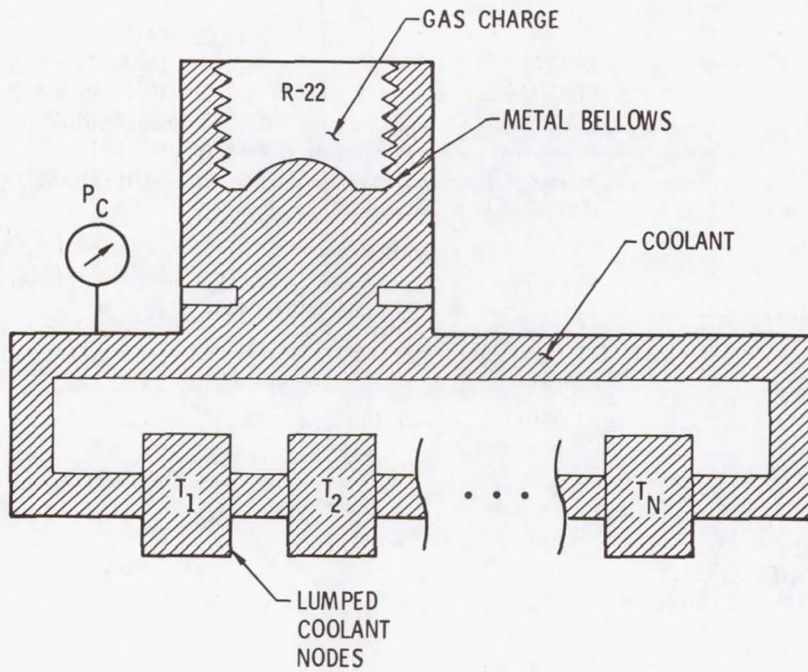
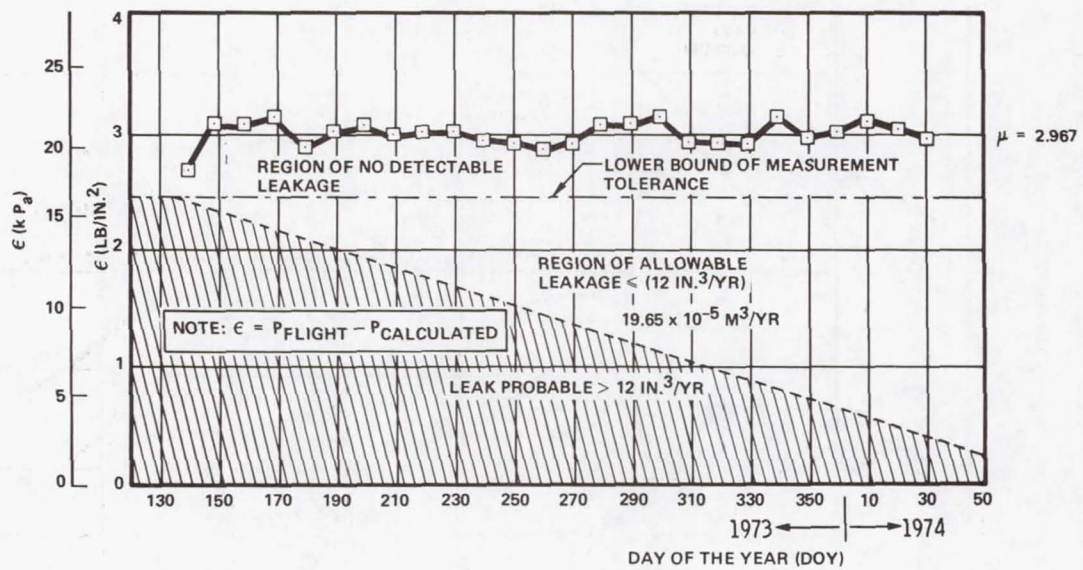


Figure 5. Refrigeration System Symbolic Coolant Loop



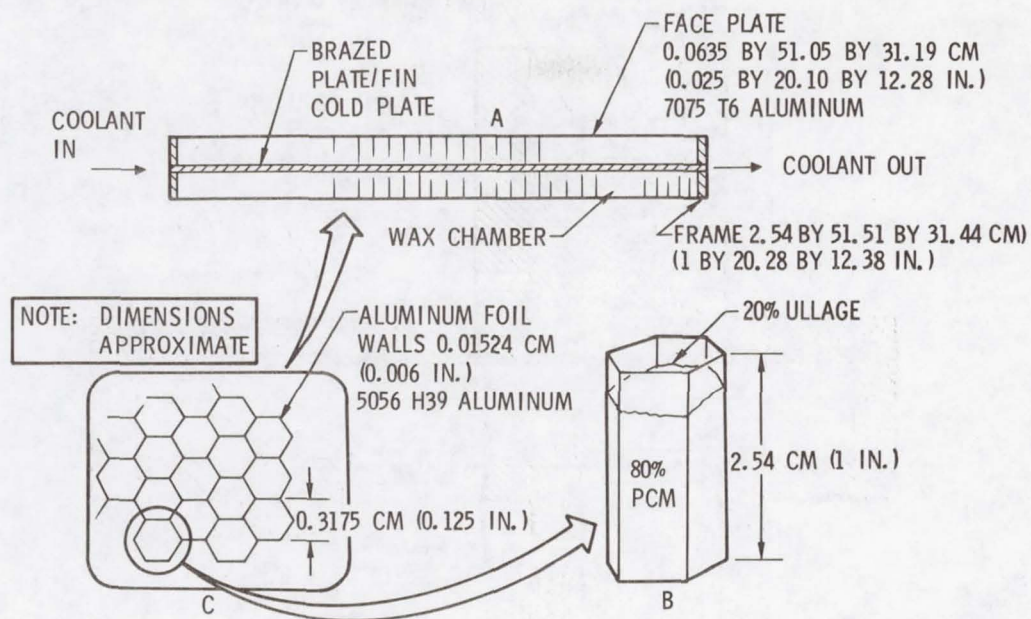


Figure 7. Refrigeration System Thermal Capacitor Segment

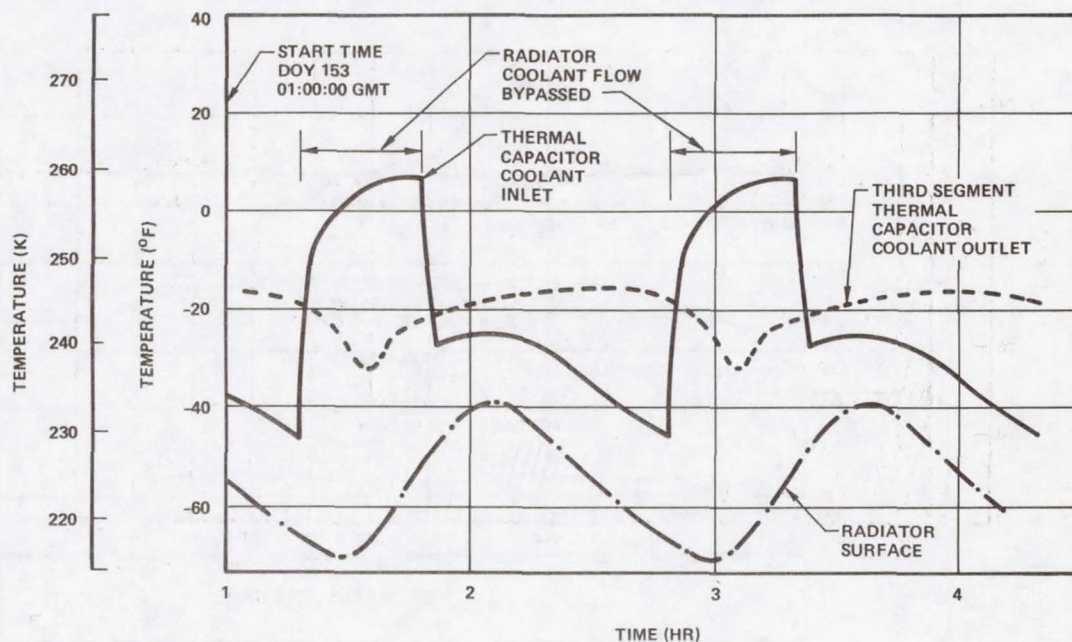


Figure 8. Refrigeration System Thermal Capacitor Performance Temperatures

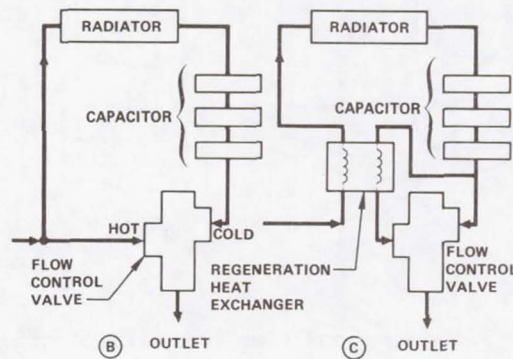
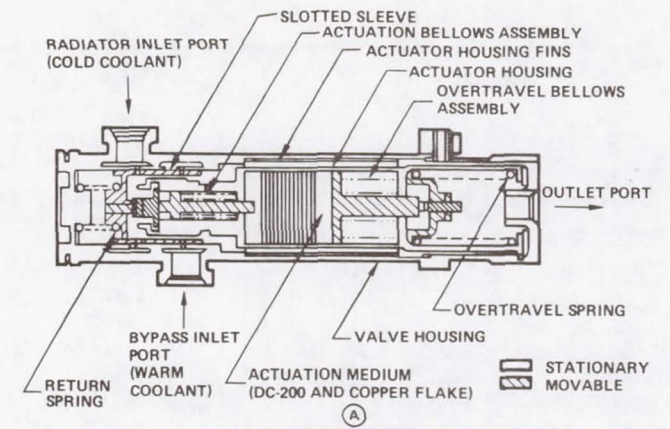


Figure 9. Low-Temperature Flow Control Valve

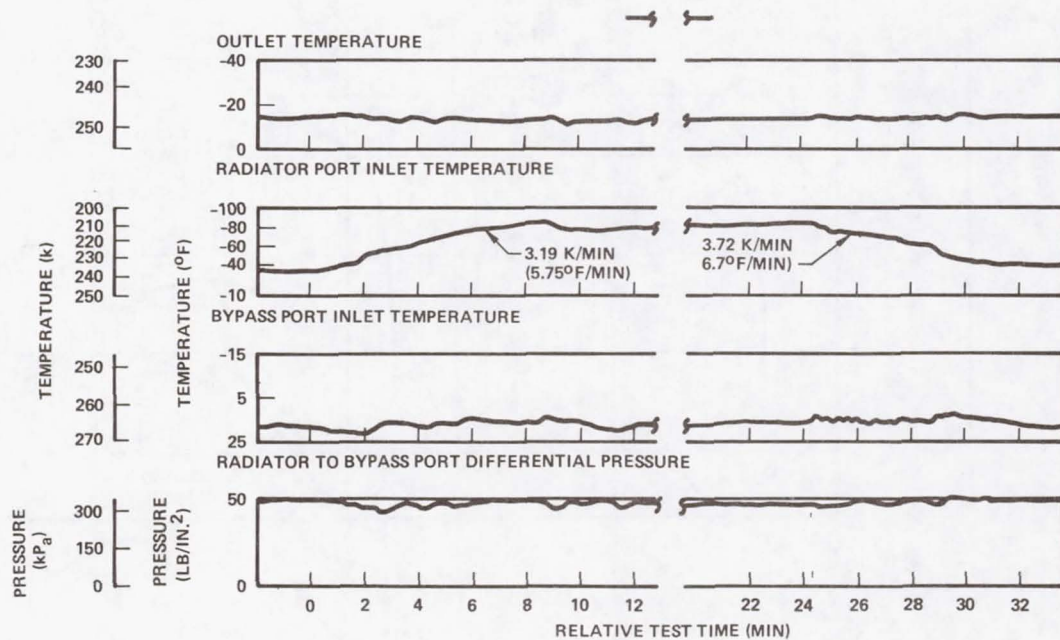


Figure 10. Radiator Control Valve Performance Maximum Hot Port Differential Pressure

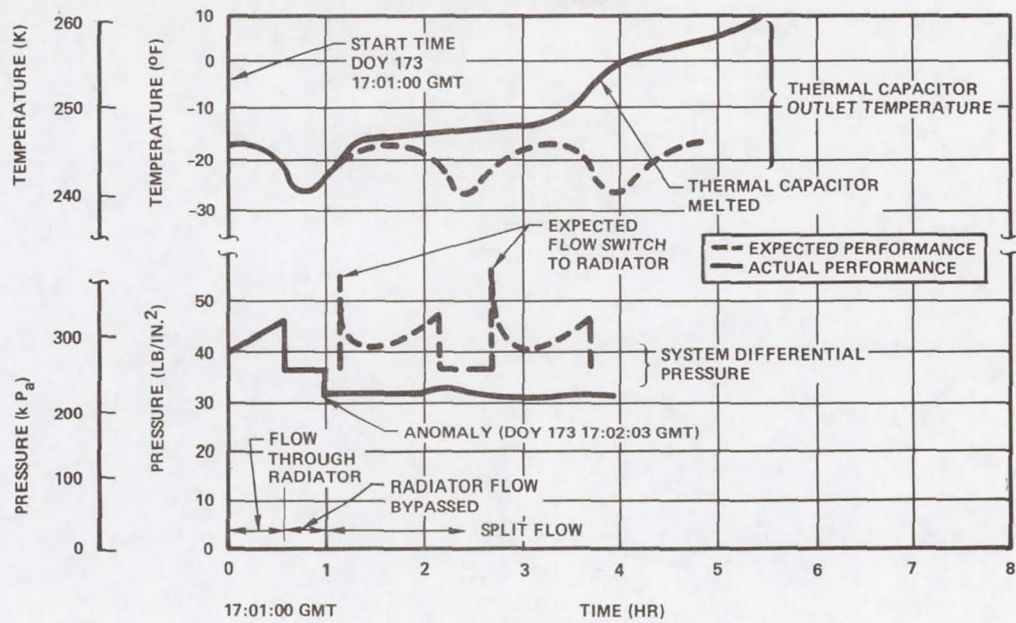


Figure 11. Refrigeration System Performance Anomaly

10. REFURBISHMENT OF THE CRYOGENIC COOLERS FOR THE SKYLAB

EARTH RESOURCES EXPERIMENT PACKAGE

By Jerry C. Smithson and Norman C. Luksa

Lyndon B. Johnson Space Center

SUMMARY

Two of the Skylab Earth Resources Experiment Package (EREP) experiments, S191 and S192, required a cold temperature reference for operation of a spectrometer. This cold temperature reference was provided by a subminiature Stirling cycle cooler. However, the failure of the cooler to pass the qualification test, coupled with the fact that the cooler manufacturer had gone out of business made it necessary for the additional cooler development, refurbishment, and qualification to be done by the Lyndon B. Johnson Space Center (JSC). Because of the exclusive nature of the contracts between the cooler manufacturer and the experiment contractors, no drawings, assembly procedures, or manufacturing specifications were available. Furthermore, no replacement components were available for the limited number of existing coolers in the EREP program. These facts made the development of adequate procedures for both disassembly and reassembly of the cooler mandatory. Also, since these coolers were flight items, a strict quality assurance program had to be implemented. A description of the failures and the cause of these failures for each of the coolers is presented. The solutions to the various failure modes are discussed along with problems which arose during the refurbishment program. The rationale and results of various tests are presented. The successful completion of the cryogenic cooler refurbishment program resulted in four of these coolers being flown on Skylab. The system operation during the flight is presented.

INTRODUCTION

The primary objective of the Skylab mission was the study of the earth. This earth survey included agriculture, forestry, oceanography, hydrology, geology, and geography. The EREP contained the scientific instruments to conduct the investigation of these various disciplines. Two of the experiments within the EREP group were designed to investigate the infrared region of the electromagnetic wave spectrum. The S191 Infrared Spectrometer performed controlled experiments in the applicable region of the spectrum on ground sites actively acquired and tracked by the flight crew. The S192 Multispectral Scanner gathered quantitative high spatial resolution line-scan imagery data on radiation reflected and emitted by selected ground sites. One of the

features which each of these experiments had in common was their use of a nearly identical cryogenic cooler to refrigerate the infrared detector.

CYCLE DESCRIPTION

Before presenting a detailed description of the cooler, it is helpful to briefly review the operation of the cooler. Any refrigerator operating on the Stirling cycle principle must have a compression volume at a warm temperature and an expansion volume at some colder temperature. The relationship between these two volumes must be such that a fixed quantity of working fluid (helium in this case) is made to alternately pass from one volume to another through a regenerative heat exchanger. This is shown in Figure 1, which illustrates the four basic processes of an idealized Stirling cycle. In the isothermal compression process of Figure 1-A, the compression piston moves upward while the expander piston remains stationary at its top position. Heat is rejected at the compressor head (the aftercooler heat exchanger) at an intermediate temperature. Figure 1-B illustrates a constant-volume heat transfer process in which heat is stored in the regenerator. In Figure 1-C, isothermal expansion occurs by a downward movement of the expander piston with the compressor piston stationary. Heat is absorbed (from the infrared detector) at the low temperature in the cold-end heat exchanger. The cycle is completed (Figure 1-D) by a constant-volume heat transfer process in which the working fluid travels from the expansion volume to the compression side. During this process, the working fluid extracts the heat stored in the regenerator during the previous constant-volume heat transfer process.

COOLER DESCRIPTION

The cooler, shown in Figure 2a, is a subminiature Stirling cycle refrigerator which uses helium as the working fluid and has a cooling capacity of approximately 1 watt at 90°K (-297°F). Physically, the cooler is 6.35 cm (2.5 inches) in diameter and approximately 30.5 cm (12 inches) long, and weighs approximately 2.7 kg (6 lbs). The cooler consists of four working sections; they are as follows: (Figure 2b)

- a. Cold end assembly, including the cold end heat exchanger and regenerator.
- b. Cylinder head assembly, including the after-cooler heat exchanger.
- c. Cylinder block assembly, including pistons and crank assembly.
- d. Drive motor assembly and gear case.

The cold end assembly contains the refrigerating surface, which is in good thermal contact with the infrared detector. This section of the machine operates at approximately 90°K (-297°F). The cold end assembly also contains the regenerator which is the heart of a Stirling cycle refrigerator. The effectiveness of a regenerator is defined as the ratio of energy actually absorbed to the energy which could be ideally absorbed. It can be shown (Reference 1) that if the effectiveness for the regenerator is less than 94 percent, there will be no net refrigeration. Hence, great care must be exercised in working with the regenerator.

The cylinder head assembly contains the after-cooler heat exchanger. The after-cooler heat exchanger, which absorbs the heat of compression from the helium gas, consists of several very small copper tubes brazed into a bundle and inserted into the aluminum cylinder head. Heat rejection is by conduction through the heat exchanger walls and cylinder head to the cooler outer shell and finally, through the mounting brackets to the spacecraft structure.

The cylinder block assembly contains the compression and expansion cylinders plus all of the important mechanisms in the cooler. Figure 3 shows a detailed view of this assembly. A single crankshaft is utilized to drive both the compressor and expander pistons. In order to achieve the constant volume processes required for proper operation, the compression and expander pistons are approximately 90° out of phase. This phase angle is very important for the optimum performance of the cooler. The phenolic extension on the expansion piston is to provide a long heat path between the relatively hot piston rings and the cold working fluid. The pistons have four basic components; they are as follows:

- a. An aluminum body,
- b. A Rulon (glass filled Teflon) sleeve over the aluminum body,
- c. Two full-circle Rulon compression rings and,
- d. O-rings behind the Rulon compression rings to prevent gas leakage between the ring and the aluminum body.

The pistons are connected to the piston rods with wrist pins; the wrist pin bearings are needle bearings while the rod bearings and the main crankshaft bearings are ball bearings. These bearings are all packed with a commercial grade, high temperature hydrocarbon lubricant.

A 96-tooth bevel ring gear (shown in Figure 3) is attached to the crankshaft with eight screws, which are staked. The ring gear has a reduction ratio of four which results in a nominal crankshaft speed of approximately 1500 r/min. Both the ring gear and pinion gear are coated with molybdenum disulfide dry lubricant. The entire crankshaft/piston assembly is attached

to the cylinder head assembly by screws through the main bearing hangers. The bearing hangers contain pilot pins for gross alignment; shims are used to complete the precision alignment of the pistons in the cylinder.

The drive motor assembly contains the 28V d.c. motor which operates at approximately 6000 r/min or 4500 r/min. The two speeds are a requirement for the S192 experiment; S191 operates only at the higher speed. The power consumption ranges from a maximum of 45 watts operating at high speed to a minimum of 28 watts when operating at low speed. The pinion gear is mounted to the motor shaft and the set screws are safety-wired. The gear case is utilized to mate the motor drive assembly to the cylinder block assembly.

Since a long shelf life for the coolers is required, an outer case is installed over the entire cooler to prevent helium leakage. The original outer case design was an aluminum cylinder with a bimetallic joint at each end. The aluminum section provides for good heat rejection, while the stainless steel permits the outer case to be welded to the cooler. The electrical leads are soldered to a ceramic feed-through connector contained in a stainless steel end cap. The end cap is welded to the motor end of the unit making the entire cooler hermetically sealed (Figure 2a).

Physically, the only external difference between the S191 cooler and the S192 cooler is the design of the front mounting flange. In operation, the startup procedure for both coolers is the same; the motor is set to the high speed, and 28V d.c. is applied to the motor. The S191 runs continuously in this configuration. The detector temperature is controlled at a constant 82°K (-312°F) using an electrical resistor on the detector. The S192 operates differently. Once the detector reaches 90°K (-297°F), a controller in the experiment switches the motor to low speed and reduces the voltage simultaneously. The detector temperature is then controlled at approximately 92°K (-293°F) by automatically varying the motor voltage, which varies the motor speed and consequently the cooling capacity.

COOLER PROGRAM BACKGROUND

In January 1972, the cooler was undergoing component qualification testing at the S191 contractor's facility. This qualification test was for both the S191 and S192 coolers. A large portion of the qualification testing, including vibration, electromagnetic interference (EMI), exposure, etc., had been successfully accomplished. There had been some problems with the thermal performance of the S191 coolers earlier, but the S192 units were operating satisfactorily. However, during qualification testing in a thermal vacuum environment, the S191 cooler experienced several runs with degraded performance and finally failed to start. At this point in time, the manufacturer of the cooler had gone out of business, thus it was not possible to procure additional coolers nor, more importantly, was there anyone available

to conduct a failure investigation and perform the necessary corrective action. The cooler program was on a very close schedule and the qualification failure had significant impact. In order to meet the Skylab launch date, the flight cooler had to be delivered to the experiment contractor by June 1972.

The S192 coolers failed while in systems test at the experiment contractor's facility in April 1972. The primary result of the failure was the inability to cool the infrared detector to its required operating temperature. Three coolers failed within a two-week period of time. For this experiment, the flight cooler was required in July 1972, to phase into Skylab checkout without impacting the launch schedule.

Thus, JSC faced a situation where a functioning cooler was not available for either S191 or S192; the cooler was not qualified; and the schedule was critical. These facts necessitated two concurrent programs.

First, JSC embarked on a cooler refurbishment program which included additional development activities, the qualification test program, and the delivery of the required flight hardware. Because of the exclusive nature of the contracts between the cooler manufacturer and the experiment contractors, drawings, assembly procedures, manufacturing specification or names of component vendors (e.g., bearing manufacturer) were not available. Furthermore, the true performance capabilities of the cooler, including the off-nominal performance characteristics, were not available. Finally, no replacement components were available for the eight coolers in this program.

The parallel program involved the procurement of a new cooler from an alternate source. This new design had increased weight and electrical power requirements; it also entailed major changes in both the S191 and S192 cooler/experiment interfaces. In view of these facts, in addition to the Skylab budget constraints, this contracted effort was terminated as soon as the success of the JSC refurbishment effort was demonstrated.

FAILURE DESCRIPTION AND CORRECTIVE ACTION

Because the observed failure characteristics of the S191 cooler could have been due to several failure modes, the disassembly and inspection of the cooler was very methodical. The gas pressure was measured and gas analysis was performed. It was determined that the outer case did not have a proper shrink fit. The initial disassembly inspection showed large quantities of electric motor carbon brush particles. When the motor was removed, it was discovered that the brushes were so badly worn that the lead wire inside the brush had worn a groove in the commutator. The probable cause of the failure was excessive brush wear. This resulted from choosing a brush which could not provide the proper lubrication of the commutator when operating in the

dry helium atmosphere. The cooler performance degradation (prior to the final failure) was probably the result of contamination of the working fluid by brush material.

The corrective action was to redesign the motor; this included the design of a new brush which would operate properly in a helium environment. A number of the materials in the motor were changed to materials which would not out-gas as readily. The final corrective action was to incorporate the necessary quality assurance provisions in the cooler assembly procedures to preclude contamination.

When the S192 coolers were disassembled, one minor internal difference from the S191 cooler was noted. This difference was a small part secured by the main bearing hanger screw (see Figure 4a). Because of the manner in which this piece was attached, an adverse moment was imparted to the main bearings. This resulted in a premature failure of the main bearings and one of the rod bearings; the other main and rod bearings were affected, but to a lesser degree. This was the primary failure on all of the S192 coolers. Since the original function of the part in question could not be determined, it was decided to leave the part in place, but modify the mounting fixture to alleviate the adverse moment. The modification is shown in Figure 4b. The final corrective action for the S192 was to replace the original electric motors with those which had been redesigned for S191.

REFURBISHMENT PROGRAM

The preliminary activity of the JSC refurbishment program included the initial disassembly of a failed cooler and the determination of the physical characteristics. Two S191 coolers were originally delivered, a failed cooler and a disassembled cooler. The components from the disassembled cooler were used to determine the physical characteristics of the cooler components. After an extensive study of these components, a complete set of drawings was prepared. Since these coolers were flight items, a strict reliability and quality assurance program had to be implemented.

Concurrent with the component evaluation, the disassembly of the failed cooler was initiated. Since no drawings or disassembly procedures were available at this time, the disassembly of the cooler was performed very meticulously. Still photographs and movies were taken of each disassembly step. This information was used as the basis for writing both the disassembly procedure and the assembly procedure. Although drawings of the physical components were in work, a majority of the tolerances, alignments, and materials used were unknown. A program was initiated to determine materials used for piston rings, sleeves, o-rings, and lubricants. Since the source of the original bearings was not known, an investigation was performed to determine the availability of the required bearings. Then a program was initiated to

determine the type of bearing lubricant and the lubricant packing density required for optimum operation. Regenerator flow checks were made before and after disassembly to ensure proper reassembly. Extensive tests were also performed on the original piston sleeves and rings. These tests included "blow-by" tests and "pull-through" tests to evaluate the mechanical fit of the pistons in the cylinders.

After all of the subassembly tests and procedures had been determined, the assembly procedures were written. These procedures contained the step-by-step operations required to physically assemble the cooler components and instructions for various component level tests required prior to assembly. Although the majority of the assembly was straightforward, several sections were extremely critical. The most important of the areas was the block/crankshaft assembly. The criticality of this assembly was in the bearing alignment and the proper ring and pinion gear alignment. A fixture was manufactured in-house which provided for the measurement of gear mesh, and the gears were then shimmed to provide the proper tolerances.

During the course of the refurbishment program, certain failures were encountered which required component modification and are discussed below.

Outer Case.— During the installation of the first bimetallic outer case, it was discovered that a leak had developed at the bimetallic joint. The remaining bimetallic cases were examined by X-ray and dye penetrant techniques and found to contain flaws which were aggravated by the outer case installation, which was a shrink fit. However, extensive thermal analyses indicated that the heat transfer characteristics of the cooler were not adversely affected by the use of an all stainless steel case. Therefore, stainless steel outer cases were manufactured at JSC for both the S191 and S192 coolers.

End Cap.— Problems were encountered during the program with the end cap leakage. This leakage normally occurred around the electrical connector and was probably caused by repeated welding on the same end cap each time a cooler was refurbished. Therefore, the task of designing and procuring a new type of end cap was assigned to the S192 experiment contractor. These end caps were procured, delivered, and used on the S192 flight coolers and the S191 flight backup cooler. The S191 prime flight cooler was delivered with the original end cap.

Piston Rings.— When the S192 cooler was reassembled and tested, its performance still would not meet the necessary requirements. Intensive examination revealed that the Rulon piston rings were out-of-round. This condition was probably a result of the bearing failures. The corrective action for this failure was fabrication of new piston rings. However, this required an extensive effort to develop a "piston-fit" test which would provide the ring clearances necessary to achieve proper cooler performance. (The S191 flight unit was delivered with the original rings and sleeves.)

Low Temperature Start.— Testing of the S191 coolers revealed that a problem did exist on low temperature starts. Although the cooler would start, the cool-down times and minimum detector temperatures achievable were severely affected on starts which were performed at case temperatures of 288°K (60°F) or lower. This behavior was attributed to the different thermal expansion rates of the piston rings, sleeves, and cylinder walls. At the cold temperatures, the fit of the piston rings and sleeves in the cylinder did not provide compression. Tests indicated that if the piston rings were sized to provide proper compression at a case temperature of 280°K (45°F), the ring friction was excessive at the higher case temperature. Extensive thermal analysis of the normal mission duty cycle indicated the minimum case temperature would be approximately 293°K (67°F), thus an operational constraint of 292°K (65°F) for cooler starts was established.

FINAL ASSEMBLY AND CHECKOUT

When the assembly was complete, additional time was required to ensure satisfactory cooler performance prior to shipment. The procedures required after assembly, but prior to shipment of production units, are discussed below.

Helium Servicing.— These procedures specified the method for charging the cooler with helium prior to the bench and performance tests. This procedure was the same for both S191 and S192 coolers.

Bench Test.— This test provided (1) a run-in period to ensure proper ring and sleeve and motor brush seating, (2) a cooling capacity test to determine the cool-down time required to reach 90°K (-297°F) and (3) capacity test designed to determine the cold end temperature which could be maintained at 28V high speed, 24V high speed, and 24V low speed. In addition, the S192 bench test provided for a start with a cooler case temperature of 319°K (105°F) and a simulated mission profile.

Outer Shell Installation.— This procedure was the same for both experiment coolers. The procedure provided the methods for shrink fitting the outer case over the cooler and electron beam welding the flange and end cap to the outer case.

Performance Test.— After the outer shell had been installed, the helium servicing procedure was again performed, and the servicing tube was pinched to provide a hermetically sealed unit. The performance test was then performed. This test was essentially a repeat of the bench test, excluding the run-in, to verify that no cooler damage had occurred during the outer shell installation.

Final Acceptance Tests.— These tests were different on the S191 and S192 coolers because of the different design uses. The S191 test consisted of a nominal performance test (27V high speed, 317°K (110°F) environment), low voltage test (26V high speed, 317°K (110°F) environment), and a vibration test to determine the maximum displacement of the cold end during operation. The S192 acceptance test consisted of a nominal performance test (28.5V high speed start with a switch to 24V low speed at 90°K (-297°F) while maintaining a 297°K (75°F) environment), a high temperature-low voltage test (27.5V high speed start with a switch to 24V low speed at 90°K (-297°F) while maintaining a 314°K (105°F) environment), a low temperature-low voltage test (27.5V high speed start with a switch to 24V low speed at 90°K (-297°F) while maintaining a 286°K (55°F) environment and a cold end self-induced vibration test.

THERMAL QUALIFICATION TEST PROGRAM

The qualification test for the S191 coolers was performed at JSC White Sands Test Facility. The test was performed with the cooler installed in the S191 spectrometer. The test profile included temperature and voltage limits, minimum restart time, and nominal and off-limit mission duty cycles. The cooler performance for each of the tests was satisfactory except for the low temperature start. Although the cooler did start and cool down to the prescribed temperature at a case temperature of 288°K (60°F), the time required to achieve the operating temperature of 90°K (-297°F) was excessive. However, as previously mentioned, an operational constraint was imposed to reflect a minimum case temperature of 292°K (65°F); the retest for this condition was successfully accomplished. Since the operational conditions for the S191 were more severe than the S192, the qualification for the latter was by similiarity except for one test sequence. The low speed, high case temperature 314°K (105°F) condition was run with a simulated S192 experiment interface (i.e., heat pipe). This sequence completed the qualification testing for S192.

FLIGHT APPLICATION

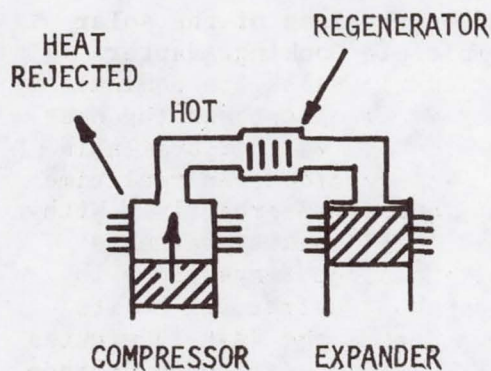
During the cooler refurbishment program, seven coolers were completely rebuilt a total of thirteen times. This included the three flight qualified coolers, two backup flight units, qualification unit, design evaluation test unit, life test cooler, and coolers for other types of test activities. For flight, the S191 had a primary flight unit and one backup cooler. The S192 experiment had two flight units, a primary and a spare which the crew could change; S192 also had a backup flight cooler. The S192 had a signal noise problem, so the backup cooler was taken up and installed by the crew of Skylab IV. The flight performance of all the coolers was excellent.

The S191 cooler had a problem during the early phases of the first Skylab mission. The problem was directly related to the loss of the solar cell panel on Skylab I. The temperature of the Multiple Docking Adapter (MDA), which contained the EREP, decreased significantly below its nominal operating temperature. This temperature reduction occurred because the heat dissipated from the EREP electronics and other subsystems was not available due to the reduced electrical power. A procedure was developed in real time to increase the cooler temperature; the unit then functioned properly. With the installation of the Skylab parasol, electrical power became available for operation of subsystems in the MDA. This increased the temperature in the MDA, and consequently, brought the cooler case and temperatures to its proper level. No further problems were encountered until the last 15 minutes of the S191 mission; at this point, the cooler performance started to degrade. The S191 was able to complete its mission, even with the degraded performance. Since the qualification design life of the cooler had been exceeded, the performance was considered out of specification, but not a failure.

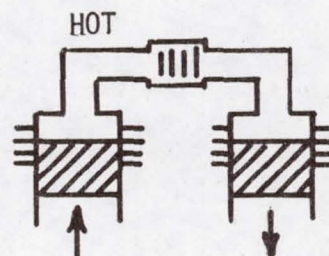
The S192 primary cooler performed with no anomalies throughout its flight life. As mentioned previously, due to a signal noise problem, the backup cooler with a detector of a new design was installed by the Skylab IV crew. This eliminated the signal noise problem, which indicated that the source of the noise was not inherent in the cooler design. The backup cooler operated satisfactorily for the remainder of the mission.

REFERENCES

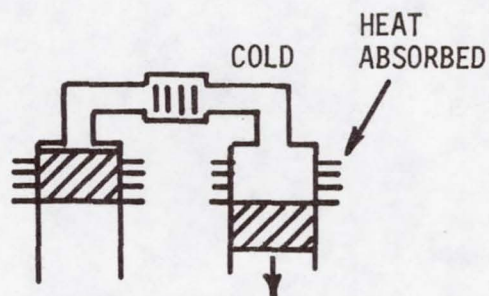
1. Barron, R.: Cryogenic Systems. McGraw-Hill Book Co., Inc., 1966.



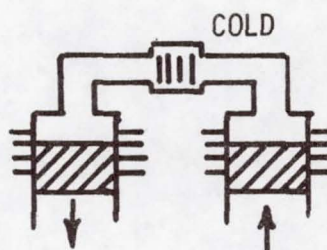
1-A. ISOTHERMAL COMPRESSION
(Heat Rejected in)
After-cooler



1-B. CONSTANT-VOLUME HEAT TRANSFER
(Heat Transfer From)
Fluid to Regenerator



1-C. ISOTHERMAL EXPANSION
(Heat Absorbed From)
Infrared Detector



1-D. CONSTANT VOLUME HEAT TRANSFER
(Heat Transfer From)
Regenerator to Fluid

Figure 1. Fundamental Thermodynamic Processes for
Stirling Cycle Refrigerator

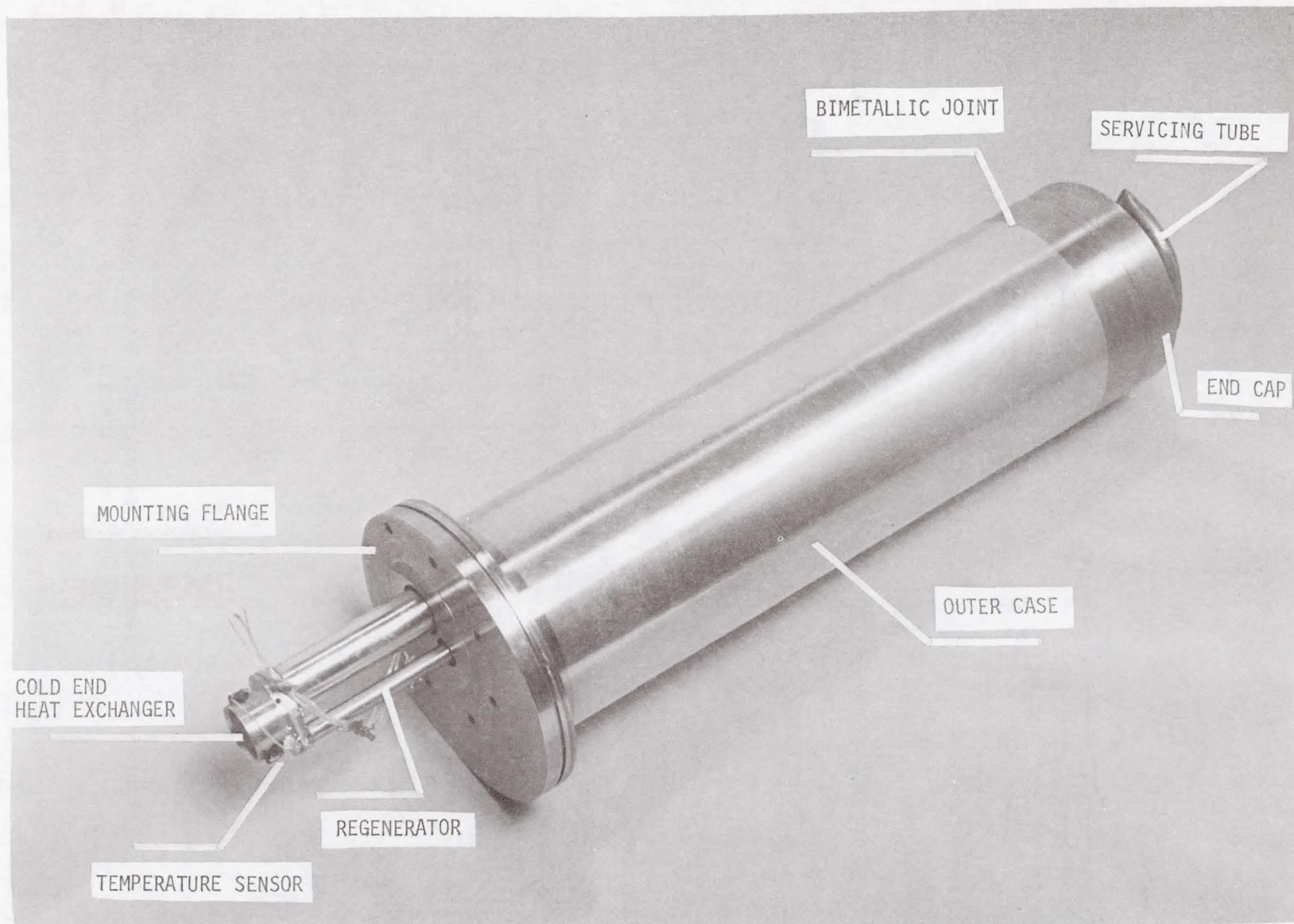


Figure 2a. Overall View of S191 Cryogenic Cooler

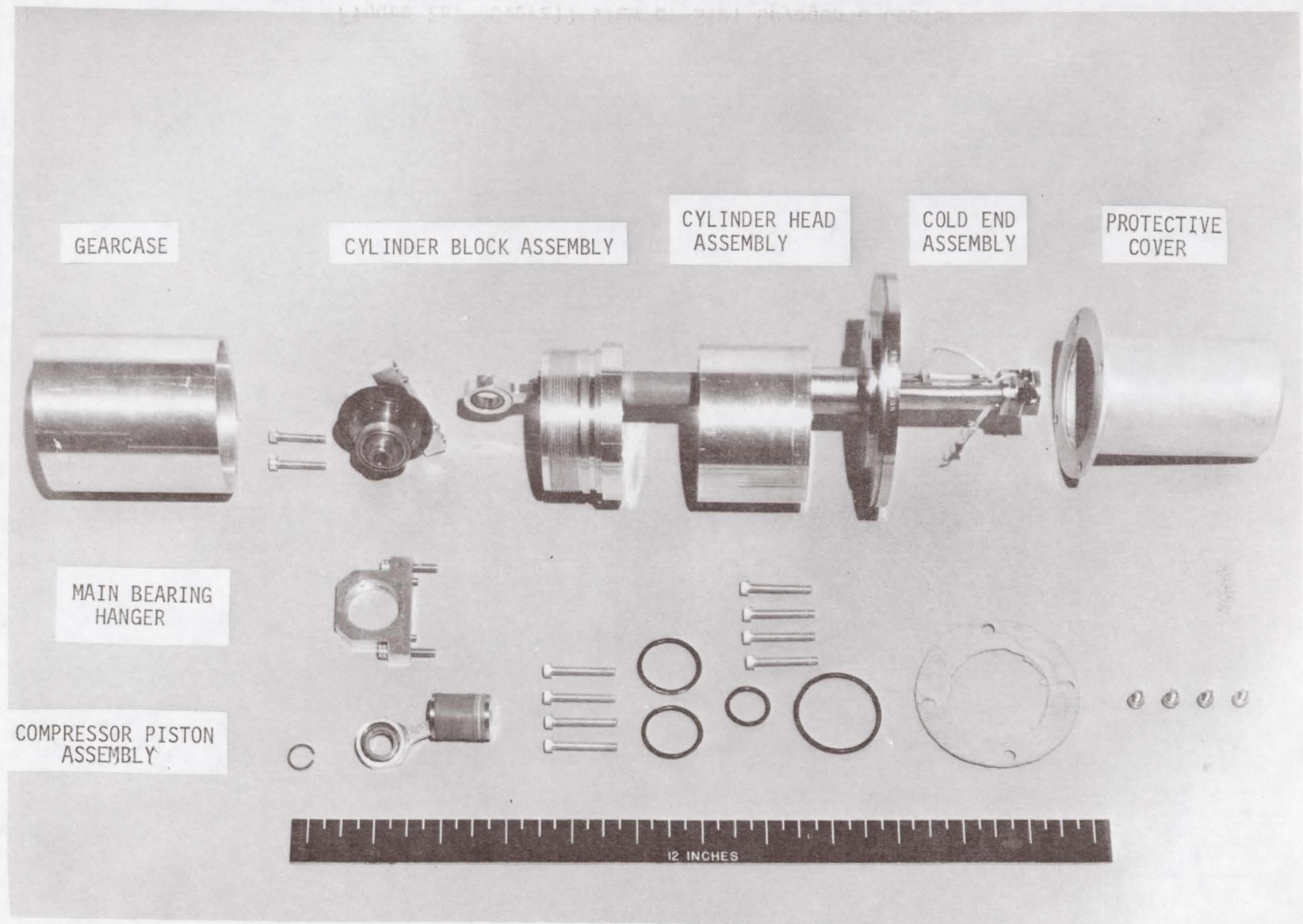


Figure 2b. Exploded View of S191 Cryogenic Cooler (Less Drive Motor and Outer Case)

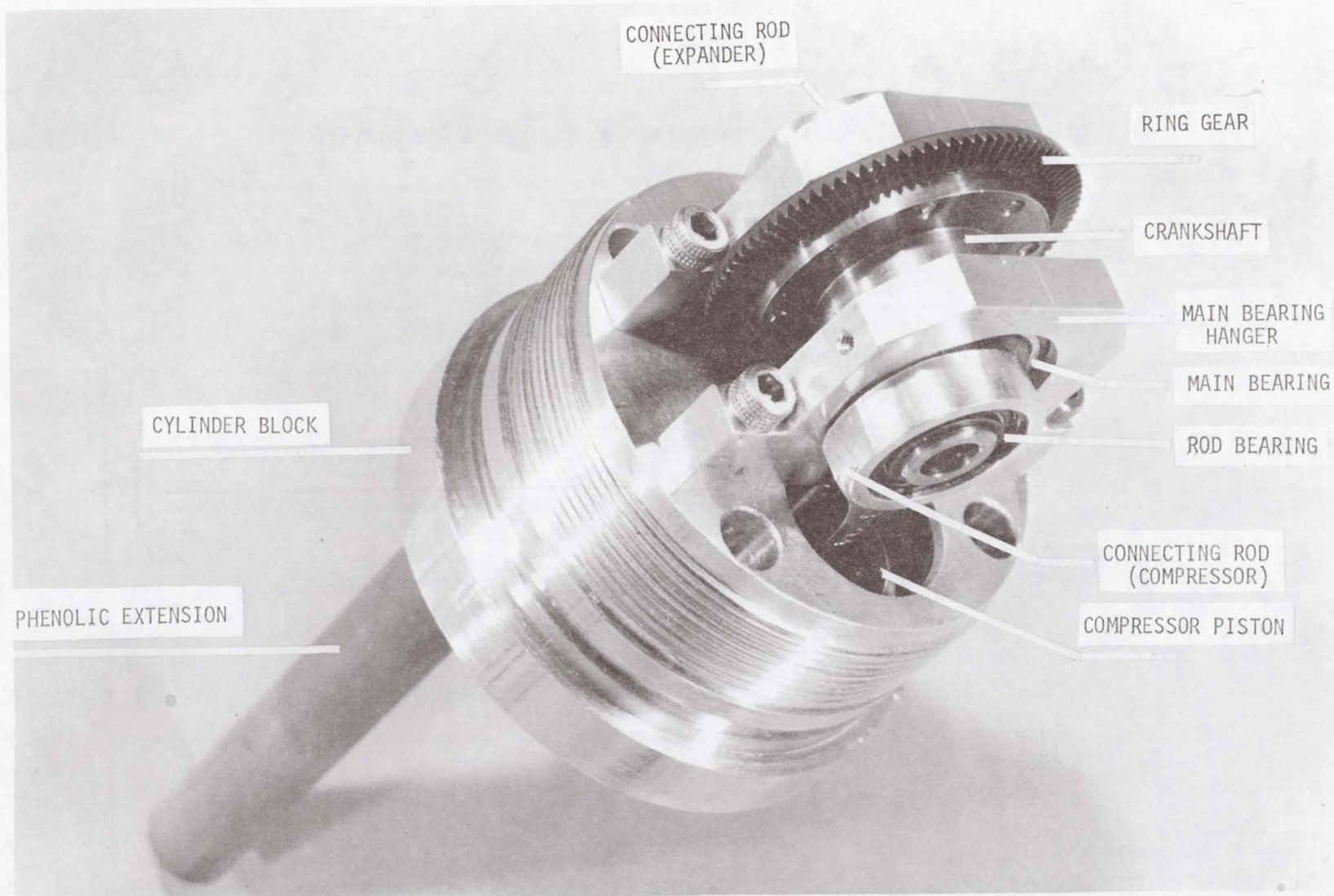


Figure 3. S191 Cylinder Block Assembly

NOTE: NOT TO SCALE - EXPANDED
TO SHOW DETAILS

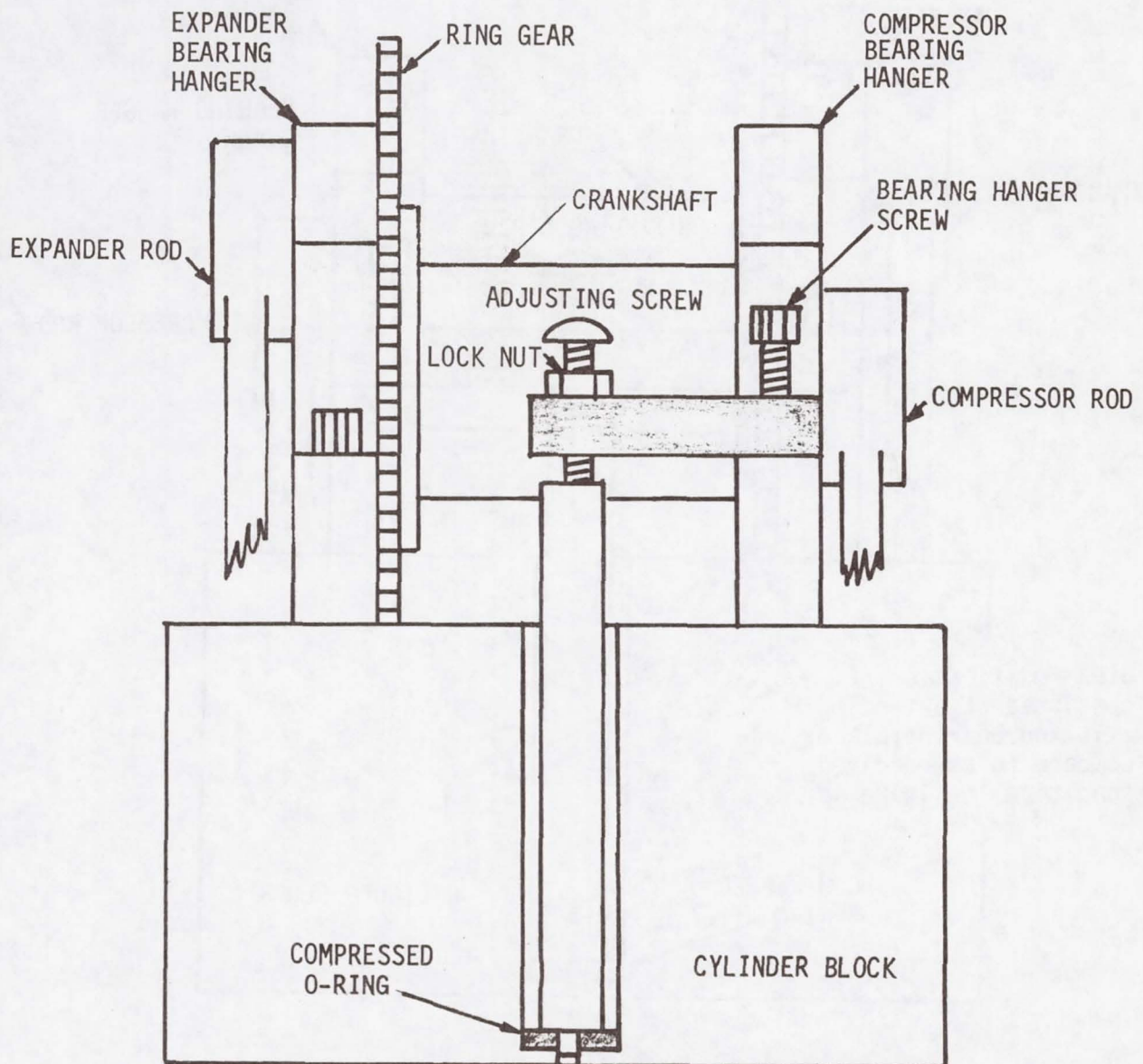


Figure 4a. S192 Cooler Main Bearing Support (As Received)

NOTE: NOT TO SCALE - EXPANDED
TO SHOW DETAILS

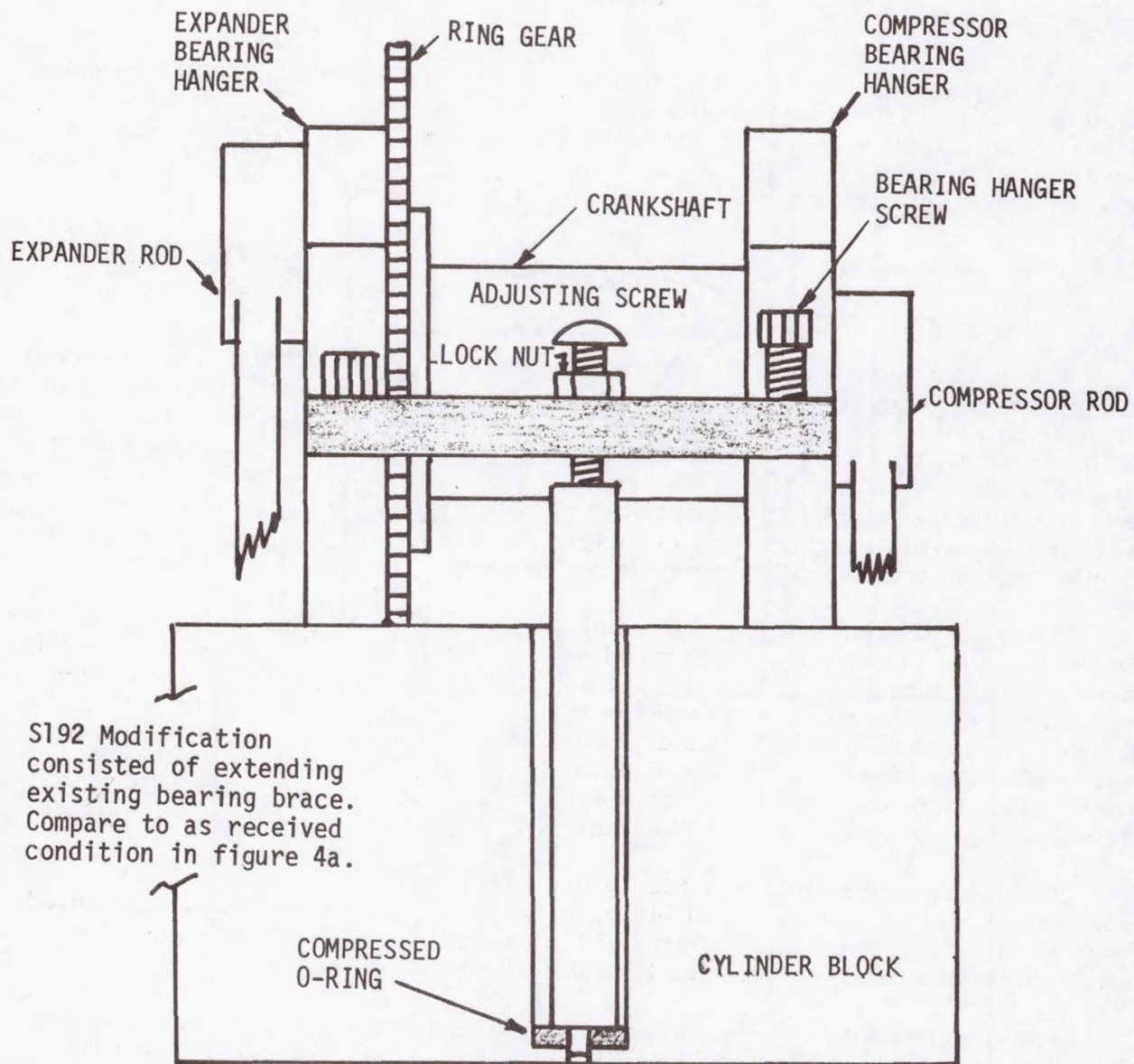


Figure 4b. S192 Cooler Main Bearing Support (As Required)

11. SKYLAB TRASH AIRLOCK*

By Larry R. Price

McDonnell Douglas Astronautics Company

SUMMARY

The Skylab Trash Airlock (TAL) was used throughout the Skylab mission to transfer trash materials that could support microbial growth from the pressurized cabin to the unpressurized waste tank. The TAL, which uses several basic mechanisms, was successfully operated daily for the 170 days of manned missions for a total of 637 cycles.

TRASH MANAGEMENT APPROACH

Trash management for Skylab was a challenging problem. The expected trash volume from three crewmen for a total of 140 days (actual duration of manned mission was approximately 170 days) was predicted to be 36.8 m^3 (1300 cubic feet). This volume was more than could be conveniently stored in the cabin. Also, much of this trash (wet wipes, food containers, urine, etc.) could support microbial growth that could be a health hazard. In addition, to avoid contamination of experiments and minimize general pollution of space, trash could not be ejected into the spacecraft environment.

The resulting approach was to collect trash in bags at specified locations in the cabin. Trash was categorized and collected separately as biologically active or not biologically active. At appropriate times, usually daily, the biologically inactive trash bags were transferred to storage areas within the pressurized volume, and the biologically active trash was transferred to an unpressurized aft portion of the Orbital Workshop identified as the waste tank. This tank was internally screened and vented so that only vapor would escape from the Spacecraft. The general configuration is shown in Figure 1.

This approach required a highly reliable device that would allow convenient and safe transfer of biologically active trash in closed but vented bags from the pressurized cabin at 34.5 kPa (5 psi) to the unpressurized waste tank at a pressure of less than 0.607 kPa (0.088 psi).

The device designed and developed to meet those requirements was the Trash Airlock Assembly, McDonnell Douglas Astronautics Company part number 1B81491-1. The airlock is mounted on the bulkhead between the cabin and the waste tank at the centerline of the spacecraft. Figure 2 shows the TAL installed in the Skylab in its launch configuration.

*This work done under the sponsorship of NASA's Marshall Space Flight Center and Johnson Space Center, Contract NAS9-6555. NASA's U.S. Patent No. 3,807,656 on the Skylab Trash Airlock is available for licensing under NASA Patent Licensing Regulations 14 CFR 1245.2 by writing Patent Counsel, George C. Marshall Space Flight Center, Alabama 35812.

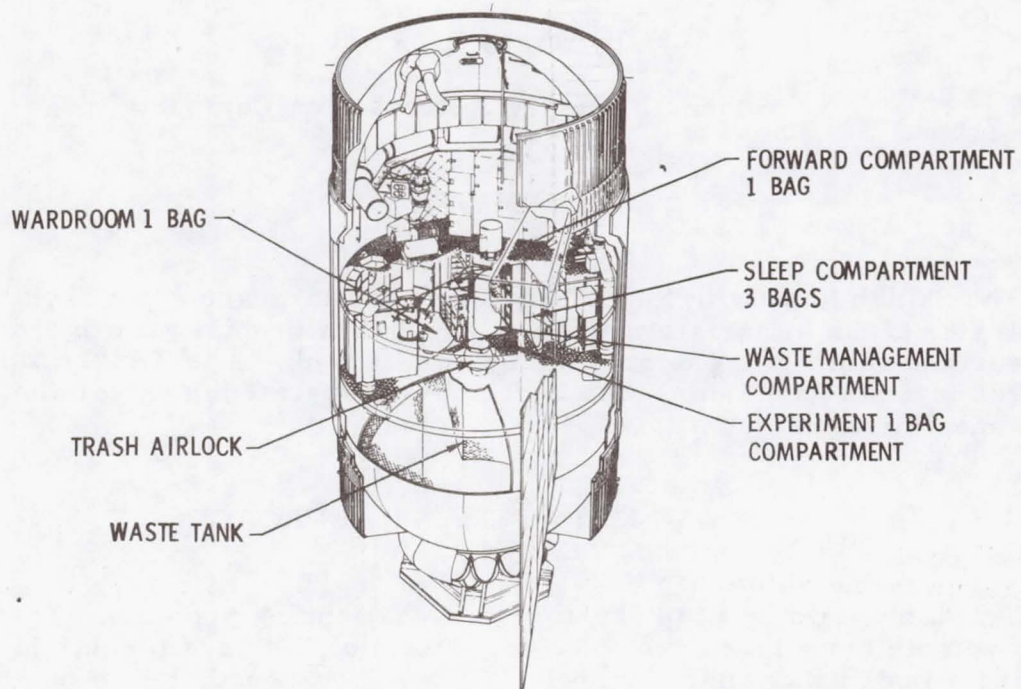


Figure 1. Trash Disposal Subsystem

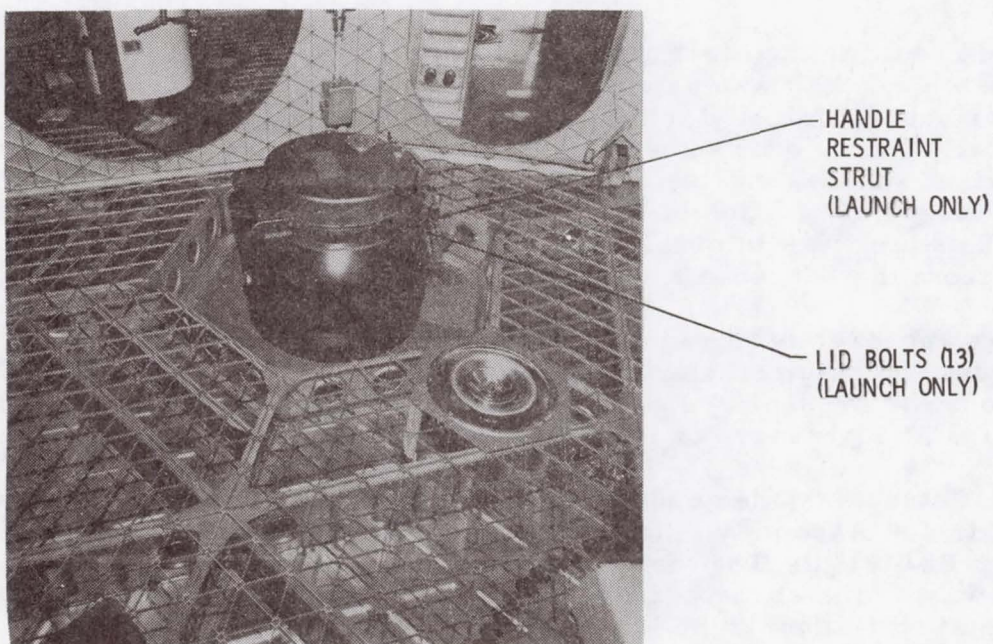


Figure 2. Launch Configuration Trash Airlock

GENERAL DESCRIPTION AND OPERATION

The trash disposal airlock assembly is a pass-through chamber built into the waste tank common bulkhead and extending through the floor into the cabin. Each side of the chamber is equipped with a hatch, forming an airlock (Figure 3). The airlock is equipped with a pressurization valve that ports the airlock to either the cabin or the waste tank, as required. On orbit, the trash disposal airlock is normally vented to the waste tank. The airlock body is spherical, approximately 610 mm (24 inches) in diameter, and has a pressure gage for viewing by the crew. It is equipped with a mechanical ejector to transfer the waste material to the waste tank. The functional steps of the operation cycle of trash disposal from the habitation area are as follows (see Figure 4):

1. Valve/outer door handle—pressure 34.5 kPa (5 psi) (verify).
2. Lid—unlock and open.
3. Insert trash bag.
4. Lid—close and lock.
5. Valve/outer door handle—close and vent [verify 3.45 kPa (0.5 psi)].
6. Valve/outer door handle—open.
7. Ejector handle—eject return to close.
8. Valve/outer door handle—close and vent.
9. Ejector handle—retract.

DESCRIPTION

The trash airlock is made up of the assemblies described below.

Lid Assembly (Figures 5 and 6)

The aluminum lid subassembly is the inboard door. It is a simple two-hinge door with a third friction hinge to maintain the lid in the open position. The lid contains a metal gasket with molded rubber seals on the top and bottom, which is removable and may be replaced with an on-orbit spare. The lid subassembly also houses the ejector mechanism.

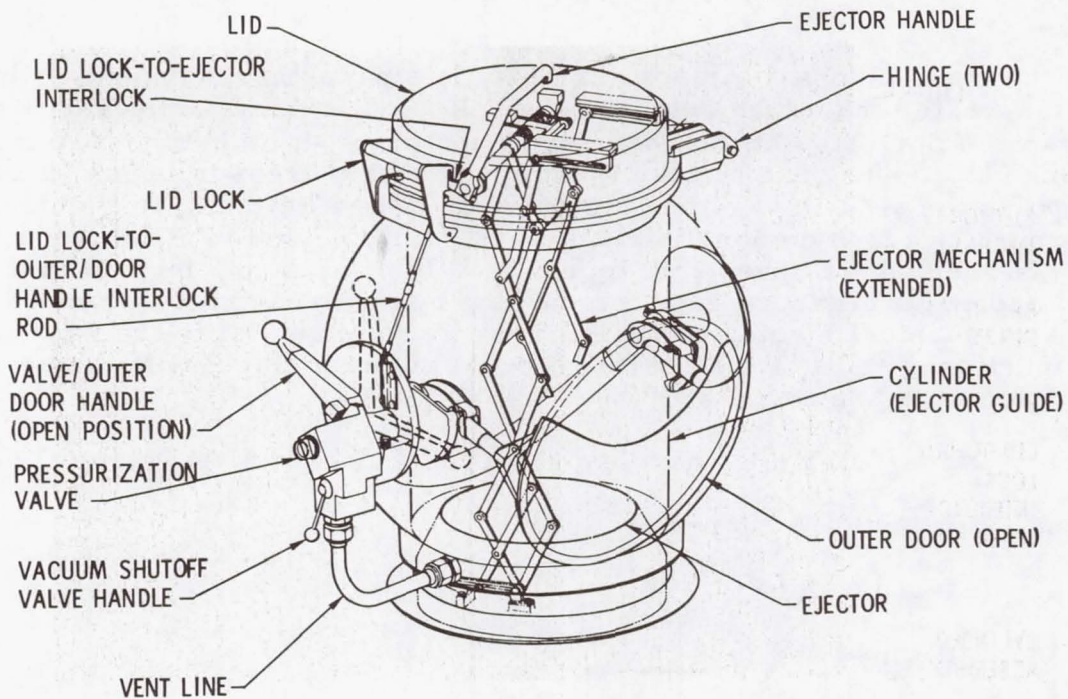


Figure 3. Trash Airlock

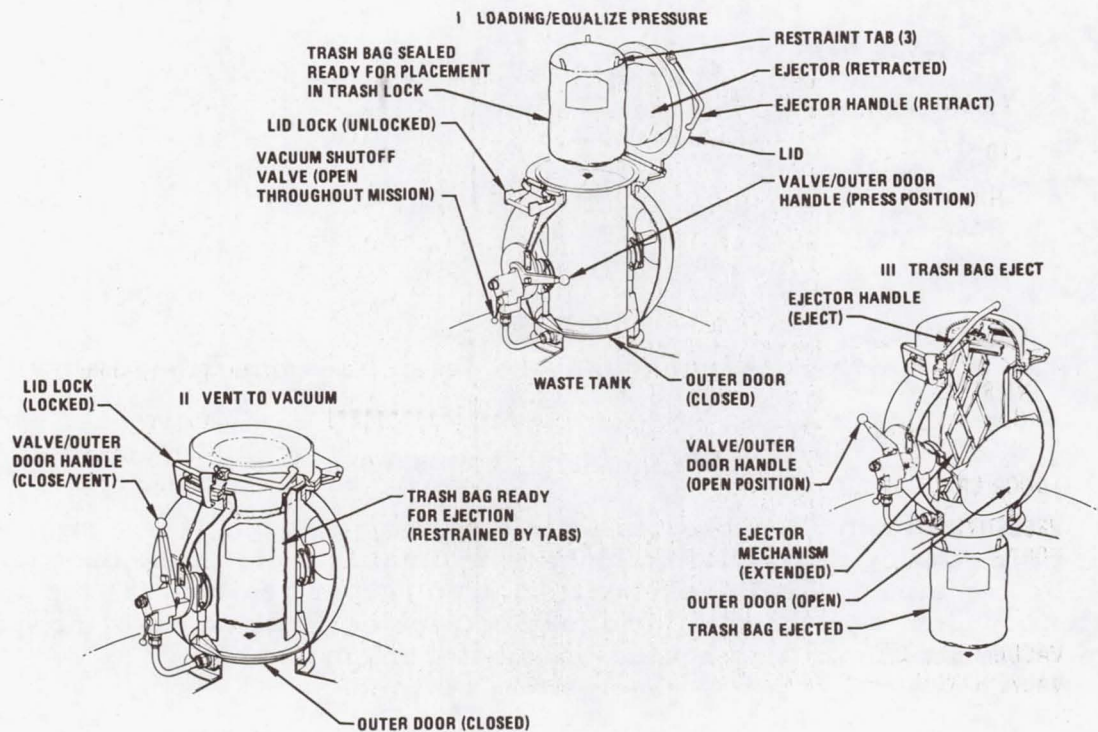


Figure 4. Operational Sequence

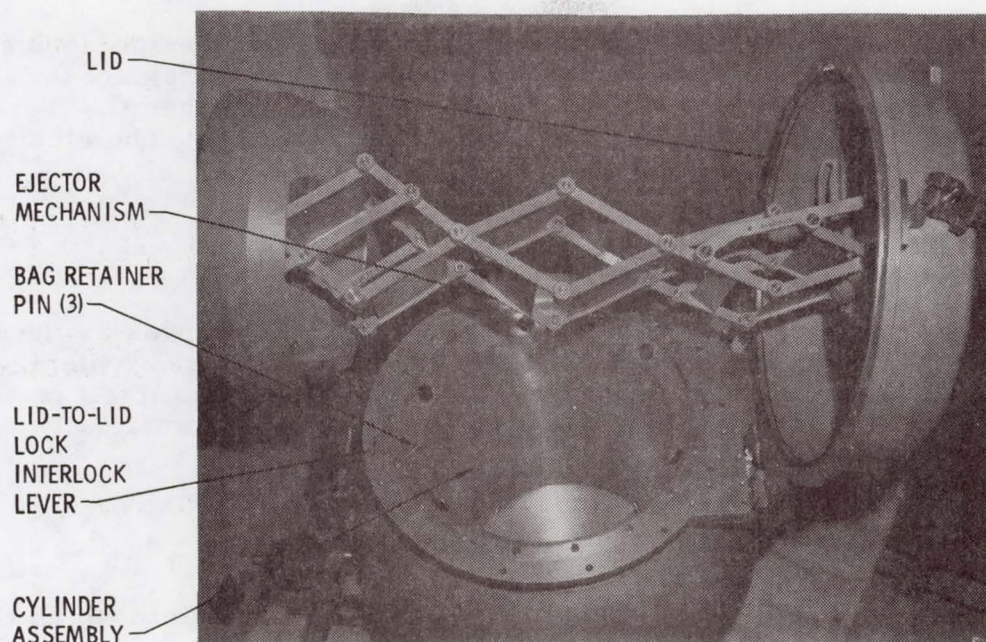


Figure 5. Lid and Ejector

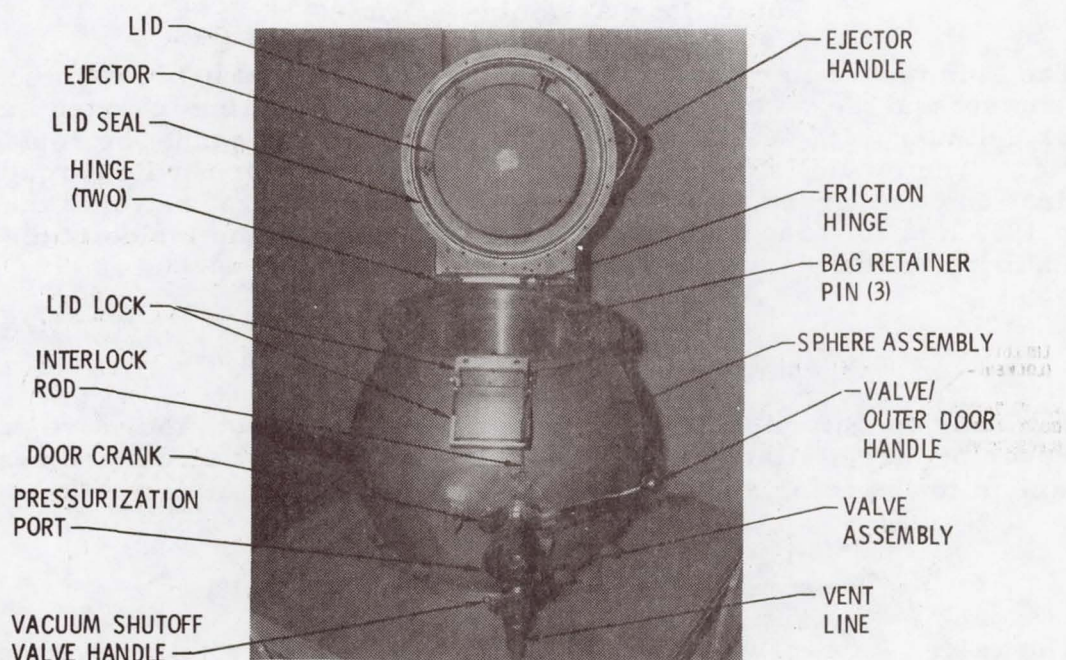


Figure 6. Trash Airlock Details

Trash Ejector Mechanism (Figure 5)

The trash ejector mechanism is a rigid scissors extension device operated by a crank arm with an overall mechanical advantage of 0.5. The mechanism is equipped with an ejection plate that pushes the trash bag into the waste tank when the ejection handle is raised. The ejector and scissors links are aluminum.

Sphere Assembly (Figure 6)

The aluminum sphere assembly is a weldment that serves as the pressure vessel and basic mounting structure for the mechanical system, which makes up the trash disposal operating system. The sphere itself is composed of six welded parts. The welds are made on an automatically programmed welding machine.

Cylinder Assembly (Figure 5)

The aluminum cylinder assembly is the compartment into which the trash bag is inserted before ejection into the waste tank. It is a smooth-walled cylinder 351.0 mm (13.81 inches) in diameter and approximately 559.0 mm (22 inches) long. Three steel pegs at the inboard circumference of the cylinder at 120 degrees hold the bag away from the outer door during opening.

Outer Door Assembly (Figure 7)

The aluminum outer door or "eyelid" forms the seal between the cabin environment and the waste tank vacuum when trash is being inserted into the airlock cylinder. Its seal is molded into the eyelid and cannot be replaced on-orbit. The eyelid is operated by the valve/outer door handle through a combination cam, crank, and over-center device that first retracts the eyelid 10.2 mm (0.4 inch) and then rotates the door on the inside of the airlock to clear the ejection port.

Valve/Outer Door Operator (Figures 8 and 9)

The door operator is a crank handle that operates both the valve and the outer door by direct attachment to the valve spool and by a cam and crank mechanism to the outer door operator. The parts are stainless steel.

Pressurization Valve Assembly (Figure 10)

The valve is a two-way, two-position valve using a rotating cylinder with O-rings to open and close ports. When the valve/outer door handle is in the PRESS position, the airlock is ported to the cabin. When the valve/outer door handle is in the VENT position, the airlock is ported to the waste

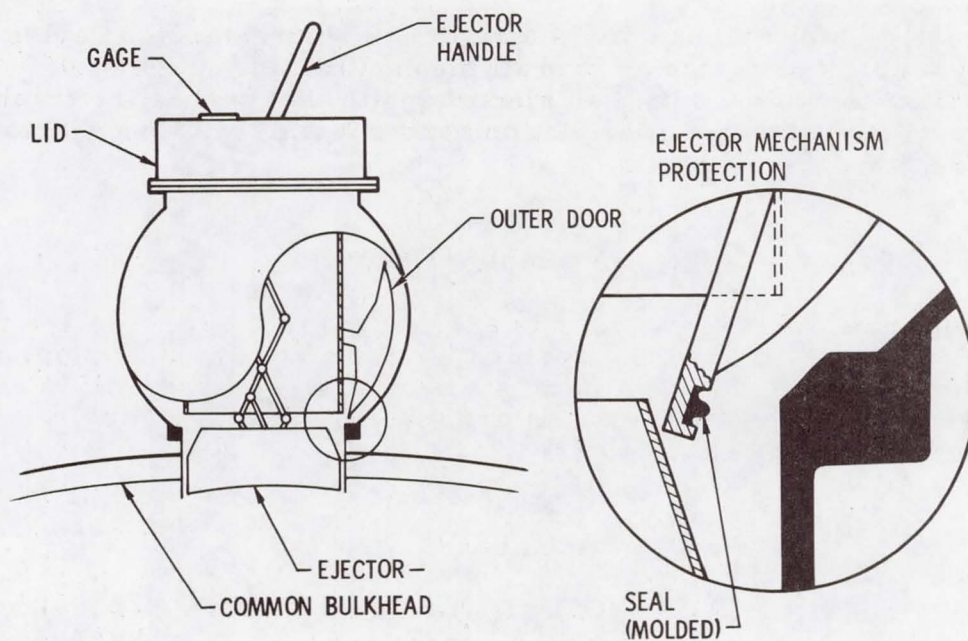


Figure 7. Outer Door and Ejector

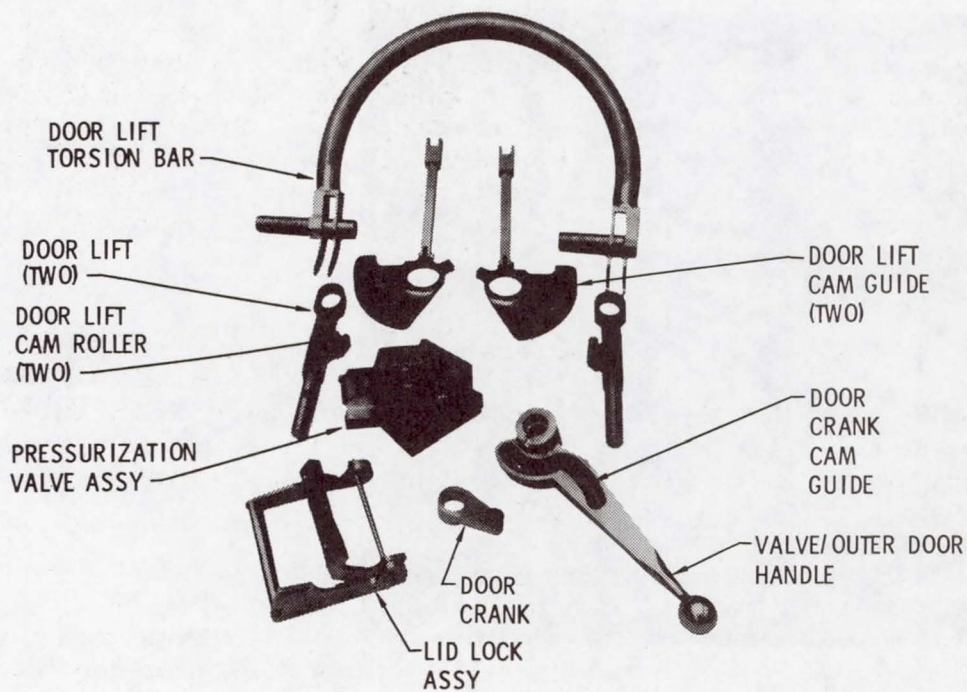


Figure 8. Trash Airlock Mechanisms

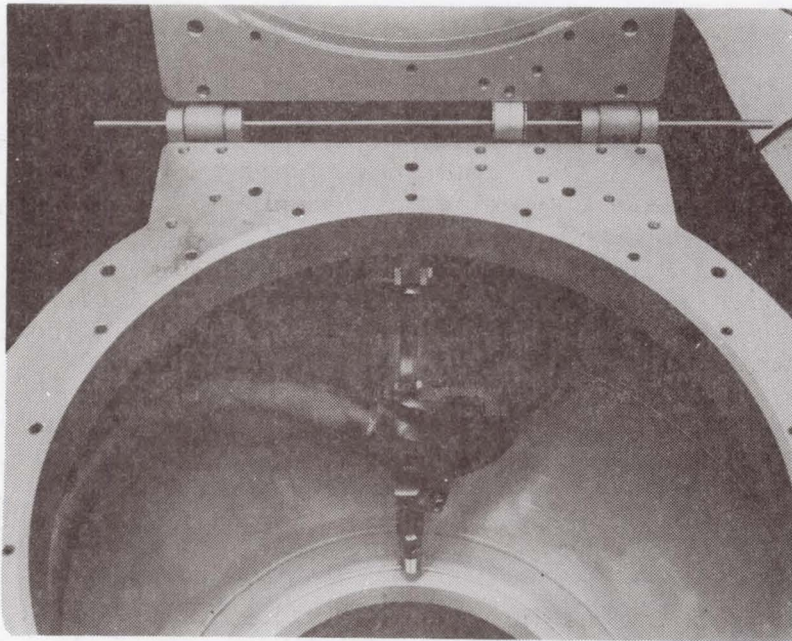
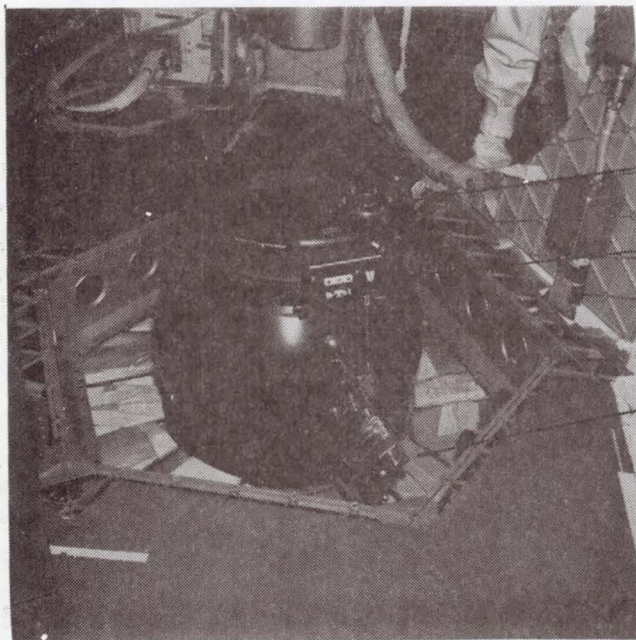


Figure 9. Door Lift Mechanism (Without Door)



PRESSURE GAGE

LID LOCK

PRESSURIZATION
VALVE ASSEMBLY

Figure 10. Operational Trash Airlock

tank. When the valve/outer door handle is rotated to the OPEN position, the airlock is still ported to the waste tank, although partially closed relative to the VENT position. The valve metal parts are stainless steel.

Absolute Pressure Gage (Figure 10)

The absolute pressure gage contains a bourdon tube pressure sensor housed in a sealed stainless steel container evacuated to provide the reference vacuum. The bourdon tube drives the needle through an amplifying linkage mechanism. The gage reads from zero to 103.4 kPa (15 psi) but will take pressures up to 310.2 kPa (45 psi) without degradation. The gage indicates when the airlock has completed pressurization or depressurization. The gage may also be used for trouble shooting for leaks by indicating pressure decay or vacuum degradation.

Lid Lock (Figures 6, 8, and 10)

The stainless steel lid lock is an over-center cam device with a large mechanical advantage. It performs the following:

1. Unlatches the lid, making it possible to raise the lid for inserting trash.
2. Provides an over-center latch to compress the lid seal to ensure a pressure seal when the airlock is exposed to the waste tank vacuum. Cabin pressure aids in compressing the seal further when the airlock is depressurized.

DESIGN FEATURES

The trash airlock is designed to perform normally in the 34.5 kPa (5 psi) cabin environment. Its life is based on five operations a day for 140 days at cabin ambient temperatures. Its proof pressure is approximately 68.9 kPa (10 psi) differential and is capable of withstanding a launch malfunction differential pressure of 179.2 kPa (26 psi) in either direction without damage.

The TAL includes the following safety interlocks:

1. Lid Lock-to-Valve/Outer Door Handle (Figure 3) — The valve/outer door handle must be in the PRESS position before the lid lock can be unlocked. This prevents opening the lid with the valve in the VENT position or with the outer door open.
2. Lid-to-Lid Lock (Figure 5) — The lid must be closed before the lid lock can be retracted. This prevents closing the lid lock with the lid open, which would allow overriding the lid lock-to-valve/outer door interlock.

3. Ejector Handle-to-Lid Lock (Figure 3) – The ejector must be retracted before the lid lock can be unlocked. This prevents unlocking and opening the lid with the ejector extended.

The following summarizes other significant features.

1. Total Gas Volume: 0.1218 m^3 (4.3 ft^3).
2. Transfer Tube Size: 350 mm (13.8 inches).
3. Trash Capacity: 350 mm dia. by 457 mm (13.8 inches dia. by 18 inches).
4. Overall Size: See Figure 11.
5. Weight: 71.7 Kgm (158 lb).
6. Microbial Control: May be evacuated between operations.

FLIGHT EXPERIENCE

The trash airlock was used successfully throughout the three missions. Although there were no malfunctions of the airlock, there were several operational difficulties that were successfully resolved. Figure 12 shows astronaut Gerald Carr operating the TAL in space.

There were two incidents of near jamming, which were attributed to overfilled trash bags. Further problems were avoided by better control of trash combinations during disposal.

It was noted during the first manned mission that the valve handle could be inadvertently kicked into or left in an intermediate position between the pressurize and vent positions, which caused a cabin atmosphere leakage of as much as 1.5 Kgm/hr (3.3 lb/hr). This problem was overcome by strapping the handle in the PRESS position between operations.

During the second manned mission, an operating characteristic of the airlock was highlighted. The manual force required to squeeze the lid during the initial portion of the latching operation is high. This high force characteristic is more significant in weightlessness because body restraint is difficult. It was found that the high force of latching could be overcome by proper technique or use of two crewmen.

Although the trash airlock was used to approximately 80% of the expected on-orbit operation with no malfunction, there are two improvements recommended for future use. First, a detent device should be added to the valve handle to positively maintain the valve handle in the PRESS or VENT positions between operations. Second, the squeeze force during latching should be reduced. This could be done by refining the hinge gap adjustment by shimming or changing to a softer rubber for the lid seal.

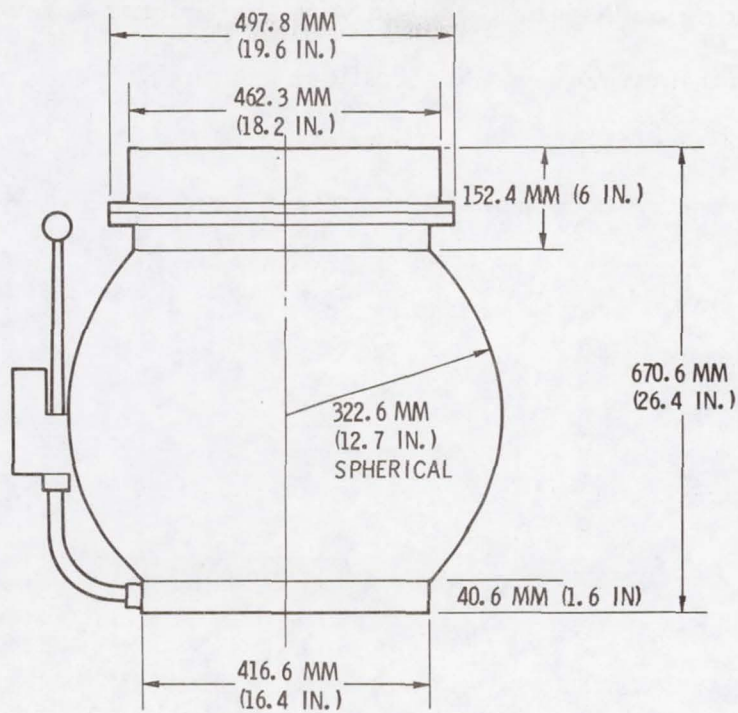


Figure 11. Overall Dimensions



Official NASA Photo

Figure 12. Astronaut Gerald Carr Operates Trash Airlock in Space

12. A PRECISION SIX-METER DEPLOYABLE BOOM FOR THE MARINER-VENUS-MERCURY '73 MAGNETOMETER EXPERIMENT

By Harry F. Burdick

Goddard Space Flight Center

SUMMARY

A unique deployable boom has been developed for accurately positioning magnetometers 6 meters (19.7 feet) from a spacecraft. Position accuracy within $\pm \frac{1}{2}^\circ$ can be maintained. Weight, mounting system, magnetic cleanliness, thermal dimensional stability, and natural frequency were critical constraints that were met. The boom was flown on Mariner 10 and deployed flawlessly. The design, development, and testing of the boom and optical alignment of the sensors are described. Design trades and problem solutions are discussed.

INTRODUCTION

A Goddard Space Flight Center Magnetic Fields Experiment was one of the science instruments on the Mariner 10 (Mariner-Venus-Mercury '73) mission launched November 3, 1973. This experiment was designed to measure the magnetic fields in interplanetary space and during Venus and Mercury encounters. Since the Mariner type spacecraft was not designed to be magnetically clean, the effect of the spacecraft field had to be determined. This was accomplished by providing a 6 meter (19.7 foot) long deployable boom that would place three orthogonal fluxgate sensors seven meters from the spacecraft Z axis and a second set of sensors 4.5 meters (14.7 feet) from this axis.

Unique design restraints were imposed by spacecraft and experiment considerations. The length of the boom when folded about its two hinged joints for launch was 3 meters (9.8 feet). This length precluded end restraint using the spacecraft structure. End tie-down was obtained by latching to the solar array tip tie via a swivel fitting and tie rod. The lack of rigid restraint of this end and the large excursions of the solar panel during ascent imposed high dynamic loads on the boom and sensors. In addition, possible dynamic interactions of a long boom with the Mariner three-axis stabilization system required a minimum natural frequency of 0.57 Hz.

REQUIREMENTS

Some significant design requirements of the boom are listed below.

1. Deploy an outboard magnetometer package to a maximum practical distance ($\geq 6\text{m}$) (19.7 ft) from the Z axis.
2. The outboard magnetometer axes should be known throughout the mission within $\pm\frac{1}{2}^\circ$ with respect to the spacecraft axes.
3. Deploy a second magnetometer package inboard of the first by approximately 2m (16.6 ft). The axes should be within $\pm\frac{1}{4}^\circ$ of the first package.
4. The natural frequency of the supporting boom should be 0.57 Hz minimum.
5. The temperature range of the sensors must be controlled.
6. The supporting boom must be compatible with the spacecraft and launch vehicle constraints.
7. Nonmagnetic materials shall be used wherever possible.

DESIGN FEATURES

A. Deployment Sequence

The boom in the prelaunch configuration is folded about its two hinged joints. One hinge (inboard hinge) is attached to an out-rigger on the spacecraft body. The other hinge (outboard hinge) joins the two tubular boom sections. Figure 1 illustrates the deployment sequence.

Simultaneously with release of the two spacecraft solar panels, the tie rod on the outboard hinge is released. The first stage of deployment takes place with the two boom elements latched together rotating through an angle of 106° . At completion of that phase, lockup of the inboard hinge takes place and the outboard element is released by a sequencing mechanism which is incorporated in the inboard hinge. The outboard element then swings through an angle of 180° and locks in place to complete the deployment. All mechanical functions were monitored by switches.

B. Deployment Mechanisms

Energy for boom deployment was provided by individual constant torque spring motors at each hinge. Figure 2 illustrates the torque spring configuration on the inboard hinge. A spool which is free to rotate on its axis is mounted to the nonrotating hinge half. A spring that is prestressed in the heat treatment process, such that it desires to coil up on this drum, applies torque to a spool fixed to the boom element. This spool is centered over the hinge pin and mounted to the rotating hinge half, thus the torque is applied to deploying the boom.

Detent mechanisms latched the hinges in the deployed position to provide the required boom alignment and stiffness. The outboard hinge detent mechanism is shown in Figure 3 in the stowed position. This hinge deploys through 180° . Stops machined into each hinge half determine the deployment angle and absorb the impact loads. A spring-driven tapered detent pin drops into a tapered hole to solidly latch the hinge. The hole and pin are angularly displaced $\frac{1}{4}^\circ$ at lockup so that the tapered pin rests on one side of the tapered hole and acts as a wedge driving the hinge stops together so that there is no play.

The sequencing mechanism that phased the deployment so that the two hinges opened sequentially is shown in the prelaunch position in Figure 4. A saddle located at the tip of the outboard boom section is locked to the inboard hinge by two sequencing pins. Completion of inboard hinge deployment allows the detent pin to drop into the hole, simultaneously withdrawing the trapezoidal-shaped wedge and releasing the spring-loaded sequencing pins so that they are withdrawn from the holes in the saddle. The saddle and outboard boom sections are then free to move away under the torque generated at the outboard hinge.

STRUCTURE

The structural design of the boom tubes was complicated by a combination of design requirements--strength (imposed by the launch environment), stiffness and weight (imposed by the spacecraft stabilization system), nonmagnetism (imposed by experiment), and straightness under solar heating (imposed by experiment axis orientation requirements and spacecraft trajectory). A graphite/epoxy composite material was selected as the best candidate material to meet these requirements. It exceeded the strength and

stiffness of aluminum with approximately one-half the weight, and had a near zero coefficient of expansion. This latter property eliminates the problem of thermal bending from being a serious concern. After completion of design trades, the design that evolved was a 38-mm (1.49-in) diameter tube with a 1.8-mm (0.07-in) wall having six longitudinal plies of high strength/low modulus graphite/epoxy and six radial plies of a synthetic fiber/epoxy.

Titanium fittings were bonded to the boom tubes for attachment of the magnetometers and hinges. Titanium was selected over aluminum and magnesium primarily because its lower coefficient of expansion creates less stress on the bond. The hinge structural parts were machined from solid blocks of aluminum to shapes resembling I beams with cross web stiffness.

In the prelaunch configuration, the boom tubes are preloaded by spacers located approximately 1 m (3.28 ft) from each end. This load is applied when the saddle (Figure 4) is latched by the sequencing mechanism. The saddle, in addition to applying the preload, also acts as a torsion restraint on the outboard boom section. The preload prevented relative motion between the tubes during vibration and increased stiffness of the boom assembly.

DYNAMICS

A. Deployment

Deployment parameters as calculated during the design phase are shown in Figure 5. For a given mass distribution and deployment angle the only independent variable is the deployment spring motor torque. The table (Figure 5) shows some of the parameters generated for a family of spring net torque values. The upper half of the table represents inboard hinge deployment and the lower half is the outboard hinge deployment. A net torque of 2.26 N·m (20 in-lb) was the upper limit because the resulting bending moment generated at the hinge was close to the design limit load. Any net positive torque would be sufficient to assure deployment. Component tests indicated the resistive torques, due to friction in the hinges and flexing of the electric cable service loop at the hinges, could vary from about 0.34 N·m (3 in-lb) to 0.79 N·m (7 in-lb) depending on deployment angle and temperature. The springs selected for flight were 1.69 N·m (15 in-lb) for the inboard hinge and 1.13 N·m (10 in-lb) for the outboard hinge.

Fifty percent higher torque springs were used for an overtest of the prototype. The maximum estimated net torque for this test was less than 2.26 N·m (20 in-lb).

B. Natural Frequency

The requirement that the deployed boom have a minimum natural frequency of 0.57 Hz proved to be the most troublesome of the design requirements. Design trades were made to maximize strength at a sacrifice in the margin of safety of predicted stiffness.

During the development, some unanticipated structural weight was added to the magnetometer packages and to the thermal blankets. This resulted in an adverse reduction of the natural frequency to 0.50 Hz.

A systematic weight reduction effort was initiated in order to raise the natural frequency. A NASTRAN model of the boom was utilized to determine the effect of the various options and combinations of options on the boom natural frequency.

The computer model proved to be responsive to load changes similar to the actual system and was very useful in selecting the weight reduction options to be implemented. Figure 6 shows the results of several runs. For successive runs, the weight reduction was cumulative. Run Numbers 013 and 014 represent reduced thermal material weights. Run Numbers 015 and 016 represent proposed redesign of the experiment packages to reduce their size and weight. Run Number 017 is a proposed structural modification to the boom that was not implemented because the weight reduction was adequate to meet the requirement. The final flight unit had a frequency of 0.61 Hz and a weight of 8.1 kg (17.8 lbs). It should be noted here that the frequency variations we were looking for were in the second decimal place of frequency. The inability to model the true system precisely enough to get this second decimal place of frequency to coincide with the absolute value obtained empirically did not seriously degrade the usefulness of the model in selecting the modifications to be implemented.

TESTING

A. Static

Static load tests were conducted on structural components such as the hinges and boom tubes to verify that they met design load

requirements. Each tube was fabricated with extra length to be cut off for test specimens. The specimens were tested to failure. These tests verified uniformity in the graphite/epoxy composite tube fabrication process.

B. Vibration

All of the vibration testing of the boom was done on the spacecraft. The complexities of the system, with mounting interfaces at each end of the folded boom having different input loads and frequencies simultaneously, made realistic testing off the spacecraft virtually impossible. The first test was conducted on an instrumented boom with mass models simulating the magnetometer packages and thermal control system. Component test specifications were generated from this test for the magnetometer packages and sun shades so that they could be tested prior to being installed on the boom. Two complete boom assemblies (the prototype and flight unit) with magnetometers were also tested on the spacecraft.

C. Deployment

Boom deployment tests were conducted under simulated "zero-G" conditions. The boom was supported in a horizontal position by overhead cables attached to the center of gravity of each boom segment. The cables were run over pulleys and counterweighted. Two setups were required for each full deployment, one to test the primary hinge deployment and the other to test the secondary, so that the overhead support point was directly above the deploying hinge. The second setup permitted an overlap of the two tests in that dynamic loads incurred during lock-in of the primary hinge were repeated. The location of the support cables over the outboard hinge created a lateral force component on the boom during the overlap portion of the test. The lock-in velocity was duplicated by releasing the boom from a position between the stowed position and inboard hinge lock-up position that gave the same boom velocity just prior to inboard hinge lock-up as that obtained with the first setup.

A functional check of the hinge mechanisms was performed following each boom vibration test by conducting a restrained "walk-out" deployment. During the first test, the sequencing pins failed to withdraw from the holes in the saddle (Figure 4) preventing release of the outboard boom section. Upon inspection, galling was noticed at the tip of the sequencing pins. In order to correct

the problem, the tip of the pins was changed from a truncated conical shape to a spherical shape. This modification prevented reoccurrence of the galling and there were no malfunctions during subsequent tests.

Low temperature deployment tests were conducted with the hinges and flexing cable service loops cooled by supplying liquid nitrogen to a thermal encasement that was removed when the desired temperature was obtained and deployment then commenced.

Strain gauges were installed on the hinges at the same locations that were monitored in the static load tests for the first series of deployment tests. These tests verified that the deployment loads did not exceed the calculated loads (Figure 5).

D. Natural Frequency

Measurement of the boom's natural frequency was performed in a test configuration similar to that used for deployment. The overhead support points were directly above the center of gravity of each boom segment. The inboard hinge was attached to a very heavy, rigid fixture. An optical tracking system monitored the tip of the boom. A voltage proportional to displacement was recorded on an oscillograph along with a precise 1 Hz reference signal. The boom was displaced and tip motion was recorded as it decayed from about 3 cm zero-to-peak (1.17 in) to less than 0.2 cm (0.79 in). The pendulum effect of the 23-m (75.5-ft) overhead support lines would tend to increase the frequency by about 0.01 Hz; this was subtracted to obtain the true zero-G natural frequency. The test was performed in two orthogonal planes - one in the plane of deployment.

The first boom assembly was also tested by a second method. The natural frequency was computed as the root mean square of two measurements taken with the boom mounted vertically - one with the tip up, and the other, tip down. It can be shown mathematically that this method's results is the zero-G frequency. It was found in this test that there were two uncoupled directions of oscillation. These were the two planes in which the horizontal tests were run. The test results for each plane were within 0.005 Hz for the horizontal and vertical test method.

ALIGNMENT

In order to meet the magnetometer axis alignment requirements, it was necessary to measure and/or simulate the boom curvature (deviations from its theoretical axis) that would occur in a zero-G field. Boom deviations in a horizontal plane were measured while the assembly was supported by floats in pans of water so that the boom was level and free to move horizontally. Measurements of curvature were made utilizing a theodolite that was collimated to a mirror which was coplanar to the boom-to-spacecraft mounting interface and perpendicular to the boom axis. The boom was then rotated 90 degrees and leveled. Straightness was measured again. The data obtained was a useful approximation of the zero-G curvature.

The magnetometer packages were then installed for alignment as shown in Figure 7. The supporting floats were adjusted in height so that the boom was forced into a curvature in a vertical plane which duplicated that shape previously measured. The boom was again free to move horizontally. A three dimensional curvature approximating that which would occur in a zero-G field was obtained. An optical alignment fixture was then installed on the magnetometer sensor packages. Alignment adjustments were made and checked using the theodolite.

CONCLUDING REMARKS

A deployable boom has been developed for positioning magnetometer sensors at a distance of 6m (19.7 ft) from a spacecraft. Use of nonmagnetic constant torque spring motors at each of the two hinges produces controlled and reliable deployment forces. A sequencing mechanism provides an orderly unfolding motion. Spring driven pins are used to keep the hinges tightly locked after deployment. Each critical mechanical function is monitored by a switch so that its status can be determined through telemetry. The boom was flown with complete success on the Mariner 10 mission.

Questions and Answers Pertaining to

Mr. Burdick's Paper (#12) Given at

9th Aerospace Mechanisms Symposium

QUESTION - Member of the audience from the Boeing Company

What sort of force margins did you attempt to maintain; that is, how much did the force available for the deployment exceed the spring torque?

ANSWER

The resistance torques as measured at the component level with a hinge and cable in a cold box varied between 3 and 7 in./lb. depending upon temperature. The lower the temperature, the more the torque, that was for the inboard hinge which had the 15 in./lb. springs. There was a smaller cable with less resistance at the outboard hinge.

QUESTION - Member of the audience

How were the bearings lubricated?

ANSWER

There were no ball bearings, just hinge pins in close tolerance holes and sliding contact lubricated with molybdenum disulfide.

QUESTION - George Sandor, RPI

Which modification of the sequencing pins helped - the stronger springs or the rounded point? Were they tested separately?

ANSWER

No, the rounded point, I am quite sure, is the one that eliminated the galling and that in itself may have done the job, but increasing the spring force gave an extra margin of safety, particularly if there were side loads on it. I didn't mention, but also, these sequencing pins and that saddle had to absorb the torsional vibration loads of the boom so it also served that function as a structural member as well as a sequencing system.

QUESTION - Gilbert

How were the hinged joints protected from the sun - a bellows arrangement?

ANSWER

The inboard hinge was protected with coatings, you can look at that on the table in the rear. The spacecraft did provide some protection for the inboard hinge. The outboard hinge was completely in full time sunlight, that had a flexible sunshade which included the same materials we used in our thermal blanket's outer layer (silver teflon coated outer layer), and it was foldable.

QUESTION - Gilbert

Was it wrapped around the hinge?

ANSWER

No, it was a flat piece held by bracketry and a frame at each end, but no framework longitudinally; it was just folded up like a sheet of paper.

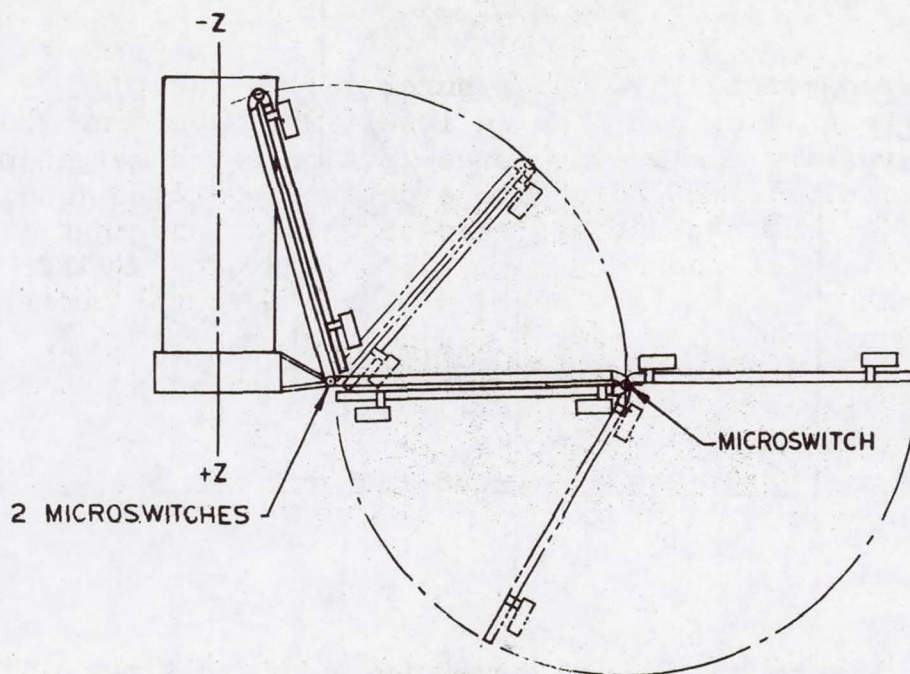


Figure 1. Deployment Sequence

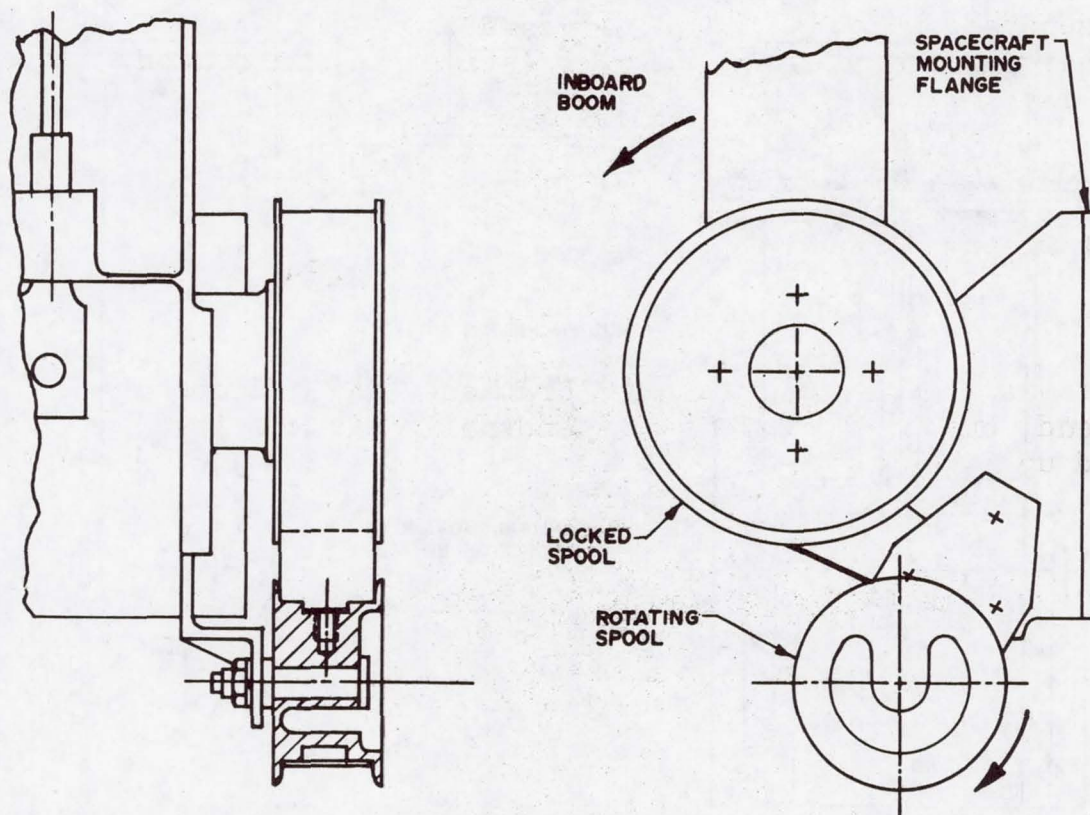


Figure 2. Torque Spring

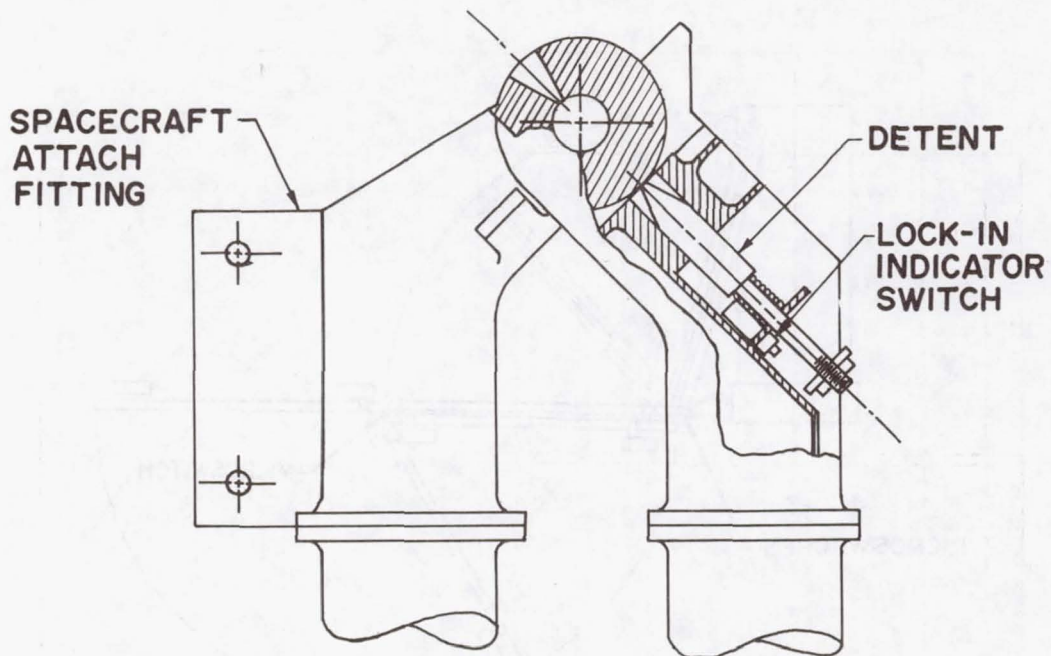


Figure 3. Detent Mechanism Outboard Hinge

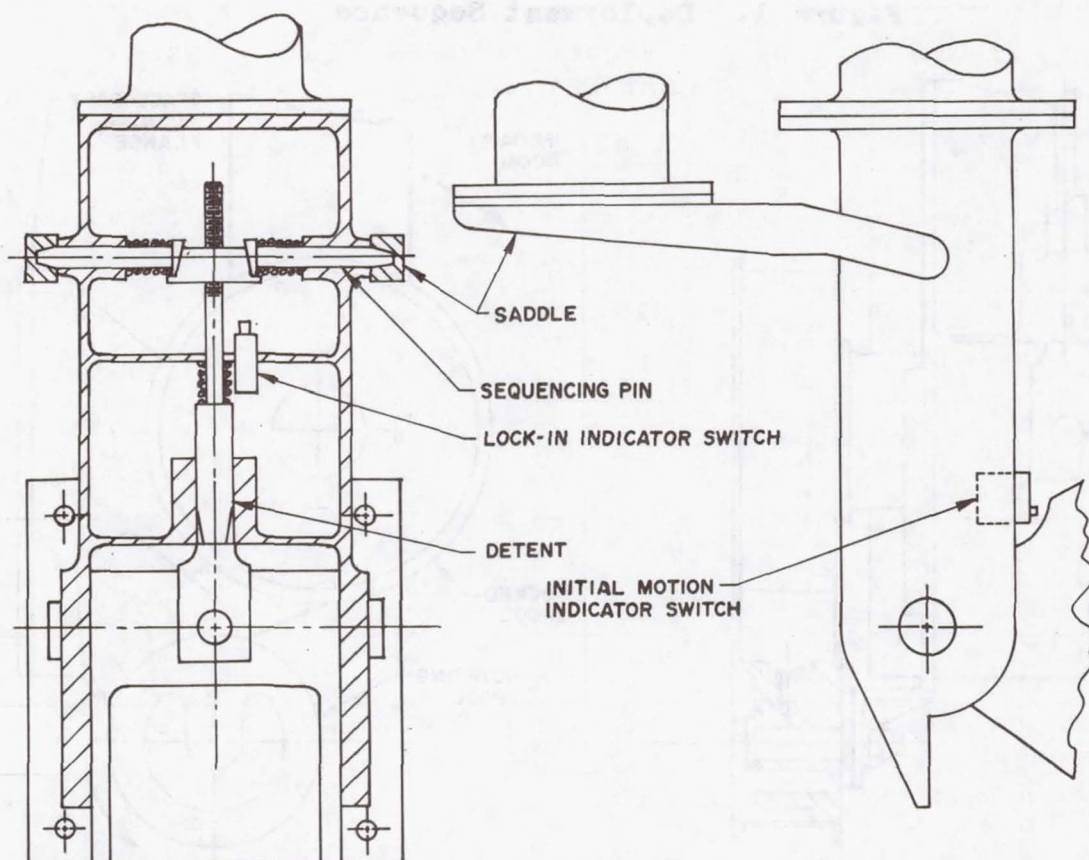


Figure 4. Sequencing Mechanism Inboard Hinge

	CASE NO	NET TORQUE	DEPLOYMENT ANGLE	DEPLOYMENT TIME	VELOCITY AT LOCKUP	MAXIMUM BENDING MOMENT	TIP DEFLECTION
		N.m (IN-LB)	DEG.	SEC.	RAD/SEC	N.m (IN-LB)	Cm.
I N B O A R D	1a	0.56 (5.0)	106.5	12.22	0.304	114 (1006)	7.2
	1b	1.13 (10.0)	106.5	8.64	0.430	161 (1422)	10.2
	1c	1.41 (12.5)	106.5	7.73	0.481	180 (1590)	11.4
	1d	1.69 (15.0)	106.5	7.06	0.527	197 (1743)	12.4
	1e	1.98 (17.5)	106.5	6.53	0.569	213 (1881)	13.4
	1f	2.26 (20.0)	106.5	6.11	0.608	227 (2010)	14.4
O U T B O A R D	2a	0.56 (5.0)	180.0	7.06	0.598	102 (906)	30.1
	2b	0.85 (7.5)	180.0	6.34	0.701	120 (1062)	36.0
	2c	1.13 (10.0)	180.0	5.82	0.790	135 (1196)	40.6
	2d	1.41 (12.5)	180.0	5.43	0.871	149 (1320)	44.7
	2e	1.69 (15.0)	180.0	5.10	0.945	162 (1432)	48.6
	2f	2.26 (20.0)	180.0	4.62	1.077	184 (1632)	55.3

Figure 5. MVM '73 Magnetometer Boom Calculated Deployment Data

RUN NO.	N(Hz)	W kg (LBS)	C.G. m (IN)	I _{TOTAL} * Kg.m ² (SLUG-FT ²)	CUMULATIVE WEIGHT REDUCTION
009	.52	9.06 (19.98)	3.55 (139.6)	141.24 (104.17)	--
013	.526	8.82 (19.45)	3.55 (139.8)	137.74 (101.59)	Removed .18 kg (.4 lb) as NSM ¹ up to O.B. Mag ² , reduced O.B. Mag ³ by .05 kg (.1 lb) and I.B. Mag ³ by .02 kg (.05 lb)
014	.539	8.40 (18.53)	3.53 (139.85)	131.33 (96.86)	Removed .30 kg (.66 lb) as NSM up to end, reduced O.B. Mag. by .07 kg (.15 lb) and I.B. Mag. by .05 kg (.10 lb)
015	.607	7.65 (16.87)	3.37 (132.68)	108.60 (80.10)	Reduced O.B. Mag. by .61 kg (1.35 lb), I.B. Snubbers re- duced .02 kg (.05 lb ea), O.B. Snubbers reduced .05 kg (.1 lb ea)
016	.618	7.17 (15.80)	3.37 (132.53)	102.98 (75.95)	Reduced I.B. Mag by .48 kg (1.063 lb)
017	.864	8.14 (17.95)	3.19 (125.67)	108.95 (80.36)	Same as 016 except with stiffeners

*Taken about inboard hinge pivot.

1. Non-Structural Mass
2. Outboard Magnetometer
3. Inboard Magnetometer

Figure 6. Results of NASTRAN Model Runs

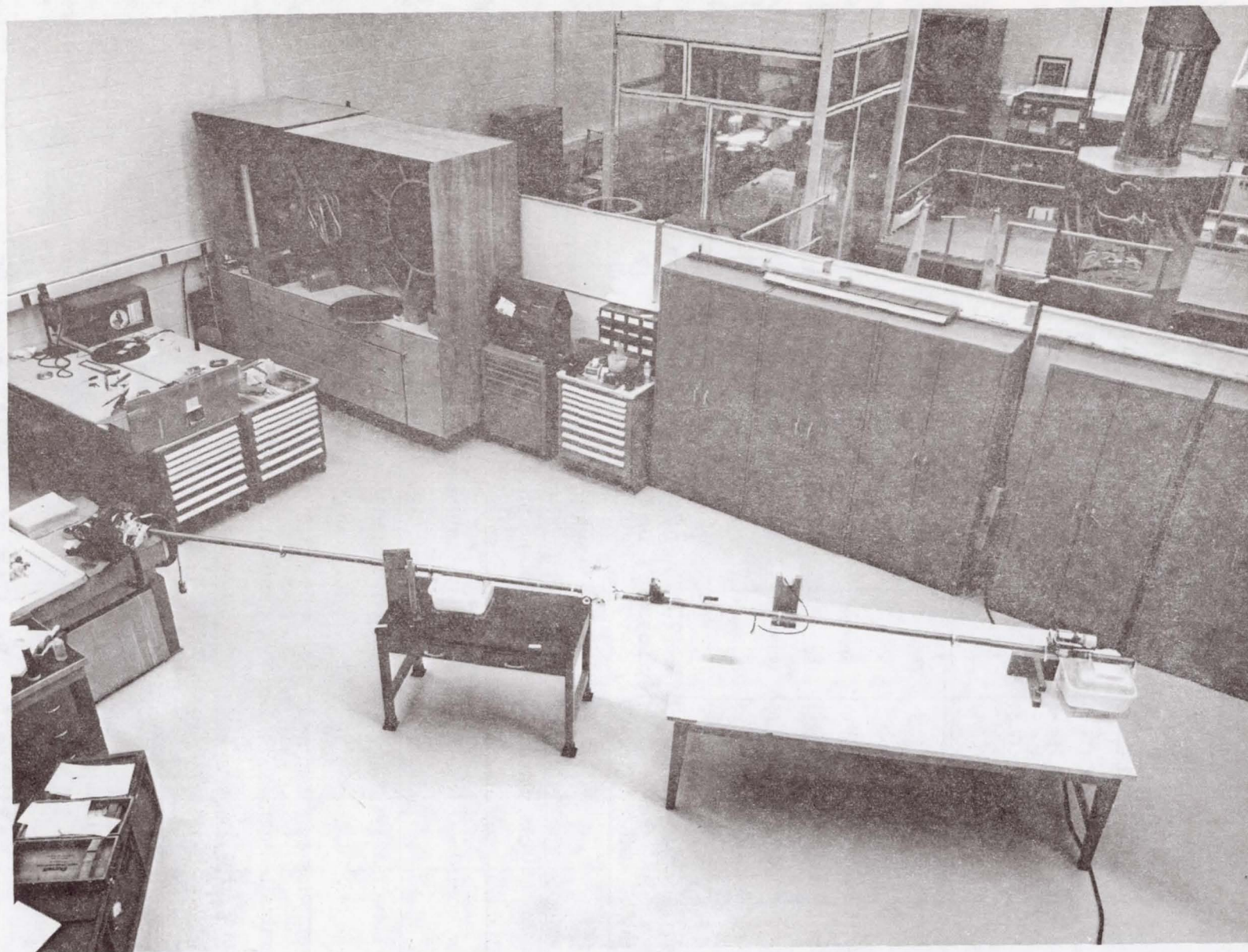


Figure 7. Magnetometer Package Alignment Installation

13. DISPERSION DEVELOPMENT PROGRAM

By

D. J. Carlson, R. J. Lusardi and W. H. Phillips

Chrysler Corporation
Defense Division

Work Sponsored By:

Army Material Command
Picatinny Arsenal
Contract: DAAA21-72-C-0030

SUMMARY

The requirement for the predictable dispersion of small munitions over large areas from ground support missile systems has resulted in the development of a fin stabilized submissile and "sling" ejection system for the Little John warhead. The progressive development of this system is traced including a comparison of simulator, sled test, and flight test results. The results indicate that it is not only necessary but also possible to eject long slender bodies, from a missile warhead at Mach 1, in a stable, uniform and predictable manner.

INTRODUCTION

The Little John warhead was selected as a test bed for this development because of its availability and scaling factor relationship between submissile, munition, and missile when compared to larger missile systems (such as Lance). To maintain development cost at a minimum, the aft section only of the warhead was selected for packaging of the submissiles. By modifying the aft bulkhead it was possible to have a cylindrical cargo bay 76.2 cm long by 30.48 cm in diameter. Packaging of two sizes of sub-assemblies carrying munitions with a 3.96 cm diameter was desirable. Therefore, submissiles containing four (4) munitions and one (1) munition in cross section were selected for development. This resulted in submissiles with equivalent length to diameter (L/D) ratios of 8 and 16 respectively. Figure 1 illustrates the Little John warhead with the submissiles in the aft cargo bay.

The cargo is ejected from the warhead at event by the "sling" action generated when the two skin panels separate pulling the "sling" taut. Figure 2 illustrates this technique.

Once the preliminary submissile packaging envelope was defined, the design of the submissile was undertaken based upon design criteria generated from prior development programs involving other missile and aircraft dispenser systems. The development process included an aerodynamic analysis to define the ballistic characteristics of the two submissiles to obtain uniform ballistic characteristics and to define the fin size to provide a stable body over the flight environment design criteria specified. In addition to the aerodynamics of the submissile after it was in the air stream, it was necessary to predict its characteristics when ejected from the warhead with a sling system. Scaled simulator tests were conducted to investigate various ejection techniques prior to high speed (Mach 1) sled tests at the Naval Weapons Center (NWC). After the ejection technique and submissile dynamics were verified by sled tests, full scale flight tests were conducted at White Sands Missile Range (WSMR).

Design Criteria

Systems requirements for the design were for the submissile to survive warhead event at Mach 1.5. The submissile was to withstand the loads imposed should it see a 90° angle of attack and axial forces of 80 g's as defined by the Little John system during launch.

Submissile fin deployment was desirable in less than 40 milliseconds to prevent the submissile from tumbling through one (1) revolution prior to stable flight should it see high pitch rates at ejection. Tumbling is not conducive to repeatable characteristics over the various flight region anticipated.

Submissile Design

As mentioned earlier the submissile envelopes were defined by the missile cargo bay and the munition diameter. The use of a submissile containing four (4) munitions in cross section (quad submissile) resulted in a basic square body configuration and because of the requirement for an explosive release technique for the munitions, the single cross section submissile was also designed as a square body. The submissiles were 8.44 cm and 4.33 cm in cross section for the quad and single submissiles, respectively. The requirement for rapidly opening fins dictated more torque than available from conventional springs which could be packaged within the available space. Therefore, a high torque torsion mechanism was designed which increased the opening torque by a factor of 6 over springs.

Sizing of the fins for the submissiles was based on the results of an aerodynamic analysis for a round body of equivalent diameter at both small and large angles of attacks. Estimates of pertinent aerodynamic parameters were made to allow computer simulations of dart flight.

Figure 3 shows the assembled submissiles and their characteristics are contained in the following table:

	<u>Quad</u>	<u>Single</u>
Length (cm)	74.0	72.4
Cross flats (cm)	8.44	4.33
Weight - grams	8285	2385
Center Gravity off base (cm)	35.7	36.9
Fin area (cm ² /fin)	69.0	47.7

Ejection System Design

As a tool to assist in the investigation of ejection characteristics, a one-half scale model ejection simulator was developed. The simulator consisted of a "bungee" cord arrangement to provide the force for exercising the sling system and a quick release system. The submissile simulators were constructed from wood with ballast added to obtain the proper weight and center of gravity. The submissile simulators did not contain fins and therefore the effect of fin torque was not included in the test program. A series of tests were conducted to determine the effects of sling length, sling shape, sling-to-warhead attachment point, sling size, ejection force, and load distribution.

Figure 4 illustrates the effect of sling shaping upon the pitch rate induced on the simulators. It varied from 2 rps nose first to 2 rps tail first. Based upon these tests, conditions which should give a near parallel ejection attitude were selected for sled tests.

The importance of the controllability of ejection conditions must not be neglected. For a vehicle constrained to pitching and heaving motion, figure 5, the linearized equations of motion may be written as

$$Z_a \ddot{a} + Z_q \dot{q} + Z_{\dot{a}} \dot{a} = m \ddot{Z}$$

$$M_a \ddot{a} + M_q \dot{q} + M_{\dot{a}} \dot{a} = I \ddot{\theta}$$

where

Z_i, M_i ($i = \alpha, \dot{\alpha}, q$) are stability derivatives for forces and moments due to the respective aerodynamic phenomena

m is the mass of the vehicle

I is the transverse moment of inertia

This system may be solved for $\theta(t)$ and $\alpha(t)$ once the geometric constraints, figure 5, have been substituted. The oscillatory solutions obtained for θ and α may be used to determine the lateral coordinate, i.e.,

$$\begin{aligned} Z(t) &= V \int (\alpha - \theta) dt \\ &= k_1 e^{\phi_1 t} + k_2 e^{\phi_2 t} + k_4 t + k_5 \end{aligned}$$

Thus, the vehicle is moving away from its initial heading due to the time dependent k_4 term. The motion may be described as an oscillation which occurs on a time dependent trim line, figure 6.

An approximate solution for the k_4 term is given by

$$k_4 = -\theta_0 + \alpha_0 - \left[\frac{Z_q + Z_{\dot{\alpha}}}{mv} \right] \alpha_0 - \left[\frac{IZ_{\alpha}}{mVM} \right] \dot{\alpha}_0$$

and the angle of dispersion, called the jump angle, is given by k_4/V .

Note that the magnitude of the jump angle, and hence the dispersion, is dependent on the initial attitude and the initial angular rate. In particular, for a finned vehicle, such as a dart, the effect of the $\dot{\alpha}_0$ term is dominant, and large initial angular rates will cause large dispersion.

This behavior is also exemplified by the lateral ejection velocity (LEV) history as the vehicles travel down range. Figure 7 presents LEV histories showing the characteristics that the curves may have for various dart ejection attitudes. Thus it is possible that a dart may suffer LEV "speed-up" for "slow-down" as a result of initial attitude. This will greatly influence pattern characteristics.

Sled Test

The Little John warhead was attached to an expended Tiny Tim booster and accelerated down the SNORT track at NWC by five (5) Zuni rocket motors. The test was arranged so the warhead did not function until it was in free flight off the end of the rail. A pit 3.6 meters wide by 2.4 meters deep was located at track end to reduce shock wave

interference characteristics.

Two (2) tests were conducted at approximately Mach 1. On the first test the sling system tore loose of the warhead skin panel at warhead event. This was caused by the primacord which curled the skin back pulling the sling attachment loose. The submissiles did not see the proper ejection characteristics and were subjected to high initial pitch conditions since the sling caught the submissile tails. However, the submissiles were ejected and flew stable without any tumbling. The sling skin panel interface was reinforced for the second test and the sling system operated properly. Figures 8 and 9 illustrate the submissile behavior at event and over the first 100 meters of flight. It should be noted that the submissiles come out with a slight nose down attitude and tend to oscillate ± 10 degrees about the horizontal during their observed flight of 1.5 seconds or 450 meters. Also it can be noted that the submissile fins are open prior to 0.05 seconds when they become distinguishable in the photographs. Comparing the average event conditions of all submissiles for the simulator and sled tests gives a good correlation considering the limited number of test points. The average pitch rate predicted from the simulator tests was -0.01 rps and the sled test result was -0.37 rps (negative sign indicates tail first ejection). This shift was in the direction anticipated because of the fin action which was not included in simulator tests. The ejection velocities were 7.6 and 6.8 meters per second respectively for the simulator and sled tests. This comparison is also good since the sled test results include effects of dynamic lifts which were in the negative direction as a result of the nose down ejection attitude.

Analysis of sled test data supplied sufficient data to compare the predicted submissile drag characteristics with test results. A comparison of static moment stability derivative coefficient (Cm_{α}) was also obtained. Test data provided a value of -10.9 radian⁻¹ compared to a predicted value of approximately -11.0 radian⁻¹.

Flight Tests

Three flight tests were conducted at WSMR to demonstrate the capabilities of this system to disperse small low ballistic factor munitions over large areas. Two basic event conditions were selected for test purposes. These were missile dive angles of 57 and 17 degrees at a velocity of approximately Mach 1. These two angles were selected to illustrate the system's capabilities to provide near constant patterns independent of missile dive conditions and without need to vary the functioning time of the submissiles.

The pattern size obtained is a function of the time the submissiles fly prior to release of their cargo. For this series of tests a flight time of 1.25 seconds was used. Analysis of the limited photographic coverage obtained on these tests indicated that the 4 rps roll rate of the missile at time of event was not detrimental to overall system performance. The actual patterns obtained were slightly larger than predicted. This increase in pattern size is attributed to the increased dispersion from each submissile obtained because of the roll rate induced in the submissile by the asymmetry of the fins from assembly tolerances. This additional dispersion is a desirable condition and could be intentionally increased for future applications.

CONCLUSIONS

Slender body submissiles can be ejected from missile systems in a stable and predictable manner. They can also be used to provide dispersion of munitions over large areas with a minimum munition flight time and with the munition pattern shape relatively independent of missile event conditions.

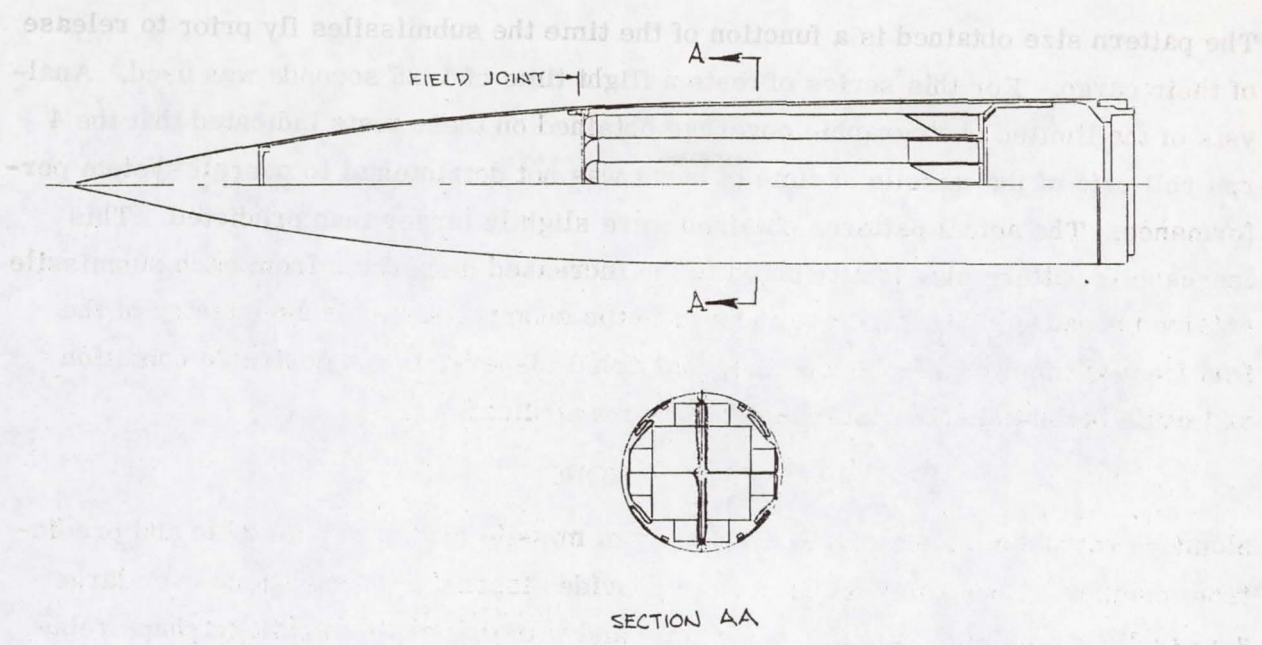


Figure 1 Little John Configuration

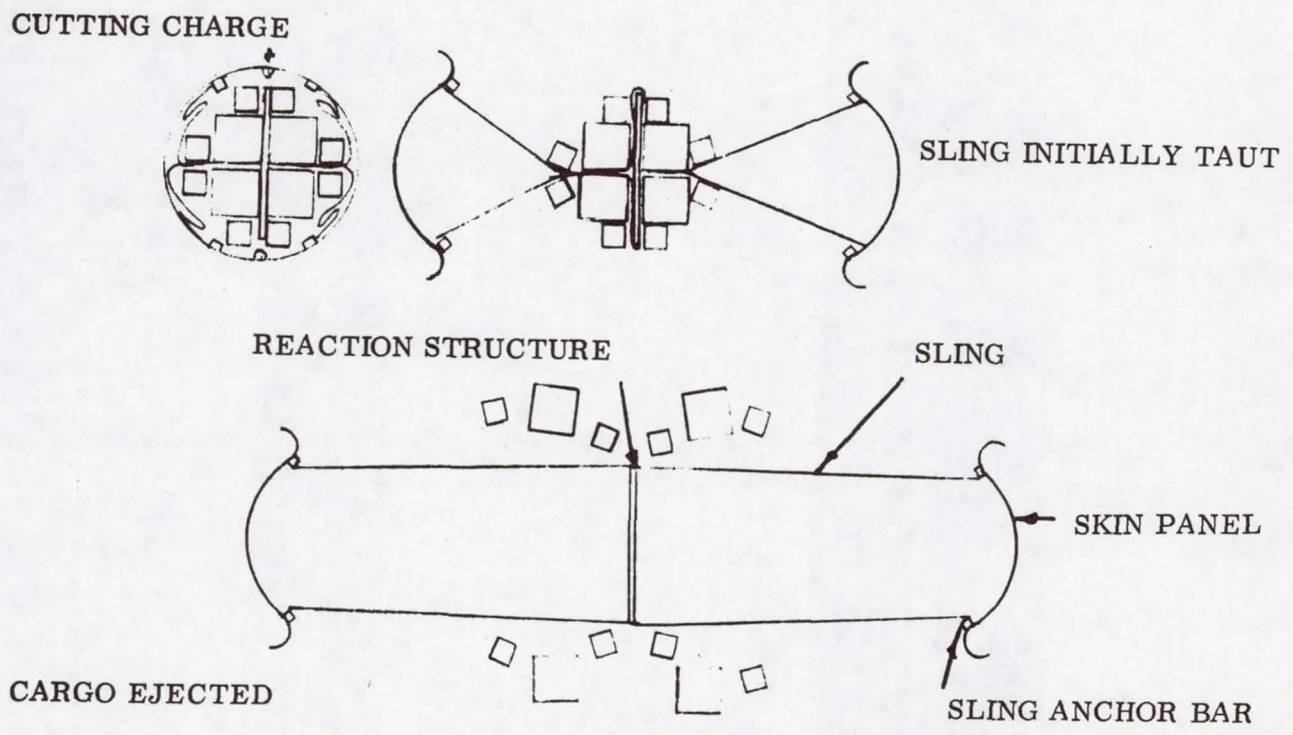
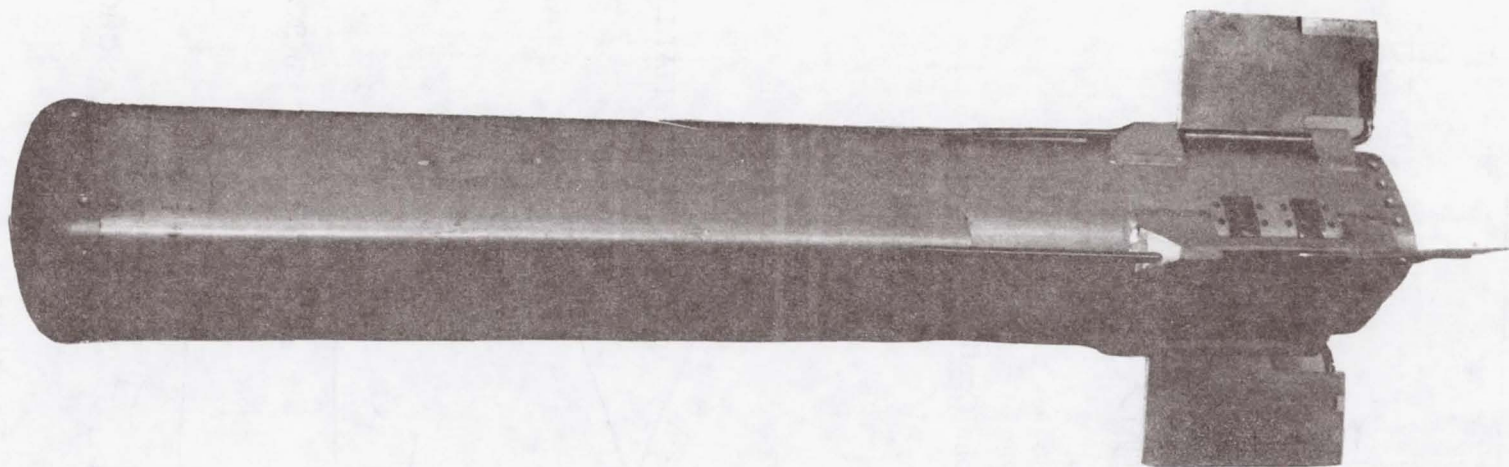
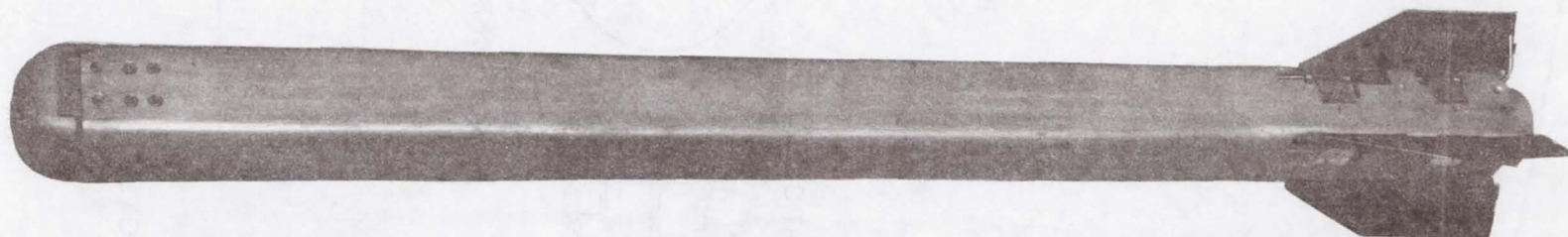


Figure 2 Sling Technique

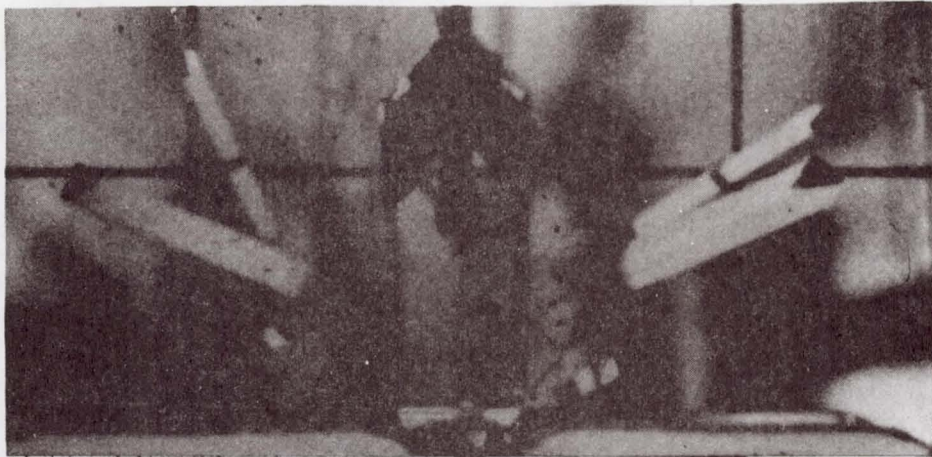


QUAD

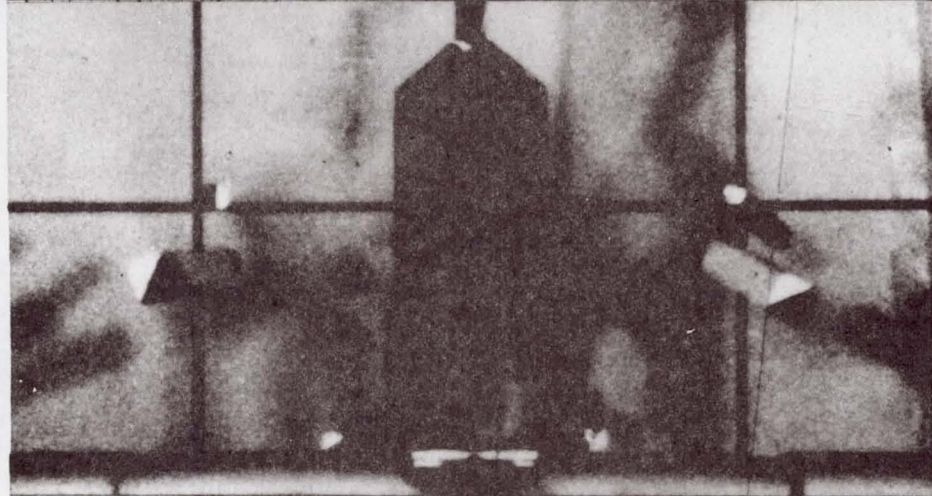


SINGLE

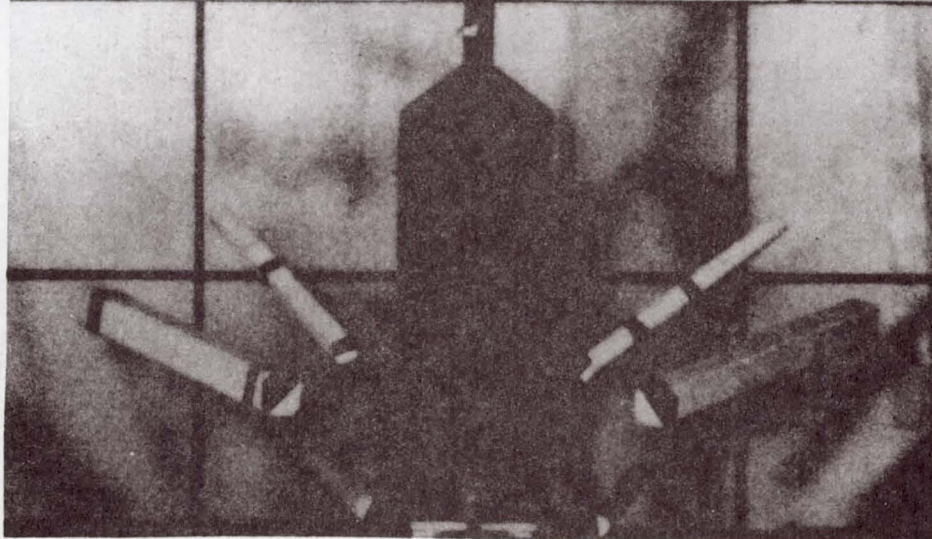
Figure 3 Submissiles



2 rps
NOSE FIRST

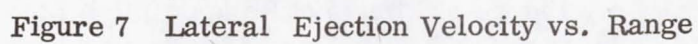
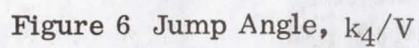
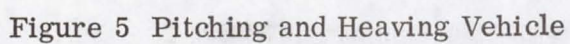


1/2 rps
NOSE FIRST



2 rps
TAIL FIRST

Figure 4 Effects of Sling on Pitch Rate



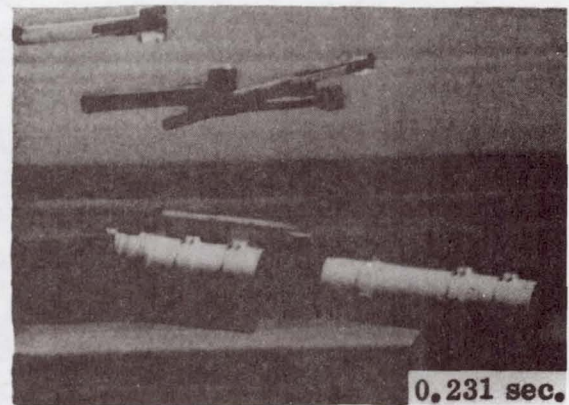
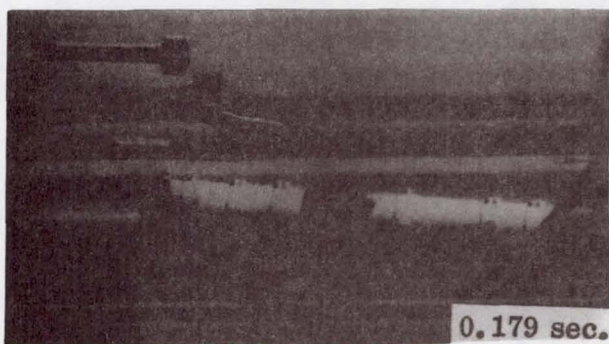
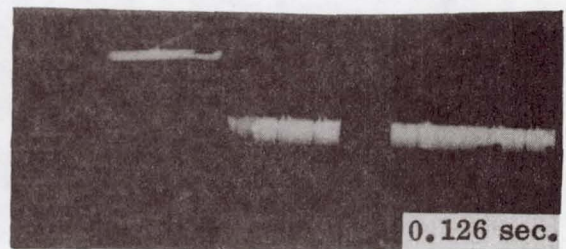
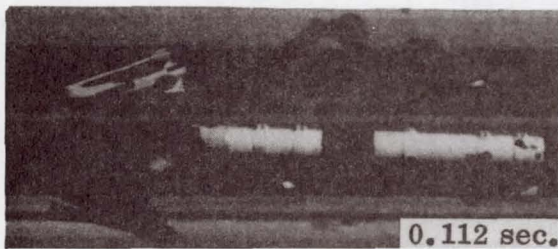


Figure 8 Sled Test Results

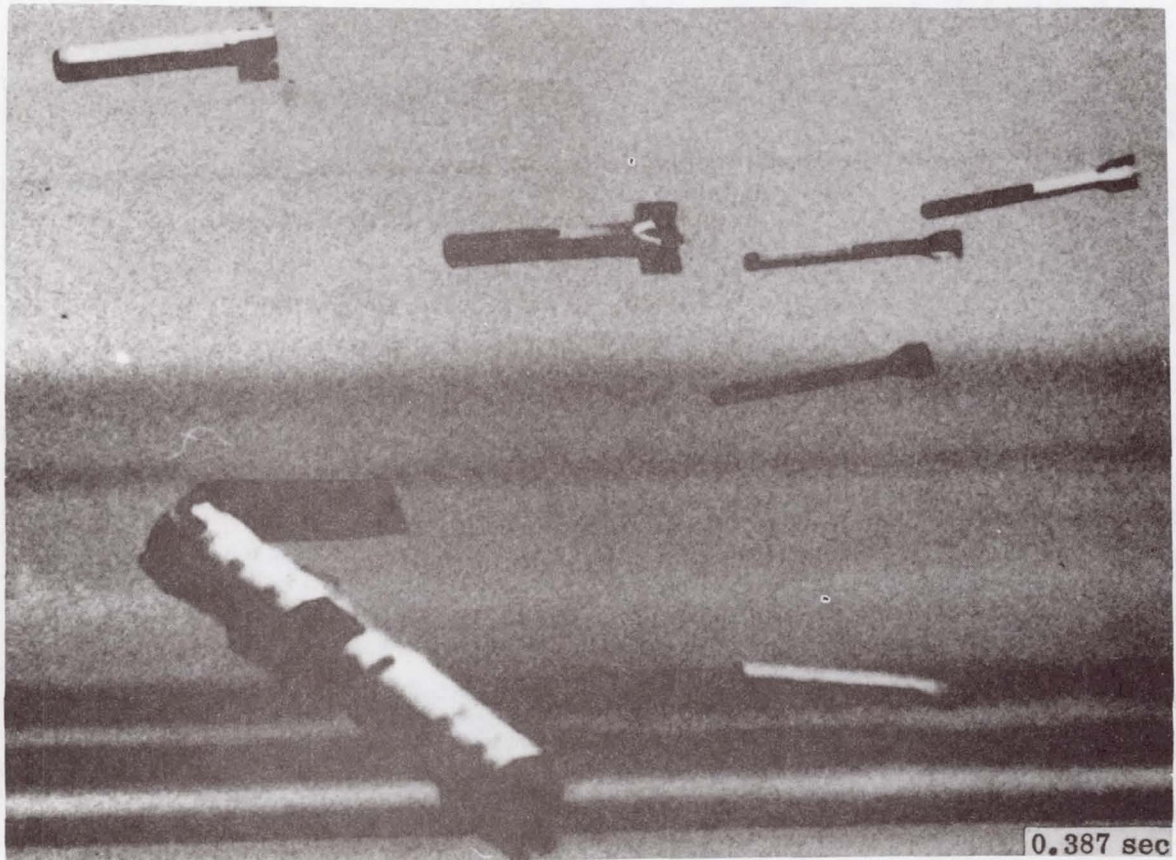
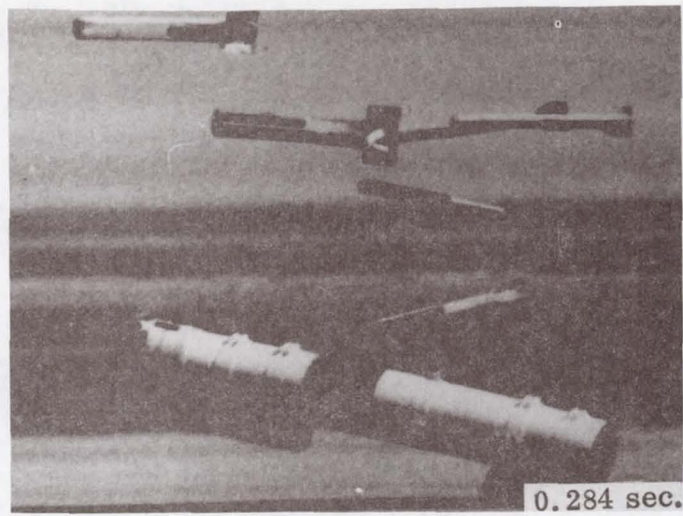


Figure 9 Sled Test Results Continued

14. A NEW CONCEPT FOR ACTUATING SPACE MECHANISMS

By William C. Stange

NASA Goddard Space Flight Center

SUMMARY

A two-position (0° and 180°) actuating mechanism driven by two alternately-heated opposing flat NITINOL springs is proposed for rotating the low field triaxial fluxgate magnetometer experiment on the 1977 Mariner Jupiter-Saturn spacecraft to its 0° and 180° positions. The magnetic field, power requirements, weight and, and volume of this device are very restrictive. The problems encountered in design and development of this device are presented.

INTRODUCTION

The purpose of this experiment is to provide precise, accurate, and rapid vector measurements (from 0.01γ to 20 gauss, $1\gamma = 10^{-5}$ gauss) of the magnetic fields of Jupiter and Saturn in interplanetary space to them and beyond. These data extend in situ studies of the solar wind interaction with Jupiter and characteristics of its magnetic field and yield first studies of Saturn's field and its interactions if the solar wind extends to 10 AU.

Performing accurate measurements of magnetic fields on a spacecraft not fabricated magnetically clean is a major problem. A moderately long boom will be used to place two low-field ($\leq 6400 \gamma$) triaxial fluxgate magnetometers at remote distances from the spacecraft. Simultaneous measurements will yield separate estimates of the spacecraft field and the ambient field.

The purpose of this essentially nonmagnetic actuator is in-flight calibration of the triaxial fluxgate magnetometers. This calibration, which determines the sensor zero point, is accomplished by periodically flipping the magnetometers by 180 degrees.

The advantages of this mechanism are that it satisfies more than any other known device, the constraints of volume, weight, nonmagnetic materials, and power in relation to the requirements of high torque, fast cycling and long life. These properties are derived solely from the unique mechanical qualities of 55-NITINOL. This actuator will provide cyclical bi-directional rotary motion under varying environmental temperatures (-45°C to $+40^\circ\text{C}$) in a vacuum for periods up to five years.

This paper describes the mechanical and electrical functions of the design which evolved, as well as the problems encountered. The objectives achieved are evaluated and other possible applications are presented.

OBJECTIVE

The objective was to develop an actuator which would meet the following requirements.

1. Rotate 180 degrees \pm 15 minutes of arc.
2. Remain at the indexing stop until again actuated.
3. Have a permanent magnetic field (when not being powered) less than 0.1 γ at 2.54 cm (1 in).
4. Have a minimum capability of 300 cycles during a period of five years.
5. Complete the rotational indexing within 30 seconds of initiation.
6. Require not more than 8 watts of power for less than 30 seconds.
7. Weigh less than 0.227 kg (0.5 lb).
8. Fail-safe indexing, i.e., the actuator must not stop in any position other than 0 or 180 degrees.
9. Operate within the temperature range of -45°C to $+40^{\circ}\text{C}$.
10. Operate in a vacuum.

DESIGN

The selection of a design approach required the consideration of other feasible concepts. Among those reviewed were bimorph piezoelectric devices, opposing coil solenoids (without cores), nonmagnetic electric motors, Freon state conversion bellows, and wax pellet actuators.

A concept utilizing 55-NITINOL was adopted because it appears to most reliably meet the above design requirements.

55-NITINOL

About ten years ago, Buehler and Wiley of the U. S. Naval Ordnance Laboratory developed a special purpose nickel-titanium alloy (55-NITINOL) that possesses "mechanical memory" (see reference 1). The phenomenon is caused by a thermally induced atomic shear transformation which occurs in 55-NITINOL. The salient property of this alloy is its memory of shapes imposed on it at a characteristic "annealing" temperature T_a . This effect is manifested, after return to an arbitrary lower temperature T_1 at which plastic deformation ($\leq 8\%$ strain, fig. 1) has been induced, by its forceful return to the originally imparted shape (at T_a) following heating to the transition temperature T_t ($T_1 < T_t < T_a$). Simply stated, this means that any shape formed at the "annealing" temperature can be thermally induced to reoccur in spite of deformations ($\leq 8\%$ strain) imposed at lower temperatures.

The 55-NITINOL used in this mechanism has a $T_a = 500^\circ\text{C}$ and $T_t = 80^\circ\text{C}$. The transition temperature T_t is a function of material composition and cold working and can range from -100°C to $+300^\circ\text{C}$. The onset of restoring stress (memory) is not sharply defined (figs. 1 and 2), rather T_t is a temperature range ($\approx 10^\circ$) over which the restoring stress increases by a factor of four and the modulus by a factor of four, as illustrated in fig. 2. If the 55-NITINOL flat springs were unrestrained they would assume the shape of a straight strip (memory shape) at 90°C (upper T_t range). The spring torque of this actuator varies directly with the yield stress of the NITINOL which is solely dependent on whether its temperature is above or below the transition temperature range. The springs used in this test model will provide 0.029 kg-m (40 in-oz) of gross torque. After about 1,000 cycles the gross torque output should level off at about 95% of the initial value.

MECHANICAL OPERATION

The mechanism as shown in figs. 3 and 4 is simply an experiment container which can be bi-directionally rotated by two opposing NITINOL flat springs with bonded heater strips, whose indexing is biased by two over-center Flexator springs. To operate the actuator, the appropriate NITINOL spring (fig. 3, section A-A) is heated to its transition temperature range ($+80^\circ\text{C}$ to $+90^\circ\text{C}$), increasing the modulus of elasticity from $27.6 \times 10^6 \text{ N/m}^2$ to $82.7 \times 10^6 \text{ N/m}^2$ (4,000,000 psi to 12,000,000 psi) (fig. 2), providing a torque greater than the unheated spring. This action drives the toggled spring crank (figs. 3 and 4) and the pinned crank arm clockwise from the position shown. After 90 degrees rotation, the two Flexator springs drive the crank arm, fail safe, to the opposing stop, 180 degrees from where it started. The shaft rotates the experiment in its container and acknowledges the indexing through a cam-actuated microswitch as shown in fig. 3. When the heater is turned off by telemetry and the NITINOL spring falls below the transition temperature, the crank arm is held against the indexing stop by the two Flexator springs. The rotation is reversed by applying electrical power to the heater

strip which is bonded to the NITINOL flat spring shown in section A-A, fig. 3. This drives the crank arm counter clockwise back to where it started.

MATERIALS

The prime considerations in the selection of materials for this mechanism were low magnetic permeability (< 1.001), volume and weight. The Flexator springs were made of Elgiloy, the bushings, housing and experiment container from Delrin, and the shafts and other hardware from titanium alloy, beryllium copper, aluminum and brass.

ALTERNATIVE USES

Other mechanisms utilizing NITINOL in different configurations are currently being designed and fabricated. Devices utilizing NITINOL can be competitively employed in many areas requiring relatively quick response and high driving force with severe limitations on the permanent magnetic field, weight and volume.

CONCLUSION

The mechanism described in this paper provides positive, cyclical indexing for a sensor rotating 180 degrees ± 15 minutes; the permanent magnetic field is less than 0.1 γ at 2.54 cm (one in), the power consumed is less than 240 watt-seconds, the weight is less than 0.168 kg (6 oz), and the volume (less the experiment container) is less than 3.6×10^5 cubic meters (2.25 cubic inches). Two mechanisms of the type described in this paper have been fabricated for feasibility testing. Eight additional units will be built, two of which it is contemplated will go aboard the 1977 Mariner Jupiter-Saturn spacecraft as the actuating mechanism for the low field triaxial fluxgate magnetometer experiment.

REFERENCE

1. Jackson, C. M., Wagner, H. J., and Wasilewski, R. J., "55-NITINOL — The Alloy with a Memory: Its Physical Metallurgy, Properties, and Applications." NASA-SP5110, 1972.

ADDENDUM

The actuator described in the Mechanical Operation Section of this paper (figure 4) has been modified as shown in figures 5 and 6. Refinement of the conceptual design necessary for the development of flight hardware has wrought most of the changes. However, one basic addition has been incorporated into the original concept; and that is the feature of a position lock.

This addition was necessitated because of the tendency of the NITINOL springs, after $> 1,000$ flips and especially at low temperatures, to return to their strained shape upon cooling and therefore pull the crank arm off its position stop (figure 5).

The concept shown in figure 4 was modified to incorporate a mechanism which locks the crank arm in either its 0° or 180° position. As shown in figure 5 the outboard end of either NITINOL spring is reacted by a pivot arm which also carries two cam springs (tension), a follower and an arm stop. The two followers interface with a cam which has one slot. In figure 5 the left follower has engaged the cam slot and bears against the lower slot face thus eliminating play and locking the crank arm against its position stop.

When the NITINOL spring on the left is heated, its increased modulus reacts with the locked toggled spring crank on the right and the pivot arm on the left. As the force of the two cam springs is overcome the pivot arm and its slaved follower move counter clockwise, thus ultimately releasing the cam. The toggled spring crank is now free to be driven clockwise as in the previous concept (figure 4) and the crank arm rotates 180° to the left stop. The spring loaded right follower detents with the cam and locks the crank arm and its associated hardware in this position until it is again flipped back to the position as shown in figure 5.

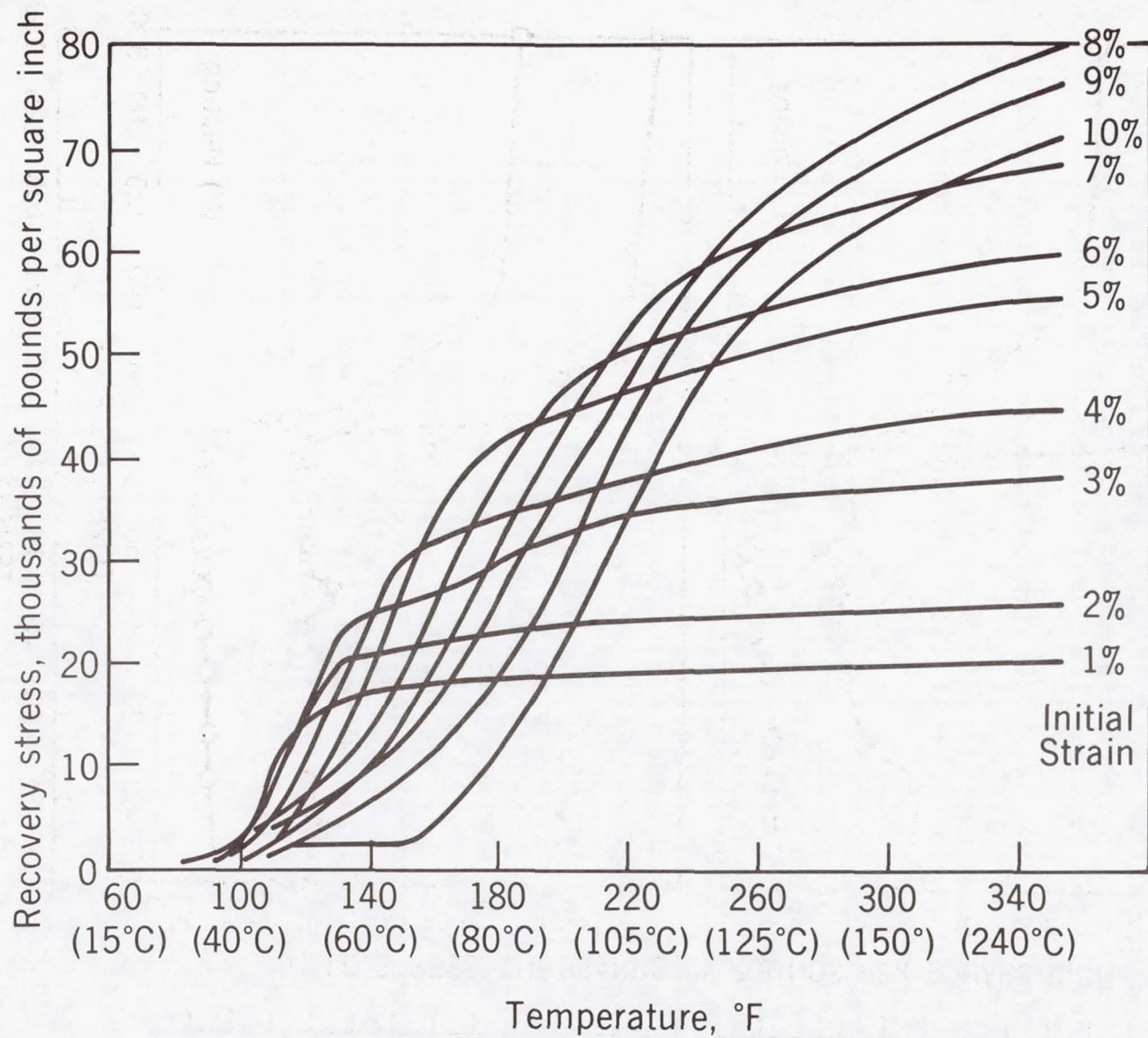


Figure 1. Typical Tensile-Recover-Stress Vs. Temperature Curves¹

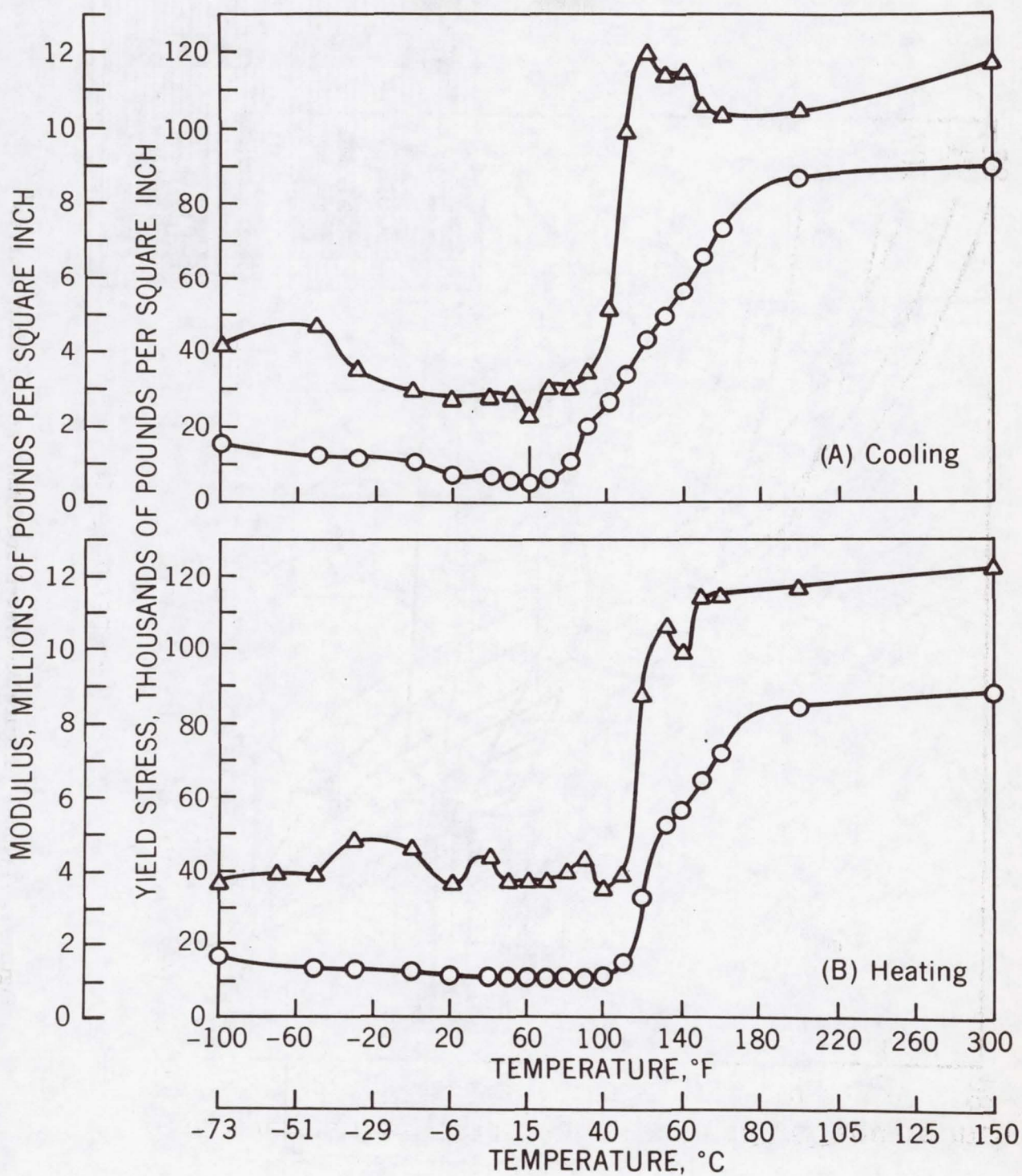


Figure 2. Typical Temperature Effect on Yield Stress and Modulus of Elasticity

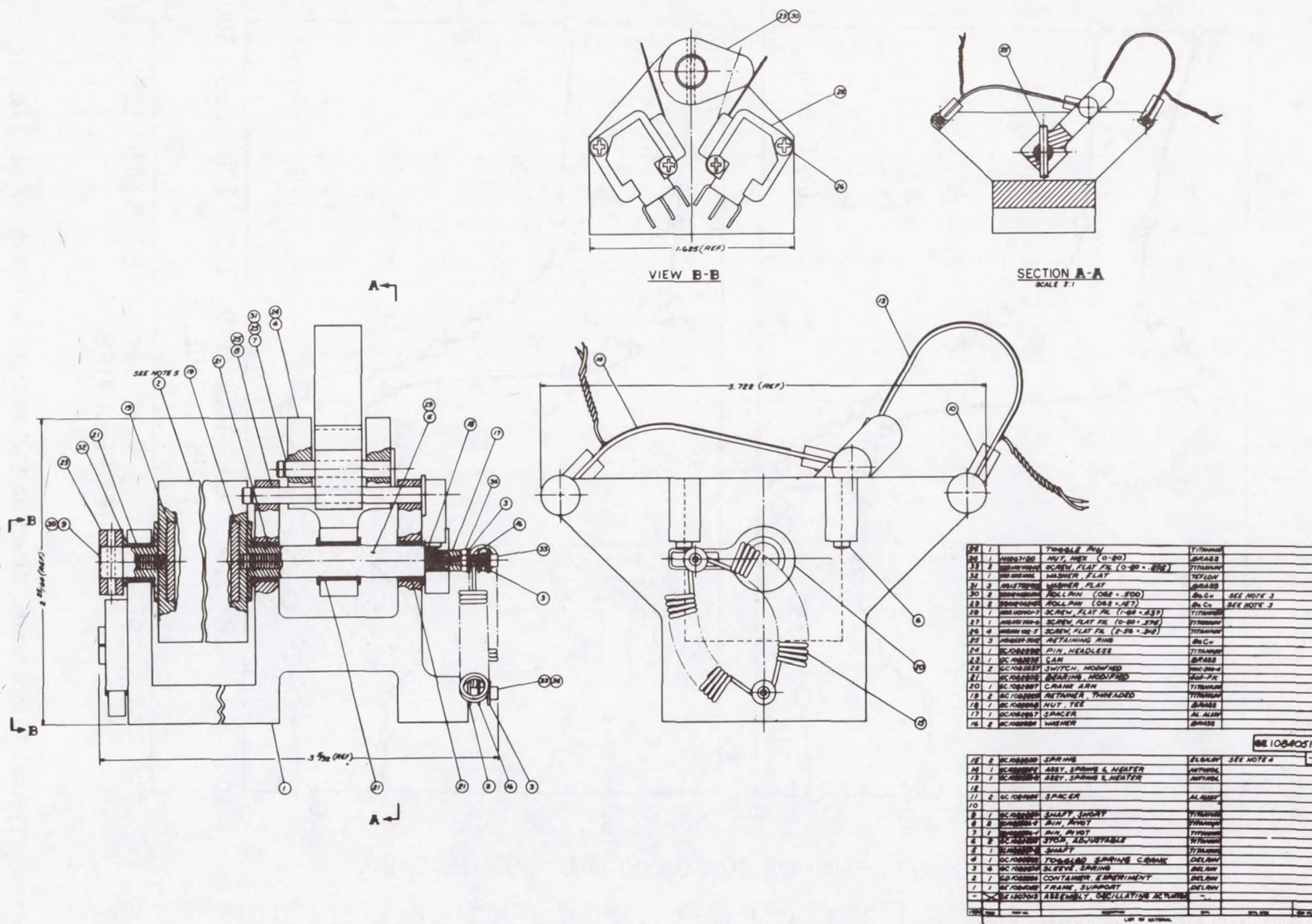
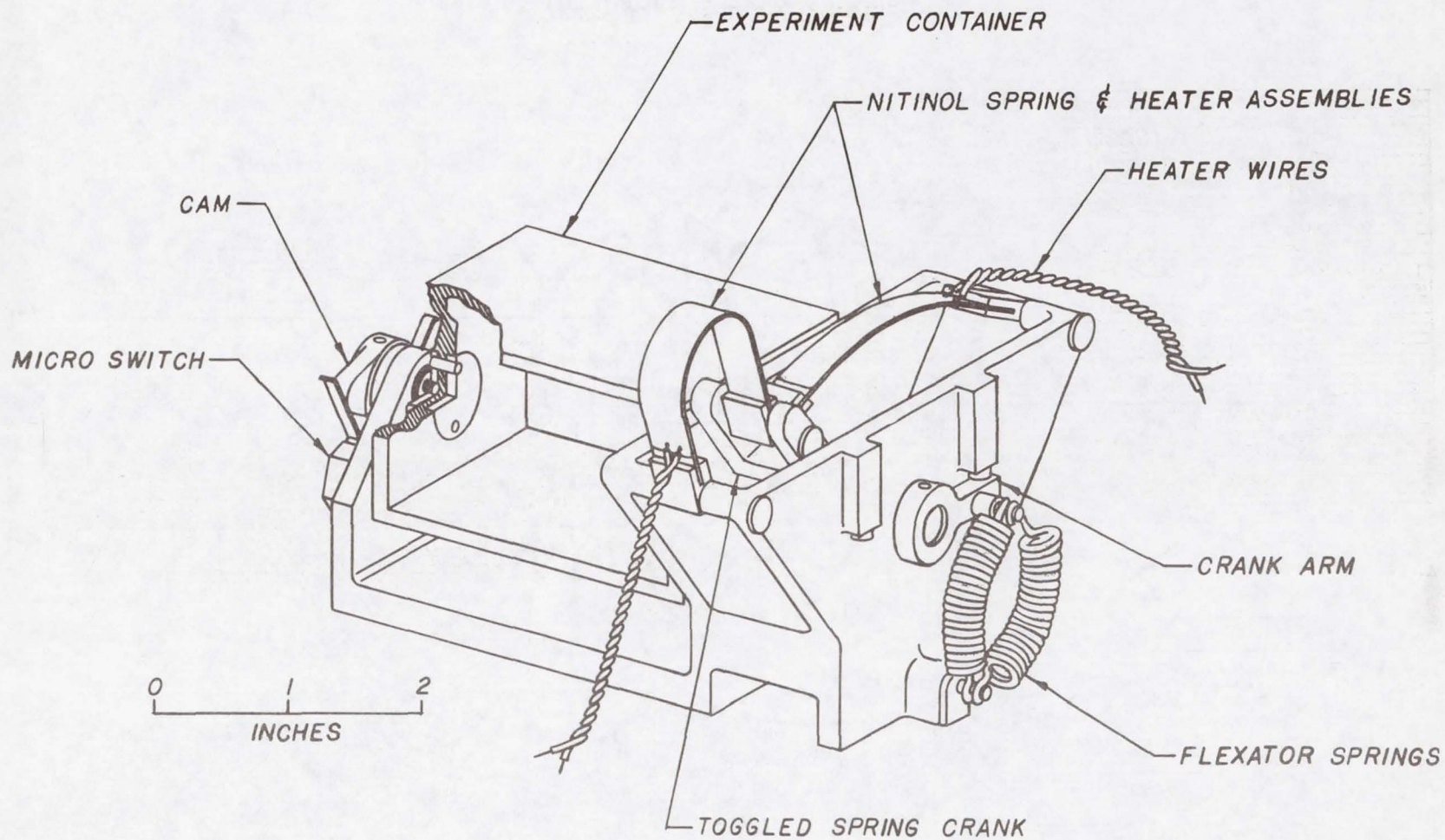


Figure 3. Assembly Drawing



OSCILLATING ACTUATOR ASSEMBLY
FIGURE 4

Figure 4. Oscillating Actuator Assembly

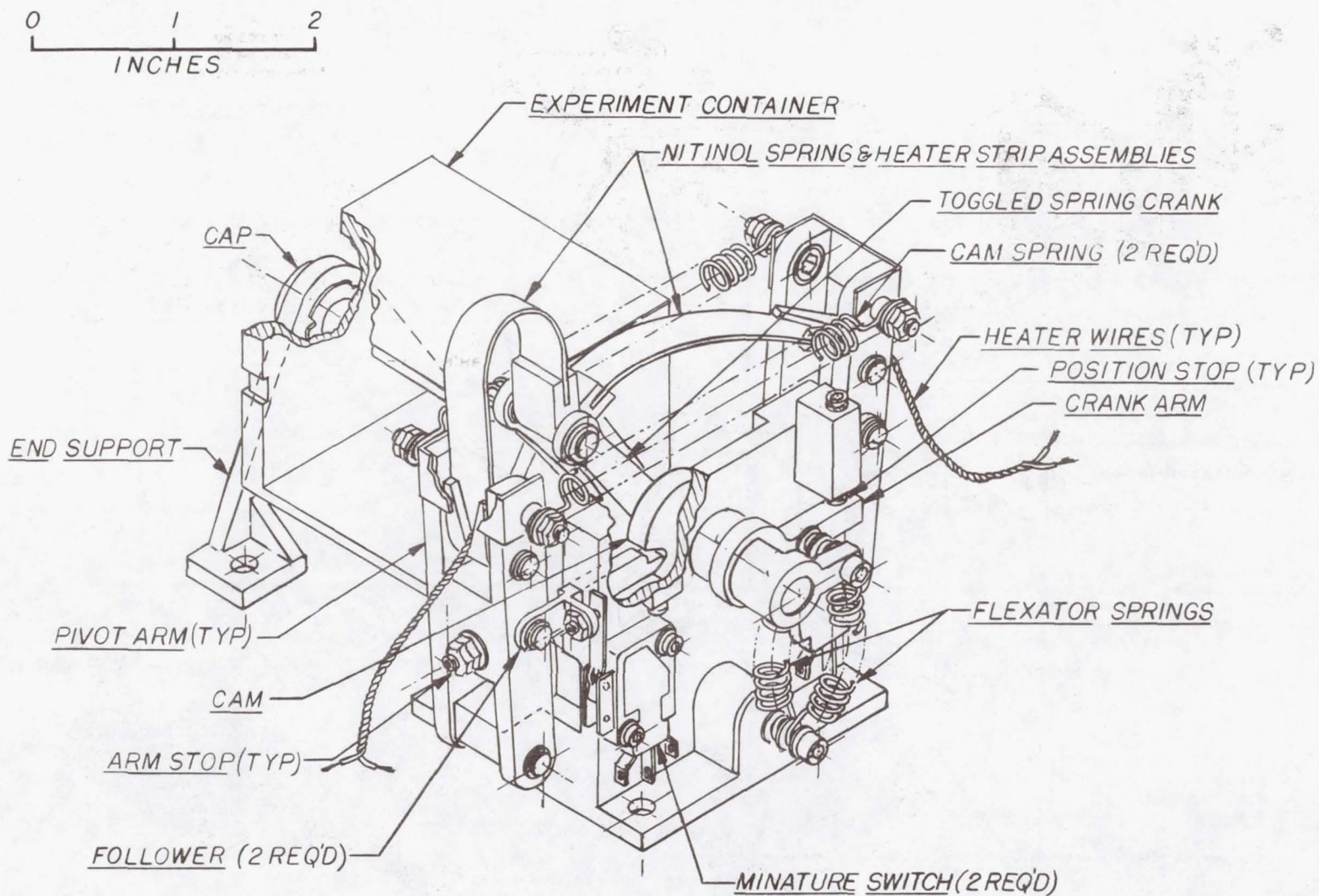


Figure 5. Oscillating Actuator Assembly

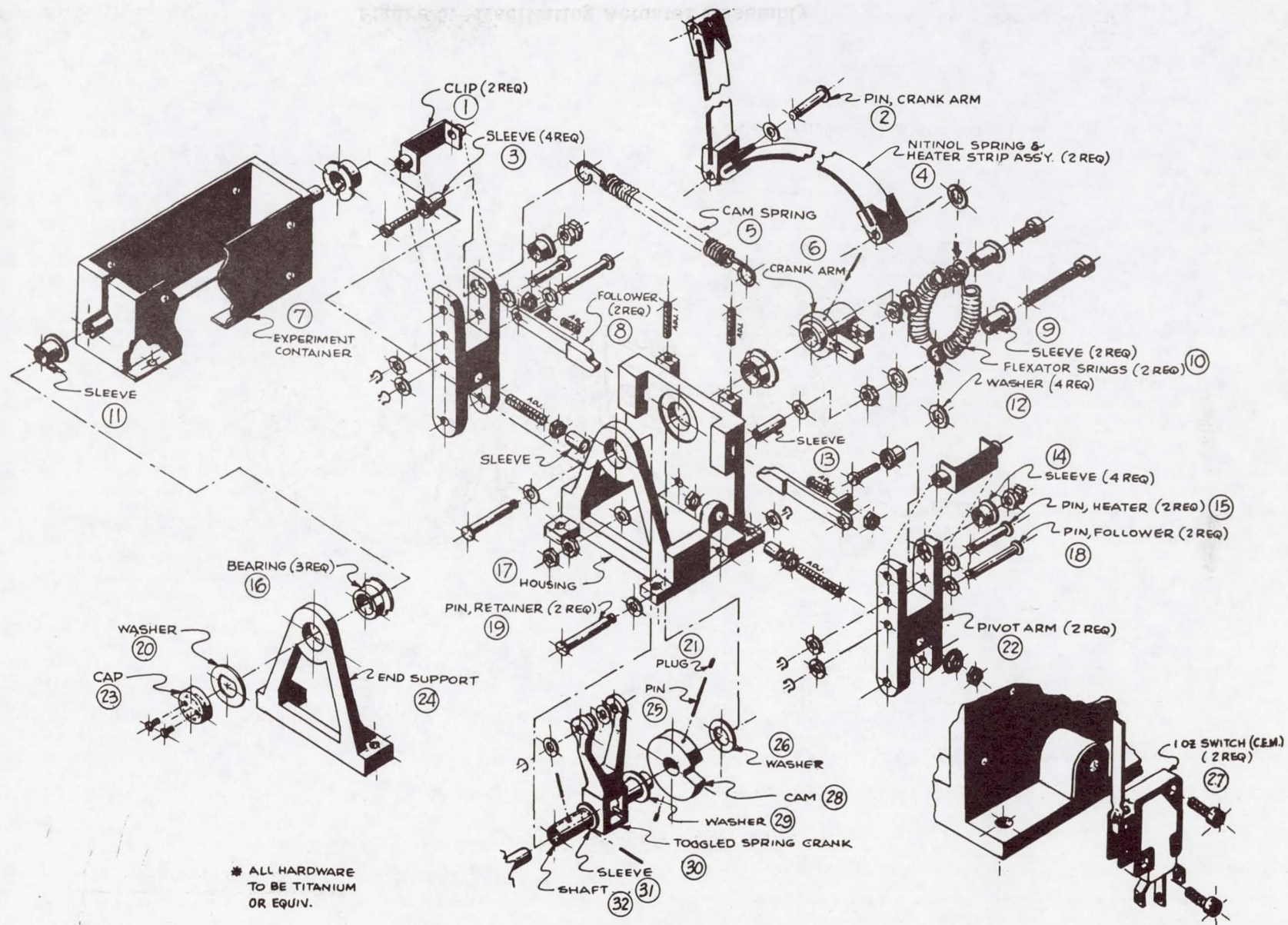


Figure 6. Exploded View-Oscillating Actuator Assembly

15. THE MECHANICAL DESIGN OF AN IMAGING PHOTOPOLARIMETER FOR THE JUPITER MISSIONS

(PIONEER 10 AND 11)

By James C. Kodak

Santa Barbara Research Center
Goleta, California

SUMMARY

This paper discusses the mechanical design and fabrication of the Imaging Photopolarimeter (IPP), a multifunction space-qualified instrument used on the Jupiter Pioneer Missions. The extreme environmental requirements for the structural design, optical system, and mechanisms are described with detailed discussion of some of the design and fabrication problems encountered.

INTRODUCTION

An Imaging Photopolarimeter (IPP) was launched aboard Pioneer 10 in March of 1972 and, after 21 months of travel through space, passed by the planet Jupiter in December of 1973. During this time, the instrument passed through the asteroid belt and the intense radiation and magnetic fields of Jupiter to successfully fulfill its mission. The interplanetary portion of the mission was utilized to generate sky maps of brightness and polarization of the zodiacal light. During the Jovian encounter, the IPP produced two-color images of Jupiter with resolution and at viewing angles unobtainable from earth. In addition, it measured the brightness and polarization of light reflected from the planet from which, for example, details regarding the size and shape of the particles composing the atmosphere can be deduced.

A second IPP launched aboard Pioneer 11 in April of 1973 will pass by Jupiter in December of 1974 to accumulate additional data at viewing and approach angles different from those of Pioneer 10. Since Pioneer 10 fulfilled its main objectives and successfully survived the Jovian radiation belts, Pioneer 11 has been retargeted so as to pass by Saturn nearly five years after the December 1974 encounter with Jupiter. This will provide significant bonuses with only relatively minor compromises, e. g., somewhat less favorable imaging geometry at Jupiter.

The IPP is a multifunction instrument designed to: 1) map the zodiacal light (faint light measurement); 2) measure the brightness and polarization of light in two spectral bands (colors) reflected from the planet Jupiter; and 3) produce two-color images of Jupiter. The instrument (see Figure 1) consists of an electronics module and a scanning electro-optics assembly. The instrument is mounted aboard a spinning spacecraft (see Figure 2) and utilizes the 4.9-rpm spin of the spacecraft to scan a narrow strip across the planet (or across the sky in the case of the zodiacal light mode) during each revolution. The electro-optics assembly may also be positioned in 0.5-mrad steps in the direction of flight from 29° from the earthward direction to 170° from the earthward direction. This stepping allows scanning of contiguous strips which can be recombined during ground data processing. The various optical modes are achieved by inserting various field-defining apertures, polarization-analyzing optics, and calibration sources into the optical path at the focal plane. The optical system is a complex combination of mirrors, lenses, prisms, multilayer coatings, and filters that separate the viewed scene into four beams, two red and two blue, with each colored pair orthogonally polarized. The four beams are then individually imaged onto individual cathodes of two dual-channel detectors. The red and blue light is quantized into 64 intensity levels (imaging mode) and 1024 levels (photopolarimeter and zodiacal light modes) and then transmitted to earth as coded numbers. The signals are reconstructed and enhanced by computer to provide two-dimensional displays of the data (spectacular color images and brightness and polarization maps).

ENVIRONMENTAL AND INTERFACE REQUIREMENTS

The IPP was designed to withstand the normal launch environment of most spaceborne instruments and to survive the almost two-year journey through space and passage through the Jovian radiation belts. In addition, the presence of a magnetometer aboard the spacecraft made it necessary to produce a virtually nonmagnetic instrument.

The instrument is located on the spacecraft to take advantage of the 4.9-rpm spin and to provide as optically clear a field of view as possible. The IPP is mounted in the spacecraft instrument compartment with the electro-optics assembly extending through the side of the compartment wall. As a result, the electronics are maintained at close to ambient temperature and the electro-optics assembly is exposed to the sub-zero temperatures of deep space. This mounting configuration caused some concern among the experimenters involved because the exposed telescope could readily collect dust and debris during launch. Dust would create extensive light scattering and could jeopardize the faint light experiment. Maintaining cleanliness of the optics was mandatory during fabrication, assembly, and launch as well as in flight to Jupiter.

The total weight of the IPP is less than 10 pounds and the power requirement is approximately 2 watts.

MATERIAL CONSIDERATIONS

The IPP was designed to be constructed almost entirely of beryllium. This material was selected primarily to minimize weight. All materials used were considered for their radiation resistance and nonmagnetic characteristics. Materials considered suspect were exposed to specific doses of radiation and evaluated for damage. Radiation problems had their most significant impact in the electronics and optics areas. The most serious problem in the optics area was discoloration or phosphorescence. In the initial design concept, the detectors were mounted with the electronics, close to the high-voltage supply, and the optical beams were relayed to the detectors through fiber optics. However, all the fiber optics materials that were flexible enough to allow the telescope scanning would discolor when exposed to the levels of radiation anticipated during the Jovian encounter. As a result, the fiber optics were eliminated and the detectors mounted directly on the electro-optics assembly. The high voltage was then routed from the electronics module through a specially fabricated flat cable to the detectors on the electro-optics assembly.

Another problem was encountered with the calcite material selected for the three-segment Wollaston prism. Because of its large size, artificially grown calcite was not available and material had to be obtained from naturally occurring crystals. Natural crystals generally contain impurity ions which discolor or phosphoresce when exposed to high energy radiation. As a result, it was necessary to irradiate various small samples cut from large crystals to find a sufficient quantity of material unaffected by the radiation.

Most mechanical materials are not affected significantly by radiation. However, the use of organic materials was potentially a problem. While most epoxies tend to harden a minor amount, teflon and nylon, for example, are severely affected. All materials and components utilized were checked for magnetic characteristics to ensure that some magnetic item was not inadvertently assembled. One magnetic screw or washer could make the system so "hot" that disassembly would be necessary. The glass feedthroughs on the detectors and other electronic components were another problem. These feedthroughs were fabricated of low nickel alloys so that their thermal expansion coefficients closely matched that of glass. It was necessary to clip the magnetic leads off as close to the glass as possible and weld nonmagnetic wire in place of them.

Gimbal bearings were fabricated of Composition 125 and Berylco 25. Small instrument bearings did not cause any significant problems and were therefore screened and used as is.

INSTRUMENT CONFIGURATION

The instrument (see Figure 1) has two major components, the electronics module and the scanning electro-optics assembly. An integral mounting platform was configured to provide a direct thermal path from the electronics and from the scanning optical telescope to the spacecraft without interference from other components or one another. Spacecraft thermal control therefore exerts a direct effect in controlling the environment of these assemblies. The mounting platform was fabricated of black anodized beryllium. Critical interfaces were gold-plated to enhance thermal and electrical transfer. The mounting platform was fabricated of four separate structures and screwed and bonded together to form an assembly. The bonded joints were located such that they do not interrupt the thermal path nor are they solely relied on to carry the structural loading. This four-piece assembly was designed to allow fabrication of the structure from small sections of beryllium plate in lieu of the less available and more costly large beryllium block.

The electro-optics assembly (see Figure 3) is supported from the mounting platform by two gimbal bearings specially fabricated of nonmagnetic materials and dry lubricated with molybdenum disulfide. One gimbal bearing is installed directly between the optics assembly and the mounting platform and the other is installed in the platform-mounted telescope drive assembly which positions the optics along its 160° scan. A flexible braided thermal strap was connected between the optics assembly and the mounting platform to enhance thermal balance between the cold optics assembly and internally heated electronics housing. Thermal conductivity of the braid is considerably greater than that of the bearing assembly.

The electro-optics assembly consists of a Maksutov telescope, a six-position focal plane aperture actuator, a Wollaston prism, various optical elements, and two dual-channel Channeltron detectors (see Figure 4).

The Maksutov telescope consists of a primary mirror, secondary mirror, and spacer installed between the mirrors. The spacer is fabricated of the same fused silica material as the mirrors to minimize focal plane shift as a result of thermal expansion. The entrance aperture is 2.5 cm in diameter and is located at the primary mirror. Contact pressure is maintained between these components by a Viton O-ring installed on the outside of the

secondary mirror (corrector). The entire telescope is housed in a machined black anodized beryllium tube which contains integral "knife-edge" baffles for stray light suppression.

The six-position aperture actuator is driven by a stepper motor specially designed to minimize static and dynamic magnetic fields. The actuator design integrates the aperture carrier into the basic structure and provides a receptacle for bonding in place the aperture plate and the focal plane optics.

The aperture plate contains the **field-defining** apertures which vary in size from a 0.5-mrad square (0.038-mm square) to a 40-mrad square. The aperture is fabricated of beryllium copper, plated with black chrome and photoetched. Because of the design change that required that the detectors be mounted on the moving optics, the space allocated for the aperture actuator was limited and resulted in an actuator configuration with a limited bi-directional rotation ($\pm 50^\circ$). As a result, the damping and calibration required to achieve desired detenting within the specified response times and voltage range, and over the required temperature range, were extremely difficult. It is felt that this type of design should be discarded on future designs in favor of unidirectional continuous rotation configurations where space permits.

The Wollaston prism (see Figure 5) is constructed of three segments of calcite. Calcite is a material possessing an anisotropic thermal expansion coefficient, $25 \times 10^{-6}/^\circ\text{C}$ parallel to its optical axis and $-6 \times 10^{-6}/^\circ\text{C}$ perpendicular to its optical axis. It is necessarily (optically) configured such that the thermal expansion coefficient of each segment differs from other adjacent segments along the same axis. The three segments of the prisms are bonded to each other and suspended in an aluminum housing by an elastomeric encapsulant. Aluminum was selected for the housing because the combined thermal expansion coefficients of the calcite and the elastomer closely match the expansion coefficient of aluminum when used in the subject configuration. As a result, the prism remains essentially stress free. Calcite is a very fragile material and must be handled with special precautions. Care must be exercised to shroud the material when thermal cycling, as even mild thermal shocks were shown to produce fractures in the raw material.

Two dual-channel detectors were mounted on the optics assembly in an aluminum housing with a semi-flexible adhesive. Aluminum was selected for this housing as it provided more radiation protection for the detectors than beryllium.

The various mirrors and lenses in the optics assembly were fabricated of radiation-resistant glass and bonded to the beryllium housings by a semi-flexible adhesive. All mirror and lens positions were individually adjustable

by replacement of premachined shims to allow optimum positioning of the optical images on each detector.

The completed optics assembly is shrouded by a low emissivity polished aluminum drum which eliminates the excessive heat loss that would result from direct exposure to deep space. It is gimballed between the platform-mounted telescope drive motor and platform-mounted bearing assembly.

The telescope drive actuator (see Figure 6) which produces the 160° scan is a special sealed drive system designed to transmit rotational motion through a welded hermetic seal. Thus, suitable lubricants were completely contained within the active mechanical portion of the drive to assure reliable operation over the lengthy Jupiter mission.

The gear configuration is divided into two stages such that it converts 15° steps at the rotor to 0.5-mrad steps at the output. The first-stage gear reduction of 7.3:1 is accomplished in two passes of conventional gearing. The second-stage gear reduction of 72:1 is accomplished through a harmonic drive.* The harmonic drive consists of three basic parts: the wave generator, flexspline, and rigid spline. The wave generator is an elliptical cam which deforms the flexspline into an ellipse causing it to engage with the circular rigid spline at two points of contact. The flexspline is fixed and the wave generator is rotated by the first-stage gearing. As the wave generator rotates, tooth engagement between the flex and rigid spline follows the rotation of the wave generator. The number of teeth in the flexspline differs from the number of teeth in the rigid spline by two. As the wave generator makes one rotation, the flex and rigid spline are displaced with respect to each other by two teeth. With a 144-tooth flexspline, this produces a 144:2 reduction.

The stepping accuracy (0.5 ± 0.1 mrad) required was pushing the state of the art for this size actuator. The windup in the flexible spline (variation in resisting torque as a result of discontinuities in the deflection member) resulted in somewhat worse accuracy than required in the initial unit. This problem was minimized by matching flexsplines to wave generators and by the ultimate addition of a torsional spring to the output shaft of the actuator. This spring loading put a higher torque on the drive and made the variation in torque caused by flexspline windup less significant.

*Gear Systems Division, United Shoe Machinery Corporation, Beverly, Massachusetts.

An input encoder was built into the motor to indicate stepper motor rotor position; this is used in conjunction with an output shaft encoder to indicate telescope position. The input encoder thus acts as a vernier position readout. An output (brush type) position encoder is mounted directly on the motor output shaft and is indexed to the main mounting platform and the telescope. This encoder provides the coarse positional readout.

An important actuator design consideration was that of magnetic field suppression so as not to interfere with the extremely sensitive spacecraft magnetometer. This was accomplished by special design of tightly coupled flux paths and the use of magnetic materials of very low remanence characteristics.* Both motor-driven actuators in the IPP exhibit magnetic cleanliness characteristics of approximately 10% of the allowable Pioneer specified values, thus confirming the validity of these techniques. For example, the aperture actuator which contains no shielding measured less than 0.1 gamma at 0.9 meter (3 feet) static and 0.2 gamma in the worst axis while stepping at maximum rate. The telescope drive assembly with a mu-metal shield measured 0.3 gamma at 0.9 meter (3 feet) depermed, 1.2 gamma at 0.9 meter (3 feet) after 25 gauss exposure and 0.06 gamma depermed and operating at maximum rate.

ACKNOWLEDGMENTS

The work reported in this paper was conducted at Santa Barbara Research Center, Goleta, California, a subsidiary of Hughes Aircraft Company for NASA/Ames Research Center under NAS-2-5605.

*Designed under subcontract by Schaeffer Magnetics, Inc., Chatsworth, California.

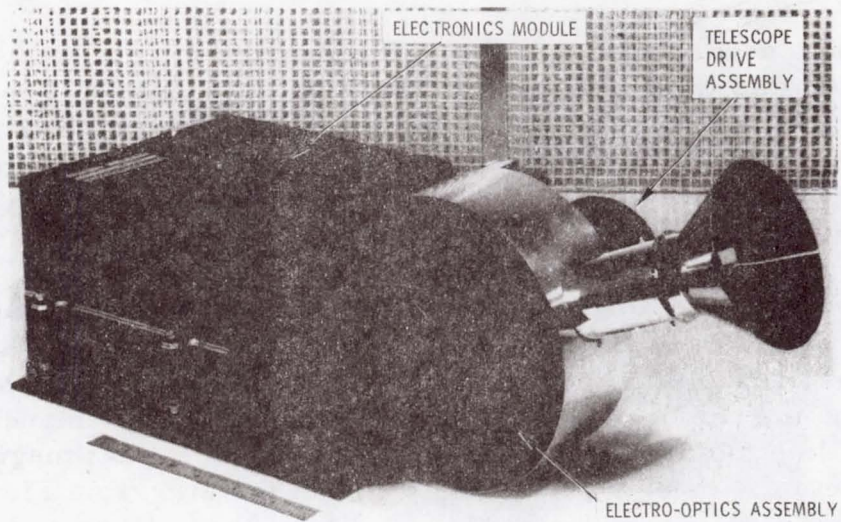


Figure 1. Imaging Photopolarimeter

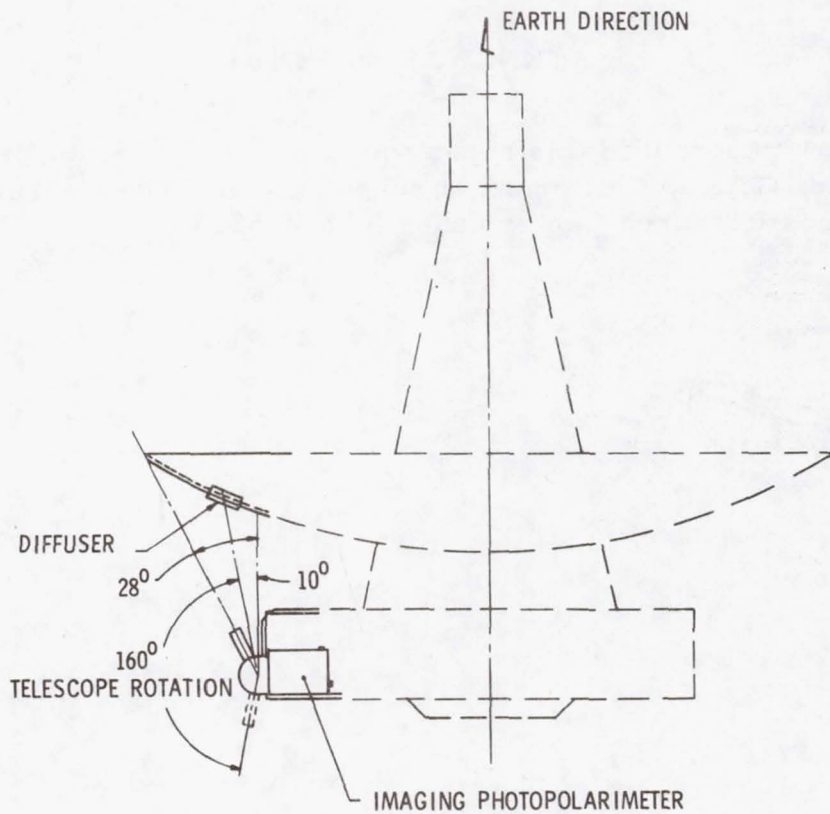


Figure 2. Imaging Photopolarimeter Orientation on Pioneer 10 and 11 Spacecraft

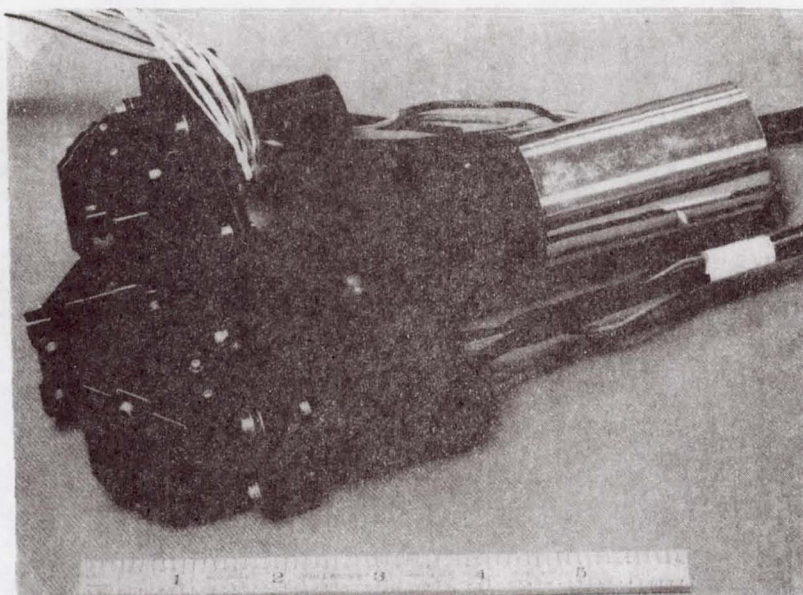


Figure 3. Electro-Optics Assembly

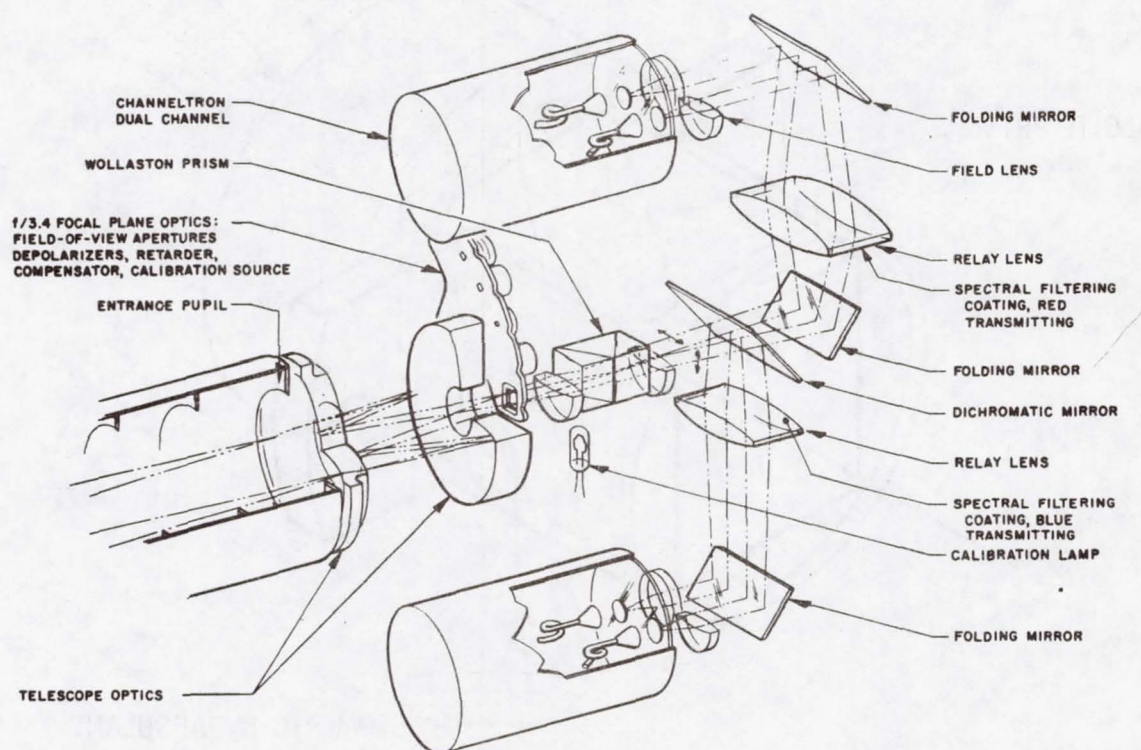


Figure 4. Optical System of the Pioneer Jupiter Imaging Photopolarimeter (Analysis of two orthogonally polarized beams into two colors, red and blue, is shown.)

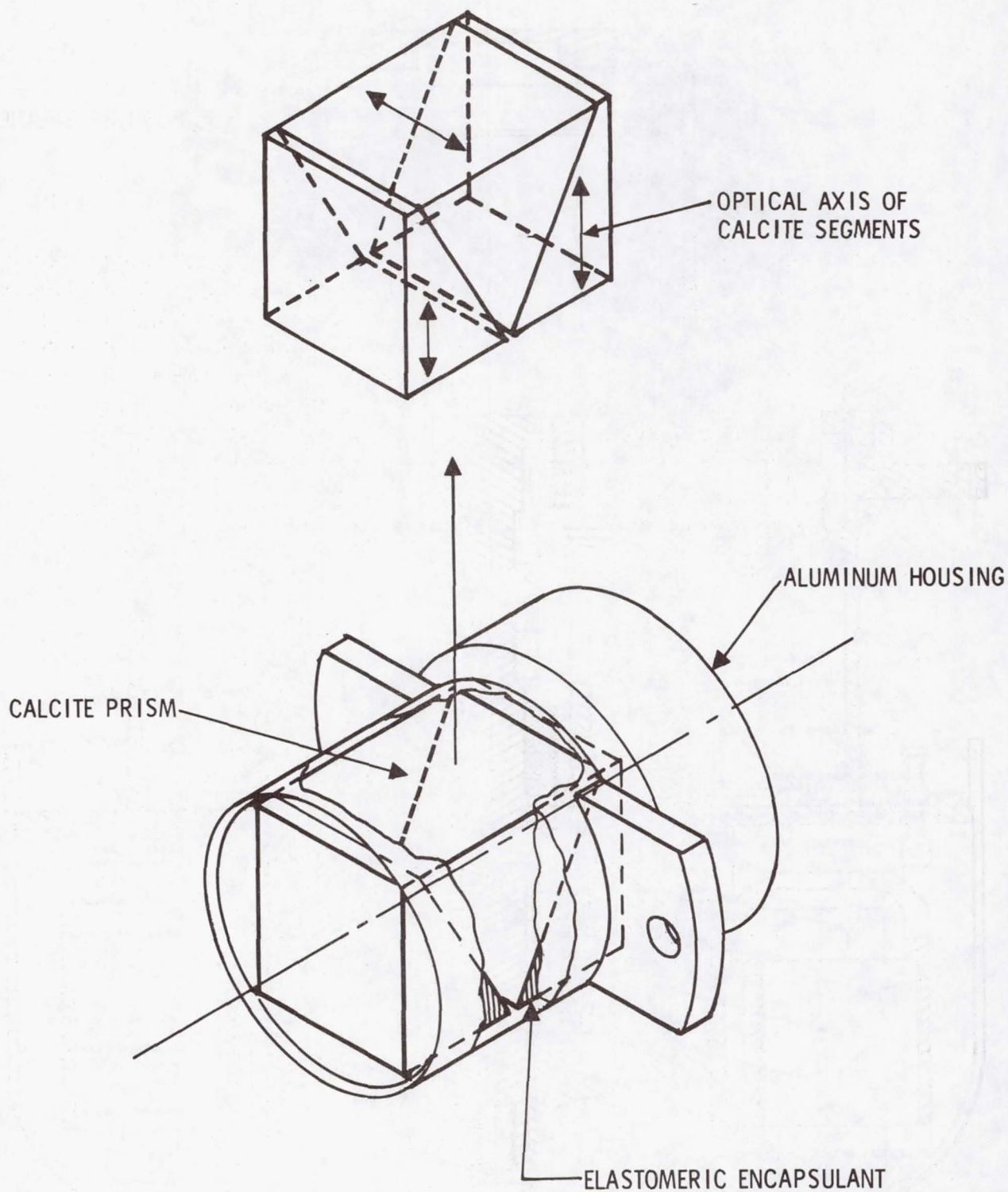


Figure 5. Wollaston Prism Mounting Configuration

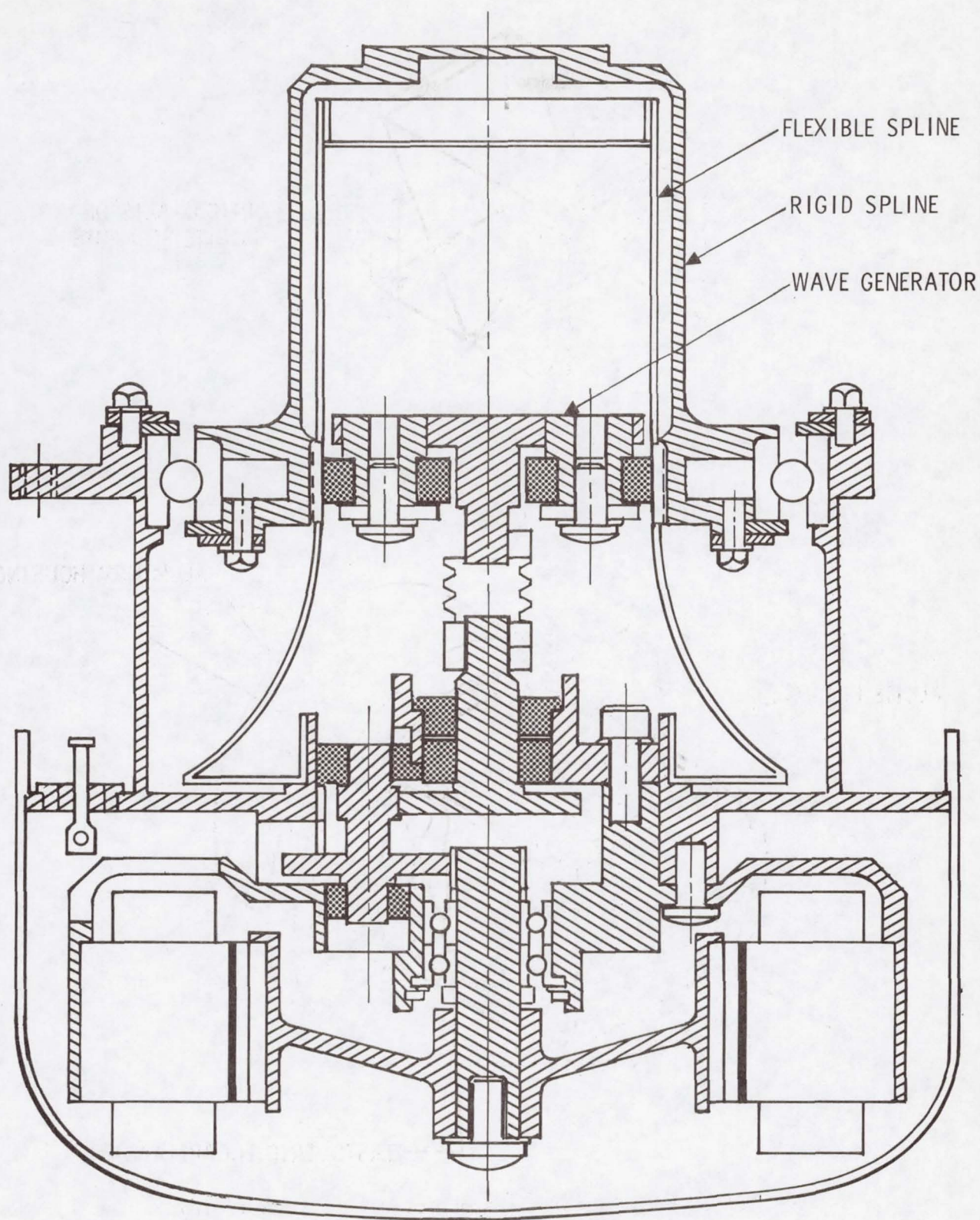


Figure 6. Telescope Drive Actuator

16. MAGNETICALLY SUSPENDED REACTION WHEELS

By Ajit V. Sabnis, George L. Stocking and, Joe B. Dendy

Sperry Flight Systems, Phoenix, Arizona

SUMMARY

Recent developments in the technology of magnetic suspensions point to an imminent application to spacecraft systems where long life is a requirement. Magnetic suspensions offer several advantages over conventional bearings, arising because of the contactless nature of the load support. In application to spacecraft reaction wheels, the advantages are: low drag torque, wear-free, unlubricated, vacuum-compatible operation and unlimited life. In addition, by the provision of redundancy in the control electronics, single-point failures may be eliminated. The rationale for selection of a passive radial, active axial, dc magnetic suspension is presented, and the relative merits of 3-loop and single-loop magnetic suspensions are discussed. The design of a .678 N-m-sec (.5 ft-lb-sec) reaction wheel using the single-loop magnetic suspension is developed; the design compares favorably with current ball bearing wheels in terms of weight and power.

INTRODUCTION

In application to reaction wheels for spacecraft, the primary advantages of magnetic suspensions are: low drag torque, wear-free, unlubricated, vacuum-compatible operation and unlimited life. Operation in the neighborhood of zero speed poses no problems since the suspension capacity is independent of rotational speed, there are no lubrication anomalies, and drag is virtually zero (70.7×10^{-6} N-m/1000 rpm) (.01 oz-in./1000 rpm). In addition, by the provision of redundancy in the control electronics, single-point failures may be eliminated. Pioneering work in the development of magnetic suspensions was done at the University of Virginia, under the direction of Beams (reference 1). The earliest suspensions date back to 1937. Since then, magnetic suspensions of various configurations have been constructed. Recent developments in the technology of magnetic suspensions have been spurred by advancements in magnetic materials and microelectronics, and point to applications in spacecraft systems where long life is a requirement. Some recent designs with the viewpoint of an ultimate spacecraft application were reviewed by Henrikson et al (reference 2) and the design of a 1085 N-m-sec (800 ft-lb-sec) momentum wheel assembly was described in (reference 3).

MAGNETIC SUSPENSION CHARACTERISTICS

Magnetic suspension offers many advantages for rotational equipment, but as may be expected, some limitations are also incurred. A summary of these characteristics is presented in Table 1.

TABLE 1

MAGNETIC SUSPENSION CHARACTERISTICS

ADVANTAGES

- High reliability (no wear, lubrication, or fatigue)
- Low torque (starting, drag and ripple)
- High speed capability
- Low noise and vibration
- No single-point failures (with redundant electronics)
- Compatible with vacuum environment (no lubricant)
- Insensitive to thermal conditions (large gaps)

DISADVANTAGES

- Lower capacity per unit weight
- Control electronics required

The advantages arise from the basic nature of contactless suspension (non-bearing). High reliability is possible because of the elimination of the lubrication, wear and fatigue characteristics normally associated with ball or fluid bearings; however, a control system must be provided, and its failure rate must be accounted for in the reliability calculation. In connection with this point, it is of interest to note that redundancy can easily be incorporated in the control system electronics; thus, single point failures can be eliminated in the entire system without duplication of the mechanical and structural elements (rotor, housing, etc).

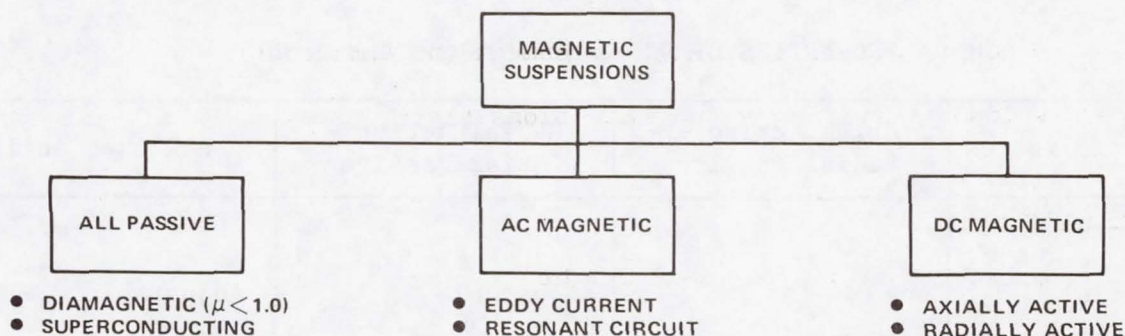
The limitation of capacity is a result of the physics of magnetic force generation: a pair of magnetized surfaces can develop a load capability of $1.6 \times 10^{-6} \text{ N/m}^2$ (232 psi) at a flux level of 2 Wb/m^2 (near saturation level

for iron). When compared with the $2065 \times 10^6 \text{ N/m}^2$ (300,000 psi) design limit for ball bearing steels, it can be appreciated that substantially more material must be provided to obtain the same total load capacity. In order to minimize total system weight, it is therefore very important to design the suspensions for the minimum required capacity and/or stiffness.

SELECTION OF MAGNETIC SUSPENSION TYPE

The achievement of entirely contactless suspension is subject to the fundamental restriction of Earnshaw's theorem (reference 4), which specifies sufficient conditions for instability in inverse-square force fields. The practical consequence of the theorem is that stability under magnetostatic fields is impossible unless diamagnetic or superconducting materials are employed. In the presence of ferromagnetic materials, there is at least one statically unstable coordinate direction, and suitable time-varying fields must be generated to assure stable suspension.

Magnetic suspensions can, in general, be placed in three categories:



444-8-5

The all-passive systems are magnetostatically stable and therefore do not require an active control system. However, diamagnetic suspensions have very low specific load capacity because their permeability is very close to unity. Superconducting suspensions require the added weight and complexity of a cryogenic cooling system. Of the active systems, ac systems (both eddy-current repulsion and ac resonant) are characterized by high power loss and poor damping characteristics. For application to reaction wheels, the choice therefore narrows to one of the dc magnetic systems.

Comparison of DC Magnetic Suspension Types

DC magnetic suspensions were first so termed because a steady-state current was used to provide passive magnetic restoring forces, with modulation of this current used to provide total (3-dimensional) stability and levitation. This category has since been extended to include systems in which the passive restoring forces are provided solely by permanent magnets. Rotational dc magnetic suspensions may be divided into three classes:

- Axial active, radial passive (1 degree-of-freedom is actively controlled)
- Radial active, axial passive (2 to 4 degrees-of-freedom are actively controlled)
- All-active (5 degrees-of-freedom are actively controlled)

The comparative characteristics of the three types of systems are summarized in Table 2.

TABLE 2
PROPERTIES OF DC MAGNETIC SUSPENSIONS

Characteristics	Axial Active - Radial Passive	Radial Active - Axial Passive	All Axes Active
Stiffness			
Radial	Low	Adjustable	Adjustable
Axial	Adjustable	Low	Adjustable
Drag Torque	Lowest	Low	Low
Power Loss	Low	High	High
Control System	1 degree-of-freedom	2 to 4 degrees-of-freedom	5 degrees-of-freedom
Reliability	High	Low	Lowest

The principal advantage of using passive means to obtain restoring forces is inherent simplicity and reliability; neither sensors, electronics, nor control coils are required. When the quiescent field used to obtain the passive restoring forces is provided by permanent magnets, the power losses due to

constant coil currents are eliminated. However, the suspension stiffness is entirely determined by the passive magnetics and, unless separate means are provided, cannot be altered from the original value. Additional damping forces (e.g., from eddy-currents) must be provided in order to ensure satisfactory dynamic response and well-bounded amplitudes at resonant conditions.

Active means of obtaining magnetic support forces have the advantage of adjustable stiffness and damping characteristics, which are obtainable by variation of control system parameters. The disadvantages are that sensors, electronics, and forcing coils are required, with a resultant lowering of reliability. Moreover, an active system requires suspension power not only during dynamic-load conditions, but also standby electronics power during static-load conditions.

Selection of a particular suspension type depends heavily on application requirements. In one important area, reliability, the axially active/radially passive suspension is superior to the other types. The reason for this is the smaller number of degrees of freedom required in the control system. Thus, it is primarily for the reliability consideration that the active axial-passive radial suspension was chosen for reaction wheels. It should be noted, however, that, for the same radial stiffness, the weight of this type of suspension is higher than for an active system, and that specific attention must be directed to designing for the minimum allowable radial spring rate for each application.

Consideration is now given to the nature of the passive-radial suspension and to the method of axial control force generation for it.

Repulsion Versus Attraction

Schematic illustrations of passive repulsion and attraction suspension techniques are shown in Figures 1 and 2, along with a listing of advantages and disadvantages. In the repulsion system, the radial restoring force is generated by the reaction between like magnetic poles. In the attraction system, the radial restoring force is caused by the tendency of the rotor to be in a position of minimum reluctance of the magnetic circuit.

In comparing the relative merits of these techniques, two significant factors can be noted:

- The flux is contained within the magnetic circuit in the attraction suspension, but is forced to be external in the repulsive suspension. This flux containment results in reduced drag torques, and also minimizes unwanted vehicle disturbance torques that would otherwise be generated by interaction with the ambient magnetic field.

- In the repulsion suspension, a separate means (such as a dual-acting solenoid) must be provided to generate bi-directional axial control forces; in the attractive suspension, it is possible to modulate (increase or decrease) the existing magnetic field to generate axial control forces. In addition, non-uniformities in the permanent magnets cause periodic forces and large runouts, and large drag torques.

A comparison of the other features listed in Figures 1 and 2 also favors the attractive system.

To summarize, the preferred suspension for spacecraft reaction wheels:

- Is dc magnetic
- Is active-axial, passive-radial
- Uses an attractive magnetic circuit.

CONTROL CONCEPTS FOR THE ACTIVE AXIS

As a consequence of Earnshaw's theorem, the radial restoring stiffness of the passive magnetics is accompanied by instability in the axial direction. Because this unbalance force is a function of the difference between the squares of two terms, the net force in the axial direction is a linear function of axial displacement near the equilibrium position. The axial equation of motion of the magnetic suspension is thereby given by

$$M \ddot{z} - K_u z = F$$

where

z = axial displacement from the equilibrium position

M = suspended mass

K_u = unbalance stiffness

F = applied force (total)

Axial stability can be obtained by controlling the current to the control coils to generate forces in the proper direction. Thus, if the control force includes rate-plus-displacement feedback given by

$$F_c = -B \dot{z} - K z,$$

then the axial equation of motion becomes

$$M \ddot{z} + B \dot{z} + (K - K_u) z = F_e$$

where F_e is the external force. This equation indicates system stability can be obtained for $K > K_u$, a net static stiffness of $(K - K_u)$, and results in a power loss under external axial loads. In practice, the rate sensor may be avoided by using lead compensation of the position signal. A block diagram of the axial control system is shown in Figure 3, and the root locus in Figure 4.

In addition to the lead compensation, a minor loop integrator can be added (shown by dashed lines in Figure 3) in order that the unbalance stiffness of the passive magnetics can be used to advantage in overcoming constant external loads. The integrator also enables long-term, low-power operation by correcting for drift in any of the electronic components, including the position sensor. With integral feedback, the static axial stiffness is negative; the root locus of this system is shown in Figure 5.

MAGNETIC SUSPENSION DEVELOPMENT

Three-loop magnetic suspensions and their application to a large momentum wheel were reported in reference 3, where the nomenclature "3-loop" was selected because of the 3-loop magnetic circuit.

A 1-loop suspension model (Figure A-1) based on the configuration evolved for the reaction wheel (Figure 7) was fabricated and tested in order to confirm the design approaches and obtain preliminary data. The model has been operated successfully through resonance speeds and has shown extremely low drag torques. Test results are discussed in the Appendix.

APPLICATION TO REACTION WHEELS

The use of reaction wheels is a proven and accepted technique for control of spacecraft attitude. In a typical system, three orthogonally mounted wheels are employed, each developing bidirectional control torques in response to commands from the attitude control sensors.

The total momentum exchange system can be configured as having a nominal zero bias, or else can have a finite momentum along a particular spacecraft axis. In the case of a zero bias system, which is of particular interest here,

the wheels must be capable of operation in both directions of rotation, including the region about zero speed. Although ball bearing supported wheels have achieved lifetimes in the neighborhood of 4 to 5 years, their use for longer missions is highly questionable. The main reason for this is the necessity of assuring the presence of a lubricant in the ball contact area over this period of time, and of providing a load-carrying film (or boundary lubrication) in the near-zero speed region. Also, while statistical proof of long life can be accomplished on a design basis for a ball bearing system, it is virtually impossible to guarantee its existence on each individual wheel.

The obvious solution to the ball bearing problem is to avoid contact of the bearing elements, and to eliminate the need for a lubricant supply. Magnetic suspension constitutes such a contactless support system, and forms the basis for the reaction wheel design described in this paper.

Design Requirements

Each application of reaction wheels to a spacecraft attitude control system has its own particular set of requirements. For the purpose of this development, the requirements were based on an interplanetary spacecraft. These requirements and the values achieved are listed in Table 3.

The motor torque is the net (accelerating/decelerating) torque applied to the wheel, and its reaction is usable for vehicle control purposes. This torque must be delivered upon command in either direction over the total angular momentum range of the wheel. The maximum motor power of 8 watts includes that required for suspension and windage drag, in addition to the net torque delivered to the vehicle.

The suspension system peak power is consumed only momentarily, during initial levitation ($< .01$ sec).

The cross axis rate input causes a deflection at each bearing due to gyroscopic effects. The interpretation of this requirement is that there be no physical contact of the touchdown bearing elements during this condition. The weight and volume requirements include the reaction wheel plus one channel of suspension control electronics.

Meeting the performance requirements at low ambient pressure and over the stated temperature range should not be a problem as it can be with ball bearing wheels. Because magnetic suspensions are low power devices and are directly compatible with hard vacuum, the housing can be vented directly to space with no adverse effects on the wheel. Performance over the temperature range should also be readily achieved because of the absence of lubricants and the use of sizable clearances. In fact, there should be no significant variation in performance from the standard test conditions.

TABLE 3
.678 N-M-SEC REACTION WHEEL CHARACTERISTICS

Parameter	Design Requirements	Design Value Attained
Angular Momentum	$\pm .678$ N-m-sec	$\pm .678$ N-m-sec
Motor Torque (min)	$\pm .0136$ N-m	$\pm .0149$ N-m
Motor Power (max)	8 watts	7 watts
Suspension Power		
Peak	8 watts	8 watts
Average	1 watt	.5 watt
Max Cross Axis Rate Input	.0175 rad/sec	.83 rad/sec
Weight	3.62 Kg	2.54 Kg
Volume	.004095 m ³	.001965 m ³
Environment		
Temperature	+20°C to +75°C	+20°C to +75°C
Pressure	10 ⁻¹⁴ torr	10 ⁻¹⁴ torr
Life	10 years, operating	unlimited
Vibration	.1 G ² /Hz	> .1 G ² /Hz

The 10-year life requirement does not apply in the normal mechanical sense because no wearout mechanisms are present. Thus, the definition of life is reduced to determining the reliability of the suspension control system based on constant failure rates.

Magnetic Suspension

Three-loop and 1-loop suspensions were considered for this application. The 1-loop configuration is shown in Figure 6. It is the simplest of the designs in which a permanent magnet field is modulated to provide control forces; the permanent magnet and the control coil establish magnetic flux in the same

magnetic circuit loop. Passive radial stiffness is attained through the action (minimum reluctance) of opposed concentric rings. Bidirectional control forces are provided by controlling the current in the coil.

The primary disadvantage of the 1-loop configuration compared to the 3-loop configuration is that the control current must counter the reluctance of the permanent magnet in the 1-loop design. This means that larger control currents are necessary to produce the same axial force, entailing larger power loss under dynamic loads. In addition, high-coercivity permanent magnet materials such as the rare earth cobalts are essential to prevent the possibility of demagnetization. Analysis shows that the reduction of the force-to-current gain is only 50 percent for the case when the magnet is designed for minimum volume, and can be even lower with an increase in magnet volume.

Since the passive radial stiffness is proportional to the square of the flux density, it is desirable to provide as high a bias flux density as possible, allowing sufficient modulation margin before saturation occurs. Considering that the flux density at saturation for soft material such as electromagnet iron is in the range 1.6 to 2.0 Wb/m^2 , a bias density level of 1.4 Wb/m^2 is a suitable value for design; this leaves adequate margin for modulation to develop axial control forces.

The minimum radial stiffness required for the .5 ft-lb-sec reaction wheel was determined to be in the range $12,270 \text{ N/m}$ (70 lb/in.) to $29,250 \text{ N/m}$ (167 lb/in.), corresponding to a rotor weight in the range of .453 (1 lb) to 1.36 Kg (3 lbs). The following constraints on radial stiffness were considered in determining these values:

- Suspension without touchdown in any attitude, in both 0-g and 1-g environments.
- Radial and angular rigid-body resonance frequencies to be above 20 Hz.
- No touchdown under cross-axis rates up to $.0175 \text{ rad/sec.}$

Previous testing on a 3-loop suspension model had demonstrated that the resonance speeds could be dwelt on for extended periods without significant effect on motor or suspension power. For this reason, the possible location of resonance speeds in the operating speed range was deemed acceptable, and no additional constraints were imposed.

Sizing 1-loop and 3-loop suspensions for the expected stiffness range revealed that the former were lighter by a factor of nearly 3:1. The weight comparison, the design simplicity, the fewer number of machined parts and ease of manufacture and assembly were the basis for selecting the 1-loop design for the reaction wheel. Iterations in the design process determined the rotor weight

to be .816 Kg (1.8 lbs) and the corresponding value of radial stiffness, 19,280 N/m (110 lb/in.). The suspension was sized accordingly and is shown in the wheel layout of Figure 7.

RWA Design Description

A minimum weight design was achieved by optimization of the rotor radius and the maximum operating speed [88.9mm (3.5 in.) rotor radius at 1500 rpm)]. Several variations of the spin motor configuration, when combined with the rotor, housing, and suspension tradeoff data, showed that the minimum weight design utilized a segmented spin motor, with its cage serving as the major RWA inertia element.

The spin motor is made up of two 40-degree segments, thus leaving ample circumferential room for the provision of redundancy (common cage feature). The motor characteristics are shown in Figure 8. The magnetic suspension configuration completely contains the permanent magnets, thus eliminating the potential problem of flaking due to the existence of microcracks in the material. The spacer ring is sized to transmit all the mechanical loads rather than the magnets. The design permits the parts to be machined with relatively loose tolerances, the pole piece clearances and the touchdown bearing clearances being set at assembly.

The touchdown system must be capable of absorbing the impact at touchdown, and also capable of dissipating the energy in the wheel. The use of journal bearings was chosen for the reaction wheel design. A survey of potential materials was made and a Garlock product, DU, was chosen. DU is a prefinished, inert, high performance bearing material that requires no lubricant, and presents no outgassing problem. In this application the calculated life is 255 hours at the maximum RWA speed of 1500 rpm.

Normal contact of the touchdown bearings as a sequenced event occurs at zero wheel speed. However, in the case of unscheduled touchdown at maximum speed, the wheel energy must be dissipated thermally. If this energy is contained within the volume of a single bearing, the calculated temperature rise is 38°C; at the upper ambient of 75°, the resulting touchdown bearing temperature of 113°C is well within the allowable material limit of 280°C.

The magnetic suspension has a radial stiffness of 19,280 N/m (110 lb/in.) and an axial stiffness of 175,000 N/m (1000 lb/in.). The axial stiffness can be varied from 0 to 350,000 N/m (2000 lb/in.) electronically. The permanent magnets used for the suspension are made from samarium cobalt because of its reversible, straight-line demagnetization characteristic and high intrinsic coercive force. This is especially important in the 1-loop design, because the control flux, which goes through the magnet, opposes the permanent

magnet flux when it is desired to decrease the flux density in the gap. The B-H characteristic also enables the magnet to be magnetized prior to assembly and eliminates the need for keepers. The weight breakdown of the system is given in Table 4.

TABLE 4
.5 FT-LB-SEC REACTION WHEEL WEIGHT BREAKDOWN

Element	Weight Kg (lbs)
Housing	.860 (1.9)
Rotor (including cage) Motor Cage	.815 (1.8)
Magnetic Suspension	.453 (1.0)
Motor Stator (2 segments)	.272 (.6)
Electronics	.090 (.2)
Vent Valve	.045 (.1)
Connector	.045 (.1)
	<hr/> 2.58 Kg (5.7 lbs)

SUSPENSION ELECTRONICS

The suspension electronics provides control forces to maintain levitation of the rotor in the axial direction. The main components, as shown in Figure 9, are the axial position sensor, compensation network, power amplifier, and an integrator. The primary design considerations are maximum reliability and minimum power consumption.

Position Sensors

Various types of position sensors are capable of measuring distances on the order of .128 to 1.28 mm (.005 to .050 inch) as required in this application. Of these, the eddy-current sensor offers a number of advantages making it very attractive. It has a high sensitivity providing a good signal to noise ratio; the sensing probe is small, thus minimizing mounting problems; and the electronics is very simple.

In the eddy-current sensor an ac source excites the probe which is simply a coil of wire oriented so that the induced field intersects the sensed surface. The surface must be a conductor so that eddy currents can be induced in it. The closer the probe to the sensed surface, the greater are the eddy currents. An electronic circuit converts the eddy current variation to a dc signal. An ac oscillator excites the probe through a high source impedance. The voltage across the probe then varies as the probe impedance changes with the varying eddy currents. The voltage is converted to dc by rectification and filtering. The eddy-current sensor can provide a typical output scale factor of .3 volt per mil and has good linearity. It is somewhat sensitive to temperature and excitation frequency changes, but in the closed loop magnetic suspension application this is not a disadvantage.

Compensation

Compensation consists of a lead/lag network which is required to stabilize the static unbalance in the axial direction. Enough phase lead must be added to lift the phase curve up above -180 degrees at the zero dB gain crossover frequency. Approximately 40 degrees of lead at 100 Hz is adequate. This will result in increased gain at high frequencies, tending to excite mechanical resonances. Thus, the lag is used to keep the high frequency gain as low as possible without introducing excessive phase lag at crossover.

An integrator is used, with positive feedback to minimize steady-state power consumption and to eliminate the effects of control electronics or position sensor drift. It operates very slowly so that it does not interfere with the dominant dynamics of the suspension system. Steady-state coil currents are integrated and added to the position signal, thus moving the position command to a point where the rotor is at a force equilibrium with the permanent magnet forces. At this point no coil current is required.

Power Amplifier

The power amplifier consists of a linear power bridge which controls current in either direction through the coils in response to the compensated position error signal. A current feedback loop is incorporated because the magnetic force is provided by current rather than voltage. A high gain loop minimizes the effects of coil inductance.

The amplifier operates from a +28-volt dc power source. A small ± 8 -volt power supply is included in the suspension electronics for the I.C. operational amplifiers. The use of this supply is selected over the more conventional ± 15 volts to conserve power. Each operational amplifier uses less than 5 mw of power. The power consumption of the suspension electronics with the wheel at operating speed is .4 watt. Some power, about .1 watt, is lost due to

pickup of rotor frequency by the suspension electronics. Thus, the total standby power loss is .5 watt. The lift-off power consumption is 8 watts.

The electronics is packaged in three cordwood modules within the wheel housing. Since there is no thermal dissipation or severe vibration, the modules are not embedded with epoxy. This minimizes the weight of the modules, to about .023 Kg (.05 lb) each.

CONCLUSIONS

The application of magnetic suspension to spacecraft reaction wheels offers several advantages as compared to conventional bearings, arising from the contactless load support. These advantages are: lower drag torque 70.7×10^{-6} N-m/1000 rpm (.01 oz-in./1000 rpm), no lubricant required, the lack of any wear-out mechanism provides virtually unlimited life, no increase in power at low temperature, lower steady-state power, no single point failure mechanism in the unit (with redundant suspension electronics and spin motor), launch loads are not taken by the on-orbit bearing surfaces, and the unit is unaffected by vacuum operation.

The design is competitive with ball bearing reaction wheels in terms of weight and power. All the concepts used in the reaction wheel design have been either utilized in flight hardware, or, as in the case of the magnetic suspension, have been demonstrated in development hardware. The sensitivity of the design to peak motor power is .136 Kg/watt (.3 lb/watt) and to momentum, .803 Kg/N-m-sec (2.4 lb/ft-lb-sec).

The advantages of magnetic suspensions summarized here apply to other momentum devices, such as bias wheels and energy wheels.

ACKNOWLEDGMENT

A portion of this work was performed for the Jet Propulsion Laboratory, California Institute of Technology, sponsored by the National Aeronautics and Space Agency under Contract NAS7-100.

REFERENCES

1. J. W. Beams, "Magnetic Bearings," Society of Automotive Engineers, Automotive Engineering Congress, Detroit, Michigan, Paper 810A, January 13-17, 1964.
2. C. H. Henrikson, J. Lyman and P. A. Studer, "Magnetically Suspended Momentum Wheels for Spacecraft Stabilization," AIAA 12th Aerospace Sciences Meeting, Washington, D.C., January 30 - February 1, 1974.
3. A. V. Sabnis, J. B. Dendy, and F. M. Schmitt, "Magnetically Suspended Large Momentum Wheels," AIAA Mechanics and Control of Flight Conference, Anaheim, California, August 5-9, 1974.
4. S. Earnshaw, "On the Nature of Molecular Forces," Trans. Cambridge Phil. Society 7, pp. 97-112, 1842.

NOTE

Customary units were used in the preparation of this paper.

APPENDIX

The design of a magnetic suspension model and its principal test results are described in this appendix. The model (photograph, Figure A-1) employs the radial-passive, axial-active, 1-loop suspension configuration shown in Figure 6. The model incorporated the suspension evolved in the reaction wheel design. The model was different from the configuration of Figure 7 in that an existing non-segmented ac induction motor was used rather than the segmented motor, no cover was fabricated, and the electronics were external, in breadboard form. However, the suspension system was the same as that developed for the reaction wheel design, and the results are therefore representative. The axial control system utilizes a single lead-lag network for compensation, with a current amplifier to drive the control coils. Provisions were made for tests with or without the positive integral feedback technique. An eddy-current proximitator was used for axial position sensing. Sliding-contact touchdown bearings made from a teflon-based material were provided.

Test Results

The test model has been successfully levitated and operated at speeds up to 3200 rpm (design speed being 1500 rpm). Successful operation of the touchdown system has also been achieved over this speed range. Very stable suspension has been attained, with minimal power loss under both ambient conditions and steady external loads, achieved by the use of positive integral feedback of control current.

The measured model characteristics are summarized in Table A-1.

TABLE A-1
ONE-LOOP MODEL CHARACTERISTICS

Momentum (1500 rpm)	.19 N-m-sec (.14 ft-lb-sec.)
Drag Torque Coefficient	10.6×10^{-6} (N-m/1000 rpm (.0015 oz-in/1000 rpm)
Stiffness	
Radial (each end)	17,500 N/m (100 lb/in.)
Axial Unbalance	-250,000 N/m (1430 lb/in.)
Suspension Power	
Lift Off	12 watts
Operating	.5 watt
Rotor Weight	0.68 kg (1.5 lb)

The net axial stiffness and damping were continuously adjustable, depending on the feedback gain settings. It was possible to operate from both control coils simultaneously (series or parallel), or from only one coil at a time. The frequency response was in good agreement with analysis.

The tests have demonstrated the viability of the one-loop suspension concept and its application to reaction wheels.

- ADVANTAGES

- LOWER UNBALANCE STIFFNESS RATIO ($K_U/K_R \approx -2$)

- DISADVANTAGES

- STRAY FIELDS
 - HIGHER DRAG TORQUES
 - INTERACTION WITH ADJACENT COMPONENTS
- SEPARATE AXIAL CONTROL TECHNIQUE REQUIRED
- LOWER CAPACITY
- MAGNETS ON SHAFT
 - SPEED LIMITATION

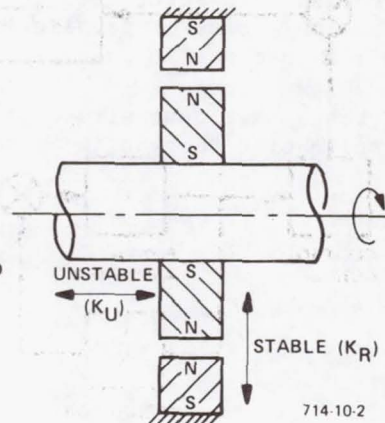


Figure 1
Passive Radial Suspension, Repulsion

- RESTORING FORCE DUE TO VARIATION OF RELUCTANCE

- ADVANTAGES

- CONTAINED FIELDS
- FIELD MODULATION FOR AXIAL CONTROL
- HIGHER CAPACITY
- MAGNETS STATIONARY

- DISADVANTAGES

- HIGHER UNBALANCE STIFFNESS RATIO ($K_U/K_R \approx -8$)
- COIL MUST OVERCOME MAGNET RELUCTANCE

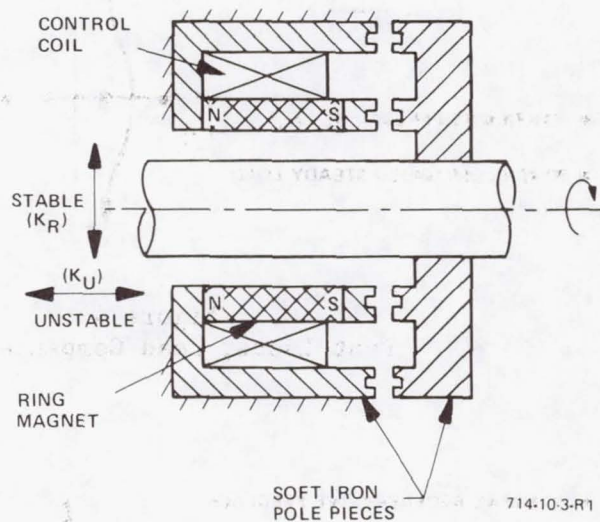
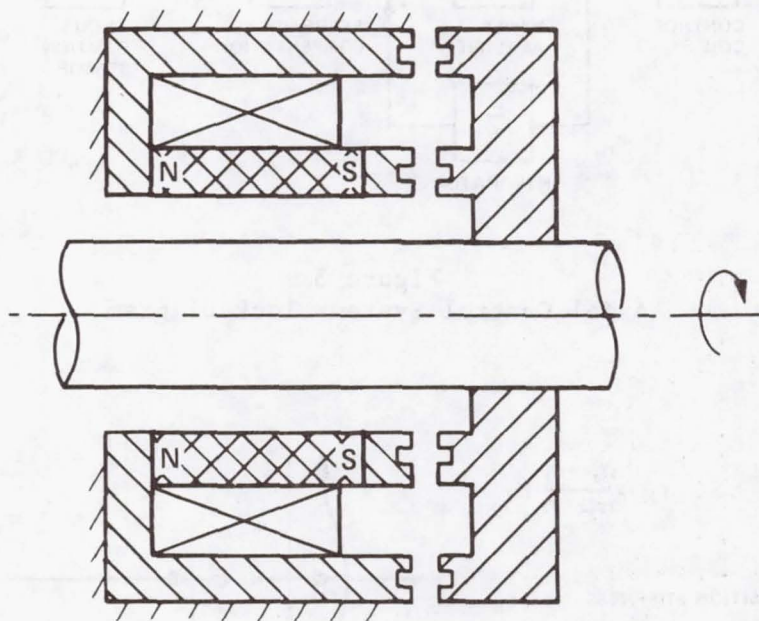


Figure 2
Passive Radial Suspension, Attraction



714-21-22

Figure 6
One-Loop Suspension Configuration

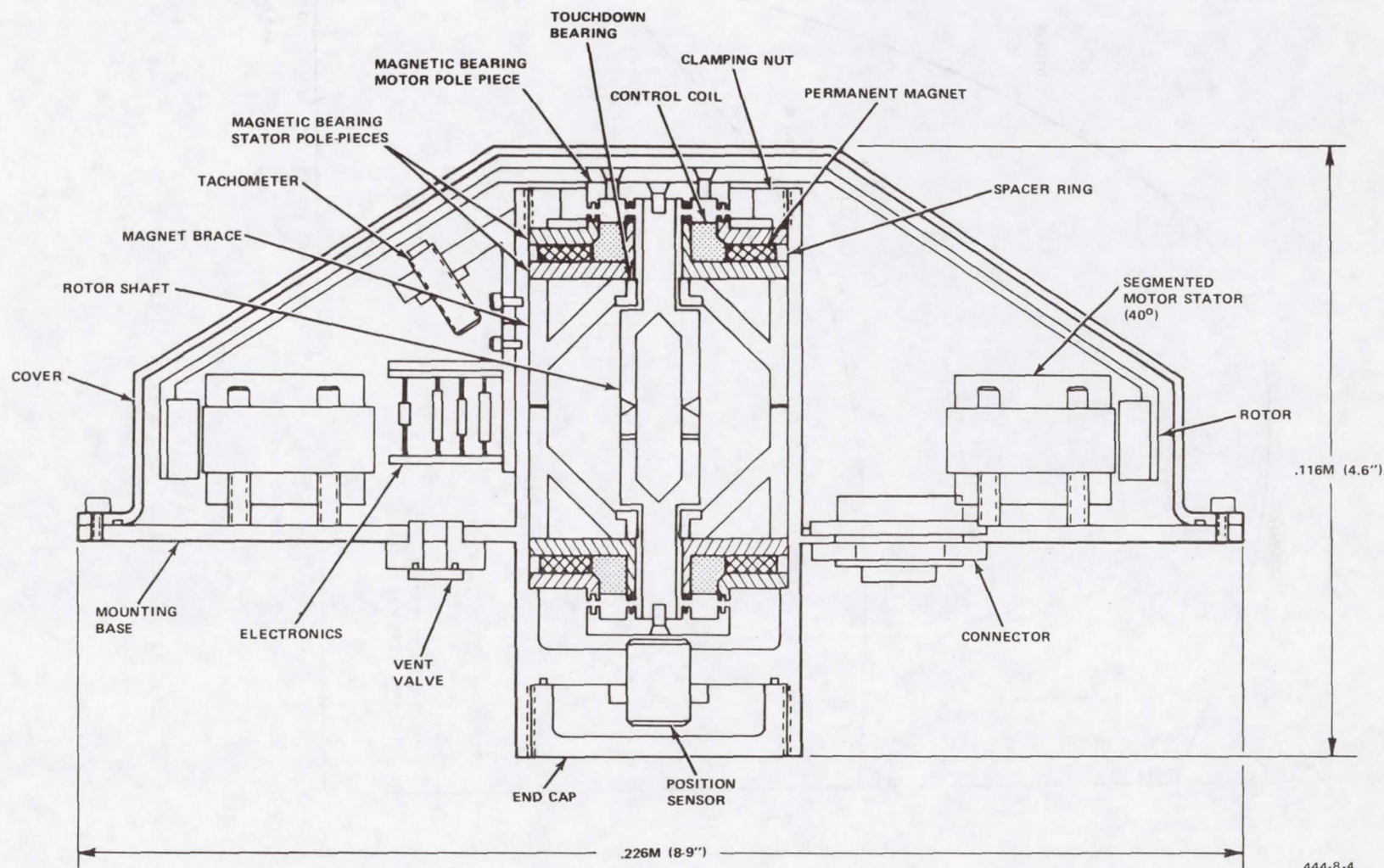


Figure 7
Preliminary RWA Design Layout

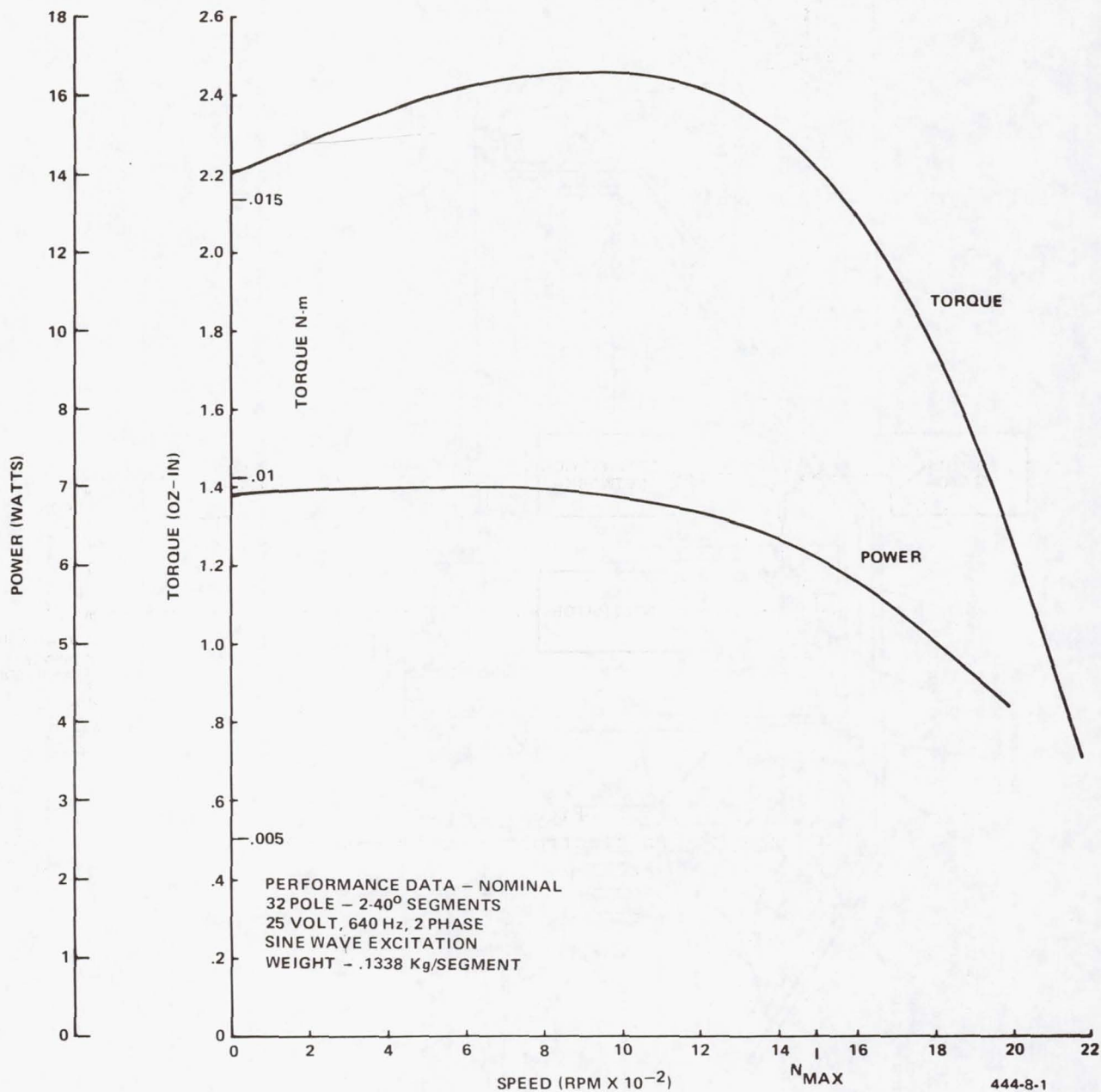


Figure 8
 Performance Data, Segmented Spin Motor

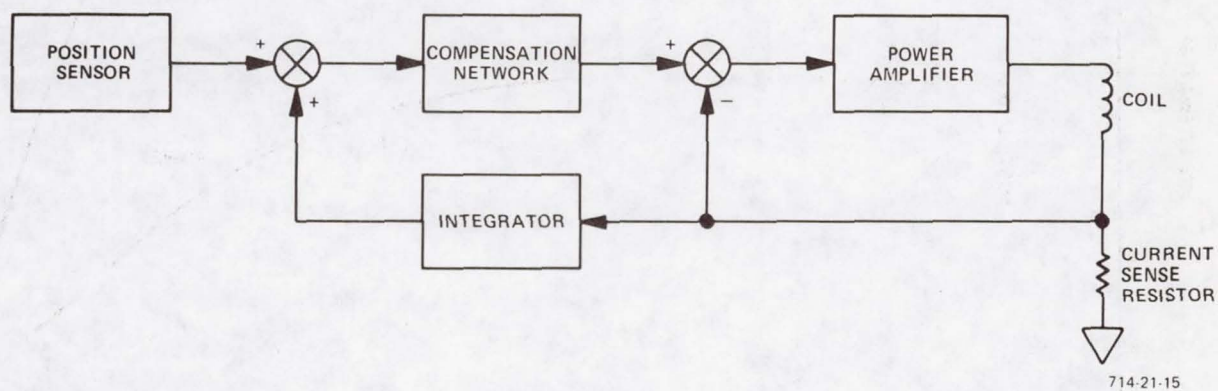
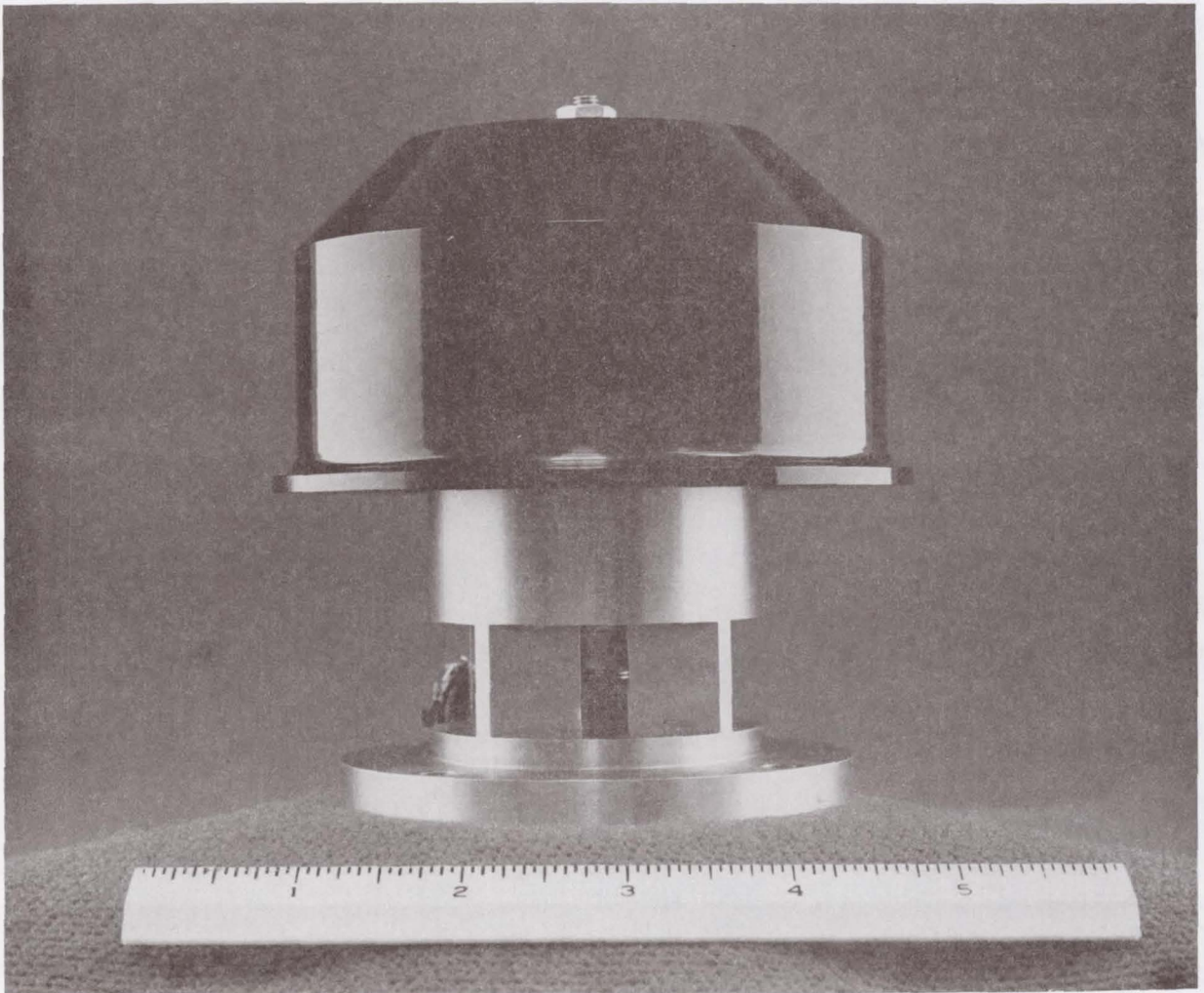


Figure 9
Suspension Electronics Block Diagram



814-44-4

Figure A-1
One Loop Magnetic Suspension Model

17. USE OF COMPUTER MODELING TO INVESTIGATE A DYNAMIC INTERACTION PROBLEM IN THE SKYLAB TACS QUAD-VALVE PACKAGE

By Raymond J. Hesser and Robert Gershman

Propulsion/Mechanical Department
McDonnell Douglas Astronautics Company
Huntington Beach, California

SUMMARY

This paper describes a valve opening-response problem encountered during development of a control valve for the Skylab thruster attitude control system (TACS). The problem involved effects of dynamic interaction among valves in the quad-redundant valve package. Also described is a detailed computer simulation of the quad-valve package that was very helpful in resolving the problem.

ACKNOWLEDGMENT

Portions of the work described here were performed by McDonnell Douglas Astronautics Company for the NASA Marshall Space Flight Center under Contract NAS9-6555.

INTRODUCTION

The Skylab thruster attitude control system was a cold-gas blowdown system using nitrogen as the propellant. Flow to each of the six thrusters was controlled by a quad-redundant valve package, as illustrated by the schematic in Figure 1. A sketch of the Skylab showing the location of the TACS control valves and other components is shown in Figure 2.

The TACS control valve had to be designed to meet a unique combination of requirements that included very low leakage, high flow rates, a wide range of operating pressures and temperatures, capability to operate down to zero pressure, quick response for both opening and closing, limited current draw, and capability to withstand launch vibration loads. The allowable leakage for the valve had to be consistent with the nine-month duration of the Skylab mission and was set at 2 sccm. Since the TACS was a blowdown system, and since it was desirable that all the loaded gas be usable, the valve was required to operate with inlet pressures ranging from 0 n/m^2 to $2.2 \times 10^4 \text{ n/m}^2$ (0 to 3200 psia). A wide range of operating temperatures -66° to $+93^\circ \text{ C}$ (-150° to $+200^\circ \text{ F}$) was also encountered as a result of the Skylab's solar-inertial attitude, since three of the TACS thrusters were mounted on the solar side of the vehicle

and the other three were on the antisolar side. An opening response requirement of 46 ms was established for compatibility with the control system.

This combination of requirements precluded use of any off-the-shelf valve and led to the design shown in Figure 3. The valve was a pilot-operated solenoid type constructed of stainless steel with integral mounting provisions. A small pilot valve, integral and coaxial with the main poppet, was used to control pressure forces for opening and closing. The pilot poppet and main poppet were linked so that energizing the solenoid coil would create opening forces sufficient for full opening of both poppets at low pressure. In the closed condition, both poppets were pressure-unbalanced closed to assure leak-tight sealing.

Development of this valve was a difficult task, but the process led to some rare insights into operation of this type of component.

VALVE INTERACTION PROBLEM

During development testing, it was found that when four valves were operated in the quad (series-parallel) setup, the opening response of the downstream valves was very erratic, sometimes to the point of not opening at all. The same behavior was observed with two valves in series, but not in single-valve operation.

Figure 4 shows data on valve current and valve outlet pressure (thruster chamber pressure) for an abnormal series-valve opening case. Normal opening data are also shown for comparison. It can be seen that in the abnormal case, the pilot valve opened normally and the main poppet started to open, but then closed. The downstream valve would usually (but not always) open within 100 ms, but since the Skylab control-system computers sent out 50 ms pulses, this delayed opening was unacceptable.

The opening anomaly occurred in about one quarter of the pulses, with the frequency of occurrence varying from one set of valves to another. The frequency appeared to be independent of whether one or both legs of a quad-valve package were operating, but the problem disappeared completely when the upstream valves were held open and the downstream valves were cycled individually. The anomaly was also strongly dependent on pressure, being more prevalent at higher inlet pressures.

The investigation of the erratic opening problem included extensive valve testing under a variety of operating conditions and a detailed examination of several of the valves that exhibited the anomaly. Also, since the problem appeared to involve interactions between the upstream and downstream valves for which no qualitative explanation was evident, it was decided to prepare a computer model of the quad-valve package that would be capable of simulating the motion of all three moving parts in each valve.

COMPUTER MODEL

A block diagram of the TACS valve digital computer model is shown in Figure 5. The model simulated the electrical, mechanical, pneumatic, and body forces on the moving parts (Figure 6) of each valve. The gas-flow model is shown in Figure 7.

The subscripts of the model variables were chosen so that each valve could be modeled to conform to a unique set of design parameters. This permitted investigation of the effects of variations in orifice size, solenoid air gap, piston stroke, etc. from valve to valve.

Real-gas properties were considered using a special subroutine based on Reference 1 to determine the effect of the changing thermodynamic properties on flow rate and compressibility. In regions near the critical point, the real-gas flow rate and compressibility differed from a perfect gas by more than 40 percent.

The nonlinear effects of electromagnetic iron losses, back EMF, and hysteresis were also included in the electrical portion of the model. An electromagnetic circuit algorithm based on methods from Reference 2 was included. The mechanical portion of the model took into account the effects of external acceleration loads as well as sliding friction forces on the motion of the valve parts.

A modified backward-difference extrapolation integration technique was used for all the state variables in the system. A digital algorithm that monitored the mechanical motion of the three valve parts was used to keep these parts within the specified design travel limits for each valve. When a specified travel limit was reached, the program integration was recycled to compute a collision using a specified coefficient of restitution.

RESULTS OF VALVE INVESTIGATION

The valve investigation disclosed two possible causes of the abnormal behavior described above. Testing showed that a small amount of leakage past the lip seal (Figure 6) existed in all valves. It was hypothesized that the pressure surge from opening of the upstream valve caused a cocking of the poppet that could increase this leakage to the point where drainage of the volume behind the main poppet would be too slow to permit immediate opening.

The second possible cause was bending of the small flange attached to the plunger (Figure 8). Disassembly of the valves that exhibited problems showed the downstream valve flange to be bent in all cases. The bent flange would interfere with valve opening, both by reducing pilot valve flow area and by leaving the flow passage through the main poppet open. It was believed that the flanges became bent as a result of a testing procedure in which the downstream valves were held open while the upstream valves were cycled. Under

this condition, the pressure surge from upstream valve opening would push the main poppet against the flange. This situation could be relieved by adding a stop to prevent the main poppet from contacting the bottom of the flange with the plunger at maximum travel.

Further testing of the valves revealed that the problem could be alleviated by delaying the opening of the upstream valve relative to the downstream valve by 5 to 10 ms. This phenomenon also defied qualitative explanation.

COMPUTER MODEL RESULTS

The computer model was refined until it could accurately predict normal valve operation, as illustrated in Figure 9. It was then used to investigate the effects of lip-seal leakage and bent flanges on valve operation. The model verified that both of these mechanisms could lead to the anomalous behavior observed in tests. Figures 10 and 11 show computer results for single-valve (upstream valve held open) and series-valve operation for a case in which the downstream valve had flange bent back by 0.0203 cm (0.008 inch). Single-valve operation is shown to be normal, but the series-valve results are similar to the data in Figure 4. Figure 12 shows the results of adding a 10-ms delay in upstream valve opening for the case covered by Figure 11. The model predicted that this would allow the downstream valve to open normally.

The data on pneumatic and electrical forces obtained from the computer model provided an apparent explanation for a valve that would not open properly in the series case but functioned normally in the single- and delayed-upstream-valve cases. In the series case, the upstream valve would open first as a result of having a smaller pressure differential across it. This would cause a pressure surge against the downstream main poppet that would push it open before the solenoid current buildup could provide enough force to compress the button spring at the top of the solenoid plunger. The surge on the main poppet would push it away from the plunger flange, thus opening the inlet to the volume upstream of the pilot and concurrently closing the pilot poppet. When this occurred, the pressure inside the volume upstream of the pilot would increase rapidly. The main poppet would then close, and the draining of the volume behind it would be recycled, but this time from the high surge pressure rather than from the initial pressure level. The lip-seal leakage, or the inability to open the pilot fully due to the bent flange, would then delay or prevent main-poppet opening.

In the single-valve and delayed-upstream cases, the simulations showed that the solenoid force would build up to a level where the plunger could complete its movement before the main poppet could move away from it, thus avoiding a pressure buildup in the volume upstream of the pilot that could push the main poppet closed.

RESOLUTION OF THE PROBLEM

Because of pressing schedules, it was decided to incorporate remedies for both potential problem mechanisms into the valve and also to add a timer to delay upstream-valve opening. A redundant seal was added at the point of suspected lip-seal leakage, and the computer model was used to optimize a poppet stop that would prevent bending of the flange (see Figure 13). Because of tolerance buildup, it was necessary to restrict main-poppet movement severely to assure that the poppet would not contact the flange. This caused concern that the pressure drop across the valve would increase excessively, but the computer model showed that excessive pressure drop would not occur because the main poppet had been only about half open at steady state without the poppet stop (see Figure 14).

After incorporation of these changes, no additional response problems were encountered, and the TACS performed perfectly throughout the 9-month Skylab mission.

CONCLUDING REMARKS

This effort proved the value of detailed computer models in dealing with complex component development problems. The model described here was also useful in resolving a later valve-test problem (in which an upstream valve was damaged by backflow when another thruster was cycled) and in providing flight-performance predictions.

REFERENCES

1. Johnson, A. C., "Real Gas Effects in Critical Flow through Nozzles, and Thermodynamic Properties of Nitrogen and Helium at Pressures to 300×10^5 Newtons/Square Meter," NASA SP-3046, U. S. Government Printing Office, 1968.
2. Rotors, H. C., Electromagnetic Devices, Wiley, New York, 1941.

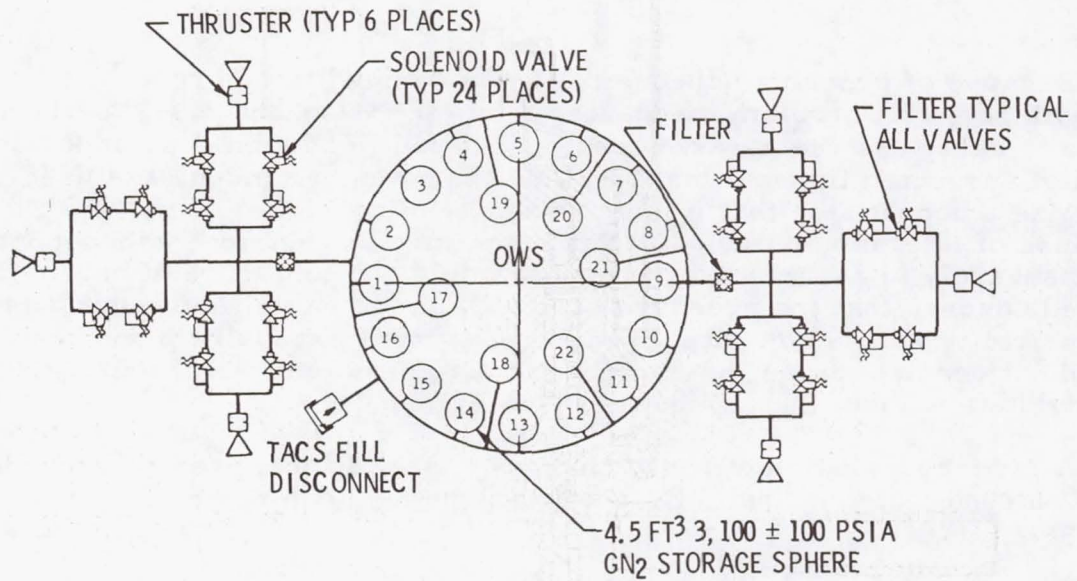


Figure 1. TACS Schematic

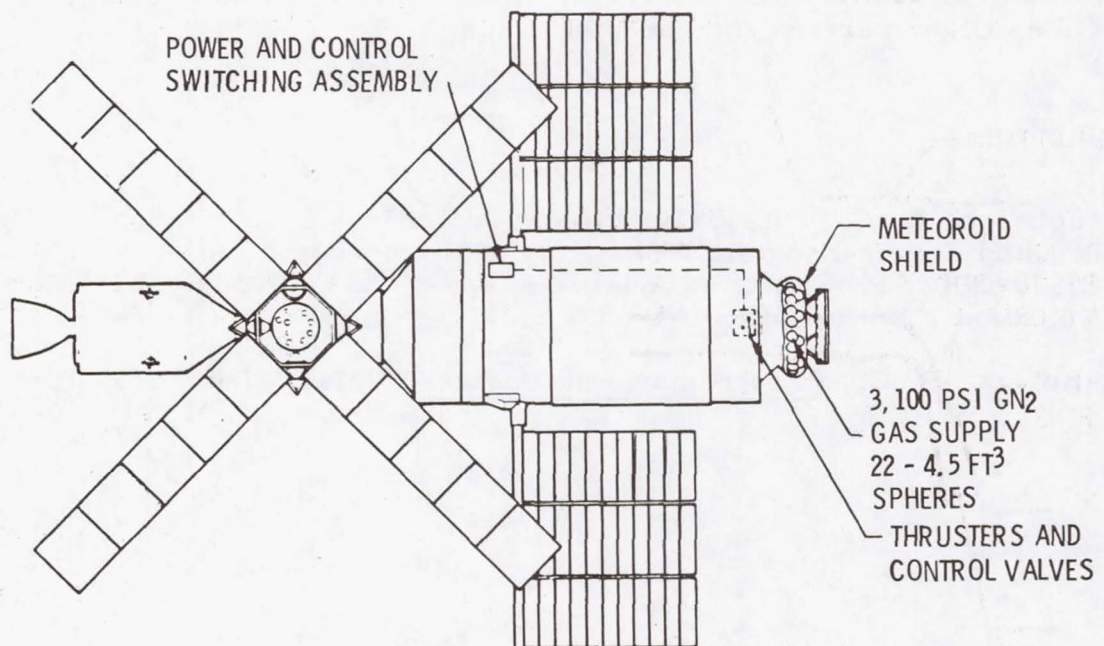


Figure 2. TACS Component Locations

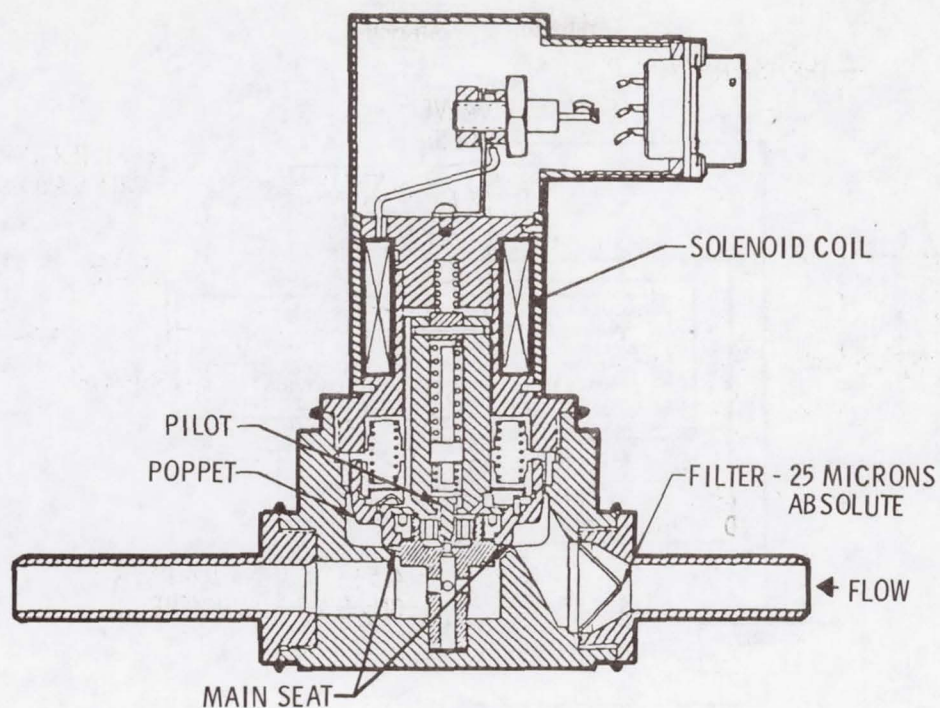


Figure 3. TACS Control Valve

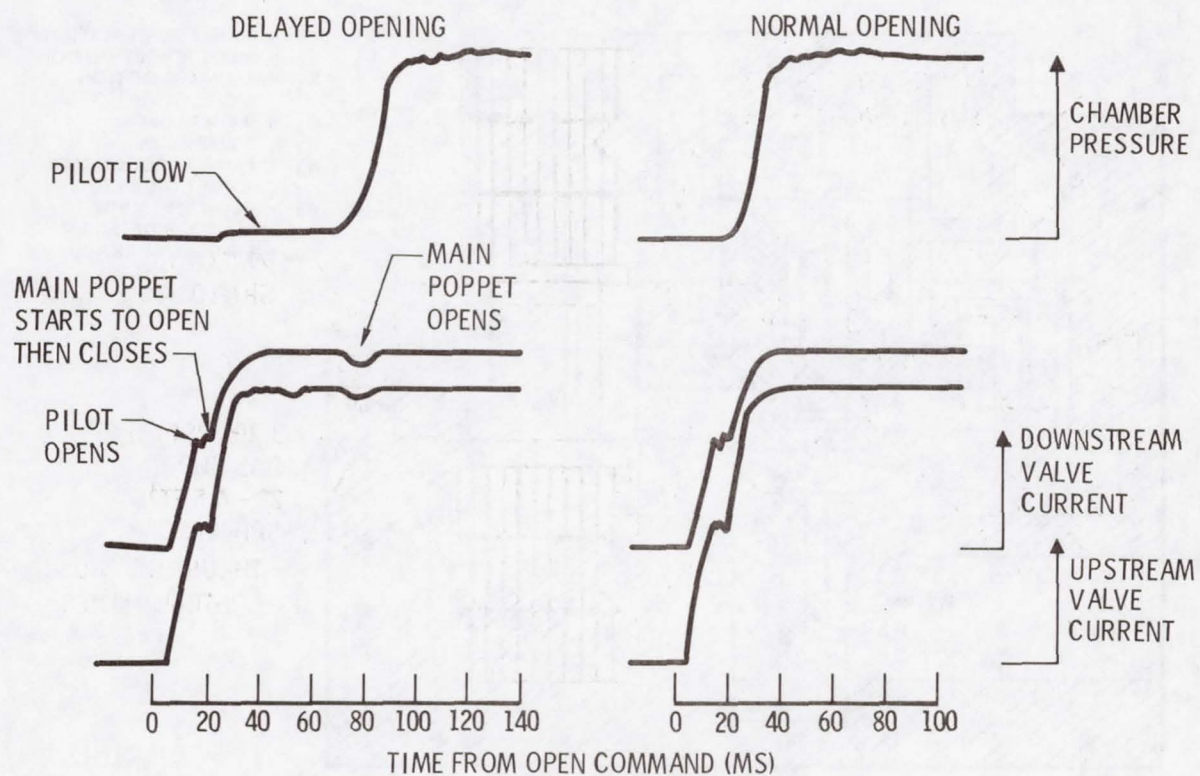


Figure 4. Valve Response Problem

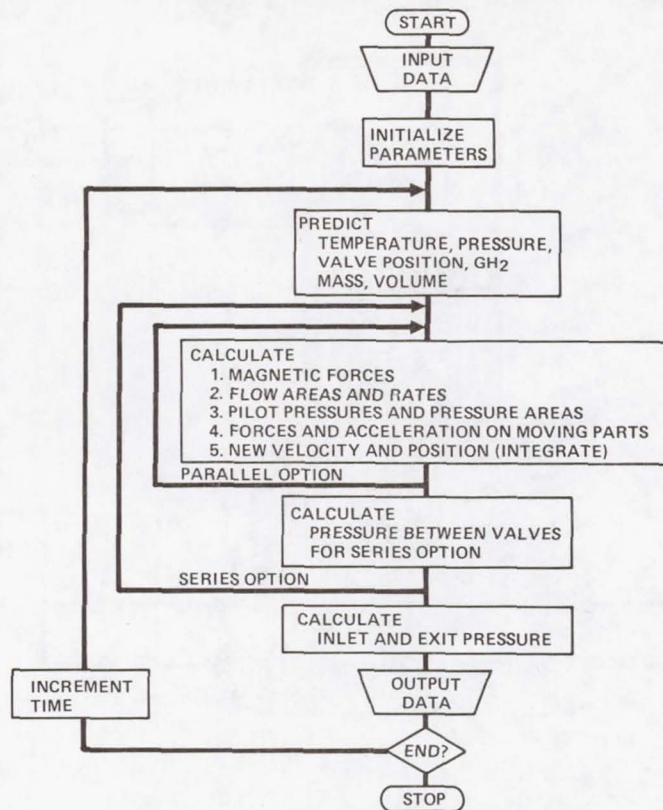
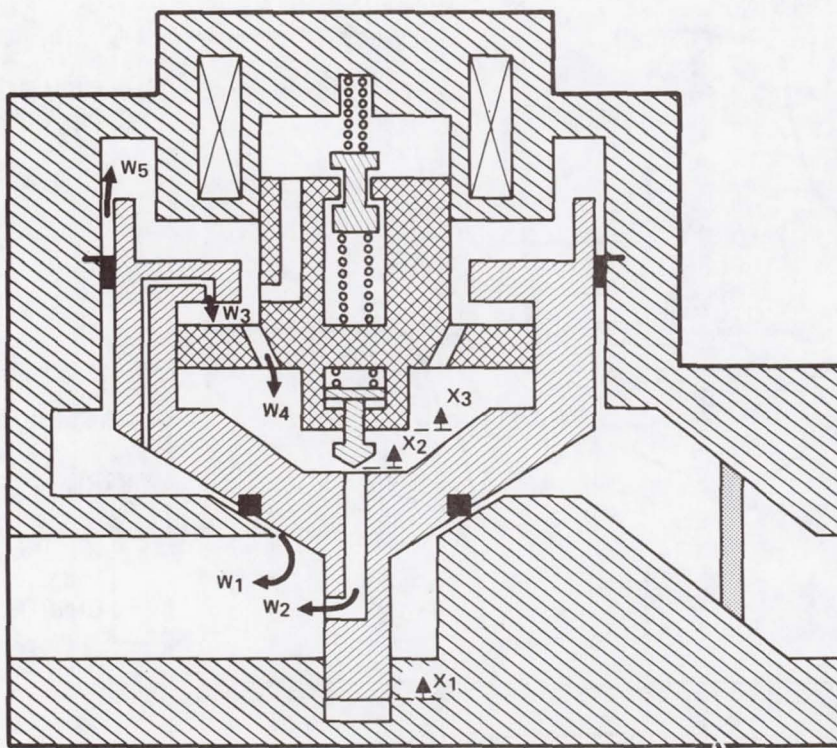


Figure 5. Valve Program Flow Diagram



X1 = MAIN POPPET MOTION
 X2 = PILOT POPPET MOTION
 X3 = PLUNGER MOTION

W1 = MAIN FLOW
 W2 = PILOT FLOW
 W3 = FLOW THROUGH MAIN
 POPPET ORIFICE
 W4 = FLOW THROUGH
 PLUNGER ORIFICES
 W5 = LIP-SEAL LEAKAGE

Figure 6. Valve Schematic

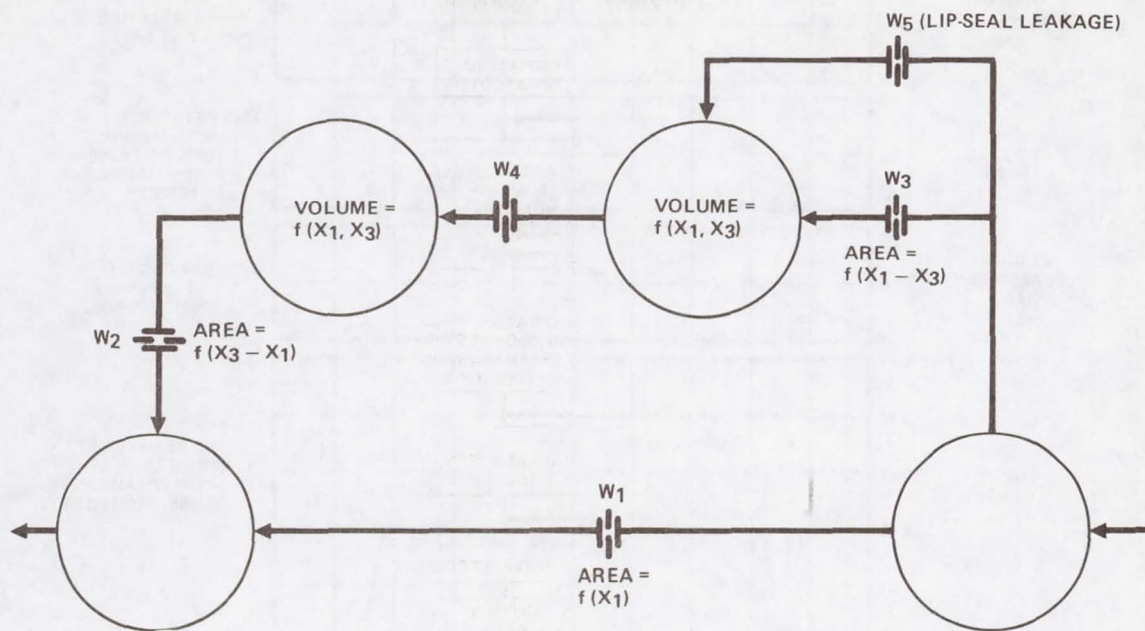


Figure 7. Valve Gas-Flow Model

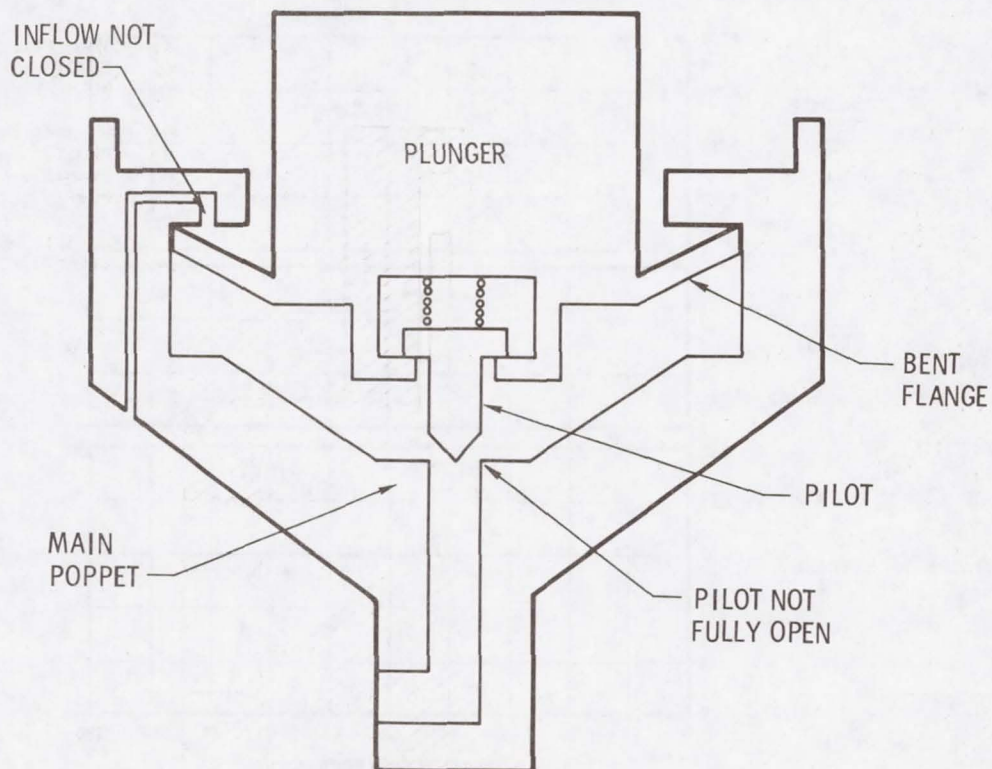


Figure 8. Effects of Bent Flange

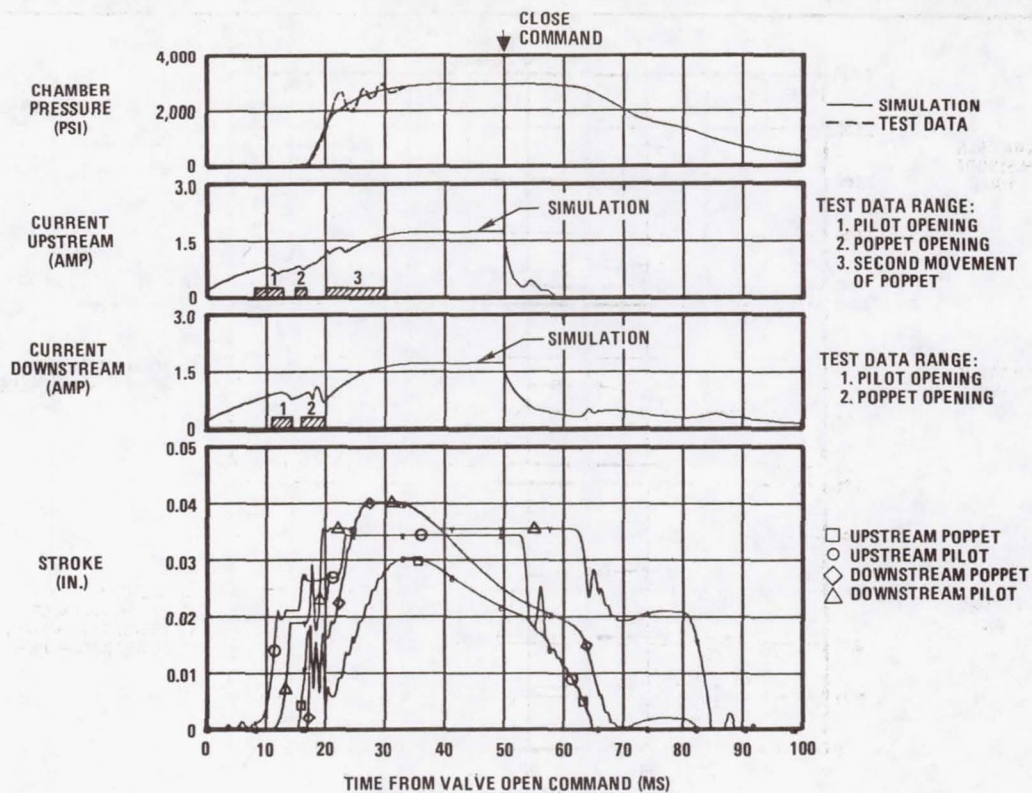


Figure 9. Simulation of Normal Quad-Valve Operation

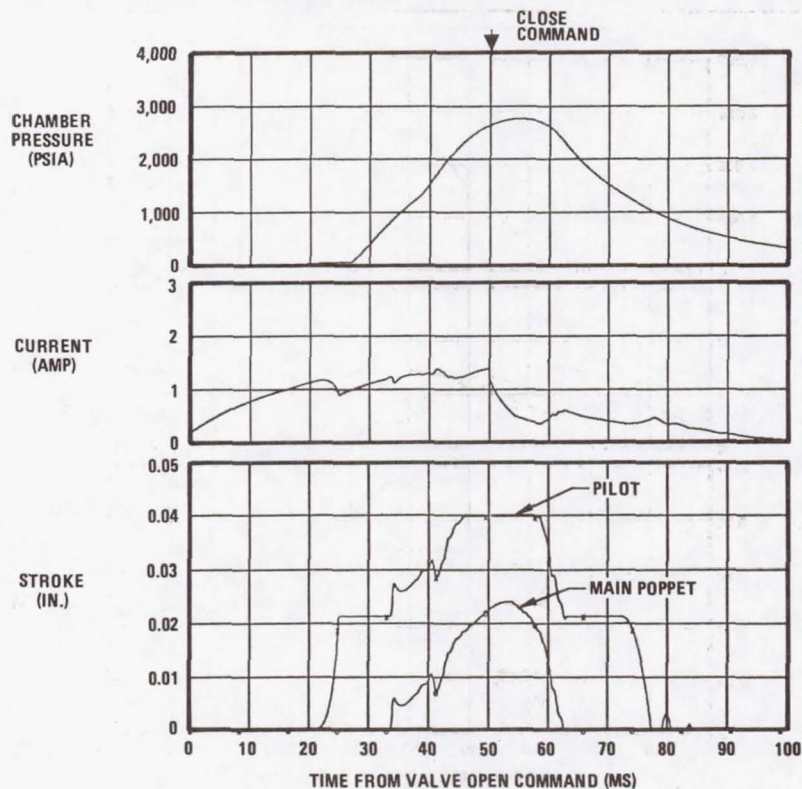


Figure 10. Simulation of Single-Valve Operation with Bent Flange

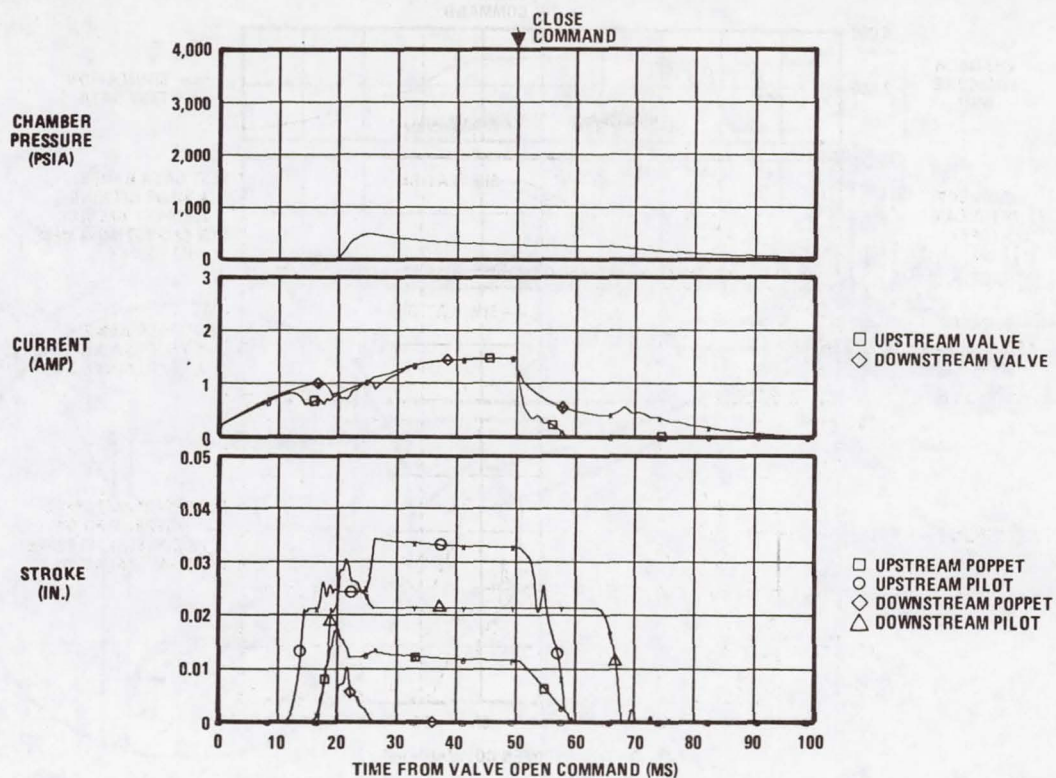


Figure 11. Simulation of Dual-Valve Operation with Bent Flange in Downstream Valve

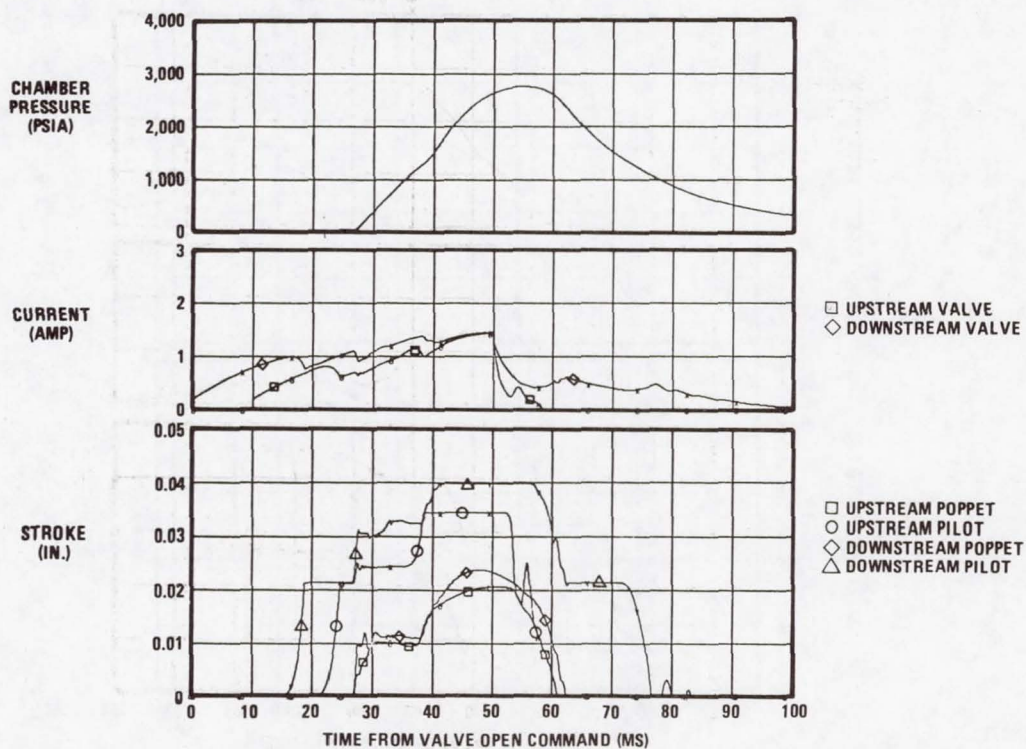


Figure 12. Simulation of Dual-Valve Operation with Bent Flange in Downstream Valve and Delay of Upstream Valve Opening

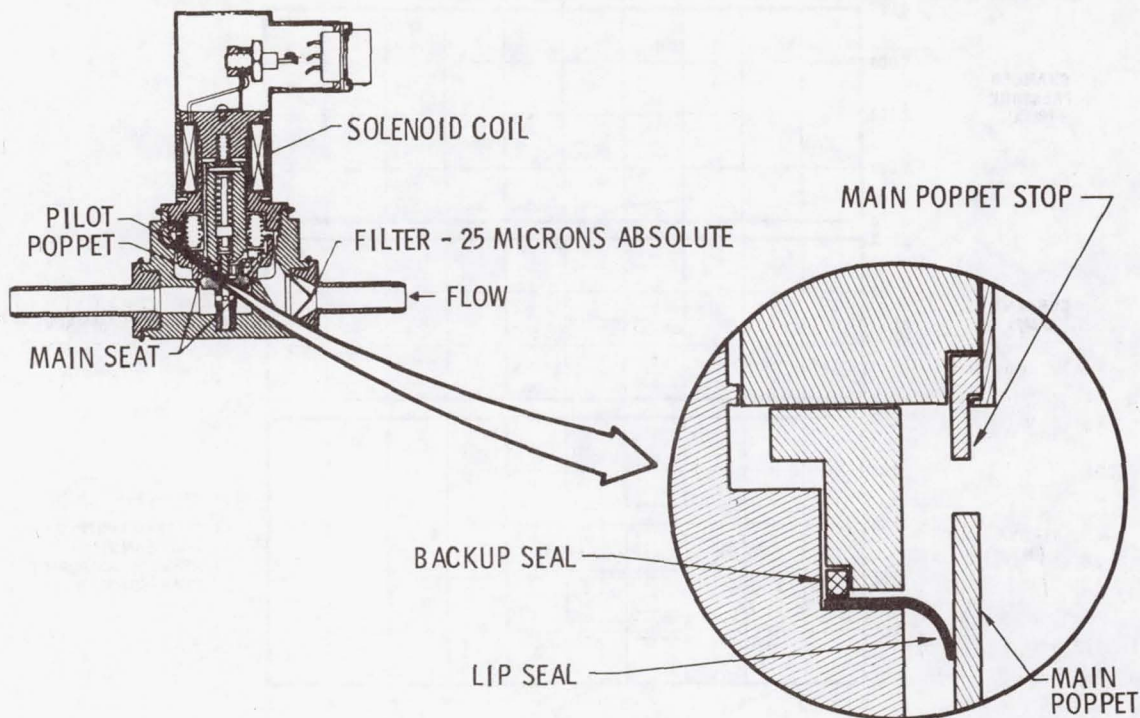


Figure 13. Valve Modifications

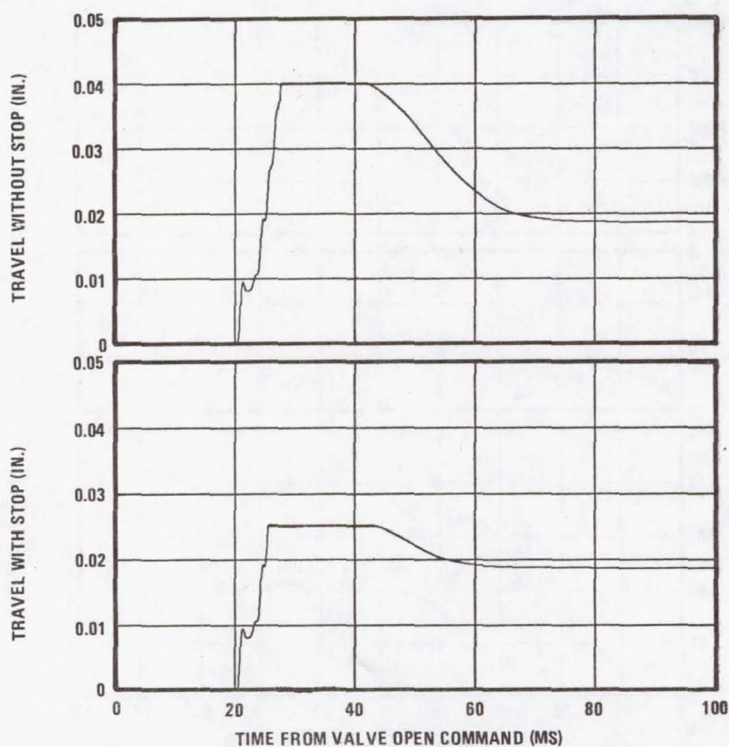


Figure 14. Main Poppet Travel With and Without Poppet Stop

18. MODERN MECHANISMS MAKE MANLESS MARTIAN MISSION MOBILE --

SPIN-OFF SPELLS STAIRCLIMBING SELF-SUFFICIENCY

FOR EARTHBOUND HANDICAPPED

By George N. Sandor, David R. Hassel
and Philip F. Marino

Rensselaer Polytechnic Institute

SUMMARY

Sponsored by NASA at Rensselaer Polytechnic Institute in Troy, New York, under Mission-Hardware Research Grant No. NGL 33-018-091, an annually changing group of undergraduate and graduate students under Dr. Sandor's direction have developed concepts for three wheel chairs, progressively improving designs of a proposed unmanned roving vehicle for the surface exploration of Mars and, as a spin-off, have generated a concept for a stair-climbing wheel chair. The mechanisms employed in these are described in this paper. The Mars mission is envisioned using the booster rockets and aeroshell of the Viking missions.

INTRODUCTION

Rensselaer Polytechnic Institute's (RPI) first concept was a four-wheeled dragster-like rover with the weight of a single payload package carried largely by the driven rear wheels (refs. 1-5, 8, 9, and 11). The undriven front wheels, which were well ahead, served for "wagon steering" and for obstacle detection. In case one or both front wheels dropped in a crevasse or over a ridge, the vehicle would stop and perform an emergency maneuver extricating its front end from the obstacle.

The wheels were a new RPI design: "toroidal" all-metal elastic wheels with crosswise hoop-spokes hinged to, but spaced apart from the flexible, grousened rim, which provides for a large footprint and avoids "stone-crushing" between rim and spokes (refs. 6, 7, and 12).

The second-generation vehicle could be folded to about two-thirds of its length for launch, with the payload at one end.

MECHANISMS OF THE MARS ROVER

RPI's present third-generation Martian Roving Vehicle (MRV) design is a four-wheel, single payload vehicle. Its demonstration model is shown in the

folded "launch-and-land" configuration in Figure 1. When fully deployed, approximately 70% of the weight is carried on the driven rear wheels, assuring good traction.

To fit inside the existing Viking aeroshell, the vehicle is much smaller in the folded configuration than in its roving mode. This collapsibility allows a relatively large volume for the payload of the vehicle and a larger vehicle wheelbase and wider track than would otherwise be possible. Once on the surface of Mars, the vehicle must be able to deploy itself into the roving configuration. As will be seen, this is accomplished by the use of motor and gear assemblies which are used for other purposes during the vehicle's roving phase. Thus no additional weight and complexity is required for self-powered deployment.

RPI's MRV is capable of raising and lowering the payload and changing the payload attitude by the use of two motor-gear assemblies within the vehicle. On the demonstration model, each of these consists of an internally geared permanent-magnet "pancake" motor working with a worm-and-gear pair (Fig. 2). These two assemblies control rotation between the front section of the vehicle and the payload box, and rotation between the rear struts and the payload box. The rear struts are rotated by a torsion bar running across the payload box, keyed at the center to the smaller worm gear in Figure 2 and driven by a worm mounted in bearings attached to the gearbox floor. Each half of the torsion bar provides elastic suspension for its respective rear strut. The front section of the vehicle is rotated by a split torque-tube concentric with and surrounding the rear-strut torsion bar. The right and left sections of the tube leave room for the worm-gear mounted in the middle on the torsion bar. A rigid inverted U-shaped crossover piece connects these two half-tubes (Fig. 2), lending torsional rigidity to the assembly of the right and left tubes. Both half-tubes are driven simultaneously by a worm-gear mounted to the right side of the U-shaped crossover as shown in Figure 2.

When roving, directional control is accomplished by "wagon steering" of the front axle, which rotates about a single vertical axis at its center (Fig. 3), turned by a worm-and-gear pair powered by an internally geared permanent-magnet motor. A precision potentiometer senses the position of the front axle and feeds this information back to the steering and rear-wheel drive control systems of the vehicle. The individual rear-wheel drives adjust their speeds to match the turning radius. When the front axle is turned 90° from its straight-ahead position, the rear wheels are driven in opposite directions and the vehicle can swing around with the center of turn at the mid-point between the two rear wheels.

Four-wheel ground contact on rough terrain is assured: the front axle swings about a horizontal pivot. Its swing is centered and limited by steel bands and leaf springs (Fig. 3).

The entire front axle and steering system is mounted on a horizontal-transverse shaft and can be rotated to any position within an arc of 240° by a motorized worm-and-gear pair (Fig. 3). This extra rotation (so-called "flipover") capability enables the front axle to flip to an "up" or "down"

position and keep its steering axis vertical regardless of the attitude of the front struts.

The front and rear strut rotation systems and the front axle flipping system assist in deploying the vehicle from its folded launch-land configuration. They also enable the vehicle to perform an emergency flip-over maneuver. In addition, they provide a sequence which allows the vehicle to climb up a step which is higher than one wheel diameter.

As can be seen in Figure 4, which shows the vehicle at the beginning of the deployment sequence, the front struts are articulated to permit folding. The locking mechanism chosen to keep the front end in its deployed position is a spring loaded locking plunger of square cross section, which fits within the hollow square-tube front-strut frame members (Fig. 5a). The plunger is automatically released and locks when the front strut articulation reaches a straightened-out position (Figs. 5b and 6).

THE DEPLOYMENT MANEUVER

To deploy the front section, the forward strut attitude motor (Fig. 2 front) is utilized to drive the rear section of the forward strut forward while the front wheels roll forward on the ground (Figs. 7 and 8). This straightens the front struts to a position where the automatic latching devices (Fig. 5) lock the articulation in the straightened-out position (Fig. 9).

The front axle flipping motor then changes the angle between the front struts and the axle to its normal attitude with the steering axle vertical (Fig. 3).

To deploy the rear wheels, the hub-mounted individual rear-wheel propulsion drive motors are actuated in the forward direction. As the rear wheels roll on the ground, they straighten out the articulated rear struts (Fig. 10), while the payload box still rests on the ground. Once straightened out, the rear strut articulation hinges are locked in the extended position (Fig. 11).

On the demonstration model, commands for deployment and maneuvering are sent to the vehicle from a manned console by way of a radio link. They are received on the demonstration model by an on-board radio receiver and control system. The deployment commands necessary to unfold the vehicle and make it ready for roving are sequences of commands normally used in roving. For example, to deploy the rear wheels, the rear torsion bar motor is commanded to drive the rear wheels downward into contact with the surface, same as would be used to raise the payload. Then both rear wheels are commanded to roll forward at low speed, thus swinging the hinged part of the rear struts forward and locking them into position (Figs. 10 and 11).

By driving both front and rear struts downward, the payload is now raised off the ground and the vehicle becomes fully operational (Figs. 12 and 13).

EMERGENCY MANEUVER

A useful feature of the RPI-MRV is its ability to extricate its front wheels from a pit or depression. If the front wheels are driven over the edge of a cliff, the vehicle lifts both front and rear sections off the ground while the bottom of the payload rests on the ground. The front and rear wheels are interchanged by swinging the struts overhead (Fig. 14). Once this interchange is completed, all four wheels are once again on solid ground, because the rear struts are much shorter than the front section, and the vehicle can drive away from the edge of the cliff.

THE RPI WHEEL

The RPI-MRV's all-metal elastic toroidal wheel is shown in Figure 15 (refs. 6, 7 and 12). Large footprint and elasticity of suspension is achieved by hinged connections between the hoop-shaped spring spokes and the flexible rim.

A "SPIN-OFF": STAIR-CLIMBING WHEEL CHAIR

One of the most interesting spin-offs of the RPI-MRV Project was the development of a design concept for a stair-climbing wheel chair (refs. 13-15). At a previous presentation concerning the Martian Rover (ref. 3) a member of the audience suggested the possibility of adapting its unique undercarriage to a stair-climbing wheel chair. The suggestion was welcomed, and resulted in a preliminary proposal in the form of a paper submitted to the Medical Society of the State of New York (ref. 15). The publication of that paper (ref. 14) resulted in numerous inquiries directed to its author, Dr. G. N. Sandor. Noting this interest, Dr. Sandor took this idea to one of his classes and proposed that the class take on the development of the design concept for the "stair-climbing wheel chair" as a term project. The response was enthusiastic, and work began in February 1974.

The idea of a central pivot and four struts was adopted directly from the rover. The flexible wheel (Fig. 16A), however, was deemed impractical for stair climbing. The problem encountered was one of approaching the first step. It was felt that the step would have to touch the wheel somewhere below the point at which a tangent to the wheel made a 45° angle with the ground. Such a wheel would have a minimum diameter of about 30". Four 30" wheels did not seem practical. An alternate solution was to provide any desired attack angle by means of a track (Fig. 16B). At the right side of this

figure there would be internal guide wheels at top and bottom. Changing the relative positions of these two wheels allows generation of any attack angle desired. Figures 16C, 16D and 16E represent three other solutions which were proposed. Figure 16C is the "lobed wheel." This particular shape is one used on a prototype stair-climbing wheel chair built several years ago. Figure 16D is the "cam wheel." The cam, on the left, contacts the step and lifts the wheel up behind itself, then folds away and allows the wheel to roll. Figure 16E represents three versions of a dual-wheel concept which arose halfway through the project. In the first version, the two wheels turn about their own axes and also about the pivot between them, similar to a lobed wheel with 2 lobes. In the second version, the auxiliary pivot is moved out from between the wheels. The rightmost wheel would rise, engage the next higher step, lift the whole chair one step, roll forward, and repeat. Version three has the same action, using linear actuators or hydraulic cylinders to provide the lifting action. In evaluating the mechanisms, "A" was considered too big, and "C" was deemed unsuitable for varying stair sizes. "D" and "E", although of reasonable size and excellent adaptability, were thought to be much more complex than a track and were held in reserve in case a suitable track brought on too many complications of its own. It was decided that the individual inventors (student members of the class) would pursue the concepts represented by Figures 16D and 16E, and the rest of the group would set to work on a track-type stair climber, with two 3 to 4 inch wide tracks, one on each side.

At this point a 1/6-scale plastic and balsa wood model was constructed, resembling Figure 17. Using this model as a rough guide, eleven teams were formed to tackle various aspects of the design. Some of the best technical solutions came from team members who were also "Martians," that is, involved in the Martian Rover Project. The resulting design is shown in a simplified form in Figure 18.

DESIGN CONCEPT OF THE WHEEL CHAIR

The fully motorized chair would be 10.1 centimeters (42 inches) long and 6.4 centimeters (25 inches) wide overall, about the size of present conventional wheel chairs. Seat height would be variable by the occupant at will from the height of a normal chair to a height at which a person in the chair would be at eye level with a standing person. This restoration of the vertical dimension of movement is highly desirable to the disabled, especially when he confronts a pay phone, supermarket, library, or overhead kitchen cabinets. Vertical movement is accomplished by pivoting the main struts. In doing so, the inner, or level-travel wheels lose contact with the ground and the chair rests on the stable wide stance of the tracks.

CLIMBING STAIRS

In public buildings, stair climbing between floors is usually made unnecessary by elevators. Getting into public buildings and private homes is

another matter, however. There is invariably a curb between the parking lot and the entrance sidewalk and building entrance. The more athletic wheel chair users can jump curbs, but two or three steps might as well be a locked and barred gate to a conventional wheel chair user. The stair-climbing chair will tackle 5 or 6 inch curbs head on. Stairs will be climbed backwards, to keep a low center of gravity.

DESCENDING STAIRS

Descent gives rise to the wheel chair user's greatest apprehension and fear of falling. To overcome this, the chair will face downhill giving good visibility, which is reassuring as well as necessary in avoiding loose objects. To assure sufficient stair clearance, two four-bar mechanisms were proposed which retract the inner wheels when the chair support strut is moved fully rearward for stair climbing or descending. The mechanism for retracting the front castered wheels, shown schematically in Figure 18, is detailed in Figures 19A and 19B. Figure 19A represents level travel and 19B shows the wheel retracted as in Figure 18.

DRIVE SYSTEMS

Two separate drive systems were incorporated. The track-drive motors will be hub-mounted in the forward track guide wheels and have manual shoe type brakes. The level drive, in the configuration of Figure 17, would be powered at the two rear wheels, steering by varying the speed ratio of these wheels. By driving the two rear wheels in opposite directions, a turn in place can be accomplished.

The strut pivots of the Martian Rover used nearly self-locking worm gears. To keep down weight and expense, while improving efficiency, a gear-motor ("M" in Fig. 19C) and spur gear combination was found which met the torque and power requirements. The motors would fit inside the aluminum box beam struts (Fig. 19C). A small, low-torque brake, mounted on the free end of the motor rotor shaft, would provide locking action.

Chair leveling is to be accomplished by the combined motions of the chair-support strut and a motor-driven ballscrew connecting the side of the chair to a pivoted nut on the chair-support strut (Shown in Fig. 18).

It is thought that the chair itself, the speed control system and the power supply could be adopted with minor alterations from present electric wheel chairs. The track, struts, chair-leveling mechanism and wheel retractors are all unique items which need to be tested in a prototype to confirm estimated power, strength, and dimensional aspects.

In addition to the purely mechanical aspects of the design, some work was done evaluating the dynamic stability of the complete vehicle with the turning radius, speed and surface inclination as parameters. This work governs optimization of the wheel base and wheel track dimensions.

The human side of the problem was considered early in the project and was a governing consideration throughout. Contacts were made with professional rehabilitation personnel, potential vendors and potential users. These contacts showed that once a prototype is made, a large effort must be devoted to assuring adaptability of the device to a particular user's abilities and disabilities. Careful consideration must be given to operating characteristics and aesthetic appearance, thus facilitating acceptance by the user as well as by the general public.

The idea of a stair-climbing wheel chair, while not unique in itself, has inspired some very original mechanisms which hopefully may make this stair climber the first to gain wide acceptance. In rehabilitation work, a distinction is made between the disabled and the handicapped. A disability is only a handicap to the extent that it prevents a person from being a full participant in society. A handicap is imposed and may be removed or overcome. The purpose of this wheel chair would be to remove such handicap.

ACKNOWLEDGMENT

The authors wish to express their appreciation for the support of the Mars Roving Vehicle project under NASA Grant No. NGL 33-018-091 at Rensselaer Polytechnic Institute, sponsored by the branch of NASA in charge of new mission hardware development headed by Mr. Paul Tarver.

Both the Mars Rover and the stair-climbing wheel chair design had many contributors among RPI's students: ten or more on the Mars project and fifteen in connection with the wheel chair. Their enthusiasm and youthful energy were inspirations to the authors.

The first author wishes to acknowledge the sponsorship of the Alcoa Foundation in support of his chair, the Alcoa Foundation Professorship of Mechanical Design at Rensselaer Polytechnic Institute.

All three authors are indebted to Mrs. Frances K. Willson for suggestions for the clarity of the text and her meticulous typing of the paper.

REFERENCES

1. Sandor, G.N., and Rayfield, W.P., "Dragster on Mars," ASME News, Hudson Mohawk Section, Vol. 7, No. 3, Jan.-Feb., 1970, pp. 3-7.
2. Grupe, J.A., (G.N. Sandor, Adv.), "Propulsion System for a Martian Roving Vehicle: Power Supply Analysis, Mr. of Engrg. Rept., RPI, June 1970, 33 pp.

3. Sandor, G.N. and Rayfield, W.P., "Rensselaer's Roving Vehicle for Mars," Proceedings of the First Western Space Congress, VANDERBERG SCIENTIFIC AND TECH. SOCIETIES COUNCIL, Santa Maria, Calif., Oct. 1970, pp. 838-855.
4. Rayfield, W.P. and Sandor, G.N., "Design of a Roving Vehicle for Mars," Invited Paper, ASME Design Engrg. Conf., N.Y.C., April 1971.
5. Koehler, R.C., (G.N. Sandor, Adv.) "Automatic Steering and Leveling Control for an Unmanned Martian Roving Vehicle," Mr. of Engrg. Rept., RPI, June 1971, 36 pp.
6. Simon, R.L., (G.N. Sandor, Adv.), "Design of a Toroidal Wheel for a Martian Roving Vehicle," Mr. of Engrg. Rept., RPI, June 1971, 148 pp.
7. Klette, C.E., (G.N. Sandor, Adv.), "Martian Roving Vehicle Wheel Test Apparatus," Mr. of Engrg. Rept., RPI, June 1972.
8. Rayfield, W.P., (G.N. Sandor, Adv.), "The Conceptual Design of an Unmanned Roving Vehicle for Surface Exploration of Mars," Doctoral Dissertation, RPI, June 1972, 149 pp.
9. Cobb, W.A., (G.N. Sandor, Adv.), "Dynamic Evaluation of a Scaled 4 Wheel Martian Roving Vehicle," Mr. of Engrg. Rept., RPI, June 1972, 78 pp.
10. Janes, T.M., Jr., (G.N. Sandor, Adv.), "Collapsibility/Deployment of an Unmanned Martian Roving Vehicle," Mr. of Engrg. Rept., RPI, July 1972, 56 pp.
11. Rayfield, W.P., (G.N. Sandor, Adv.), "Roving Vehicle for Mars," 2nd Graduate Award (\$1,500 to student, plus grant to RPI), Div. II, Oct. 1970, The Lincoln Foundation's 1970 Engrg. Student Design Competition, sponsored by the Jas. F. Lincoln Arc Welding Fdn., Cleveland, Ohio
12. Simon, R.L., (G.N. Sandor, Adv.), "Design of a Toroidal Wheel for a Martian Roving Vehicle," 2nd Graduate Award (\$1,500 to student, plus grant to RPI), Div. II, Nov. 1971, The Lincoln Foundation's 1971 Engrg. Student Design Competition, sponsored by the Jas. F. Lincoln Arc Welding Fdn., Cleveland, Ohio.
13. Sandor, G.N., "Motorized Wheel Chair Can Even Climb Stairs," (German), Medical Tribune, an international weekly, German language issue for West Germany, Vol. 7, No. 11, Mar. 1972, published in Wiesbaden, pp. 1 & 48; and also in the German language issue of the same weekly published in Baden for Switzerland, Vol. 5, No. 11, Mar. 1972, pp. 1 & 20.
14. Sandor, G.N., "Wheel Chair Can Elevate to Eye Level," Chronic Disease Management, Vol. 6, No. 4, April 1972, p. 18.
15. Sandor, G.N., "Unmanned Martian Roving Vehicle Inspires Stair-Climbing Wheel Chair," N.Y.S. Journal of Medicine, Dec. 1973, Vol. 73, No. 24, pp. 2880-2883.
16. Redkey, Henry, "Rehabilitation Practices in Germany," Rehabilitation Record, July-Aug. 1963, pp. 12-14.

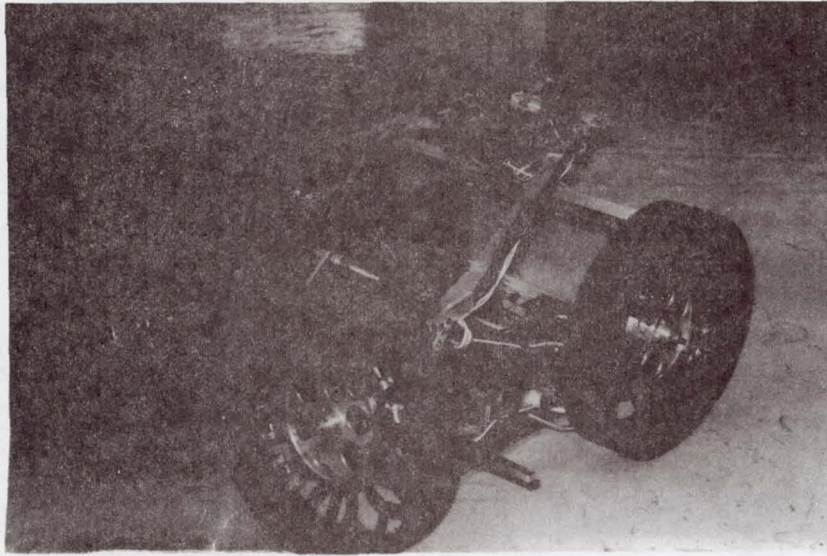


Figure 1. RPI MRV demonstration model in folded "launch and land" configuration.

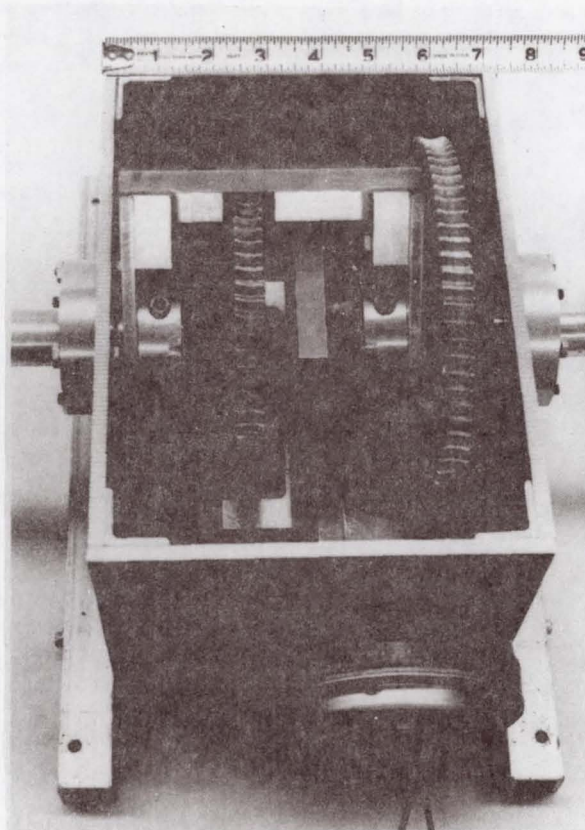


Figure 2. Strut-rotation gearbox in center of payload box. Rear strut worm gear at left, front strut gear at right, pancake motor in front. Similar pancake motor, hidden in back, rotates rear struts.

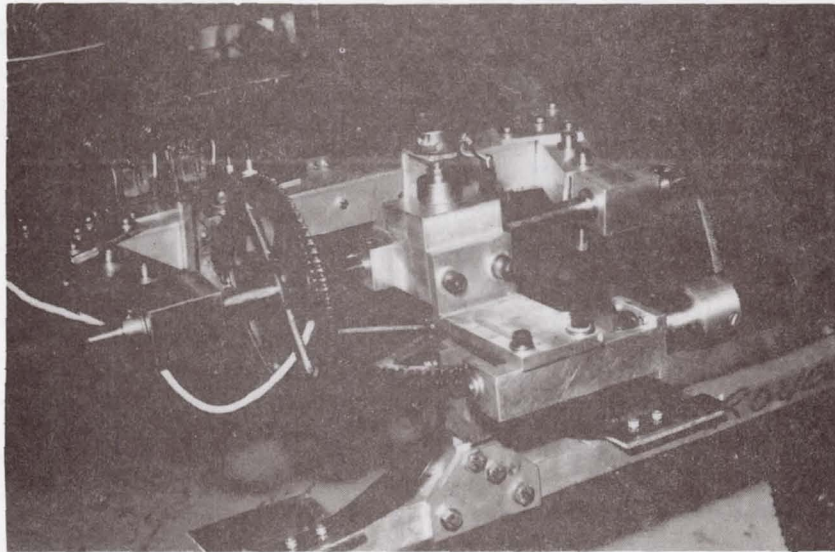


Figure 3. Front end of the RPI MRV with "flip-over" worm and worm gear (left) and steering gear (center).

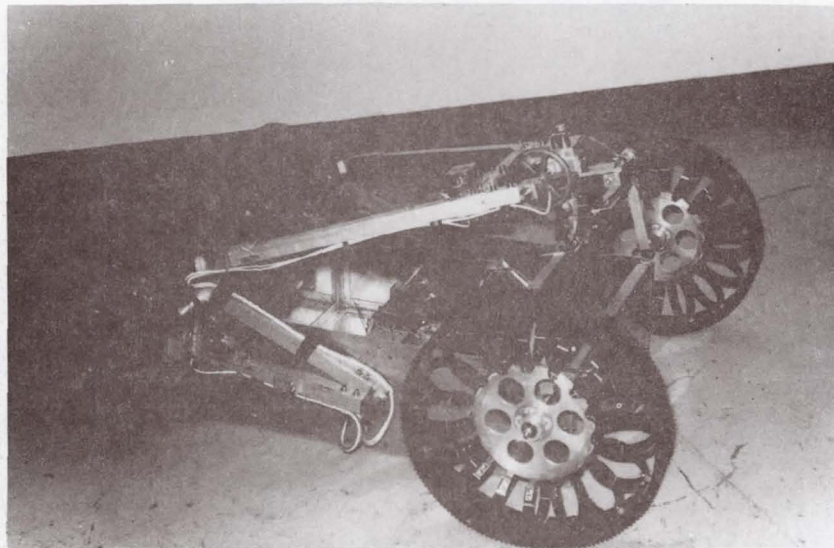


Figure 4. Side view of the MRV demonstration model in the first stage of deployment from its folded launch-land configuration, showing articulation of front struts. The front wheels are at the right.

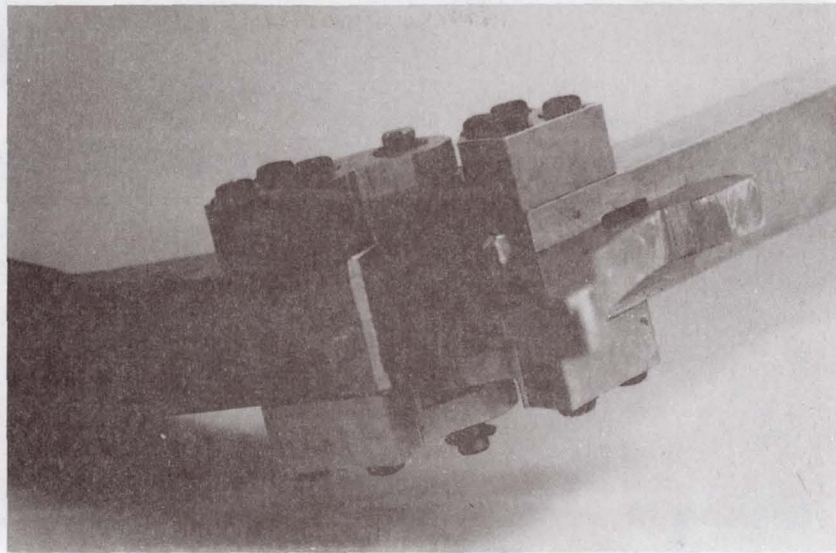


Figure 5a. Close-up of mechanism in unlocked position showing spring loaded locking plunger and release member.

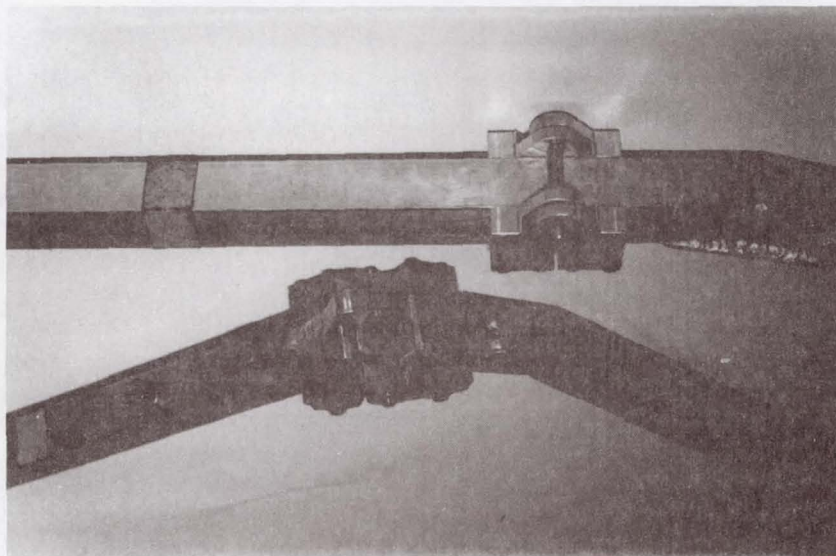


Figure 5b. Front strut articulation and locking mechanism in locked position (top) and before locking (bottom).

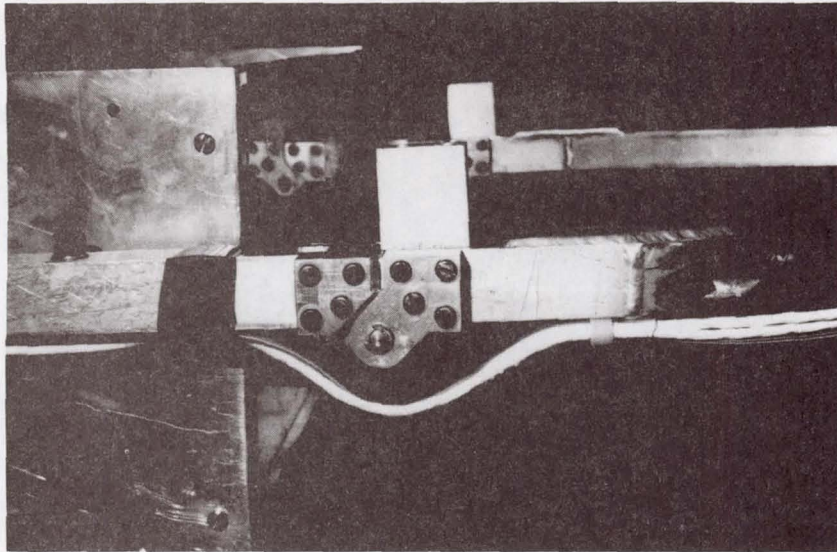


Figure 6. The front strut articulation hinge in the straightened-out position, locked by the square plunger inside the square-tube frame member.

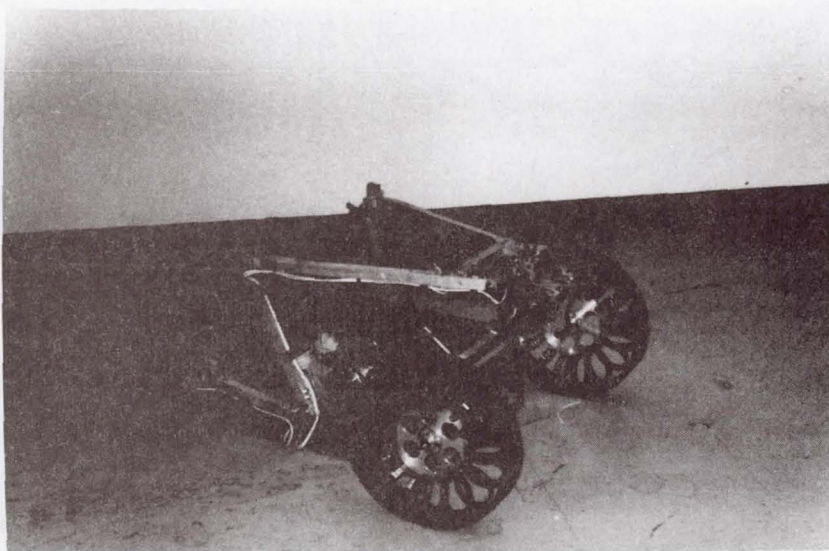


Figure 7. While the payload box rests on the ground, deployment starts by rotating the rear section of the articulated forward strut clockwise as shown here.

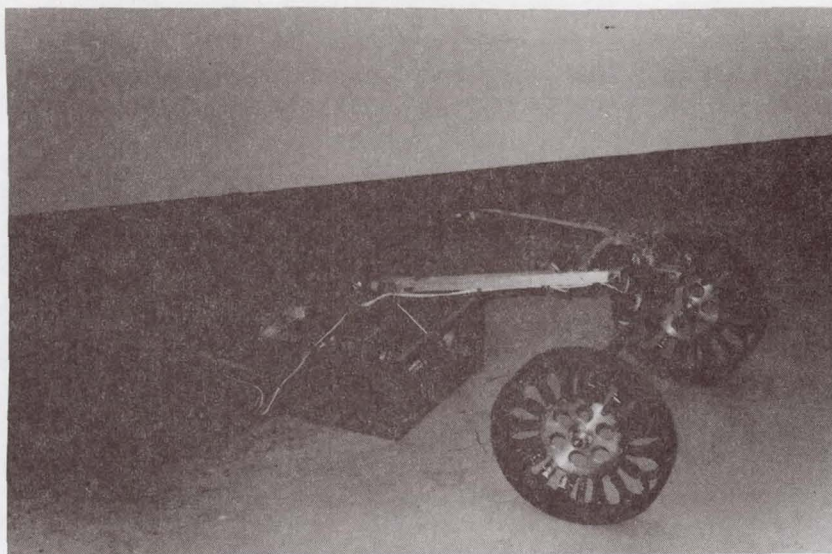


Figure 8. With the payload box still on the ground, the front struts are approaching the locking position while the front wheels roll on the ground in the course of deployment.

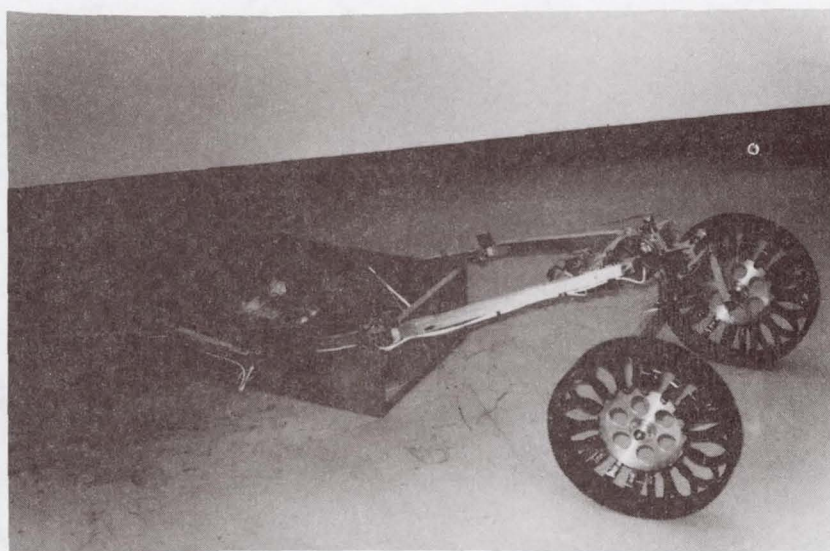


Figure 9. The MRV during deployment, shown just after the front-strut articulation has been locked in the straightened-out position. The payload box still rests on the ground.

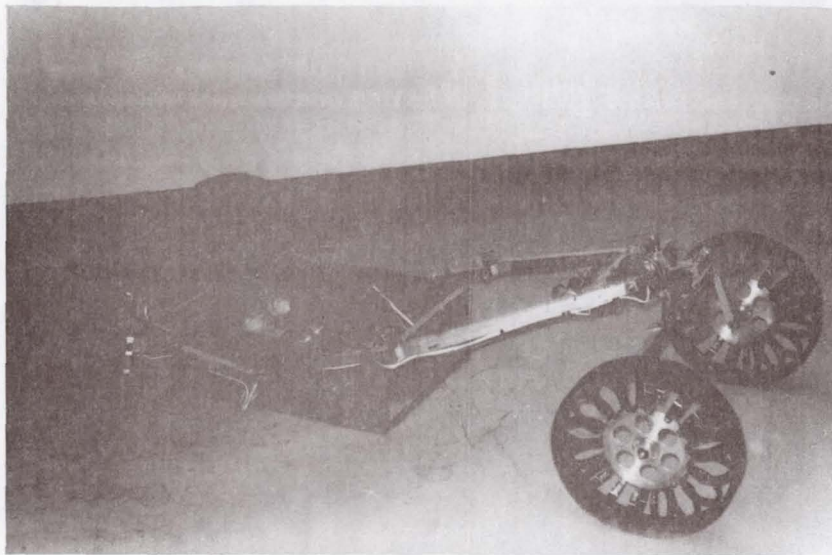


Figure 10. The RPI MRV in the process of "walking" the rear wheels from folded into deployed position. The payload box is still resting on the ground.

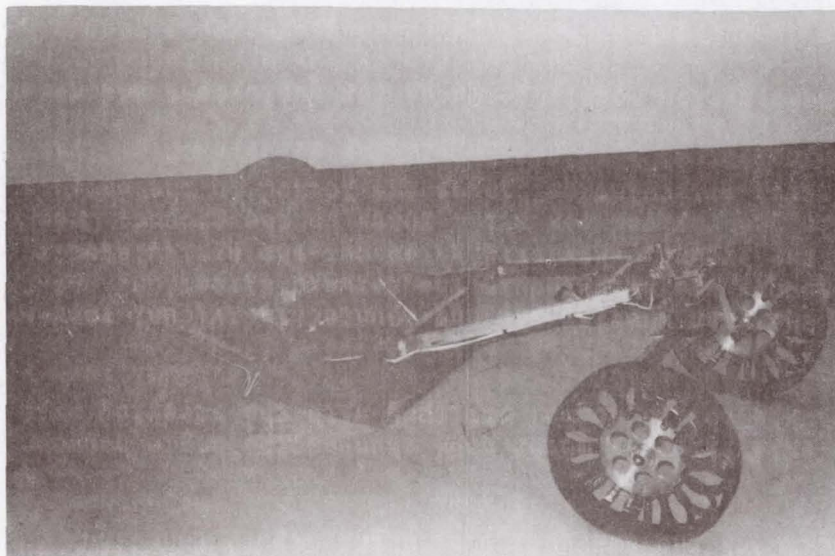


Figure 11. After completing the rear wheel deployment, the MRV is ready to lift its payload box off the ground.

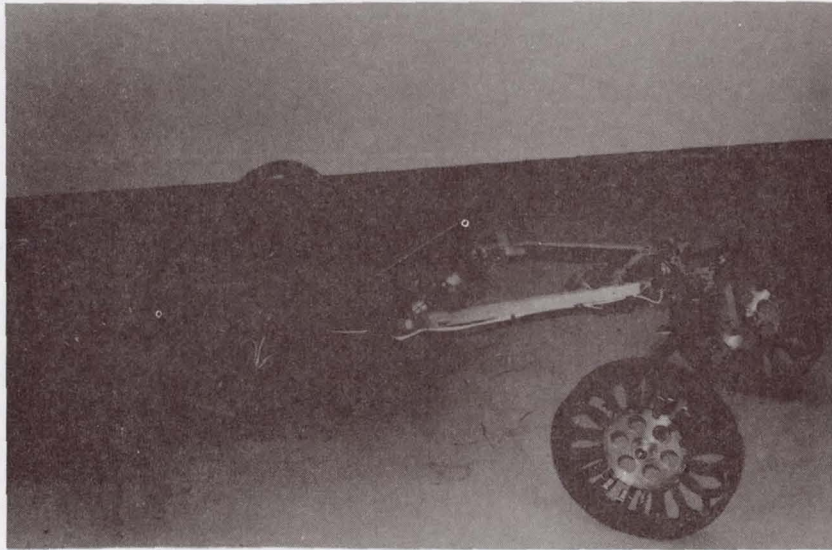


Figure 12. The front struts have been rotated downward, lifting the front of the payload box off the ground.

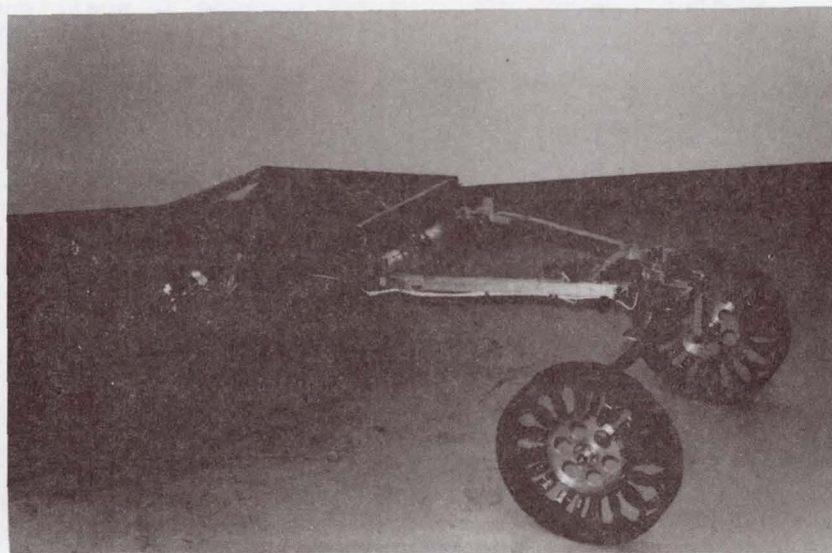


Figure 13. Rear struts having been rotated downward, the payload box is off the ground and the RPI MRV is fully deployed in the roving configuration.



Figure 14. The RPI MRV executing an emergency maneuver. The front and rear struts are exchanging positions, clearing each other as they pass overhead.

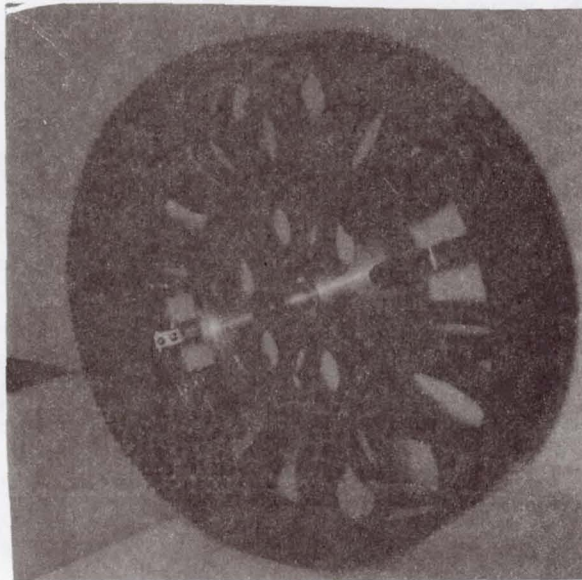
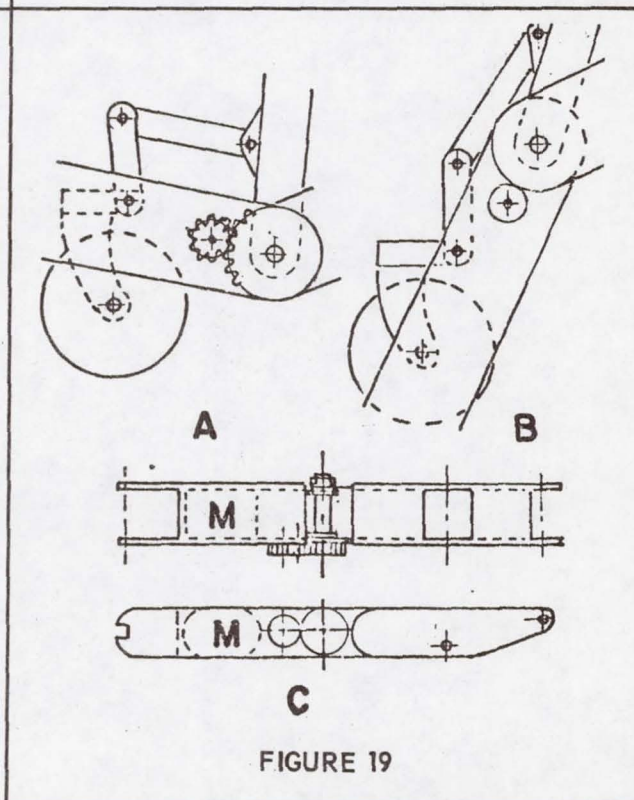
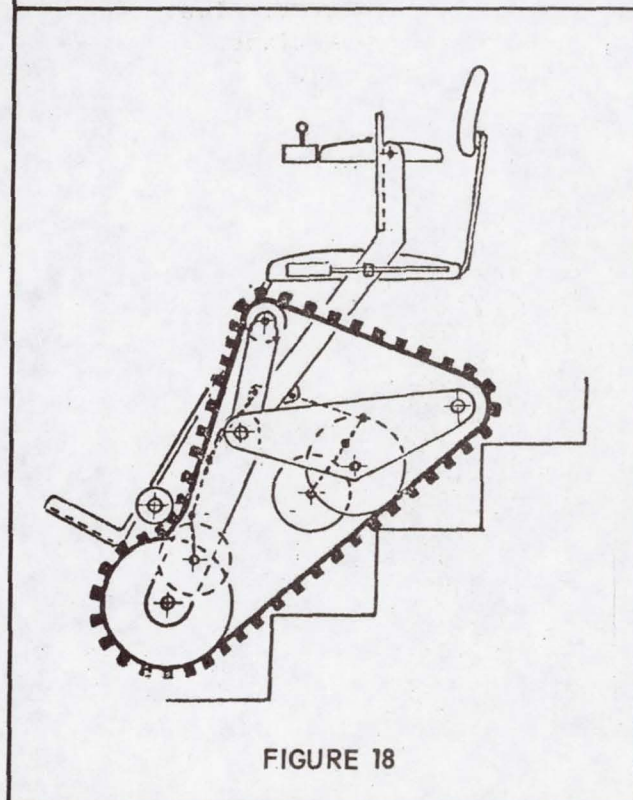
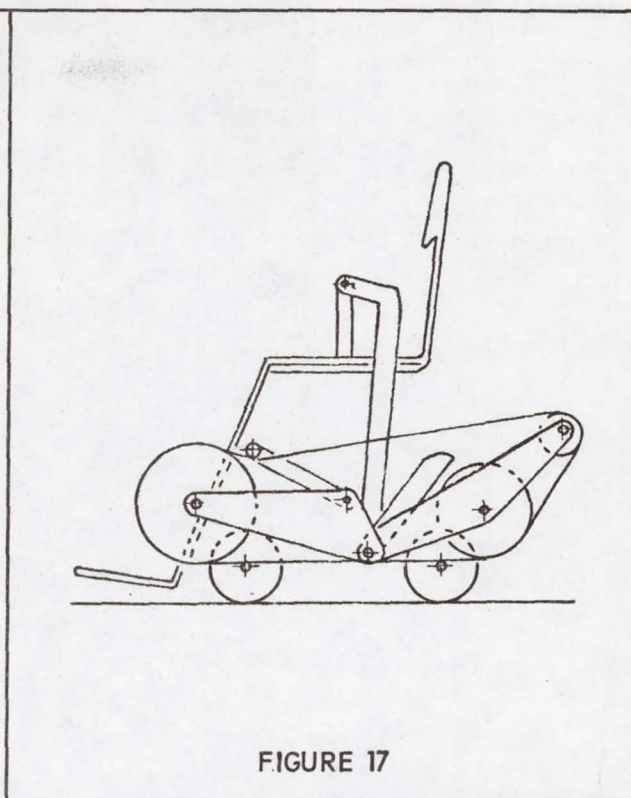
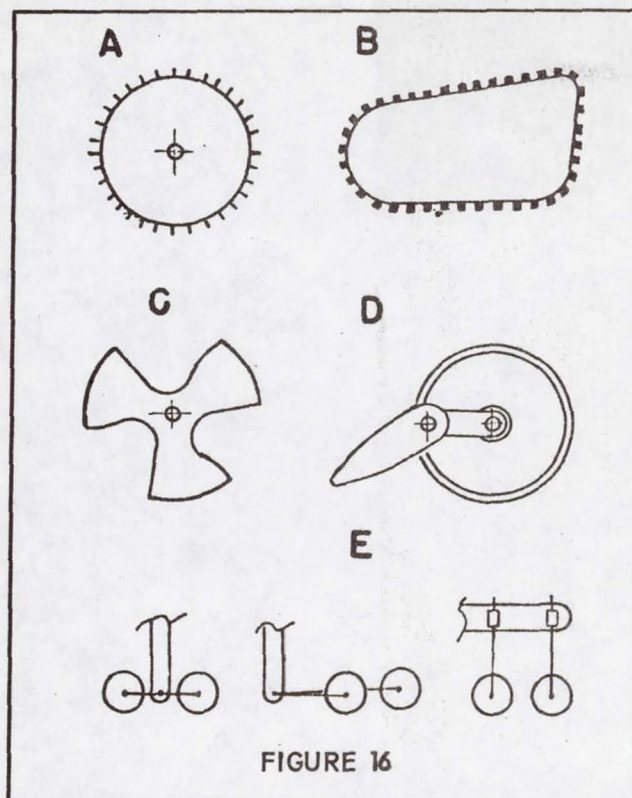


Figure 15. The RPI "all-metal elastic" toroidal wheel.



Figures 16 to 19. RPI's stair-climbing wheel chair design..

19. LOADCELL SUPPORTS FOR A DYNAMIC FORCE PLATE

By C. W. Keller and L. M. Musil
Lockheed Missiles and Space Company, Inc.
Sunnyvale, California

and

By John L. Hagy
Shriners Hospital for Crippled Children
San Francisco, California

SUMMARY

An apparatus was developed to accurately measure components of force along three mutually perpendicular axes, torque, and the center of pressure imposed by the foot of a subject walking over its surface. The data obtained are used to supplement high-speed motion picture and electromyographic (EMG) data for in-depth studies of normal or abnormal human gait. Significant features of the design--in particular, the mechanisms used to support the load-cell transducers--are described. Results of the development program and typical data obtained with the device are presented and discussed.

INTRODUCTION

Since 1965, a group of orthopedic surgeons, medical researchers, and aerospace engineers have worked together* to develop and perfect the equipment and techniques needed to thoroughly characterize and quantize human gait parameters. Early efforts by Sutherland and Hagy (Ref. 1) were focused on the use of high-speed motion picture cameras and a multi-channel EMG system to acquire data on angular motions and neuro-muscular activities of the lower extremities during walking. As these efforts progressed, the need for force, torque, and center of pressure measurements which were correlated in time with the motion picture and EMG data, became increasingly obvious. Consequently, in 1971, a device designated as the Dynamic Force Plate† was conceived and built. With this device, precise measurements of

*The work described herein was sponsored by the Shriners Hospital for Crippled Children, San Francisco, California

†U. S. Patent pending. Development models are currently in operation at Shriners Hospital, San Francisco, California; the Mayo Clinic, Rochester, Minnesota; and Children's Health Center, San Diego, California

vertical force, forward-aft shear force, medial-lateral shear force, torque, and center of pressure location are obtained as functions of the percent of walk cycle (time) while the subject's foot is in contact with the plate.

During the design and development of the force plate system, the most critical problem encountered was that of devising loadcell support mechanisms which were suitably rigid, yet which permitted the six degrees of freedom needed to obtain the desired measurements. These supports were required to provide relatively high load capability, minimum misalignment, and negligible friction. Three different support mechanism concepts were developed and evaluated during the program. In the chronological order of their development, these were: (1) sliding friction supports, (2) ball-joint/conical pivot supports, and (3) spherical segment rocker supports. The latter were found to be superior in terms of accuracy, repeatability, low-friction, low-noise, and high-load capabilities. Moreover, installation and calibration procedures were significantly simplified with this design.

SYSTEM DESCRIPTION

The Dynamic Force Plate is shown in the photograph and cut-away perspective drawing of Figs. 1 and 2, respectively. Application of current aerospace instrumentation technology to the design of the system resulted in selection of piezoelectric quartz crystal loadcell transducers to obtain the necessary measurements. Originally developed for the adverse environments and demanding requirements of unique aerospace applications, these rugged loadcells extend heretofore unavailable measurement capabilities to the medical community. Compared to more conventional strain gage loadcells, the piezoelectric devices offer the following advantages: (1) passive operation (i. e. , no active excitation power supply is required), (2) a wider load range for a given load rating, (3) a higher sensitivity due to higher output voltage, (4) a higher frequency response, (5) a higher structural rigidity, (6) a wider operating temperature range, and (7) a smaller physical size envelope.

The particular loadcell transducers selected provide up to ± 10 -volt output signals over a load range from approximately 0.09N to 2.2kN (0.02 to 500 lbf) with a frequency response from near DC (static force) to approximately 200 hz*. Once installed, they require little or no maintenance or recalibration. Output signals are generated only in response to changes in the applied load; consequently, they are summed electronically using a charge amplifier in order to determine the total net force applied at any particular instant in time.

*The value given is representative of the total system and depends primarily upon the mass and rigidity of the plate; the upper limit of response for the transducer alone is 5000 hz.

Development models feature use of a transparent plexiglas plate in order to permit photographing of the footprint pressure patterns from beneath the walk-way surface as shown in Fig. 3. However, high-load, high-frequency-response models now being planned for use in large animal gait studies will require metal or composite plates in order to accommodate vertical forces of up to 17.8 kN (4000 lbf) and to provide system frequency responses of up to 1000 hz or higher.

The Dynamic Force Plate system, as demonstrated by the existing developmental models, is eminently suited to automatic data acquisition and modern, high-speed computer reduction, analysis, and display techniques. In the installation at Shriners Hospital, for example, force, torque, and center of pressure data are recorded, processed, and plotted in engineering units within approximately 7 minutes after any given walk cycle. This is accomplished using an Electronic Processors, Inc. general purpose EPI-118 minicomputer which is connected directly to the force plate system (Ref. 2).

LOADCELL SUPPORTS

Fig. 4 shows a closeup view of one corner of the force plate assembly. One of the two loadcells provided to measure forward-aft shear and torque, and the single loadcell used to determine medial-lateral shear, can be seen as installed within the load frame. This photograph, taken looking down on the device with the cover plate removed, actually shows the load cells assembled with the original sliding friction supports. However, it is also representative of the installation for the ball-joint/conical pivot supports and the spherical segment rocker supports developed later. Details of each of these support mechanism concepts are presented and discussed in the following paragraphs.

Sliding Friction Supports

Exploded views of the shear/torque force link assembly (on the left) and the compression spring assembly (on the right) are shown in Fig. 5 for the sliding friction support concept. The force link assembly shown is typical for any one of the three shear/torque loadcells and for any one of the four vertical loadcells, although detail dimensions do vary for the shear/torque and the vertical force applications. Each of the three shear/torque loadcell assemblies is pre-loaded in compression by one of the three spring assemblies provided. This permits measurement of load in both directions using a single loadcell transducer at each location. The output is zeroed electronically after the preload is adjusted to the desired value.

With this concept, all force link (loadcell) and compression spring assemblies are mounted rigidly to the load frame through the threaded mounting studs. In order to load any given transducer, the plate must be free to deflect in the direction of the applied load. This requires sliding of the microseal bearing surfaces normal to the loadcell axis (see detail shown in Fig. 5) for all of the system transducers mounted perpendicular to the

applied load axis. A potential error in measuring the applied load is thus introduced due to the frictional reactions imposed by the transverse-axis loadcells. A secondary source of error also results from the side load imposed on any given loadcell transducer due to the sliding friction.

During the development program, an analysis was performed to predict the magnitude of potential errors due to friction. A coefficient of static friction of 0.02 was assumed in the analysis based on a data sheet supplied by the Microseal Corporation for the appropriate materials and surface finish. Results of the analysis indicated that an error in a measured shear load of approximately 17.8N (4.0 lbf) could occur due to frictional resistance of the vertical force loadcells with a 90.7-kg (200-lbm) subject on the plate. This magnitude of error was considered to be unacceptable, and the design of the loadcell supports was modified. Experimental results obtained with the sliding friction support concept showed that the errors in measured vertical force were not significant, but that those observed for shear loads were indeed high compared to the range of the expected loads.

Ball-Joint/Conical Pivot Supports

The loadcell support concept shown in Fig. 6 differs from the sliding friction support concept in that each loadcell assembly can rotate in order to achieve transverse-axis deflections. An adapter with a conical pivot is used in conjunction with a ball-joint swivel to provide the necessary rotational freedom.

Experimental results obtained with this system showed a marked improvement in accuracy. Errors due to internal friction within the mechanisms were reduced to negligible values. However, it was found that the initial calibration of the system was quite difficult due to a lack of axial rigidity within the neoprene washers used to align and cushion the swivel ball joint. Moreover, the maximum load capability of the system was limited by yielding of the conical pivot due to its extremely small contact area.

Spherical Segment Rocker Supports

The final loadcell support system concept that was evaluated during the development program is shown in Fig. 7. Using this concept, rotational freedom is provided by spherical segment rockers without sacrificing axial load capability. In addition, the difficulty encountered previously in calibrating the system due to the lack of axial rigidity was eliminated. In order to better provide the geometry envelope needed for the rocker segments, conical disc washer springs were used in lieu of the coiled compression springs.

TYPICAL FORCE PLATE DATA OUTPUTS

The data shown in Figs. 8 through 12 were obtained to illustrate the general capability of the Dynamic Force Plate system. Five walks with the right foot of one normal subject were evaluated using the force plate system currently in operation at Shriners Hospital for Crippled Children, San Francisco. Since this force plate is connected directly on-line to an EPI-118 minicomputer, the data were recorded, processed, and machine-plotted automatically.

In Figs. 8 through 11, force and torque data, obtained at a nominal cadence of 50 walk cycles per minute, are presented as a function of percent of walk cycle (time). A walk cycle is defined as the period of time which elapses between consecutive heel strikes of a particular foot (in this case the right foot), and is, therefore, the reciprocal of cadence. As shown in the figures, the initial heel strike occurs at 0 percent of the walk cycle, toe off occurs (typically) at 62 percent, and the final heel strike occurs at 100 percent. Vertical force, forward-aft shear force, and medial-lateral shear force components are presented in Figs. 8 through 10, respectively, in terms of the percent of body weight. Actual force values can be determined simply by multiplying the percent of body weight values by the actual body weight which was 66.2 kg (146 lb) for this particular subject. Torque values are presented directly as Nm (in. -lb) in Fig. 11.

Inspection of the data presented in Figs. 8 through 11 reveals the remarkable repeatability of the force and torque components generated by the foot of a normal subject while in contact with the plate during successive walk cycles. Studies conducted at the Shriners Hospital Gait Analysis Laboratory have shown that the corresponding plots are generally quite similar for different normal subjects, although unique gait characteristics can be distinguished by comparison of the data for different subjects, and even by comparing those obtained for the left foot and for the right foot of a given subject. Moreover, significant variations have been noted between normal average plots (i. e., composites of the data for a representative number of normal subjects) and the corresponding plots obtained for an abnormal subject. It is this capability to quickly and accurately distinguish and compare specific details of the normal and abnormal gait data, provided by the Dynamic Force Plate system, which illustrates its great value as a diagnostic and evaluative tool.

Another characteristic data output of the Dynamic Force Plate system is the center of pressure (CP)-time history. Fig. 12 shows CP-Time histories for the 5 normal-subject walk cycles discussed above. In this graph, the X and Y coordinate values refer to the position of the CP on the surface of the force plate with respect to a fixed reference point ($X=0$, $Y=0$) at one corner of the plate. Percent of walk cycle (time) values are shown in the circles for each walk cycle. Since the X and Y coordinates are computed from measured vertical force values, and since (by definition) the vertical force values are zero at 0 and 62 percent of the walk cycle, the CP-Time histories shown range from approximately 1 to approximately 59 percent of the walk cycle.

CONCLUDING REMARKS

The application of aerospace instrumentation technology to the measurement of body forces imposed on a walk-way during normal or abnormal gait has resulted in the development of a unique medical research apparatus. Using the spherical segment rocker support mechanism concept developed during the program, the accuracy and repeatability of the data obtained are significantly enhanced. Similar force plate designs can be developed and used to obtain reliable gait data for other human or animal studies where force measurement capabilities of up to 17.8 kN (4000 lbf) are required.

REFERENCES

1. Sutherland, David H., M. D., and Hagy, John L.: Measurement of Gait Movements from Motion Picture Film. *The Journal of Bone and Joint Surgery*, Vol. 54-A, No. 4, pp. 787-797, June, 1972.
2. Computer Applications; *Medical Electronics and Equipment News*, August, 1973.

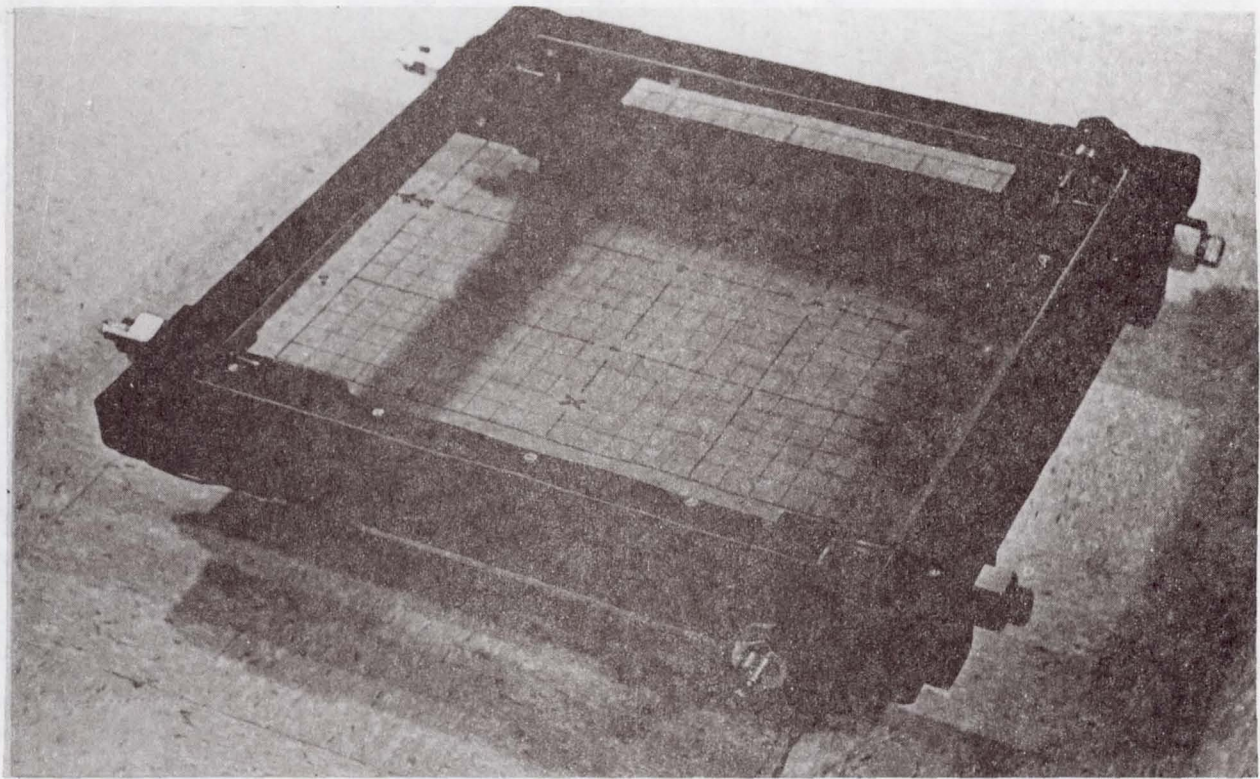


Figure 1. A Dynamic Force Plate Assembly

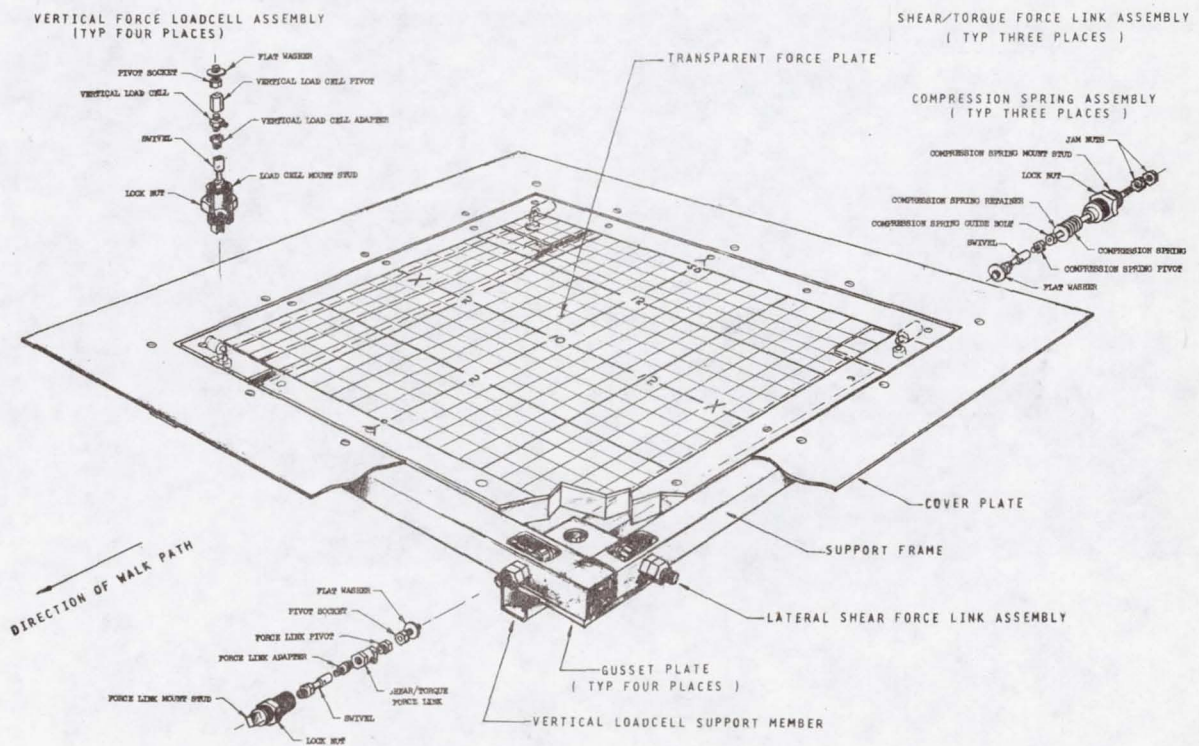


Figure 2. Cut-Away Perspective Drawing of the Dynamic Force Plate

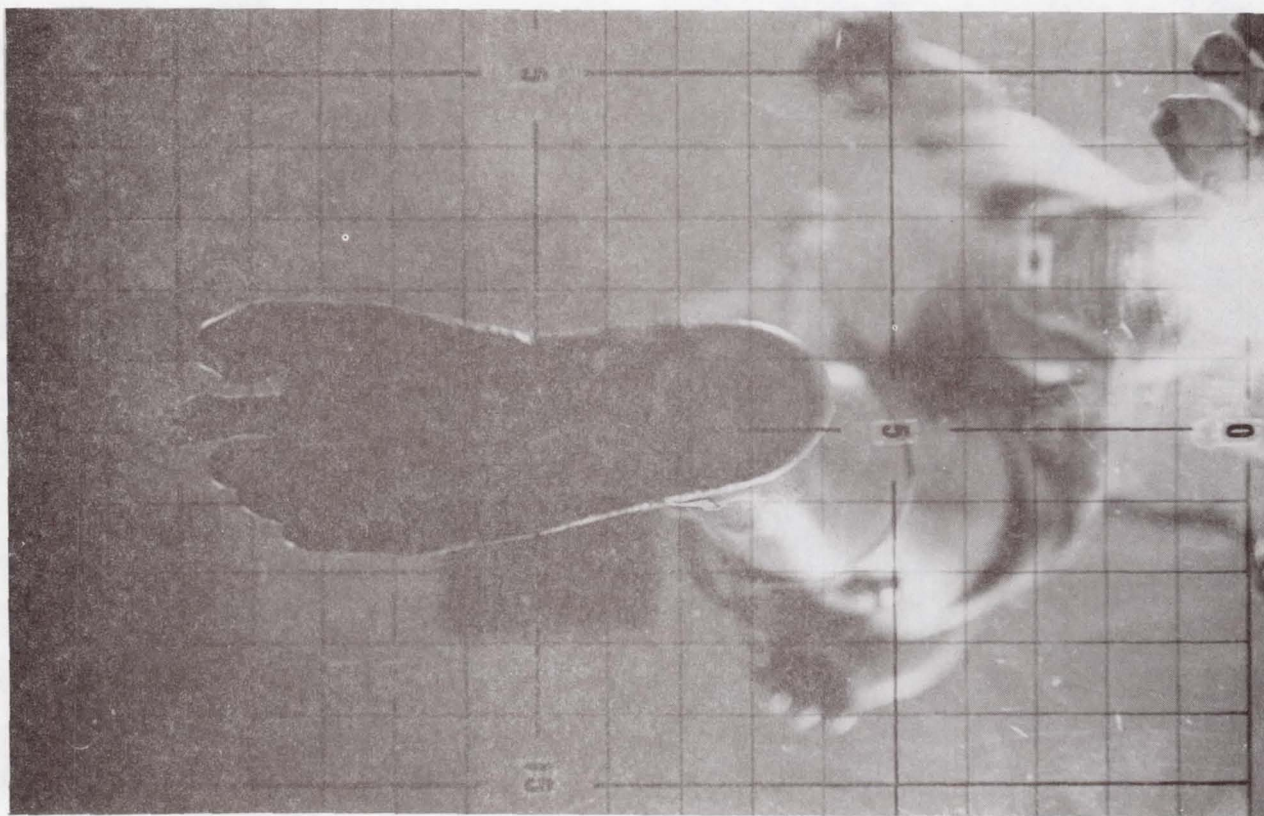


Figure 3. View of the Footprint Pressure Pattern

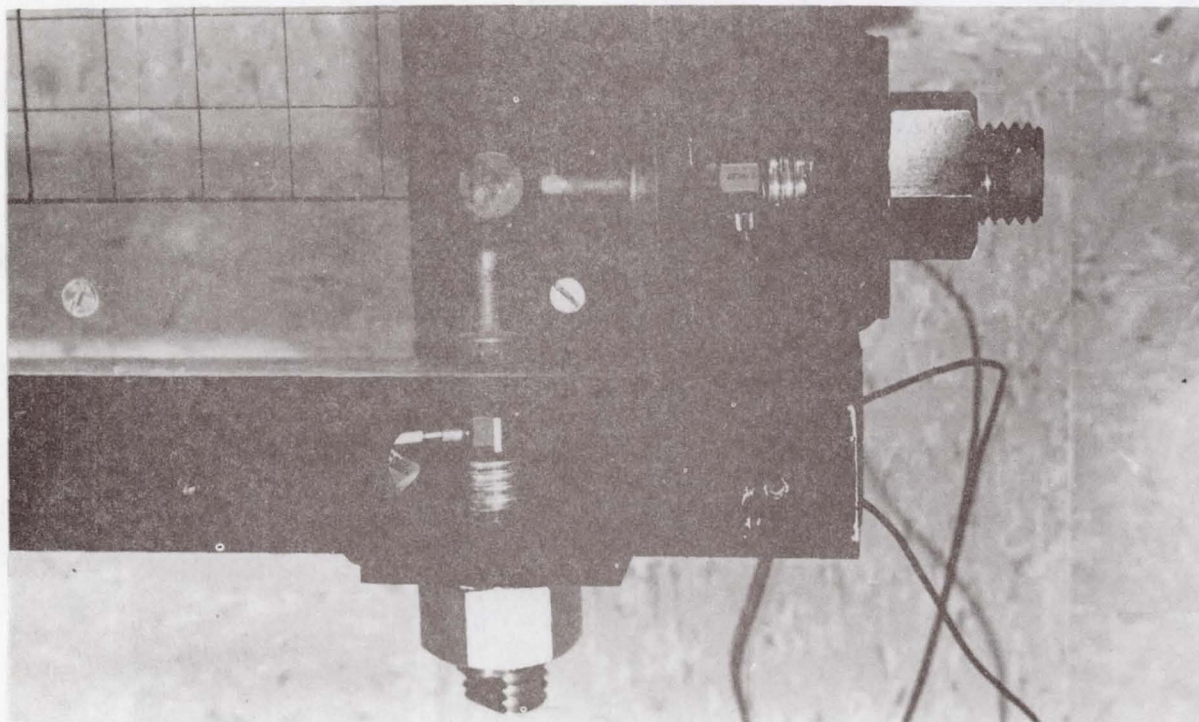


Figure 4. Closeup View of the Loadcell Support Installation

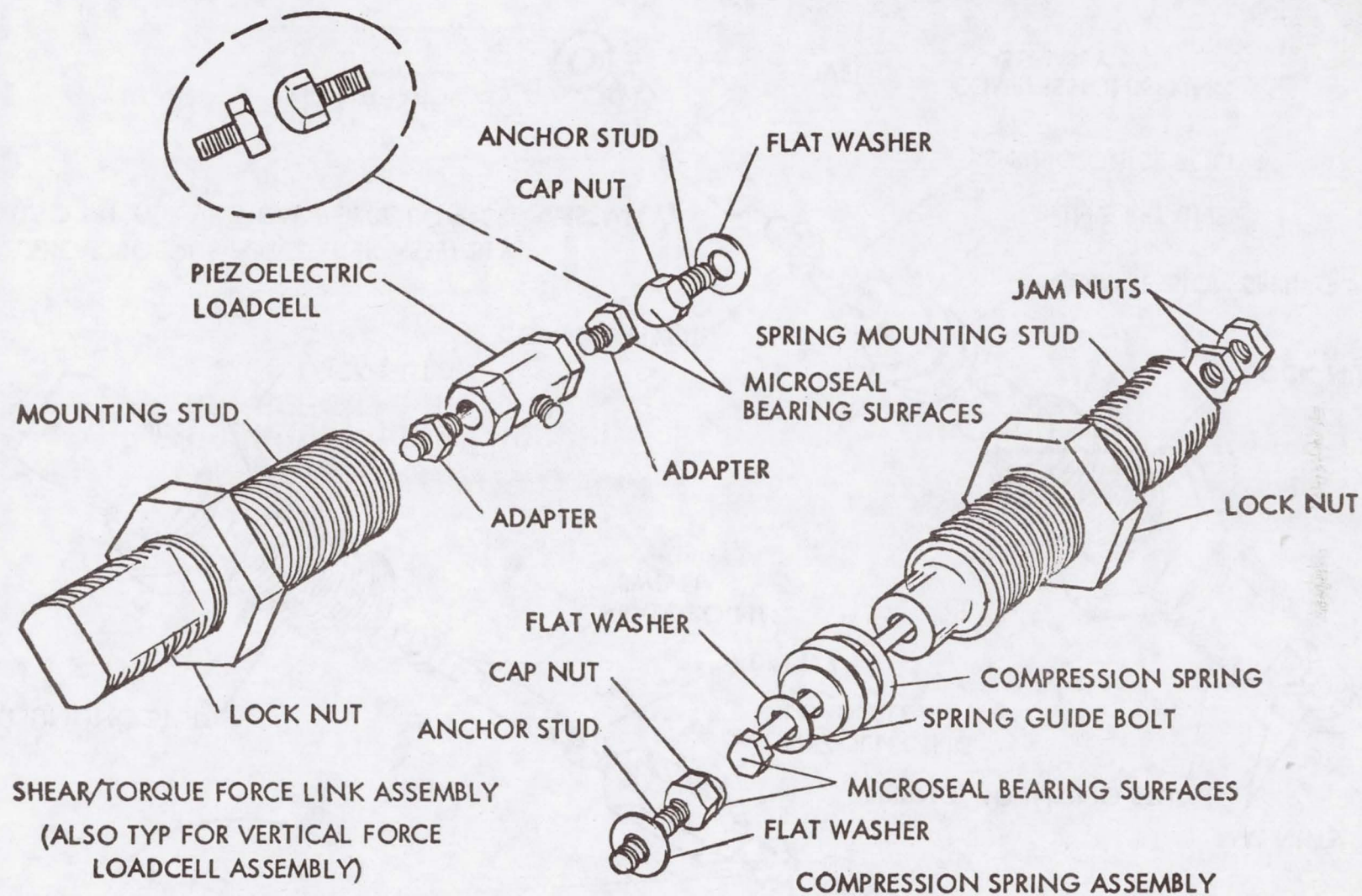


Figure 5. Details of the Sliding Friction Support Concept

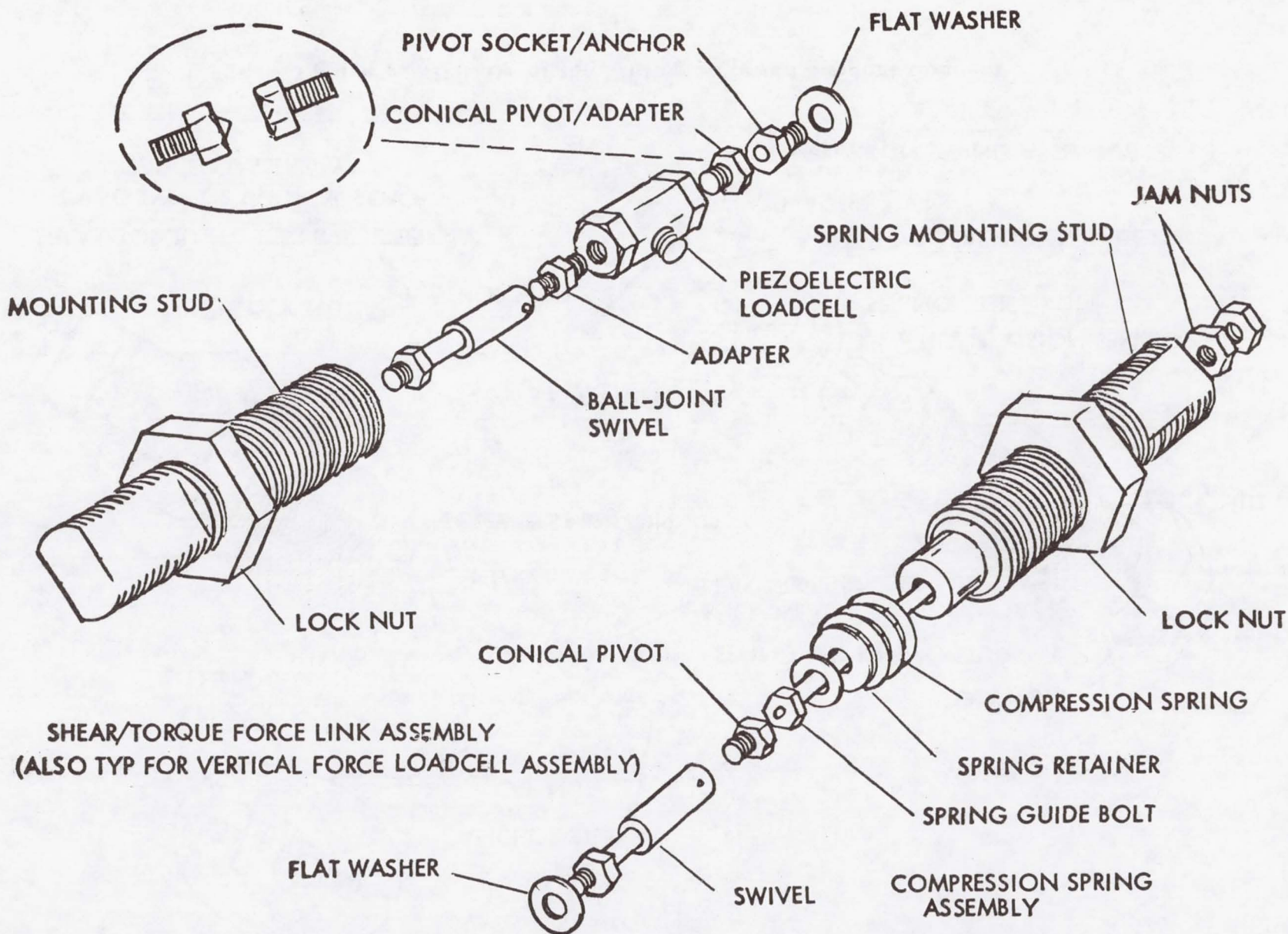


Figure 6. Details of the Ball-Joint/Conical Pivot Support Concept

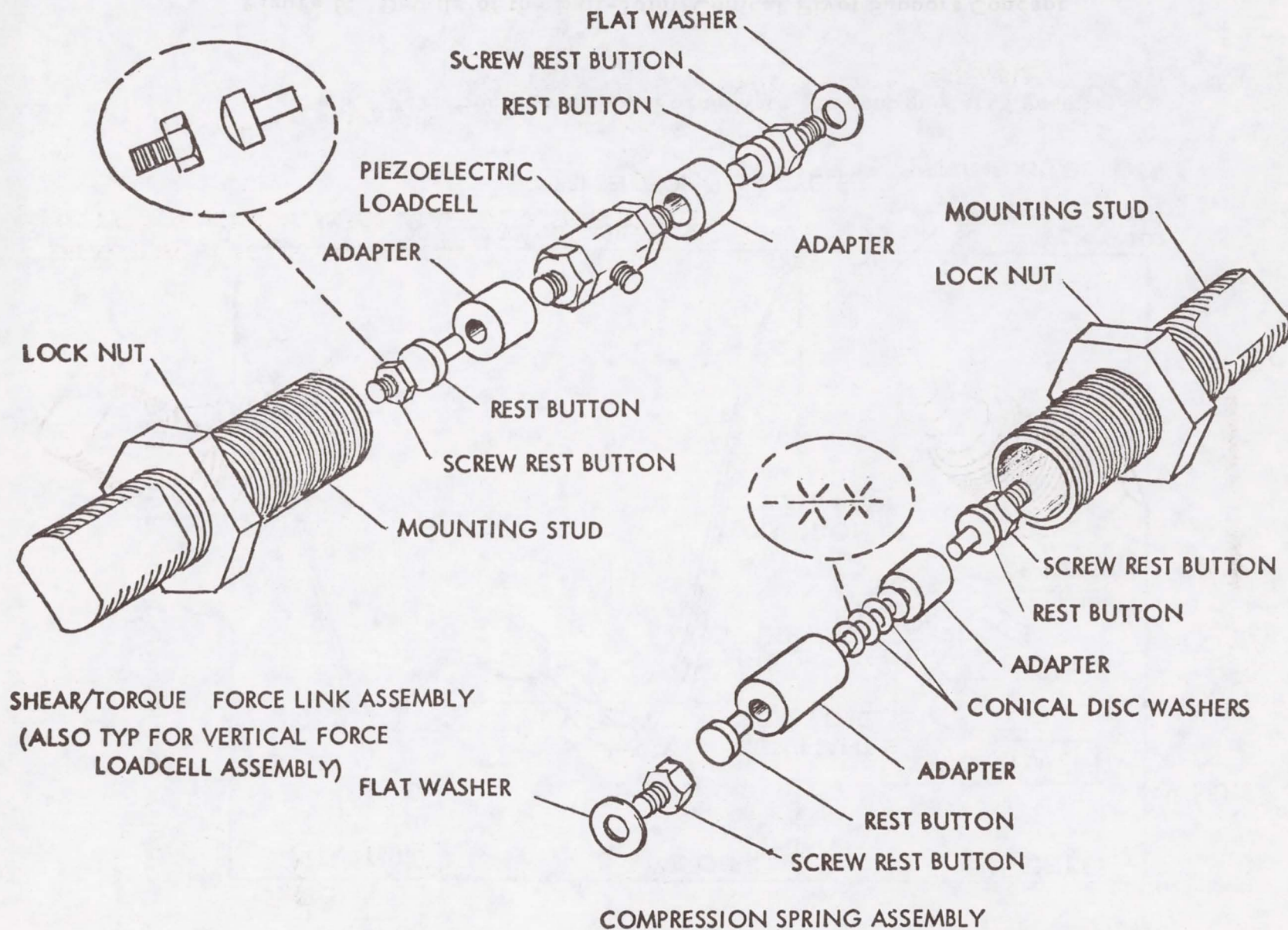


Figure 7. Details of the Spherical Segment Rocker Support Concept

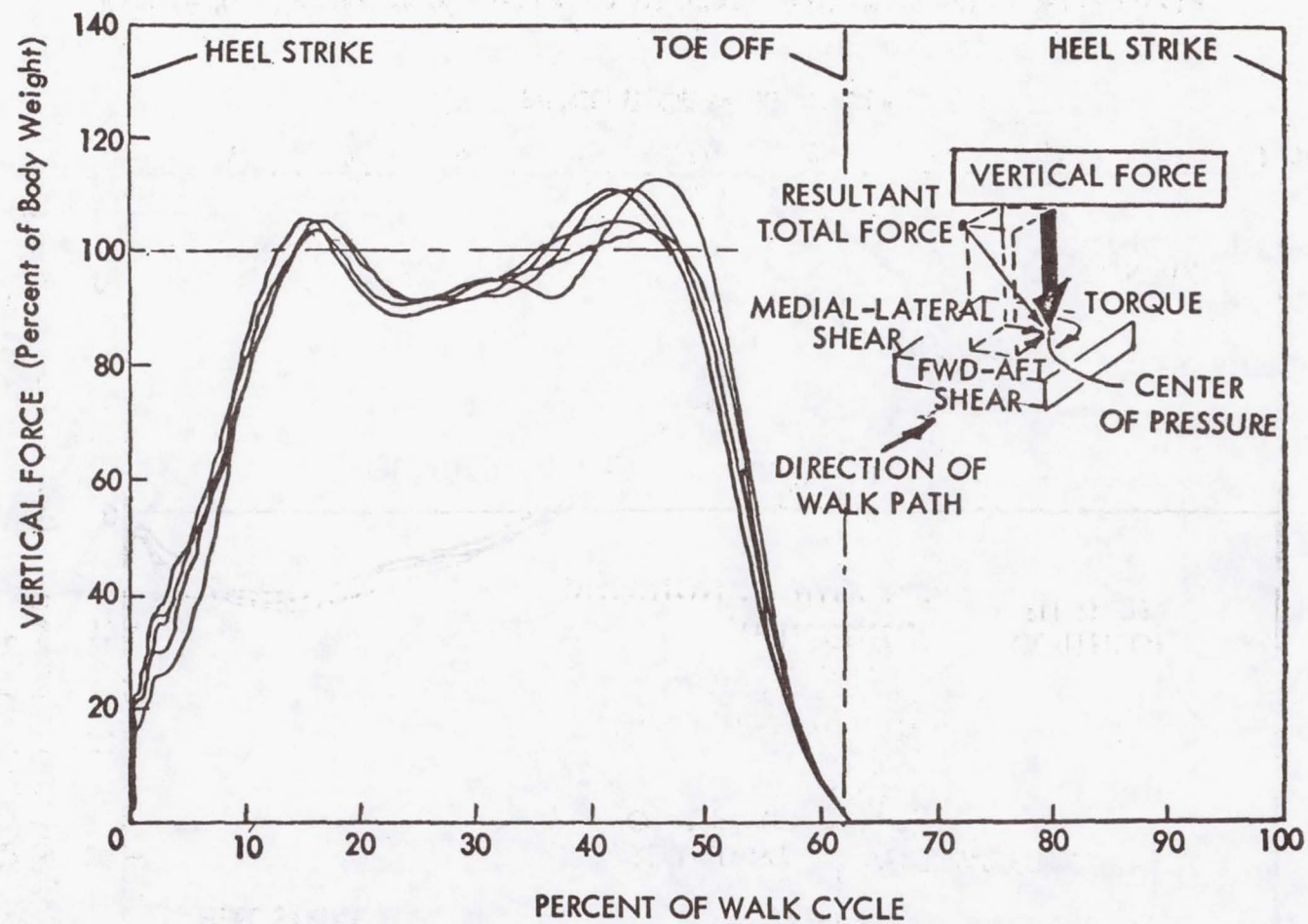


Figure 8. Variation of Vertical Force With Percent of Walk Cycle

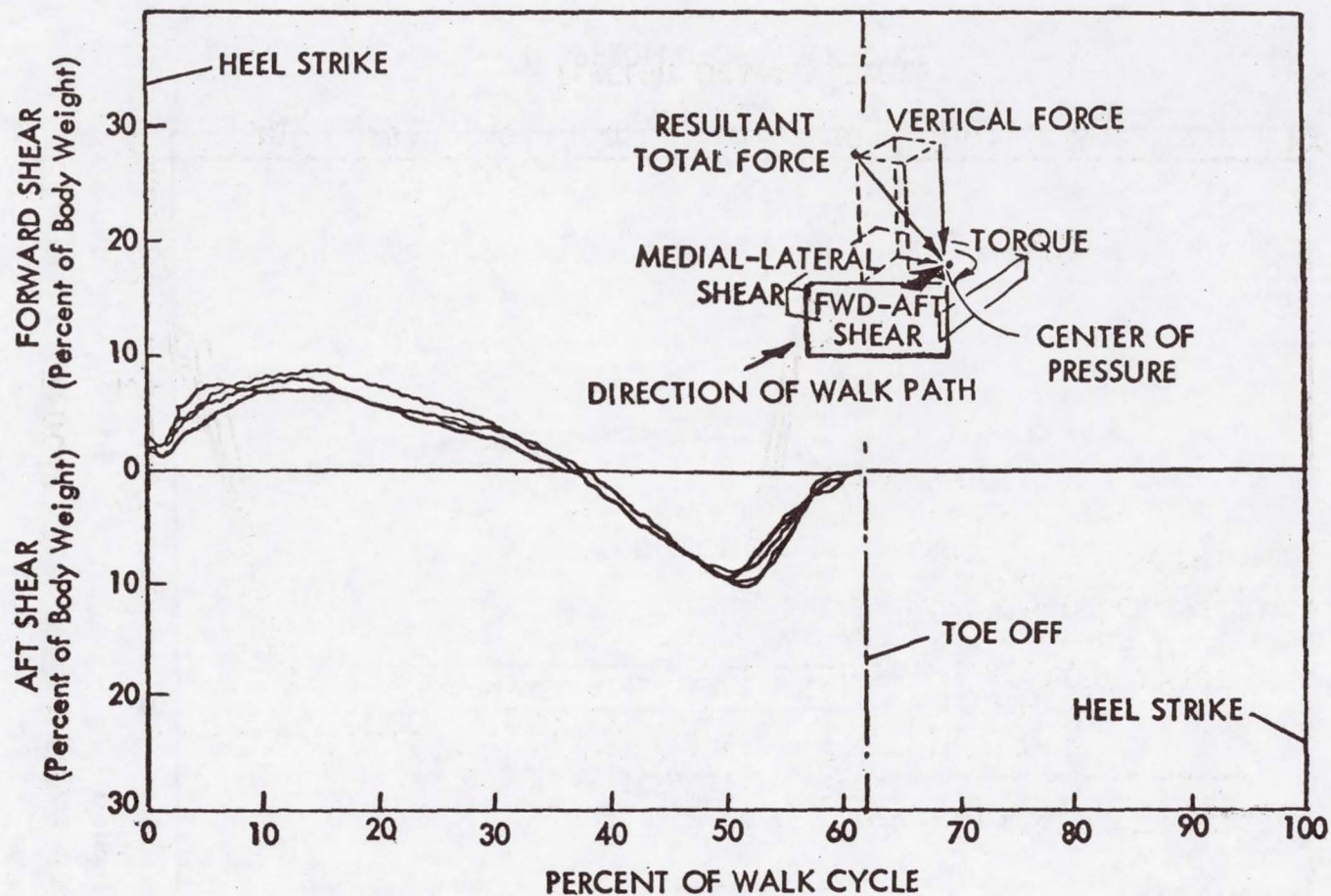


Figure 9. Variation of Forward-Aft Shear With Percent of Walk Cycle

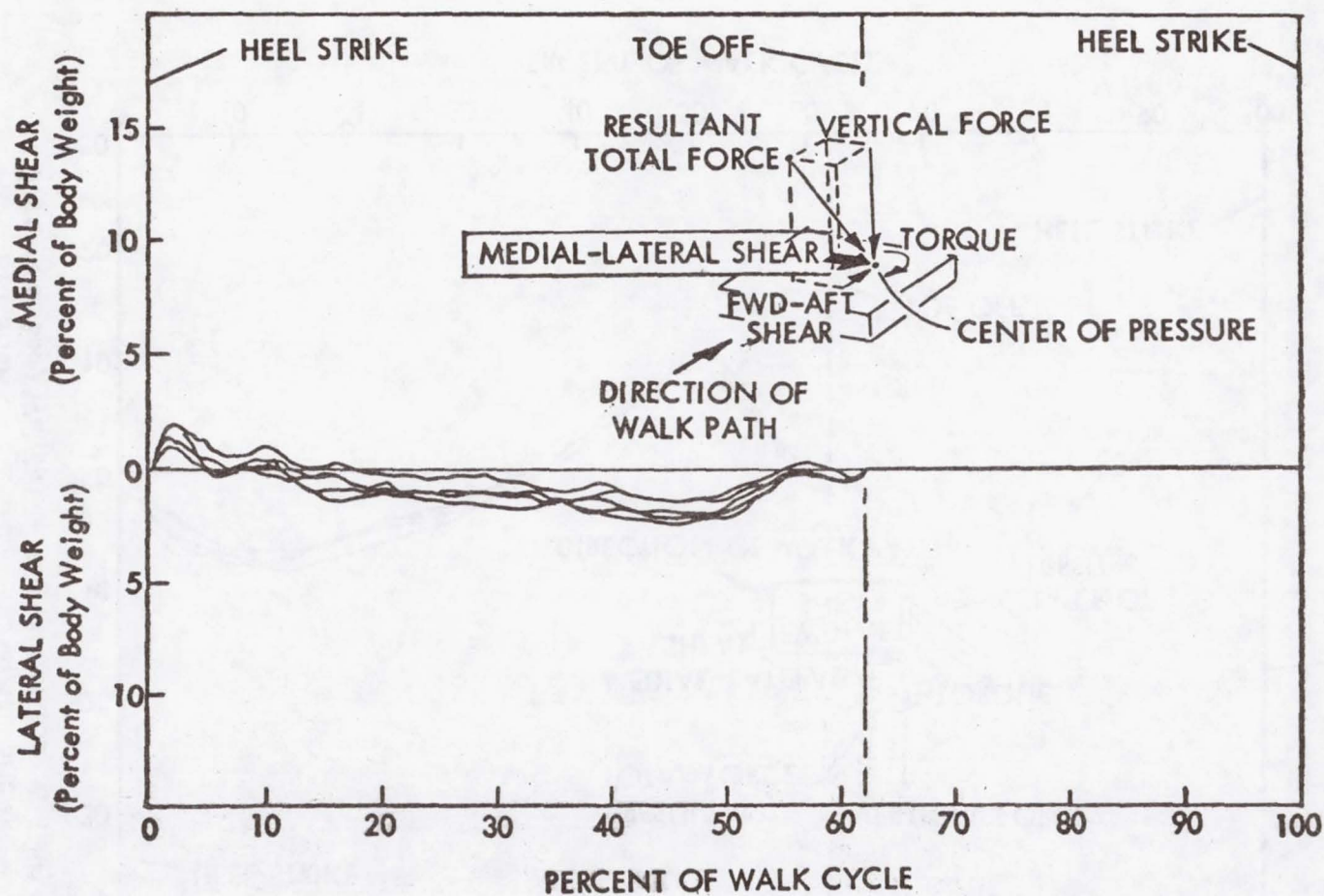


Figure 10. Variation of Medial-Lateral Shear With Percent of Walk Cycle

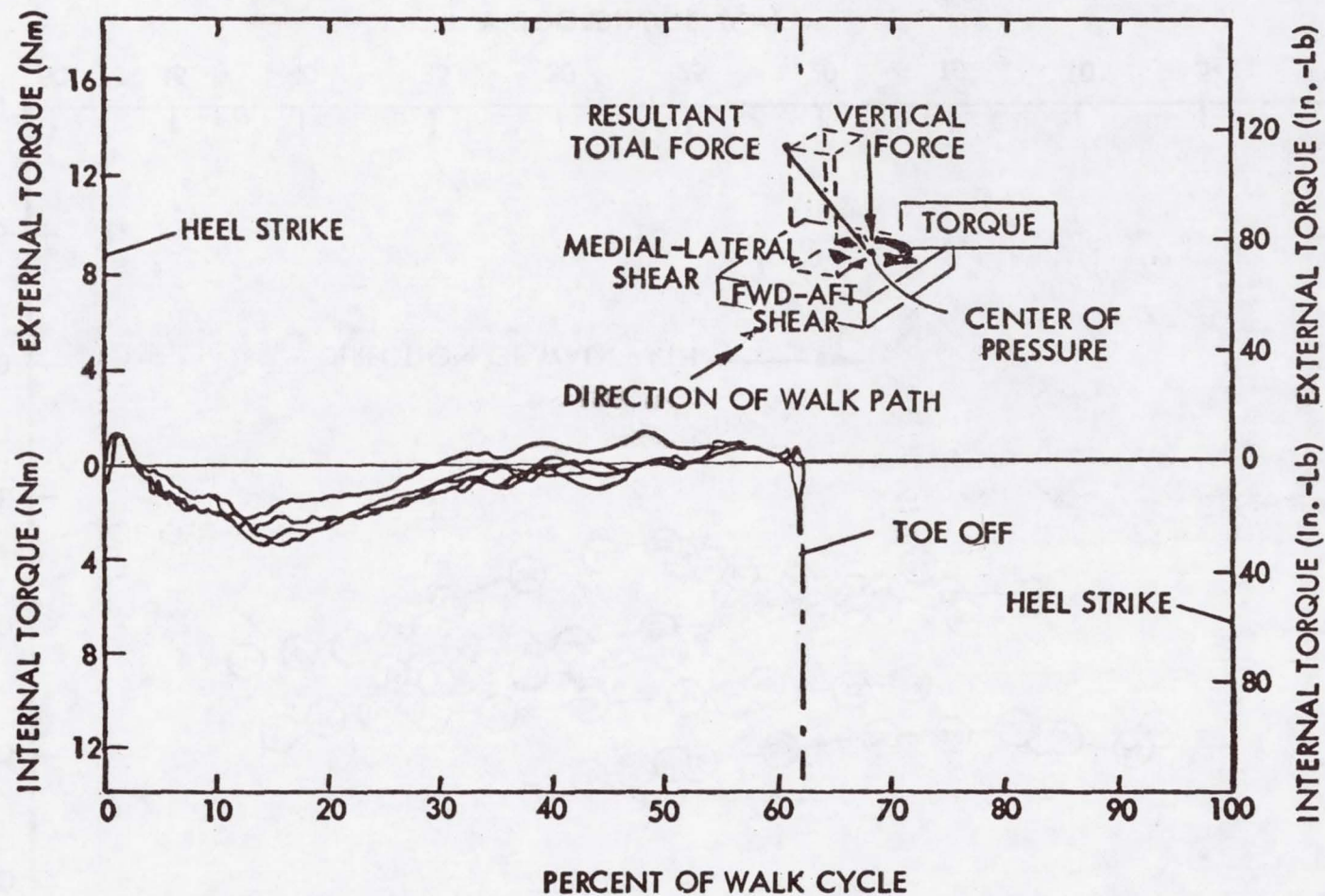


Figure 11. Variation of Torque With Percent of Walk Cycle

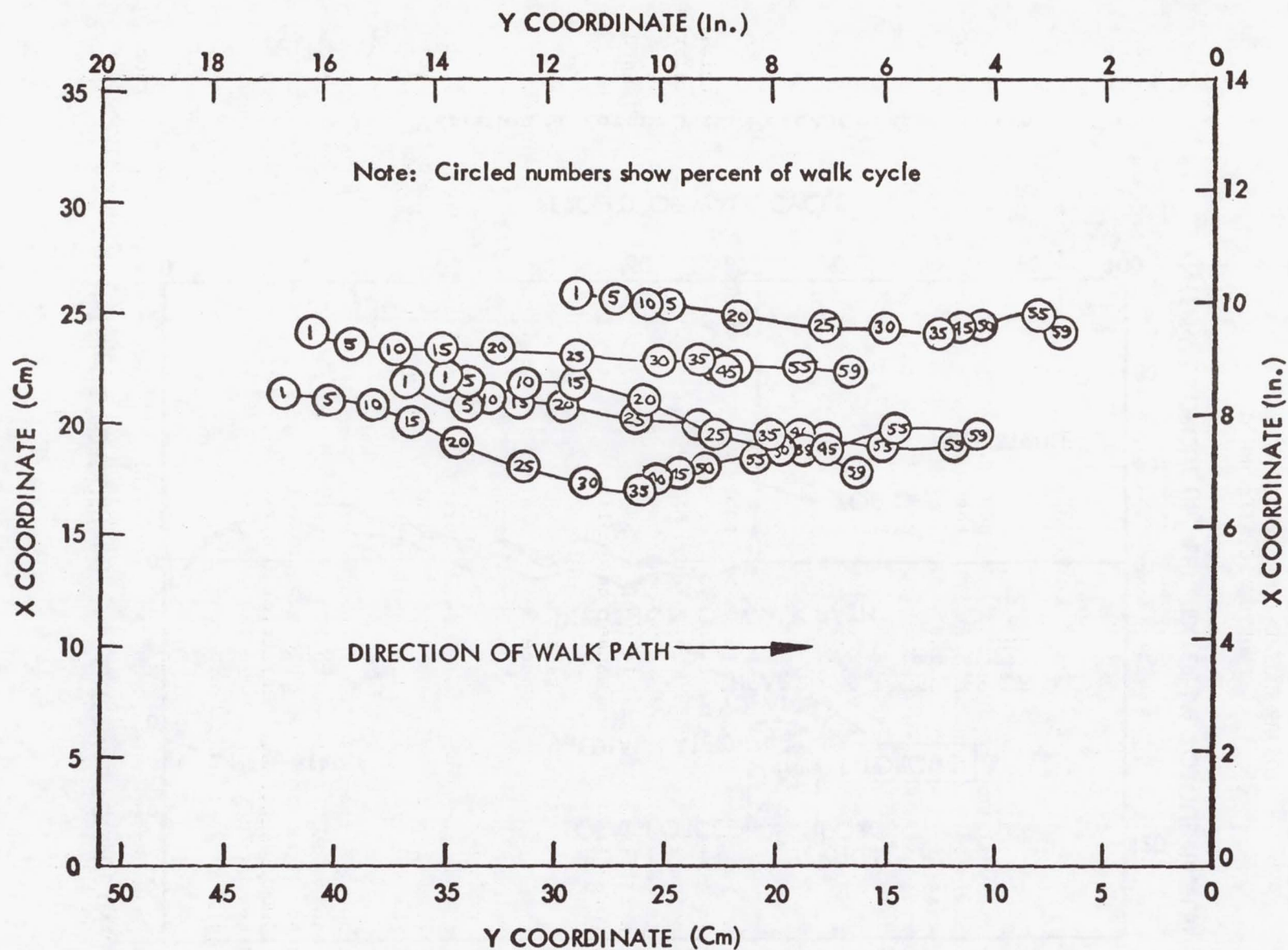


Figure 12. Center of Pressure - Time History

20. DEVELOPMENT OF A BONE-FIXATION PROSTHETIC ATTACHMENT

By Lester J. Owens
NASA Kennedy Space Center

SUMMARY

The first of what promises to be a new generation of prosthetic devices--an artificial limb attached directly to the bone by a quick-disconnect coupling--is undergoing in-place testing at a California medical rehabilitation center. This paper describes its design concept and development, made possible by multiple spinoffs of aerospace technology.

INTRODUCTION

Man's experience in the design and fabrication of prostheses dates to prehistoric times, when some cave-dwelling amputee created the first artificial leg by binding a piece of tree branch to his stump. Since then, and particularly within this century, many advances have been made in the state of the art. However, artificial arms and legs of today still have to be strapped or clamped on the amputee's stump in a manner not unlike that of the olden days.

Thus, it was with a considerable sense of challenge that the writer, a member of the NASA Kennedy Space Center Design Engineering staff, responded to a request to help design a quick-connect, strapless prosthesis. The request was made by Dr. David B. Hartmann, a member of the staff of Rancho Los Amigos Hospital in Downey, California, during a visit to KSC in March, 1973. Over a period of years this Los Angeles County hospital has worked closely with NASA and the aerospace industry in a continuing technological exchange.

Months ago, the hospital's Amputee and Fracture Service chief, Dr. Vert Mooney, announced that research at the institution had shown the feasibility of using aerospace-developed biocompatible carbon for "direct skeletal attachment of limb prostheses." Heretofore, direct prosthetic attachment had been thwarted by the body's tendency to reject foreign materials and the failure of the skin to form a hygienic seal around otherwise compatible material.

Now, the medical researchers hoped for a workable prosthetic design utilizing a bone-implanted connector accessible through a biocompatible carbon collar around which the flesh and skin would heal. This led to Dr. Hartmann's request and the launching of the project described herein.

CONCEPT DEVELOPMENT

Development of the new prosthetic attachment concept began with consideration of the basic problem of finding a quick-disconnect method suitable for use with a person's bone. Aerospace technology quickly suggested the ball-lock connector, a familiar item in missile and space programs for several years. These quick-disconnect devices have served reliably to hold umbilicals and even complete space vehicles in place until the desired instant of release.

The ball-lock mechanism is simple and effective. In a typical device, balls captivated in holes near the point of the locking pin are forced to protrude from the shaft surface by a spring-loaded rod inside the pin. When the pin is inserted into its receiver, the balls encounter and lock into an annular groove. The pin cannot then be withdrawn until a release is pressed, moving the rod inside the pin to permit the balls to retract into cavities in the rod shaft.

Ball-lock devices are made in a variety of styles for aerospace applications. They normally range in diameter from 3/16 inch to 1 inch, although the Saturn V is released by four 3 1/2-inch pins. A four-ball stainless-steel ball lock of 1/2-inch pin diameter can carry approximately 102,300 newtons (23,000 pounds) in shear and 6,670 newtons (1500 pounds) in tension.

The medical researchers quickly accepted the simplicity of a ball-lock prosthetic disconnect, and the conceptualization of the new prosthesis was expedited as follows:

The male half of the disconnect device, containing the ball-lock pin and release mechanism, would be part of the prosthetic limb. The female half--the receiver--would be implanted surgically in the medullary canal of the bone remaining in the amputee's stump. A sleeve or collar of biocompatible carbon would be bonded around the distal end of the receiver insert to provide a permanent passage through the skin.

This connection concept would be usable wherever stump size permitted a receiver implant, including arm and leg locations above and below the elbow and knee. Hopefully, it would benefit many amputees with stumps too short for conventional strap-on or clamp-on prosthetic limbs.

DESIGN DEVELOPMENT

The announcement early this spring that an amputee at Rancho Los Amigos Hospital had volunteered for implant surgery spurred the development of a working prototype of the quick-disconnect prosthesis. Work was concentrated at KSC to provide a suitable ball-lock receiver and subsequently the associated hardware for a lower-leg prosthesis. A basic design was standardized using ball locks of three pin sizes: 1/4-, 5/16-, and 3/8-inch.

The receiver design (Figure 1) was influenced by consideration of Young's modulus of bone elasticity and corresponding moduli for the steel implant and an acrylic plastic, methylmethacrylate, which would be used as an insulator and bond between the implant and the surrounding bone. These moduli were calculated to be approximately 2×10^{10} , 2×10^{11} , and 4×10^9 newtons/meter² respectively. The lower modulus of the methylmethacrylate allows a transfer of bearing loads between the implant and the bone; the ogival contouring of the receiver was designed to provide decreasing load transfer toward the bone end and to avoid stress concentrations. The toothed, grooved shaft of the receiver enhances its seating in the bone canal with optimum distribution of the semi-fluid methylmethacrylate and gives mechanical interference with the plastic against pull-out and rotation within the bone.

Type 316-L stainless steel, previously proven biocompatible, was selected as the receiver material. Implant dimensions were determined by the writer through reference to Gray's Anatomy; they were subsequently approved by hospital personnel. The interior design provides a second ball-locking groove against the possibility that wear or future adjustments might require this backup feature, as the receiver could not easily be replaced. The unused groove would be filled in with an epoxy that could be removed cleanly with a dental pick when required. The epoxy would prevent wearing of the groove and facilitate cleaning of the receiver, which could be done simply with a swab and alcohol.

The finished implant device, complete with its biocompatible carbon collar and plastic plug, is shown in Figure 2. The protective plug would be used during the implant operation and recovery period and could be used afterwards during periods of prosthetic disconnection. The carbon collar was manufactured by Gulf General Atomic Corporation. Hospital experts developed the collar design to provide optimum healing and implant support. The circumferential holes are intended to promote tissue growth about the stump end.

The remaining design work was encouraged by the initial success of the implant operation, which was undertaken in March of this year. Figure 3 is a view of the healing leg stump showing the receiver in place.

Development of the prosthetic attachment involved the writer in a design effort to produce a mounting assembly containing not only the male portion of the ball-lock mechanism but also adequate shock-isolation provisions. The importance of the latter was emphasized by the belief that rejection of previously attempted implants may have resulted from shocks and stresses to the bone at the implant interface. It was decided to provide a coaxial shock absorber mount extending from just below the connection point into the main support column of the prosthesis.

Experimentation with various techniques and materials led to the development of the shear-radial isolation mount shown in Figure 4. This is formed by bonding an elastomer (silastic rubber) between aluminum cylinders that are threaded to provide adjustment capability.

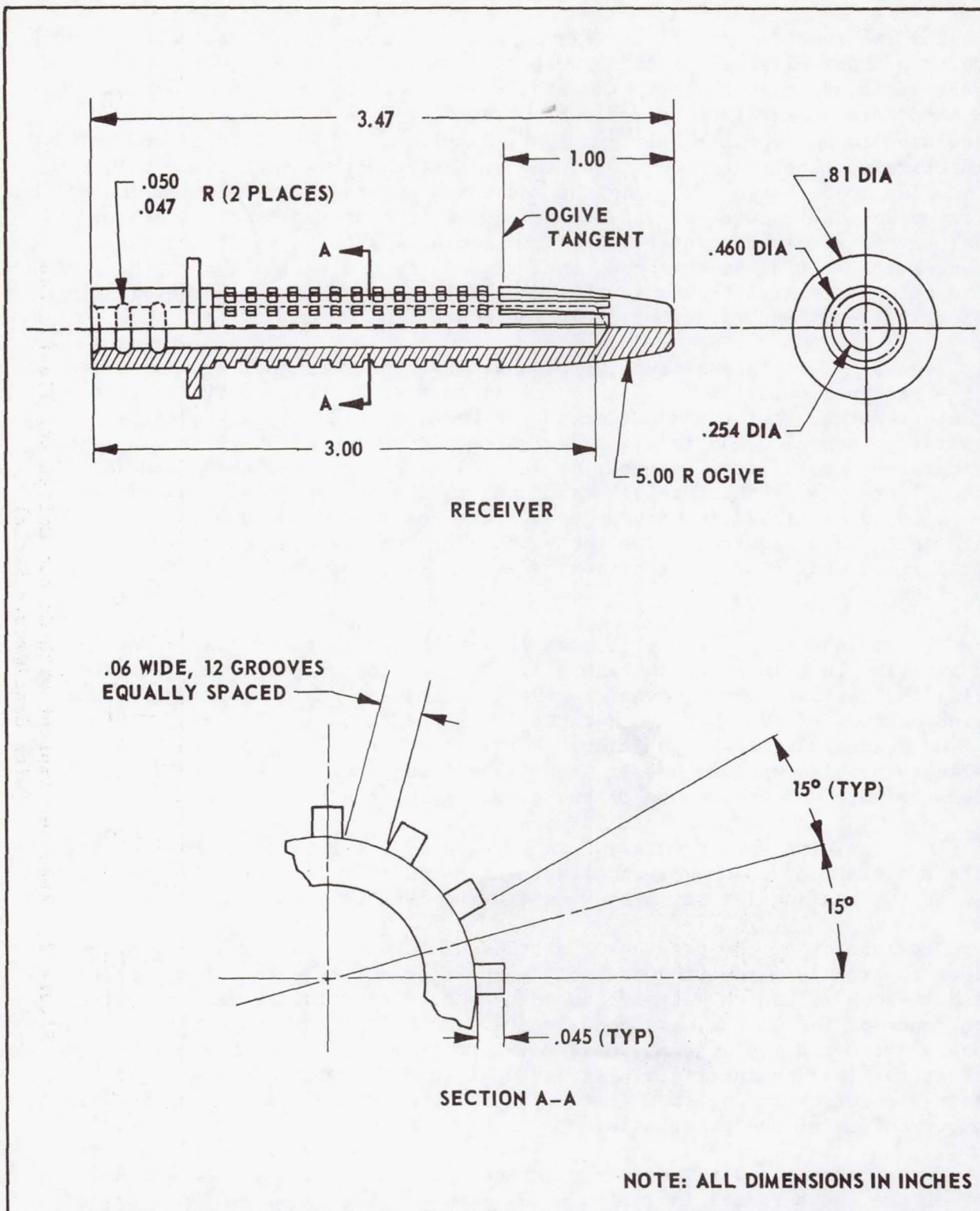


Figure 1. Receiver Implant Design (Extracted from Manufacturing Drawing)

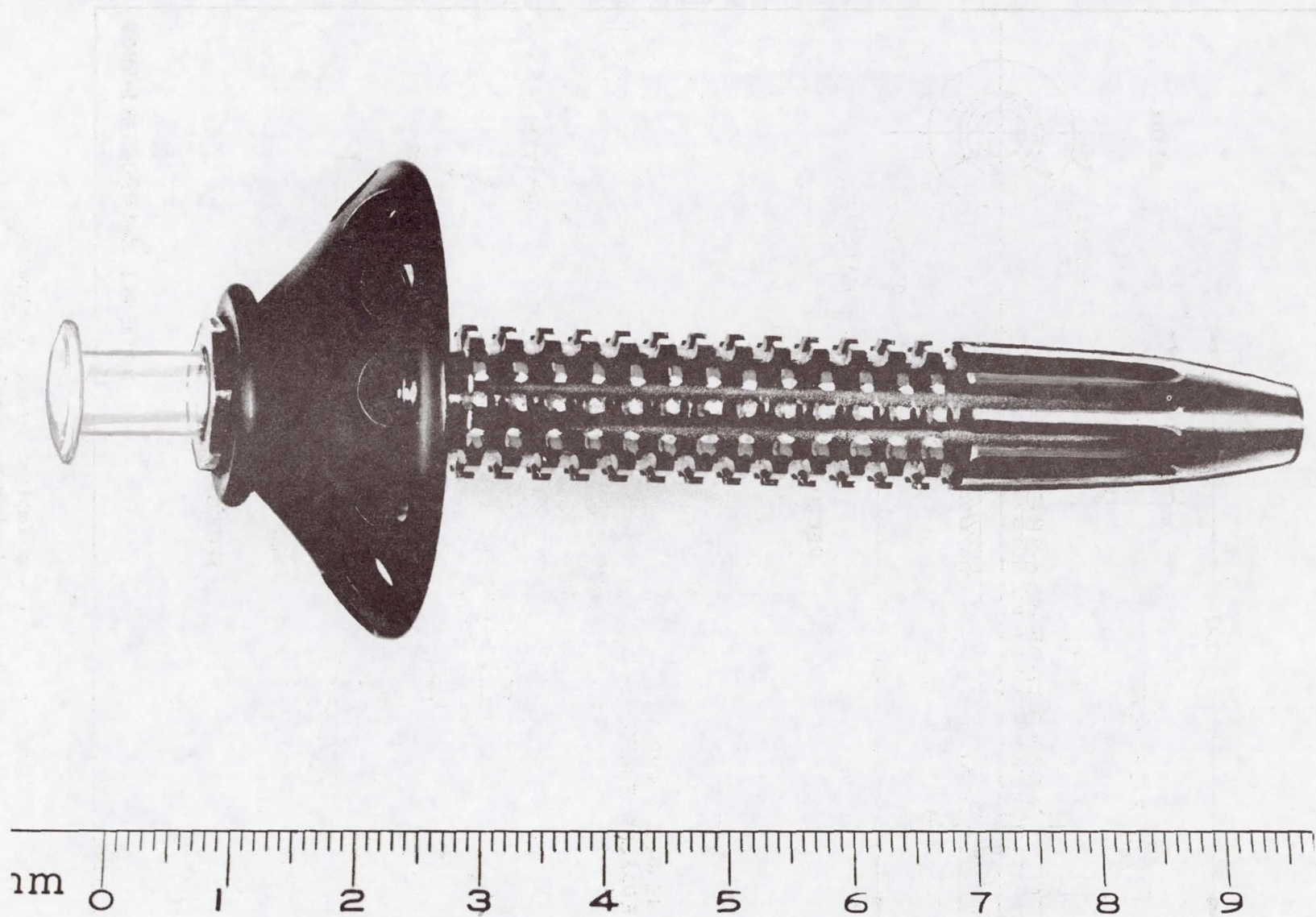


Figure 2. Receiver Implant with Carbon Collar and Plastic Cap
(with Centimetric Scale)

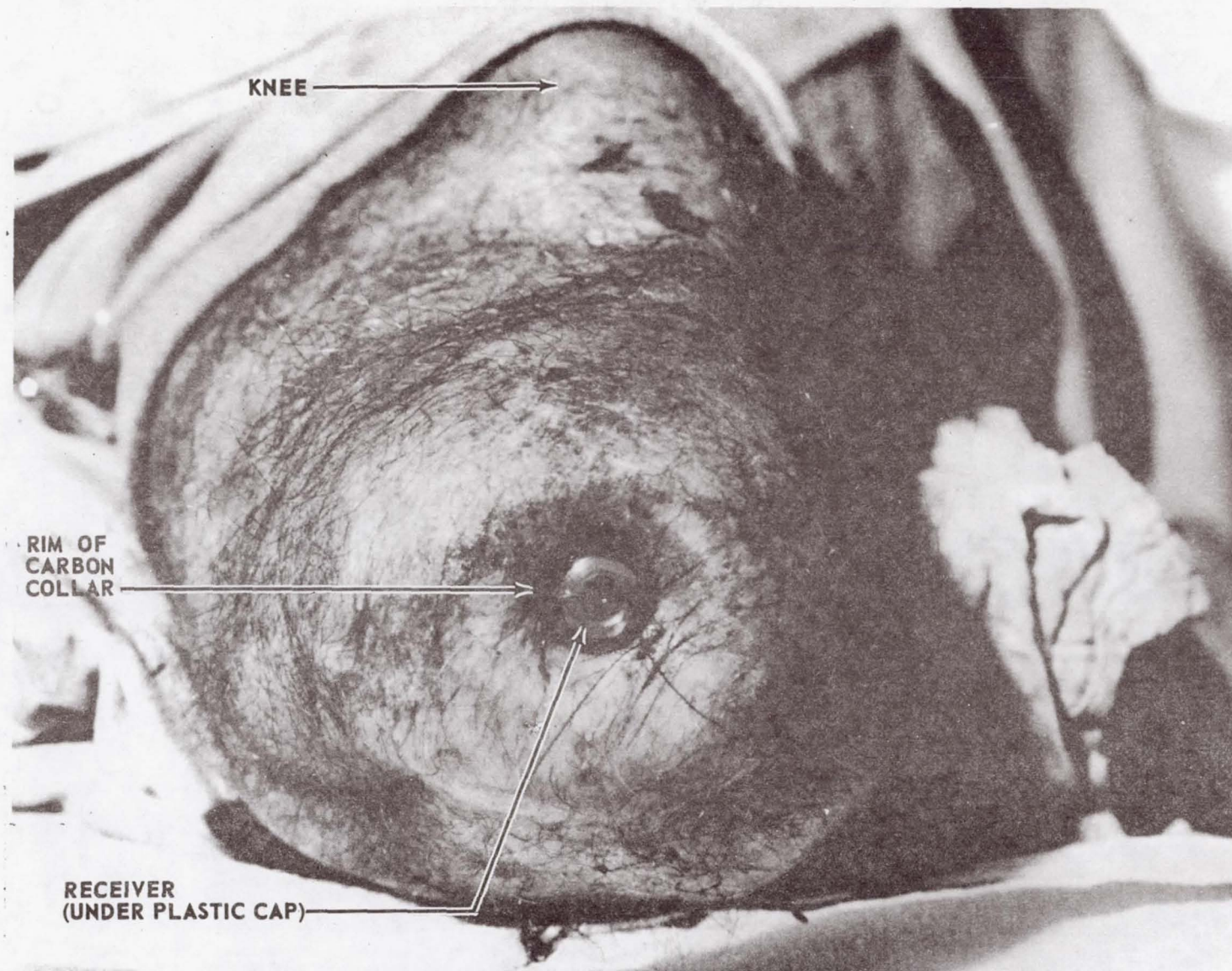
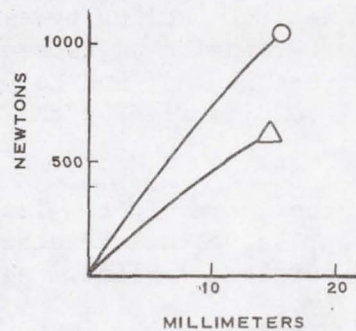
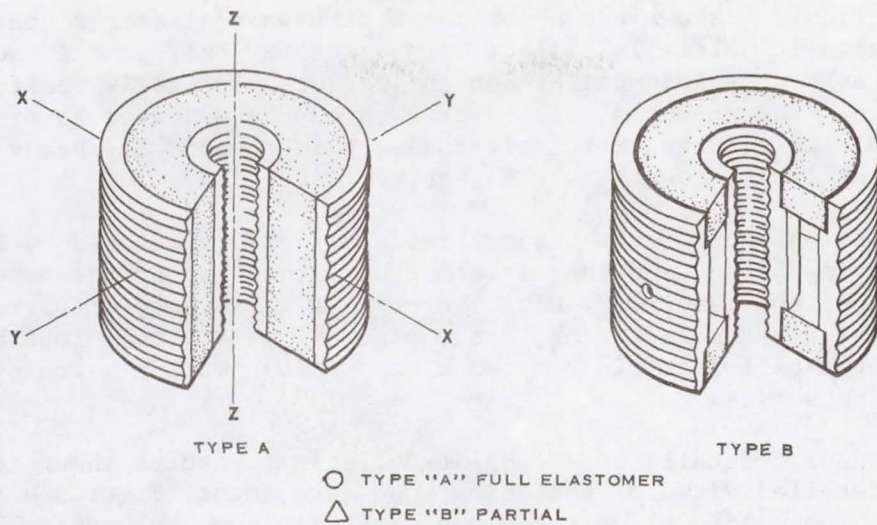
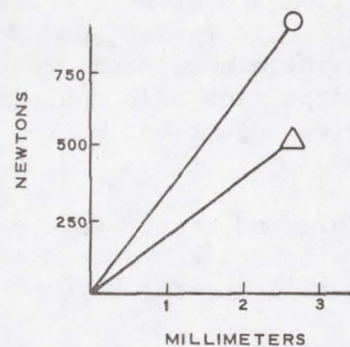


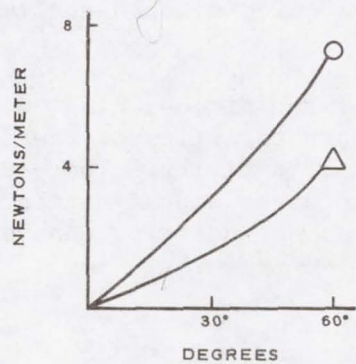
Figure 3. Leg Stump with Implant



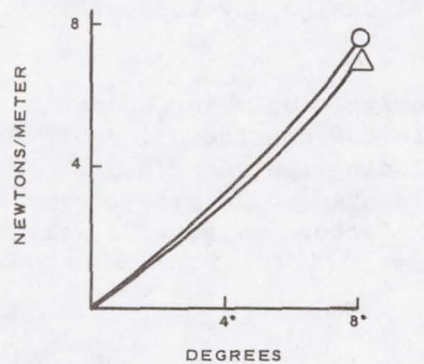
LOAD DEFLECTION (ALONG Z-Z AXIS)



LOAD DEFLECTION (ALONG X-X AND Y-Y AXES)



ROTATION (ABOUT Z-Z AXIS)



ROTATION (ABOUT X-X AND Y-Y AXES)

Figure 4. Shock Mount Design Characteristics

View A of Figure 4 shows the shock mount with full elastomer content while View B shows it partially filled, with elastomer only at the ends. The accompanying graphs give load-deflection and torque characteristics for both conditions shown. The amount of elastomer used may be adjusted to produce design variations as required for individual applications. For heavy, active individuals, even larger mounts may be required.

Metal and nylon parts for the shock isolator were fabricated by the Development Testing Branch and the elastomer was processed by the Materials Testing Branch of the Laboratory Division of NASA's KSC Support Operations Directorate. Avibank Manufacturing, Inc., contributed the ball-lock head design. Figure 5 shows the ball-lock pin and shock mount along with a matching receiver and mounting accessories.

Remaining design details were completed with the results shown in the pictorial and detailed views of the below-knee attachment (Figures 6 and 7 respectively). The molded plastic stump socket, designed by hospital staff members and made from a cast of the actual stump, assures custom-fitting and maximum support. It is designed to impart natural feeling by assisting the wearer in sensing minute pressure variations. Tension adjustments on the KSC-engineered portion also contribute toward this end, and to patient comfort, by allowing adjustment of the ratio of load carried by the socket and the connection.

Overall comfort and safety were carefully considered in the design to achieve an integration of components with a progressive failure scheme providing maximum protection to the amputee and the surgical implant.

The yoke-shaped support column of the prosthesis is one of the design variables. Most leg prostheses would require this feature for structural strength, whereas artificial arms hopefully would derive most of their strength from the structural properties of the prosthesis proper. In general, however, the conceptual design developed for the initial quick-disconnect limb would be usable.

Exact design, including cosmetic treatment and dimensioning, would necessarily follow consideration of various characteristics of the individual amputee, including age, sex, build, and degree of activity. The modularity of the basic design would provide for ease of changes and adjustments necessitated by such factors as growth, weight changes, and activity changes in the individual user. Figure 8 shows an attached prosthesis.

CONCLUDING REMARKS

It is the writer's privilege to report completion of the first phase of the quick-disconnect prosthetic design project with the shipment of the leg mechanism in late June, 1974. While it is still too early to assess the impact of this development on the prosthetic state of the art, the hope is great and the hospital reports are enthusiastic. The designers would like to feel that their work, with a major boost from the technology development to help man walk on the moon, is destined to help many more walk, and perform, on earth.

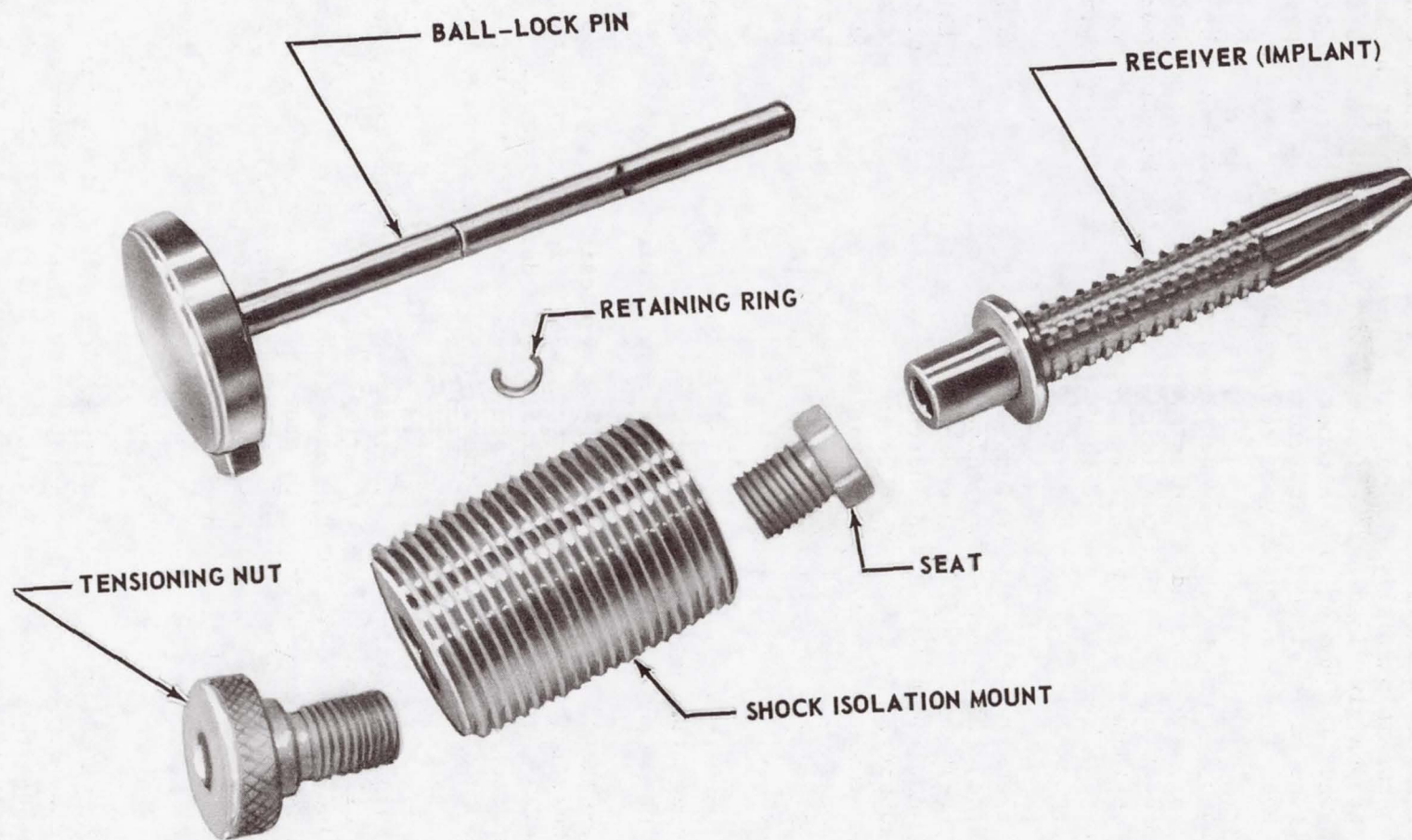


Figure 5. Prosthetic Connector and Shock Mount Components

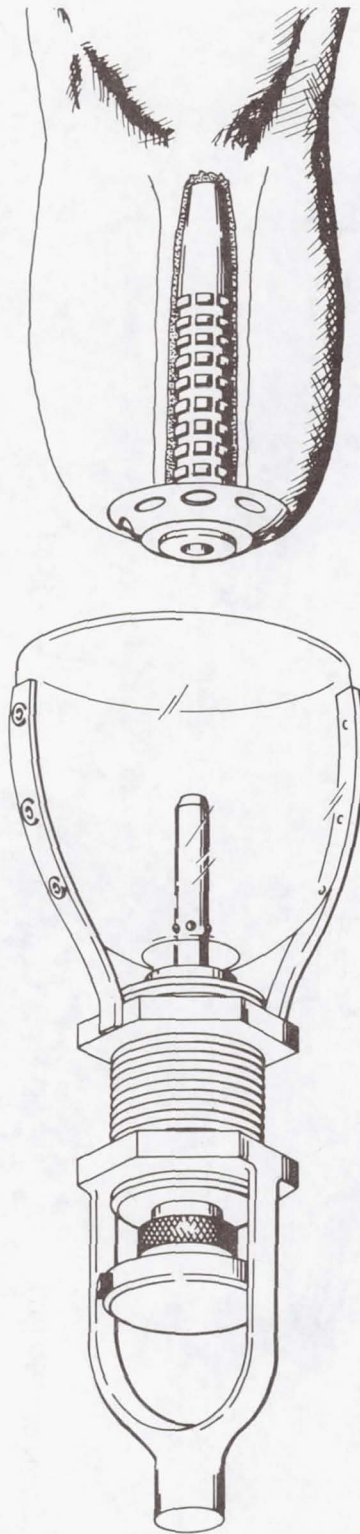


Figure 6. Below the Knee Prosthetic Attachment (Pictorial View)

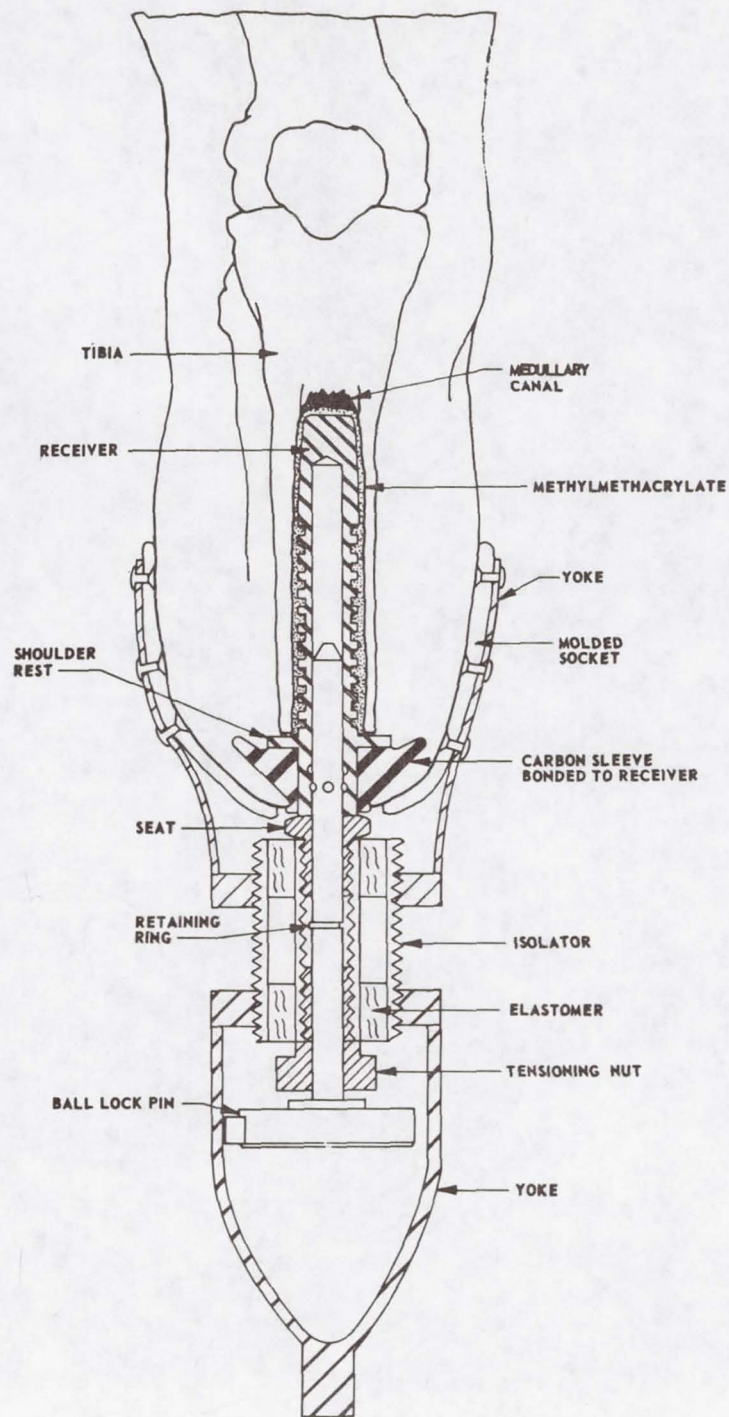


Figure 7. Below the Knee Prosthetic Attachment (Detail View)



Figure 8. First User

CREDITS

The success of the design effort must be credited to the efforts and contributions of several individuals, including Drs. Hartmann and Mooney, already mentioned. Others who contributed significantly were Dr. Michael Raklewicz, who performed the first KSC implant, and Dr. James Reswick, Director of the Rehabilitation Engineering Center, both of Rancho Los Amigos Hospital; John Duran, Avibank Manufacturing, Inc.; Jack Bokros, Ph.D., Medical Device Division, Gulf General Atomic Corporation; James Harrell, Miles Hollingsworth, Charles Bright, Frank Markley, William Jones, Glenn Roberts, and Otto Fedor, all of Kennedy Space Center; members of the Logistics Section of the KSC Systems Engineering Division; and Walter Parsons and Donald Buchanan of KSC Design Engineering management. Thanks must also go to Larry McGrath of Planning Research Corporation for assistance in preparing this paper.

21. A UNIQUE CHALLENGE: EMERGENCY EGRESS

AND LIFE SUPPORT EQUIPMENT AT KSC

By Henry M. Waddell, Jr.

Rockwell International

In early 1968, there were some unusual problems related to emergency egress and rescue of Apollo astronauts from atop the Saturn V rocket on the launch pad. The huge quantities of hazardous propellants in the launch vehicle and spacecraft required that all ground personnel be cleared from the launch danger area; yet the fastest possible action would be required should rescue become necessary. This had been dramatically demonstrated by the January 1967 fire, which took the lives of three astronauts. As a result of the investigation following the fire, new materials were developed, flight hardware was modified, and test procedures were rewritten--establishing the framework within which a more effective rescue concept was to be developed. The target date for implementing the new rescue operation, including equipment changes and the training of personnel, was October 1968, when Apollo 7 was scheduled to lift off.

FACTORS AFFECTING RESCUE

Distances, heights, and the limited space within which ground personnel have to work were critical factors to launch-pad rescue. Figure 1, which shows Saturn V on the launch pad with the White Room and Mobile Launcher swing arms in place, illustrates how high above the ground the command module sat at launch. This was the way things were when the six-man closeout crew placed the astronauts in their couches and closed out the command module for lift-off. The White Room, about 109.7 meters (360 feet) above the ground, required some 2.5 minutes to reach from the base of the launcher.

Figure 2 is a ground plan of the KSC launch pads. The closeout crew left this area, at Roadblock 5A, about the time the cryogenic oxygen and hydrogen propellant loading of the launch vehicle was completed. From here, the closeout crew went up to prepare the command module for the astronauts, who arrived approximately an hour later. During this time and throughout the launch, a special KSC Fire Department rescue team was stationed about 610 meters (2000 feet) from the launch pad. It normally took this crew about 2.5 minutes to go from its station to the base of the launcher. This time plus the time required for the crew to ascend the umbilical tower to the command module level totaled five minutes. Actually, this time had been bettered, but under ideal drill conditions and after much practice. This five-minute response was a crucial factor because the human brain has little chance of surviving without damage after four minutes with no oxygen.

So time and space became the principal factors in developing the new rescue operation. It would be necessary to reach an incapacitated astronaut quickly with equipment small enough to function in the limited space of the White Room

and command module, and the first thing that would have to be done would be to get oxygen into his lungs to replace the toxic fumes or smoke that he had inhaled.

Figure 3 shows the full-scale training mockup of the command module and White Room. The White Room, with launch support equipment installed, is about one half the size of a 2.7- by 3.6-meter (9- by 12-foot) room. The command module, with a 0.67- by 0.79-meter (26- by 31-inch) opening and suited crew in place is shown in Figure 4. From the beginning of launch operations, the size of this hatch had been the most severely limiting space factor in crew rescue. It created a problem because a rescuer had to be equipped with an independent air supply to prevent his being overcome by an atmosphere that would disable an astronaut. As can be seen in Figure 5, which illustrates a typical rescue exercise conducted by the Space Division contingency crew, it would have been very difficult for a man to enter the command module wearing an air pack. In fact, at the time the new rescue procedures were being developed, a self-contained air pack as described was not available at KSC for a rescue man to wear when entering the command module.

TESTING THE CONCEPT

The first test rescue was conducted in March 1968. There were two major test requirements: fast reaction time in getting an oxygen resuscitator on an incapacitated astronaut and ability of a rescuer to enter the command module without being overcome.

After two astronauts and a NASA life support engineer, all wearing bulky space suits, entered the command module mockup, the hatch was closed. Three standard 15.9-kilogram (35-pound) oxygen resuscitator units were hung on the mockup access arm, and the oral-nasal masks were connected to hoses long enough to reach into the command module. At the GO signal, six firemen entered the White Room. Each was outfitted in full rig with 0.44-kilogram (14-ounce) felt turnout coat and wore a low-profile rebreather chest pack. Each carried a 3-meter (10-foot) breathing air hose, which could be plugged into an air manifold on the White Room ceiling. Three carried the resuscitator oral-nasal masks, which were equipped with rubber straps that could be attached to the "incapacitated" astronauts.

The test rescue plan was as follows: Once the hatch was opened, a fireman was to enter the command module, remove the plastic helmet from each of the astronauts, and apply the resuscitator oral-nasal masks. The astronauts were not to be removed from the command module. As it turned out, the rescue left much to be desired. It took over four minutes to apply the first resuscitator and nearly eight minutes to put on the last one.

THE SEARCH FOR BETTER EQUIPMENT

Clearly, better life support equipment was necessary. Over the next several days, every life support-related trade magazine was searched and many telephone calls were made to life support equipment companies and military installations. A miniature resuscitator, made for military field use, was finally located. Because it was small, it mixed a quantity of ambient air with the oxygen in the supply bottle to extend its period of operation to 30 minutes. Its size was attractive, but the mixing would not do; during a fire, the ambient air in the command module may be toxic. However, the unit did use some oxygen, the necessary ingredient and the miniature size was required.

The resuscitator company was asked if it could eliminate the air mixing and use pure oxygen without shortening the operating time by more than half. It was felt that if oxygen could be given quickly to the astronauts to stabilize their breathing, the chance of rescuing them would be greatly increased. A 15-minute resuscitator operation was sufficient for either removing the astronauts to safety or for obtaining another oxygen supply. The resuscitator company was very cooperative; it modified the unit and sent one to KSC.

Meanwhile, a way was developed by which the time required to get help to a disabled astronaut could be shortened. Since the closeout crew was with the astronauts until about 55 minutes before launch, time would be saved if they were trained to handle most incapacitating contingencies that occurred during closeout. The Fire Rescue Team would stand by at its usual place to respond if the situation got out of hand and could be responsible for its normal role after the closeout crew departed.

While this procedure was excellent for saving time, it had its drawbacks. Rather strict cleanliness standards were required for the command module interior and White Room. While these requirements would not apply in an emergency, the dirty residue from standard flame-retardant-treated coveralls could not be tolerated for normal closeout operations. On the other hand, the use of highly flammable Dacron clean room clothing used by past closeout crews had to be discontinued. The TV coverage of White Room activities also presented a problem. Emergency rescue or fire-fighting equipment had never been shown during astronaut insertion operations. Whatever was found to protect the closeout crew from fire or other hazards had to be clean and look normal or be stowed out of sight.

THE SEARCH FOR BETTER MATERIALS

Thus began another search, a tough one that continued into the early summer. No progress was made except to consider ordering the same cotton poplin coveralls fire jumpers wear. In an issue of Safety News magazine was an article on the results that Longhorn Arsenal, in Texas, had obtained in testing Nomex, a new, clean, fire-retardant material made by Du Pont. Coincidentally, the KSC Fire and Rescue Service was testing a new aluminized Nomex proximity fire suit.

The individual in charge of developing Nomex for industrial use had achieved some success in outfitting race car drivers with flame-retardant coveralls, so he did not require much explanation to understand the rescue problem at KSC. His advice and help were sought, and the next day at 10 a.m. investigators at KSC concerned with astronaut rescue were looking at his samples and reviewing material test data. By 3 p.m., a garment had been designed and a supplier contacted.

The resultant closeout-crew coveralls are shown in Figure 6. Actually, the suit was a protective clothing system. The elements were a miner's bump cap, race driver's gloves, heavy shoes, and inherently flame-retardant coveralls with Velcro closure and a protective hood that folds into a quick-opening pouch on the back of the coveralls.

The suit looked good, and the fabric tested better than was anticipated. However, one problem had to be corrected before the suit could be used. Like all nylon garments, the coveralls could build up sufficient static electricity to discharge a spark. In the oxygen-rich atmosphere surrounding closeout operations, a spark could have a catastrophic effect. The Nomex developer was aware of this problem and provided a wetting agent. By allowing the coveralls to soak in a washing machine filled with water and the agent, the fibers were coated with a thin film of hygroscopic material that ensured a conductive surface to dissipate static electricity before it built up.

MORE PROBLEMS

Two problems had been resolved, but two others remained. No one had found a low-profile breathing unit small enough to be worn by a rescuer through the command module hatch opening nor had they found an efficient way to apply the rubber straps of the resuscitator mask while the astronauts were in their couches.

Only the resuscitators used on incapacitated personnel supplied pure breathing oxygen. In the interest of safety, rescuers breathe air. Thus the literature and telephone search was continued for a small, reliable self-contained air pack. In late summer, a small unit that appeared promising was located. Three were ordered for test and support of the Apollo 7 launch, and they arrived in time to be submitted to Bendix, the life support equipment contractor, for servicing and cleaning. Unfortunately, the unit not only was too dirty to service but did not meet the flow rates and time specifications claimed by the manufacturer. It was made to work, however, in time to support the launch.

The inadequacy of this unit focused attention on a problem that had been overlooked, one with possible serious consequences. The desire to obtain miniature, long-duration breathing equipment had caused the investigators to proceed in many directions attempting to combine the best features of several manufacturers' equipment. The Fire and Rescue Service was virtually building its

own equipment. At KSC, fortunately, a single function was responsible for servicing, testing, and certifying all life support equipment. As the different combinations of masks, regulators, tanks, hoses, and valves began to arrive for servicing, the life support technicians became increasingly concerned that the combinations might not be interchangeable. Enough workable equipment was put together to support the Apollo launch but it still needed improvement. As it turned out, the search for good rescue breathing equipment that satisfied the varied requirements of the several astronaut rescue configurations was to last a number of years.

Meanwhile, the miniresuscitator was being tested by the astronaut flight surgeon at KSC and by the life support contractor. The unit worked fairly well except for two difficulties: (1) the standard rubber-strap arrangement was still time consuming and (2) the seal around the oral-nasal mask was inflatable.

The latter became evident when the unit's compatibility with the altitude chamber was tested. One of the requirements in checking out an Apollo spacecraft was to run it through manned simulated missions in the steel vacuum chamber. Here the systems that had to operate in the vacuum of space were tested by the astronauts who would man them. The chamber simulates an environment of about 60.8 kilometers (20×10^5 feet) and, since this was a hazardous test, emergency egress requirements had to be met. Significant to the mask seal design was that rescue was programmed to occur at a simulated altitude of 7.57 kilometers (2.5×10^4 feet). Ingress and egress were made through an airlock. The problem with the inflatable rubber seal was that it changed size and shape when subjected to outside pressure changes. A seal inflated to fit an astronaut at 7.57 kilometers (2.5×10^4 feet), which is 37.9 newtons/meter² (5.5 pounds/inch²), would have been a poor seal at sea level.

This problem was solved when, on a trip to the home plant in Downey, California, one of the investigators was shown some of the life support equipment trailers that the Space Division physiologist had set up to support altitude chamber operations. The system included a large trailer with five or six seats at which breathing oxygen was available through a sweep-on head harness. (This arrangement is used by commercial airline pilots in the event of inadvertent cabin depressurization. In the airline operation, oxygen under light pressure is supplied through the mask.) The harness was of sturdy, nonflammable plastic that held the breathing mask tight against a person's face. The question was, would it also hold a resuscitator unit against a person's face while the mechanism force-breathed him? It was obvious that the sweep-on feature could be applied much faster than could the rubber-strap configuration.

The harness was quickly modified so that the miniresuscitator head could be securely attached (Figure 7). In forced breathing or resuscitation, there is a significant difference between the inflation resistance of the lungs of a conscious person and that of an unconscious one. Since it was impossible to get a volunteer to be an unconscious test subject, the investigators called on the expertise of the KSC physiologist, who simulated an unconscious victim as closely as possible. The astronaut flight surgeon and the physiologist tested the rig and it worked.

So a miniature, quick-don resuscitator was available for the Apollo 7 launch. This little unit supplied oxygen for 15 minutes at both sea level and 7.57 kilometers (2.5×10^4 feet); weighed 3.63 kilograms (8 pounds) (compared with 15.9 kilograms (35 pounds) for the usual unit); could be securely installed on an incapacitated person in less than 15 seconds (compared with several minutes for the standard oral-nasal mask); and its face seal was self-venting at any altitude. These attributes met the needs of the new rescue procedure, but another problem was to arise (described later) that set off a new cycle of investigation.

DEVELOPING THE BREATHING UNIT

Developing a lightweight, low-profile rescue breathing unit was a concerted effort by a team of NASA and Space Division personnel. Each team member was responsible for peculiar requirements in his own phase of the rescue operations, and all had made several false starts on inadequate or incompatible units. The missing link was a set of requirements and specifications that encompassed all needs and used available hardware of proven compatibility. A task team was set up to develop these requirements and specifications. Users, designers, testers, procurement specialists, and medical personnel combined their ideas in an effort to produce the best unit. The Surviv-Air Company, a division of U.S. Divers, presented the best combination of hardware that met the requirements.

There were two designs of a lightweight, low-profile mobile rescue apparatus that provided a 15-minute air supply and a self-contained, two-way communications assembly. One, called Astronaut Rescue Air Pack (ARAP), was worn by the Fire and Rescue Team that stood by from the time the astronauts were placed in their couches through launch. If rescue should be necessary before launch, the team would rush up the umbilical tower to the command module and pull the astronauts to safety. Figure 8 shows a fire rescue man in ARAP, which he put on before entering the hazardous area.

The second unit, called Emergency Egress Air Pack (EEAP), was placed on the command module level, and could be quickly donned by the closeout crew in the event that a fire or a toxic propellant leak suddenly made the atmosphere in the White Room unbreathable. The astronauts could also use the EEAP as a breathing unit if they had to leave the command module in an emergency without assistance from the Fire and Rescue Team or the closeout crew. They would remove their protective plastic helmets before putting on the unit. Figure 9 shows a closeout crewman in protective coveralls wearing the EEAP.

Both the ARAP and the EEAP units used had a quick-don Wilson Tite-Seal mask to which 7.9 cubic centimeters (2.8 cubic feet) per minute of air was supplied at null pressure of 0 millimeter of water. To exclude toxic vapors, the face mask incorporated an exhalation valve with a cracking pressure of 58.42 ± 7.62 millimeters (2.3 ± 0.3 inches) of water, thus maintaining a positive gage pressure at all times. A low-profile alarm whistle warned the operator when the pressure in the cylinders indicated the breathing air remaining was

down to about two minutes. This allowed time to reach a place with better air or to get another set of air cylinders. (More complete descriptions of these units, as well as recommended areas of use, are included in NASA Tech Brief 70-10680, which is available from the KSC Technology Utilization Officer.)

DEBUGGING THE RESUSCITATOR

The miniresuscitator, as previously stated, uses pure breathing oxygen. In terms of benefitting a person who is overcome from inhaling smoke or toxic fumes, pure oxygen is quite a different gas than air, which contains 20 percent oxygen. But oxygen presents a handling problem because of the ease with which certain materials ignite in its presence and because it greatly increases their burning rates. Indeed, these properties of oxygen caused an incident that complicated the investigation.

One night a life support technician was preparing a miniresuscitator for use. He stripped it, cleaned and checked the inner workings of the main regulator, reassembled it, and turned on the oxygen valve to test the unit. As he turned on the valve, a blue flame jetted from the regulator. Fortunately, no one was injured, but the investigation that followed revealed that the soft goods, the valve seats, and the regulator body were not compatible with oxygen.

In searching for a replacement regulator, it was found that no resuscitator on the market used materials compatible with oxygen. Moreover, there had been regulator fires, but injury or damage had not been of an extent that resulted in a demand for replacement of the incompatible materials with safer but more expensive materials. In addition, it was discovered that, while the U.S. Bureau of Mines closely checked portable breathing equipment, no federal agency regulated the safety of high-pressure oxygen resuscitators. The construction, flow rates, and cycling times were left to the manufacturer. This situation put KSC into the business of manufacturing oxygen equipment long enough to make the needed number of safe units. The Bureau of Mines and the National Institute of Occupational Safety and Health are trying to solve the problem, but it is a slow process.

The compact miniresuscitator now being used at KSC is shown in Figure 10. It is operated by turning one valve, which starts the process of automatically inflating and deflating a victim's lungs if he cannot breathe, thus supplying life-giving oxygen. A clear plastic window in the top of the oral-nasal mask permits the operator to observe whether the patient has spit up anything that might block his breathing. (A more complete description of the miniresuscitator is included in NASA Tech Brief 69-10319, which may be obtained from the KSC Technology Utilization Officer.)

Fortunately, there has been no reason to use the resuscitator, the rescue equipment, the procedures, or the training developed since the Apollo fire. This has not diminished their value, however. The concerted NASA-Space Division efforts have not only greatly improved the probability of a successful rescue on the launch pad, but may have benefited other rescues having no connection with the space program.

SPACE SHUTTLE: A NEW CHALLENGE

Today at KSC, plans are being made for launching and landing the Space Shuttle. This vehicle, which is launched like a rocket, will ferry payloads and passengers to and from earth orbit on missions lasting from 7 to 30 days. The Shuttle Orbiter makes a controlled landing like an airplane on a runway. There the similarity to an airplane ends, however, because when it is approached for safing and servicing, it will be like no airplane ever flown. Having just entered the earth's atmosphere at orbital speed and, through a series of glide maneuvers, it will have slowed to about 346 km/hr (215 mph) and made a controlled dead-stick touchdown. It will be spewing ammonia fumes from several outlets, as well as gaseous hydrogen, nitrogen, and possibly highly toxic hydrazine and nitrogen tetroxide vapors. Parts of the Orbiter will have been heated by the friction of entry to temperatures in excess of 3632°C (2000°F). This much frictional heat may be accompanied by a large static charge on the nonconductive ceramic tile surface.

The first tasks of the ground crew, after verifying that the Orbiter is not leaking propellants, will be to attach cold Freon lines and large air ducts to commence cooling the internal voids and compartments and the underside of the Orbiter's thermal-protective skin. Many ground-servicing tasks will follow, and they raise some important questions. What protective equipment will be required? What equipment is now in inventory to satisfy these requirements? What new equipment will have to be developed? One of the most important lessons learned from Apollo was to start answering such questions early, to keep pace with the program to ensure that its requirements were understood, and to work long lead-time items as soon as they become apparent. One Shuttle need already known, for example, is a new type of glove that will protect the landing-area technician's hands from heat and burns from propellant spills, yet not impair the dexterity required to perform the demanding task of connecting the cooling lines and ducts.

There will be other special requirements for protecting personnel during various hazardous tasks throughout Shuttle launch and landing operations. A team is already at work on these requirements. When the time comes, both personnel and procedures will be ready.

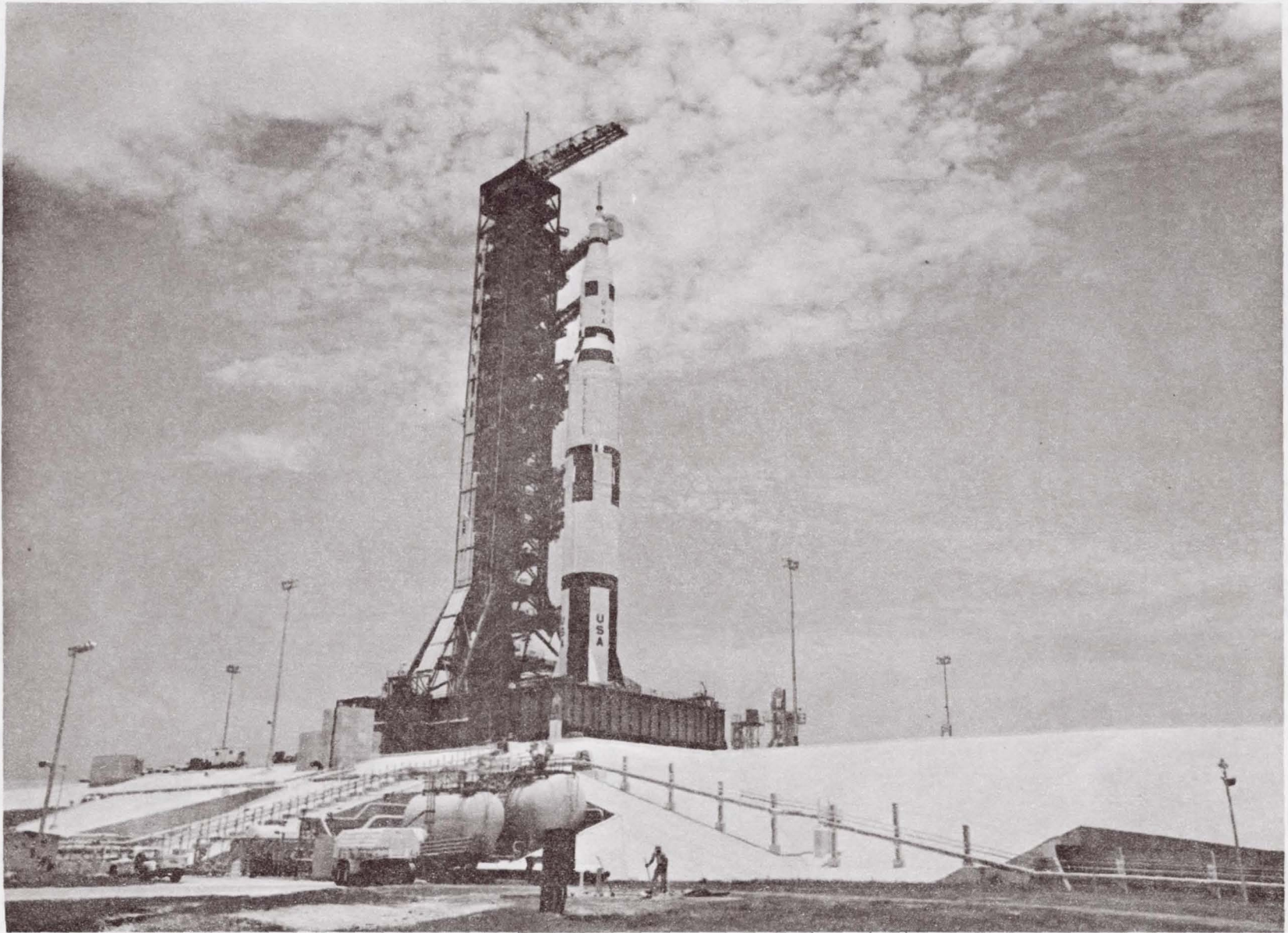


Figure 1. Apollo and Saturn V on Launch Pad

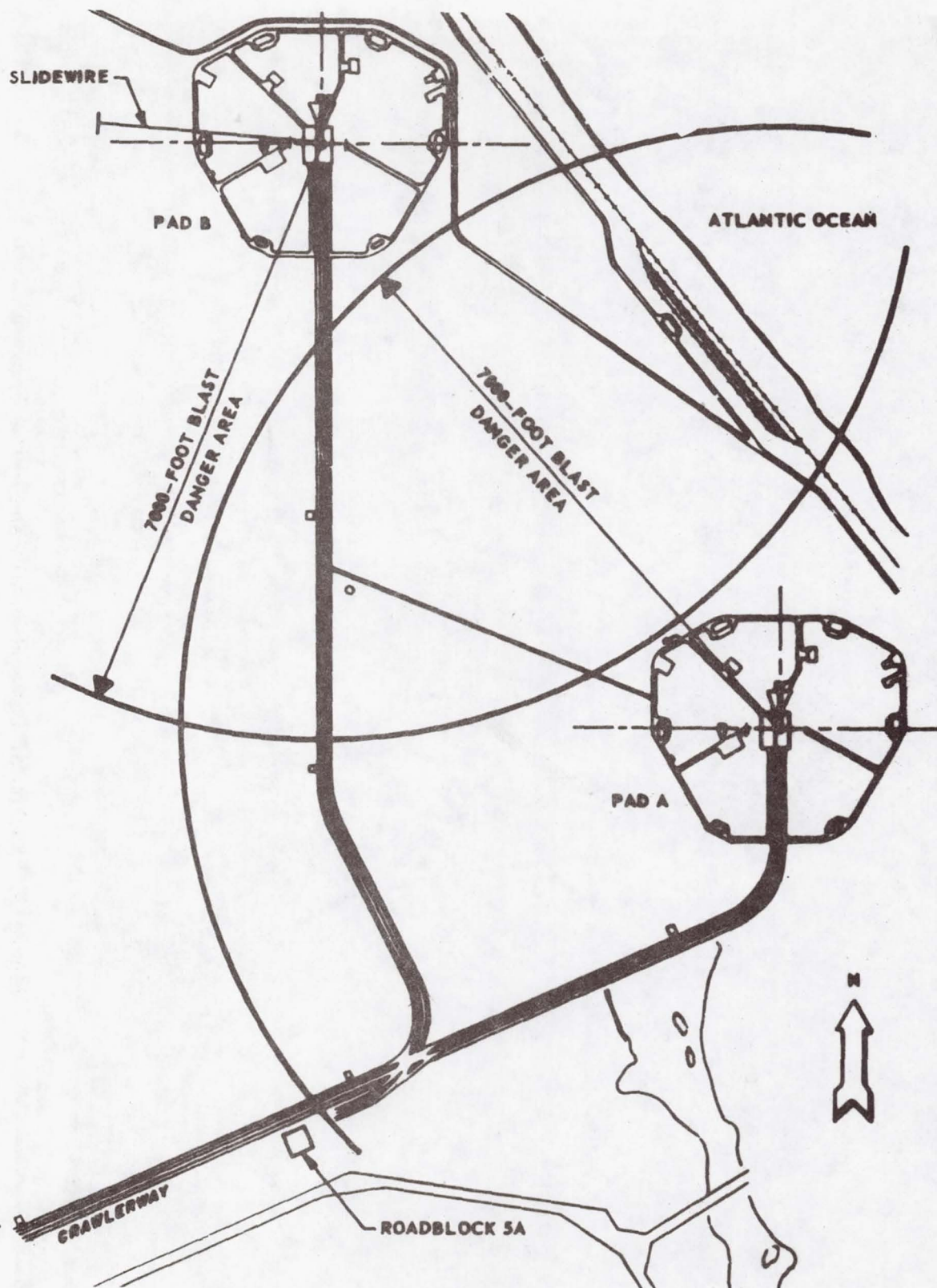


Figure 2. Launch Pad Ground Plan

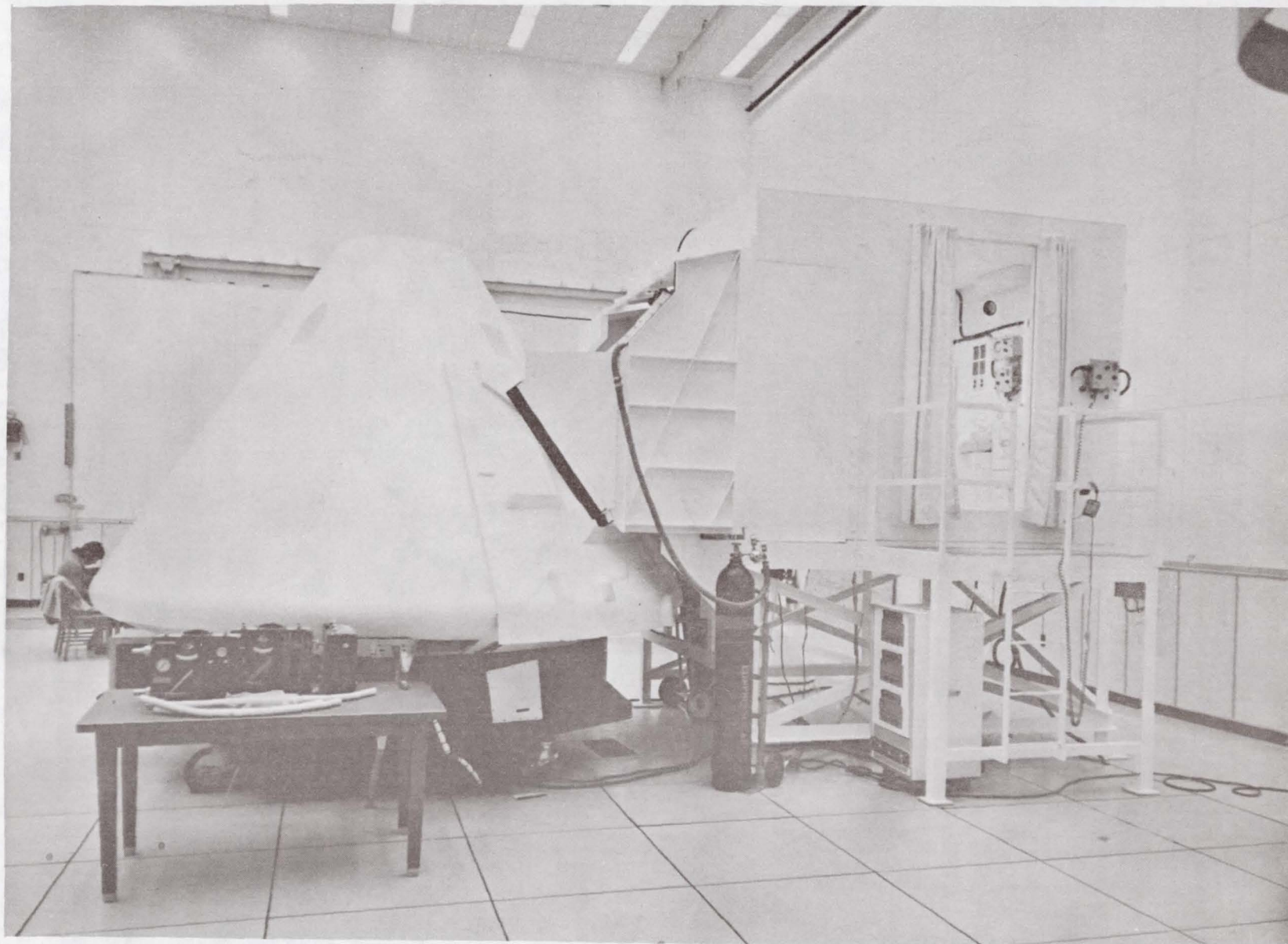


Figure 3. Mockup of Command Module and White Room

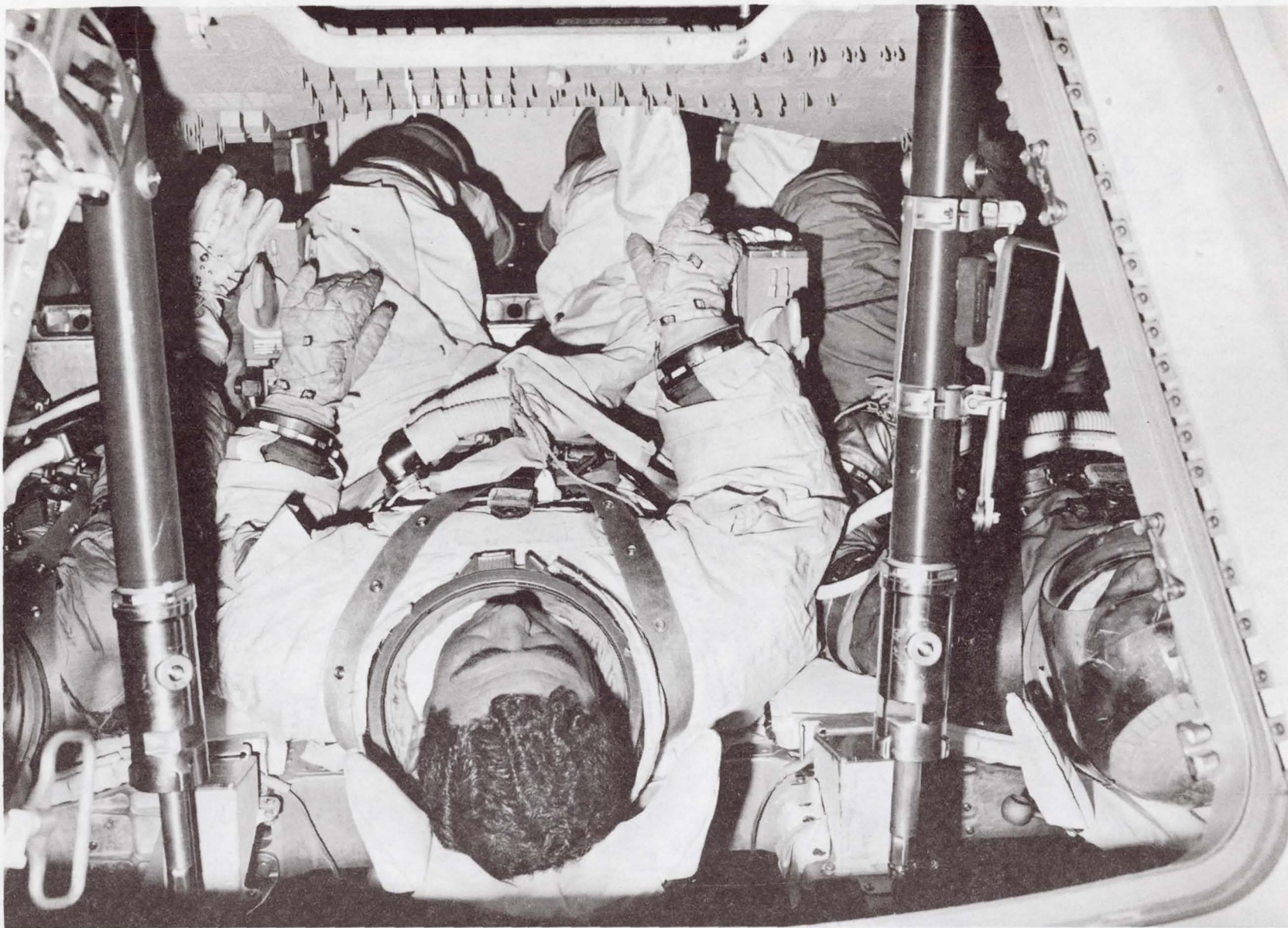


Figure 4. Command Module Entrance Hatch



Figure 5. Test Rescuers, Wearing Scott Air Packs, Pulling "Victim" From Command Module Mockup



Figure 6. Closeout Crewman Dressed in Closeout Protective Clothing System

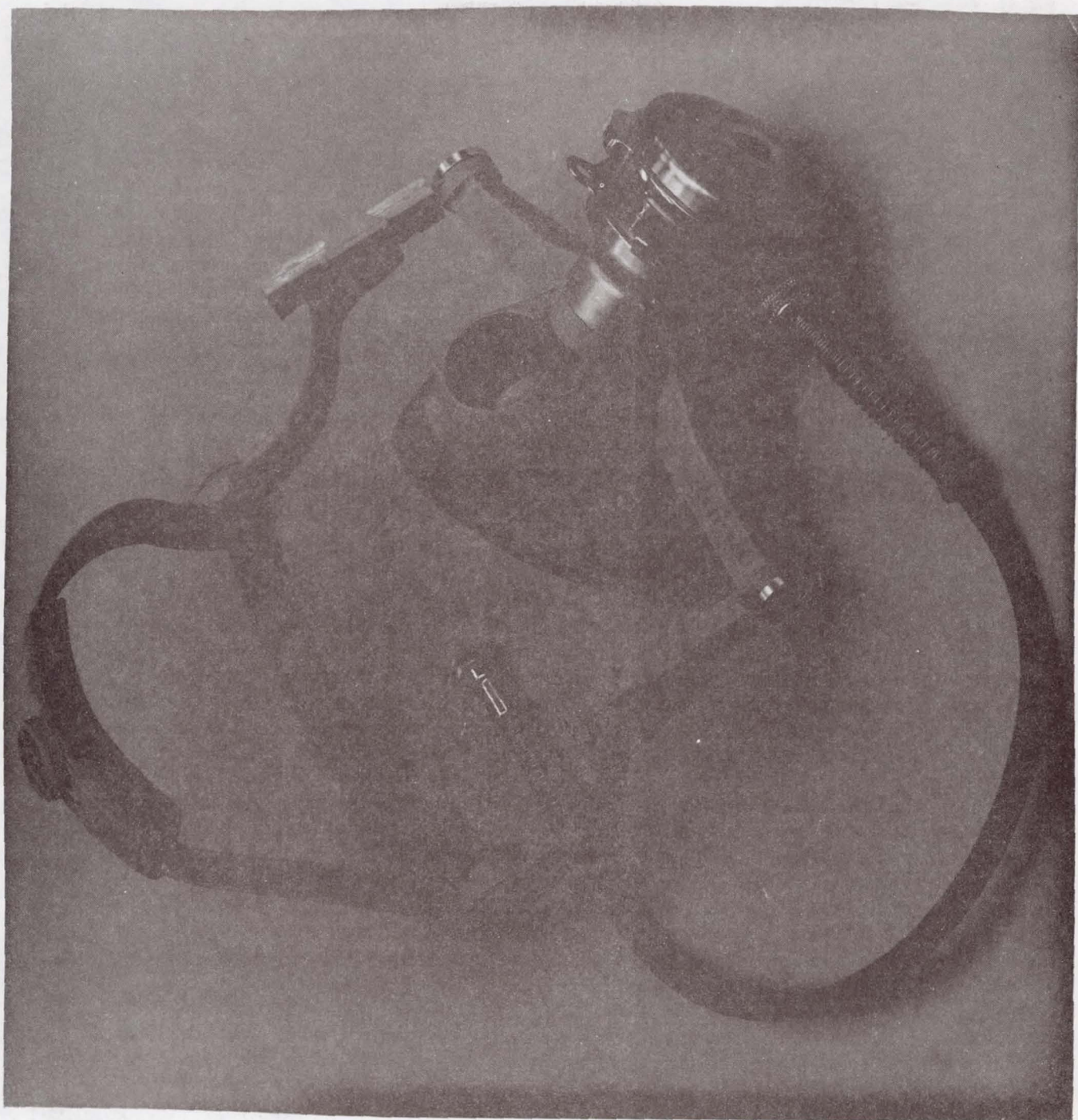


Figure 7. Puritan Sweep-On Head Harness With Resuscitator Head Attached



Figure 8. KSC Fire Rescue Technician Dressed in Aluminized Nomex Proximity Protective Clothing and Wearing ARAP



Figure 9. KSC Closeout Technician Dressed in Nomex Protective Coveralls and Wearing EEAP

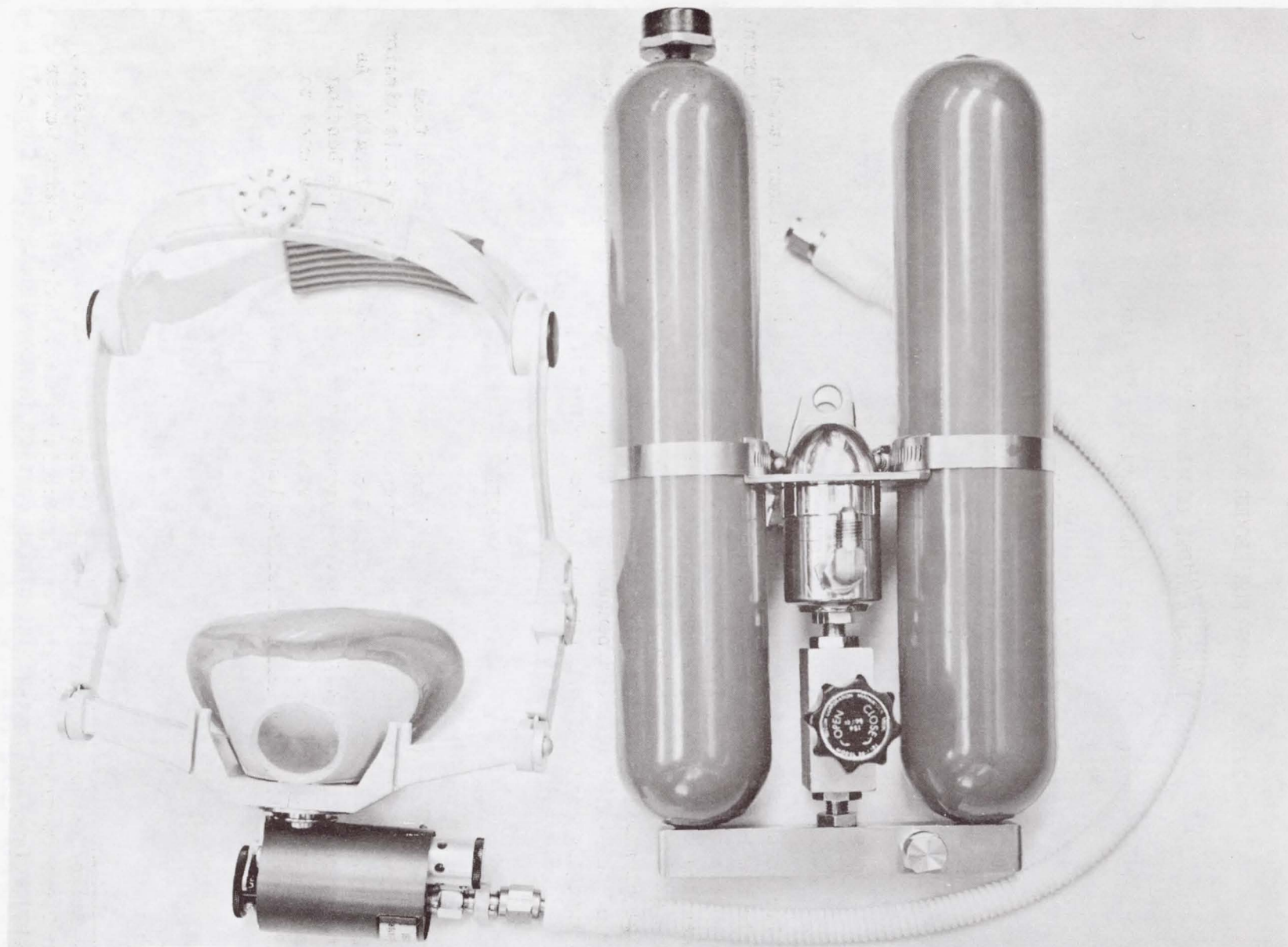


Figure 10. KSC Miniresuscitator

22. A DAMPER FOR GROUND WIND-INDUCED

LAUNCH VEHICLE OSCILLATIONS

By John G. Bodle and David S. Hackley

GENERAL DYNAMICS CORPORATION

Convair Aerospace Division

San Diego operation

SUMMARY

Prelaunch oscillatory bending deflections of the Atlas/Centaur launch vehicle are restrained by a damper mechanism mounted on the end of a horizontal boom supported from the umbilical tower. A single vertical pin on the vehicle engages the mechanism. The damper is connected to the vehicle until liftoff. As the attach pin rises with the vehicle, a retractable arm mechanism provides initial clearance. An explosive release mechanism allows the boom to swing clear of the vehicle like a pendulum. A snubber mechanism decelerates the free swinging boom and damper mechanism to a safe stop.

INTRODUCTION

The Atlas/Centaur* launch vehicle shown in figure 1 has evolved from initial development as booster for "Surveyor" to present day versatile mission capability. This evolution has produced a 5.5 meter increase in length. As length increased, potential for severe ground wind induced vehicle bending loads became acute. Restrictive ground wind velocity limits threatened to reduce availability for small effective launch windows.

* The Atlas/Centaur is built by General Dynamics Convair Aerospace Division, San Diego operation. Program management is by NASA Lewis Research Center (LeRC), Cleveland, Ohio.

Ground wind aerodynamic forces on the Atlas/Centaur launch vehicle produce bending deflections. The phenomenon of vortex shedding creates oscillatory deflections which reach maximum amplitude within a plane normal to the wind direction. The allowable bending moment limit for the vehicle may be reached at 50% lower wind speed when oscillatory deflections are combined with the steady state deflections. Addition of a damper to reduce oscillatory deflection thus became a prime objective.

In 1972, under the direction of NASA LeRC, General Dynamics Convair Aerospace (GDCA) developed a system concept for an oscillation damper for Atlas/Centaur. In April 1973, NASA LeRC directed GDCA to implement the oscillation damper system at Cape Kennedy, Launch Complexes 36A and 36B to provide for the October 1973 launch window of Mariner 10.

The system was to be designed to remain in place until vehicle liftoff. Adequate clearance was to be provided during vehicle liftoff to preclude the addition of restrictions on vehicle drift. The retraction system was to be redundant. Extension and engagement with the vehicle was to be performed manually only. The damper was required to permit unrestricted operation for actual ground wind speed up to 33.6 knots for all tanking conditions with the Atlas fuel tank full.

The two basic system functions are described. First, the damper system, which performs the required damping until liftoff. Second, the retraction system which retracts the damper mechanism and support boom at liftoff.

DAMPER SYSTEM DESCRIPTION

The installed damper system is shown in figure 2. The two main elements of the system are the damper mechanism and the support boom with its counterweight. The system is installed on the umbilical tower below the level of the Centaur stage umbilical booms. The damper mechanism is connected to the vehicle by a single attach pin near the lower end of the interstage adapter. This is not the most advantageous point for applying the damping force, but was dictated by the limited height of the Complex 36A umbilical tower. Attachment near the forward end of the vehicle would have provided a longer moment arm for the applied damping force for more efficient damping.

The damper mechanism, shown in figure 3, is a linkage differential mechanism, formed by three equidistant parallel sliding bars pinned to a cross bar. The center bar is a linear ball bearing guided splined shaft. The spline prevents rotation of the mechanism about the centerline of the shaft. The ball bearings are essential to minimize friction forces. The two outboard sliding bars are the piston shafts of balanced double acting hydraulic

dashpots. The dashpots have the same damping coefficient in both directions of travel. The cross bar, referred to as the cross head, and the retractable arms form a rigid bellcrank when the vehicle attach pin is fully engaged. The vehicle attach pin and the dashpot rod end bearing centers are located an equal distance from the pivot pin in the splined shaft. The error due to dashpot angular motion is negligible for the small amplitude oscillatory travel of the attach pin (5.77 cm, zero to peak maximum).

The damper mechanism is mounted on the end of a rigid support boom. The boom is hinged at the base to swing vertically. A cable is connected at one end near the end of the boom, routed through a pulley elevated on the umbilical tower, and connected at the opposite end to a counterweight. This counterweight not only supports the weight of the horizontal boom, but maintains an upload on the end of the boom to keep the damper mechanism fully engaged with the vehicle attach pin until liftoff.

DAMPER SYSTEM DESIGN

Damping Coefficient

The Atlas/Centaur launch vehicle deflects like a cantilever beam from drag and lift loads induced by ground wind. This deflection includes a steady state (static) component and an oscillatory component as illustrated in figure 5. The oscillatory component is not linear due to the individual components of lift and drag. When added vectorially, the total resultant deflection must not exceed the limits allowed by the strength of the vehicle and launcher. The relative characteristics of ground wind loads are shown in figure 6. The damper has no effect on static deflections. The oscillatory deflections, which create the most severe wind velocity constraints, are significantly reduced with a damper.

The damper was required to increase the modal damping factor of the vehicle from an average value of 0.03 to 0.43 for the most critical case where only the Atlas fuel tank is filled. A viscous damping coefficient range of 840.6 to 1,260.9 N/cm/s was computed for the damper. A design load of 8900 N maximum was established for the vehicle attach pin and the local structure of the interstage adapter wall. This required the damper to be force limited as a precaution against structural damage in the event the wind loading exceeded the maximum design requirement. The damping coefficient and force limit for each dashpot in the mechanism is half the total required. The resulting damping characteristic envelope for the dashpots is shown in figure 10.

The computed viscous damping coefficient for the damper mechanism was derived assuming an infinitely stiff umbilical tower. A simple test of the overall system was performed at Complex 36B. The vehicle was manually deflected, then suddenly released. The decaying oscillatory response was then recorded. This test indicated the umbilical tower was less rigid than anticipated. The derived viscous damping coefficient was, however, found to be satisfactory.

Damping Force and Direction

Vehicle oscillation in any direction is damped by an opposing force at the attach pin proportional to pin velocity. The constant of the proportionality is the viscous damping coefficient. When the attach pin moves there is, in most cases, a component of force normal to the direction of travel as shown in figure 4. The magnitude of the normal force component is a function of the following factors:

- 1) Difference in damping coefficient between the two dashpots due to tolerances on the specified damping coefficient.
- 2) Bearing friction on the splined shaft.
- 3) Inertia loads of the mass and mass moment of inertia of the cross head and arms assembly and the mass of the piston rods and splined shaft.
- 4) Initial offset of the neutral position of the attach pin from the splined shaft centerline caused by vehicle misalignment, umbilical tower deflections and steady state wind deflections of the vehicle.

Examples of computed damper mechanism force dispersions are shown in figures 8 and 9. A linear sinusoidal displacement of the attach pin is applied in directions between $\beta = 0$ and $\beta = \frac{\pi}{2}$ rad. A typical difference in dashpot damping coefficients in both the linear and load limiting range was used. Friction, dashpot hysteresis and force deadband due to bearing clearances are neglected. Forced oscillation tests of the damper mechanism proved these effects to be minor. The mechanism is assumed to be rigidly supported.

In figure 8, both dashpots are operating in the proportional range. The maximum normal force is 8.5% of the corresponding collinear force for a 5.08 cm initial offset in the worst direction. This is 6.2% greater than for zero off-

set. The variation in collinear force with direction of travel is primarily caused by the difference in damping coefficient between the dashpots. With the travel at $\beta = \frac{\pi}{4}$ rad, only one dashpot is working. In this particular case, it is the one with the greater damping coefficient. Thus, the collinear force is greatest when $\beta = \frac{\pi}{4}$ rad.

Figure 9 shows the force dispersions in the force limiting range of operation at maximum design velocity for two directions of travel. The normal forces for the directions shown are less than 9% of the collinear force. For intermediate directions of travel, e.g., $\beta = \frac{\pi}{3}$ and $\frac{\pi}{6}$ rad, normal forces of nearly 43% of the collinear force occur due to the unbalancing action of one damper going to force limit while the second damper is operating in the proportional range. Collinear force is the least when $\beta = \frac{\pi}{4}$ rad in this case because the force limiting velocity of the working dashpot is reached earlier in the pin travel.

In actual operation, the oscillatory motion at the vehicle attach pin is nonlinear and random rather than linear and sinusoidal. The nature of the motion does not change the force response of the damper mechanism. Analysis has shown the direction of the total damping force does not always coincide with the direction of attach pin motion. In the load limiting range, this difference may tend to change the direction of travel. This is another form of damping since the mechanism is transferring work energy to the vehicle. The effects of this action have not been fully explored.

Travel Limits

The limits of travel of the attach pin are a function of the stroke of the dashpots. The criteria for establishing travel limits were as follows:

- 1) The damper must never limit the bending deflection of the vehicle to less than that calculated from allowable bending moments for the vehicle. This is represented by a circular envelope 23.1 cm in diameter.
- 2) An allowable vehicle vertical misalignment of 2.54 cm in any direction, plus a locating dimensional tolerance for the damper mechanism were included.

- 3) Damper displacement due to thermal deflection of the umbilical tower caused by solar heating. This was measured at the appropriate tower station and found to be a total of 1.8 cm maximum for the conditions prevailing during one day in May.

A travel limit envelope consisting of a 30.48 cm diameter circle was selected to satisfy the criteria. Although this does not accommodate the sum of all of the criteria, it was considered improbable that all conditions would occur simultaneously in the same direction.

A 43.18 cm dashpot stroke is required for the damper travel to include a 30.48 cm diameter envelope. Figure 7 shows the boundary of actual travel limit of the attach pin traced by the mechanism.

Dashpot Design

The hydraulic dashpot shown schematically in Figure 11 is a self contained system. The proportional damping and force limiting characteristic is controlled by a pressure modulated spool valve with specially shaped orifice slots. The heat produced by the fluid pressure and shear work across the orifice is dissipated to atmosphere through cooling fins in the aluminum dashpot body. A relief valve allows excess fluid volume from thermal expansion to transfer to a spring loaded accumulator. The accumulator also provides fluid make-up for thermal contraction and leakage loss. Pressure isolation of the primary damping circuit and accumulator is provided by check valves.

The spring nulled spool valve displacement is proportional to the pressure differential (ΔP) across the piston. As the spool moves from the null position, one orifice slot is covered while the other is opened to increase flow area. The exponential shape of the slot provides the proper flow area at each ΔP to produce a flow rate directly proportional to ΔP . The slope of the force vs velocity curve is thus constant within the desired force range. When ΔP has increased to the limit value during piston acceleration, the slot suddenly widens and one spring is relaxed. The slope of the force vs velocity curve is thus reduced abruptly as shown in Figure 11. The reverse sequence takes place as the piston decelerates with some variation due to hysteresis effects.

Attach Pin Design

The attach pin shown in figure 3 connects the vehicle to the damping system. The functions performed by the attach pin are as follows:

- 1) The pin reacts the damping loads.

2. The pin is pulled by vehicle rise without jamming in the arms under all expected motions and deflections.
3. The pin holds the retractable arms extended.
4. Pulling of the pin provides instant release of the arms.
5. The pin support sustains the static and dynamic vertical loads applied by the counterweight through the boom and arms.

These requirements resulted in a cylindrical 17-4 PH pin with an enlarged ellipsoid shaped section in its middle, centrally located in a beryllium copper alloy bushing in the end of the arms. The bushing is the pivot bearing in the outboard joint of the arms. The ellipsoid shape insures localized contact in the bushing without possibility of binding under misalignments and deflections. The lower end of the pin locks the arms in place. The pin is mounted on the lower face of a machined bracket fastened to the side of the vehicle inter-stage adapter.

The boom is preloaded against the vehicle to prevent early release and retraction during vehicle longitudinal oscillations at engine start-up. A counterweight provides this preload by overbalancing the mass of the boom through a cable-pulley system as shown in figure 12. The counterweight must be heavy enough to keep the boom in contact with the pin during vehicle upward acceleration with engine ignition. It must not be so heavy that excessive vertical loads are applied as the vehicle accelerates downward during the thrust buildup transient. Figure 12 also provides mathematical equations for determining the relationship between the boom weight and the weight of the counterweight.

Environmental Protection

The dashpots and adjacent structures could be exposed to a wide range of environmental temperature influences varying from direct sunlight at $+44^{\circ}\text{C}$ ambient temperature to impingement by liquid oxygen boiloff gas at -180°C from the vehicle. Such extreme variations would have a significant effect on design and final costs. To provide a more controlled, consistent environment, the end of the system nearest the vehicle has a tubular frame around it, over which is stretched a covering made of chloroprene coated nylon fabric. This covered area is continuously purged with ambient air supplied from a centrifugal blower mounted on the umbilical tower. Thus the dashpots, mechanism, and structure within the covered section are maintained at ambient temperature.

RETRACTION SYSTEM

Retraction System Description

It was decided early in the design to provide a system which would give an "instantaneous" clearance of about two feet between the boom and the vehicle with an ever-increasing, but slower, clearance build-up between two feet and nine feet. The retractable arms mechanism shown in figure 13 accomplishes the instantaneous two-foot clearance portion. The retractable arms mechanism consists of two pivoted, springloaded arms, three spring, cable, and pulley assemblies, a crosshead on which the arms pivot and the afore-described attach pin. The two to nine-foot portion of the clearance is provided by separating the cable which supports the support boom and allowing the boom to freely swing about its hinges until it engages a snubber mechanism. When the release mechanism, located as shown in figure 2, separates the cable, the counterweight is also released. The counterweight falls approximately 15 cm where it is stopped by two small shock absorbers.

The sequence of retraction is for the vehicle to begin to liftoff, the boom/damper mechanism assembly accelerates up with the vehicle until limited by a restraint chain, at which time the pin is pulled releasing the arms to provide a two-foot clearance. Simultaneous with vehicle rise, an electrical signal is sent to the boom release mechanism which separates the cable into detached parts as shown in figure 14, permitting the boom and counterweight to fall by gravity, independently. The boom falls onto the snubber mechanism provided to absorb the energy in the falling boom.

Retractable Arms Mechanism

The retractable arms mechanism (figure 13) is made up of two pivoted arms. The left hand arm is one-piece. The right hand arm is pinned to a pivoting link about one-third of its length. This pivoting link is adjacent to, and in parallel with, a fixed section of the right hand arm so that, when the arm is extended and the attach pin (figure 3) is inserted through the outboard arm bushing, the pin engages the fixed section, in effect bypassing the pivoting link out of the system. When the pin is engaged through the bushing far enough to engage the rigid portion of this arm, then the "four bar" linkage becomes a rigid triangle. However, as the vehicle rises and the pin disengages from the rigid portion of the right hand arm, this arm becomes articulated around the pivot link. The right arm is retracted by the double springs shown, whereas the left arm is retracted by being pulled in by the right hand arm and by the single spring. When retracted, the arms nest together and are latched tightly against the crosshead to prevent centripetal force from extending them as the boom retracts.

The arms are machined from 17-4 PH steel billets and are shaped primarily by a stiffness requirement in reacting the dynamic (vertical) preload. The crosshead is a built up, box-reinforced channel made of A36 steel. A small shock absorbing rubber washer on the end of the arms, concentric with the outboard pivot bushing, is installed between the arms and the attach pin support housing as seen in figure 3. The washer is provided to dampen out any higher frequency vibrations and prevent shock loading between the arms and the attach pin housing. The washer is hard silicon rubber with cupped metal washers protecting its flat contact surfaces. The washer-cup assembly is fastened to the left arm by screws.

Release Mechanism

Figure 14 shows the boom release mechanism. This mechanism is in the vertical run of cable between the boom and the counterweight. Its purpose is to separate the cable upon command to permit the boom to drop. The mechanism consists of an upper plate, lower block, two clamping blocks, and two explosive bolts. The upper plate is attached to the lower end of the vertical cable run. At the lower end of the upper plate is an enlarged, triangular, wedge-shaped section. This wedge-shaped section is held hard against the lower block by the two clamping blocks as shown. The lower block is attached to the counterweight by a steel rod. The explosive bolts each hold one clamping block to the lower block. The explosive bolts each have redundant squibs and are fired by redundant circuits activated by redundant switches in the launcher system which releases the vehicle for launch. Thus, the release of the ground wind damper system is not initiated until the vehicle has been committed to launch. Firing of either squib in either bolt releases a clamping block which permits the wedge-shaped portion of the upper plate to come free. The released clamping blocks are retained by wire rope cable tethers to the lower block.

When the release mechanism is fired, the upper plate is freed. The cable runs over the pulley, permitting the boom to drop against its snubber. It also releases the counterweight which drops down about 15cm, guided by two tracks onto two shock absorbers. To "recock" the release mechanism for the next launch, a hand winch lifts the boom back out to its horizontal position and a hand-jacking system raises the counterweight back to its operating position. The release mechanism can again be assembled. Set-up bolts and straps are used to hold the release mechanism together until the explosive bolts are installed on launch day. At this time, the set-up bolts and straps are removed.

Snubber Mechanism

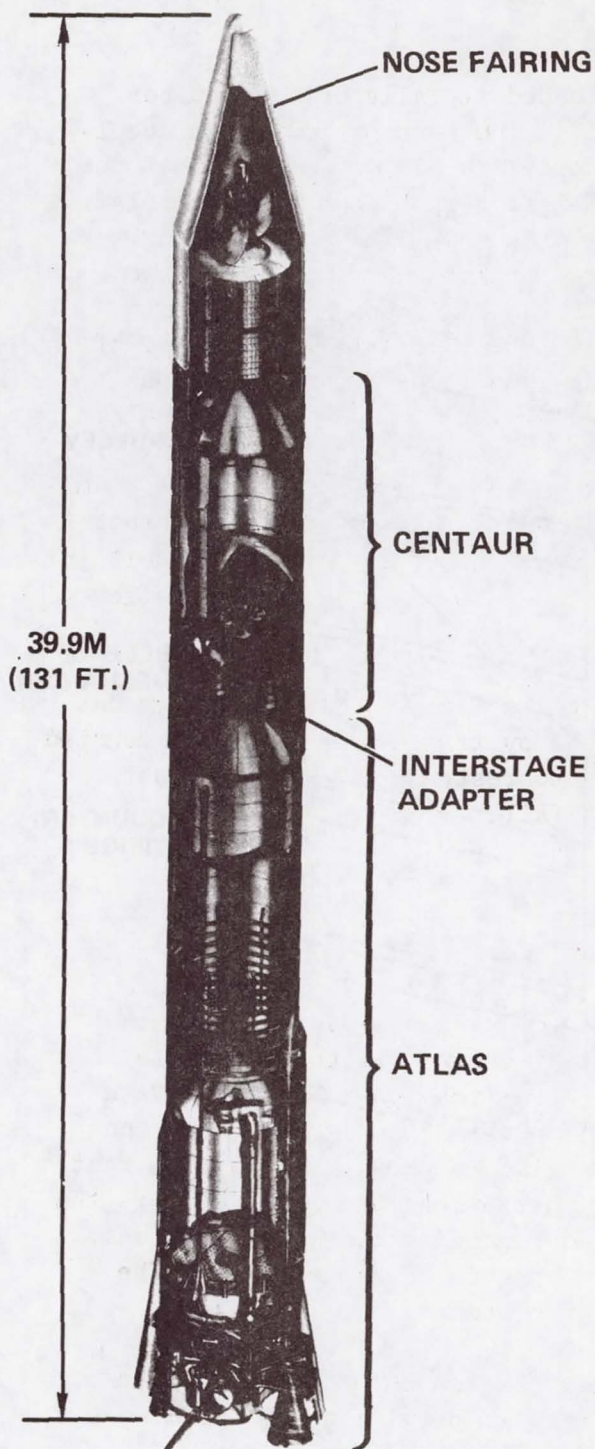
As stated earlier, when the boom is released it falls onto a snubber mechanism which absorbs the energy of the fall. The snubber mechanism decelerates the boom at approximately 5 g's to protect the damper mechanism at the end of the boom from high side loads. Figure 15 shows the snubber mechanism. It consists of a 0.5 meter stroke shock absorber end-mounted in a housing which also forms the trunnion mount for a large bellcrank. The rod of the shock absorber is attached to the short arm of the bellcrank. A pair of rollers is mounted on the long arm of the bellcrank. On the outboard end of the boom there is an elliptical ramp which contacts these rollers when the boom has fallen to the point where it must be decelerated. The elliptical shape of the ramp was required to gently initiate motion in the bellcrank. Tests performed with a flat plate ramp produced high impact loads as the boom energy was transferred into the bellcrank to start it and the shock absorber piston in motion. Rotation of the bellcrank causes displacement of the oil in the shock absorber through orifices to absorb the 2.03×10^5 N-m of kinetic energy developed by the falling boom mass.

As the boom falls it engages a spring loaded latching arm. The arm has three barbs, any of which prevents boom rebound by trapping a catch bar mounted on the boom. The reason for multiple barbs is to restrain the boom in the farthest retracted position to which it might fall.

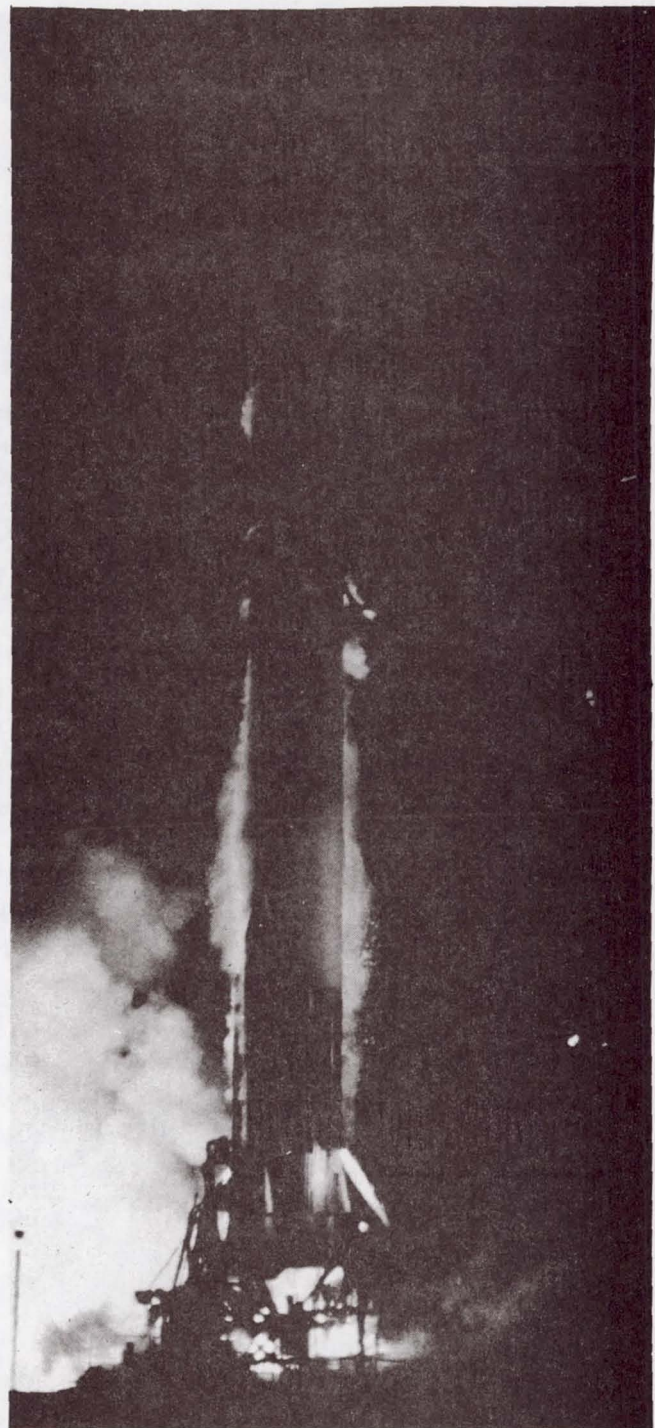
CONCLUDING REMARKS

The effectiveness of the Atlas/Centaur damper system was first demonstrated during a propellant tanking test of the Mariner 10 backup vehicle designated AC-33 in October 1973. A comparison of resultant rate gyro data from an undamped AC-26 vehicle and from AC-33 under similar ground wind conditions is shown in figure 16. The rate gyro signals shown are the resultant of vehicle pitch rate and yaw rate near the upper end of the Atlas. It is the most effective means of monitoring ground wind induced vehicle oscillations. In this case, the launch of AC-26 was delayed because of ground wind. The tanking test of AC-33 was completed in a routine manner.

The damper system successfully supported the launch of Mariner 10 on 2 November 1973. The existence of this system will provide considerable launch availability and launch safety improvements for Atlas/Centaur plus the capability for future growth in length.



ATLAS/CENTAUR/INTELSAT IV



LIFTOFF FOR VENUS AND MERCURY NOVEMBER 1973

Figure 1. Atlas/Centaur launch vehicle.

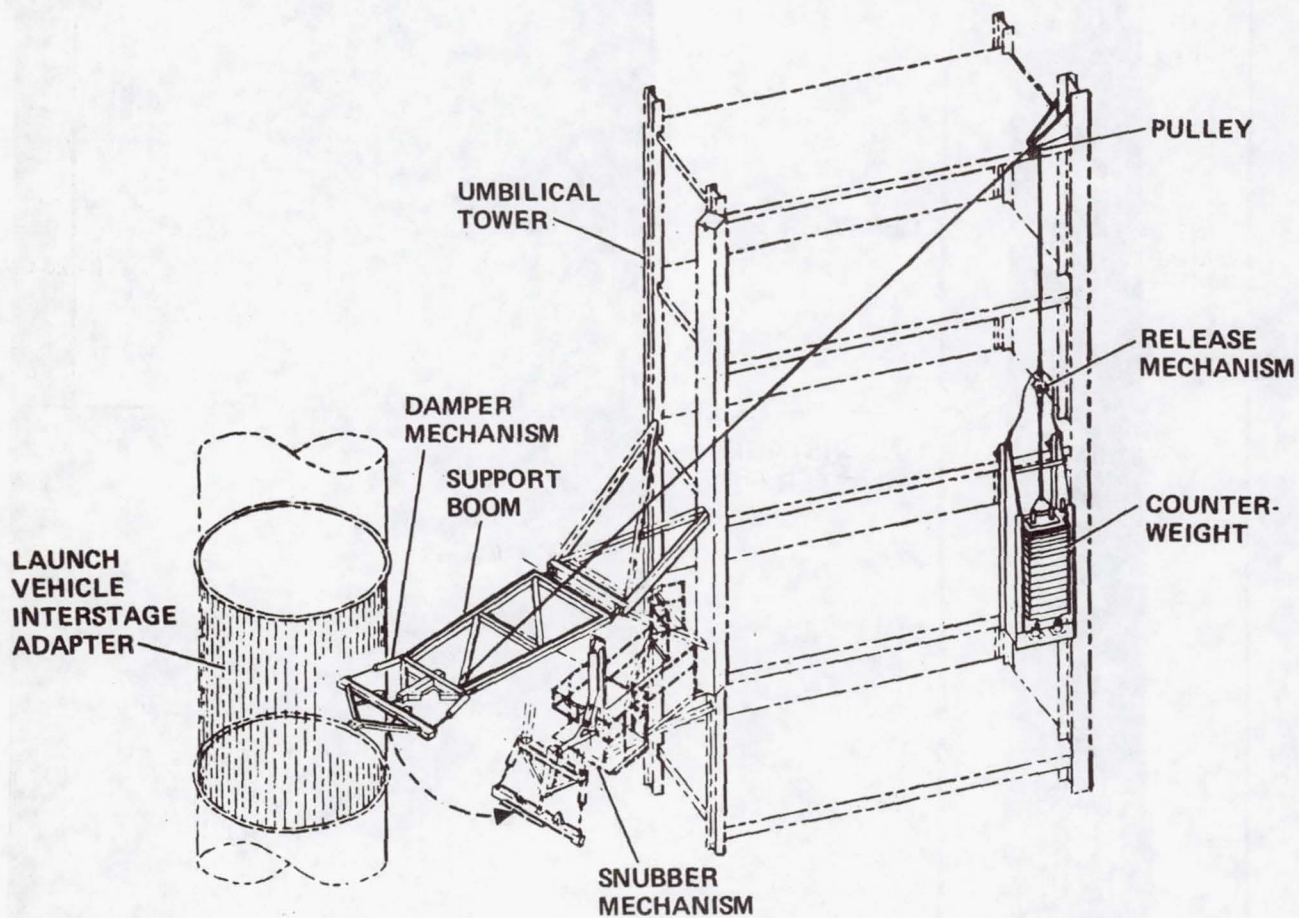
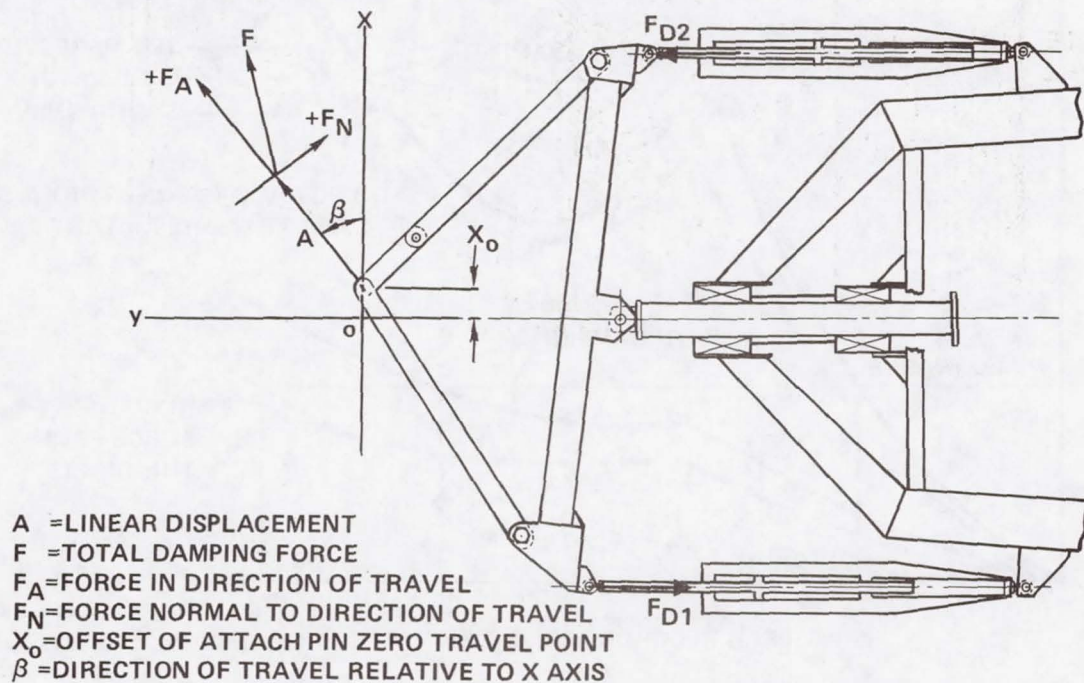
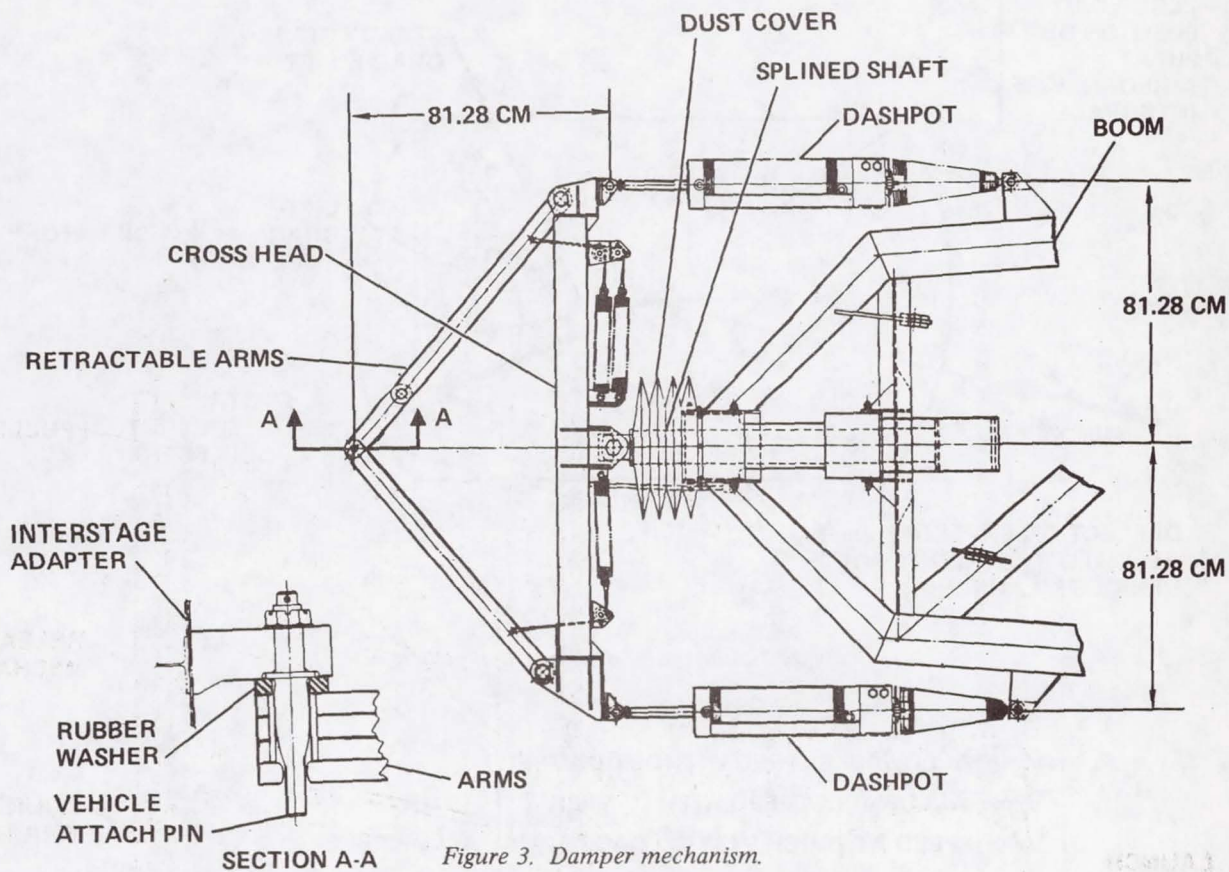


Figure 2. Installed ground wind damper system.



A = LINEAR DISPLACEMENT
 F = TOTAL DAMPING FORCE
 F_A = FORCE IN DIRECTION OF TRAVEL
 F_N = FORCE NORMAL TO DIRECTION OF TRAVEL
 X_0 = OFFSET OF ATTACH PIN ZERO TRAVEL POINT
 β = DIRECTION OF TRAVEL RELATIVE TO X AXIS

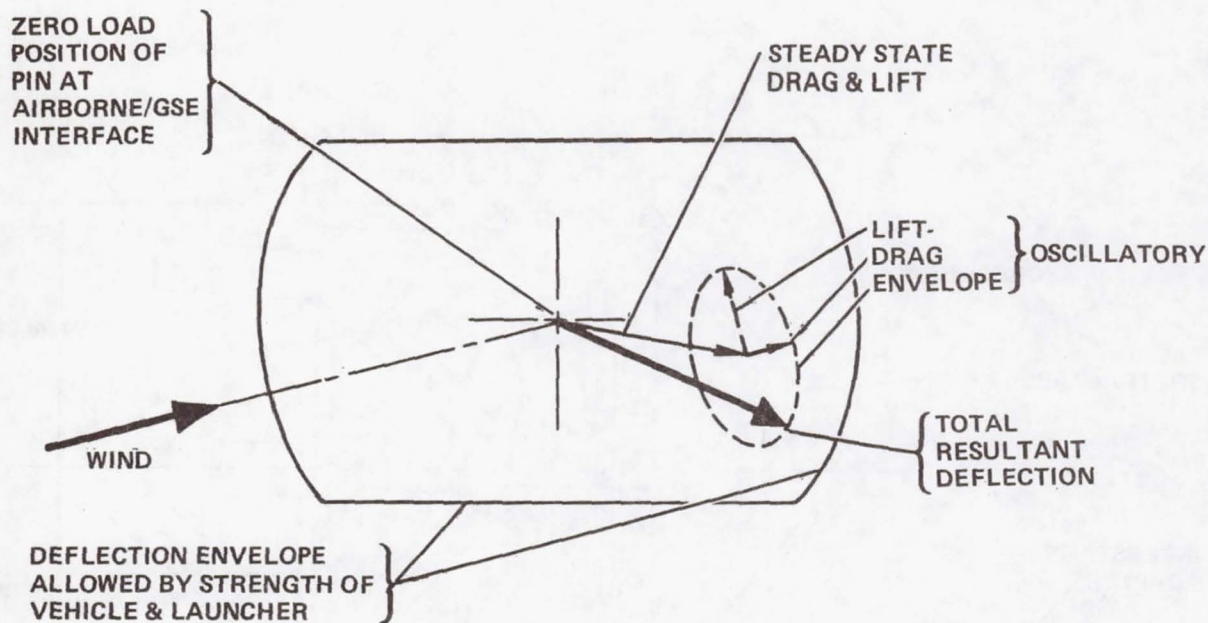


Figure 5. Illustrative description of vehicle deflections.

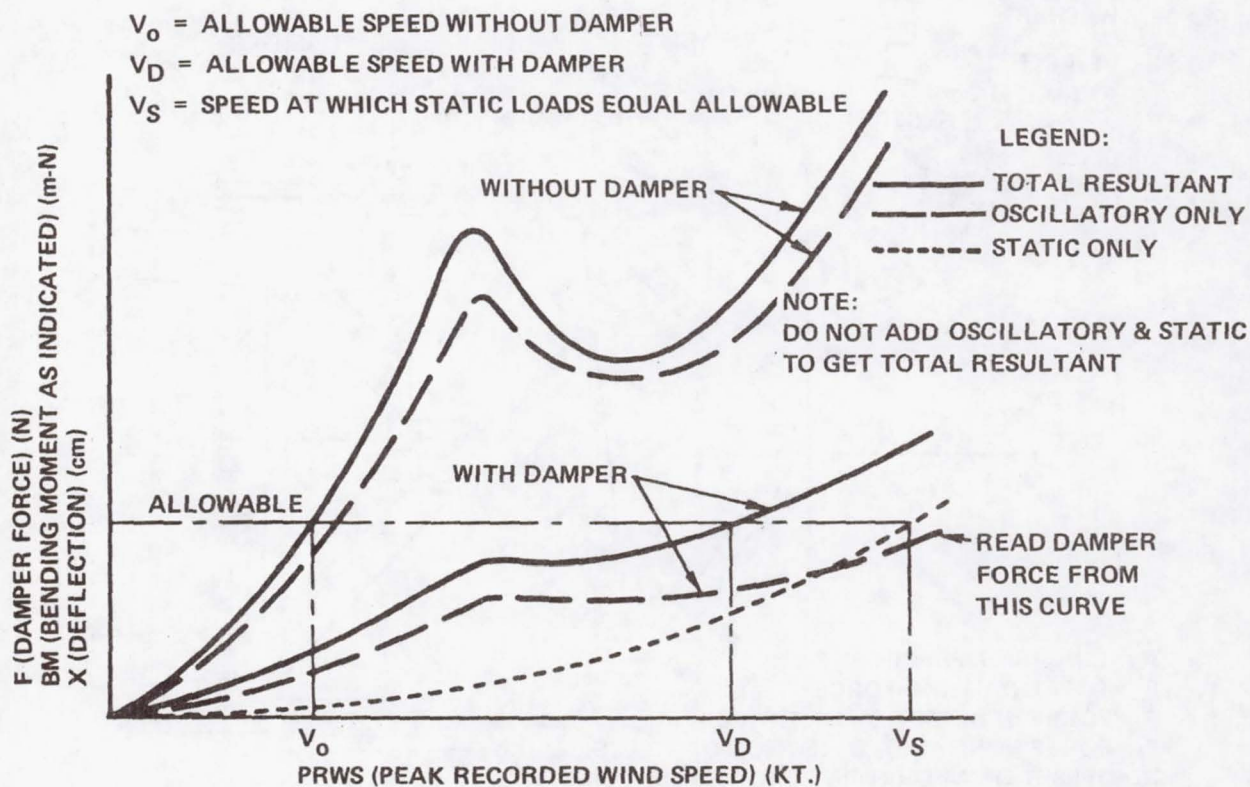


Figure 6. Characteristics of ground wind loads.

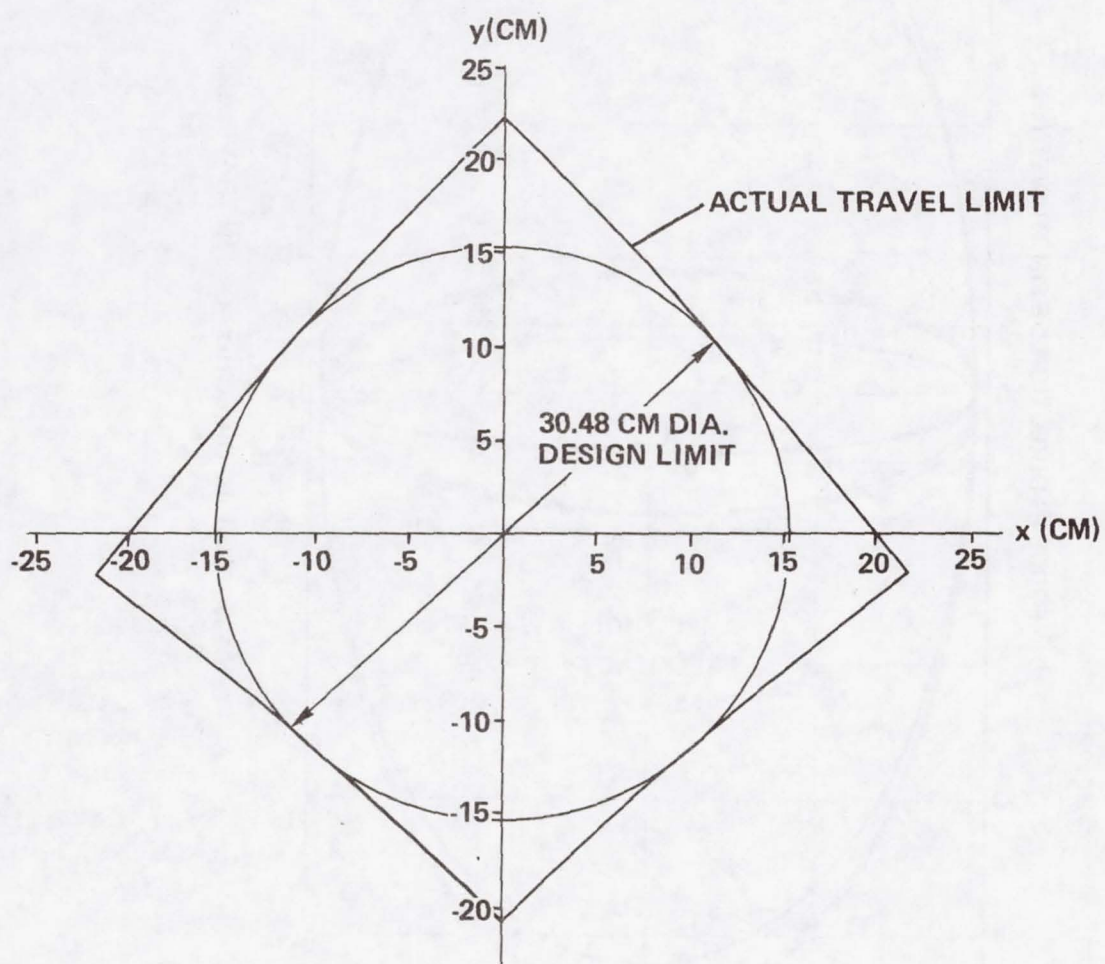


Figure 7. Damper mechanism travel limit.

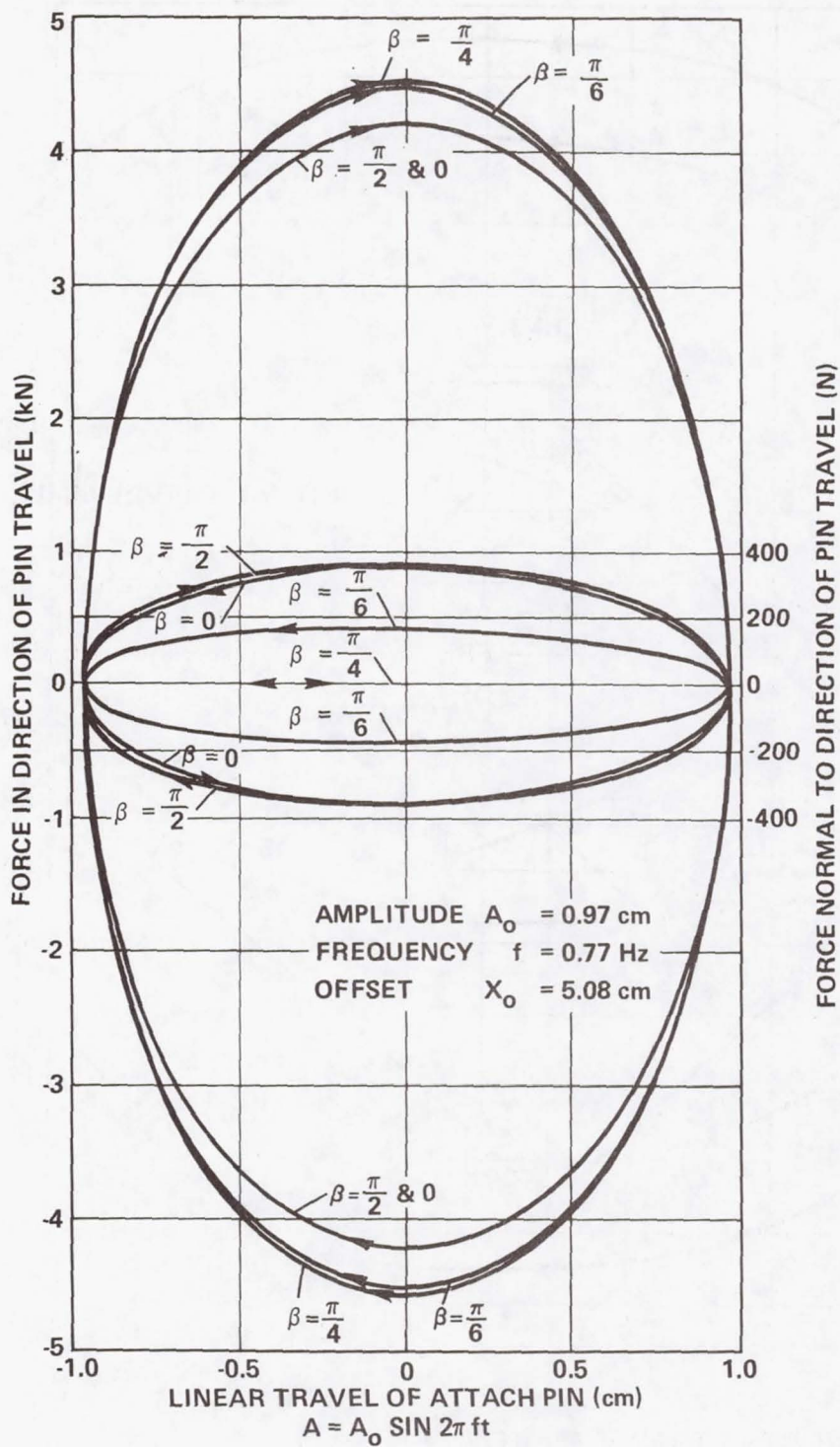


Figure 8. Proportional damping range force dispersions.

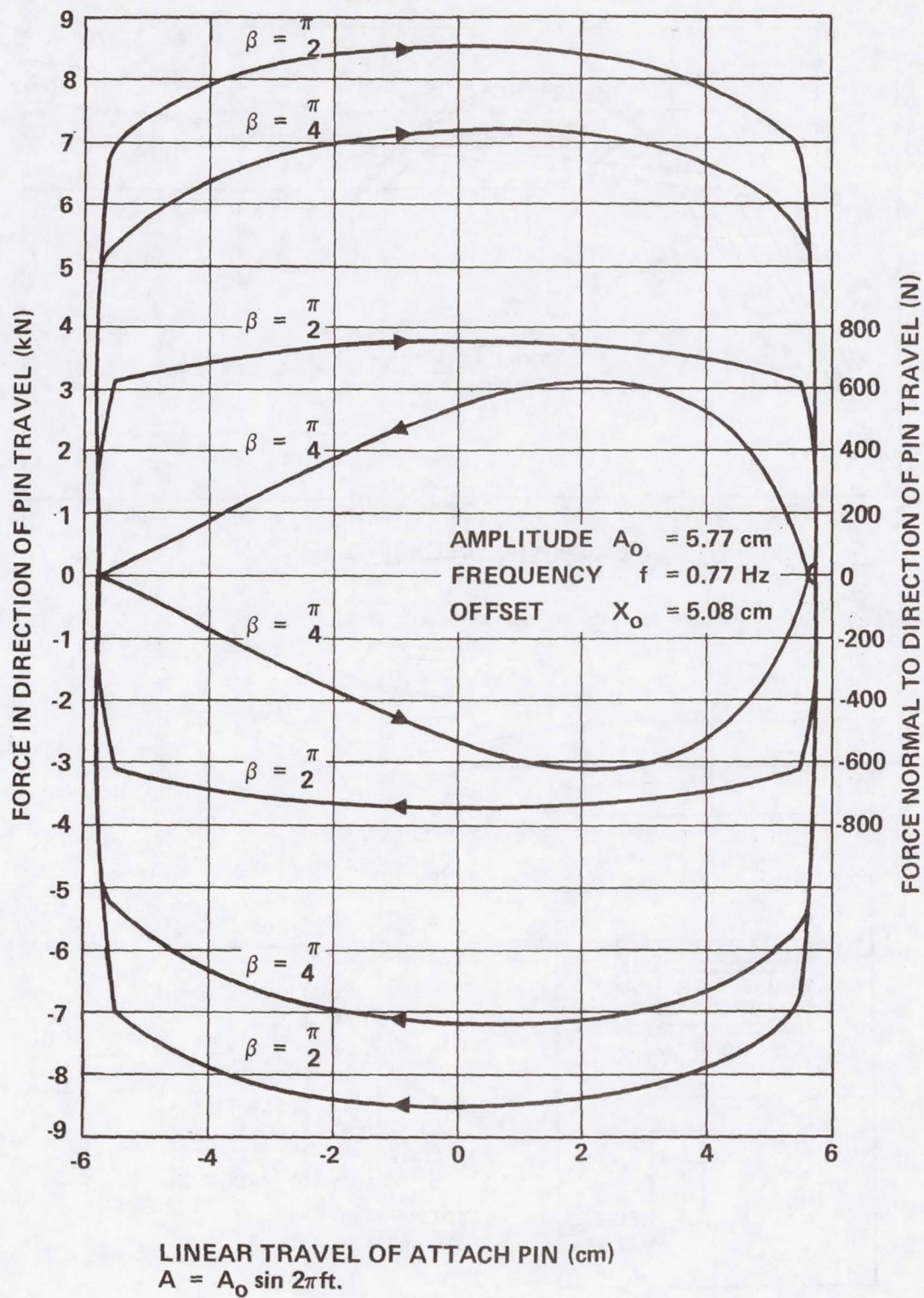


Figure 9. Force limiting range force dispersions.

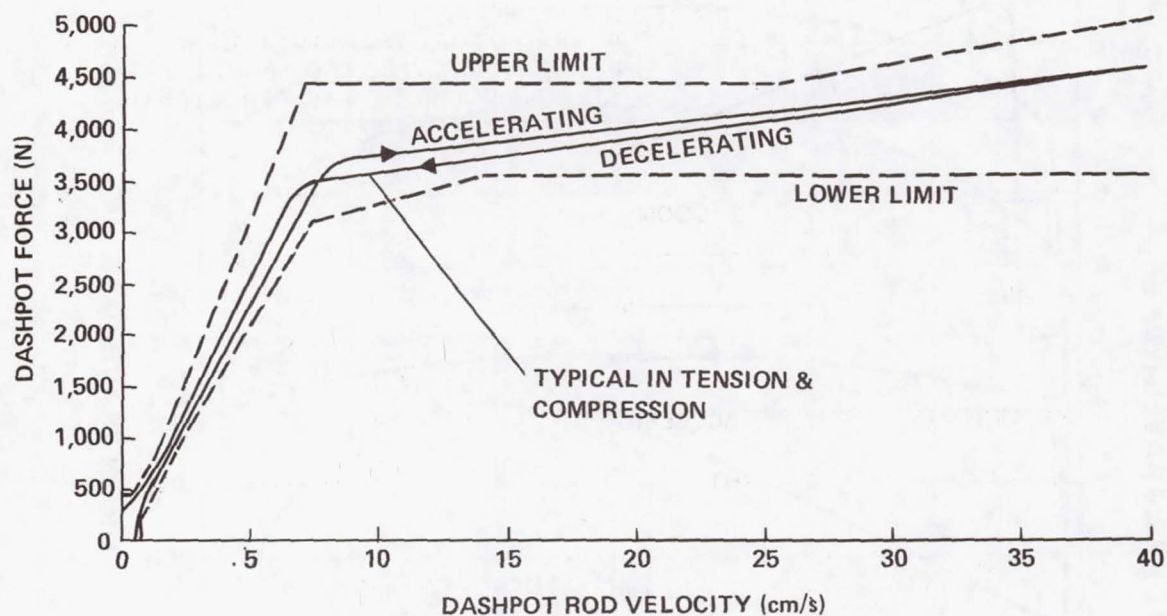


Figure 10. Dashpot damping characteristics.

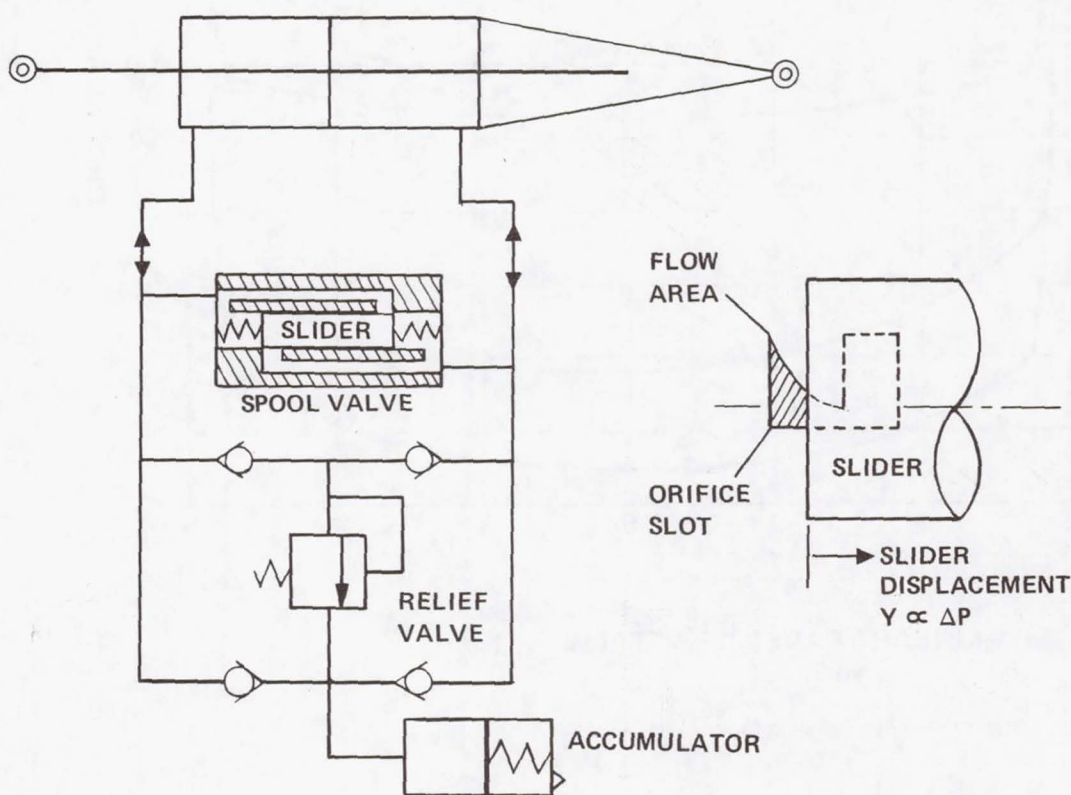
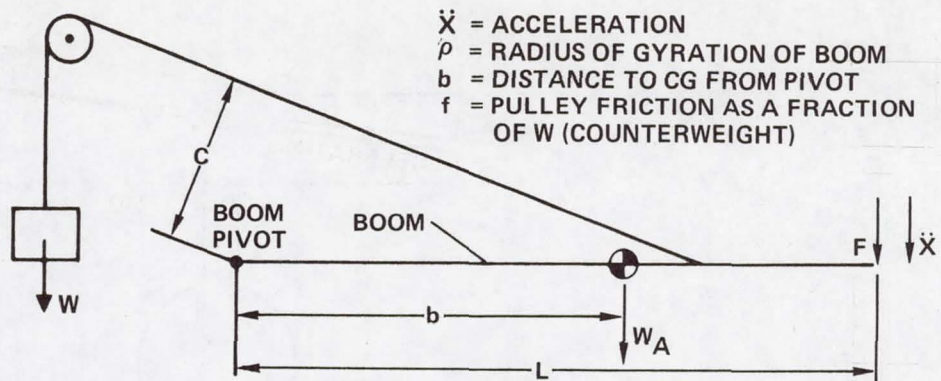


Figure 11. Dashpot schematic diagram.



REQUIREMENT: BOOM TIP ACCELERATE UP AT $1g$ WHEN FORCE F IS REMOVED.

WEIGHT OF COUNTERWEIGHT

$$W = \frac{W_A (Lb + \rho^2)}{CL (1-f) - C^2}$$

FORCE REQUIRED TO ACCELERATE END OF BOOM DOWN AT $1g$

$$F = \frac{WC (1-f) - W_A b}{L} + \frac{\ddot{X}}{gL^2} (W_A \rho^2 + WC^2)$$

Figure 12. Boom acceleration calculation.

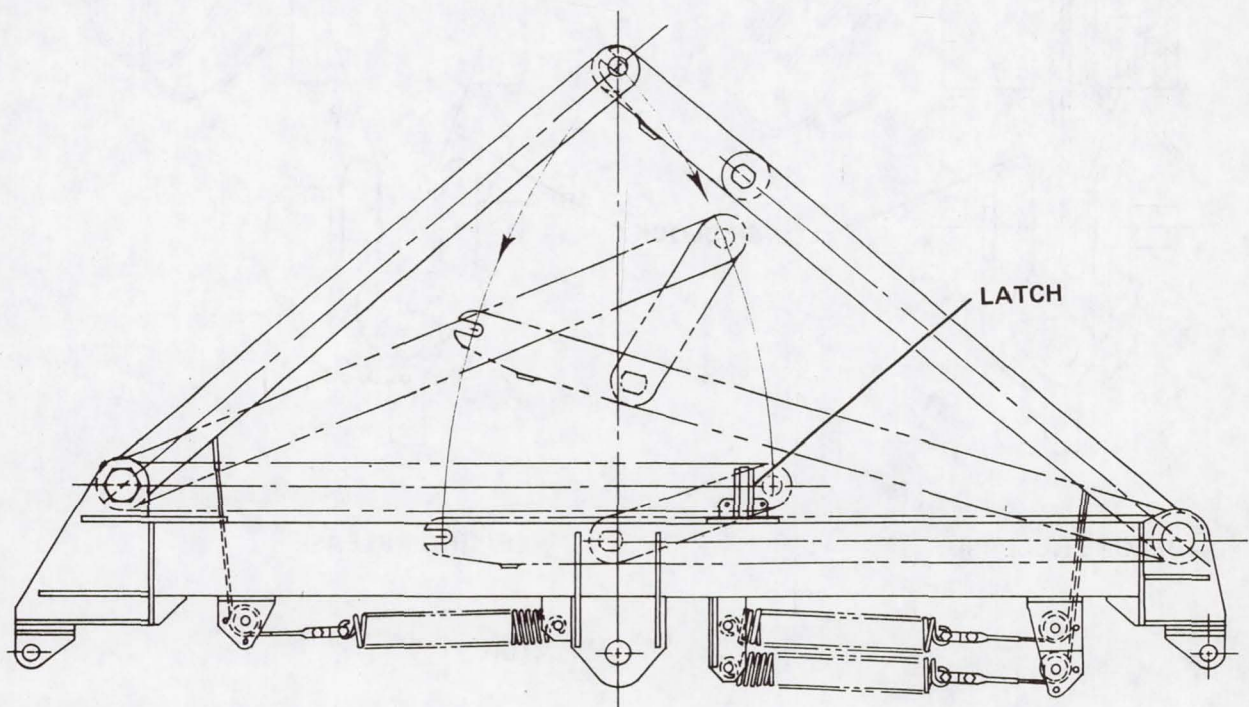


Figure 13. Retractable arms mechanism.

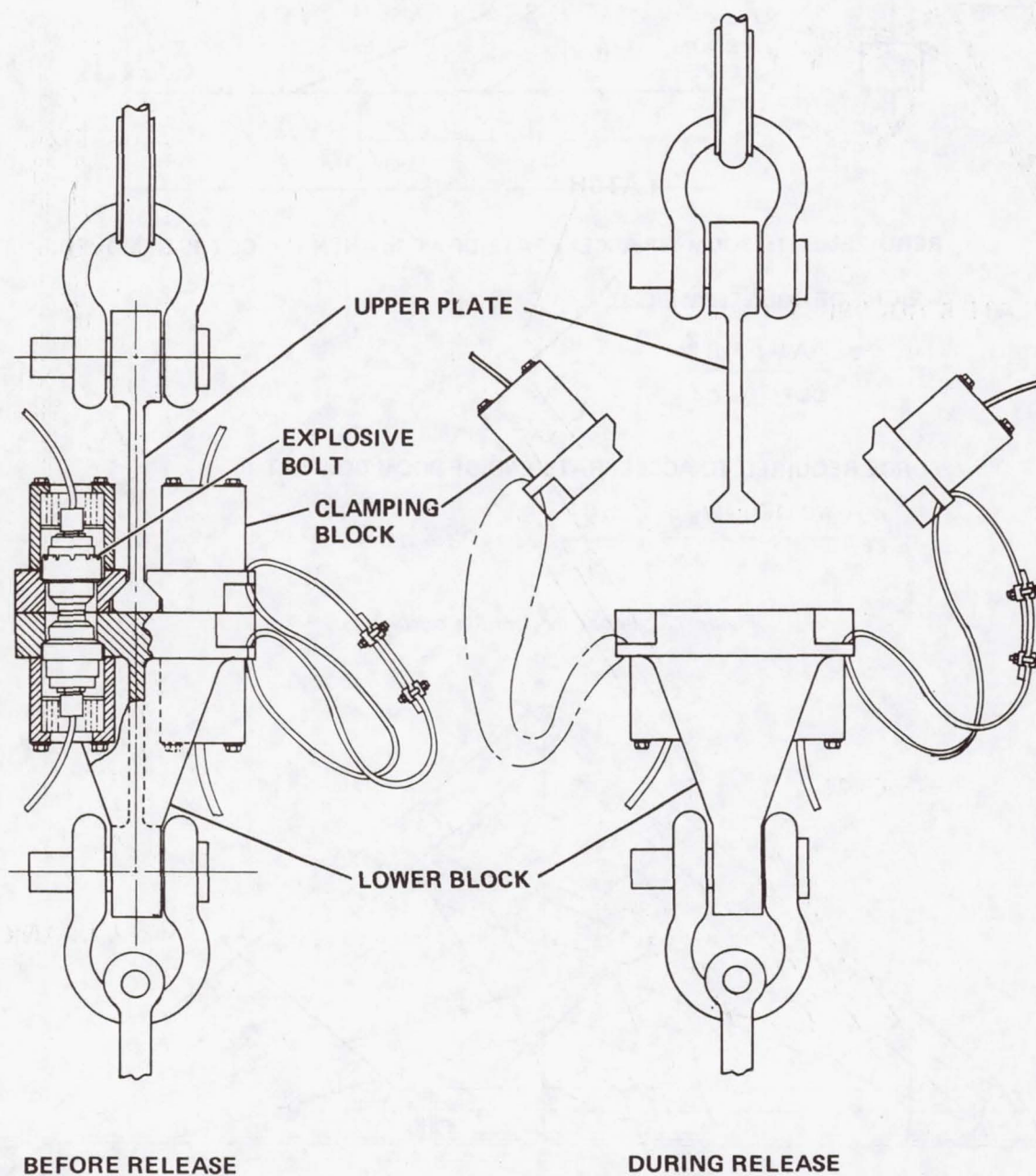


Figure 14. Boom release mechanism.

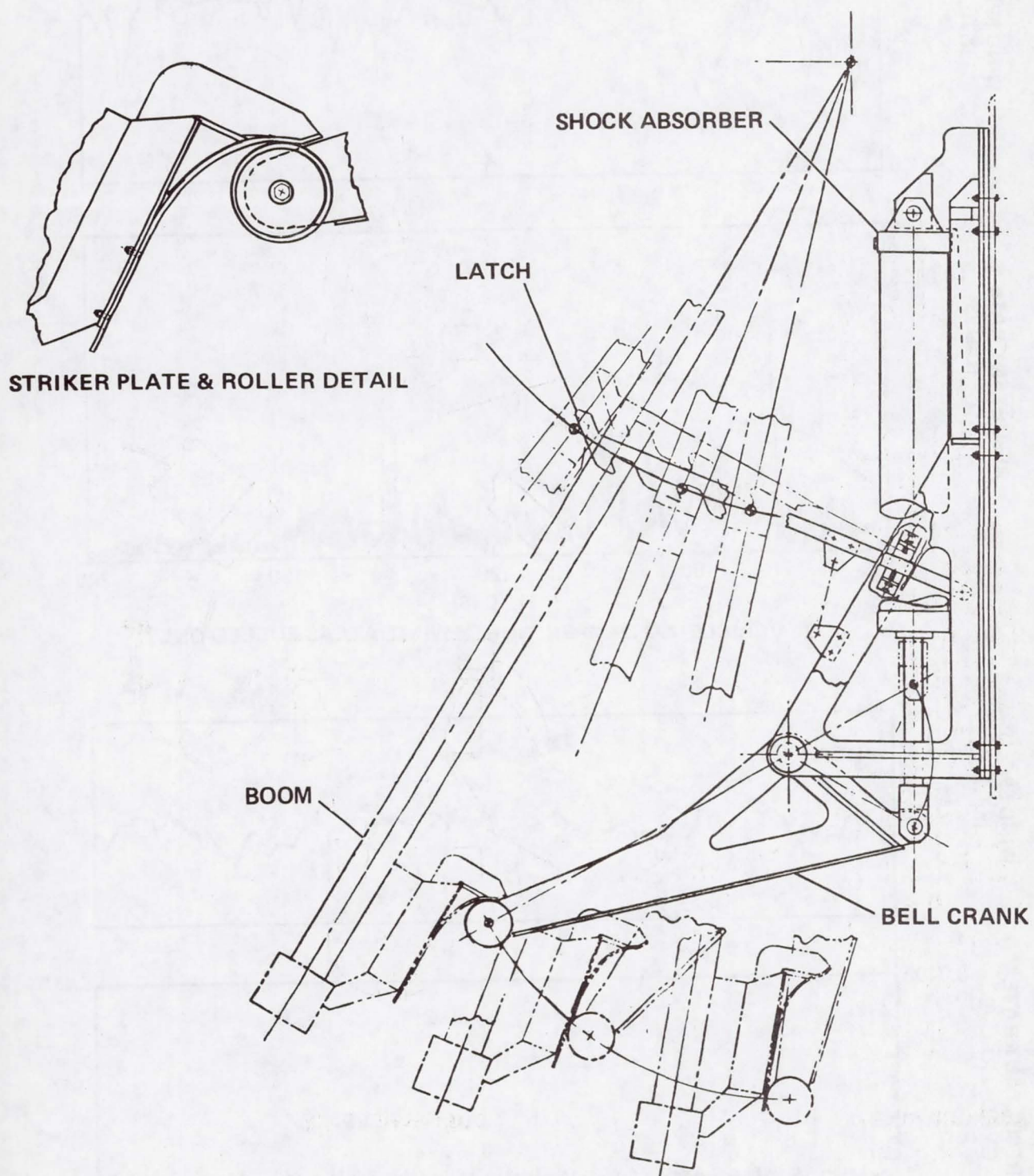
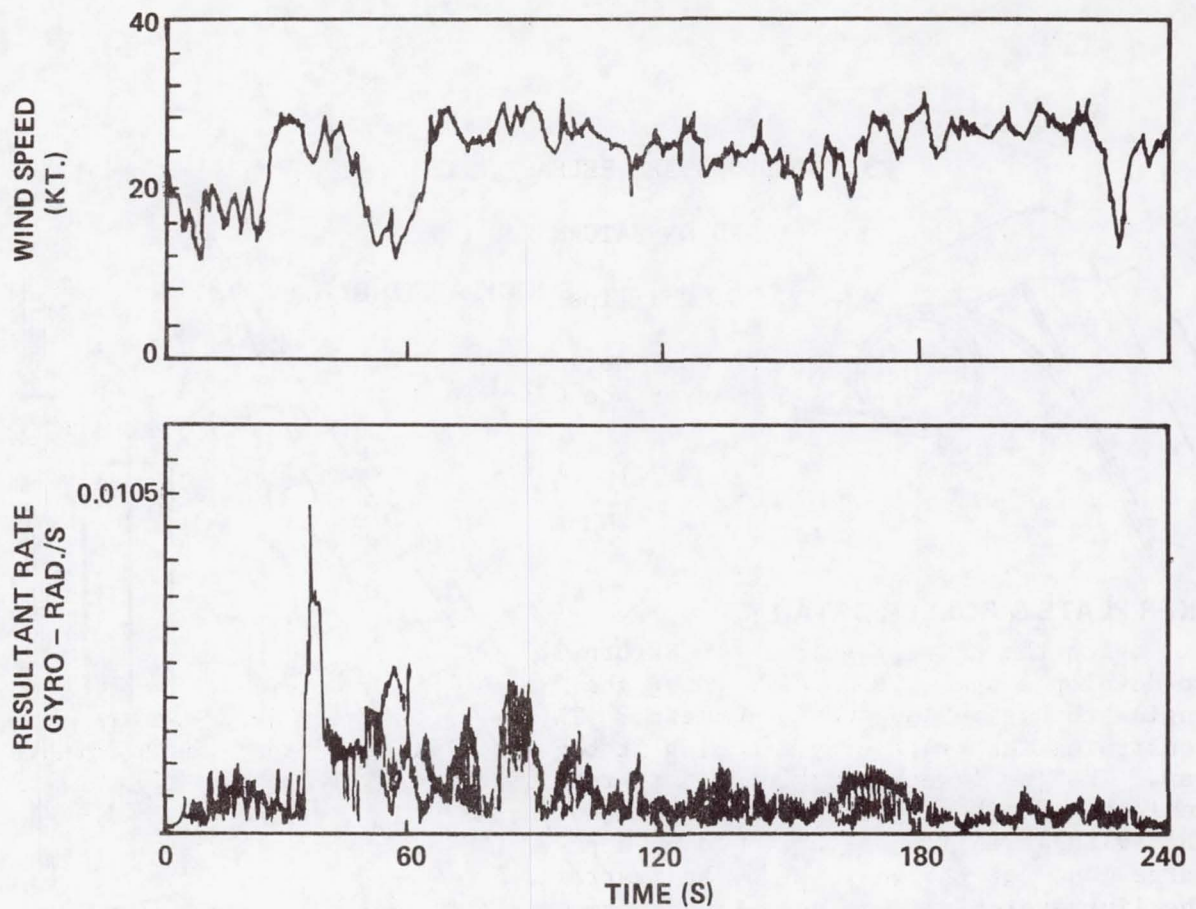
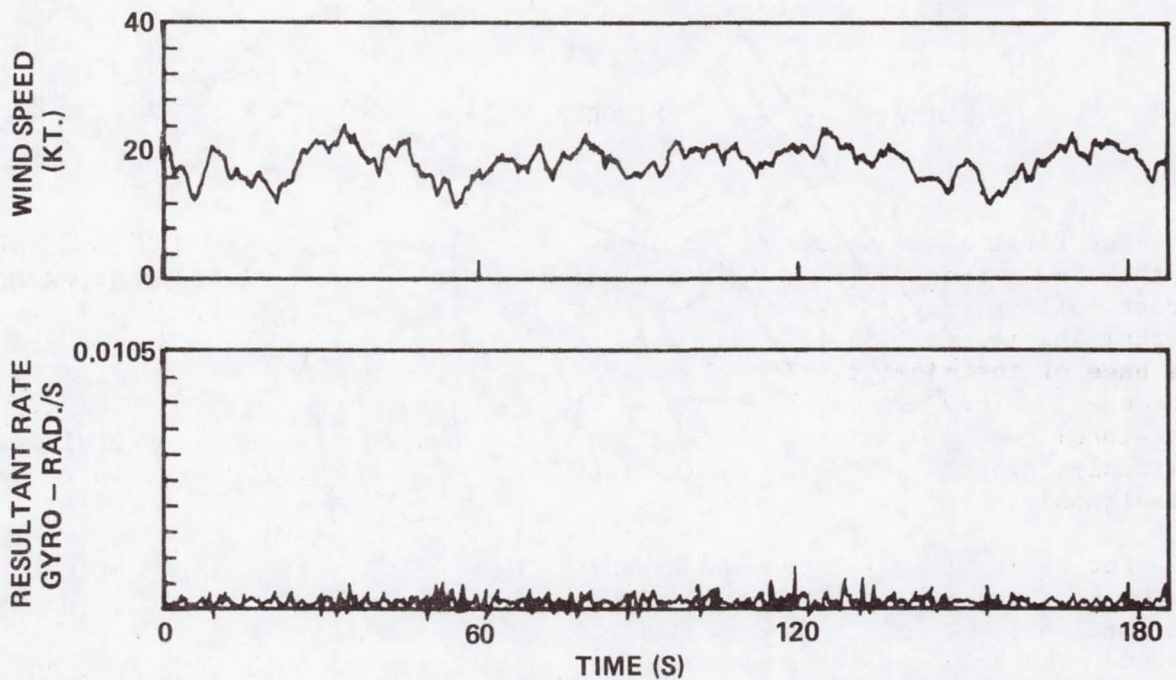


Figure 15. Snubber mechanism.



AC-26 VEHICLE, NO DAMPER, NORTH WIND, ATLAS FUELED ONLY



AC-33 VEHICLE, WITH DAMPER, NORTH WIND, ATLAS FUELED ONLY

Figure 16. Results of damper installation.

23. HOLDDOWN ARM RELEASE MECHANISM

USED ON SATURN VEHICLES

By: J. D. Phillips and B. A. Tolson

Design Engineering Directorate
Kennedy Space Center, NASA

SUMMARY

With the development of the Saturn launch vehicle, it became mandatory to develop a system for restraining the vehicle until after all checks and engine thrust buildup were completed. The basic Saturn I holddown arm constrains the vehicle by clamping it between a fixed support and a movable jaw. The jaw is on a link pinned to rotate sufficiently to release the vehicle. There are three links in the jaw (restraining) system arranged so that with a small force provided by a pneumatic separator mechanism, the large loads of the vehicle can be restrained. Design details discussed are the link system, the separator, adjustments, and the energy absorber. The function of preloading is discussed. The secondary release system is described. Finally, the design differences between the Saturn I and the Saturn V arm are described.

INTRODUCTION

The first large-scale rocket propelled vertical-fired missiles developed in the 1940's and 1950's were freestanding. Upon ignition of the engines and thrust buildup, launch was achieved when thrust exceeded missile weight. Overturning moments due to winds were countered by wind locks or clamps around the base of the missile. The clamps required removal prior to flight. Any increase in winds approaching redline values (loads where vehicle would not freestand) required personnel to return to the pad to reinstall these wind locks. Obviously, propulsion system faults that resulted in decayed thrust were catastrophic.

For the extremely large and expensive Saturn, it was mandatory that a system be developed that would safely support and restrain the vehicle on the pad until all checks, including engine start and thrust buildup, were completed. The holddown arm system was designed to fulfill this function, and is described in this paper.

NOTE: In general, this paper describes the Saturn I holddown system. The Saturn V holddown system is quite similar - differences will be pointed out at the end of the paper.

BASIC ARM

The basic Saturn I arm, as shown in Figure 1, is essentially in the shape of a pyramid and weighs approximately 3,765 kilograms (8300 pounds). Attached to the front (directly under the vehicle) is a plunger that supports the vehicle. The plunger is supported on a wedge that is moved up or down an inclined plane machined into the housing. See Figure 2. This provides the plunger with approximately 5.08 centimeters (2 inches) of vertical adjustment to level and align the vehicle. The screw that moves the wedge is turned by use of a 3-to-1 multiplying gear box that is bolted to the housing.

The main pin, which is approximately 6.98 centimeters (2.75 inches) in diameter, is aft of and slightly above the plunger. The main pin attaches the upper link to the holddown base at a point approximately one-fourth back from the front of the upper link. The center link is attached to the aft end of the upper link and to the forward end of the lower link by pins approximately 6.35 centimeters (2.5 inches) in diameter. The lower end of the lower link is fastened to the base with a pin also 6.35 centimeters (2.5 inches) in diameter. This arrangement of three links pinned to each other and to the base at two points allows the aft end of the upper link to rotate through approximately 90 degrees.

Looking at Figure 1, it can be seen that if the lower and center links are held in a vertical position such that a straight line would pass through the three pins, any load applied in the up direction at the plunger end of the upper link would be reacted through the center and lower link and would have a magnitude equal to the ratio of the moment arms about the upper link main pin. This condition, however, is unstable, because the center/lower link pin could move in either direction (fore or aft).

Stability can be gained for the linkage by moving the center/lower pin point a small distance fore or aft. By keeping the distance that the pin is moved forward small, a large load through the links can be restrained with a small horizontal load. Figure 3 is a representation of the three-link system. If the angle α that the lower/center link pin subtends is set at 3 degrees, and the length b is set at 3 times the length a , the relationship of force F to force F'' is defined as follows:

$$M \text{ about pin} = 0$$

$$F a = F' b$$

$$F' = \frac{F a}{b} \quad (1)$$

$$\frac{F''}{F'} = \tan \alpha$$

$$F' = \frac{F''}{\tan \alpha}$$

Substituting into (1) above

$$\frac{F''}{\tan \alpha} = \frac{Fa}{b}$$

$$F'' = \frac{Fa}{b} \tan \alpha$$

Substituting $\alpha = 30^\circ$; $b = 3a$

$$F = 57.2F'' \quad (2)$$

To restrain the vehicle until after thrust buildup requires that the holddown arms restrain a vertical up-load equal to the vehicle thrust minus weight of the vehicle, plus the overturning moment due to wind. This value of up-load is then preloaded into the linkage to assure no separation of the vehicle from the holddown arm plunger during engine start. For the Saturn I, the value of this load is 444,822 newtons (100,000 pounds) per holddown arm.

NOTE: Additional allowances must be made for thrust overshoot, hardover engines, and unknowns, i.e., wind gust, misaligned engines, etc.

For a load on a holddown arm of 444,822 newtons (100,000 pounds), the separator is required to provide a restraining force of approximately 7,784 newtons (1750 pounds) in tension (using equation 2 above).

SEPARATOR

The separator (Figure 4) is essentially a cylinder with a piston that includes a rod having a groove or ball race machined near its end. Ball bearings that are seated in the cylinder protrude through the cylinder wall; and in the holddown position rest on the outer end of the piston rod and in a machined race in the separation link of the separator, which is essentially a continuation of the cylinder. In the holddown position, the piston is held aft in the cylinder by spring action so that the balls protrude outside the cylinder wall into the machined race on the separation link. Tention loads can then be carried from the separation link (which is bolted to the lower link of the holddown arm) through the balls and through the cylinder to the holddown arm base.

To operate the separator, pneumatic pressure pushes the piston forward, allowing the balls to be pressed into the piston groove by the load being transmitted through the separation link. When the balls are forced into the piston groove, the separation link is no longer attached to the separator cylinder and is free to move with the lower link.

PRELOADING

To assure a tight connection between the vehicle and the holddown arm, the arm is clamped with a preload large enough to assure no separation between the vehicle and the arm plunger until release. This preload takes care of bending in the upper link and any tolerance in the linkage system. To preload the arm, the vehicle is placed on the plunger blocks and leveled. Then the holddown arm linkage is erected, using a demountable winch. The separation link is connected to the separator, and the separator rear swivel nut (Figure 1) is tightened to develop the necessary preload. Curves of torque of the swivel nut versus preload or clamping force on the vehicle have been developed. The preload value selected must be attained with the linkage in a particular geometry. For the Saturn I arm, the center/lower link pin must be located forward of a straight line between pins by approximately 3 degrees. This is measured by an alignment gage on the arm base. If either the proper preload torque value (74.7 joules) (55 ft-lbs) is not attained or the pin geometry is not obtained, the linkage is lowered and shims are added to or removed from the upper arm section pad and the torqueing procedure is repeated. The arm is now preloaded and ready for firing. The 3 degrees mentioned was selected to keep separator tension load small and assure the center/lower link pin would always be forward of the unstable point (straight line between pins).

ENERGY ABSORBER

When released under load, the linkage has kinetic energy equal to gravity plus the preload reaction. Obviously, because of the large preload, the linkage travels with great speed and must be arrested without damage to the linkage. For the Saturn I arm, a shear module (Figure 5) is used to absorb this energy. The module is essentially a housing with four shear rods staggered such that as the lower link falls, a striking plate mounted on the bottom of the lower link breaks each rod in succession, absorbing the energy.

ZERO MOMENT

Because machining of a perfectly flat plane on the base of a vehicle such as the Saturn is impossible, means must be provided to assure that moments about the plane of the linkage are not introduced. This would not only be detrimental to the linkage, but would add unnecessary loads to the vehicle as well. To assure that moments are not introduced, the attach point on the vehicle contains a spherical surface. Likewise, the forward end of the upper link also contains a spherical surface (Figure 6). The separator is designed for a straight tension pull. Bending would apply unsymmetrical loads to the separator balls. To prevent bending in the separator mechanism, spherical washers are incorporated between the separator rear swivel nut and the hold-down base (Figure 1).

SYNCHRONIZATION/RELIABILITY

To assure synchronization of the release of all eight arms, a pneumatic circuit (Figure 7) was designed that provided the same length pneumatic line to each separator from the pressure source. This concept of equal lengths of line removed the problem of orifice design that would be required because of the location of the source. For reliability, two circuits were provided to each separator, as shown in Figure 7.

Redundancy was also provided in the firing panel by installing an accumulator with sufficient gas to fire the complete circuit. The firing panel itself is made up of two solenoid-operated 3-way valves installed in a parallel circuit. With a history of several hundred firings during tests and launch, the firing panel has never fired prematurely or failed to fire on command, and a separator has never failed to release. Looking at the pure numbers of reliability, however, a single failure point exists in the separator. Reliability numbers obtained by testing cannot match the confidence provided by a second or redundant system. Therefore, a second system for holddown release was developed.

SECONDARY RELEASE SYSTEM

The secondary release system consists of an explosive nut attaching one end of the pneumatic separator to the link. Figure 8 shows an exploded view of the separator, explosive nut, and the separation link. An eyebolt connects the separation link to the lower link. The nut that holds this eyebolt to the separation link is slotted and is sufficiently long to allow attachment of an explosive charge that has enough power to split the nut.

Figure 9 is a schematic of the circuit that fires the explosives. The circuit contains three relays such that prior to start of countdown the power supply is shorted. Upon receiving the signal to release, which for both the pneumatic and the explosive system is the same signal and is furnished by vehicle ground equipment, relay contacts PK 1 close and relay contacts PK 2B open. This arms the circuit. This same signal starts a timer that closes relay contacts PK 2 after an appropriate time - 130 milliseconds in the case of the Saturn I. If the separator has operated pneumatically, the movement of the separation link forward will break the lead wires to the explosive nut, and therefore the redundant explosive system will not operate. If the pneumatic separator has not operated, the nut will blow it free and allow operation of the arm.

TIMING

It has been found during testing that helium under a pressure of 5.17×10^6 newtons per square meter (750 psi) will operate the separator in 20 milliseconds with a length of tubing containing approximately 819 cubic centimeters (50 cubic inches) volume (Saturn I). Gaseous nitrogen, on the other hand, requires approximately 69 milliseconds. Other gases possibly would be satisfactory, but have not been investigated, because helium is the lightest gas available, and therefore should be the fastest.

A normal time for release shows first arm release is approximately 130 milliseconds after signal, and the last of the eight must release in a maximum of 180 milliseconds after signal. The time for the secondary release system explosion is set such that all separators have a full chance to operate pneumatically. If the system were being designed today, it is possible that the explosive release method would be considered primary, but because of such a long history of satisfactory use (over 13 years), the pneumatic separator is considered primary. There is one important advantage to the pneumatic separator: The unit can be tested in configuration as late in the countdown as desired, while the explosive system cannot be tested.

TEST PROGRAM

Because of such high loads and the absolute necessity of sure operations, each arm is loaded in a test fixture to the design load. For the Saturn I, the down-load applied is 1.8×10^6 newtons (400,000 pounds) and the up-load applied is 1.1×10^6 newtons (250,000 pounds). In addition, once installed, all arms are fired as a system to check linkage release timing. Timing is critical, because the time span between first arm release and last arm release must not exceed 50 milliseconds.

LAUNCH ENVIRONMENT PROTECTION

The launch environment subjects the arm and system to not only the loads mentioned above but engine exhaust gases having a temperature of approximately 1649°C (3000°F) and a velocity of approximately Mach 3. Fortunately, this condition exists for only a few seconds at the most. For protection, the mass of materials must be large to serve as a heat sink, and sharp points must be eliminated or provided with protection. Water is also sprayed on the arms a short time after liftoff to absorb the heat and prevent heat-soaking deterioration. In addition, the rocket engines generate a sound level of approximately 170 decibels and generate a vibration level of 24g maximum at all frequencies up to 1500 Hz. All moving parts, such as the separator piston, must be designed with a natural frequency that is not in resonance with these vibrations.

DESIGN POINTS OF INTEREST

In a paper it is difficult to tie all points of interest into a narrative discussion, but there are a few points of interest in the design and operating experience of these arms that should be shared. It is not intended to explain the reason or theory behind each, but simply to provide the information in hope that it may be of use.

1. It has been our experience that an odd number of balls in the separator, such as 3 or 5, will give unsatisfactory results, while an even number will result in satisfactory operation.

2. The point loading of the balls on the separation link groove has always resulted in brinelling no matter how hard the material. Cutting a groove at the edge of the groove provides a place for material to flow. Then the only detrimental effect due to brinelling is the necessity of remachining the face of the groove after several operations.

3. Precipitation hardening steels, such as 17-4 PH, have been used very satisfactorily when a close-tolerance part, such as the main pins, was required. This allows machining to close tolerances after final heat treatment.

4. Stress risers in the form of sharp corners are to be avoided under all conditions. They will invariably result in a crack.

5. Sand castings for the base structures have proven very satisfactory, provided care is taken in inspecting for cracks, voids, and inclusions in the areas of stress - primarily around the main pins. Be prepared, however, to explain the surface cracks that are visible everywhere under magnetic particle or zyeglow inspection to the operating engineer.

6. If a heavily loaded structural component must be thicker than 5.08 or 7.62 centimeters (2 or 3 inches), forgings offer advantages in grain growth and eliminate the heat-treating difficulties of castings.

SATURN V HOLDDOWN ARMS

In the preliminary engineering stages of the Saturn V vehicle, it was apparent that to save flight weight, the number of supports should be four, rather than eight as used on the Saturn I. This, and the fact that the Saturn V would have a thrust and weight of five times the Saturn I, led the ground equipment engineers to re-examine the holddown scheme in detail. This examination reiterated the basic simplicity and load-carrying properties of the Saturn I arms. The decision was made to maintain the same basic designs for the Saturn V, as shown in Figure 10. Obviously, all components are larger, but the basic design has been followed very closely.

DETAIL DIFFERENCES

With such a large vertical down load (13.34×10^6 newtons) (3000 kips), it was decided to abandon the inclined plane and sliding wedge to achieve vertical adjustment and use shims instead. Figure 11, detail A, shows the shims between the adjustable head and the base. For the Saturn V, the spherical surface to assure zero moment transfer is incorporated into the adjustable head of the holddown rather than into the vehicle, as with the Saturn I. This saves flight weight with no real hardship on the ground design.

The shock absorber was also changed to a block of wood in the Saturn V program. During the test program, a piece of oak wood 20.32 by 14.61 by 63.50 centimeters (8 by 5.75 by 25 inches) was substituted for the bolt shock absorber to save costs, and this wood worked so well it was decided to adopt it for all operations.

The remaining paragraphs describe added systems for Saturn V.

CONTROLLED RELEASE SYSTEM

The holddown arm upper link system will restrain the Saturn V vehicle until launch commit and programmed release of holddown linkage. At launch, the upper link is pivoted rapidly away, releasing the restraining force at a rate which,

without design refinement, could create unallowable stresses in the vehicle structures. To provide a smooth, controlled release of the vehicle, control release devices were designed.

The controlled release mechanism consists basically of a bracket, which is bolted to the holddown arm base, and a draw pin, which is connected to the bracket and to the vehicle through a die. The die is fastened to the vehicle, and at launch the pin is drawn through the die for the first 15.2 centimeters (six inches) of vehicle travel. See Figure 12.

As the pin is drawn through the die at launch, the force decreases from 3.3×10^5 newtons (75,000 pounds) to zero after 15.2 centimeters (six inches) of travel.

PROTECTIVE HOOD

Due to increased exhaust plume characteristics for the Saturn V, a protective hood was designed to protect the holddown arm linkage and components inside the arm. The hood is actuated with a lanyard as the vehicle rises. See Figure 13.

Listed below are a few statistics and facts of the Saturn I and Saturn V holddown arms and their components.

ITEM	S-I	S-V
Load Carrying Capability	1.1×10^6 N	6.7×10^6 N
UP	(250,000 lb)	(1,500,000 lb)
DOWN	1.8×10^6 N	13.34×10^6 N
	(400,000 lb)	(3,000,000 lb)
Weight Complete Arm	3765 kg	20,412 kg
	8300 lb	45,000 lb
Base Material (Cast)	ASTM A27	ASTM A27
Upper Link Material	ASTM A487	4340 Electric
	Grade 70	Furnace Steel
	Casting	Forging

ITEM	S-I	S-V
Main Pin Material	17-4 PH	17-4 PH
Link Pin Material	Type 431 Cres	ASTM A36
Pneumatic Separator Tension Load Capability	22,240 N (5000 lb)	222,411 N (50,000 lb)
Pin Lubricant	25:1 Halocarbon and Molykote (Used because of LOX compatibility requirement.)	
Separator Lubricant	Dow-Corning Silicone DC-510-500-C-S	

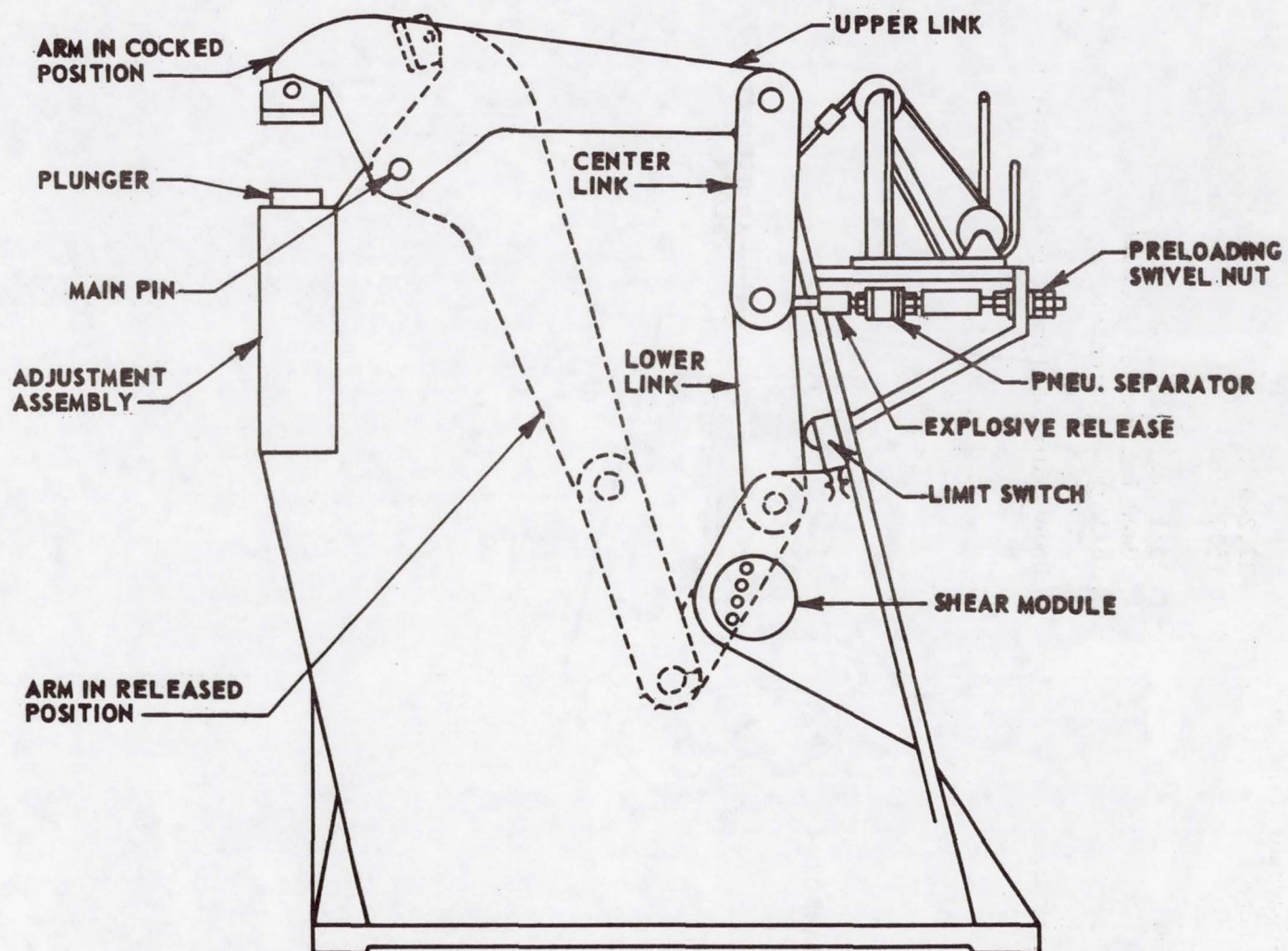


Figure 1. Holddown Arm Assembly

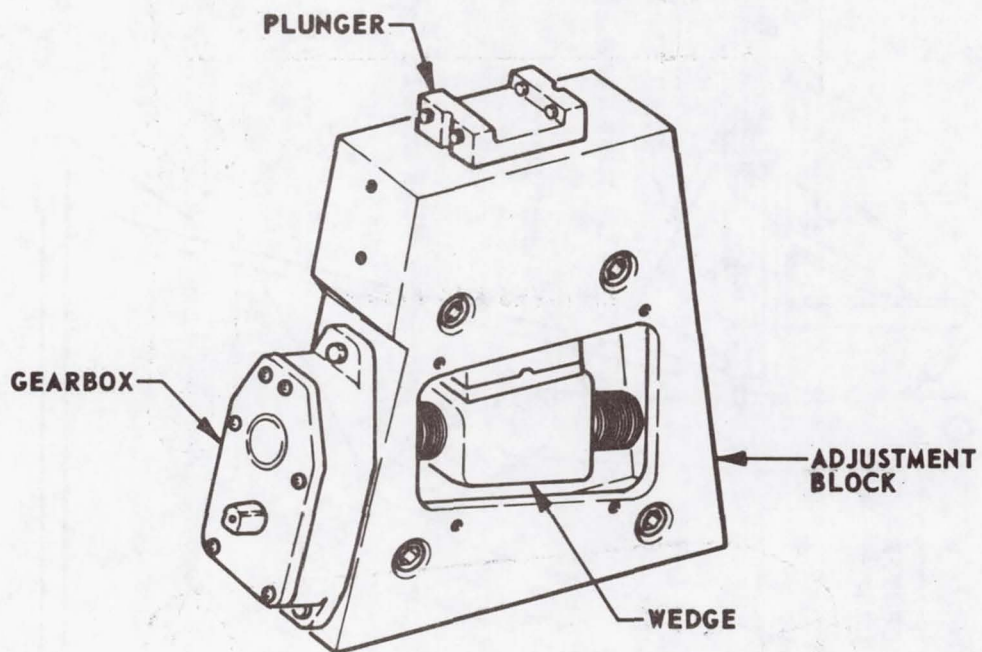
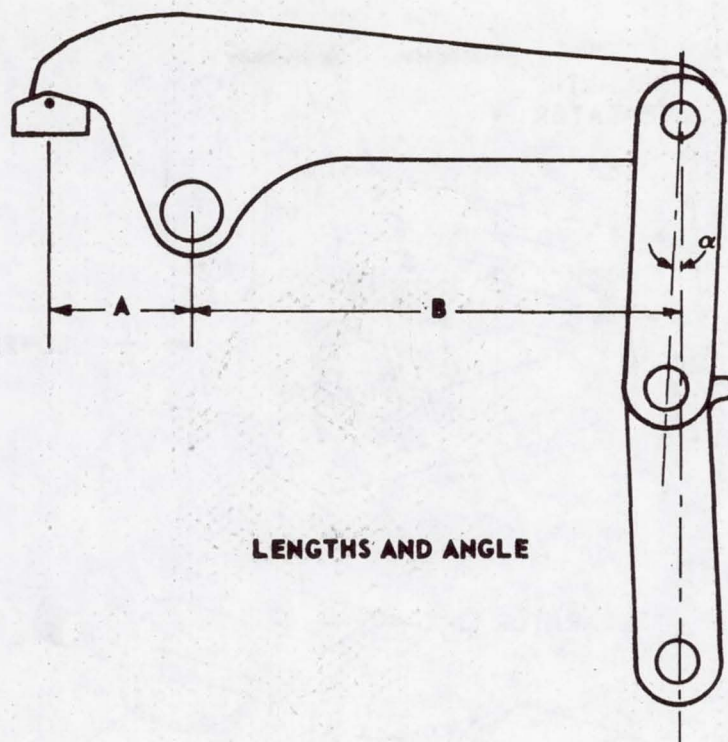
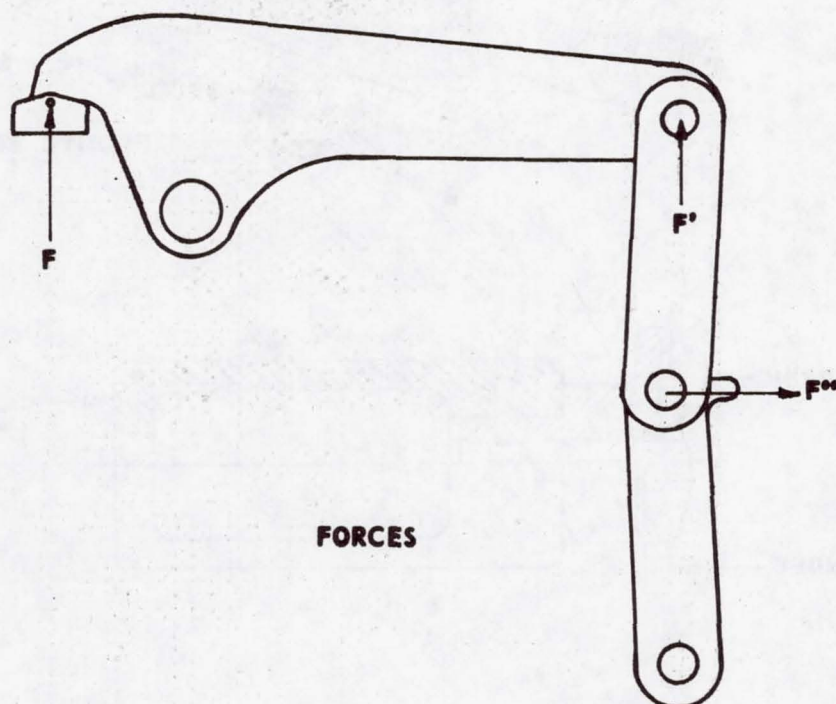


Figure 2. Adjustment Assembly



LENGTHS AND ANGLE



FORCES

Figure 3. Load Diagram

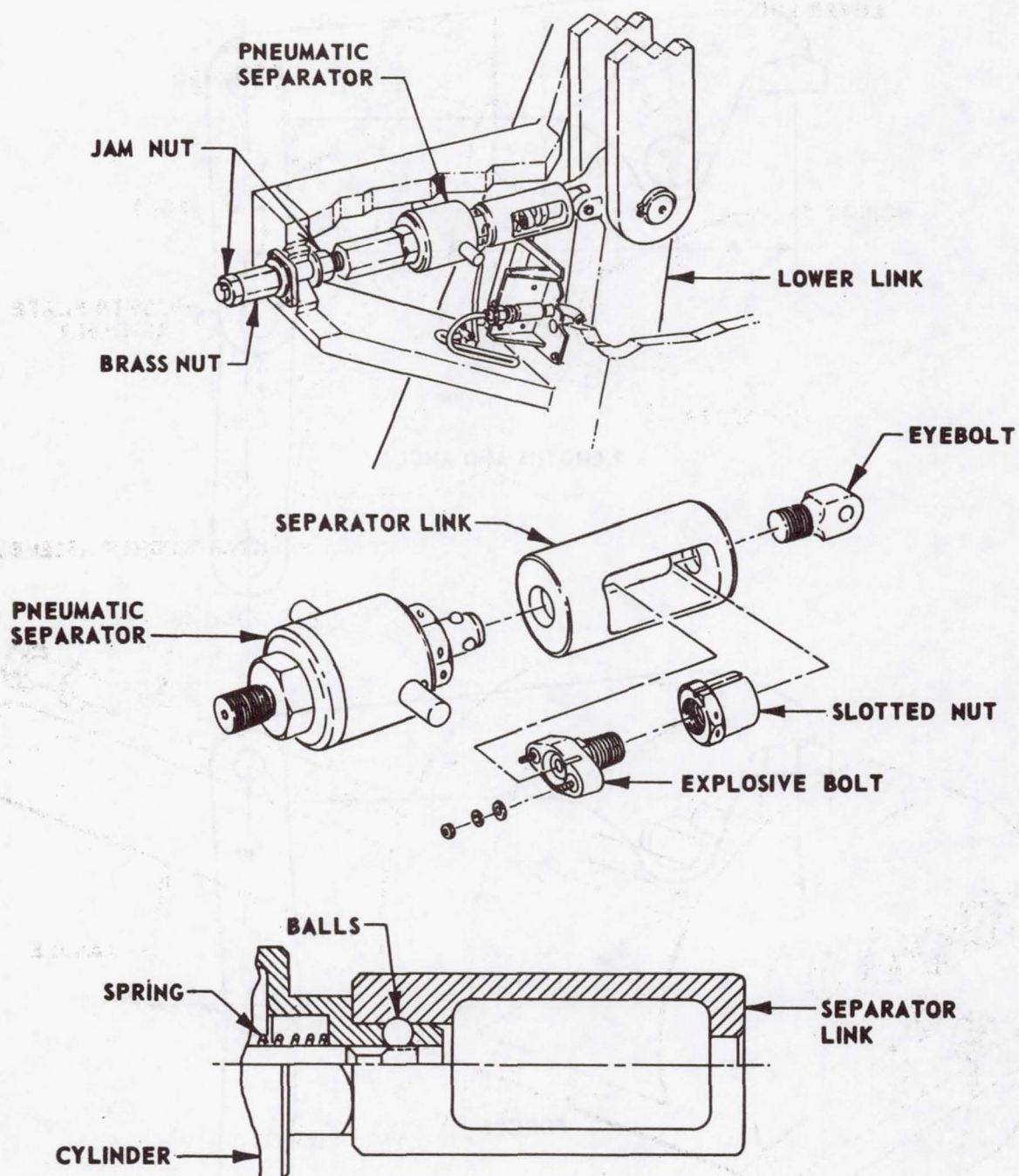


Figure 4. Pneumatic Separator Assembly

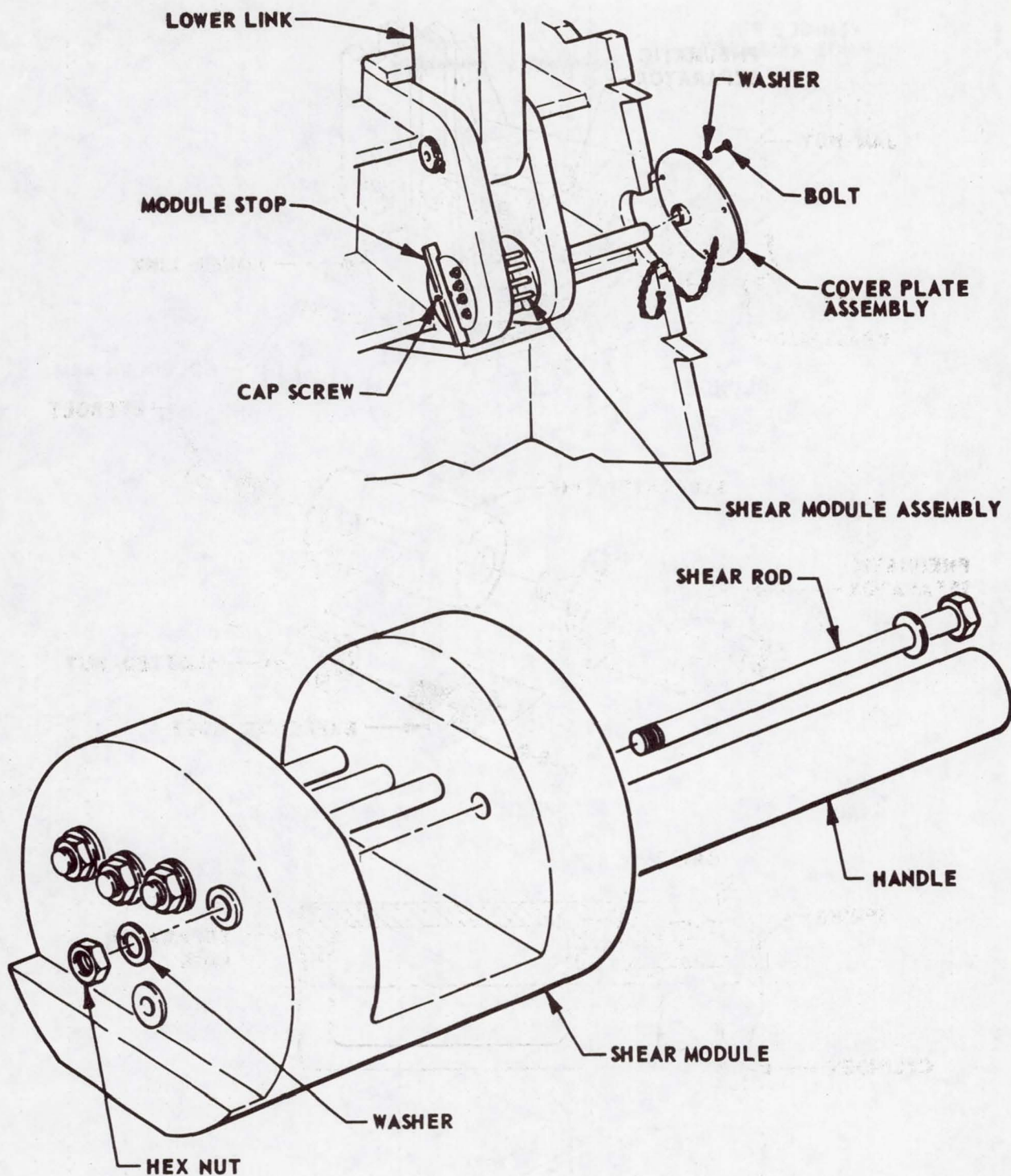


Figure 5. Shear Module Assembly

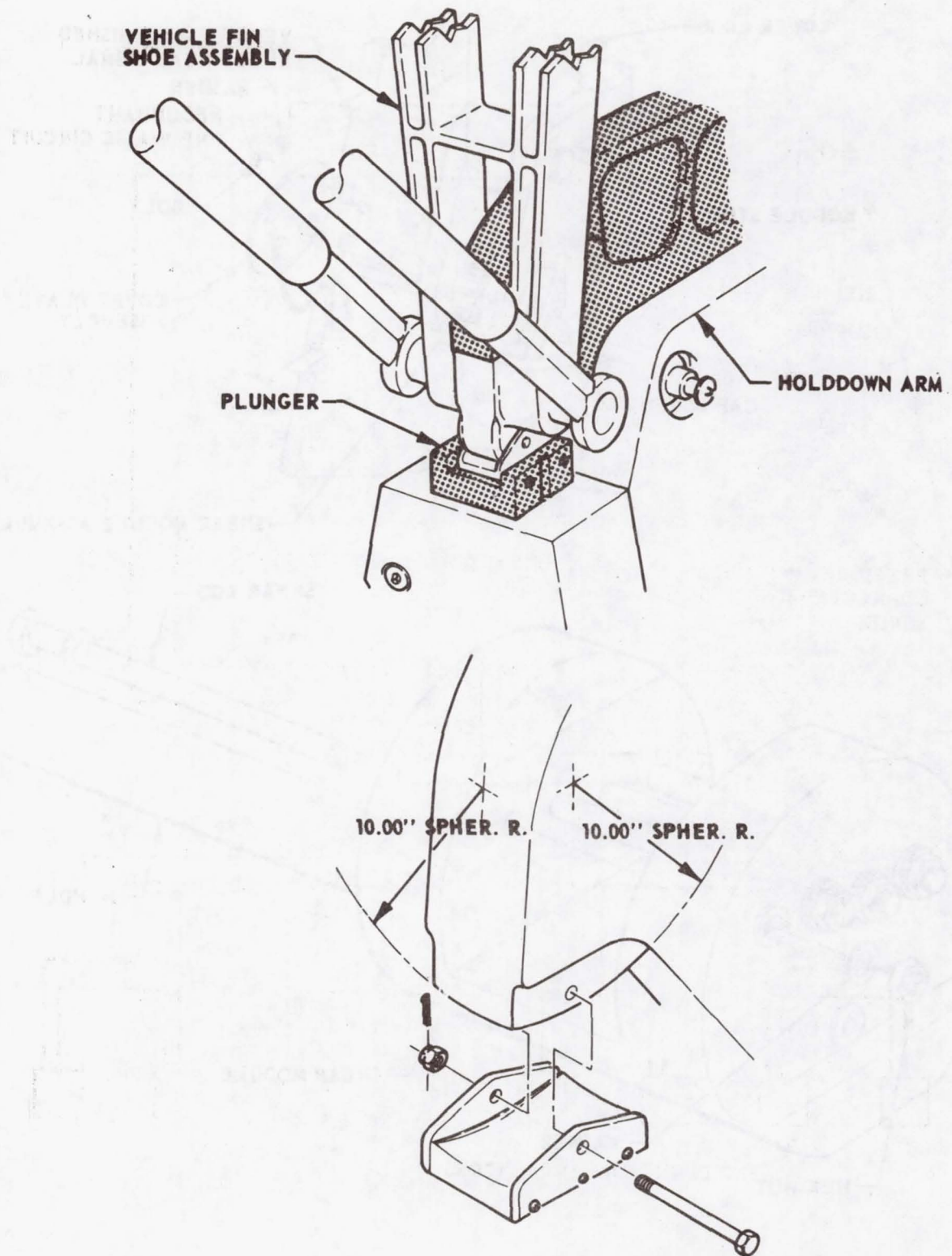


Figure 6. Spherical Surfaces at Arm Pad

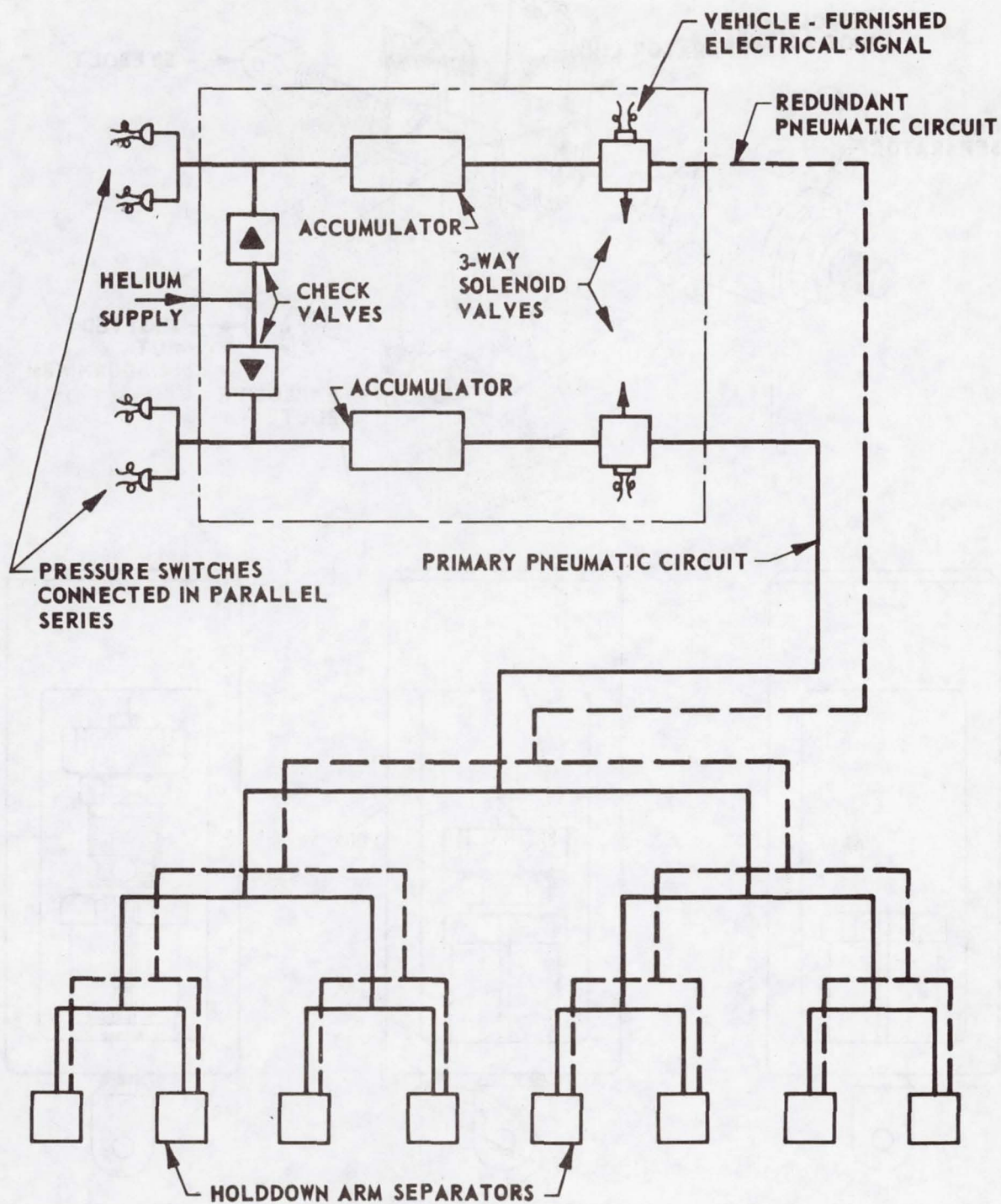
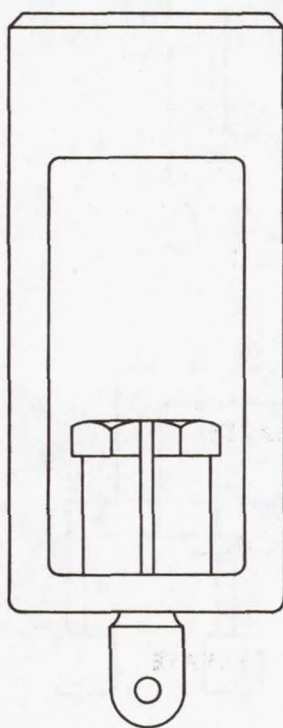
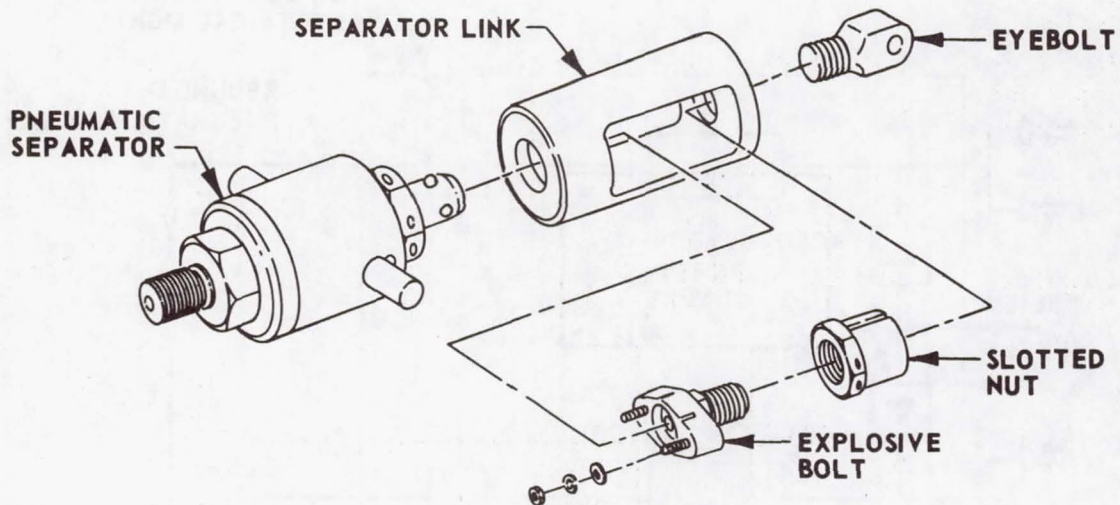
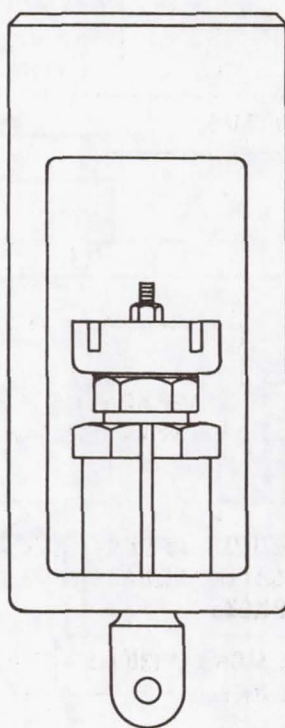


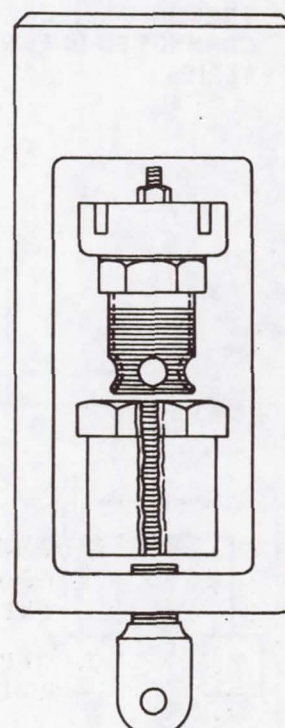
Figure 7. Pneumatic System Schematic



UNARMED

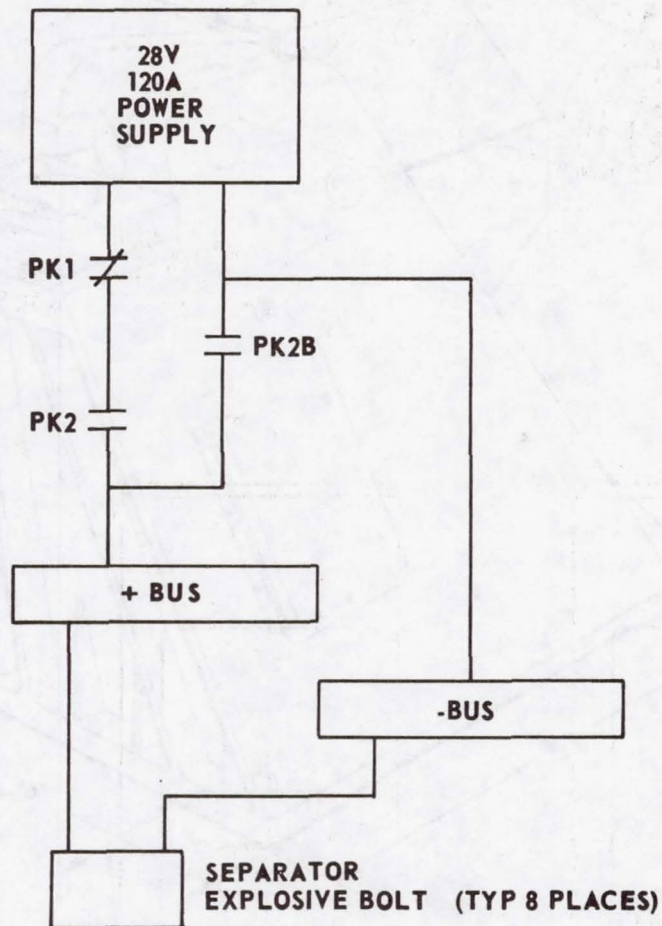


ARMED READY FOR RELEASE



AFTER DETONATION

Figure 8. Pneumatic Separator Explosive Release



1. CONTACTS SHOWN JUST AFTER VEHICLE RELEASE SIGNAL. VEHICLE - FURNISHED RELEASE SIGNAL CLOSSES PK1 AND OPENS PK2B.
2. TIMER FURNISHES SIGNAL 130 MS AFTER PNEUMATIC RELEASE SIGNAL TO CLOSE PK2.

Figure 9. Explosive Release Systems Schematic

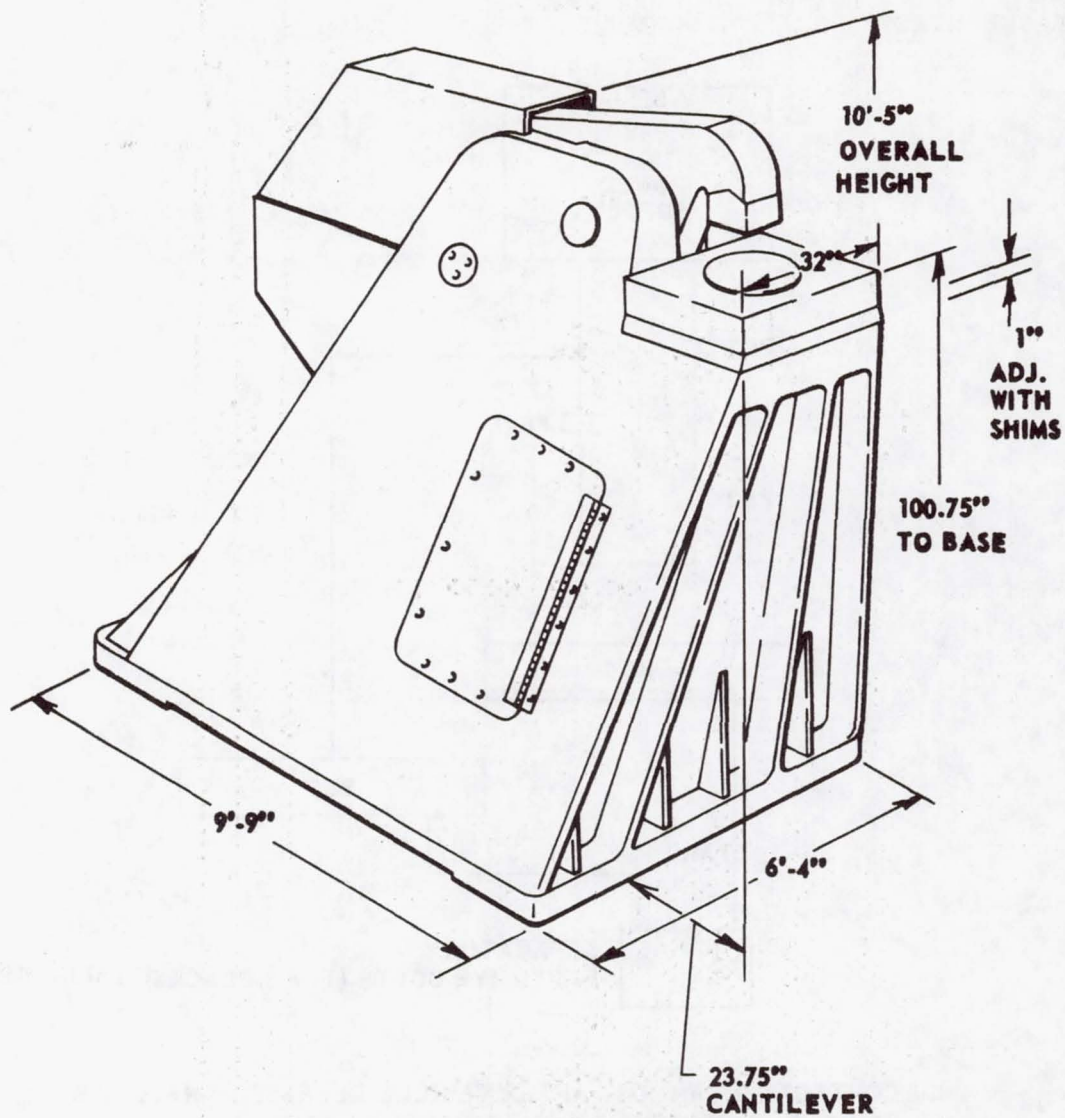


Figure 10. Saturn V Holddown Arm

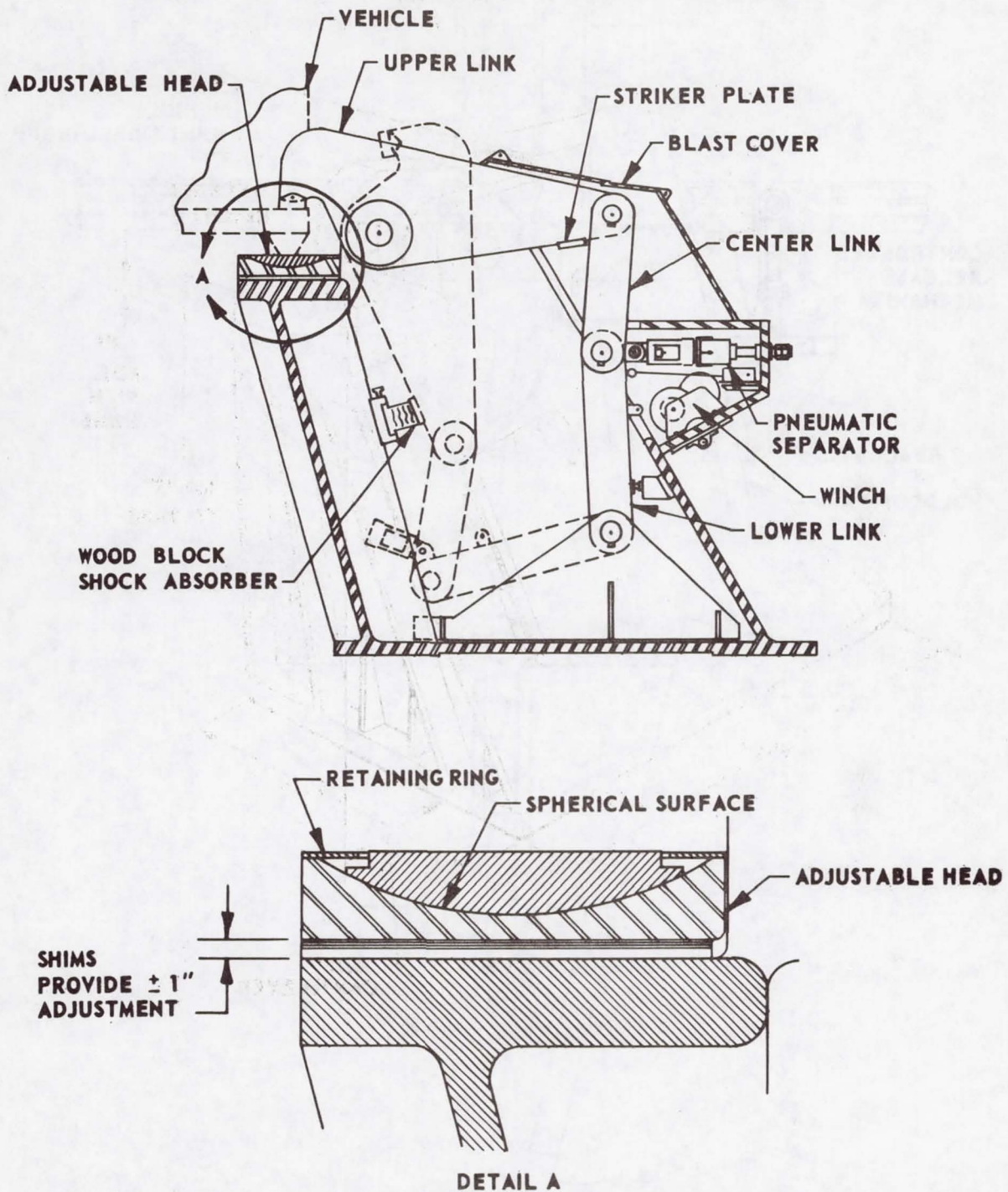


Figure 11. Holddown Arm Features

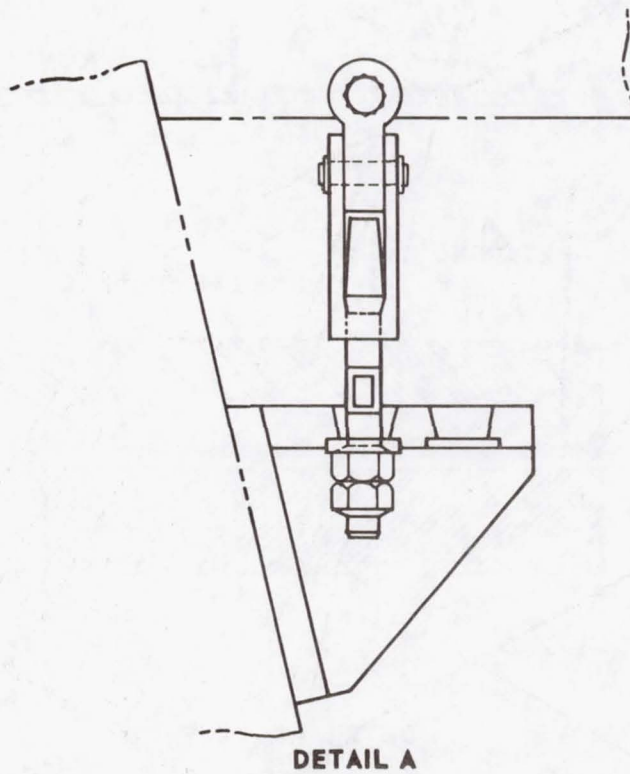
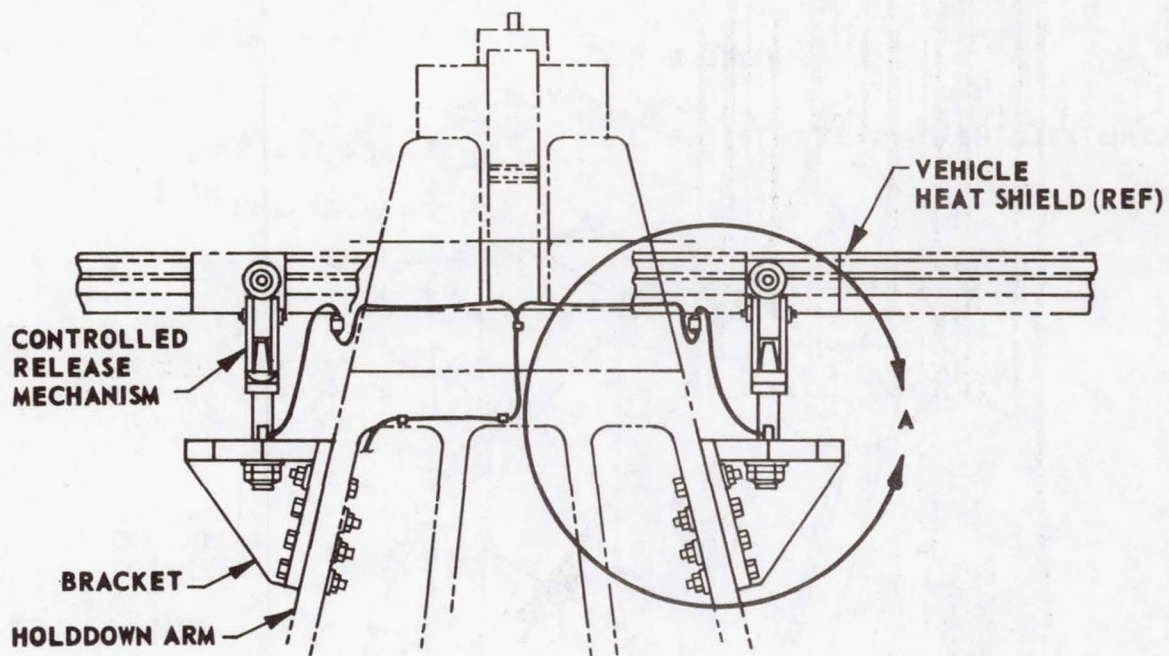


Figure 12. Controlled Release Mechanism ,

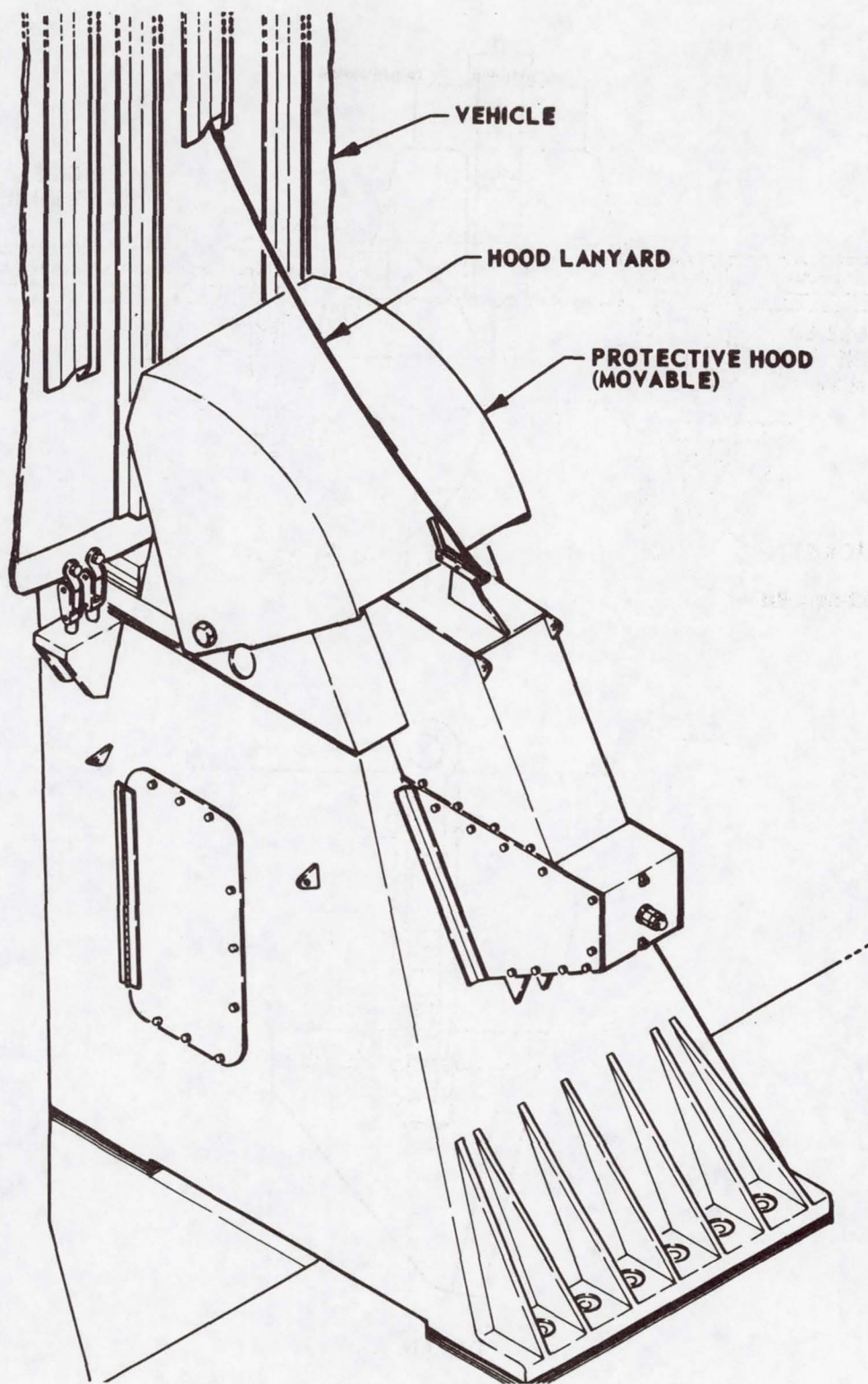


Figure 13. Protective Hood

24. CRAWLER TRANSPORTER

STEERING AND JEL SYSTEMS

By Virgil Leon Davis

John F. Kennedy Space Center

SUMMARY

A vital element to Launch Complex 39 and the Kennedy Space Center (KSC) mobile transfer operation is a culmination of many unique engineering mechanisms known as the Crawler Transporter. The Transporter is a mighty tortoise weighing 2.8 million kilograms (6.3 million pounds) used to lift a 5.7-million-kilogram (12.6-million-pound) combination of Mobile Launcher and space vehicle, transfer this load approximately 5.6 kilometers (3.5 miles) from its point of assembly, negotiate curves of 152-meter (500-foot) mean radius, climb a 5-percent grade while maintaining the 122-meter (400-foot) structure in a vertical position within 10 minutes of arc, and smoothly position this huge structure to within ± 5.1 centimeters (± 2 inches) on support pedestals at the launch pad.

INTRODUCTION

There are some unique mechanisms in the hydraulic jacking, equalization, leveling (JEL), and steering systems required by the Crawler to perform its mission. Numerous problems associated with these mechanisms have been overcome in a program requiring fabrication of operational equipment while proceeding with a developmental process. This was necessary since complete data did not exist in some phases of the design prior to construction. Besides, such an independent transporter system had never been built, and today only two such systems are in existence.

PRELIMINARY DESIGN CONSIDERATIONS

The primary impetus behind the selection of the Crawler Transporter as the prime mover during the development of facilities for the Saturn V space vehicle in 1962 was the fabrication of a similar device--a 76.2-meter (250-foot) high, 8.16-million-kilogram (18-million-pound) stripping shovel. Crawler excavators were tried and proven methods of handling large loads, some similar in magnitude to those required for the Apollo-Saturn V Program. After studying various transfer modes in detail, it was concluded that a crawler-mounted transporter would be the most advantageous method of turning the mobile concept into workable hardware.

The feasibility study of the crawler transfer concept basically proposed a crawler-mounted transporter and launcher pad in one unit. It was suggested that after the transporter and launcher pad were placed on fixed mounts, the leveling cylinder pistons could be raised, the steering cylinders and struts could be removed, and the trucks could be walked out under power. Such an undertaking involved problems associated with heavy equipment movement, as well

as problems in repositioning the crawlers under the transporter platform. Early in the analysis it became evident that there were considerable advantages to removing the crawlers from the launch platform and providing an independent crawler transporter structure.

This arrangement (see Figure 1) allowed the trucks, together with self-contained power-generating, hydraulic-leveling, and steering equipment mounted in a transporter structure, to act as an independent unit that could easily be removed from the blast area during launch. An independent crawler transporter could also be favorably positioned under the center of gravity of the Mobile Launcher platform to enable more even load distribution on the crawler trucks. Additionally, fewer transporter units were needed since one could be on the move to another area while its deposited load was undergoing testing or check-out.

To enable the Crawler Transporter to function in its unique role at Kennedy Space Center, there were many changes required to evolve from a stripping shovel prime mover concept to an independent transporter mode. Large stripping shovels were constructed on site in an excavated hole; they removed the overburden (earth) in front of them and moved over terrain smoothed by bulldozers. Behind them were power cables plugged into extended substations. If a support cylinder leaked, the hydraulic fluid was collected (in a saucer surrounding the cylinder) and pumped back into its own reservoir. If a shoe broke or some similar problem occurred, the shovels kept going until they were forced into a repair mode. This operational philosophy was not amenable to reliable fulfillment of strict launch schedules. Besides, the leveling capability of stripping shovels was designed primarily to prevent the machine from turning over and was not adaptable for the critical tolerance level required to transport a 36-story rocket while its topmost part remains within ± 5 minutes of arc, or within the dimensions of a basketball. It was essential to maintain the transported load in a level plane and to reduce acceleration, torque, and jarring forces to a minimum. Reliability of the hydraulic system and operational integrity of the equipment were absolute requirements and major design challenges. With these considerations in mind, KSC adopted the transporter configuration depicted in Figure 2. If a critical control component should fail, there would be a backup system immediately available. In the event of a serious malfunction, such as a hydraulic line rupture, the load would be kept from becoming unbalanced by automatically locking (or securing) the corner cylinders. These cylinders, in groups of four, were designed such that if one should fail, the 5.7-million-kilogram (12.6-million-pound) load could still be safely transported.

A contract for two transporters was awarded in March 1963. The procurement plan called for assembly of the first Crawler Transporter by late 1964, followed by operational testing with resultant changes or modifications to be complete by March 1965. Both Transporters became operational early in 1966. (Their final configuration is shown in Figure 3.)

Let us briefly look at a few of those unique mechanisms and discuss the design evolution in relationship to stripping shovels used in the early 1960's as well as problems that were associated with the fabrication/development process.

JEL SUSPENSION SYSTEM

Previously, chassis support of large crawler excavators was dependent upon the utilization of a single, large diameter, hydraulic cylinder (see Figure 1). In order to preclude damage to transported loads in the event of a single cylinder failure, a clustering of cylinders was designed for the transporter suspension system. A single cylinder would not only have to provide proper leveling, but it would have to resist side loads introduced by wind as well as propel and steering conditions. Horizontal forces acting on a fixed vertical cylinder produce bending, and, if forces are of significant magnitude, they will cause hydraulic oil leakage, galling, and possible failure.

To prevent introducing shearing forces into the hydraulic actuators, a unique arrangement was designed for the four double-track truck suspension system. In the center of each truck is a 1.22-meter (4-foot) diameter guide tube that slides in a spherical bearing (see Figure 4). Clustered around this guide tube are four linear single-acting hydraulic cylinders with a 508-millimeter (20-inch) bore and an extensible stroke of 2006 millimeters (79 inches). The cylinder assembly on which the weight of the transported load rests is designed to operate at a normal pressure of 20.7 million newtons/meter² (3000 psig), an emergency pressure of 33.1 million newtons/meter² (4800 psig), and to withstand 41.2 million newtons/meter² (6000 psig) proof pressure and 62.3 million newtons/meter² (9000 psig) burst pressure. The support cylinders are attached to the chassis and trucks with spherical ball bushings to assure that only vertical loads are transmitted.

Shear forces from propel, steering, or wind loads are transmitted through the guide tube and into the chassis through a spherical bearing housed on the trucks. This not only removes horizontal loads from the cylinders but provides a pivot for the truck and permits vertical movement of the chassis in relation to the crawler truck. The guide tube fits into the cylindrical inside surface of a bronze ball bushing (see Figure 5). The outside surface of the bushing is a spherical section that mates with the inside surface of a concentric bushing container. This assembly enables limited tilt of the trucks in any combination of lateral or longitudinal motion. Changes in the vertical position of the chassis and rotational positions of the crawlers are supplied to the steering and JEL servo systems by transducers mounted at the bottom of the guide tube assembly.

The extremely low vertical friction allowed by this mechanism has provided for smooth leveling and jacking operations. This unique grouping has resisted large wind loads, having carried a Saturn V test vehicle on board a mobile launcher 5.63 kilometers (3.5 miles) at 0.04 meter/second (1 mile/hour) in winds as high as 30.1 meters/second (68 miles/hour) without incident. After more than eight years of operation, there has been no hydraulic leakage from these cylinders, and none have even had to be removed or partially disassembled.

STEERING THE TRANSPORTERS

Positioning the Mobile Launcher on its support pedestals requires precise maneuverability since alignment must be within +50.8 millimeters (+2

inches). Not only is this no easy task, but special considerations had to be taken just to enable the negotiation of a 152-meter (500-foot) radius curve. Since the crawler trucks are located on 27.4-meter (90-foot) centers, there is an angular position error between the inside and outside crawler trucks during great circle steering. Experience with large shovels propelling over surfaces other than coal, upon which they are usually operated, revealed that large horizontal loads were applied to their trucks. This led to a reevaluation of the preliminary concept (depicted in Figure 1) of using a single-acting cylinder to pivot each truck about its center. The front and rear end trucks were connected by a large tie rod that pulled one truck while the opposite truck was being pushed by one single-acting steering cylinder. Since an independent transporter chassis would be much less rigid than that required for a permanently attached platform, scuffing loads introduced in skidding a crawler truck through a one-degree steering error could introduce stress levels high enough to cause severe chassis distortion. A mechanical linkage could have been designed to give the desired correction, but due to maintenance, cost, and weight considerations, it was decided to provide an Ackermann correction in the electronic servo system. Independent push-pull action was incorporated into each corner by using large double-acting hydraulic cylinders. For redundancy, these cylinders were mounted in pairs at each end of a crawler truck. These two mechanisms (electronic Ackermann correction and double-acting cylinders) allow the four trucks to be steered independently around corners in a great circle mode as well as diagonally in a crab mode.

The possible consequences of stresses introduced by the truck/road contact surface (46.5 meters^2) (500 feet^2) were areas of major concern and consequently were thoroughly investigated and analyzed. The chassis structure was designed to resist scuffing loads of 2.3-million kilograms (500,000-pounds) over those expected. A scale (1/8) model of the Crawler Transporter chassis was constructed to determine and analyze projected loads. A scale (3/8) model of the steering arm assembly (see Figure 4) was assembled and tested. A scale (3/8) model of the Crawler shoes was tested to destruction. Results of the model analyses were used to formulate design modifications to improve the load carrying capability of these structures. Since stresses are at a maximum during steering (sliding the trucks across the road surface), many tests were performed in an effort to determine a suitable, low friction, resilient roadbed. Model tests were not easy to simulate; therefore, verification was accomplished after construction. Tests on a prepared surface, sand, macadam, crushed granite, and river rock led to the selection of river rock as the minimum frictional surface for utilization on the Crawlerway.

Operational experience with the transporter disclosed that, even with a reduced frictional surface, large pressures were exerted in the hydraulic steering system. Since both corner cylinders were needed for proper steering, the required redundancy was marginal at best under full load. The loss of a cylinder under these conditions could possibly result in a launch scrub. In order to adequately provide redundancy and to increase the capabilities of the

system, two steering cylinders were added to each truck. The new cylinders work perpendicular to and are identical to the original ones. They are used in pairs extending from steering brackets mounted below the Crawler Transporter chassis to an auxiliary steering arm (see Figure 4) welded to the inside frame of each truck.

The uprated steering system was not implemented until 1969. Before proceeding with the modification, a sound engineering basis was developed through a detailed control servo system analysis, through mathematical stress analysis, and through a model evaluation program. The scale (1/8) model originally used for chassis design verification was modified and used to evaluate structural response to loads introduced by the uprated steering system. An analysis showed that the proposed hydraulically activated electro-mechanical steering network was inherently stable; testing and operations have verified this many times.

In addition to structural changes, the modification included 16 four-way two-position pilot-operated valves. In the disabled condition, these isolate selected cylinders from the hydraulic pumps. They also allow the double-acting cylinder to "float" by permitting trapped hydraulic fluid to flow back and forth from a compressed chamber into an expanded chamber. The system now has the capability of operating with one or both pump sets and with two, three, or four operating steering cylinders per corner--thus providing complete redundancy with only a small sacrifice in steering rate.

JEL SYSTEM STABILITY

Conventional leveling of large stripping shovels was accomplished by adjusting the relative height of diagonally opposite corners by sensing the height variation with crude mercury-level switches or by using large heavy pendulums to sense level changes. These mechanisms were centrally located and mounted on rigid structures. They were not considered feasible for use on an independent, flexible structure due to tighter level requirements and possible chassis deflection. A manometer-type leveling system extending across diagonal corners was proposed, and a 39.6-meter (130-foot) full-scale experimental mockup was made to determine the dynamic characteristics of acceleration forces inherent in such a system. Theoretical analyses confirmed by test results demonstrated that a closed manometer system equipped with differential pressure transducers was a feasible level sensor for Crawler Transporter applications.

Although diagonal axes may be level, they may also lie in separate planes. Design specifications required that no support point be more than 50.8 millimeters (2 inches) out of plane. Large shovels, when propelling, would connect two adjacent corners together so that the loads would be equal on one end. An off-centered load with such a three-point equalization system could set up large twisting or warping moments in the chassis. Therefore, it was proposed to use a hydraulic-equalizing system, causing the sum of corner loads on one diagonal to be equal to the corner load sum of the other diagonal.

Initial test runs during 1965 resulted in over-reaction and instability in the hydraulic servo system. A stability study and computer analysis revealed that the original pressure loop criteria had not taken into account (1) varying oil compressibility constants caused by cylinder extension nor (2) differences in the spring constant incurred by mass changes between loaded and unloaded configurations.

The problem was corrected by augmenting two additional manometers across the front and rear corners perpendicular to the travel direction. Unloaded moves are performed using only the manometer system for leveling and equalization control. During loaded moves, hydraulic-pressure transducers located at each corner are used to control platform equalization. With the Mobile Launcher on board, the manometer equalization system provides only out-of-limit warnings and shutdowns. Leveling is accomplished at all times by the mercury manometer mechanism.

CONCLUDING REMARKS

In order to meet schedule requirements of a facility of such complexity and unprecedented size, it was necessary for ground equipment design to proceed in parallel with vehicular design. The evolution from concept to operational hardware of such unique equipment was not strictly based on a theoretical approach but on reasonable criteria developed through actual experience with past design and a periodic update resulting from actual and model test results. The Crawler Transporter is an exemplification of this methodology. The end result (see Figure 6) speaks for itself. Theoretical evaluations were supplemented by model tests and these in turn by actual tests of the physical hardware--each stage of the development leading to an improved design.

Although the Crawler Transporter was designed specifically for the Apollo Program, it has supported the Skylab Program without modification, even though the Mobile Launcher pedestal addition for the Skylab 1B configuration caused a weight increase. The adaptability of the independent Crawler Transporter is evident as it has supported various platform configurations for the Apollo and Skylab Programs as well as the giant steel Mobile Service Structure (see Figure 7). The Crawler Transporters will not require modification to transport the Space Shuttle on its Mobile Launcher Platform (see Figure 8). Once again, our Space Program's success will be highly dependent on a tried and proven "mighty tortoise"!

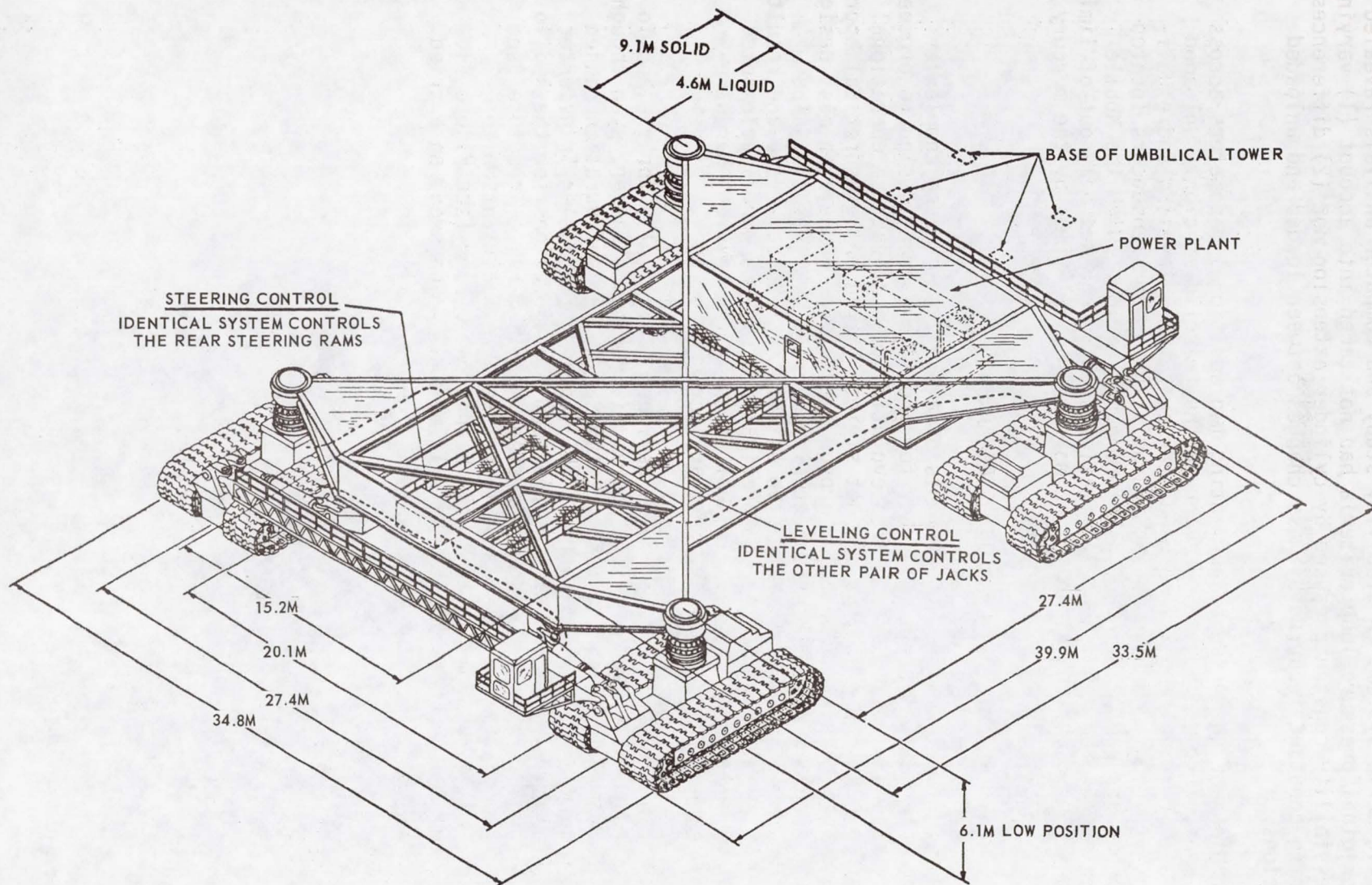


Figure 1. Preliminary Concept: Independent Crawler Transporter

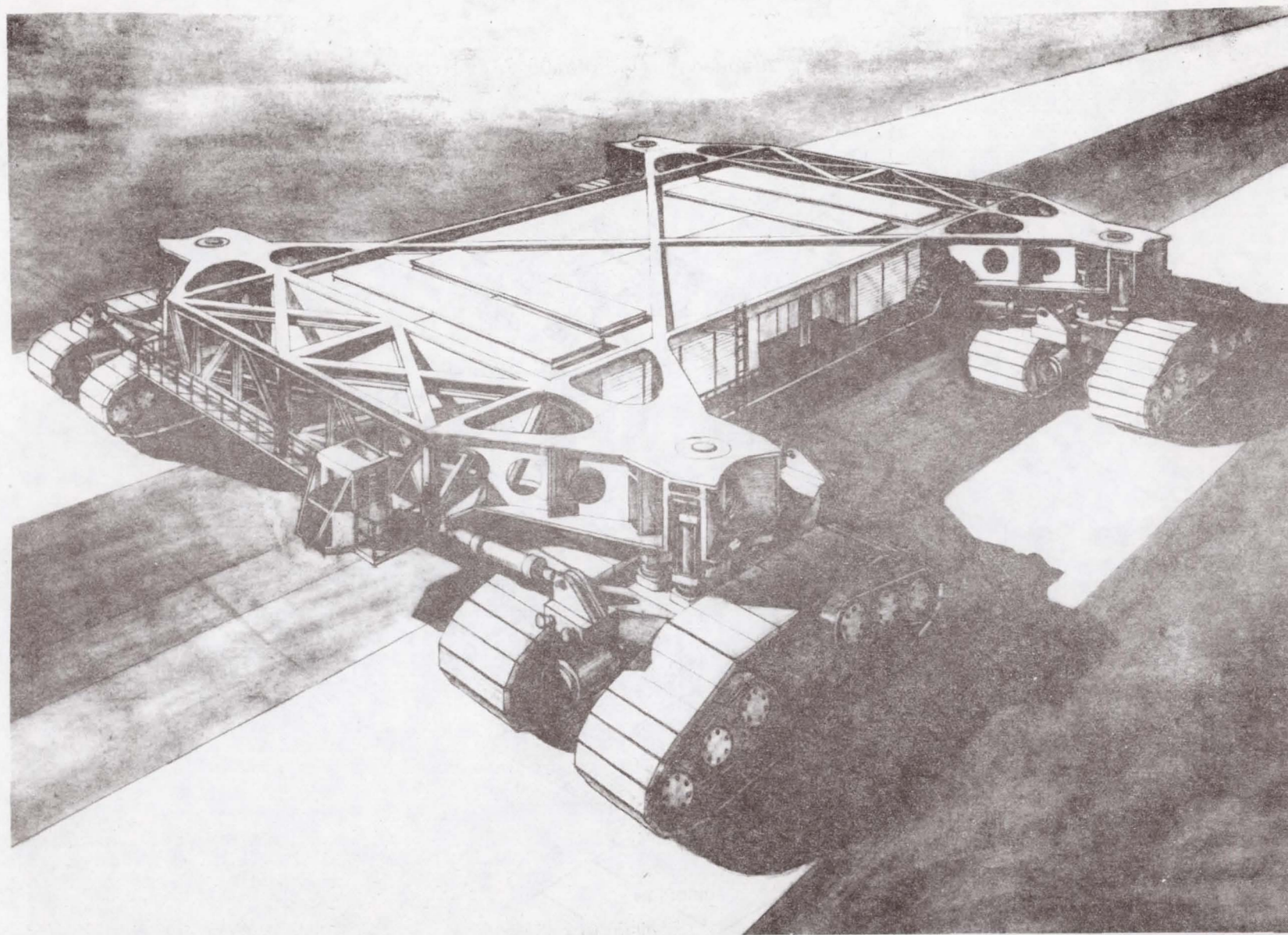


Figure 2. Approved Concept: Crawler Transporter

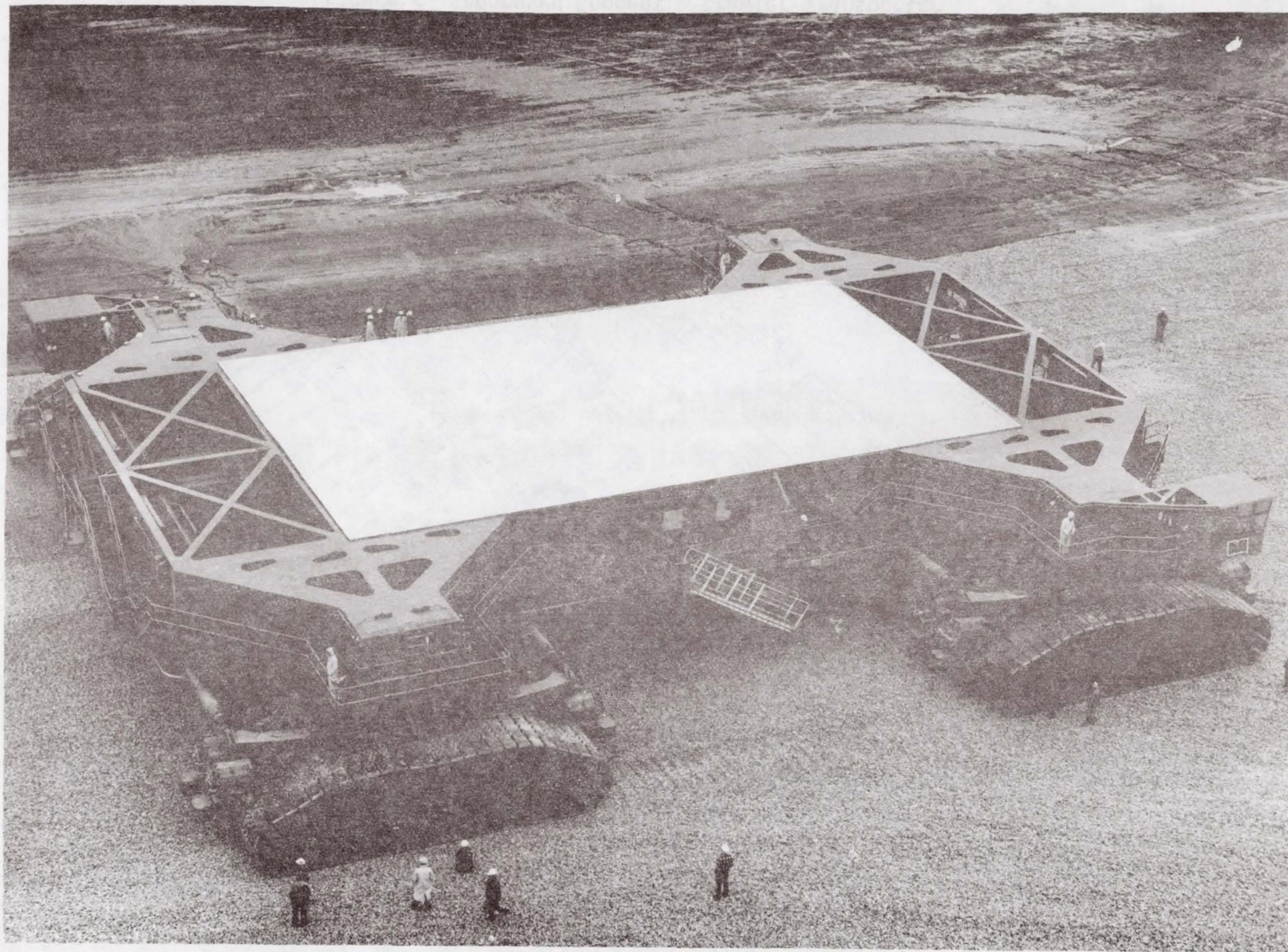


Figure 3. Crawler Transporter

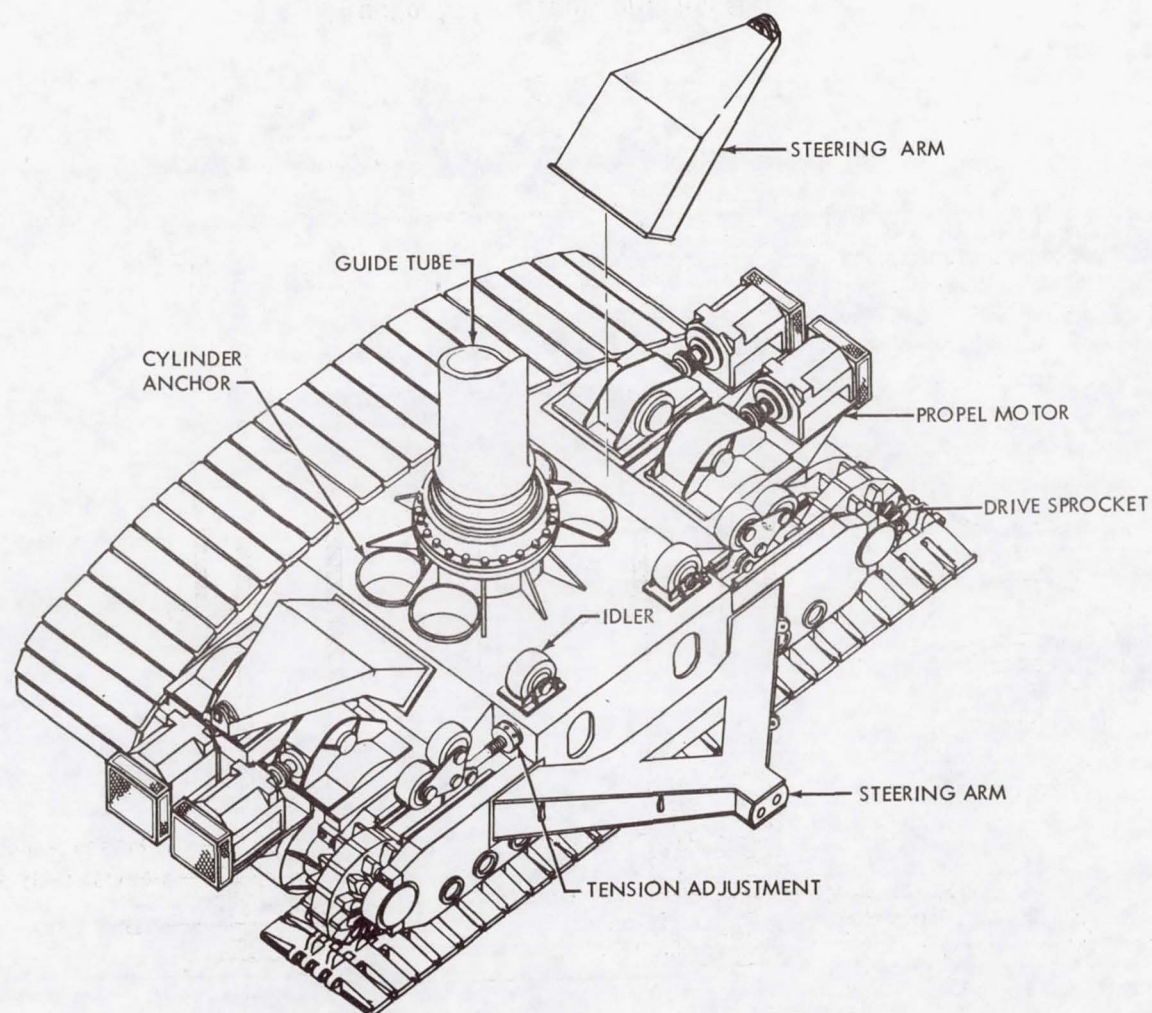


Figure 4. Crawler Truck Assembly

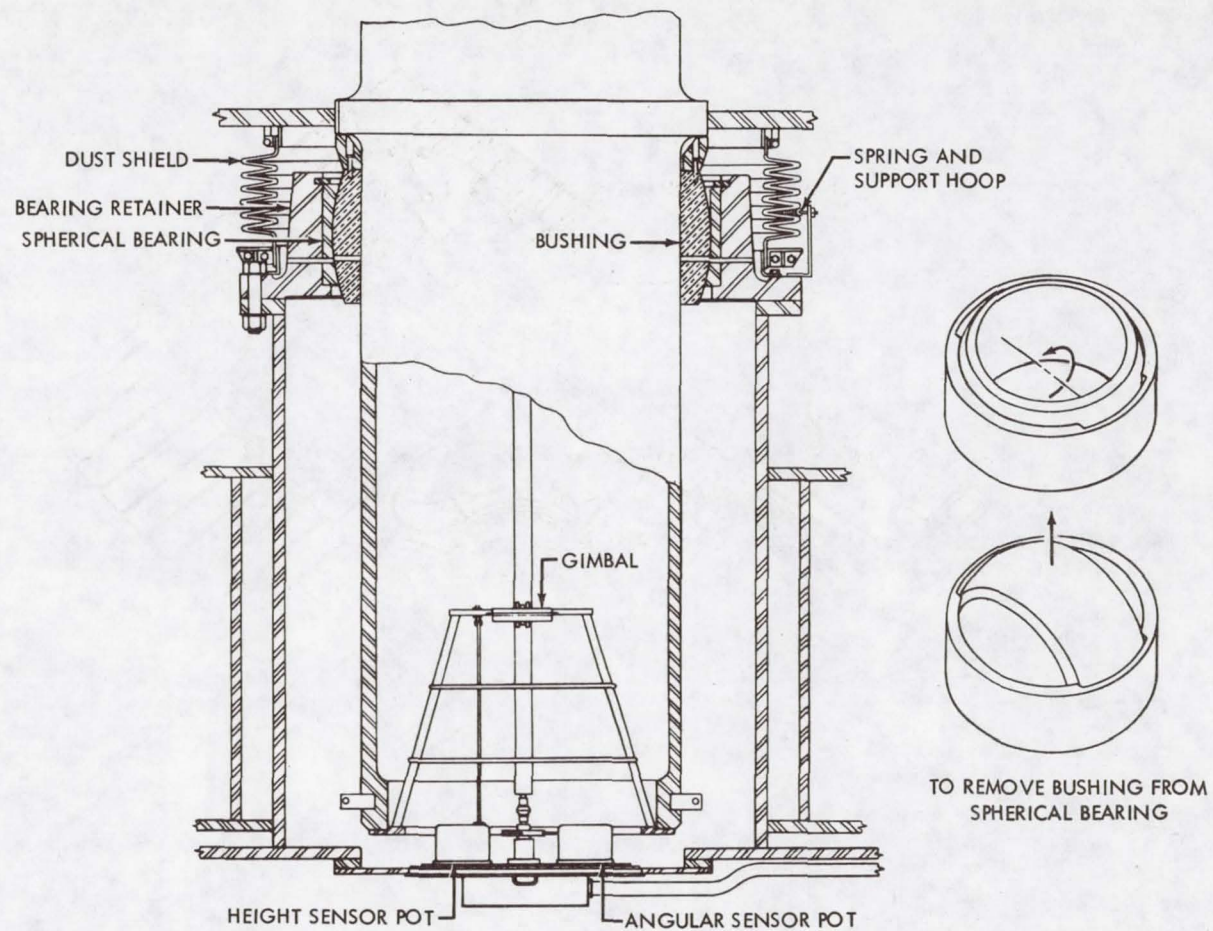


Figure 5. Guide Tube Assembly

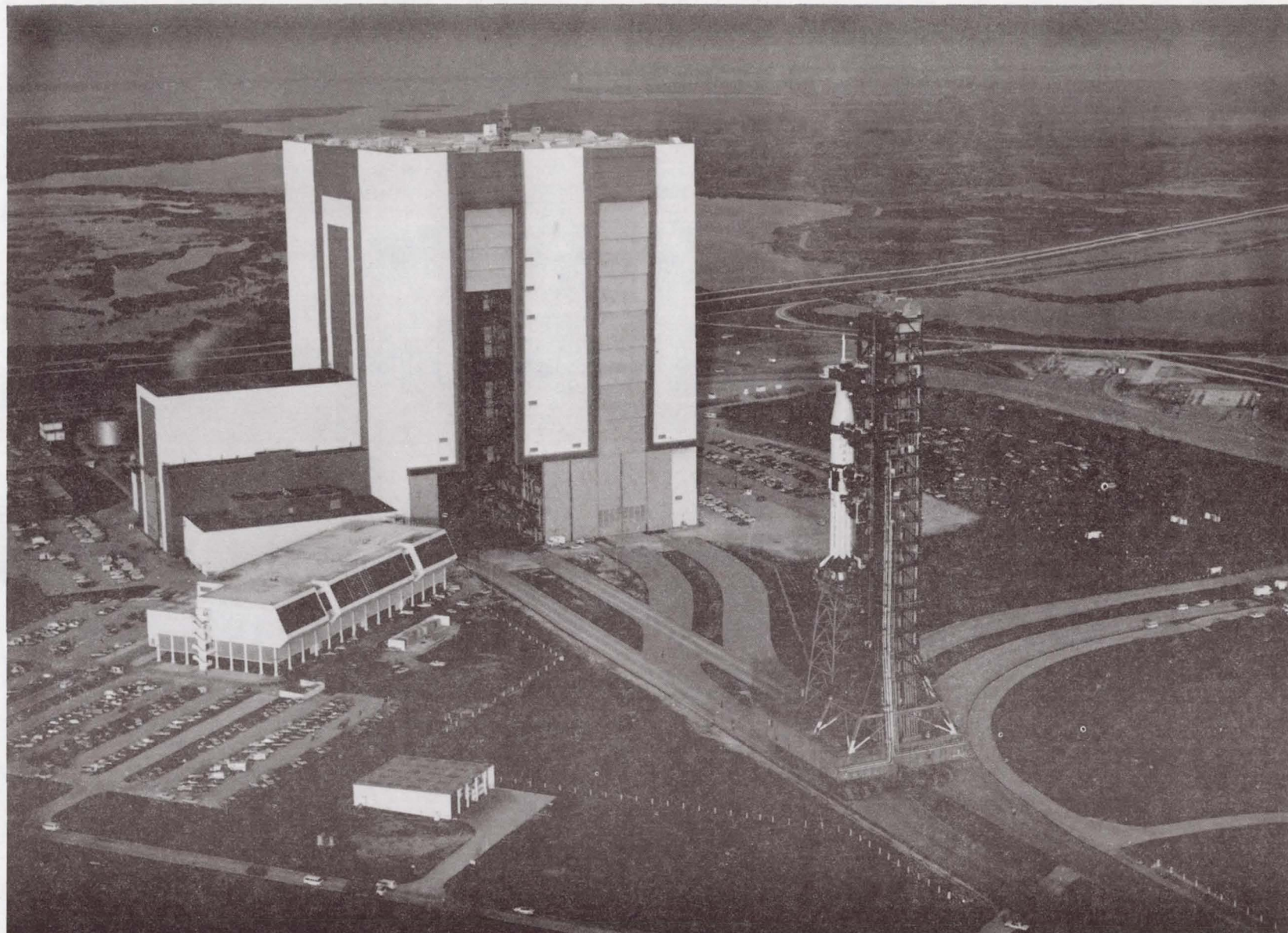


Figure 6. Crawler Transporter Moving Mobile Launcher (Adapted to Skylab II Configuration) from Vehicle Assembly Building

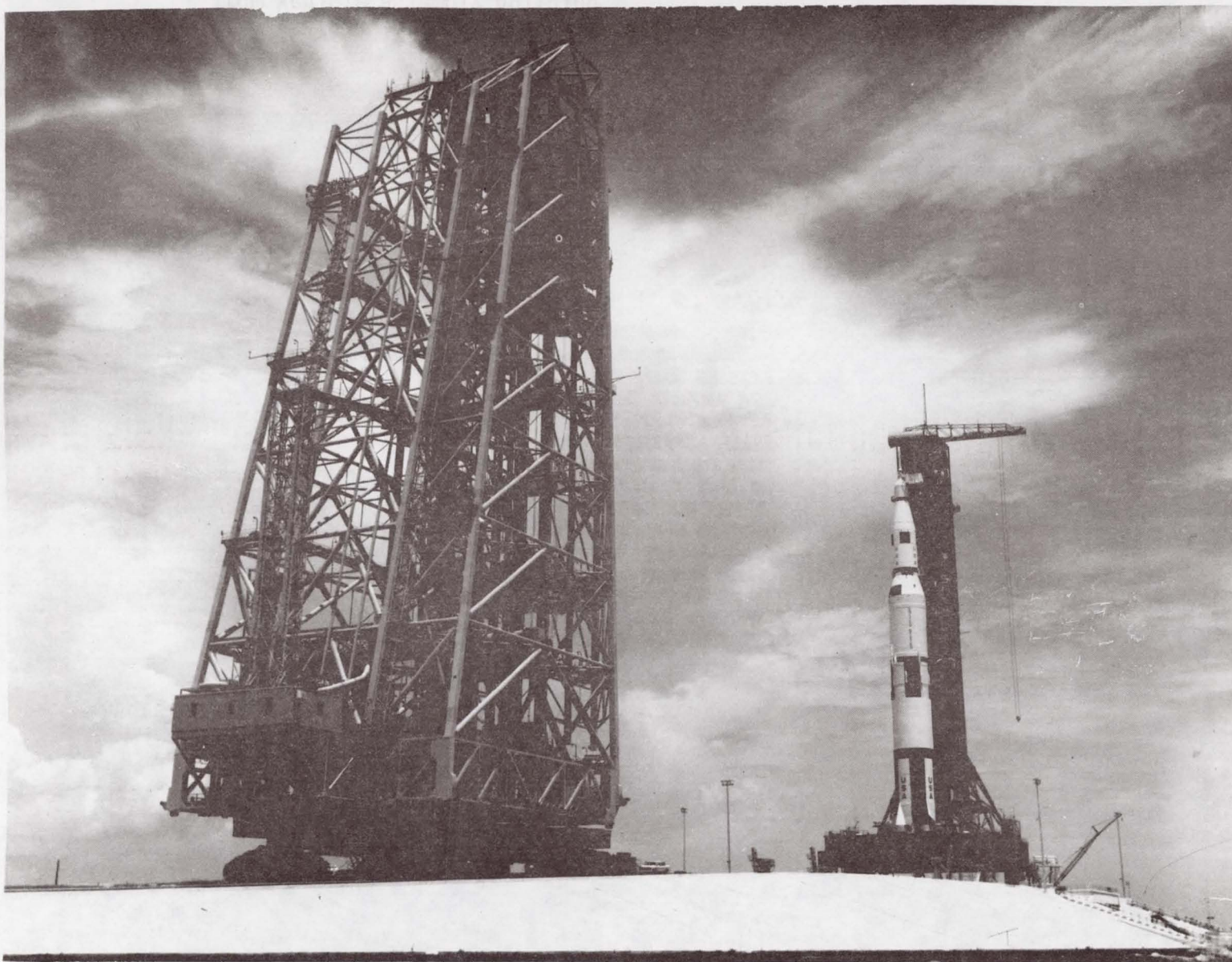


Figure 7. Crawler Transporter Carrying Mobile Service Structure Up Five Percent Slope to Saturn V Mobile Launcher

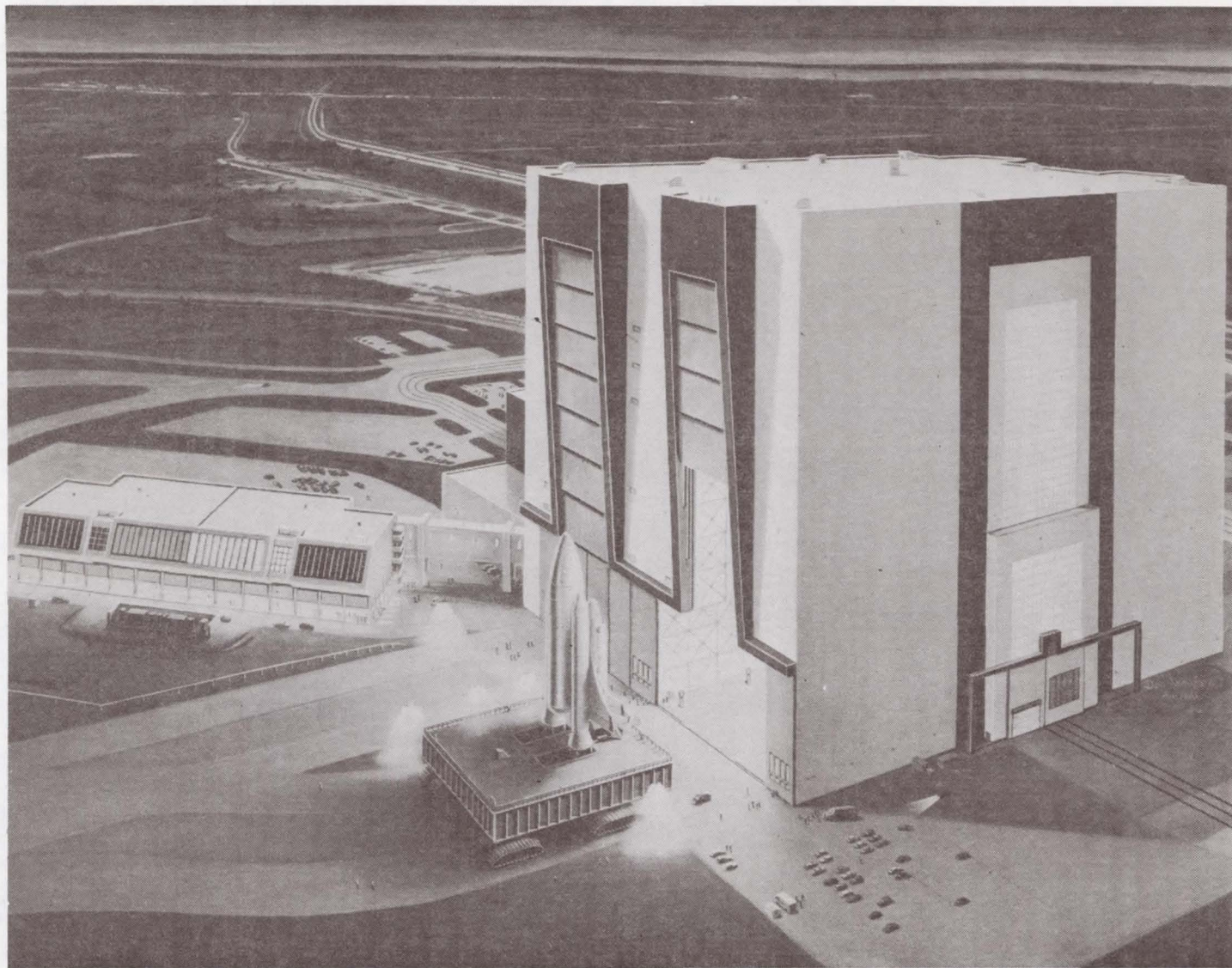


Figure 8. Sketch of Crawler Transporter Carrying ML Platform and Shuttle from VAB

25. MOUNT MECHANISMS

FOR THE SATURN V/APOLLO MOBILE LAUNCHER

AT JOHN F. KENNEDY SPACE CENTER

By Harry A. Balke

Harry Balke Engineers, Cincinnati, Ohio

SUMMARY

The expanse of the mobile launcher (ML), its operational requirements, and the environmental extremes to which it is subjected presented a difficult problem in providing it with a suitable support system. Since the crawler transporter had to pass beneath the ML to lift it for travel, the supports had to be a minimum of 6.7 meters (22 feet) above ground level with a transverse spread of 40.5 meters (133 feet). The support system had to resist hurricane wind loads at the launch pad and yet allow the supported structural frame to expand and contract freely under wide ranges of temperature. Such a support system was conceived and designed by the author. This system consists of six mount mechanisms (Types I through III), devised to meet the previously stated requirements plus a load-carrying capacity for each of 3.2-million kilograms (7-million pounds) downward and 1.6-million kilograms (3.5-million pounds) upward. A similar but lighter system of six mount mechanisms (Types IV through VI) were designed for use in the sheltered environment of the Vehicle Assembly Building (VAB). Each requirement and design result is discussed in the text, and each mount mechanism by location and type is defined with references to visual presentations.

INTRODUCTION

The launch pad, ML erection area, and VAB mount mechanisms function to support the ML and to provide clearance for the crawler transporter to pass beneath the ML. Six mount mechanisms at the launch pad support the weight of the ML and the unfueled Saturn V vehicle and accommodate those horizontal and vertical loads imposed by wind and thermal expansion. Prior to fueling, four extensible columns are placed in position to minimize the rebound effect of the ML at launch vehicle release during firing. Mount mechanisms at the erection area are similar to those at the launch pad. The VAB must be utilized in the event of impending hurricane winds when the launch vehicle is erect on the ML. Foundations at the erection area are designed for hurricane wind loads, but the VAB provides an enclosure for the ML and vehicle, reducing the foundation requirements there. The six types of mount mechanisms with their mating process are discussed in the following text. Since the mount mechanisms always mate with the ML base, the structural makeup of the ML is discussed first to explain the need for different types of mount mechanisms.

MOBILE LAUNCHER

The ML (see figure 1) is basically a huge box-like platform 40.5 meters (133 feet) wide, 48.2 meters (158 feet) long, and 7.6 meters (25 feet) deep, and structurally symmetrical about its longitudinal axis. It supports a 115.8-meter (380-foot) umbilical (service) tower at one end and furnishes support for the vertical launch vehicle 24.4 meters (80 feet) from the tower's transverse centerline. The platform has six primary supports--three mount mechanisms under each of the outside longitudinal girders. Both outside girders are supported at each end and centrally at their intersections with the main transverse girder. This girder supports the inboard legs of the tower 18.3 meters (60 feet) from the end girder that supports the outboard legs. The space between the two rows of mount mechanisms, which are 6.7 meters (22 feet) high, allows clear passage-way for the crawler transporter to pass beneath the ML to lift it for travel (see figure 2).

MOBILE LAUNCHER (BASE) DESIGN

The basic ML structural frame is rectilinear, consisting of five main girders, nominally 7.6 meters (25 feet) deep. Two outside girders are 48.2 meters (158 feet) long, framed between two end girders, 40.5 meters (133 feet) long. The fifth main girder is interior and located 18.3 meters (60 feet) from one end girder and parallel to it. One mount mechanism support point is located at each corner with a central support at each intersection of the interior girder and outside girders.

SUPPORT COLUMN ASSEMBLY DESIGN

For horizontal control of the ML's expansion and contraction, three types of support column assemblies were designed, which, to distinguish them from more conventional supports, were designated "Mount Mechanisms, Type I, Type II, and Type III." With reference to the horizontal plane of support, the Type I is fixed, the Type II allows freedom of movement either laterally or longitudinally but fixed in the other direction, and the Type III allows freedom of movement in both directions (see figure 2).

The various types of mount mechanisms are installed so that one side girder and the interior girder are fixed laterally, but free to expand and contract longitudinally with relation to their common intersection, which is fixed in the horizontal plane. The opposite side girder is fixed longitudinally at its intersection with the interior girder because the interior girder is fixed laterally. The opposite side girder is free to expand and contract longitudinally from that intersection in the direction of its intersections with the two end girders. These intersections are free to move in any horizontal direction, as the opposite ends of the end girders intersect at the side girder which is

fixed laterally. With this support system, the ML is stable and yet allowed to expand or contract without inducing secondary stresses into the girder system.

MOUNT MECHANISM DESCRIPTION

Type II Mount Mechanism (see figure 3) comprises an adjustable 914-millimeter (36-inch) tubular column braced by an adjustable 457-millimeter (18-inch) tubular diagonal. The main shaft is 4.3 meters (about 14 feet) between centers of ball joints, created by 792-millimeter (30-inch) hemispherical bearings, allowing full articulation at each end. The centerline of the diagonal intersects the centerline of the column at the top center of rotation, connecting there with a pin and clevis joint. The diagonal forms a nominal one-to-one slope with the vertical shaft, ending with a 457-millimeter (18-inch) hemispherical bearing whose center of rotation is level with the bottom center of rotation of the main shaft. This arrangement allows the shaft and diagonal brace freedom to move only in a plane about the axis through these centers of rotation. Since relatively small movements are required for operational and environmental adjustments, the main shaft's top moves rectilinearly for all practical purposes.

Each ball joint consists of a hemispherical bearing and a yoke assembly. The yoke consists of an externally threaded forging which flares out into a spherical surface that forms the outer wall of the socket for the hemispherical bearing; all spherical surfaces are centered on the ball-joint center point. A collar, whose inner surface is spherical, fits over the outer wall of the bearing socket and is securely bolted to the flange with which each ball-joint end of the main shaft and diagonal is provided. This arrangement provides ball-joint action if the member is in tension or compression.

An internally threaded boss, flanged and drilled to bolt to the underside of the ML, is screwed onto the column's top yoke. The column's bottom yoke is screwed into an internally threaded boss, an integral part of the base plate assembly, which is bolted to the foundation. A similar system is used for anchoring the strut to the foundations.

Thus, the Type II Mount Mechanism, when bolted to the bottom of the ML, allows the connected point of the ML structure to rotate freely, in flexure, about the top ball joint and move horizontally perpendicular to the nominal column-strut plane but fixed against movement parallel to that plane. The following two types have the same basic design as the Type II but include features that affect the horizontal movement of its ML connection in a different manner.

Type I Mount Mechanism (see figure 4) is simply a Type II Mount Mechanism to which an additional strut has been added that lies in a plane 1.57 radians (90 degrees) in relation to the plane of the strut/column when it is vertical. The additional strut locks the top ball joint and also the connected point of the ML in position, allowing no horizontal movement but allowing freedom for the ML structure to rotate in flexure.

Type III Mount Mechanism (see figure 5) is a Type II Mount Mechanism without any side braces, allowing the connected point of the ML freedom to move in any horizontal direction and to rotate in flexure.

On every mount mechanism, minor features are included to assist operating personnel. A ladder is welded to each column shaft leading to a work platform from which the alignment of the mount mechanism with the ML support point can be observed and the securing bolts installed. Each column is provided with two column centering jacks for adjusting the top of the column horizontally. Where a column is stabilized with a strut, the corresponding centering jack is disconnected.

When the ML is moved by the crawler transporter to its position over the mount mechanism, the ML support points are very close to the centers of the mount mechanisms. A support point is seldom as much as 50 millimeters (2 inches) off center. The mount mechanisms are positioned to receive the 228-millimeter (9-inch) diameter shear pin protruding from the bottom of the ML at each connection point by adjusting the struts or column centering jacks before the ML is lowered onto the mount mechanisms.

Each mount mechanism is designed to carry its full load with the top ball joint 152 millimeters (6 inches) off center of the column base, longitudinally and laterally, simultaneously. Each mount mechanism (Type I, II, and III) is designed for vertical loads of 3.2-million kilograms (7-million pounds) downward and 1.6-million kilograms (3.5-million pounds) upward. The struts are designed for a full hurricane wind of 200 kilometers (125 miles) per hour on the ML, the wind velocity being based on that at the 10-meter (30-foot) level.

VAB MOUNT MECHANISMS

The VAB mount mechanisms are designed and located under the ML in a pattern similar to the outdoor mount mechanisms except they are lighter and simpler because of the greatly reduced loads to which they are subjected (see figure 6).

Type IV Mount Mechanism (see figure 7) is the VAB counterpart of Type I in that it allows no horizontal movement of the connected point of the ML structure but allows freedom for that point to rotate in flexure. To conserve space, the 6.7-meter (22-foot) mount mechanism is 1680 millimeters (66 inches) square in cross section, fixed to the foundation and with a ball joint only near the top. The yoke is flanged at the top for connection to the ML and rests directly on the hemispherical bearing that can be adjusted horizontally with the linear movement of a sliding plate system that rests on the column shaft. Two mutually perpendicular screws are used to slide the bearing surfaces of an intermediate plate and the flat surface of the spherical bearing in relation with one another until the ball joint is properly aligned under the ML connection point. Since uplift is no problem in the shelter of the VAB, Type IV Mount Mechanisms are designed only for compression loads up to 1.72-million kilograms (3.8-million pounds).

Type V Mount Mechanism (see figure 8) is merely a lighter and simpler version of Type II, designed only for compression loads up to 1.72-million kilograms (3.8-million pounds).

Type VI Mount Mechanism (see figure 9) is the lighter and simpler version of Type III, designed only for compression loads up to 950-thousand kilograms (2.1-million pounds).

A nominal wind of 85 kilometers (54 miles) per hour was considered as the basis for the horizontal load used to ensure the lateral stability of the ML in the VAB. This decreased horizontal loading allowed one less strutted Type V Mount Mechanism to be used and a Type VI to be used in its place (see figure 6).

CONCLUDING REMARKS

Since the mount mechanisms were designed to support the ML and vehicle at the VAB, the erection area, and the pads, the different environments and needs at each area necessitated different type mounts. Demands of space limitations, weight, and wind loading with some freedom of movement for positioning caused each type mount to be unique but universal in function. To allow for thermal effects of the ML base, positioning during ML and vehicle transfer, and vehicle vertical positioning, various mount movements and adjustments had to be designed into the mount mechanisms. This design has proven itself through many transfers and launches of the Saturn vehicle.

ACKNOWLEDGMENT

The author wishes to acknowledge the invaluable assistance of Mr. George Walter, NASA Design Engineering Directorate at Kennedy Space Center, Florida.

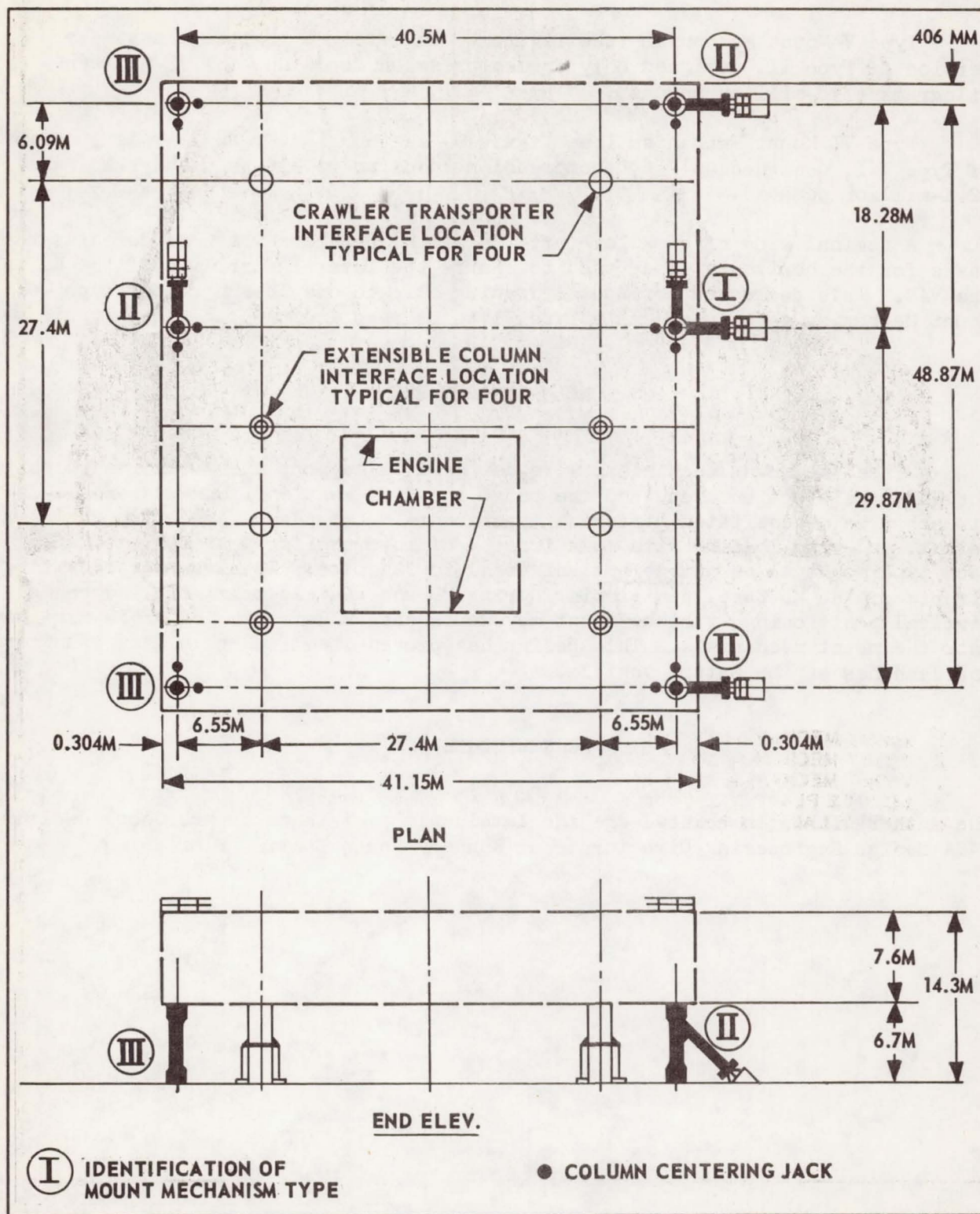
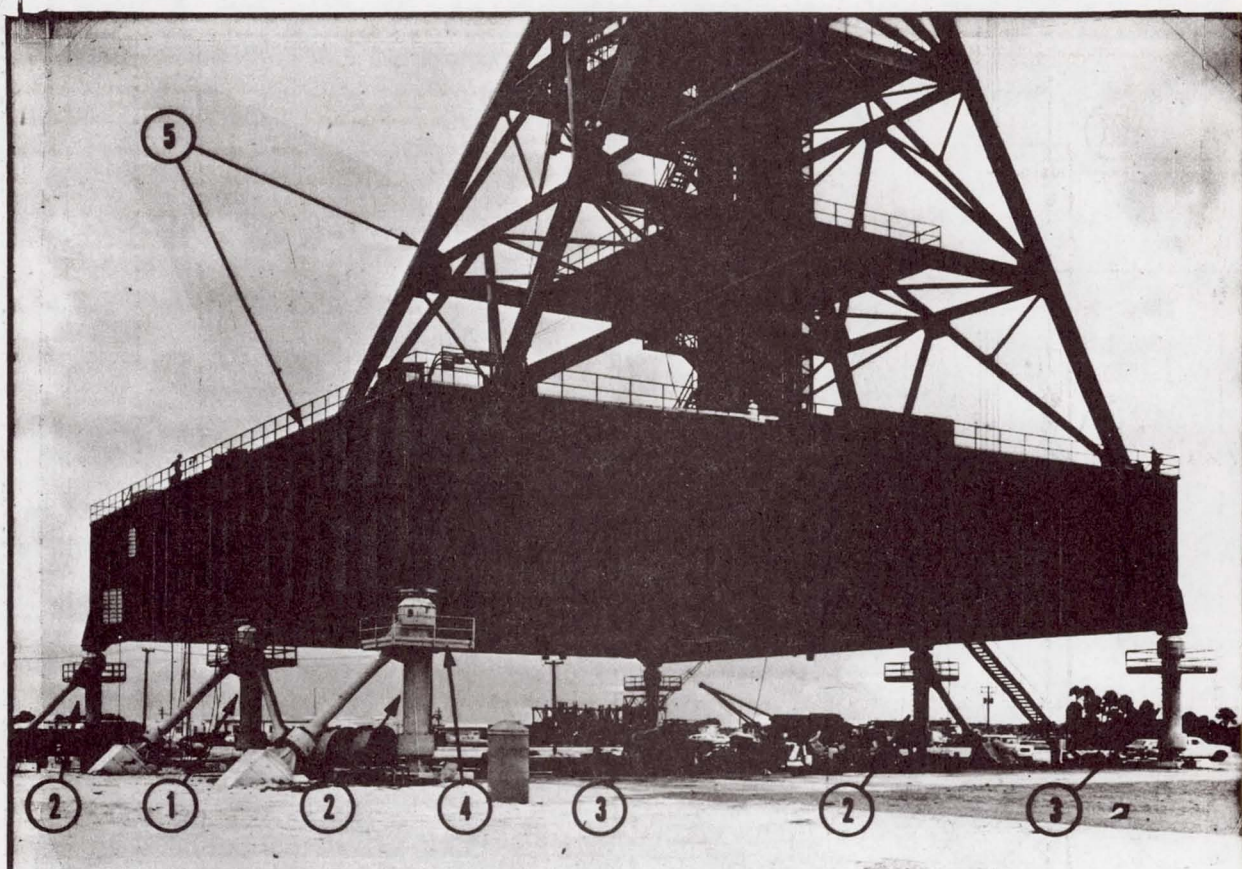


Figure 1. Mount Mechanisms - General Arrangement at the Launch Pad



1. MOUNT MECHANISM TYPE I.
2. MOUNT MECHANISM TYPE II.
3. MOUNT MECHANISM TYPE III.
4. SERVICE PLATFORM (TYPICAL FOR EACH MOUNT MECHANISM);
5. MOBILE LAUNCHER (ML).

Figure 2. Mount Mechanisms - General Arrangement in VAB

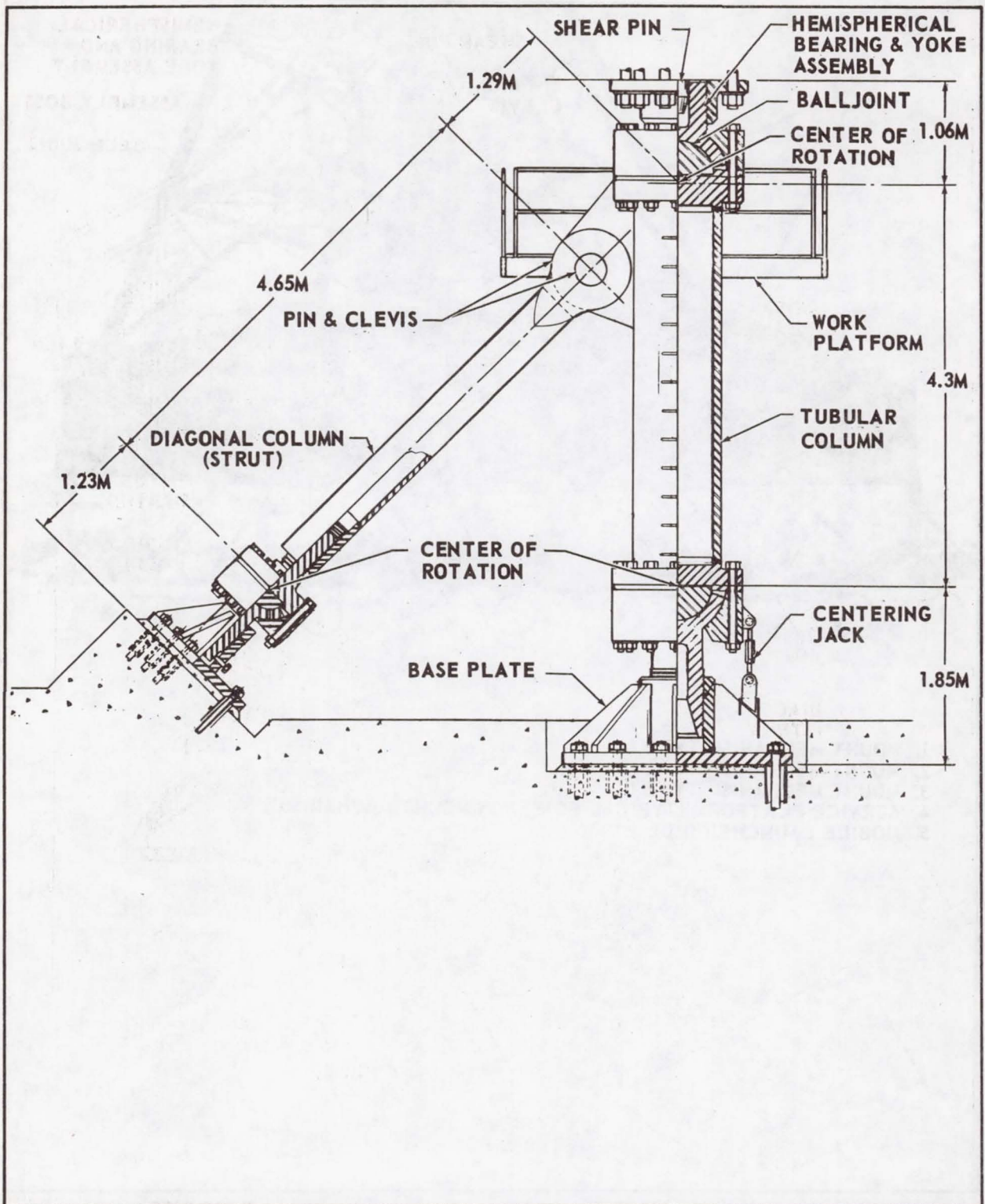


Figure 3. Mount Mechanism Type II With One Side Strut

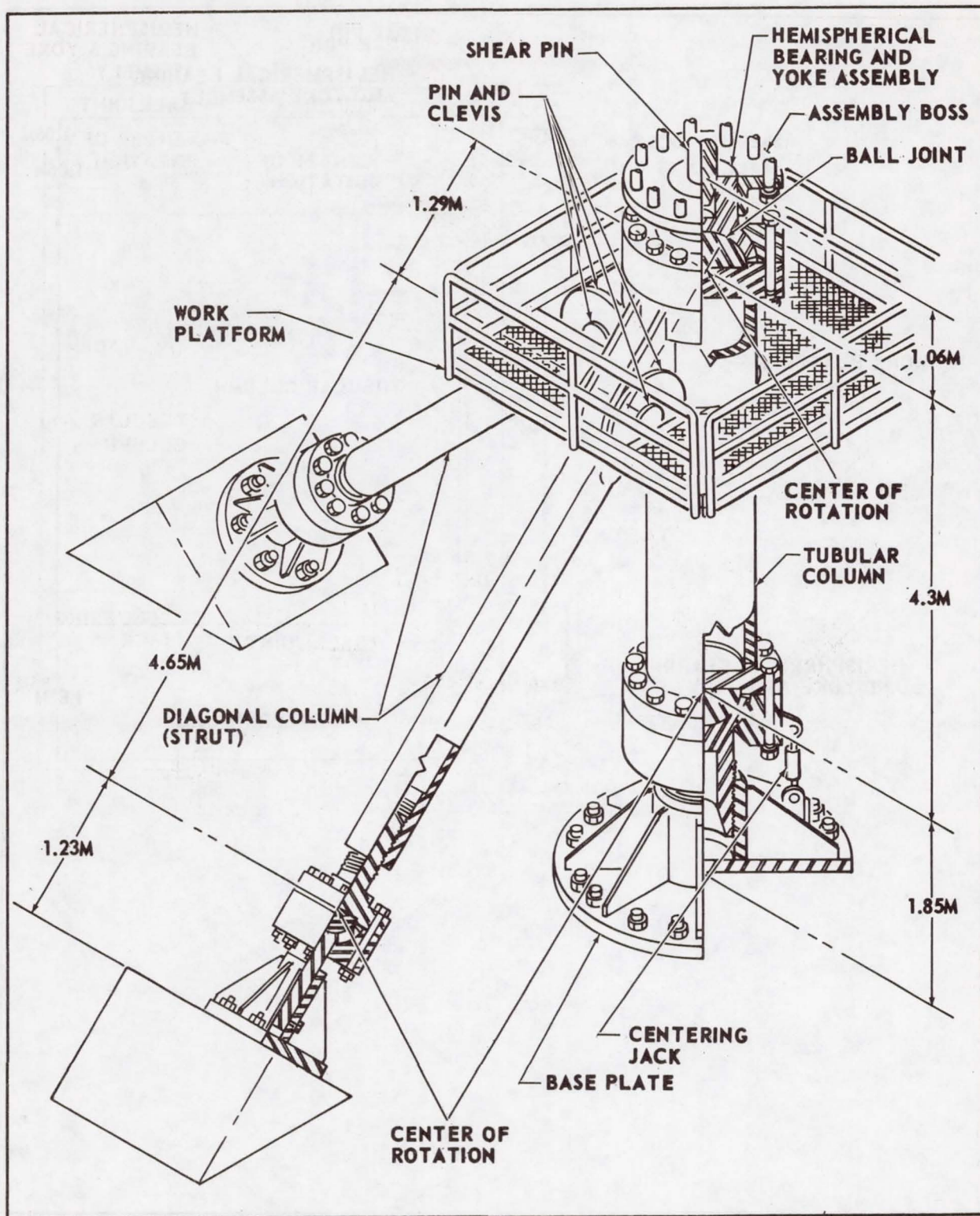


Figure 4. Mount Mechanism Type I With Two Side Struts

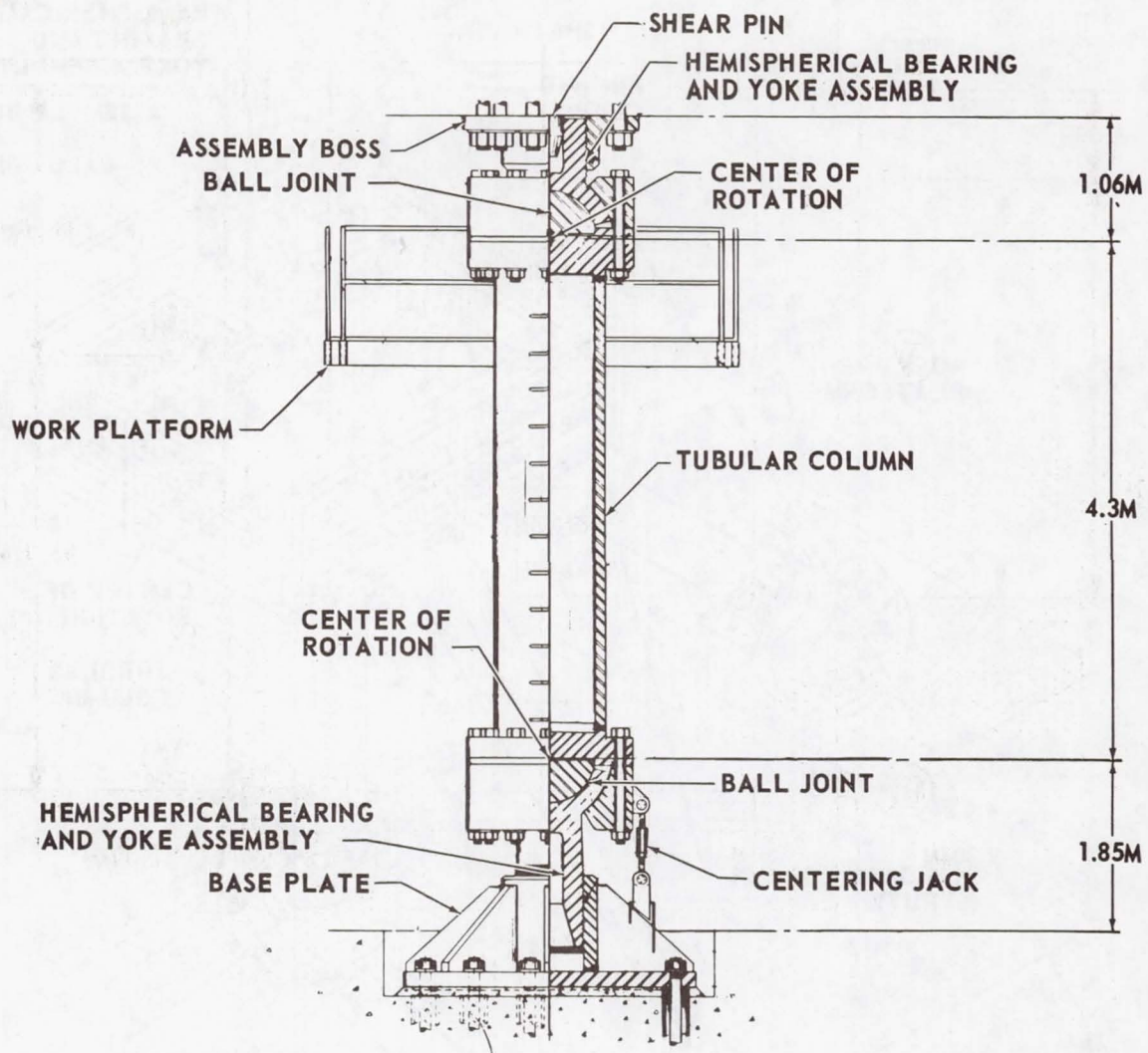


Figure 5. Mount Mechanism Type III Without Side Strut

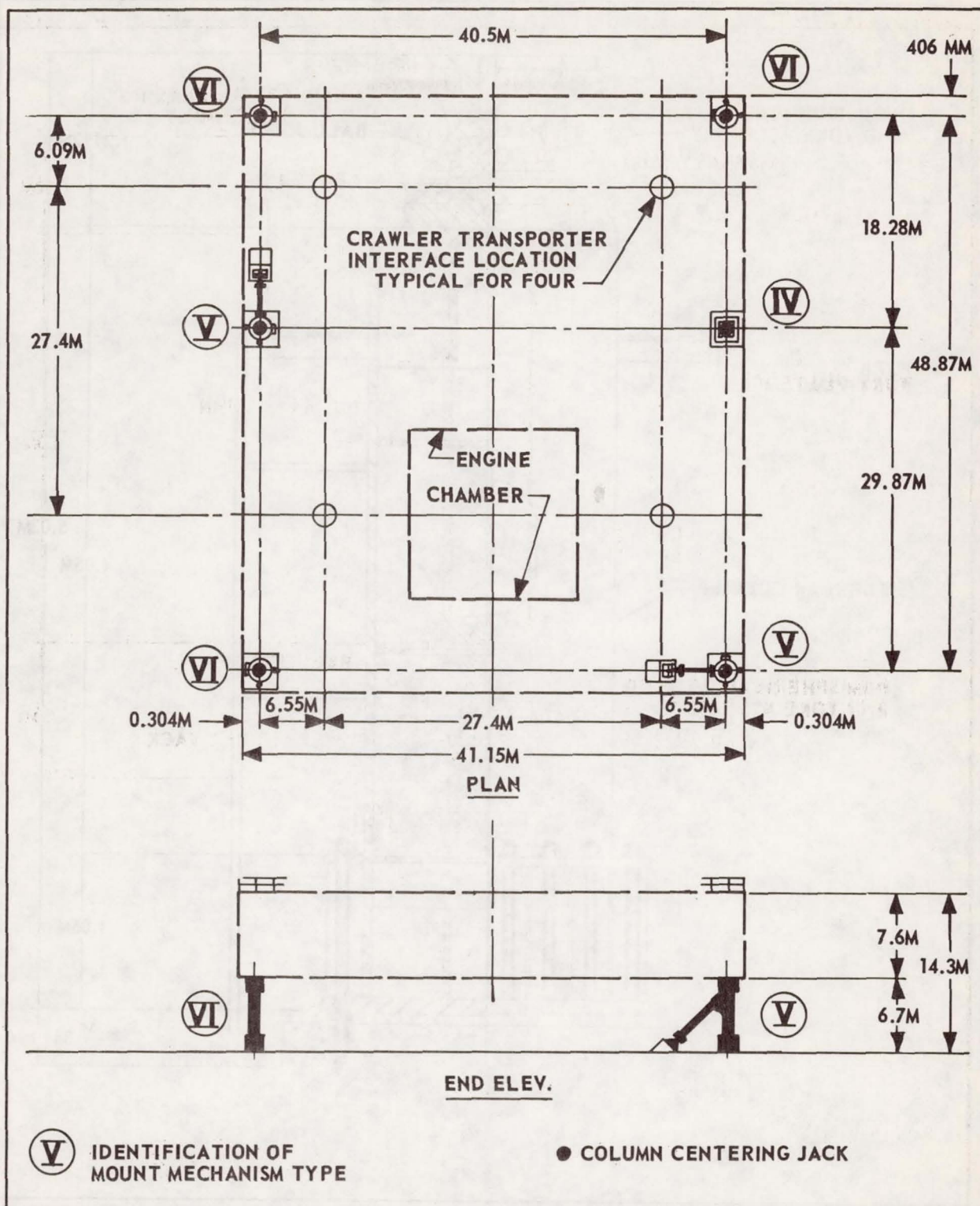


Figure 6. Mount Mechanisms - General Arrangement in VAB

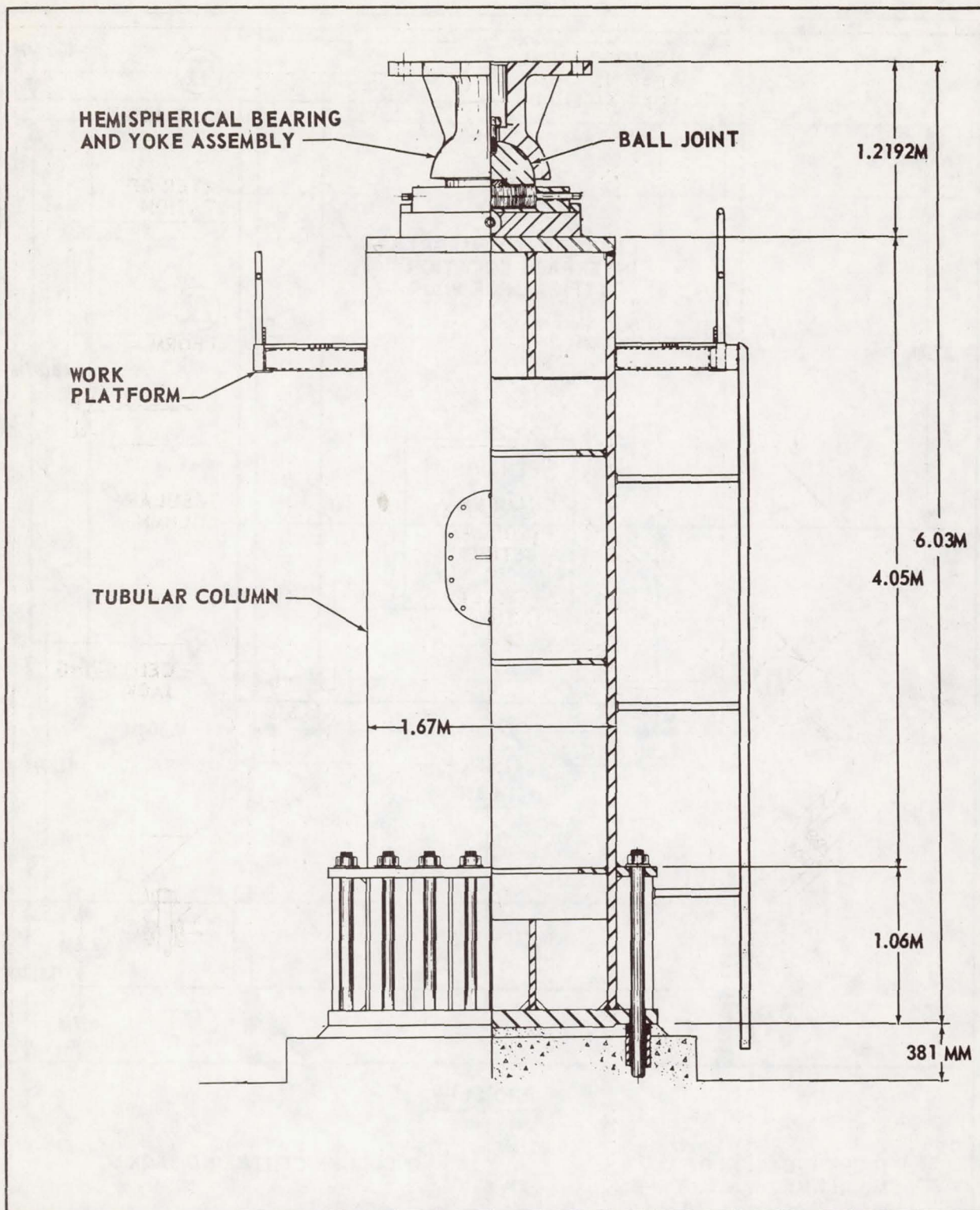


Figure 7. Mount Mechanism Type IV - Fixed Column

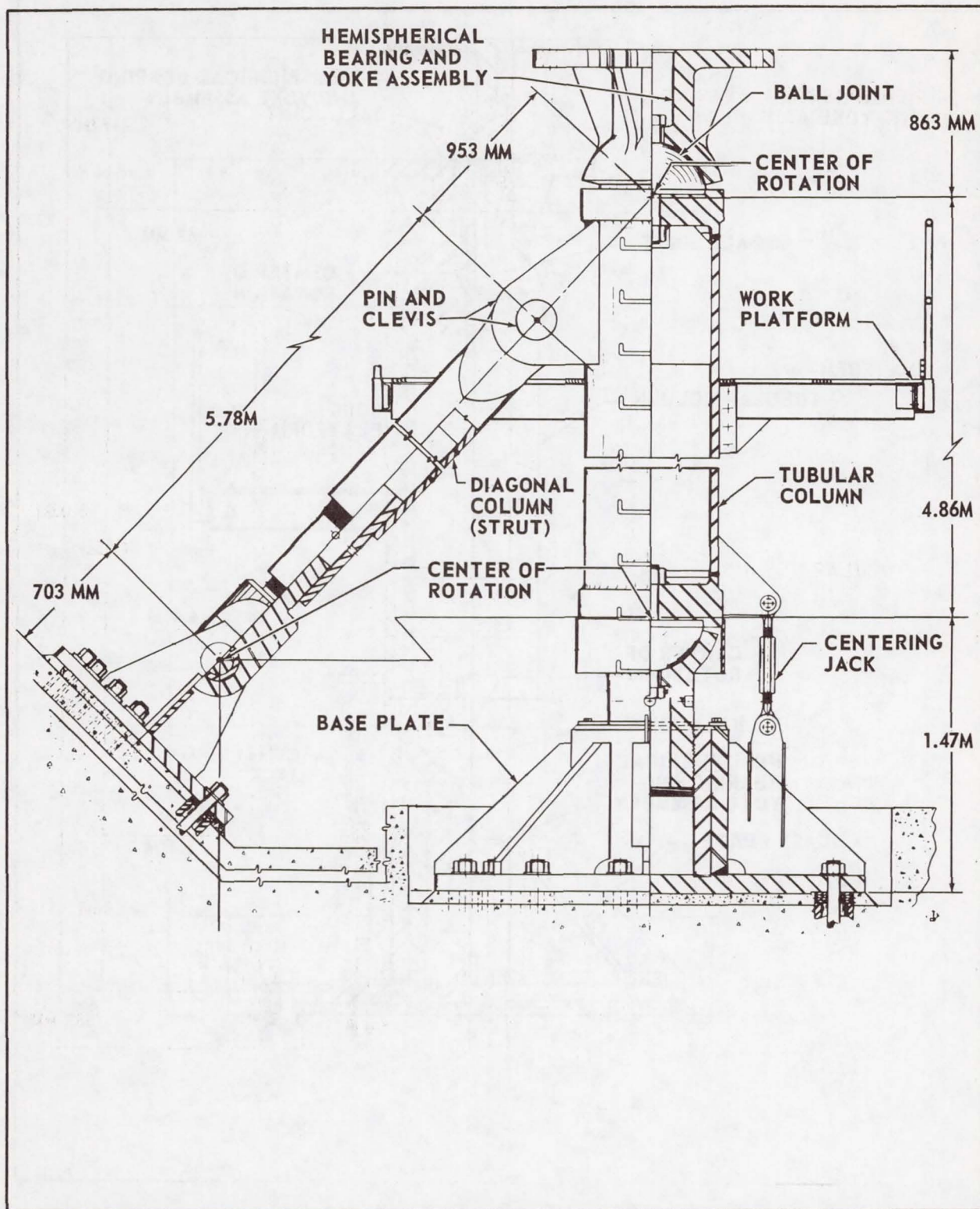


Figure 8. Mount Mechanism Type V With One Side Strut

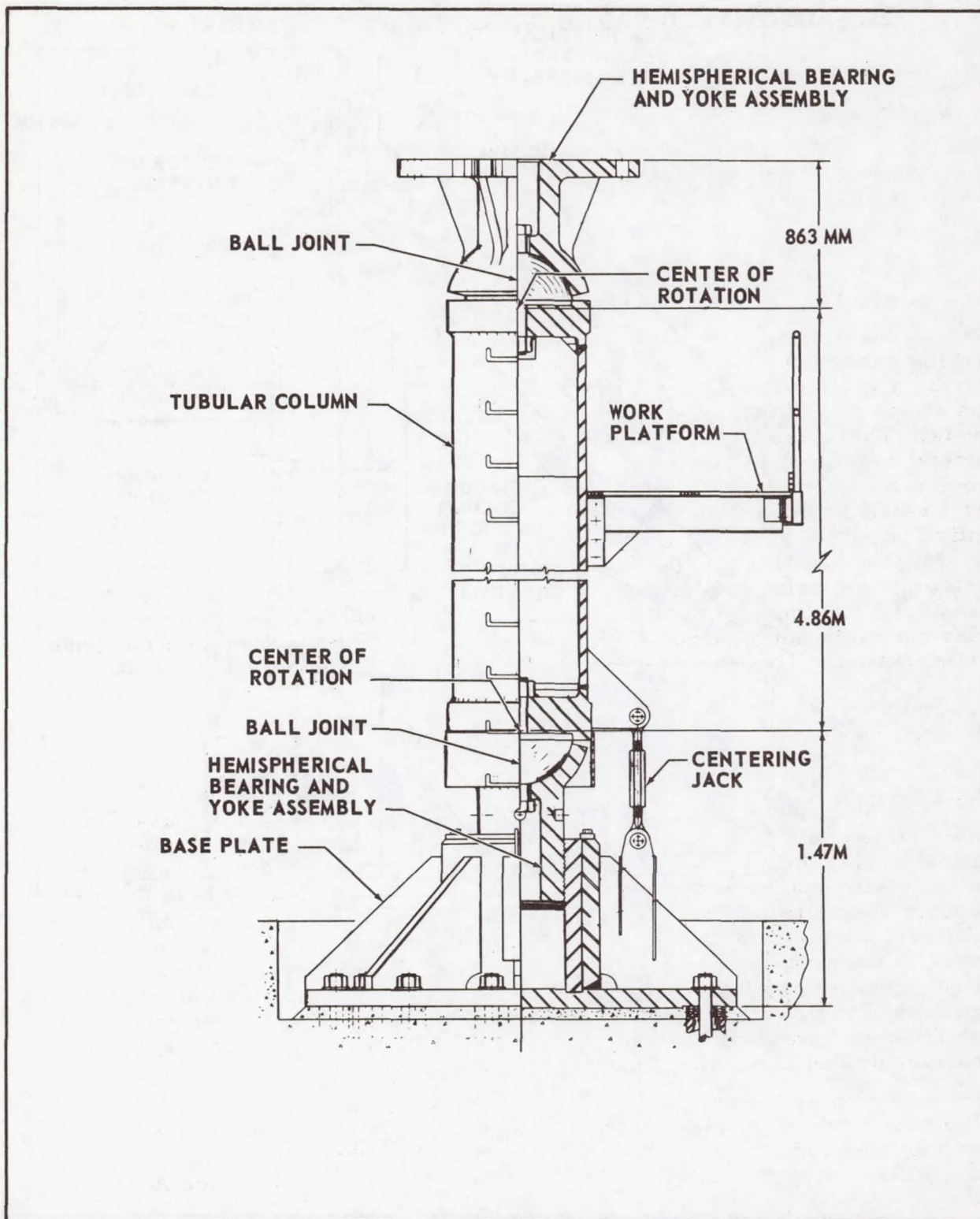


Figure 9. Mount Mechanism Type VI Without Side Strut

26. AUTOMATED PARKING GARAGE SYSTEM MODEL*

By

Earl R. Collins, Jr. **

Jet Propulsion Laboratory
California Institute of Technology
Pasadena, California

SUMMARY

A one-twenty-fifth scale model of the key components of an automated parking garage system is described. The design of the model required transferring a vehicle from an entry level, vertically (+Z, -Z), to a storage location at any one of four storage positions (+X, -X, +Y, -Y) on the storage levels. There are three primary subsystems: (1) a screw jack to provide the vertical motion of the elevator, (2) a cam-driven track-switching device to provide X to Y motion, and (3) a transfer cart to provide horizontal travel and a small amount of vertical motion for transfer to the storage location. Motive power is provided by dc permanent magnet gear motors, one each for the elevator and track switching device and two for the transfer cart drive system (one driving the cart horizontally and the other providing the vertical transfer). The control system, through the use of a microprocessor, provides complete automation. This automation is accomplished by a feedback system which utilizes sensing devices.

INTRODUCTION

The scarcity of adequate automobile parking capabilities, not only in the United States but also in Europe and Japan, has become increasingly more critical during the past decade. Increases in world automobile production and the rising standard of living have coupled with the increases in urban property values to compound this problem. The traditional solution, the multilevel ramp garage, while satisfying many of the requirements, has several disadvantages; e. g., poor volumetric efficiency. Whereas mechanical garages have been developed in the past, and nearly 1,000 patents have been issued in this field, few have been successful to even the slightest extent. Such failures have been fundamentally attributed to: (1) economics, both in construction and in service, and (2) mechanical problems.

*This paper presents the results of one phase of research performed at the Jet Propulsion Laboratory, California Institute of Technology, under Contract No. NAS7-100, sponsored by the National Aeronautics and Space Administration.

**Member of Technical Staff, Design Section, Applied Mechanics Division.

While there is no panacea to all parking problems, the criteria considered to be most critical in solving these problems are economics, volumetric efficiency, customer convenience, and reliability. The model described in this paper represents the key elements of a unique automated parking garage system that is considered by many to be superior to other forms of high density parking systems. This consideration is based upon its storage density, capital costs per space, operational costs per space, personal safety features, and optimal environmental impact.

This model was originally built for a proof-of-concept demonstration. The scale of one-twenty-fifth was selected to be compatible with available plastic scale-model automobiles, which, therefore, dictated the relatively small scale of the model.

CONFIGURATION

The basic configuration is shown in figure 1. An elevator is installed in the center core. There are three floor levels; the top is the loading or vehicle entry level and the bottom two are the storage levels. On each of the storage levels, there is a storage position on each of the four sides of the elevator. The storage levels have two sets of tracks, oriented 90° to each other, crossing at the elevator and extending into the storage positions. The transfer cart typically stays on the elevator but may travel to each of the four storage slots on each floor.

ELEVATOR

The elevator is supported from and driven by two 1/4-28 lead screws on diagonally opposed corners (see figure 2). They are kept in rotational synchronization by a toothed slip-proof belt drive. The basic drive is a small 12-volt dc permanent-magnet motor through a spur gear directly to the master lead screw. There is also a slotted-wheel mounted on the master lead screw to provide rotational counting capability, thereby elevator position, by means of an electro-optical detector. There are limit switches at the extreme elevator positions to prevent damage and to initiate and verify the electronic counter.

TRACK SWITCHING

Directional control, from X-X to Y-Y, is accomplished by means of a track switching system mounted on the elevator (the track crossing position). The track is HO model-train equipment. The segments of track, as opposing pairs within the intersections, rotate down and out to clear the unused cart wheel flanges. Also, when the track rotates up and in, close centering of the cart is provided. The switching positions are: (1) X track and Y track segments both up to lock the cart on the elevator, (2) X track segments rotated

out and down out of the way to allow Y direction travel, and similarly (3) Y segments out of the way to provide X travel. The action is provided by a small 3-volt dc gear motor driving a cam (see figure 3) that in neutral position locks the track up and when rotated 30° holds one track up and rotates the other out of the way.

Small switches are mounted on auxiliary cams, to provide information on the three operating positions.

TRANSFER CART

The transfer cart is the key element in the system. It provides horizontal travel and vertical transfer (see figure 4). The horizontal drive is provided by a miniature 2-volt dc gear motor connected to two drive wheels for each direction. Neoprene tires were added to flanged HO model-train wheels, for added traction and quieter operation. As can be seen in figure 5, X and Y drive wheels rotate together, the unused ones clearing the retracted track. This allows travel in the +X, -X, +Y, and -Y directions with one gear motor by simply controlling the + and - directions by changing the respective dc polarity to the motor and the X and Y directions through the track switching.

The vertical transfer is accomplished by means of a vertical screw jack system. To provide good stability when the platform is in the raised position, four screw jacks are used. The originally specified 6-volt motor was marginal in performance, so it was replaced by a 12-volt unit. Reducing the face width of alternate spur gears was a significant aid in minimizing gear load. The final vertical transfer drive was through a 1670 to 1 reduction gear-head to the 1/4-28 screw jacks.

COMMAND SYSTEM

The on-board electronics consist of limit switches and a diode bridge for the vertical-transfer drive, power and signal rail contacts, and position contact sensors. The system command sequencing is provided by a micro-processor containing 6 read-only memory chips containing 256 instructions each and 4 random-access memory data chips containing a total random access storage of 320 words.

Data input is through a hexadecimal keyboard with a display monitor.

The command system provides the capability of automatically storing and retrieving vehicles in random order by vehicle identification.

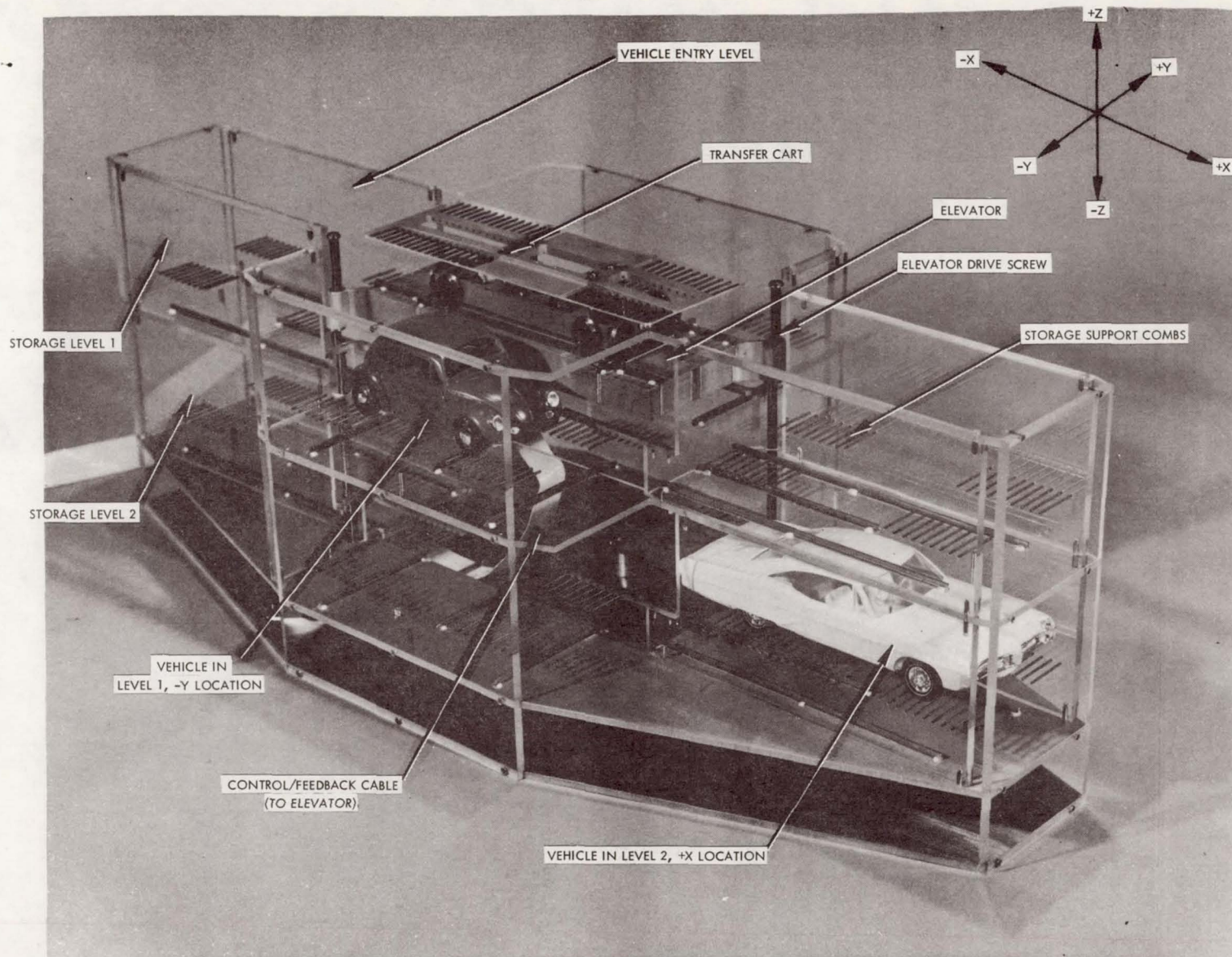


Figure 1. - Automated parking garage model configuration.

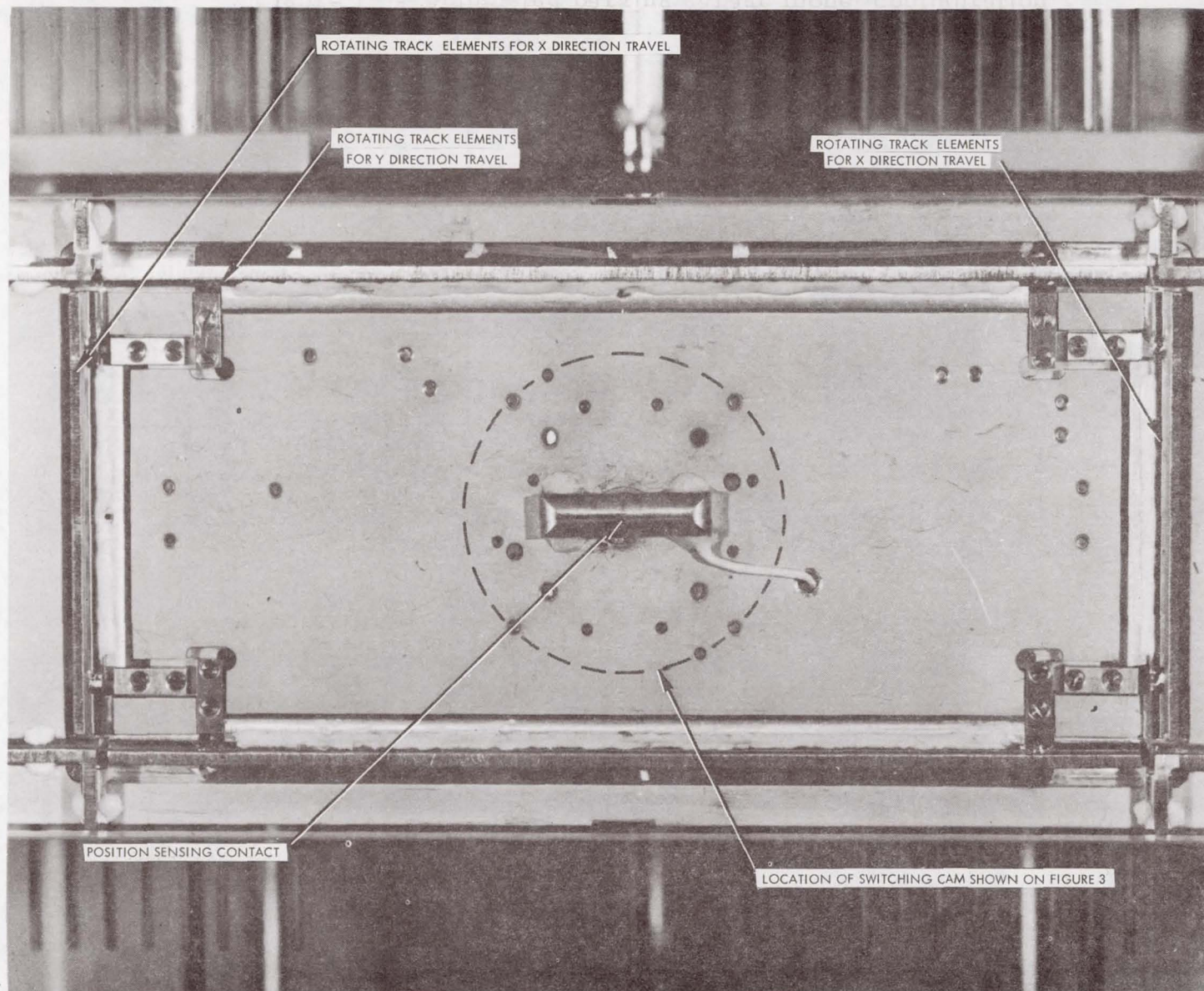


Figure 2. - Plan view of elevator.

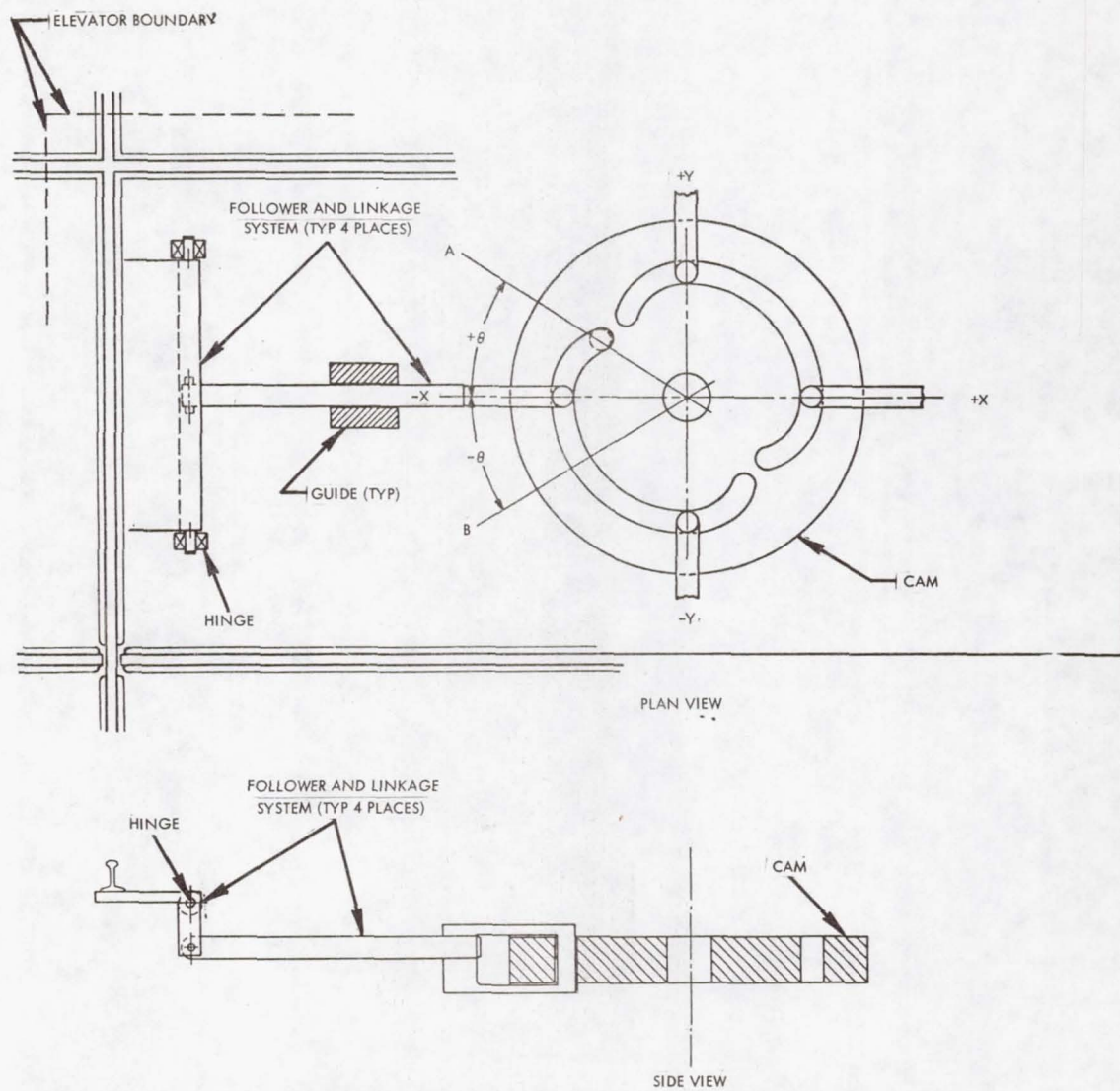


Figure 3. - Track switching mechanism.

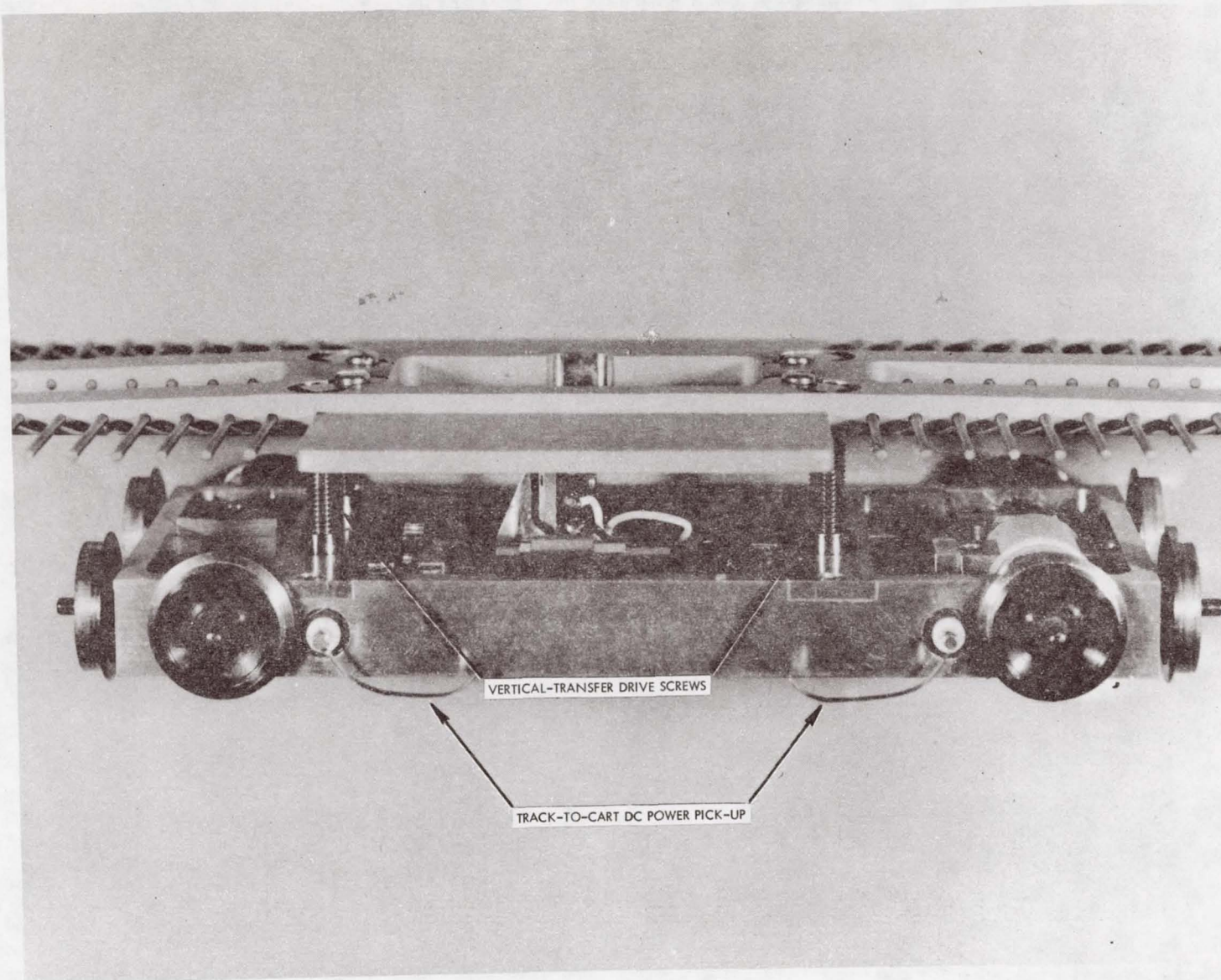


Figure 4. - Transfer cart configuration.

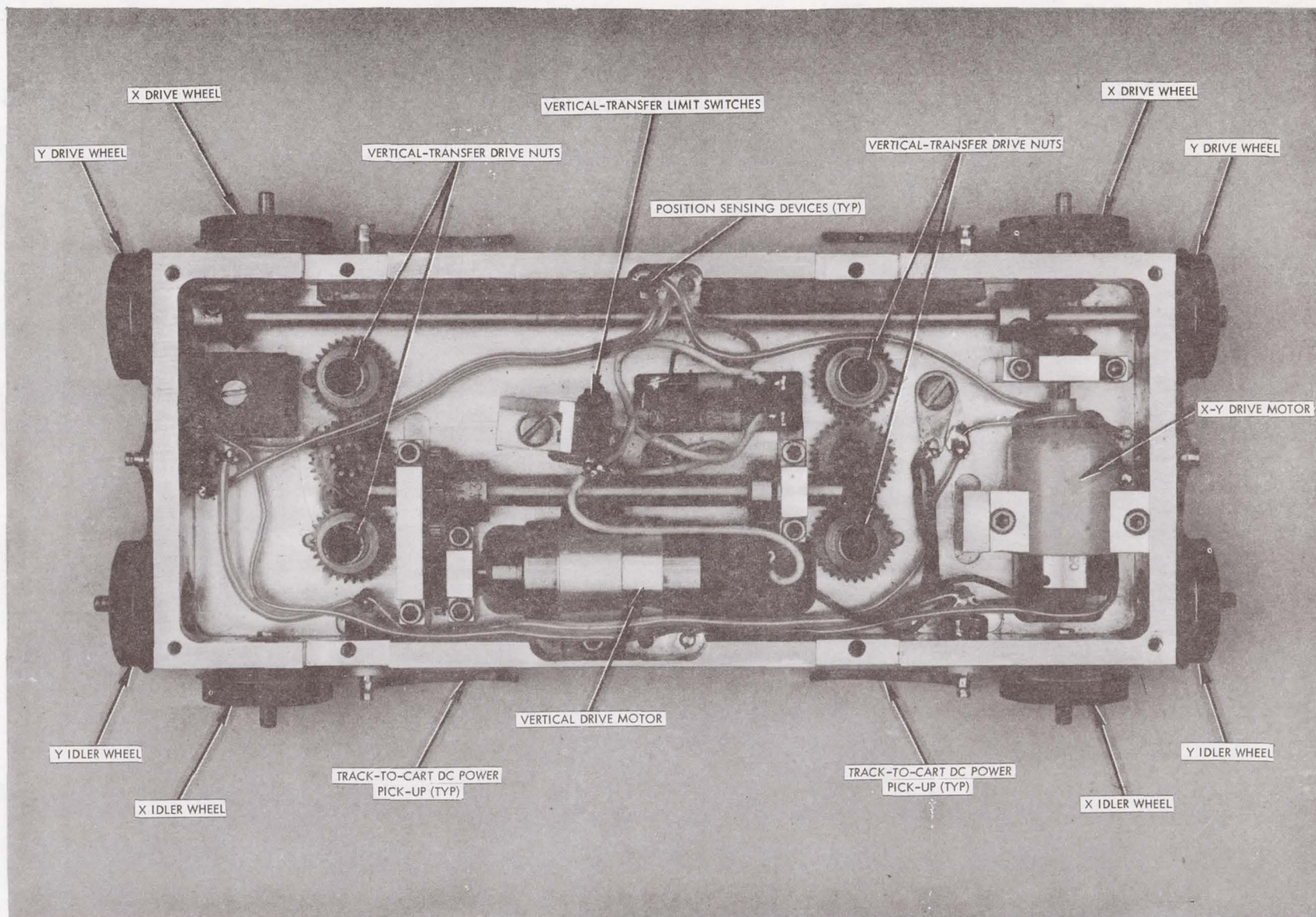


Figure 5. - Transfer cart chassis.

NATIONAL AERONAUTICS AND SPACE ADMINISTRATION
WASHINGTON, D.C. 20546

OFFICIAL BUSINESS
PENALTY FOR PRIVATE USE \$300

SPECIAL FOURTH-CLASS RATE
BOOK

POSTAGE AND FEES PAID
NATIONAL AERONAUTICS AND
SPACE ADMINISTRATION
451



POSTMASTER: If Undeliverable (Section 158
Postal Manual) Do Not Return

"The aeronautical and space activities of the United States shall be conducted so as to contribute . . . to the expansion of human knowledge of phenomena in the atmosphere and space. The Administration shall provide for the widest practicable and appropriate dissemination of information concerning its activities and the results thereof."

—NATIONAL AERONAUTICS AND SPACE ACT OF 1958

NASA SCIENTIFIC AND TECHNICAL PUBLICATIONS

TECHNICAL REPORTS: Scientific and technical information considered important, complete, and a lasting contribution to existing knowledge.

TECHNICAL NOTES: Information less broad in scope but nevertheless of importance as a contribution to existing knowledge.

TECHNICAL MEMORANDUMS: Information receiving limited distribution because of preliminary data, security classification, or other reasons. Also includes conference proceedings with either limited or unlimited distribution.

CONTRACTOR REPORTS: Scientific and technical information generated under a NASA contract or grant and considered an important contribution to existing knowledge.

TECHNICAL TRANSLATIONS: Information published in a foreign language considered to merit NASA distribution in English.

SPECIAL PUBLICATIONS: Information derived from or of value to NASA activities. Publications include final reports of major projects, monographs, data compilations, handbooks, sourcebooks, and special bibliographies.

TECHNOLOGY UTILIZATION PUBLICATIONS: Information on technology used by NASA that may be of particular interest in commercial and other non-aerospace applications. Publications include Tech Briefs, Technology Utilization Reports and Technology Surveys.

Details on the availability of these publications may be obtained from:

SCIENTIFIC AND TECHNICAL INFORMATION OFFICE
NATIONAL AERONAUTICS AND SPACE ADMINISTRATION
Washington, D.C. 20546